UAB
Universitat Autònoma de Barcelona

Simple biochemistry for complex protein-based materials

Hèctor López Laguna

ADVERTIMENT. L'accés als continguts d'aquesta tesi queda condicionat a l'acceptació de les condicions d'ús establertes per la següent llicència Creative Commons: https://creativecommons.org/licenses/?lang=ca

ADVERTENCIA. El acceso a los contenidos de esta tesis queda condicionado a la aceptación de las condiciones de uso establecidas por la siguiente licencia Creative Commons: https://creativecommons.org/licenses/?lang=es

WARNING. The access to the contents of this doctoral thesis it is limited to the acceptance of the use conditions set by the following Creative Commons license: https://creativecommons.org/licenses/?lang=en

PHD THESIS 2023

SIMPLE BIOCHEMISTRY FOR COMPLEX PROTEIN-BASED MATERIALS

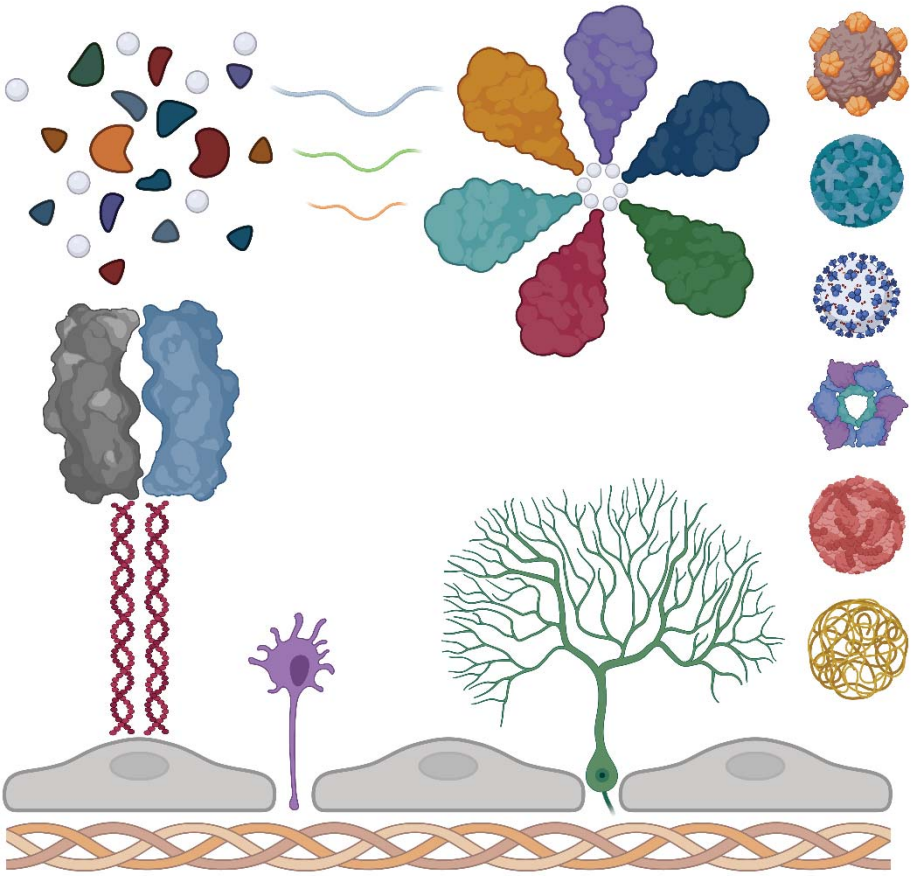

HÈCTOR LÓPEZ LAGUNA

Doctorat en Biotecnologia

Simple biochemistry for complex protein-based materials

Tesis Doctoral 2023

Departament de Genètica i de Microbiologia · Facultat de Biociències

Memòria presentada per l'Hèctor López Laguna per optar al grau de Doctor en Biotecnologia per la Universitat Autònoma de Barcelona

Hèctor López Laguna

Vist i plau dels directors de tesis:

Antonio Villaverde Corrales **Esther Vázquez Gómez** **Ugutz Unzueta Elorza**

Aquest treball s'ha dut a terme principalment a l'Institut de Biotecnologia i Biomedicina, Vicent Villar i Palasí, sota la direcció del Professor Antonio Villaverde Corrales i els Doctors Esther Vázquez Gómez i Ugutz Unzueta Elorza. Una part complementaria, però, s'ha realitzat a l'Hospital de la Santa Creu i Sant Pau (Barcelona, Espanya) sota la supervisió del Professor Ramon Mangues Bafalluy, i a la Universitat de Glasgow (Escòcia, Regne Unit) sota la supervisió del Professor Matthew Dalby.

To all of those who have accompanied me during this journey,

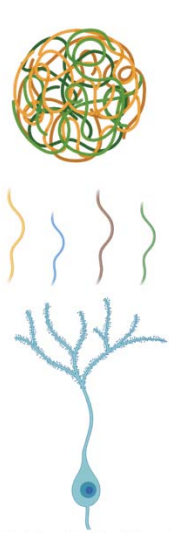

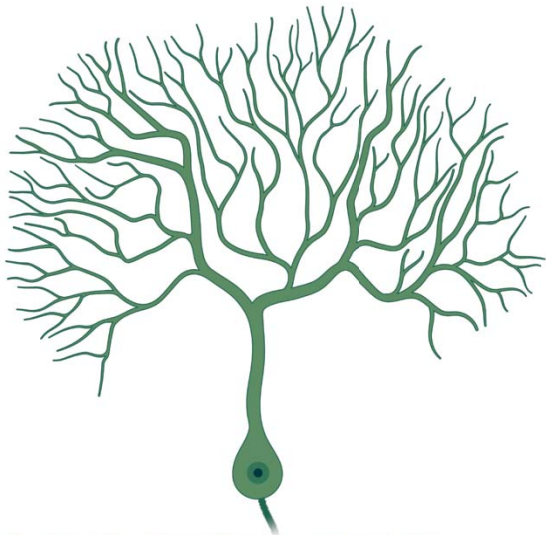

TABLE OF CONTENTS

The author has selected a variety of technical terms and abbreviations that will be explained in detail in this chapter. The intention is to maximize the scientific understanding and ease the reading of the text.

Words marked in bold refer to **keywords** and are displayed at the beginning of each chapter. They have been selected as main ideas to construct the overall storyline furtherly presented. Words marked in dark blue also contain relevant information and are generally subedited to the bold words.

ACTH: It is the adrenocorticotropic peptide hormone that acts on the adrenal gland to control the corticosteroid hormone release.

Actin: An intracellular protein structured as microfilaments and active in cellular movement, contraction, and shape.

Activation energy (E_A): It is the minimum amount of energy necessary to induce molecular changes that promote a chemical transformation or a physical transport. In biology, E_A is defined as the minimum amount of energy necessary to start a biological reaction.

Amide bond: A bond type formed when an amino group interacts with a carboxyl group resulting in the loss of a water molecule.

Amyloid-β peptides: A set of short peptides that are the main components of amyloid plaques.

AraC: Cytarabine is a chemotherapeutic drug that is usually used in acute myeloid leukemia (AML) treatment.

ATP synthase: Adenosine triphosphate (ATP) synthase is a multi-domain protein that promotes the synthesis of ATP, combining adenosine diphosphate (ADP) and inorganic phosphate (Pi) from electrochemical proton motive forces.

Avidin: A biotin-binding protein found in several organisms. It is related to antimicrobial capacities.

Bent-like conformation: A twisted protein conformation related to an inactive conformation, specially observed in integrins.

Bioinorganic chemistry: An interdisciplinary scientific field that studies inorganic entities within biological systems.

Collagen: The main structural protein observed in the skin and connective tissues with a fibrillar structure.

Coordination bond: A type of covalent bond that shares an electron pair from a single atom, especially in divalent metal ions.

Cross-β sheet motif: A structure formed by the lamination of successive β sheet layers, which are abundantly observed inside amyloid fibrils.

CXCR4: The chemokine receptor type 4 (also known as CD184) used by the human immunodeficiency virus to infect CD4+ T cells. It is also a known tumoral marker.

Cytoskeleton: A microscopic network of filaments inside living cells which gives them shape, mobility, and structure sustenance.

Disulfide bond: A bond type formed when two thiol groups couple to each other.

DITOX: A cytotoxic protein domain from *Diphtheria* toxin.

EDTA: It is the Ethylenediaminetetraacetic acid that widely binds to divalent metal ions forming water-soluble stable complexes.

Electrophile (Lewis acid): The chemical tendency to attract electrons. When a chemical compound can accept an electron pair from a donor is described as a Lewis acid.

Endorphin-β: A peptidic hormone produced in certain neurons associated with pain, thrill, hunger, sexual behavior, etc.

FDA: The Food and Drug Administration is the American agency responsible for protecting the public health and ensuring efficacy, safety, and security of human and veterinary drugs.

FdU: Floxuridine is a chemotherapeutic drug, analogue of pyrimidine, which is usually used in colorectal cancer treatment.

Fibronectin: A multifunctional adhesive structural protein related to cell attachment and motility, embryogenesis, and tissue repair.

G protein-coupled receptor (GPCR): An integral membrane protein used to convert extracellular stimuli (neurotransmitters, hormones, etc.) to intracellular responses

Genetic fusion: A molecular biology technique that artificially fuses genes from different nature.

GFP: Green fluorescent protein (GFP) is a protein that exhibits bright green fluorescence when exposed to blue light and that is used as gold standard in protein engineering.

Growth hormone (GH): A hormone protein produced in the pituitary gland which stimulates the release of fatty acids from adipose tissues and protein synthesis in muscle cells.

Homeostasis: A process of actively maintaining a fairly stable equilibrium between interdependent elements, especially in physiological processes.

Hydrolase: An enzyme that catalyzes the break of chemical bonds using water.

IMAC: Immobilized Metal ion Affinity Chromatography is a protein purification method that uses enriched metal-associated columns to coordinate histidine tagged proteins.

Insulin granule: A dense core granulated supramolecular structure constructed to store crosslinked insulin inside pancreatic cells.

Integrin: A transmembrane protein that mediates the interaction between the cellular cytoskeleton with the extracellular matrix. Thus, it is involved in cell adhesion.

IPTG: Isopropyl β- d-1-thiogalactopyranoside is a molecular compound that mimics the allolactose metabolite, which triggers the lac operon transcription.

IRFP: Near-infrared fluorescent protein (IRFP) is a protein that exhibits bright near-infrared fluorescence (NIR) preferred for in vivo imaging.

Irving-William Series: A list of ordered divalent metal ions depending on their relative stabilities when water is replaced by a ligand.

Lactic acid: An organic compound created by cells when glucose is broken down to generate energy (ATP) in the absence of oxygen.

Macromolecule: A molecule made of a very large number of atoms like nucleic acids, proteins, polymers etc.

MAPK: It is the mitogen-activated protein kinase involved in directing cellular responses induced by osmotic stress, heat shock, mitogens and proinflammatory cytokines.

Mesenchymal stem cells: A stromal cell type produced in a variety of tissues with multipotent properties essential to repair and make tissues.

Microbial cell factory (MCF): A bioengineering concept that takes advantage of microbial cells to mass produce metabolites or recombinant proteins.

Microtubule: A hollow tubular-like microscopic structure found in the cytoplasm that helps to support cell shape and chromosomic movement.

MMAE: Monomethyl auristatin E is an antimitotic chemotherapeutic drug used for cancer treatment and generally linked to a monoclonal antibody (MAb).

MPS system: The mononuclear phagocyte system which comprises a family of cells (marrow progenitors, blood monocytes, and tissue macrophages) involved in tissue repair, inflammation, and homeostasis maintenance.

Non-canonical amino acids: A set of unnatural amino acids that are not located in the genetic code of naturally occurring organisms and generally made in a laboratory.

NTA-Ni^{2+}: A chemical complex constructed by the Nitriloacetic acid (NTA) chelating divalent metal ions such as Nickel (Ni^{2+}). This complex can interact with histidines using the imidazole groups.

Nucleophile: The chemical tendency to donate electrons.

Opsonin: An extracellular protein that binds to cells or extracellular microorganisms making them more susceptible to be phagocytized by the MPS system.

Oxidase: An enzyme that catalyzes the transfer of a hydrogen atom to an oxygen molecule.

PE24: A cytotoxic protein domain from *Pseudomonas* exotoxin A.

PKA: The protein kinase A is involved in the regulation of cyclic-AMP (Adenosine monophosphate) dependent physiological processes in cells, including glycogen, sugar, and lipid metabolism regulation.

Polarization of cells: The spatial difference in cell's structure, function and shape which enables them to develop specialized functions.

Polyethylenimine (PEI): A polymer constructed by the repetition of amino groups and two carbon aliphatic spacers with a polycationic surface.

Proteome: The catalogue of proteins produced by an organism or biological system.

Quantum world: A world found in the subatomic scale (a world that we can't see), in which elements do not behave the same way as in the macroworld (a world that we can see).

Reactive Oxygen Species (ROS): A group of unstable oxygen-based molecules that easily react with other molecules inside the cell.

Recombinant cell factories: An engineered collection of cells able to produce proteins from cloned genes.

Recombinant DNA technologies: A technology that involves using enzymes and laboratory methodologies to isolate and manipulate DNA segments of interest to create new functions.

RNA: Ribonucleic acid is a nucleic acid, similar to DNA, which principally acts as a messenger molecule carrying the instructions for protein synthesis, among other related functions.

Self-assembling: A process in which a disordered system or group of molecules spontaneously organizes into a more complex and stable structure.

Sepharose: A crosslinked and beaded form of agarose used as an adsorbent in chromatography, electrophoresis, and other protein engineering techniques.

Size exclusion chromatography (SEC): A purification strategy that uses spherical beads with different pore sizes to separate proteins.

Streptavidin: A tetrameric protein, similar to avidin, which strongly interacts with biotin. It is related to antimicrobial capacities and used for purification purposes.

Supramolecular complex: A dynamic and complex architecture made off small molecular monomers able to assemble and disassemble under certain environmental conditions.

Syphilis: A bacterial based (*Treponema pallidum*) and sexually transmitted infection (STI) which causes substantial morbidity and mortality.

Talin: A high molecular weight cytoskeletal protein that acts as a key regulator of actin and extracellular matrix communication.

Theragnostic: It is a clinical strategy that combines therapeutics and diagnostics.

Transcription factors: Proteins involved in regulating and initiating the transcription of genes.

Tubulin: An intracellular protein that is the main constituent of microtubules.

Urease: An enzyme that catalyzes the hydrolysis of urea into carbon dioxide (CO_2) and ammonia.

Vimentin: A structural filamentous intracellular protein expressed in mesenchymal cells usually related to cell differentiation.

PRELUDE

There is an intrinsic need of understanding the surrounding world. A need to shell how nature has created such a beautiful environment of coexisting species; in which the only way out is a continued iterative process of trials and errors. Sometimes it feels like a constantly losing game.

As scientists, we try to create order from this chaos. We try to understand all the uncertainty that surrounds us the best way possible; as in an everyday class, and nature is our own professor.

Our work is simple, create more or less accurate hypothesis that could be experimentally tested, and from our perception extract conclusions that could be used by others. Like mounting a pyramid, piece by piece, and we are the constructors.

This thesis has been the weaving process of years of learning. The sum of answers from given questions progressively understood from nature. A conversation: I ask nature and nature responds, usually not as expected, but as it should be.

Thus, there is one thing that has become clear to me; there are not good or bad results, neither absolute truths. There are natural observations that create a pattern. A pattern that repeats in different scenarios. We have taken advantage of these repetitive observations and constructed our own scientific pyramid that allows us to create novel protein-based smart materials that may help others afterwards.

At the end, the essence of being happy may also reside on our contribution to the world. The grain of sand we leave before we depart. May these words be categorized as unusual, but for me are necessary to understand why I am doing what I am doing. Their expression gives me the energy to continue creating new stories, as this one seems to be ending. The process, not the outcome, so they say. Thank you very much for taking your time to read the following lines: they have been written following instinctive rhythms, my own rhythms. Hope you find out something from them. A journey of a thousand miles begins with a single step. So, let's start…

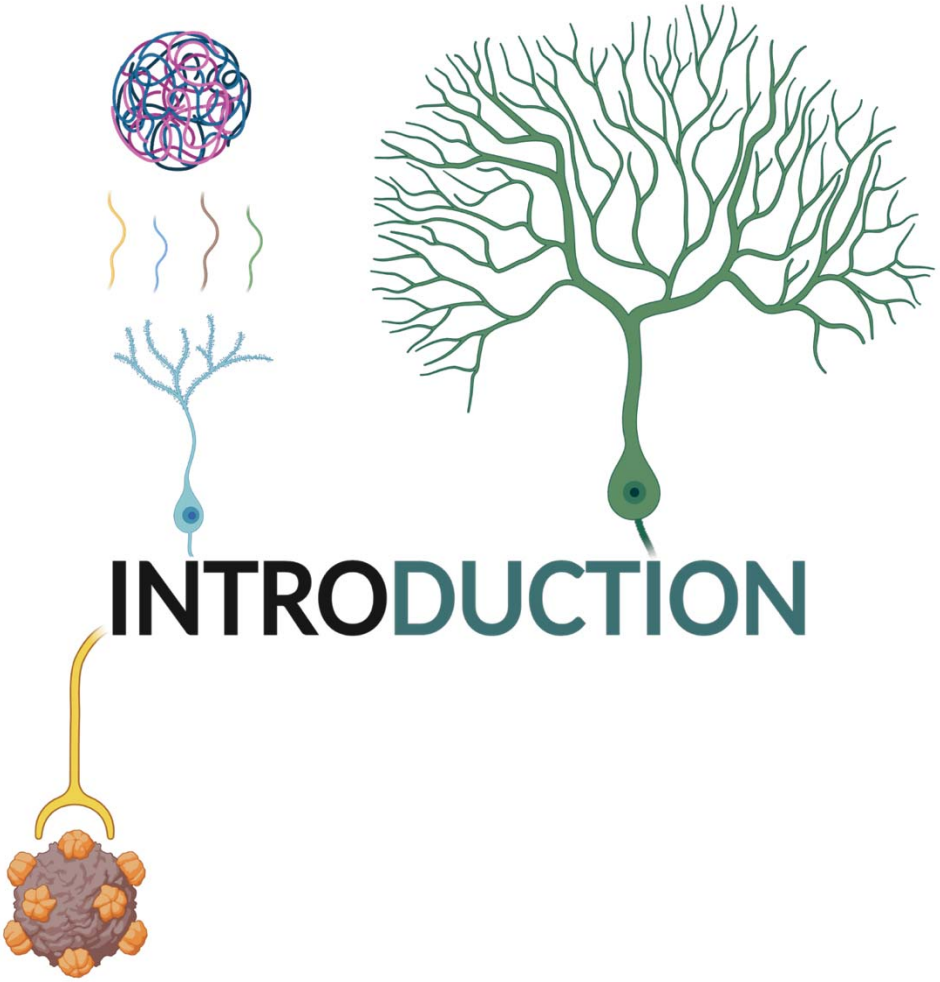

INTRODUCTION

1. The ABC of biochemistry in living systems

Keywords: Biochemistry, biomolecules, hierarchical organization, supramolecular structures, and protein-based assemblies.

1.1 The foundations of everything

It is said that the universe was created approximately fourteen billion years ago due to a cataclysmic explosion of hot energetically enrich subatomic particles (a theory in constant evolution) [1]. In just few seconds, all we today can see, hear, feel, touch, smell and predict was formed in an eye blink [2], and still remains to this day [3].

Following this timeline, around four billion years ago, an incremental complexity raised when a particular number of chemical gears matched, with the formation of the first microorganisms [4]. These new-born living creatures were able to use the simplest inorganic compounds from the antique Earth soil and sunlight, to extract energy. This survival mechanism along with the natural earthly evolution finally led to the creation of more complex **biomolecules** able to conduct highly complex functions, as organisms' complexity also increased [5]. It would be fair to say that all living organisms, including human beings, have been created from stardust [6].

In front of this astonishingly complex landscape, **biochemistry** was born to study and understand the chemistry of life, which at the end, determines the specific properties of each living organism [7]. Yet, if we can understand nature and its physical, chemical, and biological laws we would be able to use them in our advantage and design new medical approaches to solve our current most feared existential issues.

1.2 The building blocks of life

The biochemical studies carried out during the last decades have allowed to understand how biomolecules such as lipids, nucleic acids, proteins, and carbohydrates organize themselves in certain and predefined ways to establish the basic pillars of life [7]. This complex nanoscopic organization allows each entity to have a specific function, which concatenates and cooperates with the functions of their counterparts creating a system that is constantly adapting and evolving [8]. Cells appeared as the result of this complex network, being able to survive on their own through a variety of interconnected metabolic processes [9] and

constructing the building blocks of all living organism owing to a precisely established **hierarchical organization** [10]. From this first stage, it is well known how (1) the coordinated and iterative integration and polarization of cells [11], (2) the surrounding extracellular matrix [12], and (3) the mesenchymal stem cell differentiation triggered by specific transcription factors [13] can create tissues. Tissues appear as the second stage of the hierarchical organization that allows the creation of bigger and higher-in-complexity organisms [10]. A similar hierarchic process promotes the formation of organs from tissues, and systems from organs [11] that will end up constructing a whole unique living organism. Each step of this pyramid allows the execution of broader and systemic functions, and because of that, it is essential to understand the nano and microscopic worlds to be able to influence the macroscopic world. The more we understand the small, the more effective and precise our scientific inventions will be.

1.3 The world of supramolecular complexes

When scientists study cells they usually arrive to the same conclusion. Cells are incredible builders of **supramolecular structures**. Indeed, cells can specifically select a discrete set of nanoscale biomolecules to assemble bigger multifunctional suprastructures in the roots of a precise hierarchical organization [14]. In this regard, these suprastructures, known also as supramolecular complexes, coexist inside cells with biomolecules as a dynamic system (**Figure 1**) with concrete energetic restrictions [15]. These energetic landmarks allow the spontaneous self-assembling or interaction between biological molecules to create bigger structures ranging from the nano to the micro scale. Meanwhile, biomolecules are generally sustained by strong covalent bonds, such as amide and disulphide bonds linking amino acids or coordination bonds linking metal ions with proteins, supramolecular complexes are usually held together by noncovalent interactions, which are individually weak, but strong when added altogether [7]. Hydrogen bonds observed between chemical groups with different polarities, ionic interactions observed between charged opposite groups, hydrophobic interactions observed between non-polar groups in aqueous solution and van der Waals interactions observed due to London forces, are some examples of noncovalent bonds able to maintain the quaternary structure of supramolecular complexes [16,17].

Cells use a combination of covalent and noncovalent interactions to generate a dynamic and flexible system in which macromolecules are in constant architectural movement [18]. Unique

structures are rapidly assembled, held, or disassembled depending on the biological needs of cells, allowing the system to quickly adapt [19–21].

One of the most fascinating supramolecular structures observed inside cells is DNA (Deoxyribonucleic Acid). DNA consists of two strands of nucleotides held together by hydrogen bonds, creating a double-strand helical macrostructure that contains all the instructions needed for an organism to develop, reproduce, and survive [22]: a true wonder of nature.

Aside from this iconic example, there is an additional set of supramolecular complexes that comprehend crucial roles in cell functioning, such as (1) biological membranes (composed by proteins, lipids and carbohydrates, which are indispensable for the proper cell functioning) [23], (2) secretory granules (serving as storage pools for selected biomolecules; they usually take advantage of metal ions such as zinc 2+ to create this type of protein cargos, e.g. insulin granules) [24], (3) amyloids (serving as hormone storage depots ordered in fibrillar-like structures with high levels of cross-β sheet motifs, e.g. ACTH and β-endorphin amyloids; they also take advantage of metal ions to form this type of assemblies) [25,26], (4) inclusion bodies (serving as submicron dynamic proteinaceous particles formed by an unbalanced equilibrium between aggregated and soluble functional protein. They are majorly observed in recombinant cell factories and viruses) [27–29] and (5) protein assemblies (used by cells as protein-based and self-assembled macrostructures with a plethora of different functions, and architectural properties, e.g., collagen and actin) [30–32] (**Figure 1**).

Each one of these supramolecular complexes, hand in hand with its biomolecular counterpart, create a network of constant intermolecular communication that allows cells to survive [33]. But amongst all these different structures, protein assemblies appear nowadays as very attractive due to their great structural variety and multiple functionalities [34].

1.4 The world of protein-based assemblies

From all the different biomolecules that are taking part in cell biochemistry, proteins appear as the redundant actors carrying out a plethora of cellular functions [35,36]. Actually, proteins are responsible of a vast amount of colloquial tasks such as (1) inner organization, cell shape and dynamics (e.g. α and β -tubulin forming microtubules) [37], (2) intracellular response and cell proliferation (e.g. Mitogen-activated protein kinases, MAPK) [38], (3) waste and clean-up (e.g. proteases) [39], (4) reaction catalysis and energy production (e.g. ATP synthase) [40], and (5)

outer signals reception (e.g. G protein-coupled receptors) [41], etc (**Figure 1**). Since proteins exhibit a wide spectrum of different functionalities, protein variability is also huge. They can be big or small, exist as monomers or create assemblies, they can be mostly hydrophobic or hydrophilic, and they can also be constantly moving or immobile [42]. This functional versatility matches with the intrinsic structural properties, meaning that protein sequence, structure and hierarchical organization usually go hand in hand with a specific function [43]. In short, proteins end up acting as reporters that are constantly changing in response to specific inner or outer stimuli [44].

Nature takes advantage of such protein architecture to create supramolecular complexes, namely **protein-based assemblies**, able to trigger more complex and specific reactions, and to create an astonishingly huge landscape of structural diversity [34] (see table 1 in annexes, page 265).

All these understandings have allowed scientists to start exploring new ways of creating helpful biological devices, from expressing recombinant proteins (see chapter 3), to manufacturing smart materials using biomolecules (see chapter 4) and particularly using proteins (see chapter 5). But first, there is still a set of small entities that are crucial for biomolecules to work. Without them, life, as we understand it, would not be possible.

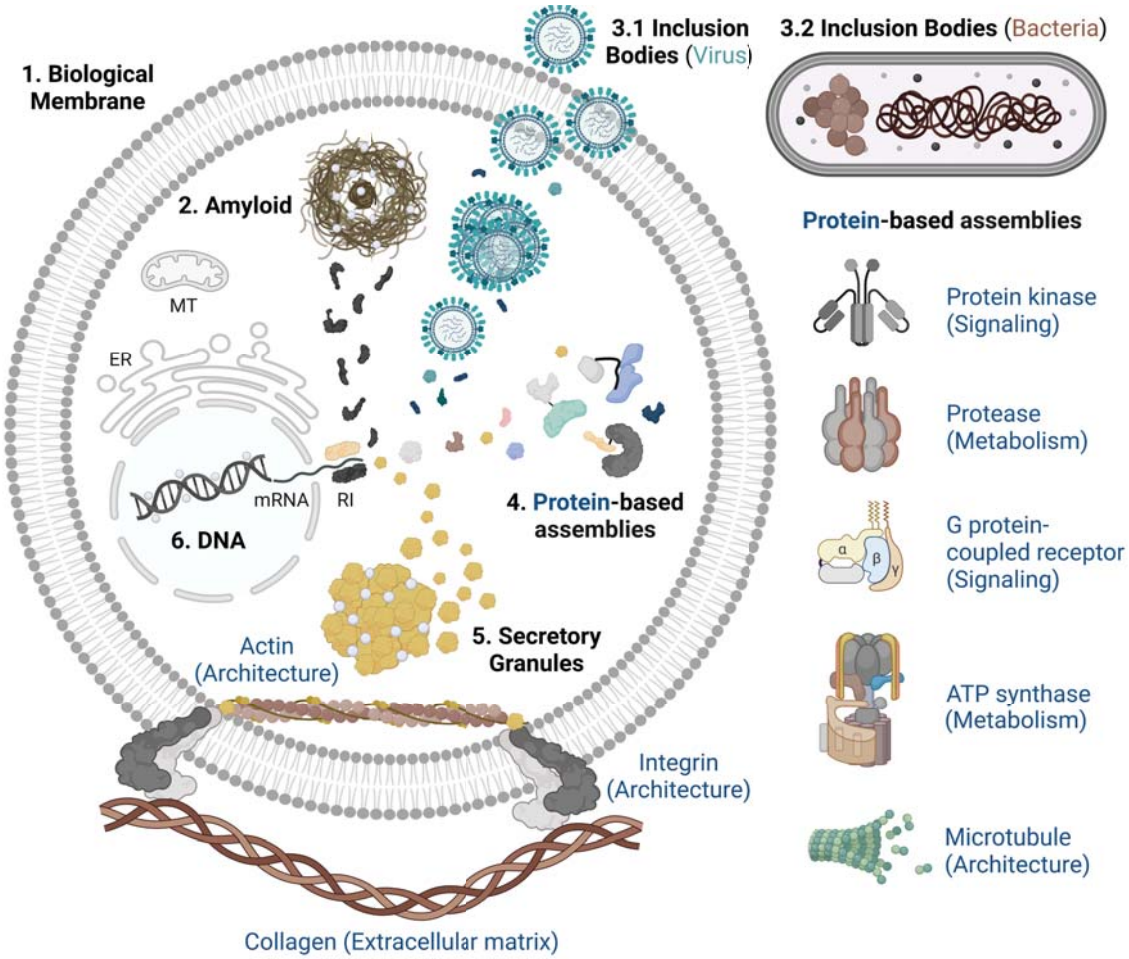

Figure 1. A schematic representation of how cells build supramolecular structures, including (1) biological membranes, (2) amyloids, (3) inclusion bodies (from both bacteria-brown and virus-blue origins; 3.1 and 3.2), (4) protein-based assemblies, (5) secretory granules and (6) DNA. Several examples of protein-based assemblies are displayed in blue with its related cellular function in brackets. Additional cell organelles such as mitochondria (MT), endoplasmic reticulum (ER), messenger RNA (mRNA) and ribosome (RI) are shown to ease the understanding of the illustration. White dots represent undetermined divalent cations. Adapted from [345].

2. Metal ions, the indispensable screws for cell functioning

Keywords: Divalent metal ions (Zn^{2+}), toxicology of metal ions, EDTA, histidine residues, and coordination bonds.

2.1 The inorganic matters

The philosophical idea that all living organisms were derived from stardust, could give credit to the relevance of inorganic chemistry in biological systems [45]. Historic experiments like the ones performed by Paul Ehrlich (Nobel Prize in Physiology and Medicine, 1908) demonstrating the importance of metals in the treatment of syphilis (Salvarsan) [46], James B. Sumner (Nobel Prize in Chemistry, 1946) crystalizing urease with nickel at its active site (1926) [47], or James Watson and Francis Crick (Novel Prize in Physiology and Medicine, 1962) demonstrating the presence of phosphate containing polymers of DNA (1953) [22], reveal and support the importance of inorganic elements in biological molecules and processes. The experimental applicability of inorganic chemistry in biology and the theoretical tools developed during this period led to the birth of the so-called *bioinorganic chemistry* in 1970-1971 [48].

It is well known that about 99% of the human body is made of oxygen, carbon, hydrogen, nitrogen, phosphor, sulfur, potassium, sodium, chlorine, and magnesium ions (classified in the periodic table as essential or beneficial nonmetal ions, **Figure 2**) [49]. These are easily identified as the simplest atomic structures essential to form the architecture of any organism. Indeed, amongst all the different possible element combinations, carbon-based bonds are the bricks from which all organic entities are constructed. In short, carbon atoms are the first stage of the hierarchical pyramid that will finally construct more complex carbon-based biological macromolecules presented in chapter 1 [50].

But most importantly, the way these bricks relate with the environment is usually determined by the presence of other less abundant ions with a metallic nature, generally described as **metal ions** (classified in the periodic table as alkali, alkaline-earth, or transition metals, from column 1 to 12, **Figure 2**) [51]. As an analogy, if we think about the Eiffel tower, the bars that hold the structure will corresponds to the carbon-based biomolecules and the metallic screws that allow the proper tightening and dynamics, the metal ions. Hence, bioinorganic chemistry appears as an interdisciplinary field that examines the roles of metal ions in biology [52] elucidating their implications in a plethora of different pathways like (1) electron-transfer

reactions (e.g. cupper II in multicopper oxidases) [53], (2) substrate binding and activation processes (e.g. zinc II and potassium I in S-adenosyl-L-homocysteine hydrolase from Pseudomonas aeruginosa) [54] and (3) atom and group transfer reactions (e.g. phosphoryl group transfer in the hydrolysis of lactic acid) [55], among others.

2.2 The chemical nature of metal ions

To understand the importance of metal ions in biological systems, their chemical reactive nature should be addressed. We could simply define these species as atomic compounds that present a net electric charge. This electric charge is created when such atoms willingly lose shallow electrons to build a positive core, these are usually depicted as cations. This scenario is usually promoted by an undergoing oxidation process, in which electrons are lost from the external orbitals reducing the metal's binding energies. Depending on the number of orbitals of the element and the intrinsic natural properties of the atom, this oxidation process varies, creating different groups of atoms classified as alkaline (column 1 in the periodic table), alkaline-earth (column 2 in the periodic table) or transition metals (from column 3 to 12) with different reactivity and oxidation states such as monovalent (+1), **divalent (+2)** and trivalent (+3), depending on the number of lost electrons [56–58]. These chemical considerations allow metal ions to coordinate or to be chemically reactive towards a huge number of different atomic species present in biomolecules or other inorganic chemicals [59].

A clear example of the relative stabilities of complexes formed by first row transition metals are the Irving-William Series (**Figure 2**) [60]. Transition metals such as manganese (Mn), iron (Fe), cobalt (Co), nickel (Ni), copper (Cu), and **zinc (Zn)** in its divalent +2 oxidation state can form stable complexes in aqueous media with other species usually called as ligands (L) [61] following a certain order (from low to high stability):

$$\text{Mn (+2)} < \text{Fe (+2)} < \text{Co (+2)} < \text{Ni (+2)} < \text{Cu (+2)} > \text{Zn (+2)}.$$

In addition to that, there are also alkaline earth elements such as calcium 2+ (Ca^{2+}), able to form coordination complexes by using their d orbitals as seen for transition metals, besides the strength of the interactions is expected to be lower [62].

In short, the coordinative chemistry observed in the Irving-William series and alkaline earth elements, altogether with the biological relevance of certain ions such as Zn^{2+} and Ca^{2+}, end up being indispensable pillars to afterwards design novel oligomerization platforms.

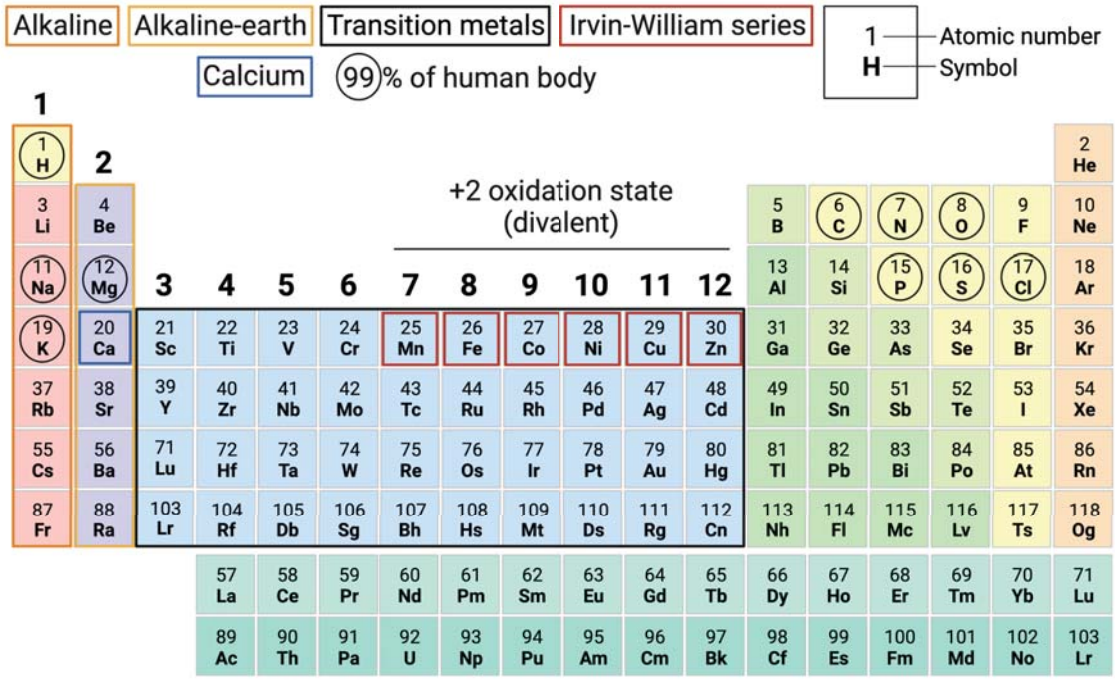

Figure 2. A modified version of the periodic table in which alkaline (dark orange), alkaline-earth (pale orange), Irvin-William series (red) and transition metallic (black) elements appear highlighted. Respective column position is additionally indicated, and the major components of the human body are circled (meaning 99 %). An interesting +2 oxidation state (divalent) is depicted for Irvin-William series' elements, as well as, for calcium (blue). Each chemical element is represented by a symbol and the atomic number on-top. The rest of the filling colors only ease the understanding of the illustration.

2.3 The dark side of metal ions

When biochemistry analyses the presence of metal ions inside organisms, only a specific set of candidates are the ones carrying out most of the biological reactions and processes [63]. Reactivity, abundance, atomic radius, oxidation states, electron configuration, atomic mass, electronegativity, or ionization energy are some examples of chemical properties that have bottlenecked certain elements for certain functions [64]. Considering the overall chemical suitability and abundance, the pool of metal ions distributed in the different cell compartments inside organisms is called metallome [64]. Thus, the metallome, in symbiosis with the proteome and genetic material [65], ensures the proper functioning of the whole living system.

The metallome landscape presents an essentiality criterion, meaning metal ions only work in certain and quite narrow concentration ranges [66]. These ranges are described as tolerance areas, in which each chemical element can promote an adequate systemic function without causing deleterious effects [63,51,52]. To exemplify it, there is a famous quote from an antique

scientist called Paracelsus which expresses that "all things are poison, and nothing is without poison, only the dose makes a thing not a poison", meaning the dose will finally be the key factor that determines toxicity [67]. A similar approach is represented in Bertrand's diagram (**Figure 3**), in which there is an optimal range of concentrations to promote the desired physiological effect. Outside from these margins, lower doses are expected to be insufficient and higher doses are toxic for the organism (**toxicology of metal ions**) [68]. That is why Recommended Dietary Allowances (RDAs) were created, to ensure an adequate daily intake of each element [69]. From a toxicological perspective, the presence or absence of certain metal ions is meticulously regulated, as not all the elements are biocompatible with the human body [70,71] (see table 2 in annexes, page 266).

The precise dose regulation of metal ions ensures body homeostasis, and so the proper functioning of the digestive, hormonal, neuromuscular, metabolic, and cardiovascular systems. Alterations in metal ion's physiological concentrations, in both deficiency and excess, triggers the development of a wide spectrum of different human illnesses [72] (see table 3 in annexes, page 267).

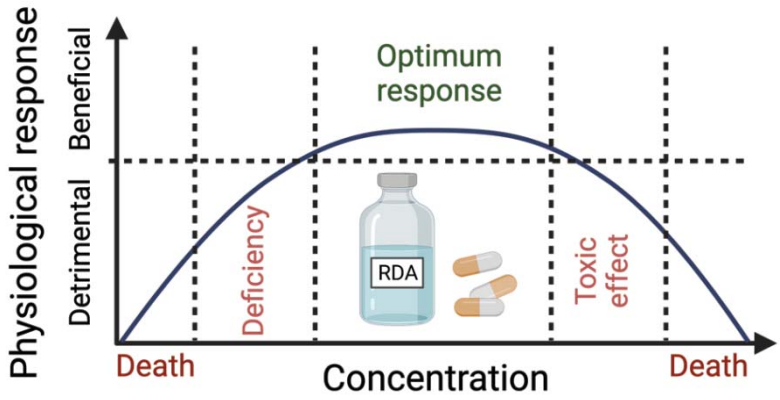

Figure 3. A graphic representation of Bertrand's diagram indicating physiological response vs concentration of metal ion. The optimum response area (green; meaning beneficial) is correlated with the Recommended Dietary Allowances (RDA) for each element. Death (dark red) is predicted in both low and high extremes, deficiency in mid-low and toxicity in mid-high concentrations (pale red; meaning detrimental).

2.4 We need metal ions to survive

Inorganic metal ions are involved in a plethora of molecular and organic structures and processes in both cellular and subcellular compartments, such as (1) cellular architecture, (2) electron transfer, (3) signaling, (4) redox catalysis, (5) biomineralization, (6) charge balance and electrolytic conductivity, (7) energy storage and (8) Bronsted acid-base buffering, in which biomolecules such as proteins, RNA, DNA, lipids and carbohydrates are involved [51,52,73] (see table 4 in annexes, page 268).

As examples, low concentrations of divalent Zn^{2+} are necessary to maintain the cell cytoskeleton's interactive capacity with vimentin filaments, which ensure the proper monitoring of several biochemical cell mechanisms [74]. On the other hand, Ca^{2+} can promote architectural changes of integrins (bent-like conformations) restructuring cell anchoring and preventing adhesion. Interestingly, cell adhesion is restored when calcium is displaced from the cytosol by the presence of magnesium (Mg^{2+}) and Mn^{2+} divalent ions (**Figure 4**) [75].

Mg^{2+}, Zn^{2+} and Mn^{2+} could be also found in directing transduction signals such as phosphoryl transfer and substrate binding in protein kinase A (PKA). Meanwhile, Mn^{2+} and Zn^{2+} stimulate a protein kinase noncatalytic conformational state, magnesium stabilizes the catalytic center accelerating the product processing (**Figure 4**) [76].

2.5 Metal ions and supramolecular protein complexes dance together

As mentioned in the previous chapter 1, cells are incredible builders of protein-based supramolecular complexes [14], and it is logic to predict that metal ions will exhibit crucial functions on its architecture or assembling processes [74–76]. Amongst them, amyloidosis is a clear example of the structural organization of highly stable fibrils (amyloid fibrils) in form of aggregates, directed through diverse aggregation routes by divalent cations [25,26]. Besides amyloidosis is usually attributed to present toxicological or pathological effects, inside-the-cell amyloid materials are also known to be functional, so-called functional amyloids, that are formed by a controlled aggregation process, being generally non-toxic structures [77].

Amongst the detrimental effects of amyloidosis, Cu^{2+} and Ca^{2+} are able to interact with α-synuclein (in particular the N-terminal histidine residue at position 50) with different affinities, promoting the structural transition from the monomer to a fast interfibrillar aggregation hold by electrostatic and hydrophobic interactions [78,79]. A similar event is observed in Alzheimer disease, where Cu^{2+} and Zn^{2+} induce the formation of a beta peptide

(Aβ) amyloid, a precursor of the plaque-like tangle structures, by also coordinating 3 histidine residues from the N-terminal of the protein [80,81].

Amongst the functional effects of amyloidosis, secretory granules (SGs) appear as biological assemblies that ensure the proper hormone storage in the human endocrine system and slowly release peptides into the bloodstream when needed (already mentioned in chapter 1). As an example, Zn^{2+} initiates the early cross beta-sheet fibrillar aggregation of the human growth hormone (GH), forming a secretory granule in the pituitary gland (confirmed by the disaggregation of the amyloid upon **EDTA** addition, **Figure 4**) [82]. In a similar way, insulin is stored inside human pancreatic cells. In this case, Zn^{2+} coordinates histidine residues from the B_{10}-chain inducing the subsequent crystallization of inactive aggregated protein hexamers at low pH. Ca^{2+} has also been reported to contribute in this hexameric formation [83,84].

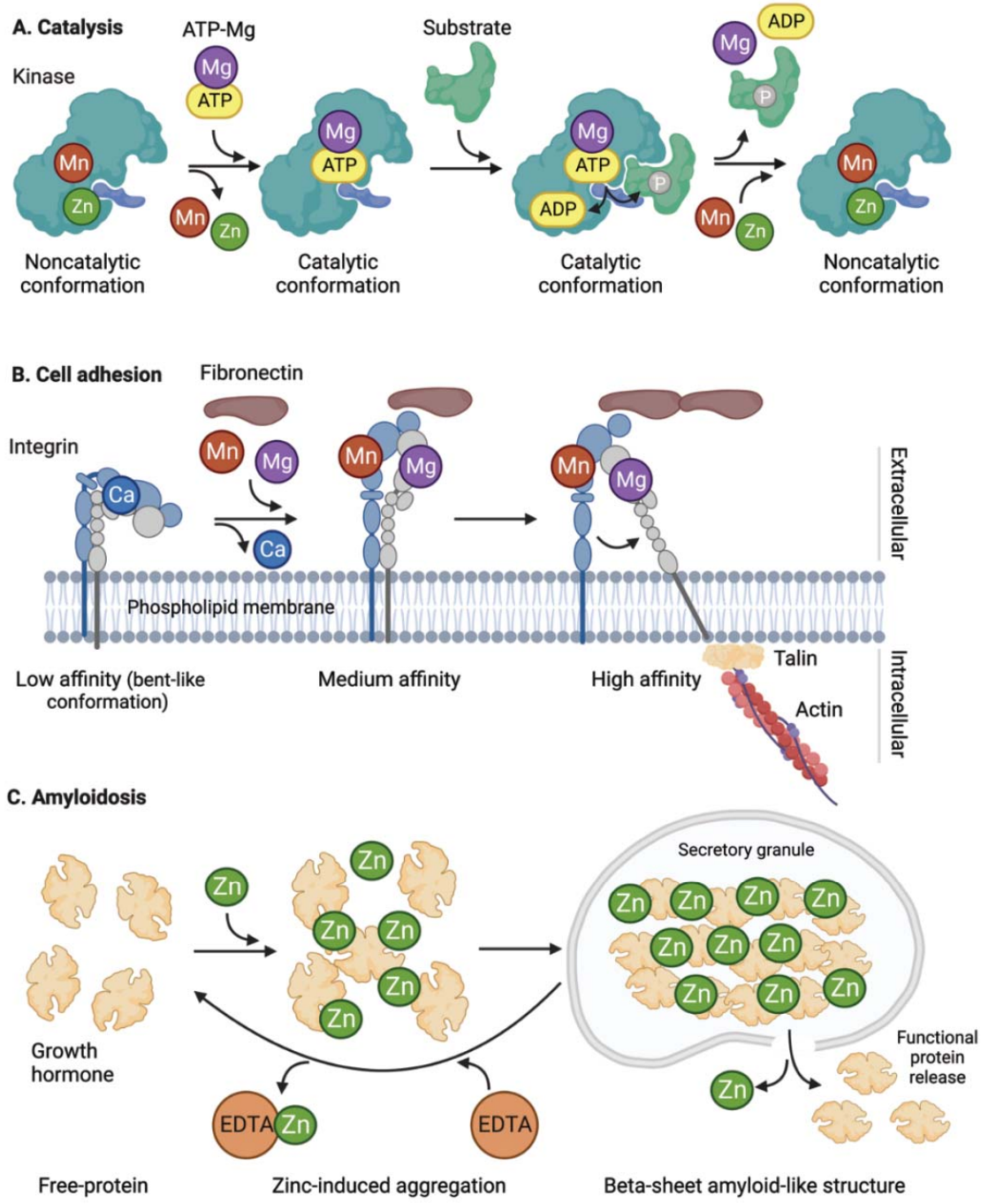

Figure 4. A short set of biochemical examples in which metal ions dance together with protein-based supramolecular complexes. (A) Catalysis: a kinase-based substrate phosphorylation process mediated by divalent cation interdependence (Mn^{2+} and Zn^{2+} trigger an enzyme non-catalytic conformation, meanwhile Mg^{2+} a catalytic conformation) [76]. (B) Cell adhesion: the extracellular integrin's binding affinity (to fibronectin) mediated by divalent cation presence (from low to high affinity, meaning, from Ca^{2+} to Mn^{2+} and Mg^{2+} respectively) [75]. (C) Amyloidosis: the zinc-based (Zn^{2+}) cross-linking of growth hormone creating a beta-sheet amyloid-like structure which releases functional protein upon an external stimulus and is reverted by EDTA addition [82].

2.6 The gluing of proteins with metal ions

With the so far described literature, divalent cations, and especially those described in the Irving-Willian series (plus Ca^{2+}), are naturally used to construct protein-based supramolecular complexes, and in particular, they tend to interact with the **histidine residues**. Because of that, histidine residues appear as suitable reactive biological species able to conform stable complexes with molecules and ions [85].

In this divalent cation and histidine type of bonding, the reaction takes place when the δ1-nitrogen atom from the histidine's imidazole ring (acting as a nucleophilic center) shares 2 unpaired electrons with the divalent cation (acting as an electrophilic Lewis acid) at physiological pH (around 7.4), creating a strong **coordination bond (Figure 5)**. The presence of adjacent proteins creates a gluing effect that triggers the formation of a supramolecular complex based on divalent cation-histidine crosslinking. Interestingly, this type of interaction is permanent and strong enough to support the physiologic mechanical forces inside the organism [86–88].

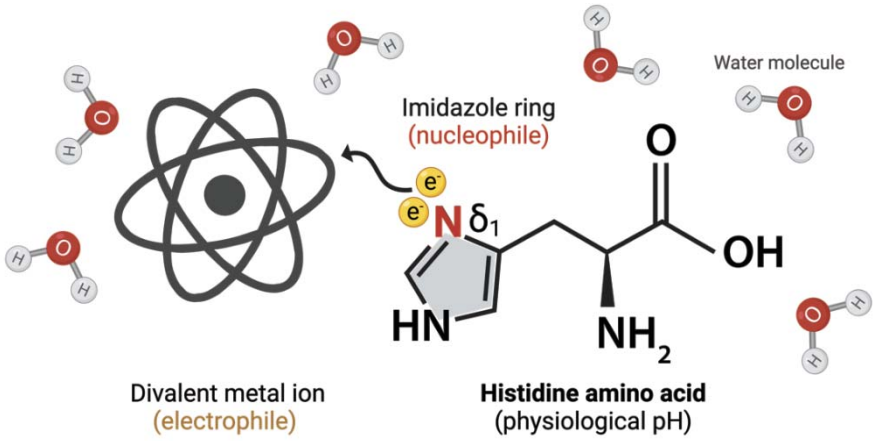

Figure 5. A simplified representation of the histidine amino acid - divalent cation coordination bond. Two unpaired electrons (yellow) are shown on top of δ1 nitrogen (acting as a nucleophilic center) and shared with divalent cation's external orbitals (acting as an electrophilic center) at physiological pH and aqueous solution (see surrounding water molecules).

3. The birth of protein engineering

Keywords: Protein production, histidine tag, protein purification, IMAC chromatography, and modular recombinant proteins.

3.1 Fundamentals

Since the discovery of the protein's essentiality in life, scientists have been fascinated by nature's capacity to develop creative ways to dynamically tailor and tune proteins [35].

Our modern society is directing a huge amount of effort into developing drugs able to mimic these natural processes [89]. Protein engineering has risen as a key player of the whole scientific development, in which proteins and enzymes are the main actors of the scene [90].

Thanks to the increasing understanding of protein chemistry and enzymatic reactions, scientist have been able to **produce proteins** (namely recombinant proteins) to address the clinical needs of our society [91]. The understanding of (1) protein folding [92] and (2) the recognition of basic protein biochemical principles [93] has prompted the creation of rationally designed protocols [94,95] and directed evolution methodologies [96,97] aimed to make new or modify existing proteins for novel functions (also called gain of function). Although there is still a long way to fully understand and trustfully predict protein structures and functions, there are remarkable stories of success. From non-natural enzymes capable of catalyzing reactions not observed in nature [98,99], to proteins with better pharmacological profiles in clinics [100,101]. Hence, the deeper the understanding of protein's biochemical properties, the better the products will be designed and manufactured by the biotechnological and pharmaceutical industries [91,90].

3.2 Histidine tag, the queen of protein engineering

At the end of the 70s, restriction enzymes were discovered, making possible the in vitro production of functional proteins by using recombinant DNA technologies [102]. From there, different expression systems such as (1) bacterial cell factories, (2) mammalian cells, (3) insect cells, (4) yeast cells and (5) microalgal cells [103–106] were used to express proteins in recombinant forms and to produce peptidic structures.

A great variety of different small protein domains and short peptides with different properties were developed to ensure an adequate downstream purification from the

expression system (e.g., Strep or GST tags, calmodulin binding peptide, maltose-binding protein, antigens, chitin binding domain, etc.) [107]. Among these strategies, the **histidine tag** (also called H6 or hexahistidine tag) placed at either N or C -terminus of the protein by genetic fusion, became the gold standard [108].

What is more, aside from being extensively used in the purification landscape, H6 or derived-H6 tags are currently being translated into other biotechnological fields. They have unexpectedly shown oblique applicability in (1) triggering catalytic reactions (due to the intrinsic imidazole ring's reactivity) [109,110] and (2) establishing novel labelling, immunodetecting, site-specific conjugation and biosensing diagnostic methods (especially when interacting with labelled NTA-Ni^{2+} complexes) [111–114].

The biochemical principles that allow this functional latitude are found in its intrinsic cross-molecular reactivity or affinity for metal ions. Indeed, this principle was already wildly spread and used by the scientific community several decades ago in the conventional **IMAC** (namely Immobilized Metal Ion Affinity Chromatography) purification strategies [115].

3.3 Affinity chromatography, the fiancé of protein engineering

Protein purification is an indispensable late downstream task flow in protein engineering that ensures the adequate product's quality (translated as purity) and scalability [116]. Indeed, affinity chromatography is an essential tool for drug development and proteomics. It is generally described as a one-step and simple isolation protocol, in which recombinant proteins are isolated from culture media or cell extracts using specific affinity peptides or small domain-based tags that interact with immobilized binder analogues (e.g., metal ions, substrate analogues, antibodies, avidin or streptavidin proteins, etc.) [115,117].

Among the different affinity purification strategies, IMAC methodology was extensively used to entrap hexahistidine tagged proteins in presence of divalent metallic ions such as Ni^{2+}, Zn^{2+}, Cu^{2+}, Co^{2+}, Fe^{2+} and Ca^{2+} (being nickel the most popular choice) [118]. The purification procedure is simple. Cell lysates, irrespective of the used cell factory, are loaded into a purification column which contains a particular set of Sepharose, or agarose beads functionalized with NTA (which chelates divalent metal ions). Starting from a heterogeneous sample, histidine-tagged proteins are attached to the immobilized resin (by a histidine-metal ion interaction), separated from the rest of the cell extract by several washes and eluted by an enriched imidazole buffer (which competes with the histidine residues for the

coordination with the metal ion) [119,120] (**Figure 6**). As an interesting fact, upon the elution steps, traces of divalent cation could be potentially dragged out from the column in a phenomenon called metal ion leakage [121]; a scenario that will be considered during the discussion afterwards.

This overall procedure has been performed during decades, proving its robustness, versatility, simplicity and fulfilling the cost-benefit requirements of protein engineering.

3.4 Recombinant protein alchemy

The complex and dynamic microenvironment cells are constantly dealing with, surely requires biomimetic drugs that also simultaneously respond to the same type of dynamic stimuli [122]. In this regard, and thanks to the development of molecular biology, the new approaches in recombinant protein manufacturing have made protein-based materials an interesting biocompatible, versatile, and economically viable option to address our current biotechnological needs [123]. From here, new methodologies have appeared in which non-canonical amino acids are fused together in a final **modular recombinant protein** construction [124,125].

The process usually starts (1) genetically designing the protein at the DNA level, in which DNA sequences (encoding for different protein domains) are consecutively placed in the desired order. Each encoding sequence refers to a different module. (2) The nucleotide-based sequences are afterwards introduced inside the desired expression system and the recombinant proteins are produced and purified (**Figure 6**). The selection of the most appropriate expression system will determine the final production outcome, and it is generally influenced by several factors such as the need of post-translational modifications, experimental yield requirements, the final protein applications, and the costs [126–129].

Each construction will present diverse functional properties depending on the type of modules added into the structure. As examples, (1) bioactive or responsive domains will facilitate the interaction between cells or biomolecules, (2) structural domains will provide stable mechanical properties, and (3) degradable or crosslinking domains could be used as responders to environmental stimuli or enable a spatiotemporal control over the material characteristics. In short, the combination of all these functions in a single entity allows the creation of an all-in-one material able to act dynamically and respond efficiently to the system

[124]. Aflibercept [130], denileukin [131] and etanercept [132] are some examples of fusion proteins approved by regulatory organizations to be used in human therapies.

Obviously, there are some technical limitations in the sequence-structure-function scheme, as the structure of the resultant modular "Frankenstein" based on the initial designed sequence, could potentially present unpredictable structures and functions [128,129,133]. That is why, the more we rationally understand and predict our primary sequence creations, the higher the quality of our final products will be.

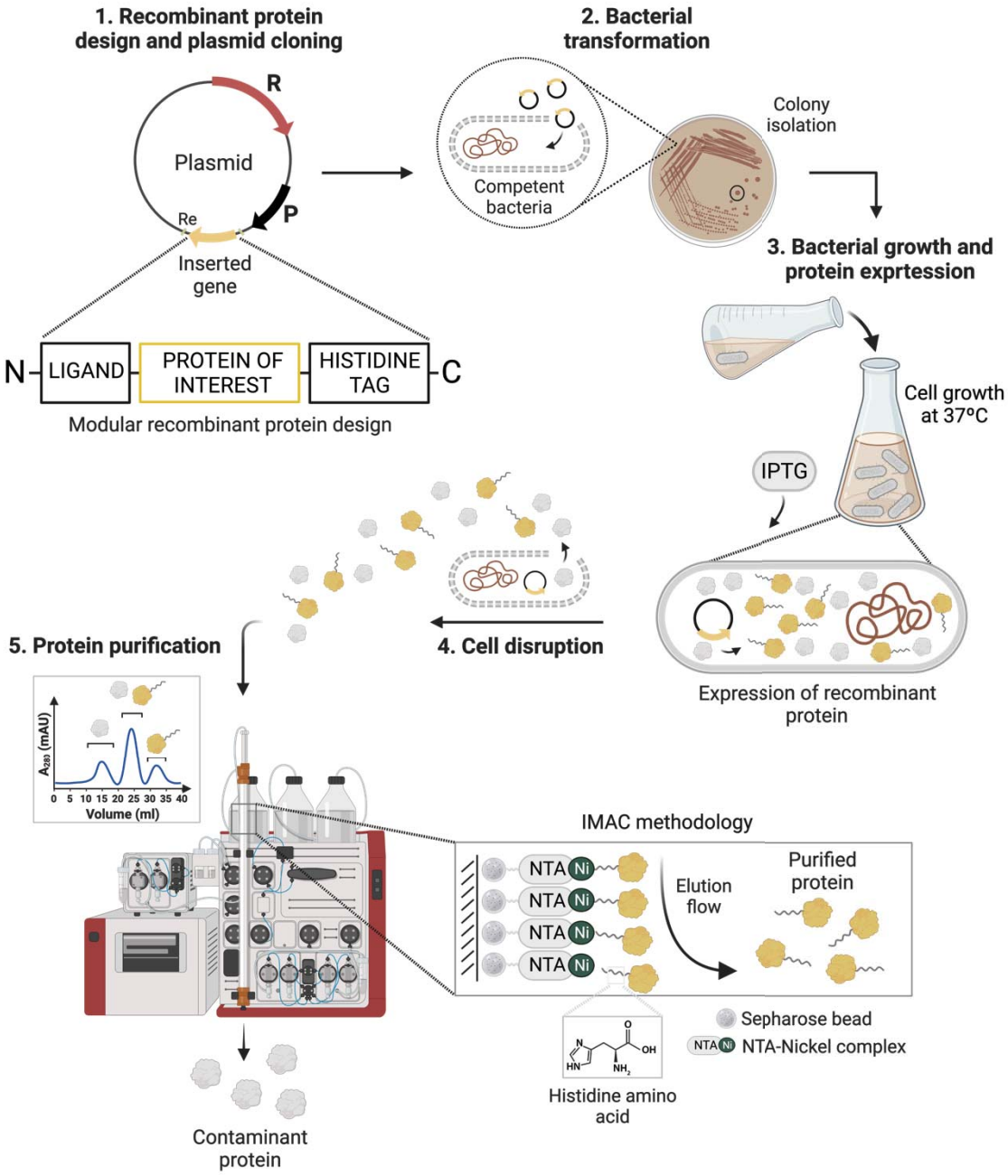

Figure 6. An extended diagram illustrating the usual workflow of recombinant protein production and purification in microbial cell factories. From (1) recombinant protein design (of multidomain proteins from N to C -terminal, meaning ligand – protein of interest – histidine tag) and plasmid cloning (using molecular biology techniques), (2) bacterial transformation and colony isolation, (3) bacterial growth (at 37 ºC) and protein expression (upon induction with IPTG), to (4) cell disruption (by sonication, or pressure-based techniques) and (5) protein purification (by NTA Ni^{2+}-based IMAC methodology). In (1), R refers to resistance, meaning, a genetic sequence encoding for a biomolecule that allows the specific bacteria selection upon plasmid transformation. P refers to promotor sequence, which allows protein expression upon the addition of a certain chemical (IPTG) at a particular time point. Re means restriction enzyme sites, used for cloning purposes. In (5), an additional inset shows the resultant protein purification chromatogram in which the unwanted (unspecific) and desired (specific) peaks are displayed after the elution step. The elution step is triggered by the addition of high concentrations of imidazole as a competitor of the Ni^{2+} histidine tag interaction. As a result of this workflow, purified recombinant protein is obtained.

4. The insights of material science

Keywords: Nanotechnology, nanotoxicology, biocompatible, self-assembly, drug delivery, biodistribution, nanoparticles, and design of drug delivery systems.

4.1 Material science is everywhere

There is a famous quote that says, "everything is made of something", and far from being obvious this idea exemplifies the fact that without this "something" nothing could be explored, understood, or transformed. Material science appears as the mother of such exploration. A tremendous interdisciplinary field able to discover and design new materials for the sake of a better human health, safety, and overall quality of life [134].

In this line, the continuous innovation has allowed to deeply understand materials' physical and chemical properties like morphology, mechanics, structure, and magnetic properties in both the macro and micro -scaled worlds [135], which allows scientists to classify materials in 5 major categories, namely (1) polymers [136], (2) semiconductors [137], (3) ceramics [138], (4) glass [139], and (5) metals [140], each one with its respective subdisciplines.

4.2 The dark side of material science

Interestingly, traditional materials are not particularly suitable to interact with biological systems, as they (1) can't be accurately delivered to specific regions of the human body due to macrometric size limitations, and (2) tend to present biocompatibility and mechanobiological issues, which dramatically compromises the efficacy of the treatment [141–143]. That is why, during the last decade, and thanks to the novel technological advances, material science has expanded its scope of action into the nanometric world (ranging from 1 to 100 nm as standard) to optimize the interactions between materials and biological compounds [144,145].

4.3 Nanotechnology, the offspring of material science

In this newborn nanoworld, matter is generally manipulated on a near-atomic scale. In this regard, the newly produced structures exhibit unique physical, chemical, and biological properties which are not observed in the macroworld. These unexpected behaviors may be feasible due to the material's proximity to the quantum world in which the scale reduction substantially increases the material's interaction surface area, meaning, a dramatic increase of

its chemical reactivity. What is more, nanomaterials also tend to be stronger, lighter, and more efficient in certain scenarios than their bigger brothers [144,146,147].

Nanotechnology takes advantage of a vast set of different disciplines namely surface science, organic and inorganic chemistry, molecular biology and engineering, and microfabrication to design and manufacture a wide range of nanoelectronic devices, biomaterials, and nanomedicines, among others [148]. There are two major strategies to create nanomaterials. A (1) bottom-up strategy, that uses small or nearly atomic components to create higher-in-complexity structures, and a (2) top-down strategy, which uses larger entities to create smaller devices, such as a sculptor does with its sculpture [147,149,150].

What is more, nanomaterials can be classified depending on their intrinsic components' nature [151]: (1) Carbon-based materials (which are composed majorly by carbon atoms. That includes ellipsoids referred as fullerenes, tubes referred as nanotubes and hollow spheres) [152–156], (2) metal-based materials (which are composed majorly by metallic atoms. That includes quantum dots, silver, metal oxide; TiO_2 and gold nanostructures) [157–160], organic-based materials (which are composed majorly by natural or synthetic organic molecules. That includes liposomes, proteins, micelles, and polymers) [161,162], (4) polymer-based materials (dendrimers, which are majorly composed by branches of molecules constructed in layers. That includes nanosized polymers built in branches) [163], and (5) composites (which are majorly composed by combinations of nanoparticles and other bulk-type materials from different origins. That includes nanoparticles constructed as nanosized clays) [164] (**Figure 7**).

Nanotechnology has raised as one of the major revolutionary forces of the 21st century due to its technical and manufacturing possibilities and transversal character, but as always, nanotechnology is not a bed of roses [165].

4.4 The dark side of nanotechnology

Up to now, there is not a clear sense if nanomaterials are creating toxic effects to both environment and human body (namely **nanotoxicology**). Indeed, over the last 15 years, the number of scientific studies addressing nanosafety issues has exponentially increased but without conclusive statements may be due to the complexity of the problem. Thus, it is important for the scientific community to report reliable end-points that need to be assessed for in every newly tested nanomaterial [166,167]. For instance, it is common to find articles discussing about the hypothetical long-term detrimental effects of nanomaterials, translated

as chronic inflammation of the immune system without proper material description, high degrees of sample polydispersity and lack of material's stability [168,169]. On the other hand, other studies have reported a rapid expulsion of nanoparticles by renal clearance that avoids this accumulation phenomenon [170–172].

In this regard, it is important to identify which nanomaterial's properties are the ones potentially toxic and establish contingency plans to minimize them. Detailed studies of material's (1) composition, (2) morphology, (3) structure, and (4) surface charge are absolutely necessary to avoid harmful consequences, and adequate recommendations should be described in terms of sample distribution, storage, use and end-of-life [173,174].

There are some insights that could be useful to consider when injecting our experimental prototypes into *in vivo* models: (1) Aggregation state [175,176], (2) cationic surface charge [177,178], (3) release of toxic ions [179,180], (4) powdered samples [181,182], (5) presence of antigens, pollutants, or allergens [183,184], (6) presence of toxic moieties or molecules [185,186], (7) hydrophobicity and clogging [187,188], (8) non desired catalytic reactions [189], and (9) lack of targeting [190] (**Figure 7**). For a furtherly detailed explanation see table 5 in annexes, page 269.

But there is still a singular biological effect that should be considered when injecting our nanomaterials into the bloodstream, namely protein corona.

4.5 A special consideration to the protein corona

As described in chapter 4, nanotechnology has developed a wide range of different nanomaterials suitable for theragnostic purposes [146,148,151,165]. In most of the cases, these materials are intravenously administered and potentially creating the already mentioned deleterious effects [166,168,169]. But there is still an aspect that requires a special consideration, namely protein corona.

This phenomenon is immediately produced when administered nanostructures encounter a biological medium full of sticky molecules. Meaning, the intrinsic chemical reactivity of the blood stream components promotes the rapid covering of the nanomaterials, creating a surface corona which impacts the final properties and functions of the device [191,192] (**Figure 7**).

The coating is able to trigger several non-desired biochemical pathways such as (1) innate immune recognition (nanomaterial opsonization and fast phagocytosis by the MPS system),

(2) immune response priming (nanomaterial interaction with immunoglobulins, that would ultimately cause immunotoxicity), and (3) physical destabilization, off-targeting and agglomeration (nanomaterial interaction with serum proteins and lipids which would change particle's size and shape, and promote different biodistribution and pharmacokinetics) [192,193]. This scenario has been proven to happen in iron [194], gold [195,196], and silica [197] nanoparticles, as well as, in organic compounds such as liposomes [198] and polymers [199], but poorly observed in proteins as no significant evidence has been described in the literature so far. Thus, it is then necessary to consider all plausible behavioral changes that could biologically occur after material's administration and develop contingency plans to minimize them.

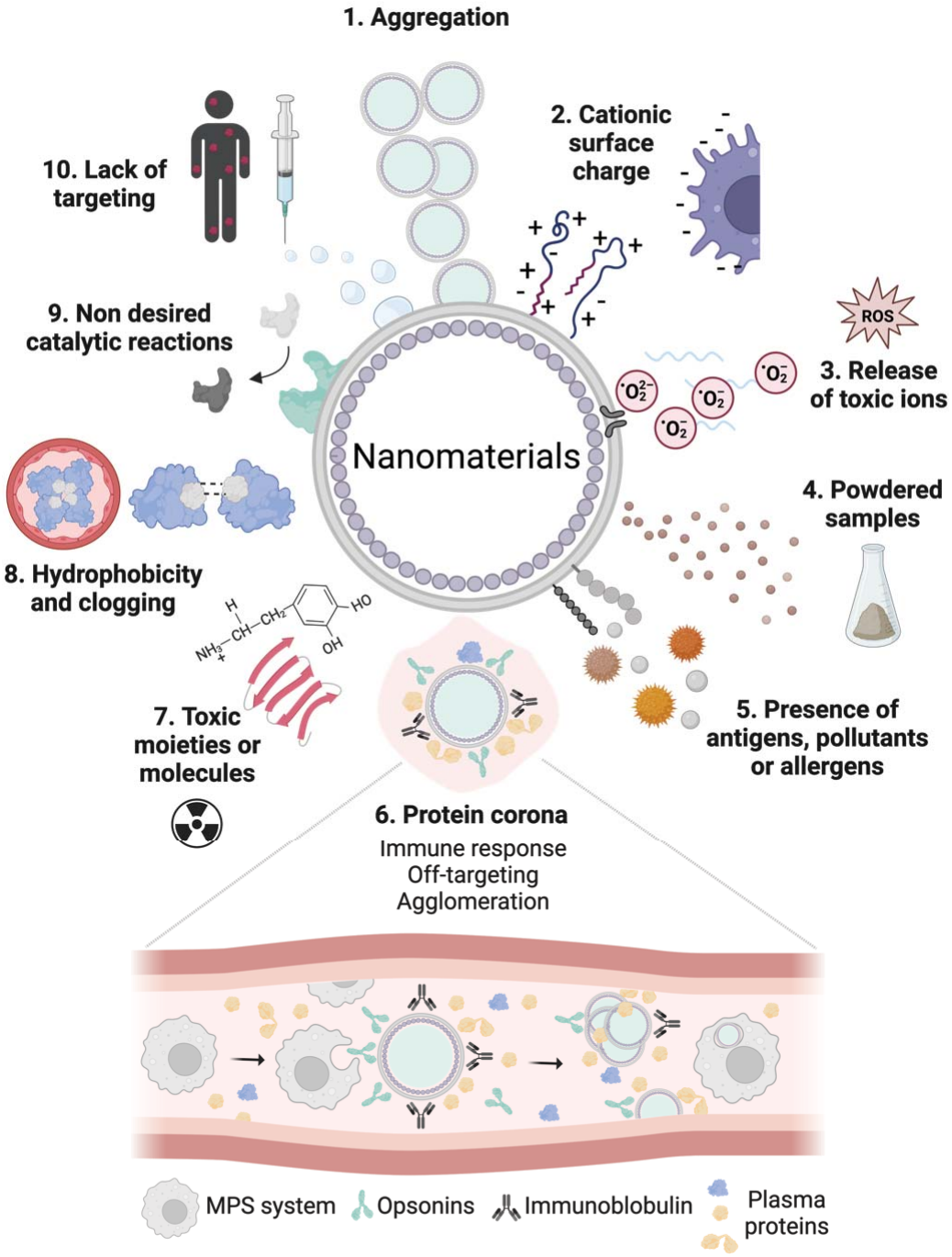

Figure 7. A simplified diagram of properties to be considered when designing novel nanomaterials for biomedical purposes. A special consideration to protein corona and consequent detrimental effects on material's behavior in the blood stream. In (3), ROS means reactive oxygen species.

4.6 Biomaterials to interact with biological systems

One of the most used contingency plans to minimize nanotoxicology and protein corona formations is the use of biological materials as bulk scaffolds. There is no better way to interact with biology than using similar-in-nature **biocompatible** devices. Indeed, the concept of biocompatibility is defined as the ability of a certain material to perform an appropriate host response, in a specific application, without causing major detrimental effects [200].

In order to define a device as biocompatible, there are several features that must be addressed once administered, such as (1) minimal or absent immune response (avoid protein corona formation and antigenic or allergenic moieties), (2) biodegradability or bioresorbability (disappear from the organism after fulfilling their action), (3) stability and hydrophobicity (avoid aggregation or exposure of hydrophobic moieties), (4) low reactivity (avoid highly cationic surfaces, undesired catalytic properties, or oxidative metal ion release), and (5) high purity (avoid the presence of allergens, toxic proteins, or pollutants in or entrapped on the material's structure). As a simplified idea, the biomaterial should be innocuous when interacting with the human tissues, but sufficiently bioactive to develop the desired action [200,201].

In short, biomaterials were created to basically solve the major drawbacks of traditional material science and nanotechnology when talking about interacting with biological tissues (e.g., artificial heart valves and ligaments, breast, bone and dental implants, skin grafts, drug delivery systems, etc.) [202–204]. It seems that the problems of some, are the basic foundations of others. The more we understand nature, the more efficient and less minacious our creations become. Maybe, we are where we started (chapter 1).

4.7 Self-assembly, an interesting approach to create biomaterials

Among the different manufacturing procedures of biomaterials, **self-assembly** is a wieldy spread process which mimics the natural assembling pathways observed in nature. Particularly, cells use this process to constantly assemble essential supramolecular complexes which ensures the maintenance of life [14,205].

From a nanotechnological perspective, self-assembly is a bottom-up strategy that creates hierarchic structures from individual units with unique physical and chemical properties. A well-directed spontaneous process that creates order from relative chaos. What is more, in

order for this process to be spontaneous, an energetic barrier must be overcomed. Biological systems use different forms of molecular interactions like Van der Waals, hydrophobic, electrostatic, coordinative, hydrogen bond or covalent interactions to minimize the resultant energy (**Figure 8**). Depending on the building block's nature, the subsequent self-assembling momentum and final properties will change [205–208].

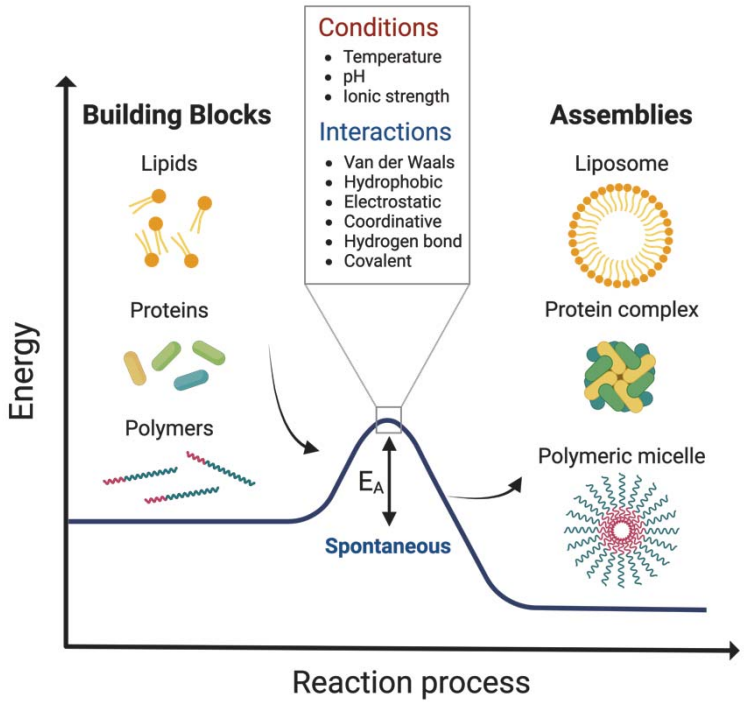

Figure 8. The energetic profile (expressed as energy vs reaction process) of simple building blocks transitioning into complex assemblies of different natures. The spontaneous transition is achieved when certain physicochemical conditions and interactions are enough to surpass the activation energy (E_A; an extended definition is shown in the vocabulary and abbreviation section).

In this regard, biomolecules such as amino acids, oligopeptides, polymers, and other π-conjugated compounds have been artificially used to build up biocompatible materials like nanofibers [209], hydrogels [210,211], vesicles [212,213], micelles [214,215], and nanotubes [216]. In all of them, size, shape, and surface chemistry can be moderately tuned depending on the final applications or needs. This creates a highly versatile manufacturing platform of biocompatible biomaterials, in which drug delivery has become the focal point [217].

4.8 Biomaterials in drug delivery, the case of nanoparticles

The use of free drugs in the treatment of many diseases, especially in cancer, is a standard practice that has taken place during decades. But although this practice has given good results, it exhibits certain therapeutic limitations like (1) limited circulation time [218], (2) undesired accumulation and penetration tendencies [219], (3) undesired interaction with proteins from the bloodstream [220], and (4) lack of targeting [221] that could be improved to

make the treatments more efficient (for a furtherly detailed explanation see table 6 in annexes, page 270).

In this regard, novel drug delivery systems were designed to minimize these non-desired tendencies and optimize drugs' **biodistribution** and pharmacokinetics. Biomaterials, and especially nano-scaled biomaterials, appear as a promising approach to enhance bioavailability, avoid ultimate drug degradation, and so improve uptake, maintain the therapeutic dose high and reduce toxicity [217,222–224].

Among all the different types of formulations, **nanoparticles** have proven to be highly versatile drug delivery systems thanks to (1) tunable particle size, shape, and surface properties (optimize drug's biodistribution and pharmacokinetics), (2) large surface/mass ratio (optimize drug's capacity to absorb high amounts of drug load on its surface), (3) targeting and cell internalization abilities (reduce off-target effects), (4) different administration routes available (parenteral, intravenous, oral, intramuscular, intra-ocular, etc.), and (5) high drug stability (optimizes drug release and reduces degradation) [225–227] (**Figure 9**).

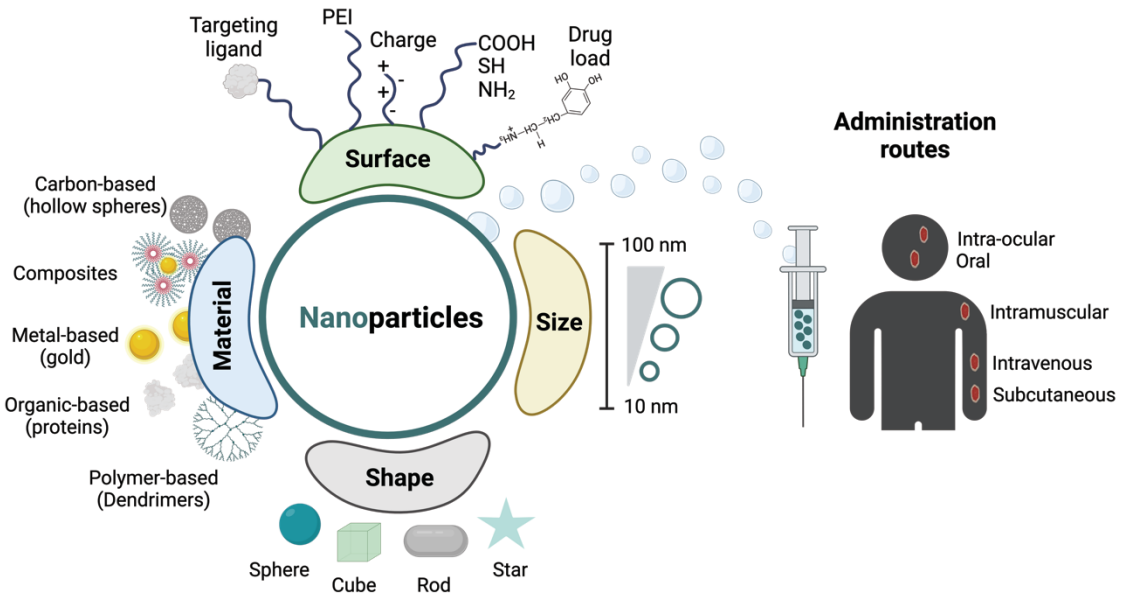

Figure 9. A schematic illustration of how nanoparticles have become highly versatile drug delivery systems in terms of (a) surface functionalization possibilities, (b) size and shape manipulability, (c) material composition, and (d) routes of administration. The proposed examples are only a few, and most used, of an extensive landscape of additional possibilities.

Abraxane is a clear example of how nanoparticles have been successfully installed in biomedicine. This biomaterial is a nanostructured complex of around 130 nm in size,

constructed by a high-pressure homogenization procedure which assembles human albumin protein with paclitaxel supported by hydrophobic interactions. The result is an FDA-approved colloidal nanoparticle suspension used for metastatic breast, pancreatic and lung cancers [228,229].

4.9 Concerns while designing biomaterials

If scientists want to achieve more cases of success like Abraxane, there are certain criteria that should be considered when trying to **design** more efficient **drug delivery systems**.

(1) Biocompatibility (biomaterials need to be non-toxic and biodegradable after performing their action), (2) proper therapeutic loading efficiency (biomaterials should be able to load enough therapeutic molecules to ensure an adequate effect and avoid re-administration), (3) physicochemical stability (biomaterials should remain stable after drug loading or injection, avoiding fast degradation or immune recognition), (4) easy to administer (biomaterials should be easily administered causing little discomfort), (5) efficient delivery and action rates (biomaterials should deliver the drug or perform its action in consistent and defined release or action profiles), (6) avoid renal cut-off (biomaterials should avoid renal cut-off to ensure optimal biodistribution. Renal cut of is approximately > 6 nm), (7) targeting possibilities (biomaterials should allow targeting modifications for site-specific delivery), and (8) simple and economic formulations (biomaterials' manufacturing should be reasonably simple, reproducible, and economic for scaling up purposes) [206,222,230].

All these considerations should be optimized depending on the application needs with the aim to ensure biomaterial's safety and efficiency (**Figure 10**).

Criteria	Status
Biocompatibility (e.g. biodegradability and low toxicity)	
Homogeneous in composition (e.g. high purity)	
Efficient delivery (e.g. targeting possibilities)	
Assembling control (e.g. controlled assembling procedure)	
Efficient biodistribution (e.g. avoid renal cut-off)	
Therapeutic versatility (e.g. applicability in different biomedical fields)	
Formulation versatility (e.g. applicability in different protein candidates)	
Product stability (e.g. chemical and thermal stability)	
Reproducibility between batches (e.g. control in size)	
Formulation in a cost-effective manner (e.g. simplicity)	

Figure 10. A list of key concerns to consider when designing novel biomaterials for clinical purposes is presented. Each main characteristic (blue) is followed by the most representative ideas in our field of study. A qualitative evaluation, meaning green (accomplished), red (not accomplished), green-red (further studies needed), and grey (not applicable) has been performed to establish the current product's overall suitability to be used in clinics. This table will be furtherly applied to evaluate the weaknesses and strengths of two state-of-the-art methodologies (figures 13 and 14).

5. Protein-based materials, a new promising approach

Keywords: Spontaneous oligomerization, rational design, protein-based nanoparticles, natural inclusion bodies, and clinical concerns.

5.1 The intersection between material science and protein engineering

Here is where the two stories intercept. So far, we have discovered the insights of protein engineering (chapter 3) and material science (chapter 4) and how both have created their roles in science. But as it usually happens in nature, things seem to be always interconnected.

A decade ago, scientists also realized that biomaterials should comprehend certain properties to be used in humans as drug delivery systems [227]. Some of them started exploiting a new set of nanoscale biomaterials such as liposomes [213,231,232], polymers [233,234], dendrimers [163,235,236], or even magnetic nanoparticles [237–239], others decided to explore proteins as key component of its structure (namely protein-based nanostructures). The new idea was to create protein-based platforms which enable a **spontaneous oligomerization** of recombinant proteins into nano or micro -particles using self-assembling strategies [240–242].

The concept aimed to give high versatility and manipulability to the new constructions, including (1) high biocompatibility (the use of human-derived proteins such as human serum albumin, allows to minimize immune response, protein corona formation, and increase biodegradability or bioresorbability), (2) high purity (the use of protein engineering purification strategies such as IMAC or SEC allows the final formulation to be free of antigenic, allergenic or pollutant moieties), (3) high stability and hydrophilicity (the use of soluble proteins mitigates their tendency to aggregate by the exposure of hydrophobic regions, presenting high stability in the bloodstream. In addition, there is a wide spectrum of stable protein candidates to be used for the therapeutic purpose, which could be engineered following recombinant protein strategies, chapter 3), (4) lack of additional components (the use of protein-only based materials allows to minimize the number of additional components such as detergents, stabilizers, matrices, or amphiphilic molecules, e.g., PEI, that could compromise sample stability or increase toxicity in vivo), (5) versatile targeting, multivalency and internalization (the use of recombinant proteins allows to easily add targeting peptides into the primary structure for site-specific delivery, and induce multivalency when assembled into protein-based nanoparticles, which will trigger receptor clustering and increase final protein internalization), (6) versatile delivery (the formulation of recombinant proteins in

different nano or microparticulated formats allow different pharmacokinetic profiles directly affecting the administration and therapeutic characteristics), (7) multiple administration routes (the use of proteins assembled as protein-based nanoparticles allows different plausible administration routes such as nasal, intravenous, pulmonary, ocular, and oral, which increases the formulation versatility and therapeutic possibilities) and (8) efficient biodistribution (the use of tunable proteins assembled as protein-based nanoparticles allows to modulate nanoparticles' size, shape, and surface chemistry, avoiding renal cut-off and non-specific interactions, and optimizing biodistribution) [243–249].

But far from being a bed of roses, the formulation procedure of protein-based materials is not predictable enough and needs a continued optimization process to ensure the adequate compliance with as many previously described properties as possible.

5.2 Two home-made manufacturing platforms of protein-based materials

Among the initial overall proposed strategies, our lab was one of the pioneers in developing two manufacturing platforms based upon **rational design** principles which recall concepts observed in nature.

Strategy 1: A cationic – Histidine tag principle for protein self-assembling

The strategy uses a novel nano-architectonic concept, which comprehends a particular way of designing fusion recombinant proteins following genetic and protein engineering techniques. The procedure is simple. (1) A cationic peptide is placed in the N -terminus of the protein genetic design, followed by a central bulk protein scaffold, and ended by a C -terminal hexahistidine tag [250]. (2) The plasmid encoding for the protein sequence is introduced by transformation into microbial cell factories and expressed and purified by an IMAC methodology. (3) Once proteins are placed in their most suitable buffers, recombinant proteins act as building blocks to spontaneously self-assemble into stable toroidal-like nanostructures (namely **protein-based nanoparticles**) of around 10 to 30 nm supported by non-covalent interactions (mainly electrostatic interactions) [251]. Interestingly, this monomeric to nanostructure protein transition is enabled by the presence of both, the cationic peptide, and the histidine tag. The lack of one prevents the self-assembling process to occur.

More than 15 positively charged peptides such as R9 (RRRRRRRRR-) [252], T22 (RRWCYRKCYKGYCYRKCR-) [253] and RK (RKRKRKRK-) [254] have been tested to

positively influence nanoparticle formation. The higher the length of the cationic peptide, the bigger the final nanoparticle size [250].

What is more, the selection of certain protein scaffold such as GFP, IRFP, or p53 [250,253], also determines the final oligomeric size (by steric features) and functional properties. Obviously, each module selection will depend on the therapeutic and drug delivery needs.

Certain positively charged peptides also present additional functions such as cell receptor interaction. Their functional duality makes them great candidates for protein assembly and drug delivery purposes [255]. A similar scenario is observed for the histidine tag, in which besides being crucial during the self-assembling, it is also needed during the purification step.

As a technical example, T22-GFP-H6 appears as the gold standard of the platform. A paradigmatic construction which describes how the system works. In this case, the used cationic peptide is T22 (a derivative peptide from Atlantic horseshoe crab *Limulus polyphemus*), followed by a GFP scaffold protein, plus a hexahistidine tag in the C -terminus. This protein sequence spontaneously forms toroidal nanoparticles of around 11 to 13 nm, and it is able to target, by specific interactions, the CXCR4 receptor, overexpressed in metastatic cancer stem cells in colorectal cancer and in many other neoplasms [255]. Indeed, T22 works as a receptor antagonist that triggers nanoparticle internalization after interaction [256]. When T22-GFP-H6 protein nanoparticles are administered to CXCR4 positive colorectal cancer mouse models, they can specifically accumulate in primary tumor cells and metastatic foci without affecting healthy tissues. The pharmacokinetic profiles suggest a fast accumulation peak 24h post-administration, requiring repeated dosage (every two days) to ensure an accumulation effect [253].

The material's high efficacy to accumulate in the desired tissue could be attributed to (1) high selectivity and affinity (promoted by the specific interaction between T22 peptide and CXCR4 receptor) [257], (2) multivalency (promoted by the T22 peptide presentation as a nanoparticle, creating a multivalent interactive surface which triggers receptor clustering and an efficient internalization in targeted cells, excluding those with a basal receptor expression; phenomenon called superselectivity) [258–260] and (3) size (promoted by the avoidance of renal clearance, expected to be at < 6nm, due to nanoparticle's oligomeric structure which increases the half-life in bloodstream and optimizes biodistribution) [170,171,261] (**Figure 11**).

From these preliminary results, our laboratory has gone one step forward and designed a set of second generation protein-based nanoparticles with therapeutic effects, by changing the GFP bulk protein with toxic domains (PE24 or DITOX) [262,263] or functionalizing the scaffold protein with chemotherapeutics (FdU, AraC and MMAE) [264–267].

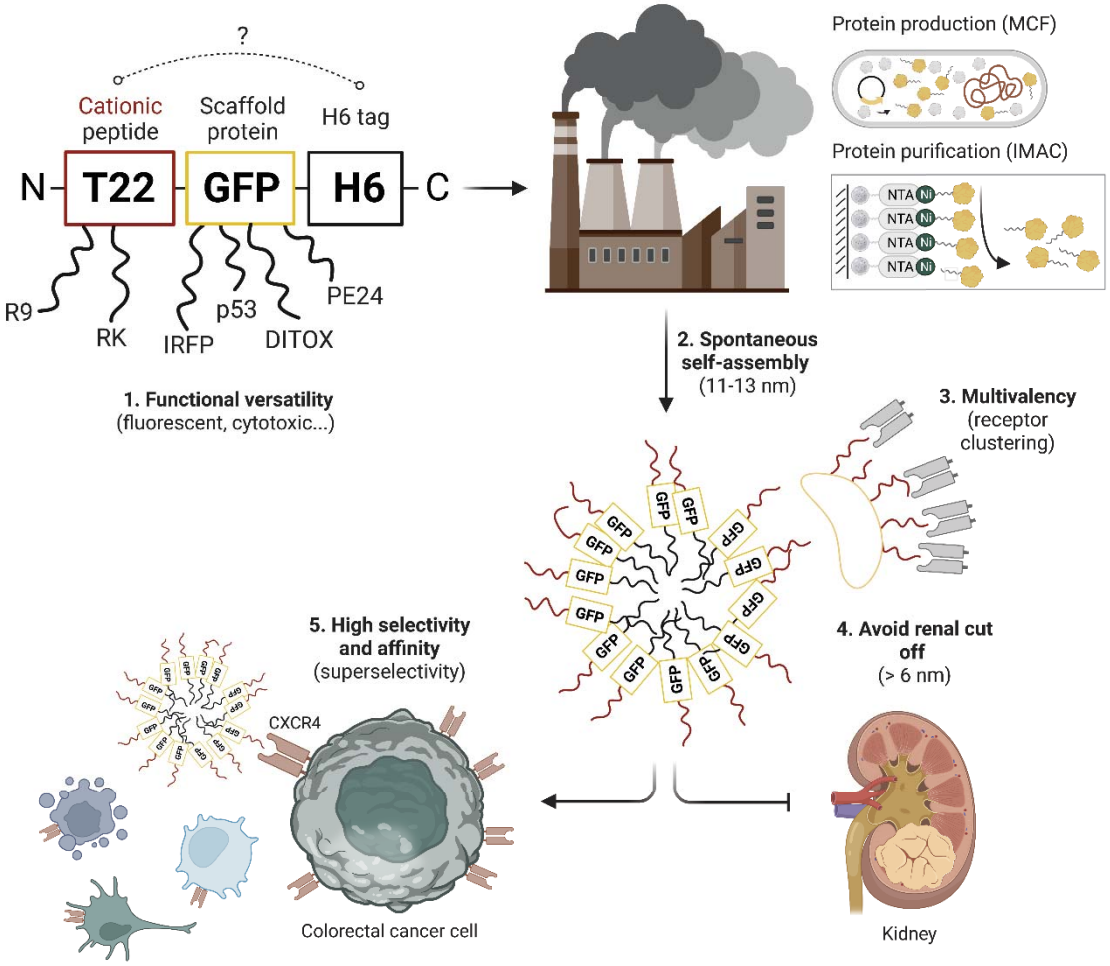

Figure 11. A concise diagram illustrating the usual workflow in microbial cell factories (MCF) and biomedical advantages of protein-based nanoparticles; meaning, (1) functional versatility (different fluorescent or cytotoxic scaffolds can be used for several theragnostic purposes), (2) spontaneous self-assembly (into toroidal-like nanoparticles of around 11 to 13 nm), (3) multivalency (multi ligand presentation which promotes receptor clustering and an efficient cell response), (4) renal cut off avoidance (optimizing biodistribution), and (5) high selectivity and affinity (specifically selecting the targeting cells over basal receptor expression in surrounding tissues). There is no clear evidence on how the cationic and histidine tags interact to conform protein-based nanoparticles (indicated with a question mark). The example is illustrated with the T22-GFP-H6 as a gold standard.

Strategy 2: A physicochemical self-assembling principle of protein-based insoluble microparticles

The second strategy takes advantage of the natural clustering tendencies of overexpressed recombinant proteins inside microbial cell factories. In this scenario, the overwhelming amount of produced protein leads to the formation of an initial colloidal population of particles, which will end up creating larger insoluble deposits (namely **natural inclusion bodies, IBs)** [241,242].

The manufacturing platform uses different physicochemical factors to trigger the micro-particularization such as (1) high temperature (around ≥ 37 ºC), (2) rapid bacterial growth rate, (3) short culturing times (between 3 to 4 hours), (4) low pH (around < 5.5), and (5) high concentration of protein expression inductors (1 mM of IPTG as an example) [268]. In addition, aggregation-prone peptides such as (VP1, MalE31 and CBDclos) can be also fused into the primary structure to promote protein clustering through hydrophobic interactions between α-helix and β-sheet moieties [269–271]; and far from being unspecific, the oligomerization process is driven by concrete interactions that follow certain patterns.

The resultant natural inclusion bodies are observed inside the cell as large refractile entities of around 0.2 to 2 μm. These microparticles are mechanically stable and formed by the combination of a heterologous population of expressed protein in different functional and folding states (meaning natively folded, partially folded, and completely unfolded). They are like sponge bulk matrixes, similar to an amyloidal fibrillar scaffold, which entrap functional recombinant proteins [269,272] (**Figure 12**).

Curiously, natural IBs were initially considered as undesirable cell by-products, but the concept evolved when different multidomain recombinant proteins were used during the formulation process creating new functions like (1) biocatalysis (able to be immobilized proteins and catalyze enzymatic reactions), (2) cell adhesion and proliferation (able to be used as topographical agents to induce changes in cell behavior), and (3) drug delivery (able to slowly release bioactive protein for several days displaying interesting pharmacokinetic profiles) [273].

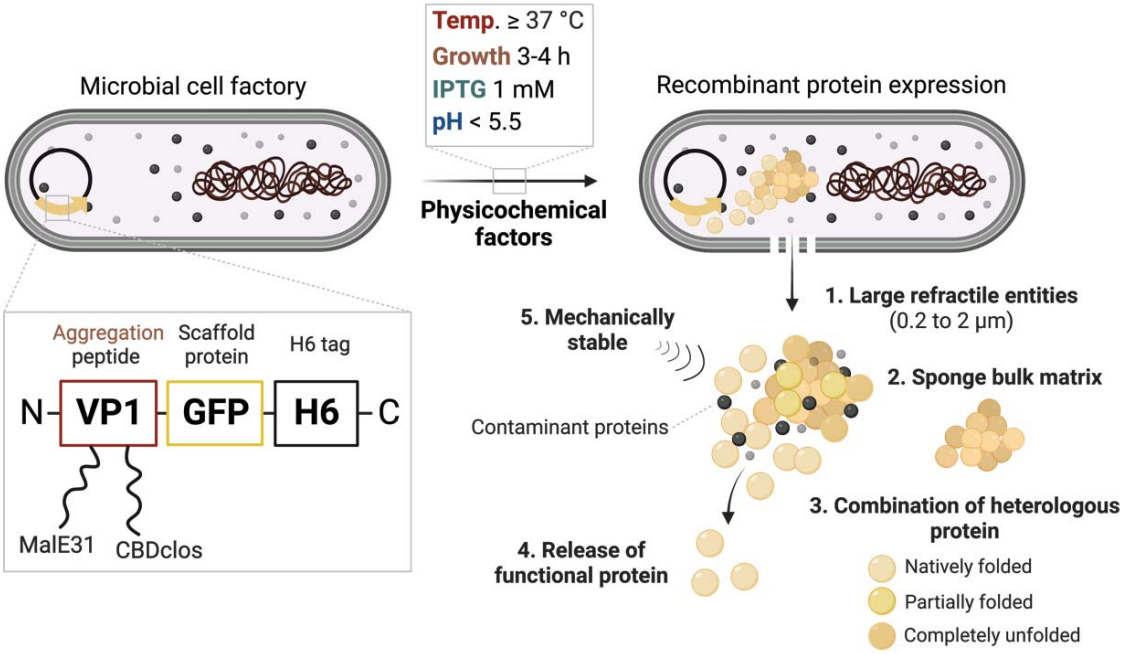

Figure 12. A schematic representation of natural IBs formulation in microbial cell factories and their physicochemical properties, meaning (1) size (large refractile entities of around 0.2 to 2 µm), (2) structure (a sponge-like bulk matrix), (3) composition (a combination of heterologous protein), (4) the capacity to release functional protein for the desired purpose, and (5) stability upon mechanical stimulation. In addition, several factors can be used to induce IBs formation including aggregation peptides, temperature, growth time, IPTG concentration and pH, depicted in the insets.

5.5 The dark side of these strategies

Both strategies were created mimicking natural processes, with the aim to display great versatility in a cost-effective manner. Thus, the protein-based nanoparticle system allows to manufacture biocompatible and pure products with efficient delivery and biodistribution capacities. On the other way around, the natural IBs system display great physicochemical stability, in conjunction with an interesting slow release profile of the therapeutic drug with great targeting and delivery possibilities. They seem to be complementary, like the two sides of the same coin.

But not all that glitters is gold, as there are also special **concerns** that must be addressed when transferring these technologies to the clinics:

Concerns of strategy 1

Although this protein-based assembling platform confers a high manipulability over the designed nanomaterial through a simple, spontaneous, and cheap manufacturing process, there is a lack of oligomerization control. Indeed, there are no clear studies that demonstrate

which are the specific interactions that trigger the nanostructuring process. This decreases the reproducibility between batches, and the size-control of the resultant material. Obviously, this scenario creates unsustainable scale up problems (for a future technology transfer) and a considerable variability between experiments. Because of that, we must find alternative biochemical approaches to optimize this oligomerization platform and ensure a reproducible well-defined set of protein-based nanoparticles, homogeneous in size, that maintain the bioactive properties, and that also are produced in a cost-effective manner (**Figure 13**).

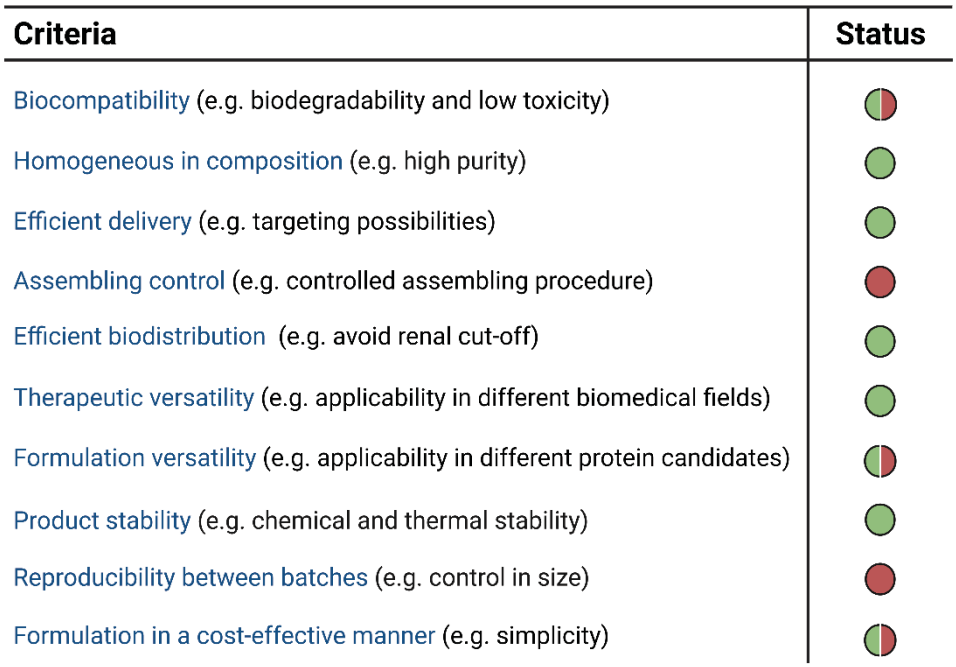

Figure 13. A qualitative evaluation following (Figure 10 list) of strategy 1 (A cationic – histidine tag principle for protein self-assembling), meaning green (accomplished), red (not accomplished), and green-red (further studies needed). This analysis was used to establish the thesis' objectives and furtherly discussed in the following sections.

Concerns of strategy 2

Naturally occurring insoluble IBs are also really versatile biomaterials for biomedicine. Meanwhile they are mainly composed by the desired overexpressed heterologous protein after several purification steps, they also contain contaminant host cell proteins, such as IbpA and IbpB (related to the cell shock response), chaperones (e.g., DNAK) and other macromolecules (e.g., phospholipids and nucleic acids) [274]. Thus, the obtained insoluble microparticles exhibit low purity levels, lack of reproducibility, and present high probability of developing inside-organisms toxic effect, mainly caused by a non-desired immune response. In this sense, this microparticularization platform should be refined, and novel

biochemical approaches considered to ensure a well-defined, highly pure, and homogeneous-in-composition product. Obviously, the novel strategy should maintain the slow release pharmacokinetic properties of the natural IBs and ensure safety in a cost-effective manner (**Figure 14**).

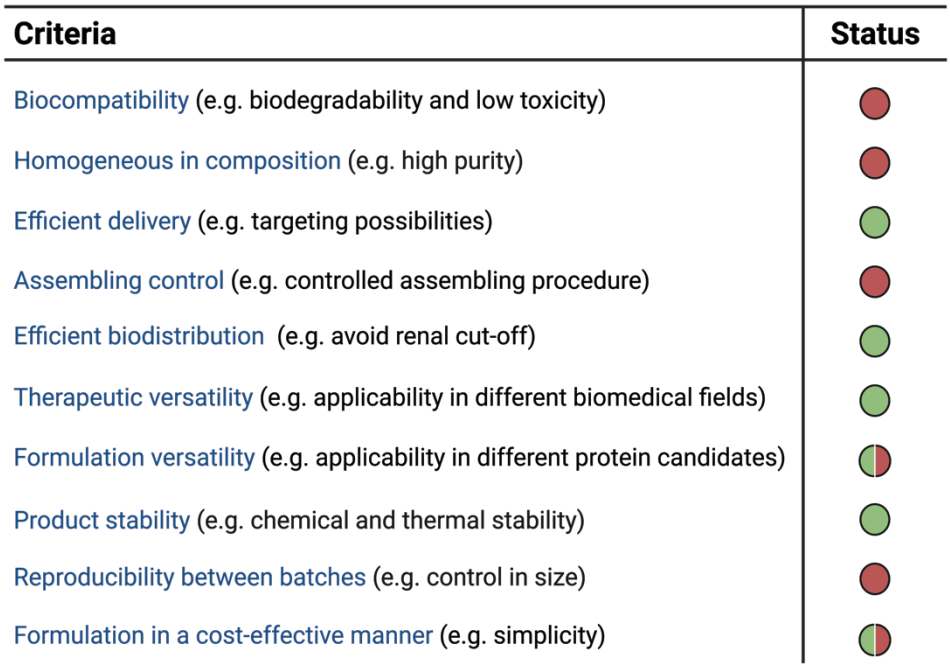

Figure 14. A qualitative evaluation following (Figure 10 list) of strategy 2 (A physicochemical self-assembling principle of protein-based insoluble microparticles), meaning green (accomplished), red (not accomplished), and green-red (further studies needed). This analysis was used to establish the thesis' objectives and furtherly discussed in the following sections.

Overview

The overall storyline has transported us through five chapters of knowledge; starting by the basic biochemical principles and moving on to our most sophisticated biomedical protein-based devices.

Chapter 1 was presented as a touchdown with biomolecules, and how cells appear as incredible builders of hierarchic supramolecular structures with pleiotropic and indispensable cell functions, being proteins-based complexes the major effectors of this vast landscape of reactions.

Chapter 2 was designed to highlight the need of ionic reactive species, namely metal ions, to ensure the adequate functioning and architecting of this protein-based complexes. As an iconic example, zinc (especially in its divalent form +2) is able to construct suprastructures such as insulin secretory granules (experimentally disassembled by EDTA) through an assembling process in which exposed histidine residues are glued by coordination bonds at defined physiological concentrations.

Chapter 3 exposes how scientist started artificially replicating natural processes. In particular, protein engineering was born as the spearhead of this technological revolution. From outsourced expression of proteins (namely recombinant protein production) to their purification by using IMAC chromatography strategies in which the histidine tag is the queen. What is more, the continued iterative optimization of protein engineering allowed scientists to design multidomain recombinant proteins with multifunctional properties.

Chapter 4 gives some light to the protein engineering limitations, and how nanotechnology (and specially nanoparticles) emerged as a viable complement to ensure proper material's biodistribution and effectiveness. It also instructs us on how nanotechnology faced its own toxicological drawbacks (such as protein corona) and how a new set of biological materials was developed, with self-assembling properties, to be used as efficient biocompatible drug delivery systems with proper biodistribution properties.

Finally, **chapter 5** presents protein-based nanoparticles and natural inclusion bodies (meaning microparticles) as versatile platforms for the rational design of biomaterials by spontaneous oligomerization principles, but still showing their clinical concerns, including low reproducibility, lack of oligomeric control, scale up limitations and toxicological issues.

OBJECTIVES

Recalling the importance of developing tunable and biocompatible drug delivery systems for our current medical needs, this thesis has been waved to explore novel and simple biochemical principles to formulate versatile, non-toxic, and efficient protein-based materials considering the already mentioned clinical concerns (figures 13 and 14).

Indeed, a set of 4 objectives were proposed at the beginning of the PhD to target each one of these weaknesses. See their correlated studies alongside:

1. To develop a new and fully transversal biochemical approach to manufacture **protein-based nanoparticles** in a well-defined, reproducible, and cost-effective regulatory compliant manner (study 1).
    a. Using multidomain proteins to construct nanoparticles (study 2).
    b. Using human microbiome proteins to construct nanoparticles (study 3).

2. To develop a new and fully transversal biochemical approach to manufacture **protein-based insoluble microparticles** in a well-defined, biocompatible, and cost-effective regulatory compliant manner (study 4).
    a. Using multidomain proteins to construct secretory granules (study 5).

3. To test the biomedical applications of these platforms (meaning divalent cation-based nano or micro -particles):
    a. In drug delivery: Zebra-fish model (study 2).
    b. In drug delivery: Mouse model (study 6).
    c. In tissue engineering: Wound healing (annex 1).
    d. In tissue engineering: Osteogenesis (annex 2).
    e. In biocatalysis (annex 3).
    f. In the treatment of infectious diseases (annex 4).

4. To review all the extracted knowledge and condense it as practical guidelines for the scientific community (study 7 and annex 5).

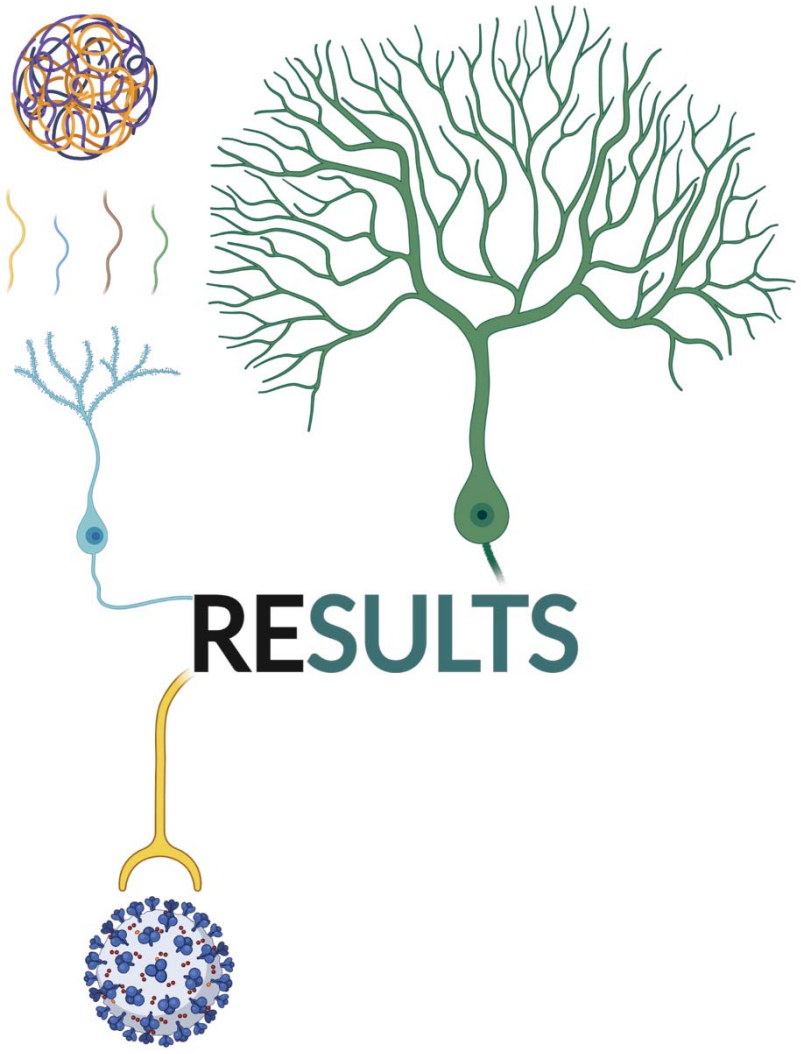

RESULTS

Study 1

Assembly of histidine-rich protein materials controlled through divalent cations

Hèctor López-Laguna, Ugutz Unzueta, Oscar Conchillo-Solé, Alejandro Sánchez-Chardi, Mireia Pesarrodona, Olivia Cano-Garrido, Eric Voltà, Laura Sánchez-García, Naroa Serna, Paolo Saccardo, Ramón Mangues, Antonio Villaverde, and Esther Vázquez

Acta Biomaterialia 2019 · Impact factor (7.242) · Quartile (Q1)

Objective 1

To develop a new and fully transversal biochemical approach to manufacture **protein-based nanoparticles** in a well-defined, reproducible, and cost-effective regulatory compliant manner.

The well-established nano-architectonic strategy 1 (A cationic – histidine tag principle for protein self-assembling) have allowed scientists to develop a new set of homogeneous in composition, efficient, versatile, and stable protein-based nanomaterials with exciting biomedical applications. However, their rational design is limited by a poor control of the assembling process, which reduces reproducibility between batches, and increases the product's complexity; meaning a huge product variability unacceptable for scale up purposes.

Thus, this work has been focused on exploring a new, well-defined, and simple biochemical principle to manufacture protein-based nanoparticles ensuring oligomeric control, and reproducibility. What is more, the cross-reactivity of histidine tagged peptides in presence of divalent cations (Irving-William series) has been studied. The obtained data shed some light on how this principle allows the assembling, disassembling (EDTA), and reassembling of protein-based nanoparticles by the simple stoichiometric manipulation of divalent cations.

Acta Biomaterialia 83 (2019) 257–264

Contents lists available at ScienceDirect

Acta Biomaterialia

journal homepage: www.elsevier.com/locate/actabiomat

Short communication

Assembly of histidine-rich protein materials controlled through divalent cations

Hèctor López-Laguna [a,b], Ugutz Unzueta [b,c,d,*], Oscar Conchillo-Solé [a], Alejandro Sánchez-Chardi [e], Mireia Pesarrodona [a,b,c,1], Olivia Cano-Garrido [a,b], Eric Voltà [a,b], Laura Sánchez-García [a,b,c], Naroa Serna [a,b,c], Paolo Saccardo [a,c,f], Ramón Mangues [c,d], Antonio Villaverde [a,b,c,*], Esther Vázquez [a,b,c,*]

[a] Institut de Biotecnologia i de Biomedicina, Universitat Autònoma de Barcelona, Bellaterra, 08193 Barcelona, Spain
[b] Departament de Genètica i de Microbiologia, Universitat Autònoma de Barcelona, Bellaterra, 08193 Barcelona, Spain
[c] CIBER de Bioingeniería, Biomateriales y Nanomedicina (CIBER-BBN), C/ Monforte de Lemos 3-5, 28029 Madrid, Spain
[d] Institut d'Investigacions Biomèdiques Sant Pau, Hospital de la Santa Creu i Sant Pau, 08025 Barcelona, Spain
[e] Servei de Microscòpia, Universitat Autònoma de Barcelona, Bellaterra, 08193 Barcelona, Spain
[f] Plataforma de Producción de Proteínas, CIBER de Bioingeniería, Biomateriales y Nanomedicina (CIBER-BBN) and Universitat Autònoma de Barcelona, Bellaterra, 08193 Cerdanyola del Vallès, Spain

ARTICLE INFO

Article history:
Received 10 June 2018
Received in revised form 29 September 2018
Accepted 22 October 2018
Available online 24 October 2018

Keywords:
Protein materials
Functional materials
Nanoparticles
Genetic design
Controlled oligomerization

ABSTRACT

Nanostructured protein materials show exciting biomedical applications, since both structure and function can be genetically programmed. In particular, self-assembling histidine-rich proteins benefit from functional plasticity that allows the generation of protein-only nanoparticles for cell targeted drug delivery. However, the rational development of constructs with improved functions is limited by a poor control of the oligomerization process. By exploring cross-interactions between histidine-tagged building blocks, we have identified a critical architectonic role of divalent cations. The obtained data instruct about how histidine-rich protein materials can be assembled, disassembled and reassembled within the nanoscale through the stoichiometric manipulation of divalent ions, in a biochemical approach to biomaterials design.

Statement of Significance

Divalent metal and non-metal cations such as Ni^{2+}, Cu^{2+} Ca^{2+} and Zn^{2+} have been identified as unexpected molecular tools to control the assembling, disassembling and reassembling of histidine-rich protein materials at the nanoscale. Their stoichiometric manipulation allows generating defined protein-protein cross-molecular contacts between building blocks, for a powerful nano-biochemical manipulation of the material's architecture.

© 2018 Acta Materialia Inc. Published by Elsevier Ltd. All rights reserved.

1. Introduction

Advanced protein engineering allows designing polypeptide chains with pre-defined cross-molecular interactivity to construct peptide- and protein-based materials [1–6]. Nanostructured homomeric oligomers with self-assembling properties are potential mimetics of complex protein structures (such as viral capsids) for *in vivo* applications in regenerative medicine [4] and drug delivery [7]. Among the diverse current approaches to construct regular oligomers [4,5,8–12], the simple combination of cationic and histidine-tag (His-tag, H6-tag or H6-tail) regions promotes the formation of functional toroidal (cyclic) nanoparticles (NPs) potentially useable for BBB-crossing [13], tumor imaging [14], tissue engineering [15] and cell-targeted drug delivery [16–19]. T22-GFP-H6, a paradigmatic representative of such engineering platform, forms robust nanoparticles of around 12 nm in size through the assembling of GFP-containing monomers produced in recombinant *Escherichia coli* [20]. These materials are targeted

* Corresponding authors at: Institut de Biotecnologia i de Biomedicina, Universitat Autònoma de Barcelona, Bellaterra, 08193 Barcelona, Spain and Institut d'Investigacions Biomèdiques Sant Pau, Hospital de la Santa Creu i Sant Pau, 08025 Barcelona, Spain.
E-mail addresses: uunzueta@santpau.cat (U. Unzueta), antoni.villaverde@uab.es (A. Villaverde), esther.vazquez@uab.es (E. Vázquez).
[1] Present address: Institute for Research in Biomedicine (IRB Barcelona), The Barcelona Institute of Science and Technology, Barcelona 08028, Spain.

https://doi.org/10.1016/j.actbio.2018.10.030
1742-7061/© 2018 Acta Materialia Inc. Published by Elsevier Ltd. All rights reserved.

to the tumoral marker CXCR4 both *in vitro* and *in vivo*, offering potential as biocompatible nanoscale vehicles for the delivery of conventional and innovative drugs [14,21]. Derivatives of this construct that contain cytotoxic protein stretches or covalently attached cytotoxic drugs have been exploited as potent, protein-only antitumoral drugs for precision oncotherapies [16–19].

While an unbalanced electrostatic charge distribution clearly contributes to self-assembly of T22-GFP-H6 and related proteins [22], His-His and His-cationic peptide contacts have also been predicted and experimentally demonstrated [14,23,24], suggesting His-tags as key architectonic players in the supramolecular architecture of this particular type of material. However, the precise mechanisms by which histidine-rich regions participate in the oligomerization process remains obscure, limiting the control over nanoparticle formation. Intervening in His-mediated protein interactions would allow a more rational design of nanostructured protein-based materials through conventional protein engineering. In particular, the possibility to manipulate the oligomerization process of His-rich building blocks (BBs) as protein-only nanoparticles would represent a powerful and versatile engineering platform for the generation of hybrid materials. Being so far a technically challenging process [24], a regulatable oligomerization platform at the nanoscale, based on *de novo* designed recombinant proteins, would have promising applications in drug co-delivery and in other biomedical fields within diagnoses and therapy [25,26].

2. Materials and methods

2.1. Protein production and purification

Genes encoding for T22-GFP-H6, GFP-H6, T22-GFP and T22-GFP-H6(Loop) proteins were designed in house and provided by Geneart (ThermoFisher) as *Escherichia coli* codon-optimized genes encoded in a pET22b plasmid. All plasmids were transformed and encoding proteins produced in *E. coli* Origami B (BL21, OmpT$^-$, Lon$^-$, TrxB, Gor$^-$; Novagen) at 20 °C overnight upon induction with 0.1 mM of Isopropyl-β-D-thiogalactopyronaside (IPTG). Bacteria cells were then harvested by centrifugation (15 min, 5.000g) and resuspended in Wash buffer (20 mM Tris, 500 mM NaCl, 10 mM Imidazole, pH = 8) for T22-GFP-H6, T22-GFP-H6(Loop) and GFP-H6; (20 mM Bis-Tris Propane, pH = 9.5) for T22-GFP in presence of protease inhibitors (Complete EDTA-Free, Roche) and DNAse (only for T22-GFP, 20 μg/mL, Roche). Cells were disrupted by two rounds at 1200 psi in a French press (Thermo FA-078A) and soluble fraction separated by centrifugation (45 min, 15.000g). Traces of DNA were eliminated using centrifugal filters (Amicon® Ultra – 15 10 K, Millipore) for T22-GFP. T22-GFP-H6, GFP-H6 and T22-GFP-H6(Loop) proteins were then purified by Immobilized Metal Affinity Chromatography (IMAC) using HiTrap Chelating HP 5 mL columns (GE Healthcare) in an ÄKTA pure system (GE Healthcare). Elution was achieved by a linear gradient of Elution buffer (20 mM Tris, 500 mM NaCl, 500 mM Imidazole, pH = 8) and eluted proteins were finally dialyzed against sodium carbonate buffer (166 mM $NaCO_3H$, pH = 8) for GFP-H6 and sodium carbonate with salt buffer (166 mM $NaCO_3H$, 333 mM NaCl, pH = 8) for T22-GFP-H6 and T22-GFP-H6(Loop). T22-GFP protein was purified by Ionic Exchange Chromatography (IEC) using HiTrap Q FF 1 mL column (GE Healthcare) in an ÄKTA pure system (GE Healthcare). Protein was eluted by a linear gradient of Elution buffer (20 mM Bis-Tris propane, 1 M NaCl, pH = 9.5) and collected protein dialyzed against sodium carbonate with salt buffer. Protein purity was determined by Sodium Dodecyl Sulfate Polyacrylamide Gel Electrophoresis (SDS-PAGE) and Western blot immunodetection with anti-GFP monoclonal antibody (Santa Cruz Biotechnology) and integrity assessed by Matrix-Assisted Laser Desorption Ionization Time-of-Flight (MALDI-TOF) mass spectrometry. Final protein concentration was determined by Bradford assay.

2.2. Dynamic light scattering

Volume size distribution of all protein versions and their size changes in presence of different chemical agents were determined by Dynamic Light Scattering (DLS) at 633 nm in a Zetasizer Nano ZS (Malvern Instruments Limited). All samples were measured in triplicate. Number size distribution (essentially matching to the volume distribution) of all DLS plots are also shown in the Supplementary Fig. 1.

2.3. Controlled disassembly and re-assembly

T22-GFP-H6 NPs were exposed to different free amino acids (L-arginine, L-tyrosine, L-histidine and L-tryptophan) at two different molar ratios (1:1 and 1:3) for 1 h at room temperature and samples analyzed by DLS in order to test their disassembling capacity. For all experiments in this work 1:1 and 1:3 ratio corresponds to 0.88 mM and 2.64 mM respectively. Alternatively, T22-GFP-H6 NPs were exposed to Ethylenediaminetetraacetic acid (EDTA) at 1:1 molar ratio for 1 h at room temperature and samples analyzed by DLS in order to test its disassembling capacity.

On the other hand, EDTA-mediated disassembled T22-GFP-H6 protein samples were exposed to different metallic divalent cations ($NiCl_2$, $CuCl_2$ and $ZnCl_2$) and monovalent cations (CsCl and KCl) at 1:1 molar ratio, and to non-metallic divalent cations ($CaCl_2$) at 1:2 molar ratio for 15 min at room temperature. Samples were then analyzed by DLS in order to test their re-assembling capacity. Alternatively, disassembled T22-GFP-H6 protein samples were exposed to increasing molar ratios of $NiCl_2$ (1:1, 1.5:1, 2:1, 2.5:1) for 15 min at room temperature and subsequently analyzed by DLS.

Reassembling was also promoted by cell extracts. Briefly, *E. coli* Origami B was grown overnight at 37 °C in Lysogeny broth (LB) medium and cells harvested by centrifugation (15 min, 5.000g). Cells were then resuspended in sodium carbonate with salt buffer, lysed by sonication (3 rounds at 10–15% amplitude for a total time of 5 min, 50% -on and 50% -off) and the bacteria soluble fraction (BSF) separated by centrifugation (45 min, 15.000g). EDTA-mediated disassembled T22-GFP-H6 protein samples were then dialyzed against BSF and resulting samples analyzed by DLS.

2.4. Non-denaturing polyacrylamide gel electrophoresis

Different protein samples were charged and run into an 8% (SDS and reducing agent-free) polyacrylamide gel. Bands were then transferred to a polyvinylidene difluoride (PVDF, Bio-Rad) membrane and proteins immunodetected with an anti-GFP monoclonal antibody (Santa Cruz Biotechnology).

2.5. Ni^{2+} determination

Nickel concentration in T22-GFP-H6 NPs and EDTA-mediated disassembled T22-GFP-H6 protein samples was estimated by Inductively Coupled Plasma Mass Spectrometry (ICP-MS), model 7500ce (Agilent Technologies). For that, samples were previously exposed to 65% suprapure nitric acid (HNO_3, Merck) in a 1:1 volume ratio and heated at 75 °C for 2 h in a heating block (DINKO D65). Disassembled T22-GFP-H6 samples had been previously dialyzed against sodium carbonate with salt buffer in order to remove EDTA-divalent cation complexes from the sample. All samples were analyzed in triplicate.

2.6. Molecular modelling

T22-GFP-H6 NPs were modelled as described elsewhere [23] and histidine surface accessibility calculated by Naccess2 software [27]. Those calculations were performed for His residues presented in the C-terminal tail of all structures in the same cluster as the selected model resulted from a previously reported docking [23] described as P1. Histidines 590 and 592 and Ni^{2+} 601 from the Crystal Structure of Na, K-ATPase N-domain from Eurasian wild boar *Sus scrofa* (pdb code 1Q3I, presented elsewhere [28] were used as a model of interaction between His and Ni^{2+} since their structure fits with previously described results [29]. Only the atoms of the main chain were superposed over the C-terminal histidines of the P1 model by using Profit software [30] based on McLachlan algorithm [31], since the side chains were expected to be very mobile.

2.7. Ultrastructural morphometry of NPs, Ni^{2+} localization and fluorescence detection

Morphometry, Ni^{2+} localization and fluorescence detection at the nanoscale were determined by Field Emission Scanning Electron Microscopy (FESEM). The analyzed samples were T22-GFP-H6 NPs, EDTA-mediated disassembled T22-GFP-H6 protein subsequently dialyzed in sodium carbonate with salt buffer, and sodium carbonate with salt buffer as negative control. Drops of 5 μL of each sample were deposited in carbon-coated gold grids (200 mesh) during 1 min, blotted, air dried and observed in a FESEM Zeiss Merlin (Zeiss) operating at 2 kV. Samples were then randomly checked with an *in-lens* secondary electron detector for morphology and with a Back-scattered Electron (BSE) detector for Ni^{2+} localization and fluorescence detection. Representative images were obtained at a wide range of high magnifications (from 200,000× to 500,000×).

2.8. Statistical analysis

Quantitative data are expressed as Standard Error of the Mean ($\bar{x} \pm$ SEM). Comparison of Ni^{2+} concentrations was made with Friedman test and pairwise comparisons were made with Wilcoxon signed rank tests. The rest of pairwise comparisons were performed with Mann–Whitney *U*-tests. Significance was accepted at $p < 0.05$ and Bonferroni correction was applied for sequential comparisons. All statistical analyses were performed with SPSS v. 18 for Windows.

3. Results

We have here investigated the involvement of His residues and cation-pi contacts in the oligomerization of the modular protein T22-GFP-H6 (Fig. 1A), that self-assembles as fluorescent, 11.7 nm NPs (Fig. 1B–D) already at the minimal protein concentration detectable by DLS, namely 0.1 mg/ml. T22-GFP-H6 and related proteins organize in form of ring-shaped oligomers (Fig. 1C) as determined by both FESEM and TEM imaging [14,32], with morphometries that fit with *in silico* protein models ([23], Fig. 1D). The presence of both the cationic peptide T22 and the H6-tail is necessary for assembly, as GFP-H6 and T22-GFP solely occur as unassembled BBs (Fig. 1A,B). To evaluate if cation-pi interactions sustain the oligomeric form of the protein through contacts between T22 and H6 tags, we attempted a controlled disassembling of the NPs through the addition of soluble L-histidine as a competitor. At the stoichiometric molar ratio of 1:1 (corresponding to 0.88 mM) and 3:1 (corresponding to 2.64 mM), the free amino acid promoted the reduction of T22-GFP-H6 NP size to 7.5 and

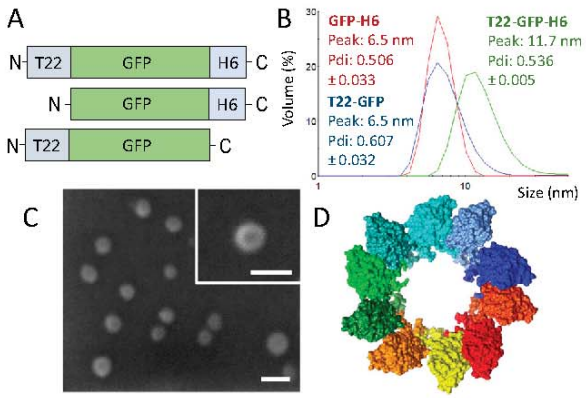

Fig. 1. Structure and architecture of T22-GFP-H6 BBs and NPs. A. Modular organization of T22-GFP-H6 and the related constructs GFP-H6 and T22-GFP. Relative sizes of boxes are only indicative. Precise details of T22-GFP-H6 NP construction can be found elsewhere [1]. The integrity and molecular masses of T22-GFP-H6, GFP-H6 and T22-GFP were confirmed by MALDI-TOF to be 30596.3, 27453.3 and 28359.6 respectively. B. Hydrodynamic size and pdi (polydispersion index) of the proteins indicated in panel A, determined by Dynamic Light Scattering (DLS). Peak values refer to the average mode of the population, that always rendered a standard error lower than 0.00. C. Representative FESEM images of purified T22-GFP-H6 NPs, showing the cyclic organization of the oligomer. White bars indicate 20 nm. D. Surface representation of a T22-GFP-H6 NP from the major purification peak in the Immobilized Metal Ion Affinity Chromatography (IMAC), in a top view (modelled with HADDOCK). Each T22-GFP-H6 protein monomer is differently coloured (modified from [23] and reproduced with permission of John Wiley and Sons). Size and organization of the model are compatible with the FESEM morphometry.

6.5 nm respectively (Fig. 2A). The His-mediated disassembling was fully compatible with the H6-tag involved in cross-molecular interactions between BBs, through the imidazole ring. To assess this hypothesis, we tried to disassemble the material with other aromatic amino acids, namely L-tryptophan and L-tyrosine, with negative results (Fig. 2A). This observation weakened the hypothesis of cation-pi interactions. In this line, free L-arginine was also unable to alter the structure of the NPs. This indicated that cationic amino acids, important to promote oligomerization, are not the unique supporters of the stability of the assembled material.

Metals remaining from the producing bacteria or residual from the Nickel II (Ni^{2+})-based chromatography might be involved in protein assembly, as in the case of amyloid fibers that interact with divalent metals [33–35]. In this regard, addition of EDTA indeed promoted efficient disassembling of the NPs (Fig. 2B). In a step further, free Ni^{2+} as well as Cu^{2+}, Ca^{2+} and Zn^{2+}, but not Cs^{+} and K^{+}, recovered the original NP size when added to the solution of disassembled BBs (Fig. 2C). Note that K^{+} is unable to promote reassembly when added at the same concentration that divalent cations but also at the same ionic strength (Fig. 2C, blue bar). Interestingly, increasing molar ratios of Ni^{2+} added to EDTA-disrupted NPs promoted the occurrence of reassembled materials with increasing sizes ($\chi^2 = 15{,}000$, $p < 0.0001$), from 10.1 to 15.6 nm (Fig. 3A). This fact confirmed an active role of Ni^{2+} in NP formation but also in the nanoscale organization of the protein material. Furthermore, the simple use and versatility of Ni^{2+} as a structural NP modulator was fully demonstrated by the consecutive removal and addition of the cation to and from the same sample of T22-GFP-H6 (Fig. 3B).

Since Ni^{2+} or other divalent cations appeared as natural molecular connectors of protein BBs, we were interested in knowing if T22-GFP-H6 NPs might be formed already in the cytoplasm of producing *E. coli* bacterial cells. Indeed, we identified a supramolecular

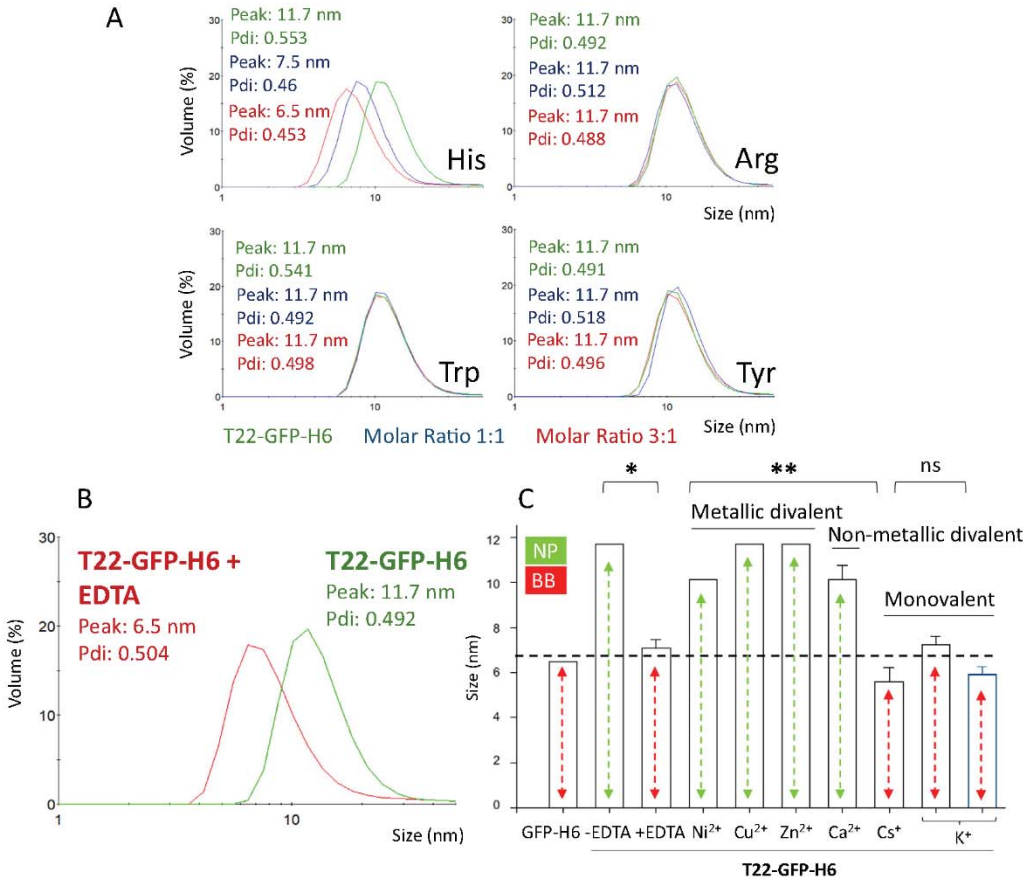

Fig. 2. Cation-mediated NP disassembling and reassembling. A. Hydrodynamic size of T22-GFP-H6 NPs in absence (control, represented in green) or in presence of different molar ratios (1:1, in blue and 3:1, in red) of diverse free amino acids. Arginine (Arg) was tested to probe electrostatic interactions while tryptophan (Trp), histidine (His) and tyrosine (Tyr) to probe cation-pi contacts. Representative DLS plots are shown, indicating the value of the peak and pdi. B. EDTA-mediated disassembling of non-treated T22-GFP-H6 NPs, in green and +EDTA, in red. C. Cation-promoted reassembling of EDTA-treated protein T22-GFP-H6 NPs. GFP-H6 and non-treated T22-GFP-H6 NPs are included as references. Bars are clustered by the type of cations used in the reassembling process, that were added to a final molar ratio of 1:1 at exception of Ca^{2+} that was used at 1:2, the minimum concentration in which reassembling was observed. K^+ was used at both the same concentration (black bar) and at the same ionic strength (blue bar) than metal ions to discard any unexpected influence or artefact. Protein complexes above the discontinuous line are considered as NPs (green) and below are considered BBs (red). Data expressed as $\bar{x} \pm$ standard error of the mean (SEM), n = 3, and statistical comparisons are in relation to +EDTA group (ns: no significant, $^{*}p < 0.05$, $^{**}p < 0.001$). (For interpretation of the references to colour in this figure legend, the reader is referred to the web version of this article.)

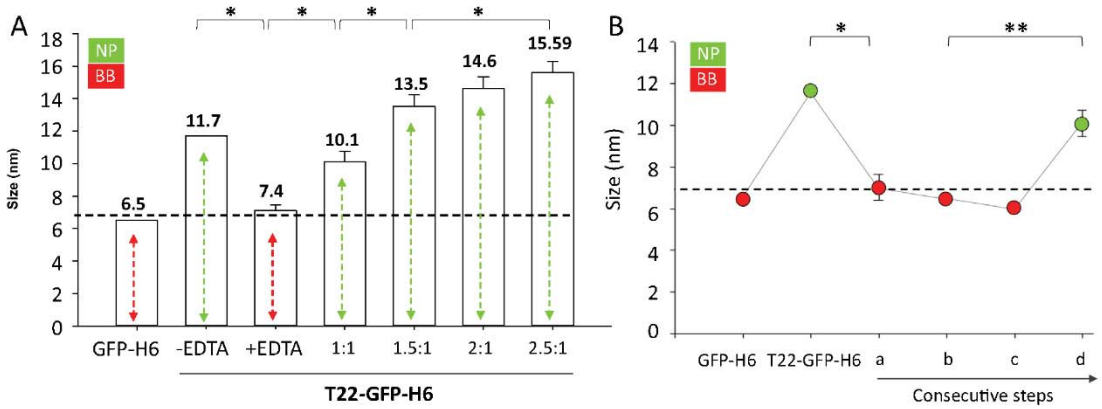

Fig. 3. Functional plasticity and manipulability of Ni^{2+} as an architectonic agent. A. Dose-dependent role of Ni^{2+} in the assembling and architecture of T22-GFP-H6 NPs, determined through the hydrodynamic size of EDTA-disassembled T22-GFP-H6 upon exposure to increasing amounts of Ni^{2+}. B. Hydrodynamic size variation of T22-GFPH6 protein when: (a) incubated with EDTA at 1:1 molar ratio for 1 h; (b) dialyzed against sodium carbonate with salt buffer and treated with Wash buffer; (c) purified with IMAC and eluted in elution buffer; (d) dialyzed against sodium carbonate with salt buffer. The experiment was performed in consecutive steps. Data expressed as $\bar{x} \pm$ SEM, n = 3, and statistical comparisons are $^{*}p < 0.05$, $^{**}p < 0.001$. The nomenclature is as in Fig. 1.

form of T22-GFP-H6 protein in cell extracts, by immunodetecting a slow migrating protein version in non-denaturing gels (Fig. 4A). In the same context, bacterial crude cell extracts were able to increase the hydrodynamic size of disassembled T22-GFP-H6 protein upon *in vitro* incubation (Fig. 4B). Finally, Ni^{2+} was analytically detected at the same stoichiometric order of magnitude (in a molar basis) for protein and ion, in samples of pure T22-GFP-H6 NPs but not in T22-GFP-H6 proteins previously treated with EDTA and further dialyzed (Fig. 4C). This fact was also confirmed by direct visualization of higher backscattered electron density (BSE). The BSE imaging only showed white-light areas where NPs occurred, reporting a correlation between protein particles and the localization of high concentrations of heavy atoms (Fig. 4C, bottom), compatible with the accumulation of Ni^{2+} in the nanoconstructs. In this regard, all these data indicated that an assembled version of T22-GFP-H6 does occur in the bacterial cytosol and that the soluble cell fraction contains sufficient divalent cations to ensure the *in vitro* assembling of the nanomaterial.

In this regard, we presumed that the metal detected in the oligomers could be coordinated with His residues, in the H6 overhanging tails oriented towards the geometrical centre of the structure and acting as a 'molecular glue' to sustain the architecture of the NP. This was modelled over the result of the previously done docking [23], by selecting all generated models belonging to the same cluster. In all these models, the surface accessibility of His residues of the C-terminal tail was calculated using the Nacces2 software. Data expressed as mean and the standard deviation were calculated to take into account the result for all the models. It was observed that the sum of the mean plus the standard deviation resulted in a surface accessibility greater than 50%, for all of them. Subsequently, His 590 and 592 and Ni^{2+} 601 of structure 1Q3I3 were selected as the His-Ni^{2+} interaction model and were superimposed by the Profit software. Only the atoms of the main chain were used for the superposition since the side chains, being so exposed to surface, were expected to be very mobile. This superposition generated an RMSD of 0.61 ± 0.29 Å, revealing that the two His residues of the His-Ni^{2+} interaction model fit perfectly on the His residues of the particle model (Fig. 5A,B). In a further approach to experimentally validate the model we argued that His residues from the H6-tail could be unavailable for cross-molecular contacts if not oriented towards the core of the NP, where metal appears to coordinate with the proteins. In this line, we generated another protein, T22-GFP-H6(Loop) (Fig. 5C), in which H6-tail was not accommodated in the C-terminus of GFP but in one of the exposed loops of GFP, that is highly permissive to peptide insertions [36,37]. As expected, T22-GFP-H6(Loop) was unable to self-assemble as NPs but it remained in a protomeric state (Fig. 5C), like T22-GFP or GFP-H6 (Fig. 1B).

4. Discussion

The potential application of divalent ions in the assembling of protein-only or protein-containing materials has been largely documented [38–41] and reviewed [42]. Among others, these architectonic principles have been applied to the construction of nanoscale materials for the delivery of drugs [1,3,6,10,43], some of them in virus-inspired formats [7,44–46]. However, the particular role of Ni^{2+} and His residues (both critical players in the purification of recombinant proteins [47]) has not been particularly addressed. Ni^{2+} had been early discussed as an important conformational arranger in biological systems (e.g., in urease) [48], as well as Zn^{2+} and Cu^{2+} that are present in carbonic anhydrase and copper B proteins [49] respectively. In fact, protein-divalent cation complexes involving Ni^{2+} and other metals have been widely described with a plethora of both catalytic and structural functions [50–55]. The configuration of electronic d orbitals in transition metals allows them to be considerable good Lewis acids for further interaction with biological molecules. Not only the d orbitals but also its geometry determines their number of possible interactions, namely an octahedral geometry for Ni^{2+} and tetrahedral for Cu^{2+} and Zn^{2+}. Those metals are able to interact with the nucleophilic

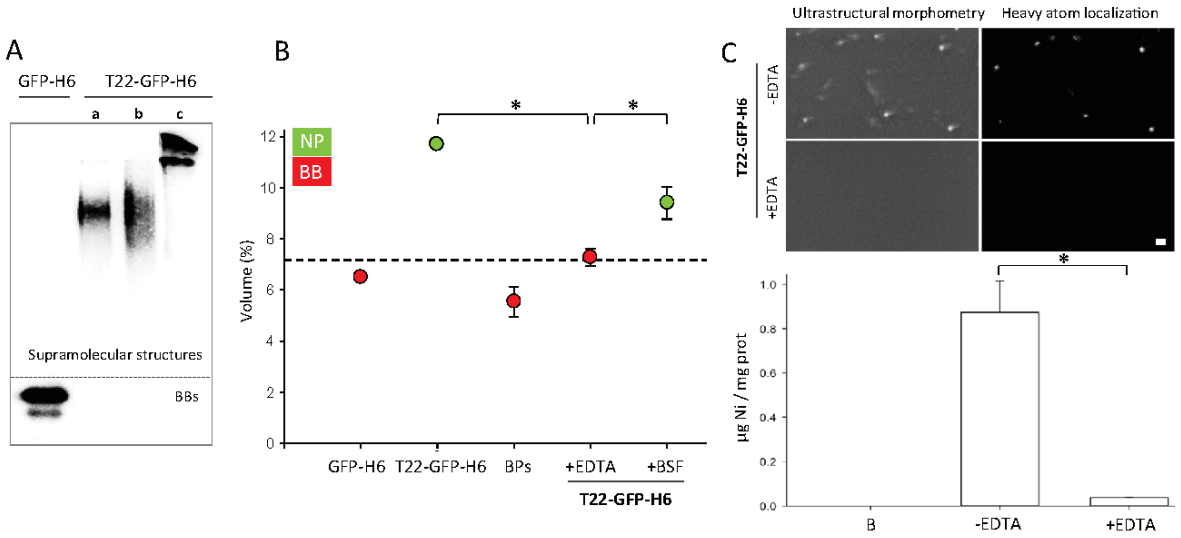

Fig. 4. Accommodation of Ni^{2+} in T22-GFP-H6 NPs. A. Immunodetection of IMAC-purified T22-GFP-H6 protein in non-denaturing gels (a), and of the same protein submitted to size-exclusion chromatography (SEC) to ensure the absence of BB and assembling intermediates that might occur in the pure protein samples (b). The bacteria soluble fraction was added to analyze the supramolecular conformation of T22-GFP-H6 protein (c). B. Hydrodynamic size of T22-GFP-H6 NPs disassembled with EDTA, and subsequently dialyzed against the crude bacteria soluble fraction (BSF). As BSF was rich in bacterial proteins (BPs), sodium carbonate with salt buffer was also dialyzed against BSF as control. Nomenclature is as in Fig. 1. Data expressed as x ± SEM, n = 3, and statistical comparisons are in relation to +EDTA group (*$p < 0.05$). C. *In situ* visualization of a backscattered electron density, compatible with Ni2+, in assembled T22-GFP-H6 NPs and EDTA-mediated disassembled T22-GFP-H6 proteins (morphometry and backscattered images). Bar indicates 20 nm. At the bottom, direct Ni^{2+} chemical analysis by ICP-MS of T22-GFP-H6 NPs and EDTA-mediated disassembled T22-GFP-H6 proteins. Sodium carbonate with salt buffer was also added as control (B). Data expressed as x ± SEM, n = 3, and statistical comparison is in relation to +EDTA group (*$p < 0.05$).

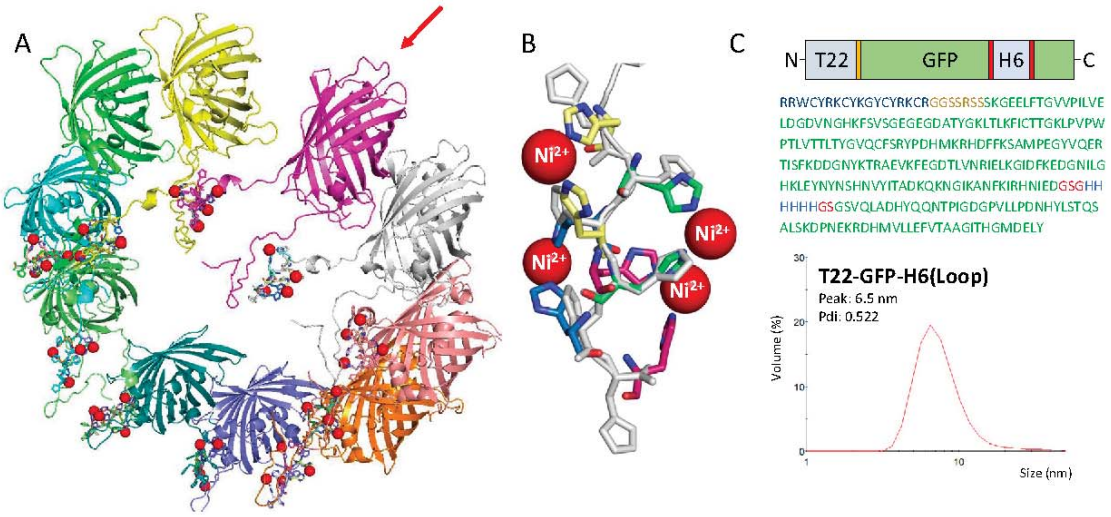

Fig. 5. A. Model of a T22-GFP-H6 NP in which all C-terminal histidine tag residues of each monomer are superimposed on the structure chosen as the His-Ni^{2+} (coloured atoms and red spheres) interaction model. The arrow indicates the GFP loop where the H6-tail segment was moved to in the construction T22-GFP-H6(Loop) (described in panel C). B. Detail of the superposition of His residues on the N-terminal tail of one of T22-GFP-H6 monomer of NPs. C. Schematic representation of T22-GFP-H6(Loop), in which the H6 segment is accommodated within the GFP, in the solvent-exposed loop indicated in panel A. The precise amino acid sequence of the protein is indicated, as well as the hydrodynamic size coincident with a disassembled form of the protein. The molecular mass of the protein was determined to be 30808.7 Da by MALDI-TOF. (For interpretation of the references to colour in this figure legend, the reader is referred to the web version of this article.)

unpaired electrons presented in the δ1-Nitrogen of histidine imidazole ring [56], being permanently and strongly held into the structure and thus supporting the mechanics of the His-tag based single-step protein purification. We have demonstrated here for the first time how the manipulation of Ni^{2+} and other metal and non-metal divalent cations allows the controlled reassembling of a family of protein-only NPs (Fig. 1C,D) with high biomedical interest in protein drug delivery [57]. The hosted histidine-rich domains participate in the oligomerization process through the coordination with ions remaining from the bacterial cell factories or upon enrichment during Ni^{2+}-based chromatographic purification (Fig. 4A). Then, NPs, once purified, can be disassembled by the removal or addition of divalent ions, in a stoichiometric proportion (Figs. 2 and 3). In this regard, keeping these NPs at a nearly physiological pH avoids δ1-Nitrogen protonation and allow divalent cation coordination, enabling robust NP formation that ensures the *in vivo* stability of the material as previously shown [14]. The capability of that Ni^{2+}, Cu^{2+} and Zn^{2+} to coordinate more than 2 His residues simultaneously [48] makes them acting as a molecular glue at the nanoscale, fully removable by easy biochemical methods such as EDTA addition. This simple approach would allow not only fine adjustments of the NP size as demonstrated here (Fig. 3), but also the easy construction of hybrid materials through the assembling of heterogeneous BBs, that might allow a functional recruitment in single nanoparticles. This is a step beyond the plain purification of biomaterials that have been already assembled in the cell factory, and it expands the versatility of the system allowing a post-production polishing and tailoring *in vitro*. Apart from the emergently discovered roles of metals in amyloid formation, protein aggregation and neurodegenerative diseases [58,59], divalent cations are a powerful and simple biochemical tool to refine and manipulate, in a controlled way, architectonic properties of self-assembling protein materials [42]. Small protein nanoparticles such as T22-GFP-H6 and related constructs are based on *de novo* designed recombinant proteins intended for cell-targeted drug delivery and imaging, once oligomerized. These entities, suitable for conventional protein engineering of their histidine tags, would be largely improved through significant functional recruitment that might be supported, at a downstream level, by a simple manipulation of divalent cation availability.

5. Conclusion

The stoichiometric manipulation of divalent metals, including Ni^{2+}, Cu^{2+} and Zn^{2+}, allows an unexpected and precise control of the assembling, disassembling and reassembling of histidine-rich recombinant proteins as functional nanoparticles. Limited by a poor control of the oligomerization process, the nanoscale development of histidine-rich protein materials has not been fully exploited, despite the enormous potential of these entities in biomedicine, especially as intrinsically functional, biocompatible and self-delivered protein drugs. The possibility to design histidine-rich proteins responsive to divalent ions represents a novel technological platform for the control of size, composition and functionalities of protein nanoparticles. In particular, the *in vitro* manipulability of BBs and their cross-interactions upon biological fabrication should allow the construction of hybrid materials for functional recruitment, what is of high interest in the context of precision medicines.

Acknowledgments

We are indebted to Agencia Estatal de Investigación (AEI) and to Fondo Europeo de Desarrollo Regional (FEDER) (grant BIO2016-76063-R, AEI/FEDER, UE), AGAUR (2017SGR-229) and CIBER-BBN (project NANOPROTHER) granted to AV, and to ISCIII (PI15/00272 co-founding FEDER) to EV. We are also indebted to the Networking Research Center on Bioengineering, Biomaterials and Nanomedicine (CIBER-BBN) that is an initiative funded by the VI National R&D&I Plan 2008–2011, Iniciativa Ingenio 2010, Consolider Program, CIBER Actions and financed by the Instituto de Salud Carlos III, with assistance from the European Regional Development Fund. Protein production has been partially performed by the ICTS "NANBIOSIS", more specifically by the Protein Production Platform of CIBER in Bioengineering, Biomaterials & Nanomedicine

(CIBER-BBN)/IBB, at the UAB sePBioEs scientific-technical service (http://www.nanbiosis.es/portfolio/u1-protein-production-platform-ppp/) and the nanoparticle size analysis by the Biomaterial Processing and Nanostructuring Unit. We are also grateful to SCAC (UAB) for cell culture facilities and assistance. LSG was supported by AGAUR (2017FI_B100063), NS by a predoctoral fellowship from the Government of Navarra and UU by PERIS program from the health department of la Generalitat de Catalunya. AV holds an ICREA ACADEMIA award.

Appendix A. Supplementary data

Supplementary data to this article can be found online at https://doi.org/10.1016/j.actbio.2018.10.030.

References

[1] J.E. Padilla, C. Colovos, T.O. Yeates, Nanohedra: using symmetry to design self assembling protein cages, layers, crystals, and filaments, PNAS 98 (2001) 2217–2221.
[2] T.O. Yeates, Geometric principles for designing highly symmetric self-assembling protein nanomaterials, Annu. Rev. Biophys. 46 (2017) 23–42.
[3] D. Peer, J.M. Karp, S. Hong, O.C. Farokhzad, R. Margalit, R. Langer, Nanocarriers as an emerging platform for cancer therapy, Nat. Nanotechnol. 2 (2007) 751–760.
[4] Y. Loo, M. Goktas, A.B. Tekinay, M.O. Guler, C.A. Hauser, A. Mitraki, Self-assembled proteins and peptides as scaffolds for tissue regeneration, Adv. Healthcare Mater. 4 (2015) 2557–2586.
[5] V.A. Kumar, B.K. Wang, S.M. Kanahara, Rational design of fiber forming supramolecular structures, Exp. Biol. Med. 241 (2016) 899–908.
[6] T.O. Yeates, Y. Liu, J. Laniado, The design of symmetric protein nanomaterials comes of age in theory and practice, Curr. Opin. Struct. Biol. 39 (2016) 134–143.
[7] U. Unzueta, M.V. Cespedes, E. Vazquez, N. Ferrer-Miralles, R. Mangues, A. Villaverde, Towards protein-based viral mimetics for cancer therapies, Trends Biotechnol. 33 (2015) 253–258.
[8] T.A.P.F. Doll, R. Dey, P. Burkhard, Design and optimization of peptide nanoparticles, J. Nanobiotechnol. (2015) 13.
[9] J.A. Fallas, G. Ueda, W. Sheffler, V. Nguyen, D.E. McNamara, B. Sankaran, et al., Computational design of self-assembling cyclic protein homo-oligomers, Nat. Chem. 9 (2017) 353–360.
[10] N. Ferrer-Miralles, E. Rodriguez-Carmona, J.L. Corchero, E. Garcia-Fruitos, E. Vazquez, A. Villaverde, Engineering protein self-assembling in protein-based nanomedicines for drug delivery and gene therapy, Crit. Rev. Biotechnol. 35 (2015) 209–221.
[11] A.P.M. Guttenplan, L.J. Young, D. Matak-Vinkovic, C.F. Kaminski, T.P.J. Knowles, L.S. Itzhaki, Nanoscale click-reactive scaffolds from peptide self-assembly, J. Nanobiotechnol. 15 (2017) 70.
[12] N. Kobayashi, R. Arai, Design and construction of self-assembling supramolecular protein complexes using artificial and fusion proteins as nanoscale building blocks, Curr. Opin. Biotechnol. 46 (2017) 57–65.
[13] N. Serna, M.V. Cespedes, P. Saccardo, Z. Xu, U. Unzueta, P. Alamo, et al., Rational engineering of single-chain polypeptides into protein-only, BBB-targeted nanoparticles, Nanomed. Nanotechnol. Biol. Med. 12 (2016) 1241–1251.
[14] M.V. Cespedes, U. Unzueta, W. Tatkiewicz, A. Sanchez-Chardi, O. Conchillo-Sole, P. Alamo, et al., In vivo architectonic stability of fully de novo designed protein-only nanoparticles, ACS Nano 8 (2014) 4166–4176.
[15] M.T. de Pinho Favaro, L. Sanchez-Garcia, A. Sanchez-Chardi, M. Roldan, U. Unzueta, N. Serna, et al., Protein nanoparticles are nontoxic, tuneable cell stressors, Nanomedicine 13 (2018) 255–268.
[16] N.C. Serna, M., L. Sánchez-García, U. Unzueta, R. Sala, A. Sánchez-Chardi, F. Cortés, N. Ferrer-Miralles, R. Mangues, E. Vázquez, A. Villaverde, Peptide-based nanostructured materials with intrinsic proapoptotic activities in CXCR4+ solid tumors, Adv. Funct. Mater. 27 (2017) 1700919.
[17] M.V. Cespedes, U. Unzueta, A. Avino, A. Gallardo, P. Alamo, R. Sala, et al., Selective depletion of metastatic stem cells as therapy for human colorectal cancer, EMBO Mol. Med. (2018).
[18] R. Diaz, V. Pallares, O. Cano-Garrido, N. Serna, L. Sanchez-Garcia, A. Falgas, et al., Selective CXCR4(+) cancer cell targeting and potent antineoplastic effect by a nanostructured version of recombinant ricin, Small (2018) e1800665.
[19] L. Sanchez-Garcia, N. Serna, P. Alamo, R. Sala, M.V. Cespedes, M. Roldan, et al., Self-assembling toxin-based nanoparticles as self-delivered antitumoral drugs, J. Controlled Release Off J. Controlled Release Soc. (2018).
[20] J.M. Sanchez, L. Sanchez-Garcia, M. Pesarrodona, N. Serna, A. Sanchez-Chardi, U. Unzueta, et al., Conformational conversion during controlled oligomerization into Nonamylogenic protein nanoparticles, Biomacromolecules 19 (2018) 3788–3797.
[21] U. Unzueta, M.V. Cespedes, N. Ferrer-Miralles, I. Casanova, J. Cedano, J.L. Corchero, et al., Intracellular CXCR4(+) cell targeting with T22-empowered protein-only nanoparticles, Int. J. Nanomed. 7 (2012) 4533–4544.
[22] U. Unzueta, N. Ferrer-Miralles, J. Cedano, X. Zikung, M. Pesarrodona, P. Saccardo, et al., Non-amyloidogenic peptide tags for the regulatable self-assembling of protein-only nanoparticles, Biomaterials 33 (2012) 8714–8722.
[23] F. Rueda, M.V. Cespedes, O. Conchillo-Sole, A. Sanchez-Chardi, J. Seras-Franzoso, R. Cubarsi, et al., Bottom-up instructive quality control in the biofabrication of smart protein materials, Adv. Mater. 27 (2015) 7816–7822.
[24] U. Unzueta, N. Serna, L. Sanchez-Garcia, M. Roldan, A. Sanchez-Chardi, R. Mangues, et al., Engineering multifunctional protein nanoparticles by in vitro disassembling and reassembling of heterologous building blocks, Nanotechnology 28 (2017) 505102.
[25] O.C. Farokhzad, R. Langer, Impact of nanotechnology on drug delivery, ACS Nano 3 (2009) 16–20.
[26] Y. Wang, S. Gao, W.H. Ye, H.S. Yoon, Y.Y. Yang, Co-delivery of drugs and DNA from cationic core-shell nanoparticles self-assembled from a biodegradable copolymer, Nat. Mater. 5 (2006) 791–796.
[27] S.J.H.J.M. Thornton, "NACCESS", Computer Program, Department of Biochemistry and Molecular Biology, University College London, 1993.
[28] K.O. Hakansson, The crystallographic structure of Na, K-ATPase N-domain at 2.6A resolution, J. Mol. Biol. 332 (2003) 1175–1182.
[29] V.M. Bolanos-Garcia, O.R. Davies, Structural analysis and classification of native proteins from E. coli commonly co-purified by immobilised metal affinity chromatography, Biochim. Biophys. Acta 1760 (2006) 1304–1313.
[30] A.C.R. Martin, http://www.bioinf.org.uk/software/profit, 2009.
[31] A.D. McLachlan, Rapid comparison of protein structures, Acta. Crystallogr. A 38 (1982) 871–873.
[32] M. Pesarrodona, N. Ferrer-Miralles, U. Unzueta, P. Gener, W. Tatkiewicz, I. Abasolo, et al., Intracellular targeting of CD44+ cells with self-assembling, protein only nanoparticles, Int. J. Pharm. 473 (2014) 286–295.
[33] M.F. Calabrese, A.D. Miranker, Metal binding sheds light on mechanisms of amyloid assembly, Prion 3 (2009) 1–4.
[34] A. Grenacs, I. Sovago, Copper(II), nickel(II) and zinc(II) complexes of the N-terminal nonapeptide fragment of amyloid-beta and its derivatives, J. Inorg. Biochem. 139 (2014) 49–56.
[35] R. Diaz-Espinoza, E. Nova, O. Monasterio, Overcoming electrostatic repulsions during amyloid assembly: effect of pH and interaction with divalent metals using model peptides, Arch. Biochem. Biophys. 621 (2017) 46–53.
[36] T. Kobayashi, N. Morone, T. Kashiyama, H. Oyamada, N. Kurebayashi, T. Murayama, Engineering a novel multifunctional green fluorescent protein tag for a wide variety of protein research, PLoS One 3 (2008) e3822.
[37] N. Soundrarajan, H.S. Cho, B. Ahn, M. Choi, M. Thong le, H. Choi, et al., Green fluorescent protein as a scaffold for high efficiency production of functional bacteriotoxic proteins in Escherichia coli, Sci. Rep. 6 (2016) 20661.
[38] P. Anzini, C. Xu, S. Hughes, E. Magnotti, T. Jiang, L. Hemmingsen, et al., Controlling self-assembly of a peptide-based material via metal-ion induced registry shift, J. Am. Chem. Soc. 135 (2013) 10278–10281.
[39] A.S. Knight, J. Larsson, J.M. Ren, R. Bou Zerdan, S. Seguin, R. Vrahas, et al., Control of amphiphile self-assembly via bioinspired metal ion coordination, J. Am. Chem. Soc. 140 (2018) 1409–1414.
[40] R. Zou, Q. Wang, J. Wu, J. Wu, C. Schmuck, H. Tian, Peptide self-assembly triggered by metal ions, Chem. Soc. Rev. 44 (2015) 5200–5219.
[41] Z. Yu, A. Erbas, F. Tantakitti, L.C. Palmer, J.A. Jackman, M. Olvera de la Cruz, et al., Co-assembly of Peptide Amphiphiles and lipids into supramolecular nanostructures driven by anion-pi interactions, J. Am. Chem. Soc. 139 (2017) 7823–7830.
[42] P.A. Sontz, W.J. Song, F.A. Tezcan, Interfacial metal coordination in engineered protein and peptide assemblies, Curr. Opin. Chem. Biol. 19 (2014) 42–49.
[43] J.L. Corchero, E. Vazquez, E. Garcia-Fruitos, N. Ferrer-Miralles, A. Villaverde, Recombinant protein materials for bioengineering and nanomedicine, Nanomedicine 9 (2014) 2817–2828.
[44] K. Matsuura, Construction of spherical virus-inspired peptide nanoassemblies, Polym. J. 44 (2012).
[45] B. Lamarre, M.G. Ryadnov, Self-assembling viral mimetics: one long journey with short steps, Macromol. Biosci. 11 (2011) 503–513.
[46] Y. Ma, R.J. Nolte, J.J. Cornelissen, Virus-based nanocarriers for drug delivery, Adv. Drug Delivery Rev. 64 (2012) 811–825.
[47] N. Ferrer-Miralles, J.L. Corchero, P. Kumar, J.A. Cedano, K.C. Gupta, A. Villaverde, et al., Biological activities of histidine-rich peptides; merging biotechnology and nanomedicine, Microb. Cell Fact. 10 (2011) 101.
[48] R.J. Williams, 16th Sir Hans Krebs lecture. The symbiosis of metal and protein functions, Eur. J. Biochem. 150 (1985) 231–248.
[49] L. Rulisek, J. Vondrasek, Coordination geometries of selected transition metal ions (Co2+, Ni2+, Cu2+, Zn2+, Cd2+, and Hg2+) in metalloproteins, J. Inorg. Biochem. 71 (1998) 115–127.
[50] D. Samorodnitsky, E.M. Nicholson, Differential effects of divalent cations on elk prion protein fibril formation and stability, Prion 12 (2018) 63–71.
[51] M. Mohammadian, A. Madadlou, Cold-set hydrogels made of whey protein nanofibrils with different divalent cations, Int. J. Biol. Macromol. 89 (2016) 499–506.
[52] S. Segawa, M. Shibamoto, M. Ogawa, S. Miyake, K. Mizumoto, A. Ohishi, et al., The effect of divalent metal cations on zinc uptake by mouse Zrt/Irt-like protein 1 (ZIP1), Life Sci. 113 (2014) 40–44.
[53] C. Zhang, Y. Zheng, L. Chen, M. Chen, S. Liang, M. Lin, et al., Regulation of basal lateral membrane mobility and permeability to divalent cations by membrane associated-protein kinase C, PLoS One 8 (2013) e80291.

[54] C.K. Wang, A. Simon, C.M. Jessen, C.L. Oliveira, L. Mack, K.H. Braunewell, et al., Divalent cations and redox conditions regulate the molecular structure and function of visinin-like protein-1, PLoS One 6 (2011) e26793.
[55] C. Baran, G.S. Smith, V.V. Bamm, G. Harauz, J.S. Lee, Divalent cations induce a compaction of intrinsically disordered myelin basic protein, Biochem. Biophys. Res. Commun. 391 (2010) 224–229.
[56] L.E. Valenti, C.P. De Pauli, C.E. Giacomelli, The binding of Ni(II) ions to hexahistidine as a model system of the interaction between nickel and His-tagged proteins, J. Inorg. Biochem. 100 (2006) 192–200.
[57] N. Serna, L. Sanchez-Garcia, U. Unzueta, R. Diaz, E. Vazquez, R. Mangues, et al., Protein-based therapeutic killing for cancer therapies, Trends Biotechnol. 36 (2018) 318–335.
[58] P. Faller, C. Hureau, O. Berthoumieu, Role of metal ions in the self-assembly of the Alzheimer's amyloid-beta peptide, Inorg. Chem. 52 (2013) 12193–12206.
[59] F. Hane, Z. Leonenko, Effect of metals on kinetic pathways of amyloid-beta aggregation, Biomolecules 4 (2014) 101–116.

Study 2

Biofabrication of functional protein nanoparticles through simple His-tag engineering

Hèctor López-Laguna*, Julieta M. Sánchez*, José Vicente Carratalá, Mauricio Rojas-Peña, Laura Sánchez-García, Eloi Parladé, Alejandro Sánchez-Chardi, Eric Voltà-Durán, Naroa Serna, Olivia Cano-Garrido, Sandra Flores, Neus Ferrer-Miralles, Verónica Nolan, Ario de Marco, Nerea Roher, Ugutz Unzueta, Esther Vázquez, and Antonio Villaverde

ACS Sustainable Chemistry & Engineering 2021 · Impact factor (9.224) · Quartile (Q1) · *Equally contributed

Objective 1.a

To develop a new and fully transversal biochemical approach to manufacture **protein-based nanoparticles** using multidomain proteins to construct nanoparticles.

Objective 3.a

To test the biomedical applications of **divalent cation-based protein nanoparticles** in Zebrafish models (Biodistribution).

From the previous findings (study 1), it seems that the histidine tag-divalent cation principle allows to formulate, in a controlled-size manner, stable protein-based nanoparticles. But these findings have been only supported by a short set of protein candidates. That is why, the same biochemical method must be explored in diverse and unrelated polypeptides to fully understand the transversality of the approach, the robustness, and the scalability of the system.

Thus, this work has been focused on using Zn^{2+} (as a gold standard divalent cation, from 0.2 to 0.5 mM) to trigger histidine tagged building blocks' (of different natures) spontaneous self-assembling. Products' physicochemical stability and function were also addressed. The obtained data resulted in all protein candidates oligomerized into regular protein-based nanoparticles ranging from 10 to 15 nm, being functional (tested in Zebrafish models), architectonically stable and serving as intermediates for a more complex assembling system namely protein-based insoluble microparticles (furtherly presented in study 4).

ACS Sustainable Chemistry & Engineering

pubs.acs.org/journal/ascecg

Research Article

Biofabrication of functional protein nanoparticles through simple His-tag engineering

Hèctor López-Laguna,△ Julieta M. Sánchez,△ José Vicente Carratalá, Mauricio Rojas-Peña, Laura Sánchez-García, Eloi Parladé, Alejandro Sánchez-Chardi, Eric Voltà-Durán, Naroa Serna, Olivia Cano-Garrido, Sandra Flores, Neus Ferrer-Miralles, Verónica Nolan, Ario de Marco, Nerea Roher, Ugutz Unzueta,* Esther Vazquez,* and Antonio Villaverde*

Cite This: *ACS Sustainable Chem. Eng.* 2021, 9, 12341−12354

Read Online

ACCESS | Metrics & More | Article Recommendations

ABSTRACT: We have developed a simple, robust, and fully transversal approach for the *a-la-carte* fabrication of functional multimeric nanoparticles with potential biomedical applications, validated here by a set of diverse and unrelated polypeptides. The proposed concept is based on the controlled coordination between Zn^{2+} ions and His residues in His-tagged proteins. This approach results in a spontaneous and reproducible protein assembly as nanoscale oligomers that keep the original functionalities of the protein building blocks. The assembly of these materials is not linked to particular polypeptide features, and it is based on an environmentally friendly and sustainable approach. The resulting nanoparticles, with dimensions ranging between 10 and 15 nm, are regular in size, are architecturally stable, are fully functional, and serve as intermediates in a more complex assembly process, resulting in the formation of microscale protein materials. Since most of the recombinant proteins produced by biochemical and biotechnological industries and intended for biomedical research are His-tagged, the green biofabrication procedure proposed here can be straightforwardly applied to a huge spectrum of protein species for their conversion into their respective nanostructured formats.

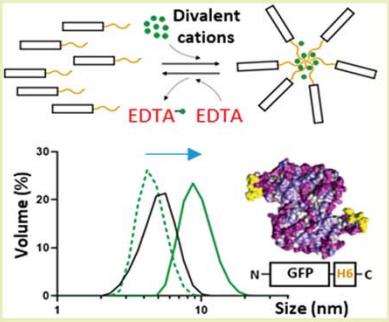

KEYWORDS: *Nanoparticles, Protein engineering, Divalent cations, Protein materials, Biomaterials design*

INTRODUCTION

Protein materials result from the controlled self-assembly of individual polypeptides under defined architectural patterns.[1,2] In contrast to other chemical categories of building blocks, proteins generate supramolecular materials that benefit from the structural and functional capabilities and the particular versatility shown by these biomolecules. Especially, their intrinsic biocompatibility and biodegradability offer a wide applicability in clinics[3−5] over alternative, potentially toxic materials such as metals, polymers, ceramics, and lipids. The interdependence between structure and function makes protein-based materials particularly appealing, since these properties can be tuned by rational genetic engineering. The formation of supramolecular protein materials out of self-assembled building blocks is common in nature. For instance, recombinant silk proteins,[6,7] viral protomers,[8] or amyloid peptides[9−11] self-organize into complex oligomeric structures because of the natural tendency of the building blocks to specifically cross-interact into defined geometries, within nano- or microscales. More complicated is conferring, on purpose, self-assembling abilities to clinically relevant polypeptides, which being intrinsically monomeric might be appealing as functional, more complex multimeric materials. In particular, innovative medicines demand biologically safe nanoscale materials that, being biologically active, might assist in a diversity of clinical fields. Cross-molecular interactions can be conferred by self-assembling protein domains recruited from nature; when they are fused to a protein of interest, they drive the organization of the whole fusion into regular oligomers.[12,13] Of course, diverse categories of chemical cross-linkers have also been explored for the construction of protein materials.[14−16] However, the design of materials usable in biological interfaces should be ideally achieved through self-assembly, with a minimal extent of protein engineering and without the addition of chemical couplers that are potentially toxic. This would minimize perturbations of the original protein conformation, preserve the full functionality, and avoid

Received: June 23, 2021
Revised: August 16, 2021
Published: August 30, 2021

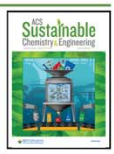

ACS Publications © 2021 American Chemical Society

https://doi.org/10.1021/acssuschemeng.1c04256
ACS Sustainable Chem. Eng. 2021, 9, 12341−12354

ACS Sustainable Chemistry & Engineering pubs.acs.org/journal/ascecg Research Article

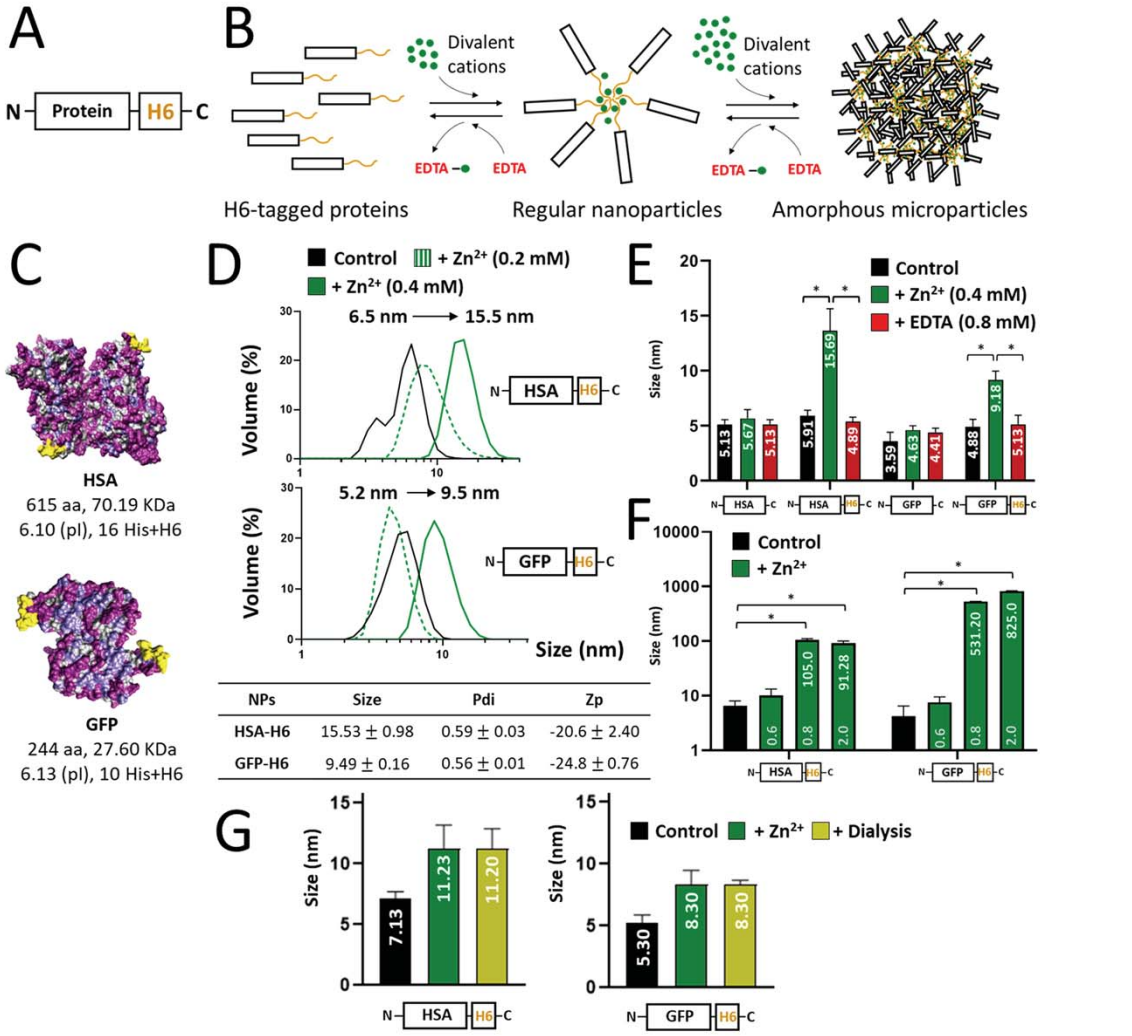

Figure 1. Proposed concept of progressive protein oligomerization supported by divalent cations and self-assembly potential of H6-tagged HSA and GFP. (A) Schematic representation of polyhistidine-tagged proteins. A histidine-rich peptide, usually the hexahistidine H6, is fused to the carboxy terminus of any recombinant protein to allow its one-step purification by affinity chromatography. Other humanized His-rich peptides are also available as efficient purification tags.[56] (B) Progressive assembly of H6-tagged proteins mediated by increasing amounts of divalent cations such as Zn^{2+}. The formation of MPs has been experimentally demonstrated,[18,19] but regular nanoparticles are expected as intermediates in the process. In each step, disassembly can be achieved by using the chemical chelator EDTA. Spontaneous disassembly of MPs has been observed under physiological conditions,[19,82] supporting the concept that such materials are mimetics of the secretory granules for peptide hormones in the mammalian endocrine system. (C) Dimeric structures (the most plausible building block forms) of HSA and GFP showing the exposed His tags in yellow. Bulk atoms are depicted in gray and cationic and hydrophilic groups in pale and deep purple, respectively. A short summary of the main biochemical properties of each construct is also displayed. (D) Hydrodynamic size (nm) of HSA-H6 and GFP-H6 in the absence and presence of Zn^{2+} at increasing concentrations, determined by DLS. The peak (Size), polydispersion index (Pdi) and Z potential (Zp, expressed in mV), in the presence of 0.4 mM Zn^{2+} are also indicated at the bottom. (E) Role of the H6 tag in protein assembly and EDTA-mediated disassembly. The hydrodynamic sizes in nm are indicated inside the histograms as white numbers. (F) Aggregation of HSA-H6 and GFP-H6 at increasing Zn^{2+} concentrations (0.6, 0.8, and 2 mM). White numbers indicate the hydrodynamic size in nm. Data are expressed as $\bar{x} \pm$ SEM with at least $n = 3$, and statistical significance is achieved when $*p < 0.05$. (G) Hydrodynamic size (nm) of Zn^{2+}-based HSA-H6 and GFP-H6 NPs extensively dialyzed against a Zn^{2+}-free buffer, determined by DLS.

the use of hazardous and recalcitrant chemicals or the application of poorly green processes.

In this context, histidine (His)-rich peptides have been recently revealed as potent and intrinsic protein cross-linkers.[17] Their coordination with divalent cations such as Zn^{2+} induces protein−protein interactions and clustering as protein-only microparticles.[18,19] The materials, essentially amorphous and having the size of a few micrometers, mimic the amyloidal architecture of bacterial inclusion bodies[20] and that of secretory granules from the mammalian endocrine system.[5,21−23] On this basis, we wondered if the controlled use of divalent cations at doses below those triggering microscale protein aggregation would represent a reliable approach to fabricate regular nanoparticles based on polyhistidine-tagged building block proteins (Figure 1A). We speculated that protein nanoparticles (NPs) might be a category of

https://doi.org/10.1021/acssuschemeng.1c04256
ACS Sustainable Chem. Eng. 2021, 9, 12341−12354

intermediates in the aggregation process that leads to the formation of amorphous microparticles (MPs, Figure 1B) and that their formation and stability might be controlled by adjusting the concentration of divalent cations in the coordination event. It must be noted that in biotechnology, recombinant proteins are commonly produced as His-tagged fusion constructs, since the short end-terminal polyhistidine stretches (such as the hexahistidine H6) do not abolish protein functionalities but permit their one-step purification by affinity chromatography from cell extracts.[24] Therefore, divalent cations, used as a molecular glue for His-tagged proteins, would straightforwardly allow the *a-la-carte* fabrication of protein nanoparticles out of most of the recombinant proteins currently available in research and pharma laboratories. This could be done without further engineering and by means of a transversal assembly platform that runs in the absence of xenobiotic cross-linkers.

MATERIALS AND METHODS

Design, Production, and Purification of Protein Constructs. β-Galactosidase (β-Gal), green fluorescent protein (GFP), and human serum albumin (HSA) were provided by Sigma-Aldrich (No, 5635), Roche (No. 11814524001), and Grifols (hemoderivative), respectively. For the other proteins, codon-optimized genes were produced by Geneart (ThermoFisher) and cloned in a pET22b vector (Novagen). Plasmids encoding GFP-H6, STM-H6, H6-GFP-T22, and BAK-GFP-H6 were transformed into *E. coli* Origami B cells (BL21, *ompT*, *lon*, TrxB, Gor$^-$; Novagen) and TRX-H6-hLIF into *E. coli* BL21 (DE3; Novagen) cells. A1-, B4-, and F7-GFP-H6 plasmids were transformed into *E. coli* BL21sox cells[2] by thermal shock at 42 °C for 45 s. Bacterial cells were grown in lysogenic broth (LB) medium, and proteins were produced overnight at 20 °C (GFP-H6, TRX-H6-hLIF, STM-H6, A1-, B4-, and F7-GFP-H6) or 37 °C for 3 h (H6-GFP-T22 and BAK-GFP-H6) upon addition of 0.1 mM isopropyl-β-D-thiogalactopyronaside (IPTG) or 1 mM IPTG (for A1-GFP-H6 production). Cells were subsequently harvested at 5000*g* for 15 min, resuspended in wash buffer (20 mM Tris-HCl, 500 mM NaCl, 10 mM imidazole, pH 8) in the presence of protease inhibitors (cOmplete EDTA-free, Roche Diagnostics), and disrupted by two rounds of 1200 psi in a French Press (Thermo FA-078A). The soluble cell fraction was recovered by centrifugation at 15000*g* for 45 min. On the other hand, a codon-optimized HSA-H6 gene was also synthesized by GeneArt (ThermoFisher Scientific), supplied into a pTriex6 plasmid, and transfected into HEK-293F mammalian cells in the presence of PEI (polyethylenimine, in the ratio 3:1), when the cell concentration reached 10^6 cells mL^{-1}. Cells were then cultured in Freestyle 293 medium and the recombinant protein was produced and excreted to the media due to a secretion peptide, in the presence of valproic acid (4 mM), for 6 days (37 °C, 70% humidity, 8% CO_2 and 120 rpm). The culture medium containing the secreted soluble protein was finally separated from the cells by centrifugation at 300*g* for 15 min.

Finally, all of the proteins were purified by immobilized metal affinity chromatography (IMAC) using HisTrap HP 1−5 mL columns (GE Healthcare) in an ÄKTA pure protein purification System (GE Healthcare) upon elution by a linear gradient of elution buffer (20 mM Tris-HCl, 500 mM NaCl, 500 mM imidazole, pH 8). The production and purification of β-Gal-H6 have been described elsewhere.[25] Recovered proteins were dialyzed against their most suitable buffer: sodium carbonate (166 mM $NaHCO_3$, pH 8) for STM-H6, GFP-H6, and HSA-H6, sodium carbonate with salt (166 mM $NaHCO_3$, 333 mM NaCl, pH 8) for A1-GFP-H6, B4-GFP-H6, F7-GFP-H6, BAK-GFP-H6, and H6-GFP-T22, Tris buffer (1 M NaCl, 50 mM Tris-HCl, pH 7.25) for TRX-H6-hLIF, and PBS (7.5 mM Na_2HPO_4, 2.5 mM NaH_2PO_4, 15 mM NaCl, pH 7.4) for β-Gal-H6. GFP, β-Gal, and HSA were commercially obtained as previously mentioned and subsequently dialyzed against compatible buffers: namely, sodium carbonate (166 mM $NaHCO_3$, 2.8 mM EDTA, pH 8), PBS (7.5 mM Na_2HPO_4, 2.5 mM NaH_2PO_4, 15 mM NaCl, pH 7.4), and sodium carbonate (166 mM $NaHCO_3$, pH 8), respectively.

Description of Protein Modules. T22 is a cationic peptide that acts as a potent ligand of the cell surface cytokine receptor CXCR4.[26] BH3 is a BAK protein domain (named here as BAK) that inhibits antiapoptotic cell proteins.[27] The human leukemia inhibitory factor (hLIF) is a well-known interleukin 6 class protein that modulates cell differentiation.[28] Thioredoxin (TRX) is an antioxidant agent that enhances protein solubility when it is used as a tag.[29] Stefin A triple mutant (named here as STM) is a human protein usable as an inert protein scaffold.[30] All of these protein domains were designed to be expressed from codon-optimized genes provided by GeneArt. A1, B4, and F7 ligands, architecturally arranged as nanobodies (VHHs), were obtained from a homemade phage display library based on naïve llama-derived nanobodies. The biopanning process was performed by confronting the library against the CXCR4 receptor overexpressed on SW1417 cells, as described elsewhere.[31,32] The most specific candidates were selected, and the recombinant proteins were produced as GFP fusions (VHH-GFP-H6).

Protein Concentration, Purity, and Integrity. The protein purity was assessed upon purification by SDS-PAGE using the TGX Stain-Free FastCast Acrylamide Kit, at 12% (BioRad). Bands were transferred to PVDF membranes by a Trans-Blot Turbo Transfer System (BioRad) and finally immunodetected by Western blot (WB) using an anti-His antibody (Ab; Santa Cruz Biotechnology) at a 1/5000 dilution. The protein integrity was determined by matrix-assisted laser desorption ionization time-of-flight (MALDI-TOF) mass spectrometry and the protein concentration by a Bradford assay.

Protein Assembly and Disassembly. Soluble proteins at 2 mg mL^{-1} (with the exception of GFP and β-Gal, adjusted at 0.5 mg mL^{-1}) in the respective optimal buffers were distributed in 50 μL aliquots. Assembly was achieved by adding a 0.22 μm filtered solution of $ZnCl_2$ (stock at 400 mM and working concentrations indicated in the figures), and the mixture was gently mixed and incubated for 5 min at room temperature (RT). Disassembly was promoted by adding a solution of ethylenediaminetetraacetic acid (EDTA) at concentrations indicated in the figures, and the mixture was gently mixed and incubated for 5 min at RT. The hydrodynamic diameter of the materials was determined by dynamic light scattering (DLS) at 25 °C and 633 nm wavelength, with a Zetasizer Nano ZS instrument (Malvern Instruments Limited) using ZEN2112 3 mm quartz batch cuvettes.

Protein Precipitation. The soluble protein was adjusted to 2 mg mL^{-1} and distributed in 250 μL aliquots (to obtain 0.5 mg of product from each aliquot, provided the precipitation would be 100% efficient). The aggregation process was promoted by adding a 0.22 μm filtered solution of $ZnCl_2$ (stock at 400 mM) at concentrations depicted in the figures, and the mixture was gently mixed and incubated for 15 min at RT. Then, samples were centrifuged at 10000*g* for 10 min at RT, and the soluble fraction was collected for further quantification by a Bradford assay. The resultant isolated and precipitated microparticles were stored at −80 °C until further use and visualized, and the protein was indirectly quantified using soluble fraction measurements. Microparticles were also analyzed by DLS at 25 °C, with short measurement time periods and using 633 nm wavelength, with a Zetasizer NanoZS instrument (Malvern Instruments Limited) using ZEN2112 3 mm quartz batch cuvettes.

Stability of Released Soluble Protein. The release of soluble protein from microparticles was promoted by the addition of 250 μL of storage buffer and subsequent resuspension at RT. Then, samples were centrifuged at 15000*g* for 5 min at RT for isolation of the soluble version. The protein size and stability were assessed at different temperatures and under thermal conditions (37 °C overnight, overnight at RT, and 4× thawing and freezing) by DLS at 25 °C and 633 nm wavelength, with a Zetasizer NanoZS instrument (Malvern Instruments Limited) using ZEN2112 3 mm quartz batch cuvettes. Protein integrity was also assessed by TGX Stain-Free electrophoretic gel (BioRad).

Determination of Z Potential. The Z potentials (Zp) of protein materials were determined by electrophoretic light scattering (ELS) at

https://doi.org/10.1021/acssuschemeng.1c04256
ACS Sustainable Chem. Eng. 2021, 9, 12341−12354

633 nm (25 °C), with a Zetasizer Nano ZS instrument using DTS10170 capillary cells and in the respective solubilization buffers.

Protein Stability. Fluorescence spectra of oligomeric and building block protein forms were recorded with a Cary Eclipse spectrofluorometer (Agilent Technologies) by using a quartz cell with 10 mm path length and a thermostatic holder. The excitation and emission slits were set at 5 nm, the excitation wavelength was set at 295 nm, and the emission spectra were acquired within ranges of 310−450 nm (for HSA-H6) and 480−550 nm (for GFP-H6). The protein concentration was adjusted to 0.2 mg mL^{-1}. We evaluated the thermal behavior of proteins within the range 25−50 °C in p/a of $ZnCl_2$ (0.4 mM). The fluorescence intensity at λ_{max} was plotted against temperature. Additional stability determinations of oligomers and building blocks were carried out by DLS as described above, within ranges of 4−50 and 4−90 °C depending on the experimental needs.

Also, the integrity of the NPs in media without Zn was evaluated in triplicate through their size upon dialysis. GFP-H6 and HSA-H6 NPs (0.15 mL), assembled as described above, were placed in dialysis cassettes (Slide A lyzer 3.5K MWCO Dialysis cassette, Thermo Fisher Scientific) and submerged in 1 L of sodium carbonate buffer (166×10^{-3} M $NaHCO_3$, pH 8.0) without $ZnCl_2$, with agitation, at 4 °C for 30 min. Then two buffer exchanges were applied, each at RT, over 30 min and against 1 L of the same buffer. Finally, the samples were removed from the cassettes and analyzed at 25 °C with a Zetasizer Advanced Pro Blue instrument (Malvern Instruments Limited) at 633 nm, using ZEN2112 3 mm quartz batch cuvettes.

Determination of Protein Activity. A 20 μL portion of a β-galactosidase−$ZnCl_2$ mixture (diluted 100-fold with respect to DLS measurements) was mixed with 5 mM *o*-nitrophenyl galactopyranoside in a 500 μL final volume of PBS. The sample was incubated for 15 min at 37 °C, the reaction was stopped by adding 200 μL of Na_2CO_3 (2.8 mM), and the product amount was determined by absorbance at 420 nm (ε_{420} = 4530 M^{-1} cm^{-1}) in a UV−vis spectrophotometer (Ultrospec 1000E, Pharmacia Biotech). The activity was expressed as the percentage with respect to the control without $ZnCl_2$.

Electron Microscopy. Ultrastructural morphometry of proteins at the nearly native state was assessed with two high-resolution techniques. Sample drops (5 μL) were deposited on silicon wafers (Ted Pella Inc.) for 2 min, air-dried, and immediately observed without coating with a Merlin field emission scanning electron microscope (FESEM) (Zeiss), operating at 1 kV and equipped with a high-resolution in-lens secondary electron detector. Representative images of general fields and nanostructure details were captured at two high magnifications (150000× and 400000×). Drops (5 μL) of the same samples were deposited for 2 min on 200 mesh copper grids coated with carbon, contrasted with 2% uranyl acetate for 2 min, air-dried, and observed with an H-7000 transmission electron microscope (TEM) (Hitachi) equipped with a CCD Gatan ES500W Erlangshen camera (Gatan). Representative images of general fields and nanostructure details were captured at two high magnifications (70000× and 200000×).

Zebrafish Husbandry and Breeding. Wild type zebrafish (*D. rerio*) were kept in a recirculating aquarium with the water temperature maintained at 28 ± 1 °C. The lighting conditions were 12 h:12 h (light:dark), and adult fish were fed twice a day at a rate of 2% body weight. Ammonia, nitrite, pH, and nitrate levels were measured once a week. Ammonia and nitrite levels were kept below the detection level, and the pH was maintained between 6.8 and 7.5. The nitrate levels were maintained to be <100 mg L^{-1}. For in-tank breeding, previously isolated individuals, one female and three males, were transferred to a breeding tank in the late afternoon. Embryos were collected the next morning and cultured in embryo medium (E3 medium) in a Petri dish (Deltalab). Fertilized eggs were separated from unfertilized eggs using a plastic pipet (Deltalab). All experiments involving zebrafish (*D. rerio*) were performed following International Guiding Principles for Research Involving Animals (EU 2010/63).

Protein Uptake by Zebrafish Larvae Assessed by Fluorescent Microscopy. Groups of 15 larvae (n = 5/condition, 72 hpf) were distributed on 96-well plates (Thermo Fisher Scientific) with one larva per well. Wells contained 200 μL of E3 medium or 50 μgmL^{-1} of unassembled or assembled GFP-H6. *In vivo* uptake after 48 h treatment was observed in anesthetized larvae (50 ppm, MS-222) using a fluorescence stereomicroscope (Nikon SMZ800) coupled with a camera (Nikon DS-Fi2). No signs of toxicity were observed during exposure.

Statistical Analyses and 3D-Model Visualization. The size increase factor (SIF) was calculated as the percentage of gained size upon oligomerization and statistically analyzed versus the presence or absence of the His tag or a peptidic ligand, the type of scaffold (GFP-based or others), or the number of histidine residues in the primary structure (more or less than 14). For all collations, an initial variety of normality and log normality tests (Anderson−Darling, D'Agostino & Pearson, Shapiro−Wilk and Kolmogorov−Smirnov) were used to stablish data normal distribution. Both t tests (single comparisons) and one-/two-way ANOVA (multiple comparisons) were used to determine the significance for parametric data, and the Mann−Whitney test was used for nonparametric data. Statistics in all data sets were performed at least in triplicate (n = 3), expressed as mean ± standard error of the mean ($\bar{x} \pm$ SEM) and significance ($^*p \leq 0.05$ or $^*p < 0.001$, respectively) in comparison to the control group. HSA and GFP models were generated using the Robetta web server[33] and visualized in UCSF Chimera.[34]

RESULTS AND DISCUSSION

Exploiting the universal H6 tag as an architectonic agent (Figure 1A) would allow the implementation of a fully transversal platform for the *on-demand* fabrication of protein nanoparticles. This would be feasible, provided divalent aggregation mediated by cations could generate regular oligomers as stable and functional intermediates in the clustering process that finally renders amorphous microparticles (Figure 1B). This possibility was initially assessed by testing two structurally dissimilar proteins commonly used in research laboratories: namely, HSA and GFP (Figure 1C). The H6-tagged forms of these proteins (HSA-H6 and GFP-H6, respectively) showed hydrodynamic sizes between 5 and 6 nm, compatible with their unassembled forms (Figure 1D). However, when these proteins were incubated with equimolar amounts of Zn^{2+} (0.4 mM), relatively monodisperse oligomers were observed of around 15 and 10 nm, respectively (Figure 1D), with a similar and slightly negative Z potential (Figure 1D, bottom). The resulting assemblies that were not built up by the wild-type protein versions lacking H6 (Figure 1E) were disassembled by the chelating agent EDTA (Figure 1E), demonstrating the relevance of the metal in the assembly process. The occurrence of several His residues in the native sequence of the proteins (Figure 1C) was not sufficient to support cation-dependent assembly, suggesting that a local His clustering was required to promote stable protein−protein contacts. Zn^{2+} concentrations above 0.4 mM resulted in a clear tendency to form large aggregates instead of regular oligomers, approaching the micrometer scale (Figure 1F). This observation supported the hypothesis that protein oligomers organized into regular NPs are intermediates in a process finally leading to the formation of amorphous MPs (Figure 1B). While protein assembly as nanoparticles would indeed be triggered by equimolar amounts of the ion (calculated with regard to the six histidine residues in the H6 tails), multivalent contacts with excess ions would induce protein aggregation as microscale complexes (Figure 1A,B). Such aggregation at higher concentrations of Zn^{2+} indicates that the amounts of ions used for NP formation were not saturating all of the available histidine residues in the proteins.

https://doi.org/10.1021/acssuschemeng.1c04256
ACS Sustainable Chem. Eng. 2021, 9, 12341−12354

ACS Sustainable Chemistry & Engineering pubs.acs.org/journal/ascecg Research Article

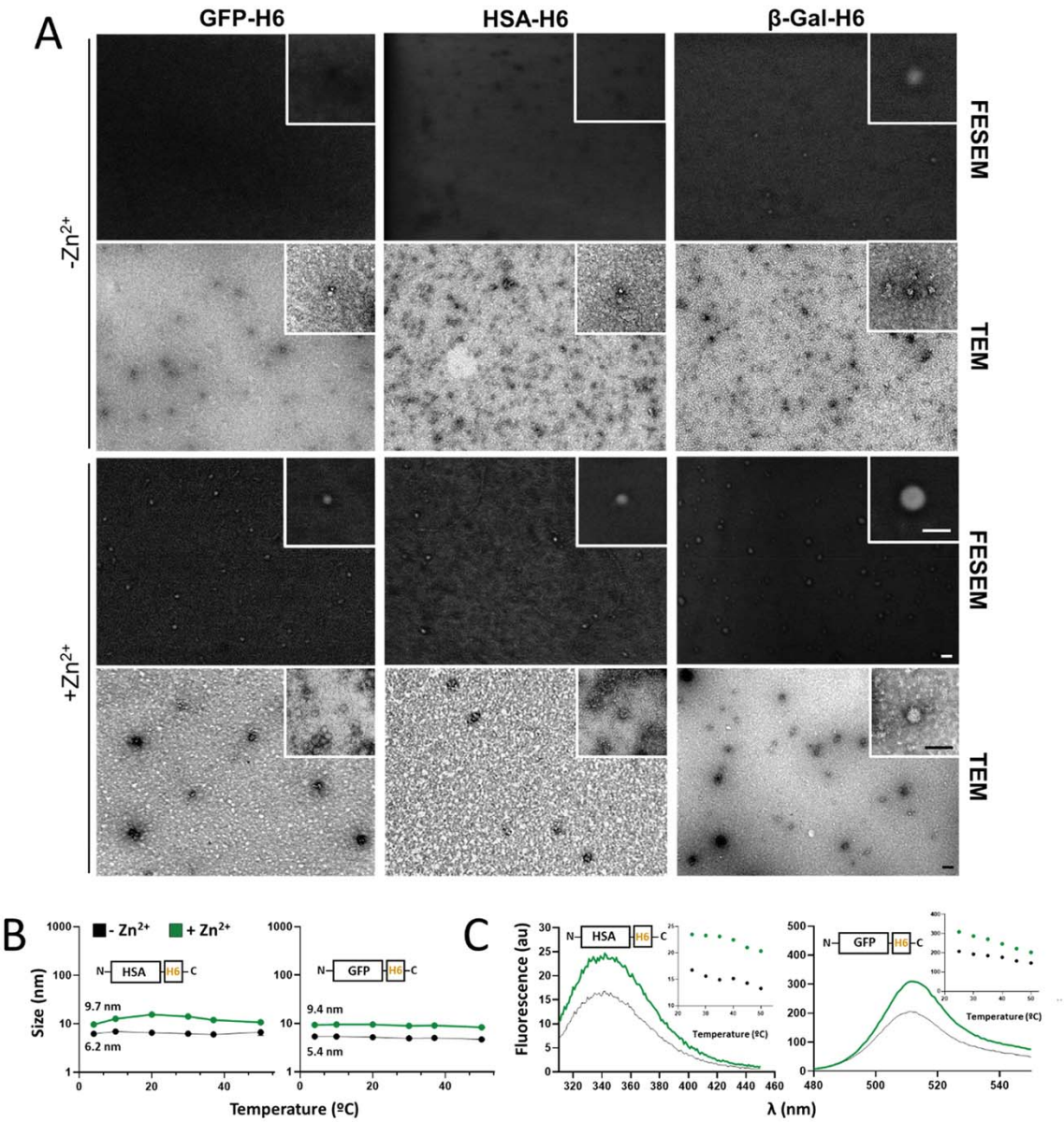

Figure 2. Structural analysis of Zn^{2+}-mediated oligomers. (A) Representative high-resolution electron microscope images (TEM and FESEM) of single monomers without Zn (−Zn^{2+}) and well-formed nanoparticles (+Zn^{2+}). Scale bar size: 25 nm. (B) Stability of the materials upon an increase in temperature (from 4 to 50 °C) in the presence (assembled, green) or absence (unassembled, black) of Zn^{2+} (at 0.4 mM). (C) Fluorescence emission spectra in the presence (assembled, green) or absence (unassembled, black) of Zn^{2+} at 25 °C and a thermal profile of the fluorescence peak (au) from 25 to 50 °C (inset).

Interestingly, the Zn-based NPs were stable, once formed, in Zn^{2+}-free media, as demonstrated by DLS for both HSA-H6 and GFP-H6 (Figure 1G). This observation indicated that the cation used for assembly formed robust interactions with His-tagged proteins and that such interactions were not resulting from an equilibrium with free cations in the media. This fact was particularly interesting, envisaging the potential *in vivo* applications of this category of material or, in general, uses in environments whose ionic composition cannot be controlled.

TEM and FESEM analyses allowed visualizing the formed oligomers as discrete NP entities with pseudospherical geometries, with sizes compatible with those observed by DLS (Figure 2A). When they were tested for stability, the assembled materials maintained the thermal resistance of the building blocks (Figure 2B). The fine analysis of protein fluorescence revealed differences in the emission profiles of building blocks and NPs (Figure 2C), which indicated structural rearrangements during oligomerization as previously observed in other assembly setups.[35] Such a structural profile was indicative of conformational adaptation to the partner subunits in the oligomer, and it was maintained over a wide temperature range (Figure 2C, insets). This fact indicated again that, once assembled, the protein NPs were structurally stable.

https://doi.org/10.1021/acssuschemeng.1c04256
ACS Sustainable Chem. Eng. 2021, 9, 12341−12354

At this point, and to confirm the transversal nature of the Zn^{2+}-mediated oligomerization and the robustness of this approach, additional H6-tagged proteins used in the laboratory, including natural and largely engineered modular species of different origins, were tested (Figure 3). These

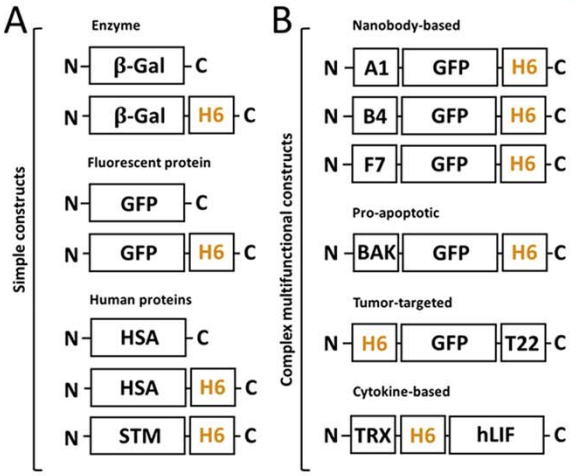

Figure 3. Comparative modular organization of the proteins tested in the study. (A) Representation of moderately engineered constructs with or without an H6 tag, categorized depending on their nature (enzyme, fluorescent, or human-based). (B) Representation of complex modular constructs developed as targeted protein drugs, categorized depending on the nature of the main functional domain (nanobody, proapoptotic, tumor-targeted, or cytokine-based). Relative box sizes are only indicative.

proteins exhibit different functionalities, and consequently, they are suitable for different applications *in vitro* and *in vivo*. For this last use, it is important to obtain nanostructured drugs with dimensions above the renal clearance threshold (around 6–7 nm),[36] which cannot be reached by the wild-type monomeric or dimeric proteins. Protein NPs offer further advantages over their plain protein versions, including enhanced proteolytic stability,[37] improved targeting,[38] and full exploitation of the enhanced permeability and retention (EPR) effect,[39] apart from the whole set of appealing physical properties associated with nanoscale materials (namely, their particular behavior between liquids and solids and their elasticity and other mechanical features[40]). As observed, all tested His-tagged proteins, but not their counterparts devoid of H6 (when available for testing), increased in hydrodynamic size in the presence of equimolar (0.2–0.5 mM) Zn^{2+} concentrations (Figure 4A,B). The assembled materials usually reached around 10 nm in size, had relatively low polydispersion indexes, and were efficiently disassembled by EDTA (Figure 4A). Interestingly, assembly occurred irrespective of the localization of H6, at the N terminus (H6-GFP-T22), at the C terminus (most of the modular proteins) or in an internal accommodation site as a linker between functional domains (TRX-H6-hLIF). Also, a structurally complex and large tetrameric enzyme, the *E. coli* β-galactosidase,[41] showed the same oligomerization profile upon exposure to the metal. The tagged version of the enzyme formed self-organized supramolecular complexes of around 40 nm in size (Figure 4C). This occurred in the absence of significant modifications in the enzymatic activity mediated by the ion, irrespective of the presence or absence of the H6 tag (Figure 4C, inset). Despite the fact that the wild-type β-galactosidase contains multiple His residues in its primary sequence,[41] these were not effective for promoting oligomerization at the tested Zn^{2+} concentrations. On the other hand, ion-mediated formation of NPs did not abort green fluorescence emission in any of the GFP-containing proteins tested here (Figure 4D), indicating the maintenance of the essential conformational patterns of the building block proteins and therefore their global functionality. Again, all of these materials were proved to be stable (Figure 5). In fact, in the case of STM and A1-based constructs, oligomerization conferred clear protection in front of thermal aggregation in comparison to the respective unassembled building blocks (Figure 5).

To explore the versatility and the *in vivo* applicability of the type of NPs generated in the present study, we first tested if divalent cations different from Zn^{2+} could also drive NP formation. As was observed (Figure 6A), Ni^{2+}, but not Ca^{2+}, Cu^{2+}, and Mg^{2+}, at the tested concentration (0.4 mM) was also able to promote oligomerization of GFP-H6. Nevertheless, Zn^{2+} was clearly the most efficient linker in the process, rendering larger materials. Interestingly, if the H6-dependent formation of NPs is an intermediate step in the formation of MPs (Figure 6B), it would be interesting to know if MPs could act as a reservoir of NPs for potential clinical applications. This potential applicability of protein MPs as protein drug depots for clinical uses has been demonstrated for a category of natural amyloids called bacterial inclusion bodies[42] and for artificial versions of such natural materials,[43] generated by clustering, either *in vivo* or *in vitro*, respectively, of receptor-targeted protein drugs. The application of 8 mM Zn^{2+} to soluble GFP-H6 resulted in polydisperse MPs peaking at around 0.5 μm but reaching sizes of over 1 μm (Figure 6C). These materials, insoluble and fully fluorescent (Figure 6C, inset), spontaneously released NPs ranging between 9 and 10 nm under different incubation conditions (Figure 6D), indistinguishable in size from those generated by the straightforward addition of 0.4 mM Zn^{2+} to soluble GFP-H6 (Figure 1D–F). The release of such NPs, which show great thermal stability (Figure 6E), confirmed that these materials are intermediates in the process of MP formation (Figure 6B), which is fully reversible under physiological conditions.

Finally, a full test of the clinical uses of the type of protein NPs generated here is beyond the scope of the present study. However, we wanted to check the stability of the NPs *in vivo* and the maintenance of their nanoscale structure in biological interfaces, using GFP-H6 NPs as a convenient model. For that, zebrafish larvae (5 dpf) were imaged after 48 h of *in vivo* exposure to GFP-H6, either in a soluble form or as assembled NPs (both at 50 μg/mL) to evaluate their uptake. We were particularly interested in checking the stability of the NP version and also in evaluating whether the nanoscale size could confer nanomaterial properties to the soluble protein and thus limit the broad diffusion in biological tissues expected for a plain unassembled polypeptide. Both biomaterials were taken up orally by the larvae (Figure 6F). While NPs accumulated uniquely in the intestine, indicative of an enhanced tissue retention expected for a nanostructured material,[44] the soluble version dispersed through the intestine and pancreas with background in other tissues (Figure 6F). Also, the NP version rendered a more intense fluorescence signal (Figure 6F), altogether indicative of the high stability of NPs and the

https://doi.org/10.1021/acssuschemeng.1c04256
ACS Sustainable Chem. Eng. 2021, 9, 12341−12354

ACS Sustainable Chemistry & Engineering pubs.acs.org/journal/ascecg Research Article

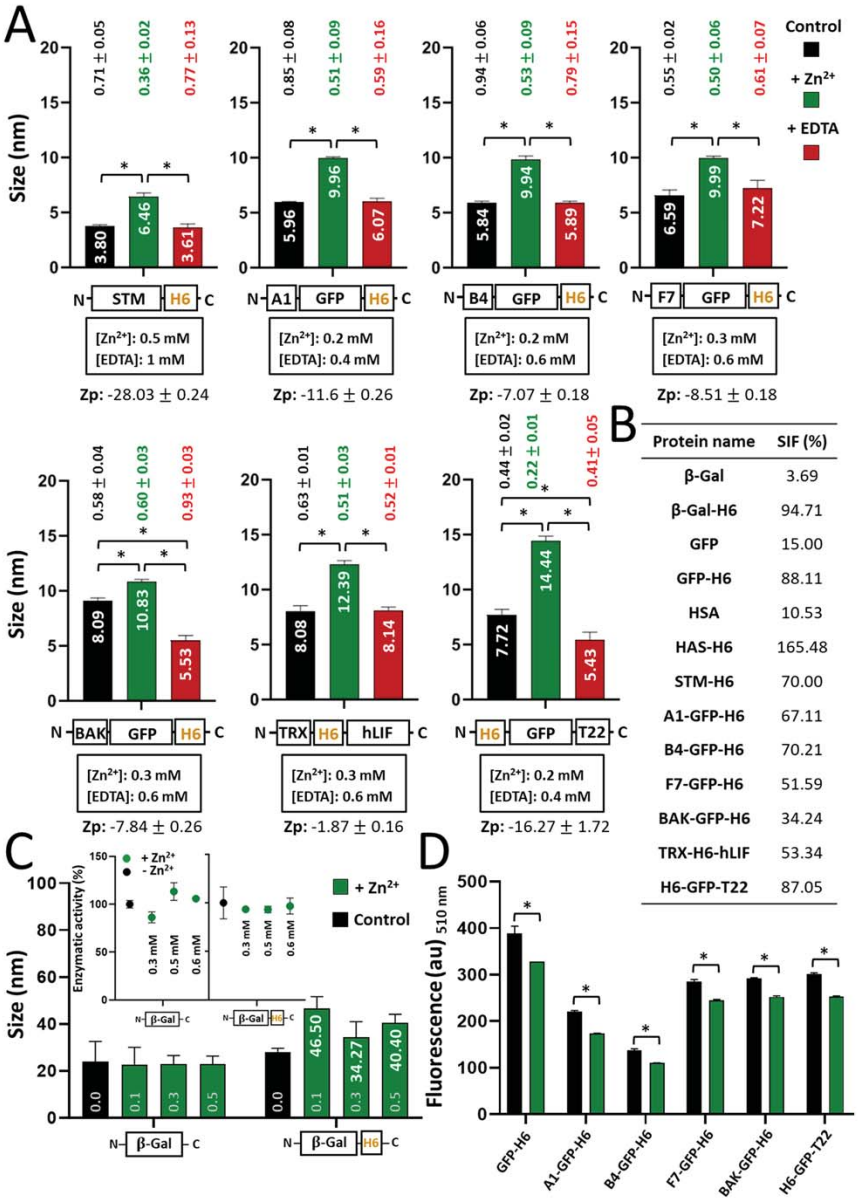

Protein name	SIF (%)
β-Gal	3.69
β-Gal-H6	94.71
GFP	15.00
GFP-H6	88.11
HSA	10.53
HAS-H6	165.48
STM-H6	70.00
A1-GFP-H6	67.11
B4-GFP-H6	70.21
F7-GFP-H6	51.59
BAK-GFP-H6	34.24
TRX-H6-hLIF	53.34
H6-GFP-T22	87.05

Figure 4. Oligomerization and biological activity of protein materials. (A) Hydrodynamic size of assembled (in the presence of Zn^{2+}, green bars) and further disassembled (with the addition of EDTA, red bars) proteins. The concentrations of Zn^{2+} and EDTA are depicted below the protein names. Protein samples without chemical agents are expressed as black bars (control). Pdi values are indicated above all samples with the respective colors, and the Zp values of samples containing Zn^{2+} are shown at the bottom expressed in mV. (B) Size increase factor (SIF), referring to the percentage of size increase observed in cation-treated proteins with reference to the unassembled material. (C) Assembly profiles of β-Gal with or without an H6 tag, at increasing Zn^{2+} concentrations (namely 0.1, 0.3, and 0.5 mM, depicted in gray). White numbers indicate the hydrodynamic sizes in nm. In the inset, the absence of the effect of Zn^{2+} on the enzymatic activity of β-Gal and β-Gal-H6. (D) Fluorescence emission measured at 510 nm of GFP-based proteins expressed in arbitrary units (au). The legend is the same as that in (C). Data sets are expressed as $\bar{x} \pm$ SEM with at least $n = 3$, and statistical significance is achieved when $^*p < 0.05$ for (A)−(C) and $^*p < 0.001$ for (D).

maintenance of their distinctive structure and fluorescent emission once in the body.

This whole set of data proved that the addition of a simple H6 tag to simple or complex protein constructs (Figure 3) allowed their controlled oligomerization into regular and reproducible nanoscale complexes, following an assembly concept of generic applicability based on divalent cation coordination. None of the main biochemical traits of the model proteins, such as the presence of a naturally interacting peptide ligand (such as T22 used for cell targeting), the type of scaffold, or the number of His residues in the native protein (excluding H6), had any influence on the assembly process (Figure 7). His residues clearly need to be clustered such as in a His-rich tag for protein assembly as nanoparticles, and consequently, oligomerization of proteins in the presence of Zn^{2+} due to naturally occurring His residues in their sequence

https://doi.org/10.1021/acssuschemeng.1c04256
ACS Sustainable Chem. Eng. 2021, 9, 12341−12354

ACS Sustainable Chemistry & Engineering pubs.acs.org/journal/ascecg Research Article

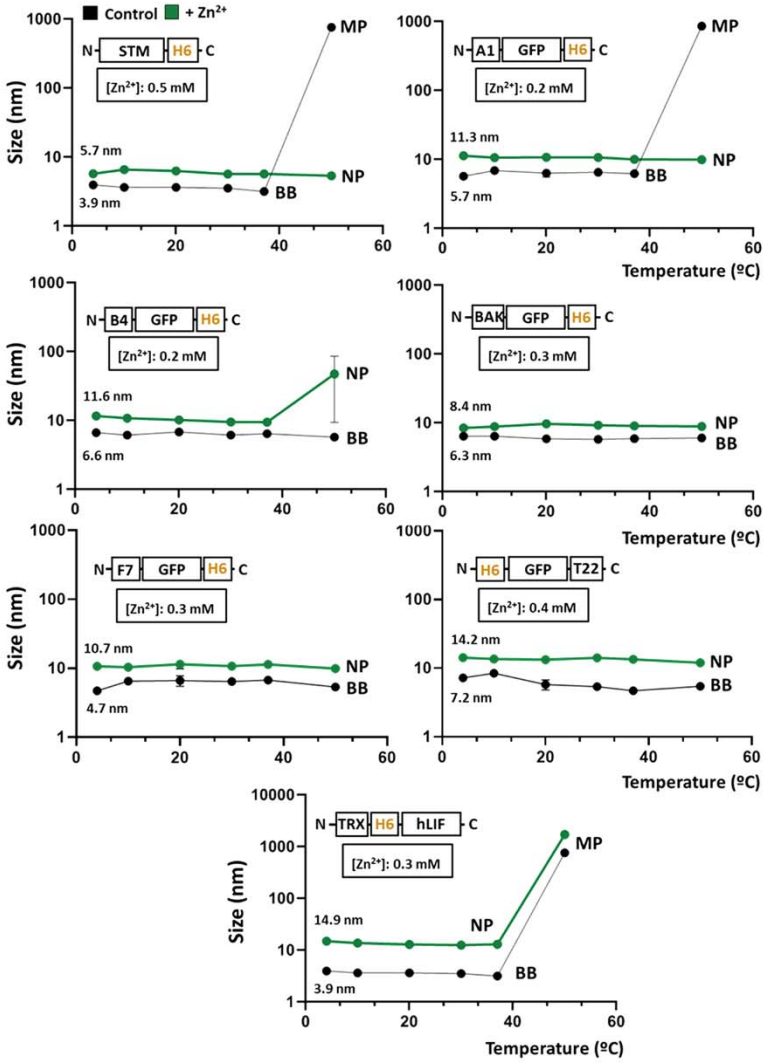

Figure 5. Oligomer stability upon thermal exposure. Size analysis of protein constructs on increases in temperature (from 4 to 50 °C) in the presence (green) or absence (black) of specific amounts of Zn^{2+} as indicated in boxes. Data sets are graphically named according to the material size as building blocks (BB), nanoparticles (NP), or microparticles (MP) and expressed as $\bar{x} \pm$ SEM with at least $n = 3$.

is not observed here and is assumed to be improbable. The single functional domains present in the building blocks preserve their biological activity once they are assembled into NPs, as tested by the GFP specific fluorescence of all GFP-containing NPs in comparison to the unassembled building blocks (Figure 4D). The experimental data showed that oligomers kept the emission capabilities of the original protein, although a tendency toward a moderated reduction was regularly observed. This could be due to quenching of the GFP fluorophore by protein−protein contacts, as previously suggested for similar GFP-based oligomers.[45,46] Interestingly, the stability of all multimeric constructs was very high. The experiments of thermal challenge (Figures 2, 5, and 6E) showed that most of the tested constructs were thermally more stable than the equivalent building block versions, proving the robustness of the resulting materials, as expected from the protein assemblies.[46] On the other hand, the clustered Zn^{2+} cation, although removable by EDTA (Figure 1E), appears to not be released from the oligomers by mere dilution, as the NPs remain stable upon dialysis against a Zn-free buffer (Figure 1G), again pointing out the structural robustness of the formed material. Interestingly, the protein NPs generated here are proved to be stable intermediates in the formation of MPs (Figure 1A). Despite the mechanical stability of the MPs (Figure 6C), the clustering process appears to be fully reversible under physiological conditions (Figure 6B,D). In this context, the MPs formed at high ion concentration released NPs that were indistinguishable from those directly formed at low ion concentrations (Figure 6D) and that are highly stable when they are challenged with high temperatures (Figure 6E). The high stability of NPs generated with clustering H6-tagged proteins has also been demonstrated *in vivo* using a fluorescent GFP-H6 material, which in the oligomeric but not in the soluble form is retained in the gut upon oral administration (Figure 6F).

Other protein oligomerization platforms for full-length proteins have been described that allow the assembly of desired polypeptides, either by the incorporation of natural

https://doi.org/10.1021/acssuschemeng.1c04256
ACS Sustainable Chem. Eng. 2021, 9, 12341−12354

ACS Sustainable Chemistry & Engineering pubs.acs.org/journal/ascecg Research Article

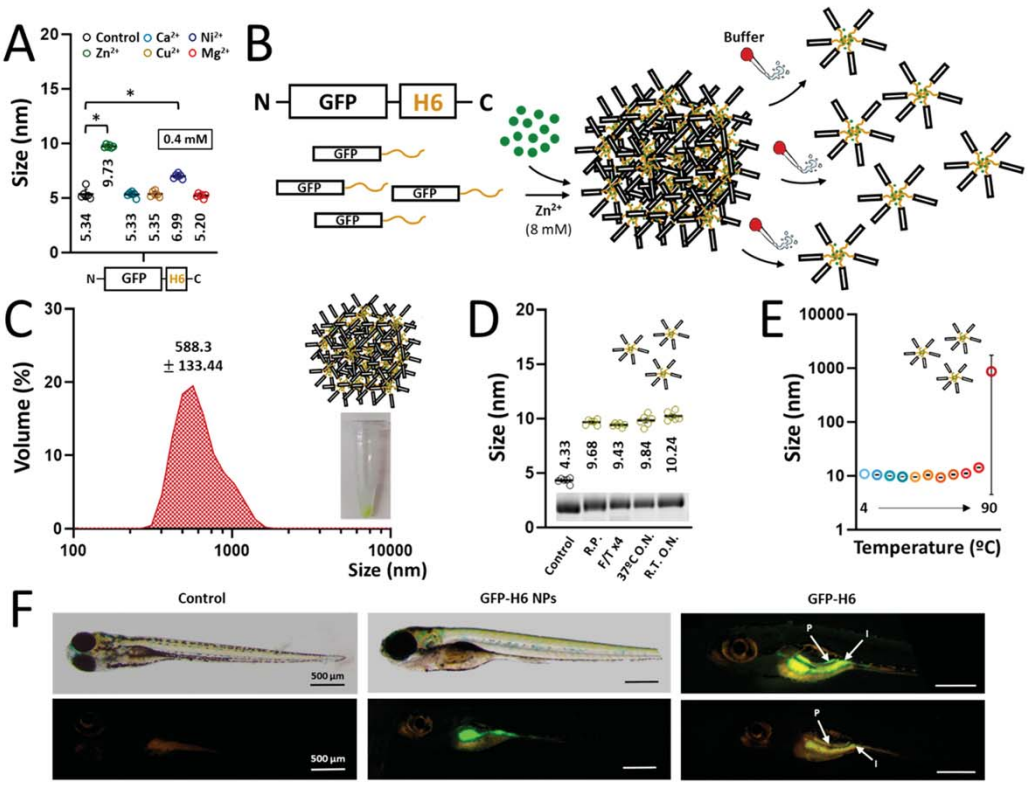

Figure 6. Manufacturing artificial GFP-H6 MPs and stability analysis of released NPs. (A) Assembly of GFP-H6 upon the addition of different divalent cations (Zn^{2+}, Ca^{2+}, Cu^{2+}, Ni^{2+} and Mg^{2+}) at 0.4 mM. Numbers refer to mean size. (B) Schematic representation of MP formation upon addition of excess (8 mM) Zn^{2+} and subsequent protein NP release after resuspension with protein storage buffer. (C) Hydrodynamic size (nm) of GFP-H6 microscaled particles at 8 mM Zn^{2+}. The inset picture shows the obtained fluorescent pellet after particle formation. (D) Hydrodynamic size (nm) of released soluble GFP-H6 NPs after MP resuspension under different thermal conditions. R.P. refers to released protein. (F/T x4) refers to freezing and thawing the sample for four cycles. 37 °C O.N. refers to protein incubation at 37 °C overnight. R.T. O.N. refers to protein incubation at RT overnight. The inset shows a TGX gel under each experimental condition. **E.** Hydrodynamic size (nm) of released soluble NPs at increasing temperatures (4, 10, 20, 30, 37, 50, 60, 70, 80, and 90 °C). (F) *In vivo* uptake experiment in 5 dpf zebra fish larvae. Larvae were immersed in 50 μgmL^{-1} of GFP-H6, either as building blocks or as NPs and thus exposed for 48 h. In the panels with quantitative data, data sets are expressed as $\bar{x} \pm$ SEM with at least $n = 3$, statistical significance (*) is achieved when $p < 0.05$, and the peak value is depicted when it applies.

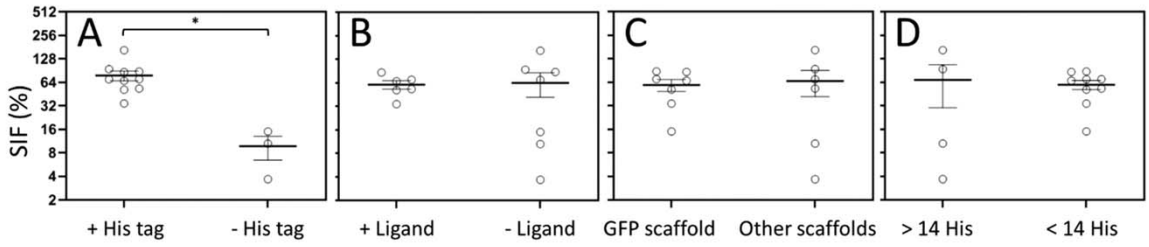

Figure 7. Effect of intrinsic protein parameters on protein self-assembly. Statistical analysis comparing the SIF upon nanoparticle formation versus intrinsic protein properties, namely the presence or absence of H6 (A), the presence or absence of targeting peptides (B), the type of protein scaffold (C), and the number of histidine residues in the native protein (D). Data sets are expressed as scattered dot plots; $\bar{x} \pm$ SEM with at least $n = 3$, and statistical significance is achieved when $*p < 0.05$. SIF is the size increasing factor.

oligomerization domains[13,47] or by the combination of several types of cationic peptides that are placed at particular accommodation sites, to promote cross-molecular interactions.[48] The technology proposed here is based on the simple natural observation that divalent cations, Zn^{2+} among others, drive the assembly of proteins into amyloidal structures,[49−51] protein reservoirs, and scaffolds,[18,23,52−55] in different biological contexts. The addition of a H6 tag to recombinant proteins is a common procedure to simplify their purification,[56−58] and therefore, most of the proteins are already suitable to undergo the assembly process described here. Such tag incorporation is the only required engineering process that, being simple and versatile, involves a minor modification of the protein properties, in most cases without a noticeable effect on their biological activity. The potential use of metals (or mixtures) others than Zn (such as Fe) in their cationic forms could, in addition, confer supplementary properties to the H6-

https://doi.org/10.1021/acssuschemeng.1c04256
ACS Sustainable Chem. Eng. 2021, 9, 12341−12354

based protein NPs such as their magnetic manipulation, which could be of particular interest in specific clinical contexts.[59]

The transversal applicability of this protein assembly approach, as demonstrated here by a broad set of unrelated proteins (Figures 1 and 3) and by the sole dependence of the H6 tag among the tested parameters (Figure 7), opens the door to the general generation of nanostructured versions of proteins of interest. In this regard, protein oligomers, built in with intrinsically biocompatible and biodegradable macromolecules, are very interesting in comparison to categories of materials such as metals, ceramics, lipids, and carbon nanotubes, which pose concerns regarding toxicity and permanence in the environment.[60−66] On the other hand, in contrast to other nanomaterials, protein NPs do not recruit protein corona upon systemic application, avoiding a critical bottleneck in the use of nonprotein nanomaterials as drug delivery systems.[67,68] This is also important because proteins are a unique category of drugs that allow their self-assembly and self-delivery in the absence of chemically heterologous drug carriers.[69] Then they fulfill, in that way, a major concept in nanomedicine aimed at preventing toxicities and increasing efficacy: that is, removing nanoscale vehicles from drug delivery systems.[70] The chemical homogeneity of proteins as increasingly approved biopharmaceuticals[71] in combination with the use of physiological linkers such as natural cations[17] makes them highly appealing, especially if they can be manipulated to gain stable nanoscale-sized functionalities, as demonstrated here (Figures 1, 2, and 6). More than 400 protein products have been approved as human drugs[71] as the result of scalable and green biofabrication processes,[72] again in contrast with less environmentally friendly nanodrug fabrication procedures.[73] Some of these protein pharmaceuticals might benefit from their administration as nanostructured multivalent forms, since we show here that the nonspecific diffusion capabilities in living tissues are restricted in such a version (Figure 6F). For cell-targeted protein drugs, the multivalent display of cell-receptor ligands has been also proved to enhance binding, internalization and delivery in target cells.[74] Also, it must be noted that chemical linkers used to generate antibody−drug conjugates and other drug constructs represent an added toxicological risk to the final product.[75−78]

Finally, the use of H6 as a clustering agent might be controversial in a clinical context due to the potential immunogenicity of H6. As a matter of discussion, no evidence of H6-linked immunopathology is available. In contrast, a simple BLAST search in the human proteome for H6 (not shown) reveals a significant list of outputs, including intracellular and extracellular proteins such as Q6UXD1,Q70CQ2, O00555, Q4VCS5, O43497, and Q9Y566 (Uniprot codes). Of course, since there is evidence which points out that other human His-rich domains might be also useful to drive protein oligomerization, fully humanized alternatives might be further explored with regard to fully biocompatible protein materials,[38,56] if this is proved to be convenient for particular cases.

CONCLUSION

On the bases of the presented data, we propose the use of divalent cations as a universal trigger of His-tag-based protein oligomerization into the nanoscale, through a simple procedure that can be applied on demand to any His-tagged polypeptide. Other strategies based on structural selection, ensuring periodicity between particular amino acids (Glu, Cys, Asp, and His[79]) or through the incorporation of artificial amino acids with high affinity for cations,[80] are also addressed to facilitate the formation of oligomeric structures. However, none of them refer to the use of a His tag as an architectonic agent for NP formation. This fact and the universal use of polyhistidines in protein production give a distinctive and totally innovative character to this new platform, which is based on fully environmentally friendly, sustainable processes supported by physiological amounts of cations present in living systems. Notably, the number of protein drugs in the market is steadily increasing[71] and this tendency will probably intensify in the future. The administration of nanoscale functional versions of otherwise monomeric drugs would provide the beneficial multivalent presentation of molecular ligands, enhanced endocytosis, and improved stability, biodistribution, and functionality. In addition, our approach fulfills the rising nanomedical concept of carrierless (or vehicle-free) nanomedicines, in which the drug itself self-organizes as nanoparticles in the absence of any heterologous vehicle.[70] The simplicity of Zn^{2+}-supported assembly[17] that uses cation doses much below the toxic threshold[17,81] allows for the immediate application of this technology in industry and biomedicine and the conversion into functional nanostructures of the huge catalogue of already existing His-tagged proteins.

AUTHOR INFORMATION

Corresponding Authors

Ugutz Unzueta − *Departament de Genètica i de Microbiologia, Universitat Autònoma de Barcelona, Barcelona 08193, Spain; CIBER de Bioingeniería, Biomateriales y Nanomedicina (CIBER-BBN), Madrid 28029, Spain; Biomedical Research Institute Sant Pau (IIB Sant Pau), Barcelona 08025, Spain;* orcid.org/0000-0001-5119-2266; Email: uunzueta@santpau.cat

Esther Vazquez − *Institut de Biotecnologia i de Biomedicina and Departament de Genètica i de Microbiologia, Universitat Autònoma de Barcelona, Barcelona 08193, Spain; CIBER de Bioingeniería, Biomateriales y Nanomedicina (CIBER-BBN), Madrid 28029, Spain;* orcid.org/0000-0003-1052-0424; Email: Esther.Vazquez@uab.cat

Antonio Villaverde − *Institut de Biotecnologia i de Biomedicina and Departament de Genètica i de Microbiologia, Universitat Autònoma de Barcelona, Barcelona 08193, Spain; CIBER de Bioingeniería, Biomateriales y Nanomedicina (CIBER-BBN), Madrid 28029, Spain;* orcid.org/0000-0002-2615-4521; Email: antonio.villaverde@uab.cat

Authors

Hèctor López-Laguna − *Institut de Biotecnologia i de Biomedicina and Departament de Genètica i de Microbiologia, Universitat Autònoma de Barcelona, Barcelona 08193, Spain; CIBER de Bioingeniería, Biomateriales y Nanomedicina (CIBER-BBN), Madrid 28029, Spain*

Julieta M. Sánchez − *Institut de Biotecnologia i de Biomedicina and Departament de Genètica i de Microbiologia, Universitat Autònoma de Barcelona, Barcelona 08193, Spain; Universidad Nacional de Córdoba, Facultad de Ciencias Exactas, Físicas y Naturales, ICTA and Departamento de Química, Córdoba 5016, Argentina; CONICET-Universidad Nacional de Córdoba, Instituto de*

https://doi.org/10.1021/acssuschemeng.1c04256
ACS Sustainable Chem. Eng. 2021, 9, 12341−12354

Investigaciones Biológicas y Tecnológicas (IIByT), Córdoba 5016, Argentina

José Vicente Carratalá − *Institut de Biotecnologia i de Biomedicina and Departament de Genètica i de Microbiologia, Universitat Autònoma de Barcelona, Barcelona 08193, Spain; CIBER de Bioingeniería, Biomateriales y Nanomedicina (CIBER-BBN), Madrid 28029, Spain*

Mauricio Rojas-Peña − *Institut de Biotecnologia i de Biomedicina, Universitat Autònoma de Barcelona, Barcelona 08193, Spain*

Laura Sánchez-García − *Institut de Biotecnologia i de Biomedicina and Departament de Genètica i de Microbiologia, Universitat Autònoma de Barcelona, Barcelona 08193, Spain; CIBER de Bioingeniería, Biomateriales y Nanomedicina (CIBER-BBN), Madrid 28029, Spain*

Eloi Parladé − *Institut de Biotecnologia i de Biomedicina and Departament de Genètica i de Microbiologia, Universitat Autònoma de Barcelona, Barcelona 08193, Spain; CIBER de Bioingeniería, Biomateriales y Nanomedicina (CIBER-BBN), Madrid 28029, Spain*

Alejandro Sánchez-Chardi − *Servei de Microscòpia, Universitat Autònoma de Barcelona, Barcelona 08193, Spain; Departament de Biologia Evolutiva, Ecologia i Ciències Ambientals, Facultat de Biologia, Universitat de Barcelona, Barcelona 08028, Spain*

Eric Voltà-Durán − *Institut de Biotecnologia i de Biomedicina and Departament de Genètica i de Microbiologia, Universitat Autònoma de Barcelona, Barcelona 08193, Spain; CIBER de Bioingeniería, Biomateriales y Nanomedicina (CIBER-BBN), Madrid 28029, Spain*

Naroa Serna − *Institut de Biotecnologia i de Biomedicina and Departament de Genètica i de Microbiologia, Universitat Autònoma de Barcelona, Barcelona 08193, Spain; CIBER de Bioingeniería, Biomateriales y Nanomedicina (CIBER-BBN), Madrid 28029, Spain;* Present Address: Nanoligent SL, Edifici Eureka, Universitat Autònoma de Barcelona, 08193 Barcelona, Spain.

Olivia Cano-Garrido − *Institut de Biotecnologia i de Biomedicina and Departament de Genètica i de Microbiologia, Universitat Autònoma de Barcelona, Barcelona 08193, Spain; CIBER de Bioingeniería, Biomateriales y Nanomedicina (CIBER-BBN), Madrid 28029, Spain;* Present Address: OCG, Nanoligent SL, Edifici Eureka, Universitat Autònoma de Barcelona, Bellaterra, 08193 Barcelona, Spain

Sandra Flores − *Universidad Nacional de Córdoba, Facultad de Ciencias Exactas, Físicas y Naturales, ICTA and Departamento de Química, Córdoba 5016, Argentina; CONICET-Universidad Nacional de Córdoba, Instituto de Investigaciones Biológicas y Tecnológicas (IIByT), Córdoba 5016, Argentina*

Neus Ferrer-Miralles − *Institut de Biotecnologia i de Biomedicina and Departament de Genètica i de Microbiologia, Universitat Autònoma de Barcelona, Barcelona 08193, Spain; CIBER de Bioingeniería, Biomateriales y Nanomedicina (CIBER-BBN), Madrid 28029, Spain;* orcid.org/0000-0003-2981-3913

Verónica Nolan − *Universidad Nacional de Córdoba, Facultad de Ciencias Exactas, Físicas y Naturales, ICTA and Departamento de Química, Córdoba 5016, Argentina; CONICET-Universidad Nacional de Córdoba, Instituto de Investigaciones Biológicas y Tecnológicas (IIByT), Córdoba 5016, Argentina*

Ario de Marco − *Laboratory for Environmental and Life Sciences, University of Nova Gorica, Nova Gorica 5000, Slovenia*

Nerea Roher − *Institut de Biotecnologia i de Biomedicina and Departament de Biologia Cel·lular, Fisiologia Animal i Immunologia, Universitat Autònoma de Barcelona, Barcelona 08193, Spain; CIBER de Bioingeniería, Biomateriales y Nanomedicina (CIBER-BBN), Madrid 28029, Spain*

Complete contact information is available at: https://pubs.acs.org/10.1021/acssuschemeng.1c04256

Author Contributions

△H.L.-L. and J.M.S. contributed equally.

Funding

We are indebted to Agencia Estatal de Investigación (AEI) and to the Fondo Europeo de Desarrollo Regional (FEDER) (grant BIO2016-76063-R, AEI/FEDER, UE to A.V., PID201-105416RB-I00/AEI/10.13039/501100011033 to E.V.), INIA RTA2015-00064-C02-02 (MINECO) and PID2019-107298RB-C22 (MINECO) to N.F.-M., AGAUR (2017SGR-229 to A.V.), ISCIII (PI20/00400, cofunded by FEDER "a way to make Europe", to U.U.) CIBERBBN (project NANO-PROTHER granted to A.V., NANOREMOTE to E.V., and NANOSCAPE to U.U.) and to the Javna Agencija za Raziskovalno dejavnost Republike Slovenije (grants ARRS/N4−0046 and ARRS/J4−9322) to A.d.M. U.U. is supported by a Miguel Servet fellowship (CP19/00028) from ISCIII cofunded by European Social Fund (ESF investing in your future). L.S.-G. and H.L.-L. were supported by a predoctoral fellowship from AGAUR (2018FI_B2_00051 and 2019FI_B00352, respectively), and E.V.-D. was supported by a predoctoral fellowship from the Ministerio de Ciencia, Innovación y Universidades (FPU18/04615).

Notes

The authors declare no competing financial interest.

■ ACKNOWLEDGMENTS

We are indebted to the CERCA Program (Generalitat de Catalunya) and to the Networking Research Center on Bioengineering, Biomaterials and Nanomedicine (CIBER-BBN) that is an initiative funded by the VI National R&D&I Plan 2008−2011, Iniciativa Ingenio 2010, Consolider Program, CIBER Actions and financed by the Instituto de Salud Carlos III, with assistance from the European Regional Development Fund. Protein production has been partially performed by the ICTS "NANBIOSIS", more specifically by the Protein Production Platform of CIBER in Bioengineering, Biomaterials & Nanomedicine (CIBER-BBN)/IBB, at the UAB sePBioEs scientific-technical service (https://www.nanbiosis.es/portfolio/u1-protein-production-platform-ppp/) and the nanoparticle size analysis by the Biomaterial Processing and Nanostructuring Unit. Electron microscopy, cell culturing, and spectrophotometric studies were performed at the UAB scientific-technical services SM, SCAC, and LLEB respectively (https://www.uab.cat/web/research/scientifictechnical-services/all-scientific-technical-services-1345667278676). A.V. received an ICREA ACADEMIA award. Molecular graphics and analyses were performed with UCSF Chimera, developed with support from NIH P41-GM103311.

■ ABBREVIATIONS

β-Gal, β-galactosidase; BB, building block; DLS, dynamic light scattering; EDTA, ethylenediaminetetraacetic acid; FESEM, field emission scanning electron microscopy; GFP, green fluorescent protein; H6, hexahistidine; hLIF, human leukemia inhibitory factor; HSA, human serum albumin; IMAC, immobilized metal affinity chromatography; IPTG, isopropyl β-D-1-thiogalactopyranoside; NP, nanoparticle; MP, microparticle; Pdi, polydispersion index; SEM, standard error of the mean; STM, stefin A triple mutant; TEM, transmission electron microscopy; TRX, thioredoxin; VHHs, nanobodies

■ REFERENCES

(1) Li, Y.; Wang, Y.; Huang, G.; Gao, J. Cooperativity Principles in Self-Assembled Nanomedicine. *Chem. Rev.* **2018**, *118*, 5359−5391.

(2) Korpi, A.; Anaya-Plaza, E.; Valimaki, S.; Kostiainen, M. Highly ordered protein cage assemblies: A toolkit for new materials. *Wiley Interdiscip. Rev.: Nanomed. Nanobiotechnol.* **2020**, *12*, No. e1578.

(3) DeFrates, K. G.; Moore, R.; Borgesi, J.; Lin, G.; Mulderig, T.; Beachley, V.; Hu, X. Protein-Based Fiber Materials in Medicine: A Review. *Nanomaterials* **2018**, *8*, 457.

(4) Hamley, I. W. Protein Assemblies: Nature-Inspired and Designed Nanostructures. *Biomacromolecules* **2019**, *20*, 1829−1848.

(5) Jacob, R.; Anoop, A.; Maji, S. *Protein Nanofibrils as Storage Forms of Peptide Drugs and Hormones*; Springer: 2019; Vol. *1174*, pp 265−290.

(6) Sutherland, T. D.; Huson, M. G.; Rapson, T. D. Rational design of new materials using recombinant structural proteins: Current state and future challenges. *J. Struct. Biol.* **2018**, *201*, 76−83.

(7) Aigner, T. B.; DeSimone, E.; Scheibel, T. Biomedical Applications of Recombinant Silk-Based Materials. *Advanced materials* **2018**, *30*, No. 1704636.

(8) Perlmutter, J. D.; Hagan, M. F. Mechanisms of Virus Assembly. *Annu. Rev. Phys. Chem.* **2015**, *66*, 217−239.

(9) Li, D.; Jones, E. M.; Sawaya, M. R.; Furukawa, H.; Luo, F.; Ivanova, M.; Sievers, S. A.; Wang, W. Y.; Yaghi, O. M.; Liu, C.; Eisenberg, D. S. Structure-Based Design of Functional Amyloid Materials. *J. Am. Chem. Soc.* **2014**, *136*, 18044−18051.

(10) Kumar, V. A.; Wang, B. K.; Kanahara, S. M. Rational design of fiber forming supramolecular structures. *Exp. Biol. Med.* **2016**, *241*, 899−908.

(11) Wei, G.; Su, Z.; Reynolds, N. P.; Arosio, P.; Hamley, I. W.; Gazit, E.; Mezzenga, R. Self-assembling peptide and protein amyloids: from structure to tailored function in nanotechnology. *Chem. Soc. Rev.* **2017**, *46*, 4661−4708.

(12) Hou, J.; Zeng, W.; Zong, Y.; Chen, Z.; Miao, C.; Wang, B.; Lou, C. Engineering the Ultrasensitive Transcription Factors by Fusing a Modular Oligomerization Domain. *ACS Synth. Biol.* **2018**, *7*, 1188−1194.

(13) Engel, J.; Kammerer, R. A. What are oligomerization domains good for? *Matrix Biol.* **2000**, *19*, 283−288.

(14) Wang, Y.; Katyal, P.; Montclare, J. K. Protein-Engineered Functional Materials. *Adv. Healthcare Mater.* **2019**, *8*, No. 1801374.

(15) Peng, Y. Y.; Glattauer, V.; Ramshaw, J. A. M. Stabilisation of Collagen Sponges by Glutaraldehyde Vapour Crosslinking. *International journal of biomaterials* **2017**, *2017*, 1.

(16) Liu, T.; Shi, L.; Gu, Z.; Dan, W.; Dan, N. A novel combined polyphenol-aldehyde crosslinking of collagen film-Applications in biomedical materials. *Int. J. Biol. Macromol.* **2017**, *101*, 889−895.

(17) López-Laguna, H.; Sánchez, J.; Unzueta, U.; Mangues, R.; Vázquez, E.; Villaverde, A. Divalent Cations: A Molecular Glue for Protein Materials. *Trends Biochem. Sci.* **2020**, *45*, 992−1003.

(18) Chen, T. Y.; Cheng, W. J.; Horng, J. C.; Hsu, H. Y. Artificial peptide-controlled protein release of Zn(2+)-triggered, self-assembled histidine-tagged protein microparticle. *Colloids Surf., B* **2020**, *187*, 110644.

(19) Sanchez, J. M.; Lopez-Laguna, H.; Alamo, P.; Serna, N.; Sanchez-Chardi, A.; Nolan, V.; Cano-Garrido, O.; Casanova, L.; Unzueta, U.; Vazquez, E.; Mangues, R.; Villaverde, A. Artificial Inclusion Bodies for Clinical Development. *Advanced science* **2020**, *7*, 1902420.

(20) Cespedes, M. V.; Cano-Garrido, O.; Alamo, P.; Sala, R.; Gallardo, A.; Serna, N.; Falgas, A.; Volta-Duran, E.; Casanova, L.; Sanchez-Chardi, A.; Lopez-Laguna, H.; Sanchez-Garcia, L.; Sanchez, J. M.; Unzueta, U.; Vazquez, E.; Mangues, R.; Villaverde, A. Engineering Secretory Amyloids for Remote and Highly Selective Destruction of Metastatic Foci. *Adv. Mater.* **2020**, *32*, No. e907348.

(21) Maji, S. K.; Perrin, M. H.; Sawaya, M. R.; Jessberger, S.; Vadodaria, K.; Rissman, R. A.; Singru, P. S.; Nilsson, K. P.; Simon, R.; Schubert, D.; Eisenberg, D.; Rivier, J.; Sawchenko, P.; Vale, W.; Riek, R. Functional amyloids as natural storage of peptide hormones in pituitary secretory granules. *Science* **2009**, *325*, 328−32.

(22) Mankar, S.; Anoop, A.; Sen, S.; Maji, S. K. Nanomaterials: amyloids reflect their brighter side. *Nano Rev.* **2011**, *2*, 6032.

(23) Jacob, R. S.; Das, S.; Ghosh, S.; Anoop, A.; Jha, N. N.; Khan, T.; Singru, P.; Kumar, A.; Maji, S. K. Amyloid formation of growth hormone in presence of zinc: Relevance to its storage in secretory granules. *Sci. Rep.* **2016**, *6*, 23370.

(24) Knecht, S.; Ricklin, D.; Eberle, A. N.; Ernst, B. Oligohis-tags: mechanisms of binding to Ni2+-NTA surfaces. *J. Mol. Recognit.* **2009**, *22*, 270−9.

(25) Flores, S. S.; Nolan, V.; Perillo, M. A.; Sánchez, J. M. Superactive β-galactosidase inclusion bodies. *Colloids Surf., B* **2019**, *173*, 769−775.

(26) Tamamura, H.; Imai, M.; Ishihara, T.; Masuda, M.; Funakoshi, H.; Oyake, H.; Murakami, T.; Arakaki, R.; Nakashima, H.; Otaka, A.; Ibuka, T.; Waki, M.; Matsumoto, A.; Yamamoto, N.; Fujii, N. Pharmacophore identification of a chemokine receptor (CXCR4) antagonist, T22 ([Tyr(5,12),Lys7]-polyphemusin II), which specifically blocks T cell-line-tropic HIV-1 infection. *Bioorg. Med. Chem.* **1998**, *6*, 1033−41.

(27) Bogner, C.; Kale, J.; Pogmore, J.; Chi, X.; Shamas-Din, A.; Fradin, C.; Leber, B.; Andrews, D. W. Allosteric Regulation of BH3 Proteins in Bcl-xL Complexes Enables Switch-like Activation of Bax. *Mol. Cell* **2020**, *77*, 901−912 e9..

(28) Pinho, V.; Fernandes, M.; da Costa, A.; Machado, R.; Gomes, A. C. Leukemia inhibitory factor: Recent advances and implications in biotechnology. *Cytokine Growth Factor Rev.* **2020**, *52*, 25−33.

(29) Rasooli, F.; Hashemi, A. Efficient expression of EpEX in the cytoplasm of Escherichia coli using thioredoxin fusion protein. *Res. Pharm. Sci.* **2019**, *14*, 554−565.

(30) Martin, J. R.; Craven, C. J.; Jerala, R.; Kroon-Zitko, L.; Zerovnik, E.; Turk, V.; Waltho, J. P. The three-dimensional solution structure of human stefin A. *J. Mol. Biol.* **1995**, *246*, 331−43.

(31) Crepin, R.; Gentien, D.; Duche, A.; Rapinat, A.; Reyes, C.; Nemati, F.; Massonnet, G.; Decaudin, D.; Djender, S.; Moutel, S.; Desrumeaux, K.; Cassoux, N.; Piperno-Neumann, S.; Amigorena, S.; Perez, F.; Roman-Roman, S.; de Marco, A. Nanobodies against surface biomarkers enable the analysis of tumor genetic heterogeneity in uveal melanoma patient-derived xenografts. *Pigm. Cell Melanoma Res.* **2017**, *30*, 317−327.

(32) Crepin, R.; Veggiani, G.; Djender, S.; Beugnet, A.; Planeix, F.; Pichon, C.; Moutel, S.; Amigorena, S.; Perez, F.; Ghinea, N.; de Marco, A. Whole-cell biopanning with a synthetic phage display library of nanobodies enabled the recovery of follicle-stimulating hormone receptor inhibitors. *Biochem. Biophys. Res. Commun.* **2017**, *493*, 1567−1572.

(33) Kim, D. E.; Chivian, D.; Baker, D. Protein structure prediction and analysis using the Robetta server. *Nucleic Acids Res.* **2004**, *32*, W526−W531.

(34) Pettersen, E. F.; Goddard, T. D.; Huang, C. C.; Couch, G. S.; Greenblatt, D. M.; Meng, E. C.; Ferrin, T. E. UCSF Chimera–a visualization system for exploratory research and analysis. *J. Comput. Chem.* **2004**, *25*, 1605−12.

https://doi.org/10.1021/acssuschemeng.1c04256
ACS Sustainable Chem. Eng. 2021, 9, 12341−12354

(35) Sanchez, J. M.; Sanchez-Garcia, L.; Pesarrodona, M.; Serna, N.; Sanchez-Chardi, A.; Unzueta, U.; Mangues, R.; Vazquez, E.; Villaverde, A. Conformational Conversion during Controlled Oligomerization into Nonamylogenic Protein Nanoparticles. *Biomacromolecules* **2018**, *19*, 3788−3797.
(36) Naumenko, V.; Nikitin, A.; Kapitanova, K.; Melnikov, P.; Vodopyanov, S.; Garanina, A.; Valikhov, M.; Ilyasov, A.; Vishnevskiy, D.; Markov, A.; Golyshev, S.; Zhukov, D.; Alieva, I.; Abakumov, M.; Chekhonin, V.; Majouga, A. Intravital microscopy reveals a novel mechanism of nanoparticles excretion in kidney. *J. Controlled Release* **2019**, *307*, 368−378.
(37) Yu, M.; Wu, J.; Shi, J.; Farokhzad, O. C. Nanotechnology for protein delivery: Overview and perspectives. *J. Controlled Release* **2016**, *240*, 24−37.
(38) López-Laguna, H.; Sala, R.; Sánchez, J. M.; Álamo, P.; Unzueta, U.; Sánchez-Chardi, A.; Serna, N.; Sánchez-García, L.; Voltà-Durán, E.; Mangues, R.; Villaverde, A.; Vázquez, E. Nanostructure Empowers Active Tumor Targeting in Ligand-Based Molecular Delivery. *Part. Part. Syst. Charact.* **2019**, *36*, 1900304.
(39) Kalyane, D.; Raval, N.; Maheshwari, R.; Tambe, V.; Kalia, K.; Tekade, R. K. Employment of enhanced permeability and retention effect (EPR): Nanoparticle-based precision tools for targeting of therapeutic and diagnostic agent in cancer. *Mater. Sci. Eng., C* **2019**, *98*, 1252−1276.
(40) Murty, B. S.; Shankar, P.; Raj, B.; Rath, B. B.; Murday, J., Unique Properties of Nanomaterials. In *Textbook of Nanoscience and Nanotechnology*; Springer: 2013; pp 29−65. DOI: 10.1007/978-3-642-28030-6_2.
(41) Jacobson, R. H.; Zhang, X. J.; DuBose, R. F.; Matthews, B. W. Three-dimensional structure of beta-galactosidase from E. coli. *Nature* **1994**, *369*, 761−6.
(42) Cespedes, M. V.; Cano-Garrido, O.; Alamo, P.; Sala, R.; Gallardo, A.; Serna, N.; Falgas, A.; Volta-Duran, E.; Casanova, I.; Sanchez-Chardi, A.; Lopez-Laguna, H.; Sanchez-Garcia, L.; Sanchez, J. M.; Unzueta, U.; Vazquez, E.; Mangues, R.; Villaverde, A. Engineering Secretory Amyloids for Remote and Highly Selective Destruction of Metastatic Foci. *Adv. Mater.* **2020**, *32*, 1907348.
(43) Sánchez, J.; López-Laguna, H.; Álamo, P.; Serna, N.; Sánchez-Chardi, A.; Nolan, V.; Cano-Garrido, O.; Casanova, I.; Unzueta, U.; Vazquez, E.; Mangues, R.; Villaverde, A. Artificial inclusion bodies for clinical development. *Advanced science* **2020**, *7*, 1902420.
(44) Nel, A.; Ruoslahti, E.; Meng, H. New Insights into "Permeability" as in the Enhanced Permeability and Retention Effect of Cancer Nanotherapeutics. *ACS Nano* **2017**, *11*, 9567−9569.
(45) Rueda, F.; Cespedes, M. V.; Conchillo-Sole, O.; Sanchez-Chardi, A.; Seras-Franzoso, J.; Cubarsi, R.; Gallardo, A.; Pesarrodona, M.; Ferrer-Miralles, N.; Daura, X.; Vazquez, E.; García-Fruitos, E.; Mangues, R.; Unzueta, U.; Villaverde, A. Bottom-Up Instructive Quality Control in the Biofabrication of Smart Protein Materials. *Adv. Mater.* **2015**, *27*, 7816−22.
(46) Unzueta, U.; Roldan, M.; Pesarrodona, M.; Benitez, R.; Sanchez-Chardi, A.; Conchillo-Sole, O.; Mangues, R.; Villaverde, A.; Vazquez, E. Self-assembling as regular nanoparticles dramatically minimizes photobleaching of tumour-targeted GFP. *Acta Biomater.* **2020**, *103*, 272−280.
(47) Yeates, T. O.; Padilla, J. E. Designing supramolecular protein assemblies. *Curr. Opin. Struct. Biol.* **2002**, *12*, 464−70.
(48) Unzueta, U.; Ferrer-Miralles, N.; Cedano, J.; Zikung, X.; Pesarrodona, M.; Saccardo, P.; García-Fruitos, E.; Domingo-Espin, J.; Kumar, P.; Gupta, K. C.; Mangues, R.; Villaverde, A.; Vazquez, E. Non-amyloidogenic peptide tags for the regulatable self-assembling of protein-only nanoparticles. *Biomaterials* **2012**, *33*, 8714−22.
(49) Faller, P.; Hureau, C.; Berthoumieu, O. Role of metal ions in the self-assembly of the Alzheimer's amyloid-beta peptide. *Inorg. Chem.* **2013**, *52*, 12193−206.
(50) Grenacs, A.; Sovago, I. Copper(II), nickel(II) and zinc(II) complexes of the N-terminal nonapeptide fragment of amyloid-beta and its derivatives. *J. Inorg. Biochem.* **2014**, *139*, 49−56.
(51) Cristovao, J. S.; Santos, R.; Gomes, C. M. Metals and Neuronal Metal Binding Proteins Implicated in Alzheimer's Disease. *Oxid. Med. Cell. Longevity* **2016**, *2016*, 1.
(52) Knight, A. S.; Larsson, J.; Ren, J. M.; Bou Zerdan, R.; Seguin, S.; Vrahas, R.; Liu, J.; Ren, G.; Hawker, C. J. Control of Amphiphile Self-Assembly via Bioinspired Metal Ion Coordination. *J. Am. Chem. Soc.* **2018**, *140*, 1409−1414.
(53) Jehle, F.; Fratzl, P.; Harrington, M. J. Metal-Tunable Self-Assembly of Hierarchical Structure in Mussel-Inspired Peptide Films. *ACS Nano* **2018**, *12*, 2160−2168.
(54) Wu, H.; Shen, Y.; Wang, D.; Herrmann, H.; Goldman, R. D.; Weitz, D. A. Effect of the divalent cations zinc and calcium on the structure and mechanics of reconstituted vimentin intermediate filaments. *bioRxiv (CSH Laboratory)* **2019**. DOI: 10.1101/844167.
(55) Maniaci, B.; Lipper, C. H.; Anipindi, D. L.; Erlandsen, H.; Cole, J. L.; Stec, B.; Huxford, T.; Love, J. J. Design of High-Affinity Metal-Controlled Protein Dimers. *Biochemistry* **2019**, *58*, 2199−2207.
(56) López-Laguna, H.; Cubarsi, R.; Unzueta, U.; Mangues, R.; Vázquez, E.; Villaverde, A. Endosomal escape of protein nanoparticles engineered through humanized histidine-rich peptides. *Science China Materials* **2020**, *63*, 644−653.
(57) Gaberc-Porekar, V.; Menart, V. Perspectives of immobilized-metal affinity chromatography. *J. Biochem. Biophys. Methods* **2001**, *49*, 335−60.
(58) Spriestersbach, A.; Kubicek, J.; Schafer, F.; Block, H.; Maertens, B. Purification of His-Tagged Proteins. *Methods Enzymol.* **2015**, *559*, 1−15.
(59) Corchero, J. L.; Villaverde, A. Biomedical applications of distally controlled magnetic nanoparticles. *Trends Biotechnol.* **2009**, *27*, 468−76.
(60) Yang, W.; Wang, L.; Mettenbrink, E. M.; DeAngelis, P. L.; Wilhelm, S. Nanoparticle Toxicology. *Annu. Rev. Pharmacol. Toxicol.* **2021**, *61*, 269−289.
(61) Bai, C.; Tang, M. Toxicological study of metal and metal oxide nanoparticles in zebrafish. *J. Appl. Toxicol.* **2020**, *40*, 37−63.
(62) De Marchi, L.; Coppola, F.; Soares, A. M. V. M.; Pretti, C.; Monserrat, J. M.; Torre, C. d.; Freitas, R. Engineered nanomaterials: From their properties and applications, to their toxicity towards marine bivalves in a changing environment. *Environ. Res.* **2019**, *178*, 108683.
(63) Raftis, J. B.; Miller, M. R. Nanoparticle translocation and multi-organ toxicity: A particularly small problem. *Nano Today* **2019**, *26*, 8−12.
(64) Sthijns, M. M.; Thongkam, W.; Albrecht, C.; Hellack, B.; Bast, A.; Haenen, G. R.; Schins, R. P. Silver nanoparticles induce hormesis in A549 human epithelial cells. *Toxicol. In Vitro* **2017**, *40*, 223−233.
(65) Liu, J.; Feng, X.; Wei, L.; Chen, L.; Song, B.; Shao, L. The toxicology of ion-shedding zinc oxide nanoparticles. *Crit. Rev. Toxicol.* **2016**, *46*, 348−84.
(66) Al Zaki, A.; Hui, J. Z.; Higbee, E.; Tsourkas, A. Biodistribution, Clearance, and Toxicology of Polymeric Micelles Loaded with 0.9 or 5 nm Gold Nanoparticles. *Journal of biomedical nanotechnology* **2015**, *11*, 1836−46.
(67) Dai, Q.; Bertleff-Zieschang, N.; Braunger, J. A.; Bjornmalm, M.; Cortez-Jugo, C.; Caruso, F. Particle Targeting in Complex Biological Media. *Adv. Healthcare Mater.* **2018**, *7*, 1700575.
(68) Shannahan, J. The biocorona: a challenge for the biomedical application of nanoparticles. *Nanotechnol. Rev.* **2017**, *6*, 345−353.
(69) Sanchez-Garcia, L.; Serna, N.; Alamo, P.; Sala, R.; Cespedes, M. V.; Roldan, M.; Sanchez-Chardi, A.; Unzueta, U.; Casanova, I.; Mangues, R.; Vazquez, E.; Villaverde, A. Self-assembling toxin-based nanoparticles as self-delivered antitumoral drugs. *J. Controlled Release* **2018**, *274*, 81−92.
(70) Shen, J.; Wolfram, J.; Ferrari, M.; Shen, H. Taking the vehicle out of drug delivery. *Mater. Today* **2017**, *20*, 95−97.
(71) Sanchez-Garcia, L.; Martin, L.; Mangues, R.; Ferrer-Miralles, N.; Vazquez, E.; Villaverde, A. Recombinant pharmaceuticals from microbial cells: a 2015 update. *Microb. Cell Fact.* **2016**, *15*, 33.

https://doi.org/10.1021/acssuschemeng.1c04256
ACS Sustainable Chem. Eng. 2021, 9, 12341−12354

(72) Corchero, J. L.; Gasser, B.; Resina, D.; Smith, W.; Parrilli, E.; Vazquez, F.; Abasolo, I.; Giuliani, M.; Jantti, J.; Ferrer, P.; Saloheimo, M.; Mattanovich, D.; Schwartz, S., Jr.; Tutino, M. L.; Villaverde, A. Unconventional microbial systems for the cost-efficient production of high-quality protein therapeutics. *Biotechnol. Adv.* **2013**, *31*, 140−53.
(73) Shamaila, S.; Sajjad, A. K. L.; Ryma, N.-u.-A.; Farooqi, S. A.; Jabeen, N.; Majeed, S.; Farooq, I. Advancements in nanoparticle fabrication by hazard free eco-friendly green routes. *Applied Materials Today* **2016**, *5*, 150−199.
(74) Xu, Z. U. U.; Roldán, M.; Mangues, R.; Sánchez-Chardi, A.; Ferrer-Miralles, N.; Villaverde, A.; Vázquez, E. Formulating tumor-homing peptides as regular nanoparticles enhances receptor-mediated cell penetrability. *Mater. Lett.* **2015**, *154*, 140−143.
(75) Beck, A.; Goetsch, L.; Dumontet, C.; Corvaia, N. Strategies and challenges for the next generation of antibody-drug conjugates. *Nat. Rev. Drug Discovery* **2017**, *16*, 315−337.
(76) Ma, L.; Wang, C.; He, Z.; Cheng, B.; Zheng, L.; Huang, K. Peptide-Drug Conjugate: A Novel Drug Design Approach. *Curr. Med. Chem.* **2017**, *24*, 3373−3396.
(77) Pillow, T. H. Novel linkers and connections for antibody-drug conjugates to treat cancer and infectious disease. *Pharm. Pat. Anal.* **2017**, *6*, 25−33.
(78) Tsuchikama, K.; An, Z. Antibody-drug conjugates: recent advances in conjugation and linker chemistries. *Protein Cell* **2018**, *9*, 33−46.
(79) Bailey, J. B.; Subramanian, R. H.; Churchfield, L. A.; Tezcan, F. A. Metal-Directed Design of Supramolecular Protein Assemblies. *Methods Enzymol.* **2016**, *580*, 223−50.
(80) Yang, M.; Song, W. J. Diverse protein assembly driven by metal and chelating amino acids with selectivity and tunability. *Nat. Commun.* **2019**, *10*, 5545.
(81) Pazirandeh, S.; Burns, D.; Griffin, U. Overview of dietary trace elements. *UpToDate* (accessed 25/07/2020).
(82) Serna, N.; Cano-Garrido, O.; Sanchez, J. M.; Sanchez-Chardi, A.; Sanchez-Garcia, L.; Lopez-Laguna, H.; Fernandez, E.; Vazquez, E.; Villaverde, A. Release of functional fibroblast growth factor-2 from artificial inclusion bodies. *J. Controlled Release* **2020**, *327*, 61−69.

https://doi.org/10.1021/acssuschemeng.1c04256
ACS Sustainable Chem. Eng. 2021, 9, 12341−12354

Study 3

Engineering Protein Nanoparticles Out from Components of the Human Microbiome

Hèctor López-Laguna, Laura Sánchez-García, Naroa Serna, Eric Voltà-Durán, Julieta M. Sánchez, Alejandro Sánchez-Chardi, Ugutz Unzueta, Marcin Łoś, Antonio Villaverde, and Esther Vázquez

Small 2020 · Impact factor (13.281) · Quartile (Q1)

Objective 1.b

To develop a new and fully transversal biochemical approach to manufacture **protein-based nanoparticles** using human microbiome proteins.

The studies (1 and 2) strongly exhibit our ability to construct protein-based nanoparticles with highly suitable physicochemical properties to be considered as efficient, versatile, cost-effective, and easy-to-manufacture drug delivery systems. But there is still one additional component that should be considered to ensure the feasibility of this platform to be translated into clinics, namely biocompatibility. In this regard, the majority of the already used scaffold proteins are not from human origin, meaning that an undesired effect on human tissues could occur.

Thus, this work has been focused on developing protein-based nanoparticles made of components of the human microbiome to ensure low interactivity with the human body, following the same histidine tag-Zn^{2+} principle. The obtained data suggested a clear oligomerization pattern and high physicochemical stability of the resultant candidates. Interestingly, temperature was also found as an additional assembling agent for some of them.

COMMUNICATION

NANO · MICRO small
www.small-journal.com

Engineering Protein Nanoparticles Out from Components of the Human Microbiome

Hèctor López-Laguna, Laura Sánchez-García, Naroa Serna, Eric Voltà-Durán, Julieta M. Sánchez, Alejandro Sánchez-Chardi, Ugutz Unzueta, Marcin Łoś, Antonio Villaverde,* and Esther Vázquez*

Nanoscale protein materials are highly convenient as vehicles for targeted drug delivery because of their structural and functional versatility. Selective binding to specific cell surface receptors and penetration into target cells require the use of targeting peptides. Such homing stretches should be incorporated to larger proteins that do not interact with body components, to prevent undesired drug release into nontarget organs. Because of their low interactivity with human body components and their tolerated immunogenicity, proteins derived from the human microbiome are appealing and fully biocompatible building blocks for the biofabrication of nonreactive, inert protein materials within the nanoscale. Several phage and phage-like bacterial proteins with natural structural roles are produced in *Escherichia coli* as polyhistidine-tagged recombinant proteins, looking for their organization as discrete, nanoscale particulate materials. While all of them self-assemble in a variety of sizes, the stability of the resulting constructs at 37 °C is found to be severely compromised. However, the fine adjustment of temperature and Zn^{2+} concentration allows the formation of robust nanomaterials, fully stable in complex media and under physiological conditions. Then, microbiome-derived proteins show promise for the regulatable construction of scaffold protein nanomaterials, which can be tailored and strengthened by simple physicochemical approaches.

Protein materials are gaining interest in nanomedicine as drug carriers[1–3] since they offer full biocompatibility and biodegradability. In addition, proteins and derived constructs are structurally and functionally versatile. Their feasible production at industrial scale by well-established recombinant DNA procedures allows their widespread clinical use.[4] In this context, hydrogels, fibers, layers but especially nanoparticles are engineered as drug-releasing systems or as carriers of drugs or imaging agents for cell-targeted delivery. Targeting can be reached by functionalization with peptidic ligands of cell surface markers[5] that allow selective cell binding and internalization. Precision drug delivery is specially needed in cancer therapies in which most of the used drugs are highly cytotoxic.[6,7] The nanoscale size of the resulting protein-drug conjugates would prevent renal filtration of the payload, usually small molecular weight chemicals, but it also favors the enhanced permeability and

H. López-Laguna, Dr. L. Sánchez-García, Dr. N. Serna, E. Voltà-Durán, Dr. J. M. Sánchez, Prof. A. Villaverde, Dr. E. Vázquez
Institut de Biotecnologia i de Biomedicina
Universitat Autònoma de Barcelona
Bellaterra, Barcelona 08193, Spain
E-mail: antoni.villaverde@uab.es

H. López-Laguna, Dr. L. Sánchez-García, Dr. N. Serna, E. Voltà-Durán, Dr. J. M. Sánchez, Dr. U. Unzueta, Prof. A. Villaverde, Dr. E. Vázquez
Departament de Genètica i de Microbiologia
Universitat Autònoma de Barcelona
Bellaterra, Barcelona 08193, Spain
E-mail: uunzueta@santpau.cat

H. López-Laguna, Dr. L. Sánchez-García, Dr. N. Serna, E. Voltà-Durán, Dr. J. M. Sánchez, Dr. U. Unzueta, Prof. A. Villaverde, Dr. E. Vázquez
CIBER de Bioingeniería
Biomateriales y Nanomedicina (CIBER-BBN)
C/Monforte de Lemos 3–5, Madrid 28029, Spain

The ORCID identification number(s) for the author(s) of this article can be found under https://doi.org/10.1002/smll.202001885.

DOI: 10.1002/smll.202001885

Dr. J. M. Sánchez
Instituto de Investigaciones Biológicas y Tecnológicas (IIBYT)
(CONICET-Universidad Nacional de Córdoba)
ICTA & Cátedra de Química Biológica
Departamento de Química
FCEFyN
UNC. Av. Velez Sarsfield 1611, Córdoba X 5016GCA, Argentina

Dr. A. Sánchez-Chardi
Servei de Microscòpia
Universitat Autònoma de Barcelona
Bellaterra, Barcelona 08193, Spain

Dr. A. Sánchez-Chardi
Departament de Biologia Evolutiva
Ecologia i Ciències Ambientals
Facultat de Biologia
Universitat de Barcelona
Av. Diagonal 643, Barcelona 08028, Spain

Dr. U. Unzueta
Institut d'Investigacions Biomèdiques Sant Pau
and Josep Carreras Research Institute
Hospital de la Santa Creu i Sant Pau
Barcelona 08041, Spain

© 2020 WILEY-VCH Verlag GmbH & Co. KGaA, Weinheim

ADVANCED SCIENCE NEWS
www.advancedsciencenews.com

NANO · MICRO small
www.small-journal.com

retention effect (EPR) in tumor tissues.[8] Among the few examples of protein-drug nanoscale complexes approved for use, Abraxane (Nab-Paclitaxel) is indicated for breast, lung and pancreas cancers.[9] In this formulation, the drug Paclitaxel is stabilized by human albumin[10] that in form of clusters of around 130 nm confers the desired nanoscale size although not receptor-mediated cancer cell targeting.[11] The albumin in such complexes is a convenient drug carrier because of its human nature and the expected absence of intrinsic immunogenicity associated to repeated administration. However, because of its multiple organic roles, human albumin is highly interactive with a large catalogue of molecules, cells and tissues of the human body.[12] This fact prevents the optimal tumor biodistribution of the drug because of the wide spectrum of multiple binding targets of the complex. The use of highly reactive human proteins would be then an obstacle for selective cell targeting even when functionalized with appropriate target cell surface ligands, that might be unable to overcome the intrinsic interactivity of the carrier protein. Ideally, for a proper utilization in clinics, protein materials aimed to assist in drug delivery (but also in other medical applications such as when used as scaffolds in tissue engineering) should be nonimmunogenic, as in the case of human albumin, but also nonreactive. At some extent, these are not matching properties since human proteins, being nonimmunogenic, have evolved to perform multiple interactions. On the other hand, nonhuman proteins, lacking strong interactions with components of the human body, should not alter the selectivity conferred by homing peptides (as recently shown with GFP-based constructs[13]), but they might potentially elicit undesired immune responses.

For a proper selection of building blocks for protein materials, a compromise between lack of reactivity and low immunogenicity can be found in the proteome of the nonpathogenic fraction of the human microbiome. In this regard, bacterial cells and their bacteriophages, being usual symbionts of the human body, are especially appealing. In the case of phages, the rising of bacterial strains with multi-resistance to antibiotics has even promoted to reconsider them as promising bacteria killing agents,[14] assuming a moderate immunogenicity acceptable at the regulatory level.[15,16] This assumption, as well as the related set of evidences in this direction supported the entry of several bacteriophage species into clinical trials, for both local and systemic applications, as antimicrobial drugs[17] (see in addition both the ongoing and already completed clinical trials NCT02116010, NCT01818206, and NCT03140085 at https://clinicaltrials.gov/).

Sustained by this concept, we selected several phage and bacterial proteins from the human microbiome (**Figure 1**A), with presumed ability to self-assemble because of their structural roles in the original microorganisms. These proteins were tagged with a hexahistidine tail (H6) for affinity purification from bacterial cell extracts and screened for their ability to self-assemble as nanostructures that should be stable under physiological conditions (namely moderated ionic strength, physiological pH and 37 °C). The selected polypeptides were the *Pseudomonas aeruginosa* HCP1 protein, an element of the type VI secretion system structurally related to the tail protein of phage lambda,[18] the major phage lambda capsid D protein (abbreviated here as PLD,[19]) and P3, a major capsid protein of phage PRD1 (abbreviated here as MCP3,[20]) that infects enterobacteria and that is also a component of the human microbiome[21] (Figure 1A). In their natural sources, all these proteins are found assembled, together with other protein partners, as rod-like structures (HCP1 and PLD proteins) or as members of icosahedral, adenovirus-like protein complexes (MCP3). HCP1-H6, MCP3-H6, and PLD-H6 were all produced in *Escherichia coli* and purified from cell extracts as proteolytically stable full-length fusions (Figure 1B). At this point, we wondered if these proteins, out of their natural context, would still keep their self-organizing properties. At exception of PLD-H6, whose hydrodynamic diameter was compatible with the unassembled monomeric form (<4 nm), the other two proteins spontaneously organized as supramolecular structures with sizes above the renal cut-off, estimated to be around 6–8 nm.[22] HCP1-H6 self-assembled as entities over 8 nm in diameter (Figure 1C,D), compatible with hexameric forms (Figure 1E) in which the protein has been naturally described.[23] On the other hand, MCP3-H6 assembled as structures of 23 nm (Figure 1C,D), over the size of the natural oligomers (Figure 1E). No differences in bacterial DNA content were observed, that might have accounted for a differential propensity to form protein complexes. Z potential was negative in all cases (Figure 1D) and far from aggregation-prone values. The molecular masses determined by MALDI-TOF were also congruent with the electrophoretic mobility of the proteins (Figure 1B,D). As a reference of the molecular size, 3D models of monomers and the natural oligomeric forms of these proteins are shown in Figure 1E.

When screening parameters potentially involved in the formation of supramolecular protein complexes, and therefore, useful to control the oligomerization process, temperature was considered as an important modulator.[24] Importantly, any protein complex should be stable at the body temperature as a necessary condition for its potential clinical use. The nanoparticles formed by HCP1-H6 were stable at 37 °C and distinguishable from microscale aggregates occurring at higher temperatures (**Figure 2**A). In contrast, MCP3-H6 nanoparticles aggregated already at 37 °C, while at this temperature PLD-H6 remained unassembled but nanoparticles were formed at 50 °C (Figure 2A). To check the temperature dependence of PLD-H6 assembly, this protein was incubated at progressively growing temperatures and the size of the resulting materials were checked in each step. As observed (Figure 2B), oligomerization of this protein started at around 40 °C and the nanoparticles remained assembled under further heating but also when cooling back to 10 °C (Figure 2B). This was indicative of an irreversible assembly process, that boosted by temperature rendered supramolecular materials stable at physiological conditions. In this context, the CD analysis of PLD-H6 (Figure S1, Supporting Information) revealed a more stable alpha helix

Dr. M. Łoś
Department of Bacterial Molecular Genetics
Faculty of Biology
University of Gdansk
Wita Stwosza Street 59, Gdansk 80–308, Poland
Dr. M. Łoś
Phage Consultants
Partyzantow Street 10/18, Gdansk 80-254, Poland

© 2020 WILEY-VCH Verlag GmbH & Co. KGaA, Weinheim

ADVANCED SCIENCE NEWS
www.advancedsciencenews.com

NANO · MICRO small
www.small-journal.com

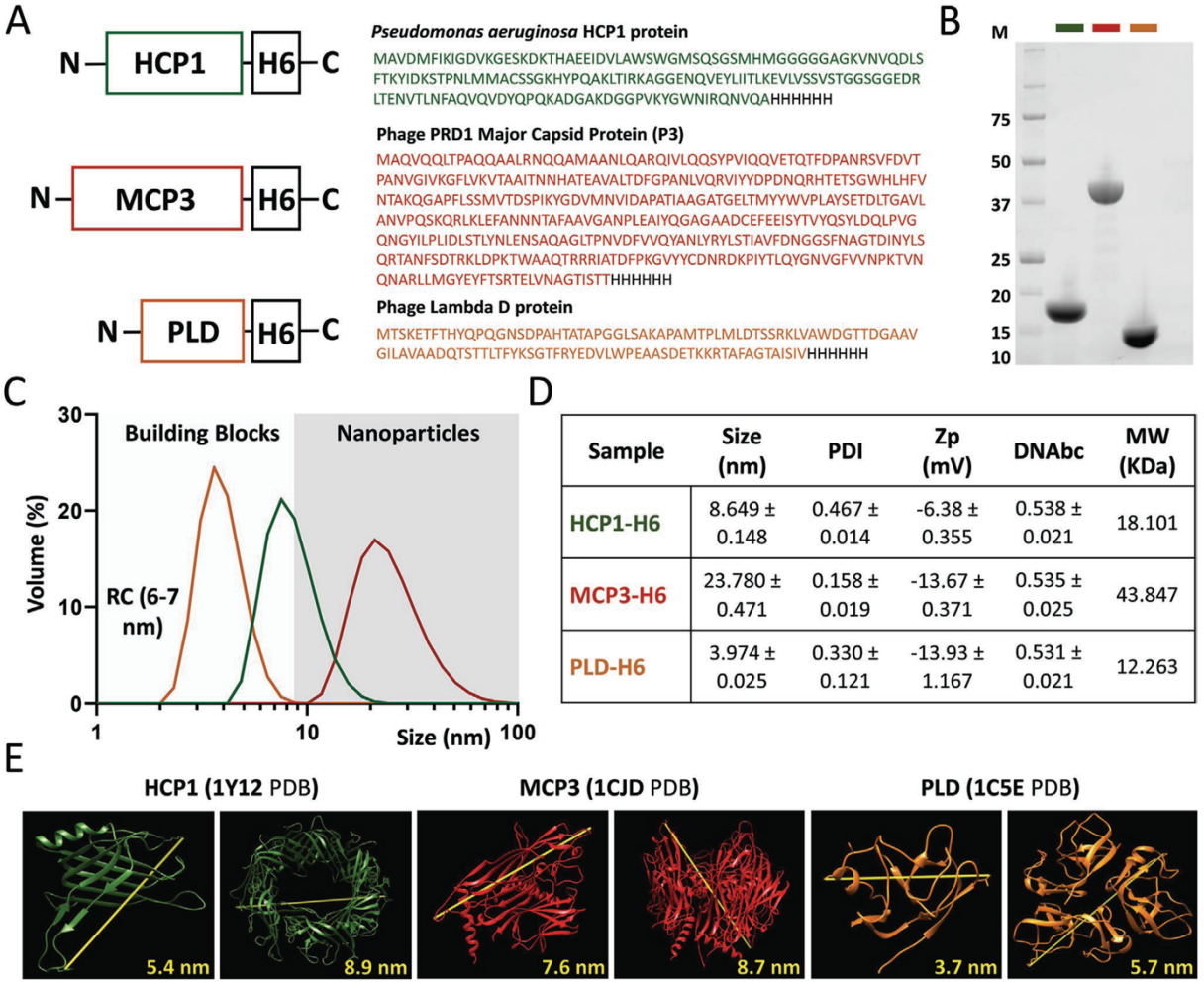

Sample	Size (nm)	PDI	Zp (mV)	DNAbc	MW (KDa)
HCP1-H6	8.649 ± 0.148	0.467 ± 0.014	-6.38 ± 0.355	0.538 ± 0.021	18.101
MCP3-H6	23.780 ± 0.471	0.158 ± 0.019	-13.67 ± 0.371	0.535 ± 0.025	43.847
PLD-H6	3.974 ± 0.025	0.330 ± 0.121	-13.93 ± 1.167	0.531 ± 0.021	12.263

Figure 1. Physicochemical characterization of H6-tagged recombinant proteins. A) Modular organization and amino acid sequences of the fusion proteins, from the amino (N) to the carboxy (C) termini. In color we indicate the protein segment from the original source, and in black, the H6 tail. Box sizes are only approximate. B) Immunodetection of the constructs through Western Blot (WB) upon affinity purification. M indicates the masses of the molecular weight marker, in KDa. C) Size distribution of pure H6-tagged HCP1, MCP3, and PLD proteins in their corresponding buffer is represented as Gaussian plots. The Renal Clearance Threshold or RC (around 8 nm[22]) is presented in pale gray and nanoparticle (NP) formation over this value, in dark gray. D) Relevant physicochemical parameters of purified proteins, namely size in nm and their corresponding Polydispersion Indexes (PDI), surface charge expressed by Zeta potential (Z_p) in mV and bicatenary DNA (DNAbc) content obtained from ratio (A_{260}/A_{280}) (values below 0.57 correspond to nearly 0% DNA content). The experimental molecular weight (MW) in kDa, obtained from MALDI-TOF assays, is also indicated. E) The monomeric as well as the trimeric or hexameric respective structures of all proteins are depicted as deposited in RCSB. MCP3 (pdb 1CJD) and PLD (pdb 1C5E) are naturally trimeric, while HCP1 (pdb 1Y12) forms hexamers.[36] Yellow lines and numbers indicate the maximum diameter of these proteins and complexes.

structure upon heating, as the two alpha helix minima became then evident (one noticeable minimum at 208 nm and an incipient one at 220 nm) simultaneous to the nanoparticle formation. The formation of these nanoparticles was observed in a wide range of protein concentrations, namely between 0.05 and 11 mg mL^{-1} (not shown), proving to be an event different from plain protein aggregation that is highly dependent on protein concentration.

On the other hand, and to test if the aggregation of MCP3-H6 at 37 °C could be prevented, we added Zn^{2+} to protein samples. Generically, divalent ions are stabilizers of protein-protein interactions mediated by histidine residues, and this principle has been recently used for the in vitro generation of protein clusters at the micro scale, using hexahistidine-tagged proteins as building blocks.[25] Indeed, physiological amounts of Zn^{2+} were able to prevent temperature- mediated aggregation of MCP3-H6 (Figure 2C), rendering stable nanoparticles of around 45 nm at 37 °C. Aggregation was then only observed at around 50 °C, far from the clinically relevant temperature range. Interestingly, Zn^{2+} had a stabilizing effect over the three tested proteins (Figure 2E), proving the effectiveness of divalent ions in regulating protein-protein contacts. The proper selection

© 2020 WILEY-VCH Verlag GmbH & Co. KGaA, Weinheim

ADVANCED SCIENCE NEWS
www.advancedsciencenews.com

NANO · MICRO small
www.small-journal.com

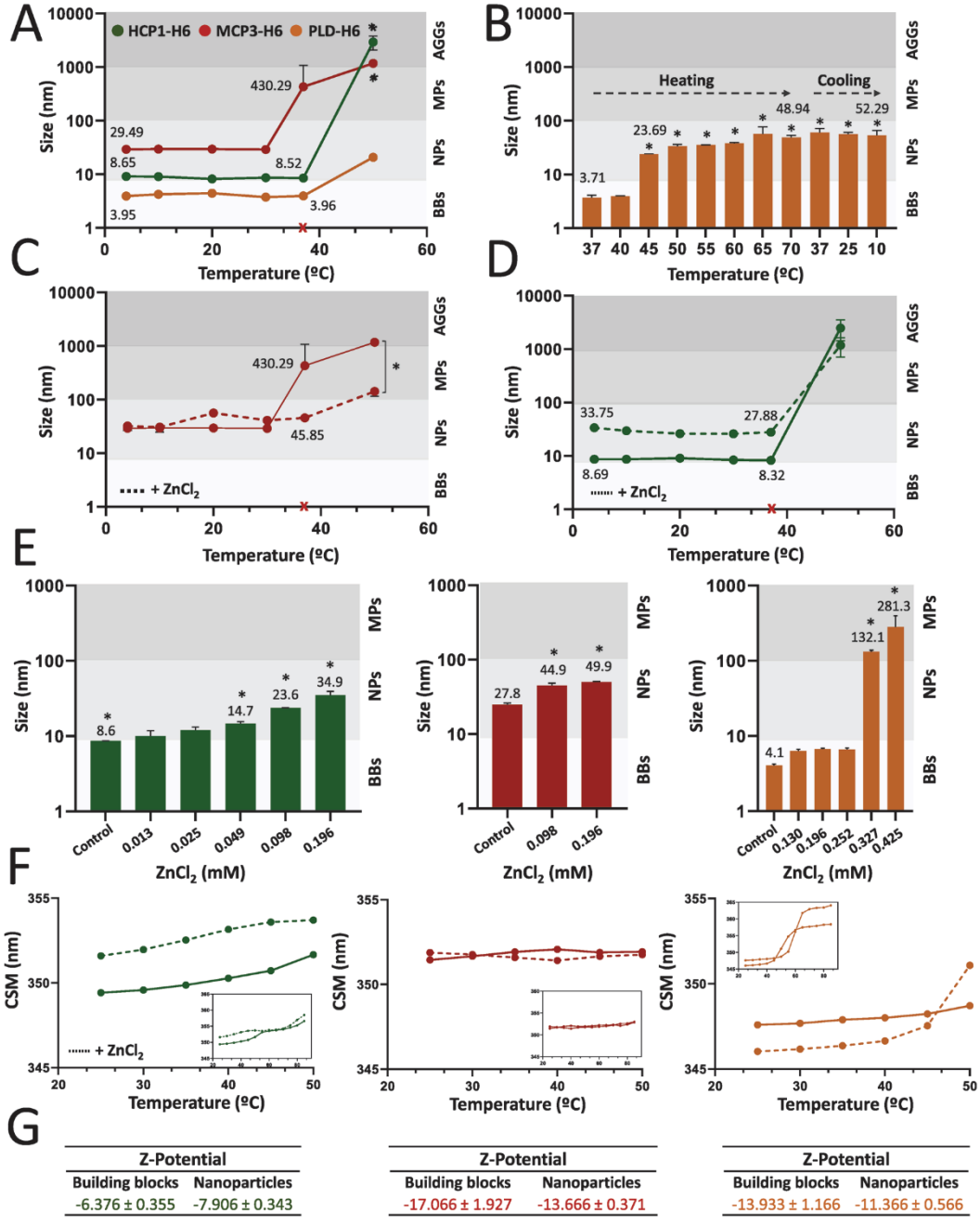

Figure 2. Protein rearrangements into oligomerized nanoscale forms. A) Size analysis of protein constructs HCP1-H6 (in green), MCP3-H6 (in red) and PLD-H6 (in orange) under increasing temperature (from 4 to 50 °C). B) Size analysis of PLD-H6 after initial heating (from 37 to 70 °C) and subsequent cooling (from 70 to 10 °C), expressed in both cases with discontinuous arrows. C) Size analysis of MCP3-H6 under increasing temperature (from 4 to 50 °C) in p/a of 0.2×10^{-3} M of $ZnCl_2$. D) Size analysis of HCP1-H6 under increasing temperature (from 4 to 50 °C) in p/a of 0.2×10^{-3} M of $ZnCl_2$. The red x in panels (A,C,D) refers to 37 °C, as a reference to the body temperature (BT). E) Size analysis of recombinant proteins after increasing concentrations of $ZnCl_2$ (from 0.013 to 0.425×10^{-3} M) at room temperature (25 °C). F) Centre of Spectral Mass (CSM) study under increasing temperature (from 25 to 50 °C) in p/a of 0.2×10^{-3} M of $ZnCl_2$. Small panels correspond to the same analysis under an extended temperature range (from 25 to 87 °C). G) Z-potential determination comparing the monomeric and nanoparticulated proteins forms. Plots are arranged in four different strata according to the material size range. Pale gray corresponds to Building Blocks (BBs), semi-pale gray to Nanoparticles (NPs), semi-strong gray to Microparticles (MPs) and strong gray to Aggregates (AGGs). Data are expressed as $\bar{x} \pm$ SEM, $n = 3$ and the statistical comparisons in relation to the starting size ($^*p < 0.05$).

© 2020 WILEY-VCH Verlag GmbH & Co. KGaA, Weinheim

ADVANCED SCIENCE NEWS
www.advancedsciencenews.com

NANO · MICRO small
www.small-journal.com

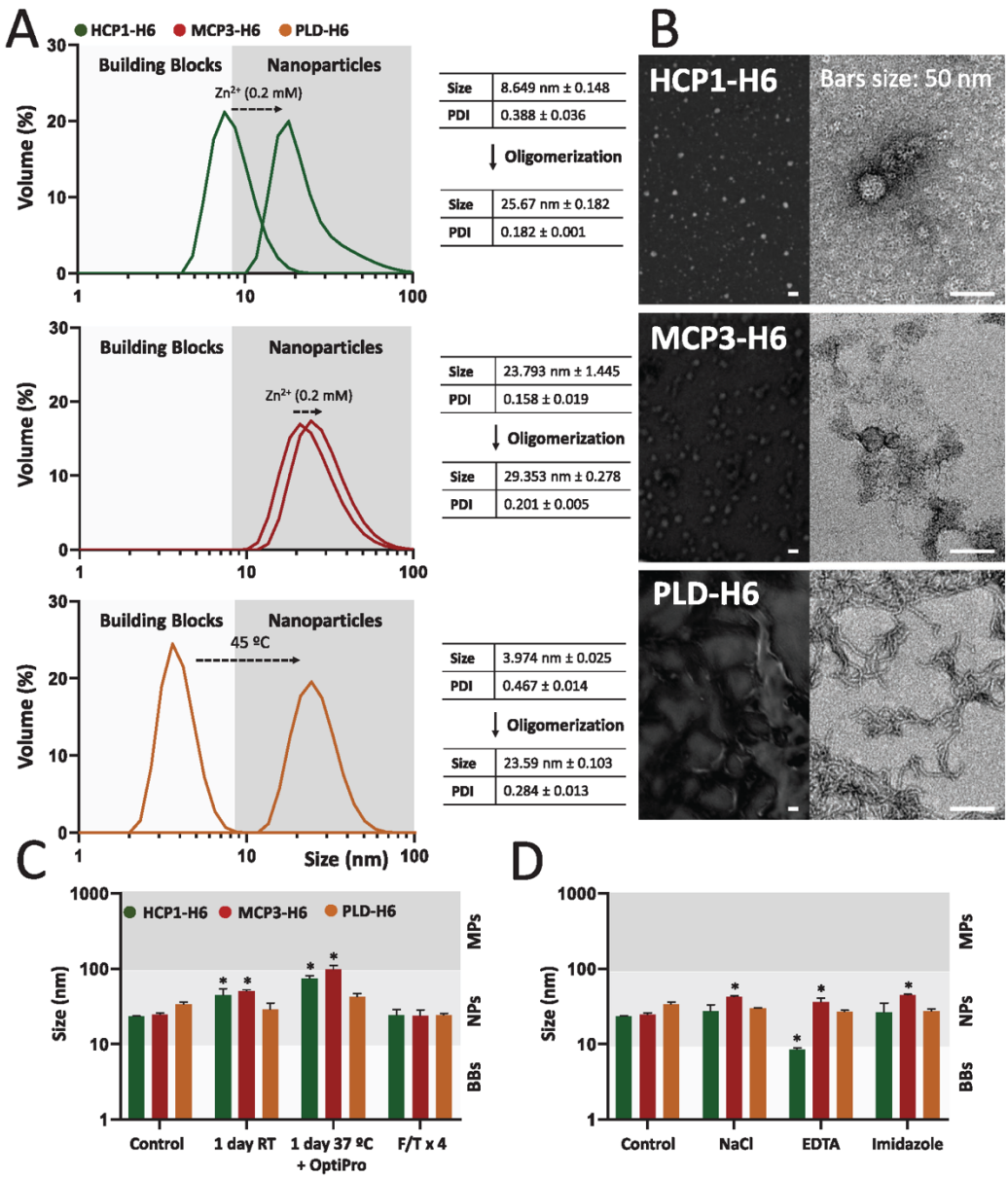

Figure 3. Oligomerization conditions and stability of nanoparticles. A) Size analysis of recombinant proteins after $ZnCl_2$ addition or temperature application. Size and PDI data are expressed in right panels. B) Visualization of previous oligomeric structures through FESEM (left) and TEM (right). C) Size analysis of all three oligomers in different temperature and complex cell medium conditions. RT corresponds to room temperature and F/T to freezing and thawing. D) The same size analysis of panel (A) but in presence of different chemical compounds such as salt (333×10^{-3} M), EDTA and imidazole at 0.2×10^{-3} M. Plots are arranged in three different strata according to the material size range. In C and D, pale gray corresponds to Building Blocks (BBs) and strong grey to Nanoparticles (NPs). Data expressed as $\bar{x} \pm$ SEM, $n = 3$ for panel (A). Data expressed as $\bar{x} \pm$ SEM, $n = 3$ and statistical comparison in relation to the control group for panels (C,D) ($*p < 0.05$).

of Zn^{2+} concentrations, always within physiological values, permitted not only preventing aggregation but also tuning the size of the supramolecular complexes (Figure 2E). At high doses, the metal promoted the collapse of PLD-H6 into aggregates (Figure 2E), probably by enhancing cross-molecular contacts above those supporting a regular supramolecular organization, in agreement with previous data.[26] Also, the optimal size range for drug delivery (between 20 and 80 nm, depending on the experimental settings) was maintained in the resulting nanoparticles, even under increasing temperatures as observed for HCP1-H6 (Figure 2D).[1,7,27] It must be noted that PLD-H6 was less responsive than the alternative constructs to size tuning.

On the other side, Zn^{2+} promoted protein oligomerization through conformational changes in the whole protein

© 2020 WILEY-VCH Verlag GmbH & Co. KGaA, Weinheim

ADVANCED SCIENCE NEWS
www.advancedsciencenews.com

NANO · MICRO small
www.small-journal.com

nanoparticles ($CSM_{+ZnCl_2} \neq CSM_{-ZnCl_2}$) (Figure 2F). Such conformational modifications were remarkable in HCP1-H6 but almost negligible for MCP3-H6, which showed the highest stability (CSM values almost unchanged). The modest increase in the CSM values of HCP1-H6 and PLD-H6 versus temperature (up to 45 °C) suggested a notable stability (Figure 2F). The presence of Zn^{2+} did not affect the whole thermal profile of any of the protein complexes (Figure 2F, insets), and the Z potential was not modified during oligomerization (Figure 2G).

A summary of optimal temperature and Zn^{2+} concentrations for the nanoscale organization of these three proteins is presented in **Figure 3**A. Interestingly, the stabilized HCP1-H6 and MCP3-H6 proteins rendered regular, discrete nanoparticles with a toroid disposition (Figure 3A,B) and compatible with their natural oligomeric forms (Figure 1E). Note that PLD-H6 generated, instead, short fibril-like structures (Figure 3B). Since amphiphilicity was not particularly evident in any of the involved proteins, their assembly would be not linked to such property (Figure S2, Supporting Information). In addition, the materials did not disassemble when incubated at 37 °C in complex cell media, neither in consecutive freezing or thawing conditions (Figure 3C), although a slight increase in the hydrodynamic size was observed. Interestingly, imidazole, known to softly disrupt histidine-based cross-interactions,[28] was also unable to disassemble the nanoparticles, and EDTA, known as a strong divalent cation chelating agent,[29] only compromised the stability of HCP1-H6 oligomers (Figure 3D). Altogether, these data indicated that Zn^{2+} contributed to the formation of the oligomers and at least partially, to their stability (Figures 2 and 3) in form of a cross-linking agent.

Protein assemblies at the nanoscale, acting as mimetics of viral capsids, are of emerging interest in nanomedicine as drug delivery systems and for applications in theragnostics because of the easy manipulability, functionality and intrinsic biocompatibility of such macromolecules.[30] However, for systemic uses, limited immunogenicity and specially poor or null reactivity with human body components are desired. Such combination of parameters cannot be accomplished by human proteins, which while devoid of immunogenicity are highly interactive with multiple ligands in the body. Components of the non-pathogenic human microbiome are particularly appealing since they are in close contact with human populations and expected to be well produced in recombinant versions as assembly-prone materials. Although whole phages or phage-derived virus-like particles have been already tested as drug carriers,[31] the differential immunogenicity exhibited by individual phage proteins[16] strongly pushes toward the construction of materials based on single selected protein species. In this context, we have tested here three microbial structural proteins with potential for self-assembling (Figure 1). We have also demonstrated how the precise but simple control of temperature and Zn^{2+} ion concentration (Figure 2) is sufficient to promote the formation of robust nanoscale structures at a wide range of protein concentrations, fully stable at the body temperature and in complex media (Figure 3) and completely different from plain protein aggregates that show microscale dimensions (Figure 2). Interestingly, Zn^{2+} is involved in the formation of robust supramolecular constructs (Figures 2C–E and 3A,D) in a concentration-dependent way (Figure 2E). Such architectonic role is specifically relevant in the case of HCP1-H6, as the oligomers formed by this construct were disassembled by EDTA through Zn^{2+} removal (Figure 3D). This can be due to the metal coordination regulating the positioning of the building blocks in the oligomers through cross-interactions with the H6 tails of HCP1-H6. Then, the metal itself appears to be an important architectonic agent. Interestingly, Zn^{2+} is also observed as a stabilizer of the materials since it prevented aggregation of MCP3-H6 at 37 °C (Figure 2C). Interestingly, in the case of PLD-H6 and irrespective of the role of Zn^{2+} (Figure 2E), the formation of stable nanoparticles is achieved through an energy influx in form of heat.

In summary, we propose here a new conceptual approach to generate biologically inert protein scaffold materials in the nanoscale, with potential for clinical applications. This concept is based on the use of protein components of the human microbiome with poor or null reactivity with human cells and tissues, that once assembled might serve as nanoscale drug vehicles for cell-targeted drug delivery. Such strategy benefits from the huge catalogue of structural proteins abounding in the phage fraction of the microbiome, which is progressively identified. The three proteins selected here are just a representative sample of such spectrum of potential building blocks, but they illustrate how the natural tendency to form nanostructures can be modulated, out of their natural context, by simple physicochemical methods. Among the strategies to generate protein nanoscale materials,[1,2,32] the microbiome-based approach is of special interest because the construction of supramolecular complexes based on structural microbial proteins does not require a fully *the novo* architectonic design but instead, it is supported by their oligomerization-prone nature.

Experimental Section

Protein Genetic Design, Production, and Purification: All protein sequences were designed as codon-optimized genes and cloned into pET22b by using NdeI and HindIII restriction enzymes. The recombinant plasmids were provided by GeneArt (ThermoFisher) and transformed into *E. coli* Origami B (BL21, OmpT–, Lon–, TrxB, Gor–; Novagen) by heat shock at 42 °C for 45 s. All encoded proteins were produced overnight at 20 °C at 250 rpm agitation, upon addition of 0.1×10^{-3} M isopropyl-β-d-thiogalactopyronaside (IPTG) when the OD_{550} reached 0.5–0.7. Cells were harvested by centrifugation at 5000 g, at 4 °C for 15 min and stored at −80 °C. For protein recovery, pellets were thawed and resuspended in wash buffer (20×10^{-3} M Tris HCl, 500×10^{-3} M NaCl, 10×10^{-3} M Imidazole, pH = 8.0) in presence of protease inhibitors (complete EDTA-free; Roche Diagnostics). Cell disruption was achieved in two rounds in a French Press (Thermo FA-078) at 1200 psi. The soluble fraction was then separated by centrifugation at 4 °C, 15 000 *g* for 45 min and the supernatant consecutively filtered through 0.45 and 0.22 µm pore filters. Proteins were purified by Immobilized Metal Affinity Chromatography (IMAC) in an ÄKTA pure system (GE Healthcare) using 5 mL HisTrap columns (GE Healthcare). Protein elution was achieved by a linear gradient of Elution buffer (20×10^{-3} M Tris HCl, 500×10^{-3} M NaCl, 500×10^{-3} M Imidazole, pH = 8.0) and the rinsed protein was dialyzed against both sodium carbonate (166×10^{-3} M $NaCO_3H$, pH = 8.0) or sodium carbonate with salt (166×10^{-3} M $NaCO_3H$ + 333×10^{-3} M NaCl, pH = 8.0) buffers.

Protein Purity, Concentration and Integrity: Protein purity was assessed by using a 12% TGX Stain-Free FastCast Acrylamide Kit (BioRad). After electrophoresis, protein bands were subsequently transferred by Trans-Blot Turbo Transfer System (BioRad) into PVDF membranes

© 2020 WILEY-VCH Verlag GmbH & Co. KGaA, Weinheim

ADVANCED SCIENCE NEWS
www.advancedsciencenews.com

NANO · MICRO small
www.small-journal.com

and immunodetected with an anti-His (Santa Cruz Biotechnology) monoclonal antibody. Protein concentration was determined by Bradford assay and their integrity checked by Matrix-assisted Laser Desorption Ionization Time-of-Flight (MALDI-TOF) mass spectrometry.

Volume Size Distribution, Surface Charge, and Ultrastructural Morphometry: The hydrodynamic diameter of proteins was determined by Dynamic Light Scattering (DLS), and protein surface charge, expressed as Z-potential (Zp) in mV, by Electrophoretic Light Scattering (ELS), both at 633 nm, in a Zetasizer Nano ZS using ZEN2112 3 mm quartz batch cuvettes and DTS10170 capillary cells, respectively, at 25 °C. The Polydispersion Index (PDI) was determined for all samples. Protein samples were deposited in silicon wafers for field emission scanning electron microscopy (FESEM)[13] and negatively stained for transmission electron microscopy (TEM).[34] Imaging was performed as previously described.[33]

DNAbc Content: Bicatenary DNA content (DNAbc) was determined from the absorbance ratio between 260 and 280 nm (A_{260}/A_{280}). All measurements were performed in a Nanodrop One System (ThermoFisher).

Oligomerization Status onto Thermal Kinetics: Protein size was analyzed at increasing temperatures (namely 4, 10, 20, 30, 37, and 50 °C) by DLS. Protein concentration was initially adjusted at 2 mg mL^{-1} in all cases.

Zinc-Mediated Protein Assembling: Proteins were exposed to increasing concentrations of $ZnCl_2$ depending on their aggregation or oligomerization tendencies. The size of the resulting materials was subsequently analyzed by DLS and data expressed in nm. Protein concentration was initially tested up to 11 mg mL^{-1} and finally adjusted at 2 mg mL^{-1} in all cases, for a convenient manipulation of ion concentrations at physiological values.

Intrinsic Fluorescence versus Temperature: Fluorescence spectra were recorded in a Cary Eclipse spectrofluorimeter (Agilent Technologies), using a quartz cell with 10 mm path length and a thermostated holder. The excitation and emission slits were set at 5 nm. Excitation wavelength (λ_{ex}) was set at 295 nm. Emission spectra were acquired between 310 and 450 nm in protein samples at 0.2 mg mL^{-1}, dissolved in sodium carbonate buffer with salt. The temperature-dependent behavior of proteins was determined between 25 and 85 °C in p/a of $ZnCl_2$ (0.196×10^{-3} M). The Centre of Spectral Mass (CSM), a weighted average of the fluorescence spectrum peaks, was calculated[34] for comparison. The CSM is also related with the relative exposure of the tryptophan (Trp) to the protein environment. The maximum red-shift in the CSM of Trp is compatible with large solvent accessibility.[35]

Thermal and Chemical Stability: Proteins, in their oligomerized form, were exposed to different temperatures (room temperature, 37 °C and freezing/thawing cycles at −80 °C) and chemical compounds (NaCl, EDTA, imidazole at 0.2×10^{-3} M final concentration and OptiPro complex cell culture media). The size of protein constructs was subsequently analyzed by DLS and data expressed in nm. Protein concentration was initially adjusted at 2 mg mL^{-1} in all cases.

Circular Dichroism: Far-UV circular dichroism (CD) was measured at 25 °C in a Jasco J-715 spectropolarimeter to assess secondary structure. Protein concentration was adjusted to 0.2 mg mL^{-1} in 166×10^{-3} M carbonate-bicarbonate, at pH 8. The CD spectra were obtained with a 0.2 mm pathlength cuvette over a wavelength range of 190–240 nm. The scan rate was 100 nm min^{-1} with a response of 2 s and a bandwidth of 1 nm, and a total of 13 scans were accumulated. The spectra were processed through a negative exponential fit with a sampling proportion of 0.1 and 1 polynomial degree.

In Silico Calculations: UCSF Chimera software was used for in silico representation, structural hydropathicity pattern visualization and theoretical measurement of distances (nm) in X-ray 3D diffraction structures of proteins. The data set was extracted from the Protein Data Bank Database (PDB) and the corresponding codes were 1Y12 for HCP1, 1CJD for MCP3 and 1C5E for PLD. The resulting analysis illustrates the sterical and physicochemical nature of protein building blocks.

Statistical Analysis: Quantitative data were expressed as mean ($\bar{x}$) ± Standard Error of the Mean (SEM) and all measurements were performed at least in triplicate ($n = 3$). In all cases, an initial normality and lognormality analyses were performed including Anderson–Darling, D'Agostino and Pearson, Shapiro–Wilk and Kolmogorov–Smirnov tests to determine the normal distribution (behavior). The parametric data were analyzed by one or two-ways ANOVA or *t*-tests depending on the number of groups and conditions. The nonparametric data were analyzed by Kruskal–Wallis tests. All comparisons were performed in relation to either the control group or the initial temperature ($^*p < 0.05$).

Supporting Information

Supporting Information is available from the Wiley Online Library or from the author.

Acknowledgements

The authors are indebted to Agencia Estatal de Investigación (AEI) and to Fondo Europeo de Desarrollo Regional (FEDER) (Grant BIO2016-76063-R, AEI/FEDER, UE) to A.V., AGAUR (2017SGR-229) to A.V. and CIBER-BBN (project NANOPROTHER) granted to A.V. The authors are also indebted to the Networking Research Center on Bioengineering, Biomaterials and Nanomedicine (CIBER-BBN) that is an initiative funded by the VI National R&D&I Plan 2008–2011, Iniciativa Ingenio 2010, Consolider Program, CIBER Actions and financed by the Instituto de Salud Carlos III, with assistance from the European Regional Development Fund. Protein production has been partially performed by the ICTS "NANBIOSIS," more specifically by the Protein Production Platform of CIBER in Bioengineering, Biomaterials & Nanomedicine (CIBER-BBN)/IBB, at the UAB sePBioEs scientific-technical service (http://www.nanbiosis.es/portfolio/u1-protein-production-platform-ppp/) and the nanoparticle size analysis by the Biomaterial Processing and Nanostructuring Unit. Electron microscopy studies were performed by the Servei de Microscòpia in the UAB. Molecular graphics and analyses were performed with UCSF Chimera, developed by the Resource for Biocomputing, Visualization, and Informatics at the University of California, San Francisco, with support from NIH P41- GM103311. A.V. received an ICREA ACADEMIA award. U.U. is supported by Miguel Servet fellowship (CP19/00028) from ISCIII (cofounding "Fondo Social Europeo"). L.S.-G. and H.L.-L. were supported by a predoctoral fellowship from AGAUR (2018FI_B2_00051 and 2019FI_B00352, respectively) and E.V.D. by a predoctoral fellowship from Ministerio de Ciencia, Innovación y Universidades (FPU18/04615).

Conflict of Interest

The authors declare no conflict of interest.

Keywords

microbiome, nanoparticles, protein engineering, protein materials, self-assembling proteins

Received: March 22, 2020
Revised: May 13, 2020
Published online:

[1] D. Verma, N. Gulati, S. Kaul, S. Mukherjee, U. Nagaich, *J. Pharm.* **2018**, 9285854.

© 2020 WILEY-VCH Verlag GmbH & Co. KGaA, Weinheim

ADVANCED SCIENCE NEWS
www.advancedsciencenews.com

NANO · MICRO small
www.small-journal.com

[2] H. M. G. Sutherland, T. D. Rapson, J. S. Church, in *Fibrous Proteins: Structures and Mechanisms*, Vol. *82* (Eds: D A. D. Parry, J. Squire), Springer, Cham **2017**.
[3] a) G. Wei, Z. Su, N. P. Reynolds, P. Arosio, I. W. Hamley, E. Gazit, R. Mezzenga, *Chem. Soc. Rev.* **2017**, *46*, 4661; b) M. Abbas, Q. Zou, S. Li, X. Yan, *Adv. Mater.* **2017**, *29*, 1605021; c) Z. Wang, K. Zhi, Z. Ding, Y. Sun, S. Li, M. Li, K. Pu, J. Zou, *Semin. Cancer Biol.* **2020**, https://doi.org/10.1016/j.semcancer.2019.11.012; d) I. Casanova, U. Unzueta, I. Arroyo-Solera, M. V. Cespedes, A. Villaverde, R. Mangues, E. Vazquez, *Curr. Opin. Pharmacol.* **2019**, *47*, 1.
[4] L. Sanchez-Garcia, L. Martin, R. Mangues, N. Ferrer-Miralles, E. Vazquez, A. Villaverde, *Microb. Cell Fact.* **2016**, *15*, 33.
[5] E. Vazquez, R. Mangues, A. Villaverde, *Nanomedicine* **2016**, *11*, 1333.
[6] K. Ozturk-Atar, H. Eroglu, S. Calis, *J. Drug Targeting* **2018**, *26*, 633.
[7] S. Raj, S. Khurana, R. Choudhari, K. K. Kesari, M. A. Kamal, N. Garg, J. Ruokolainen, B. C. Das, D. Kumar, *Semin. Cancer Biol.* **2019**, https://doi.org/10.1016/j.semcancer.2019.11.002.
[8] a) D. Kalyane, N. Raval, R. Maheshwari, V. Tambe, K. Kalia, R. K. Tekade, *Mater. Sci. Eng., C* **2019**, *98*, 1252; b) M. S. Lee, E. C. Dees, A. Z. Wang, *Oncology* **2017**, *31*, 198; c) A. Nel, E. Ruoslahti, H. Meng, *ACS Nano* **2017**, *11*, 9567.
[9] a) A. M. Sofias, M. Dunne, G. Storm, C. Allen, *Adv. Drug Delivery Rev.* **2017**, *122*, 20; b) W. J. Gradishar, *Expert Opin. Pharmacother.* **2006**, *7*, 1041.
[10] M. R. Green, G. M. Manikhas, S. Orlov, B. Afanasyev, A. M. Makhson, P. Bhar, M. J. Hawkins, *Ann. Oncol.* **2006**, *17*, 1263.
[11] B. Bhushan, V. Khanadeev, B. Khlebtsov, N. Khlebtsov, P. Gopinath, *Adv. Colloid Interface Sci.* **2017**, *246*, 13.
[12] a) K. W. Lexa, E. Dolghih, M. P. Jacobson, *PLoS One* **2014**, *9*, 93323; b) V. Arroyo, R. Garcia-Martinez, X. Salvatella, *J. Hepatol.* **2014**, *61*, 396; c) M. Taverna, A. L. Marie, J. P. Mira, B. Guidet, *Ann. Intensive Care* **2013**, *3*, 4; d) B. K. I. Meijers, B. Bammens, K. Verbeke, P. Evenepoel, *Am. J. Kidney Dis.* **2008**, *51*, 839; e) L. Philbert, W. Xiaoyang, *Curr. Pharm. Des.* **2015**, *21*, 1862.
[13] M. V. Cespedes, U. Unzueta, A. Avino, A. Gallardo, P. Alamo, R. Sala, A. Sanchez-Chardi, I. Casanova, M. A. Mangues, A. Lopez-Pousa, R. Eritja, A. Villaverde, E. Vazquez, R. Mangues, *EMBO Mol. Med.* **2018**, *10*, 8772.
[14] a) F. L. Gordillo Altamirano, J. J. Barr, *Clin. Microbiol. Rev.* **2019**, *32*; b) S. Hesse, S. Adhya, *Annu. Rev. Microbiol.* **2019**, *73*, 155.
[15] a) O. Krut, I. Bekeredjian-Ding, *J. Immunol.* **2018**, *200*, 3037; b) C. J. Cooper, M. Khan Mirzaei, A. S. Nilsson, *Front. Microbiol.* **2016**, *7*, 1209.
[16] K. Dabrowska, P. Miernikiewicz, A. Piotrowicz, K. Hodyra, B. Owczarek, D. Lecion, Z. Kazmierczak, A. Letarov, A. Gorski, *J. Virol.* **2014**, *88*, 12551.
[17] a) L. L. Furfaro, M. S. Payne, B. J. Chang, *Front. Cell. Infect. Microbiol.* **2018**, *8*, 376; b) J. Gabard, P Jault, in *Phage Therapy: A Practical Approach*, Springer, Cham, Switzerland **2019**, p. 147.
[18] A. Zoued, Y. R. Brunet, E. Durand, M. S. Aschtgen, L. Logger, B. Douzi, L. Journet, C. Cambillau, E. Cascales, *Biochim. Biophys. Acta, Mol. Cell Res.* **2014**, *1843*, 1664.
[19] S. V. Rajagopala, S. Casjens, P. Uetz, *BMC Microbiol.* **2011**, *11*, 213.
[20] S. D. Benson, J. K. Bamford, D. H. Bamford, R. M. Burnett, *Acta Crystallogr., Sect. D: Biol. Crystallogr.* **2002**, *58*, 39.
[21] S. Mantynen, L. R. Sundberg, H. M. Oksanen, M. M. Poranen, *Viruses* **2019**, *11*, 76.
[22] Y. Lu, Z. Gu, *Nat. Nanotechnol.* **2017**, *12*, 1023.
[23] J. D. Mougous, M. E. Cuff, S. Raunser, A. Shen, M. Zhou, C. A. Gifford, A. L. Goodman, G. Joachimiak, C. L. Ordonez, S. Lory, T. Walz, A. Joachimiak, J. J. Mekalanos, *Science* **2006**, *312*, 1526.
[24] J. Wang, K. Liu, R. Xing, X. Yan, *Chem. Soc. Rev.* **2016**, *45*, 5589.
[25] a) J. Sánchez, H. López-Laguna, P. Álamo, N. Serna, A. Sánchez-Chardi, V. Nolan, O. Cano-Garrido, I. Casanova, U. Unzueta, E. Vazquez, R. Mangues, A. Villaverde, *Adv. Sci.* **2020**, *7*, 1902420; b) W. Huang, P. Hao, J. Qin, S. Luo, T. Zhang, B. Peng, H. Chen, X. Zan, *Acta Biomater.* **2019**, *90*, 441; c) T. Y. Chen, W. J. Cheng, J. C. Horng, H. Y. Hsu, *Colloids Surf., B* **2019**, *187*, 110644.
[26] H. Lopez-Laguna, U. Unzueta, O. Conchillo-Sole, A. Sanchez-Chardi, M. Pesarrodona, O. Cano-Garrido, E. Volta, L. Sanchez-Garcia, N. Serna, P. Saccardo, R. Mangues, A. Villaverde, E. Vazquez, *Acta Biomater.* **2019**, *83*, 257.
[27] a) L. Deng, Z. Feng, H. Deng, Y. Jiang, K. Song, Y. Shi, S. Liu, J. Zhang, S. Bai, Z. Qin, A. Dong, *ACS Appl. Mater. Interfaces* **2019**, *11*, 31743; b) G. P. Howard, G. Verma, X. Ke, W. M. Thayer, T. Hamerly, V. K. Baxter, J. E. Lee, R. R. Dinglasan, H.-Q. Mao, *Nano Res.* **2019**, *12*, 837; c) L. Shang, K. Nienhaus, G. U. Nienhaus, *J. Nanobiotechnol.* **2014**, *12*, 5; d) N. P. Truong, M. R. Whittaker, C. W. Mak, T. P. Davis, *Expert Opin. Drug Delivery* **2015**, *12*, 129.
[28] U. Unzueta, N. Serna, L. Sanchez-Garcia, M. Roldan, A. Sanchez-Chardi, R. Mangues, A. Villaverde, E. Vazquez, *Nanotechnology* **2017**, *28*, 505102.
[29] J. B. Bailey, R. H. Subramanian, L. A. Churchfield, F. A. Tezcan, *Methods Enzymol.* **2016**, *580*, 223.
[30] a) A. Chaudhary, R. D. Yadav, *J. Nanopart. Res.* **2019**, *21*, 254; b) S. Sikder, V. Gote, M. Alshamrani, J. Sicotte, D. Pal, *Curr. Opin. Struct. Biol.* **2019**, *55*, 77; c) K. A. Cannon, J. M. Ochoa, T. O. Yeates, *Curr. Opin. Struct. Biol.* **2019**, *55*, 77; d) Y. Li, Y. Wang, G. Huang, J. Gao, *Chem. Rev.* **2018**, *118*, 5359; e) A. Maham, Z. Tang, H. Wu, J. Wang, Y. Lin, *Small* **2009**, *5*, 1706; f) U. Unzueta, M. V. Cespedes, E. Vazquez, N. Ferrer-Miralles, R. Mangues, A. Villaverde, *Trends Biotechnol.* **2015**, *33*, 253.
[31] a) Y. Ma, R. J. Nolte, J. J. Cornelissen, *Adv. Drug Delivery Rev.* **2012**, *64*, 811; b) M. Karimi, H. Mirshekari, S. M. Moosavi Basri, S. Bahrami, M. Moghoofei, M. R. Hamblin, *Adv. Drug Delivery Rev.* **2016**, *106*, 45.
[32] a) A. P. M. Guttenplan, L. J. Young, D. Matak-Vinkovic, C. F. Kaminski, T. P. J. Knowles, L. S. Itzhaki, *J. Nanobiotechnol.* **2017**, *15*, 70; b) T. O. Yeates, *Annu. Rev. Biophys.* **2017**, *46*, 23; c) T. D. Sutherland, M. G. Huson, T. D. Rapson, *J. Struct. Biol.* **2018**, *201*, 76; d) I. W. Hamley, *Biomacromolecules* **2019**, *20*, 1829.
[33] O. Cano-Garrido, E. Garcia-Fruitos, A. Villaverde, A. Sanchez-Chardi, *Biotechnol. J.* **2018**, *13*, 1700388.
[34] J. M. Sanchez, L. Sanchez-Garcia, M. Pesarrodona, N. Serna, A. Sanchez-Chardi, U. Unzueta, R. Mangues, E. Vazquez, A. Villaverde, *Biomacromolecules* **2018**, *19*, 3788.
[35] R. Mohana-Borges, J. L. Silva, J. Ruiz-Sanz, G. de Prat-Gay, *Proc. Natl. Acad. Sci. USA* **1999**, *96*, 7888.
[36] Y. R. Brunet, J. Henin, H. Celia, E. Cascales, *EMBO Rep.* **2014**, *15*, 315.

 © 2020 WILEY-VCH Verlag GmbH & Co. KGaA, Weinheim

Study 4

Artificial Inclusion Bodies for Clinical Development

Julieta M. Sánchez*, Hèctor López-Laguna*, Patricia Álamo*, Naroa Serna, Alejandro Sánchez-Chardi, Verónica Nolan, Olivia Cano-Garrido, Isolda Casanova, Ugutz Unzueta, Esther Vázquez, Ramon Mangues, and Antonio Villaverde

Advanced Science 2020 · Impact factor (16.806) · Quartile (Q1) · *Equally contributed

Objective 2

To develop a new and fully transversal biochemical approach to manufacture **protein-based insoluble microparticles** in a well-defined, biocompatible, and cost-effective regulatory compliant manner.

Objective 3.b

To test the biomedical applications of **protein-based insoluble microparticles** in mouse models (Biodistribution).

The development of natural occurring bacterial inclusion bodies (IBs, strategy 2), allowed scientists to create mechanically stable microparticles able to mimic the physiological storage of protein hormones, and to be used as drug delivery systems with a prolonged protein drug release. However, this technology is severely constrained by the lack of reproducibility between batches, biocompatibility concerns (due to bacterial traces), and lack of assembling control, which makes them susceptible to promote non-desired effects on human tissues once implanted.

Thus, this work has been focused on exploring a new well-defined, and simple biochemical approach to manufacture protein-based insoluble microparticles ensuring reproducibility, homogeneity in composition, assembling control and overall biocompatibility. In this regard, the already mentioned histidine tag-divalent cation principle was optimized to reach this aggregation requirements (meaning an increase of divalent cation's concentration during the formulation process) introduced in study 2. The obtained data showed the manufacturing process of the novo insoluble microparticles (so called artificial IBs or Secretory Granules) from pure components which ensure reproducibility, homogeneity, mechanical stability, and that replicates the intrinsic drug delivery functions observed in natural IBs.

By the way, this novel technology has been patented (see Annex 7, patent 2).

COMMUNICATION

ADVANCED SCIENCE Open Access

www.advancedscience.com

Artificial Inclusion Bodies for Clinical Development

Julieta M. Sánchez, Hèctor López-Laguna, Patricia Álamo, Naroa Serna, Alejandro Sánchez-Chardi, Verónica Nolan, Olivia Cano-Garrido, Isolda Casanova, Ugutz Unzueta, Esther Vazquez, Ramon Mangues,* and Antonio Villaverde**

Bacterial inclusion bodies (IBs) are mechanically stable protein particles in the microscale, which behave as robust, slow-protein-releasing amyloids. Upon exposure to cultured cells or upon subcutaneous or intratumor injection, these protein materials secrete functional IB polypeptides, functionally mimicking the endocrine release of peptide hormones from secretory amyloid granules. Being appealing as delivery systems for prolonged protein drug release, the development of IBs toward clinical applications is, however, severely constrained by their bacterial origin and by the undefined and protein-to-protein, batch-to-batch variable composition. In this context, the de novo fabrication of artificial IBs (ArtIBs) by simple, cell-free physicochemical methods, using pure components at defined amounts is proposed here. By this, the resulting functional protein microparticles are intriguing, chemically defined biomimetic materials that replicate relevant functionalities of natural IBs, including mammalian cell penetration and local or remote release of functional ArtIB-forming protein. In default of severe regulatory issues, the concept of ArtIBs is proposed as a novel exploitable category of biomaterials for biotechnological and biomedical applications, resulting from simple fabrication and envisaging soft developmental routes to clinics.

Bacterial inclusion bodies (IBs) are water-insoluble proteinaceous inclusions generated in the cytoplasm of recombinant bacteria,[1,2] stabilized by an amyloid fibril architecture that confers mechanical robustness.[3] They are formed by the transgene protein product plus a diversity of residual macromolecules from bacterial cells, including nucleic acids, carbohydrates, proteins, and cell wall components. Their morphology is defined by mechanical limitations imposed by the bacterial cell wall, usually at the edge of sub-micrometer and micrometer sizes. The biological activity associated to IB proteins,[4] together with the mechanical stability and high porosity of these protein particles has pushed to re-evaluate them as unconventional functional materials with a wide spectrum of applications in biotechnology and biomedicine.[5] Any functional polypeptide suitable for production in bacteria can be engineered to be packaged in form of IBs.[6] This is because IBs show a complex structure with a dual organization of the forming polypeptide chains; while around 40% of the IB protein generates a mechanically stable fibril network, the remaining fraction represents functional or quasi-functional species embedded in such stable structure.[7] This protein population is properly folded, nearly soluble, releasable under physiological conditions, and responsible for the biological activity of IBs.[1] As self-immobilized catalysts, enzyme-based IBs show high level

Dr. J. M. Sánchez, H. López-Laguna, Dr. N. Serna, Dr. O. Cano-Garrido,[+] Dr. E. Vazquez, Prof. A. Villaverde
Institut de Biotecnologia i de Biomedicina
Universitat Autònoma de Barcelona
Bellaterra, 08193 Barcelona, Spain
E-mail: Esther.Vazquez@uab.es; antoni.villaverde@uab.cat

Dr. J. M. Sánchez, Dr. V. Nolan
Instituto de Investigaciones Biológicas y Tecnológicas (IIBYT)
(CONICET-Universidad Nacional de Córdoba)
ICTA & Cátedra de Química Biológica
Departamento de Química
FCEFyN, UNC. Av. Velez Sarsfield 1611, X 5016GCA, Córdoba, Argentina

The ORCID identification number(s) for the author(s) of this article can be found under https://doi.org/10.1002/advs.201902420.

© 2019 The Authors. Published by WILEY-VCH Verlag GmbH & Co. KGaA, Weinheim. This is an open access article under the terms of the Creative Commons Attribution License, which permits use, distribution and reproduction in any medium, provided the original work is properly cited.

[+]Present address: Nanoligent SL, Edifici Eureka, Universitat Autònoma de Barcelona, Bellaterra, 08193 Barcelona, Spain

H. López-Laguna, Dr. N. Serna, Dr. O. Cano-Garrido, Dr. E. Vazquez, Prof. A. Villaverde
Departament de Genètica i de Microbiologia
Universitat Autònoma de Barcelona
Bellaterra, 08193 Barcelona, Spain

H. López-Laguna, Dr. P. Álamo, Dr. N. Serna, Dr. I. Casanova, Dr. U. Unzueta, Dr. E. Vazquez, Prof. R. Mangues, Prof. A. Villaverde
CIBER de Bioingeniería
Biomateriales y Nanomedicina (CIBER-BBN)
28029, Madrid, Spain
E-mail: rmangues@santpau.cat

Dr. P. Álamo, Dr. I. Casanova, Dr. U. Unzueta, Prof. R. Mangues
Biomedical Research Institute Sant Pau (IIB-Sant Pau) and Josep Carreras Research Institute
Hospital de la Santa Creu i Sant Pau
08041, Barcelona, Spain

Dr. A. Sánchez-Chardi
Servei de Microscòpia
Universitat Autònoma de Barcelona
Bellaterra, 08193 Barcelona, Spain

DOI: 10.1002/advs.201902420

ADVANCED SCIENCE NEWS
www.advancedsciencenews.com

ADVANCED SCIENCE Open Access
www.advancedscience.com

of operational stability and reusability.[8] In tissue engineering, they have been adapted as nontoxic topologies that provide a combination of mechanical and biological stimuli for controlled cell proliferation.[9] In a different context, IBs have been tailored as unexpected drug delivery systems or "nanopills,"[10] that mimic the functionalities of the secretory granules of the mammalian endocrine system[11] for the intracellular, local or remote delivery of functional (either untargeted or receptor-targeted) IB protein.[12] Therefore, IBs, as functional biomaterials, show promise in protein replacement therapies and in any clinical uses aimed to systemic, local or precision protein delivery.

The enormous clinical potential of bacterial IBs is, however, darkened by their heterogeneous and undefined composition.[6] Trapping an indeterminate catalogue of bacterial cell materials, clinically oriented IBs would hardly overcome the severe regulatory constraints imposed by medicament agencies. In this context, we wondered whether chemically pure IB mimetic particles (artificial IBs, ArtIBs) could be fabricated in vitro. This would imply the production of particulate microscale protein materials, made of pure and chemically controlled components, which would replicate those functionalities of natural IBs that are relevant to protein delivery. These properties are mechanical stability, absence of intrinsic cytotoxicity, mammalian cell penetrability, and the ability to release functional IB protein upon physiological conditions. Pure protein composition would be added to such functionally rich profile.

To explore the fabrication of synthetic IBs, common laboratory enzymes that form functional IBs during recombinant production, namely, β-galactosidase (β-Gal) and alkaline phosphatase (AP),[13] were selected as models for two alternative approaches to ArtIB fabrication. In one (**Figure 1**a), soluble protein was salted out plus thermally aggregated to generate amyloidal networks, further used as IB-like seeds to recruit and entrap homologous soluble protein versions. This multiple step procedure (ms), was developed to imitate the dual, sponge-like networks in natural IBs.[7] Lipids, common component of bacterial IBs were also incorporated. In a simpler single-step (ss) approach, divalent cations (Zn, in form of $ZnCl_2$), involved in amyloid formation[14] and generically, in protein–protein contacts,[15] were added to a protein solution (Figure 1a). The application of these procedures resulted in mechanically stable, discrete, and moderately disperse protein particles sizing around 1–2 µm (AP) and 2–6 µm (β-Gal) (Figure 1b,c), whose surface rugosity, size variability, and amorphous appearance remembered those of natural IBs (Figure 1b). Both enzymes, in this packaged form, were enzymatically active (Figure 1d). On the other hand, cross-β-sheet amyloid like structure (ALS) was detected by attenuated total reflectance (ATR) in AP ArtIBs at proportions (31–37%, ss and ms, respectively) matching those found in IBs.[7]

Further, we constructed new ArtIBs (**Figure 2**a) formed by the self-assembling modular proteins T22-GFP-H6[16] and

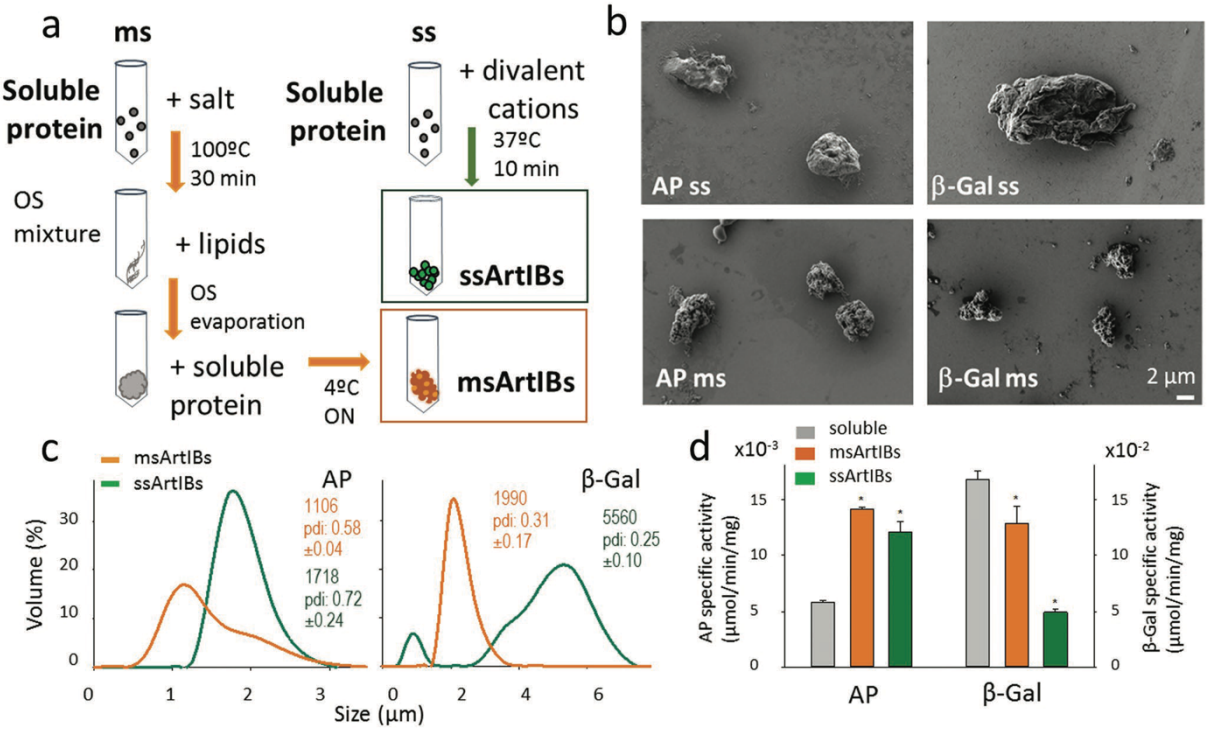

Figure 1. Fabrication of ArtIBs. a) Multiple (ms) and single (ss) step procedures for ArtIB fabrication from soluble pure protein are summarized, indicating the main operational steps (arrows). OS is organic solvent. Precise details can be found in the Experimental Section. Final products are framed. b) Representative field-emission scanning electron microscopy (FESEM) images of AP and β-Gal ArtIBs. Magnifications are equivalent in all images. c) Dynamic light scattering (DLS) size analyses of ArtIBs, indicating the mode (in nm) and the polydispersion index (pdi). d) Specific activity of both AP and β-Gal ArtIBs, compared to that of commercial soluble protein counterpart. Asterisks indicate statistically different from the specific activity of the soluble protein ($p < 0.001$, Holme–Sidak test).

© 2019 The Authors. Published by WILEY-VCH Verlag GmbH & Co. KGaA, Weinheim

ADVANCED SCIENCE NEWS
www.advancedsciencenews.com

ADVANCED SCIENCE Open Access
www.advancedscience.com

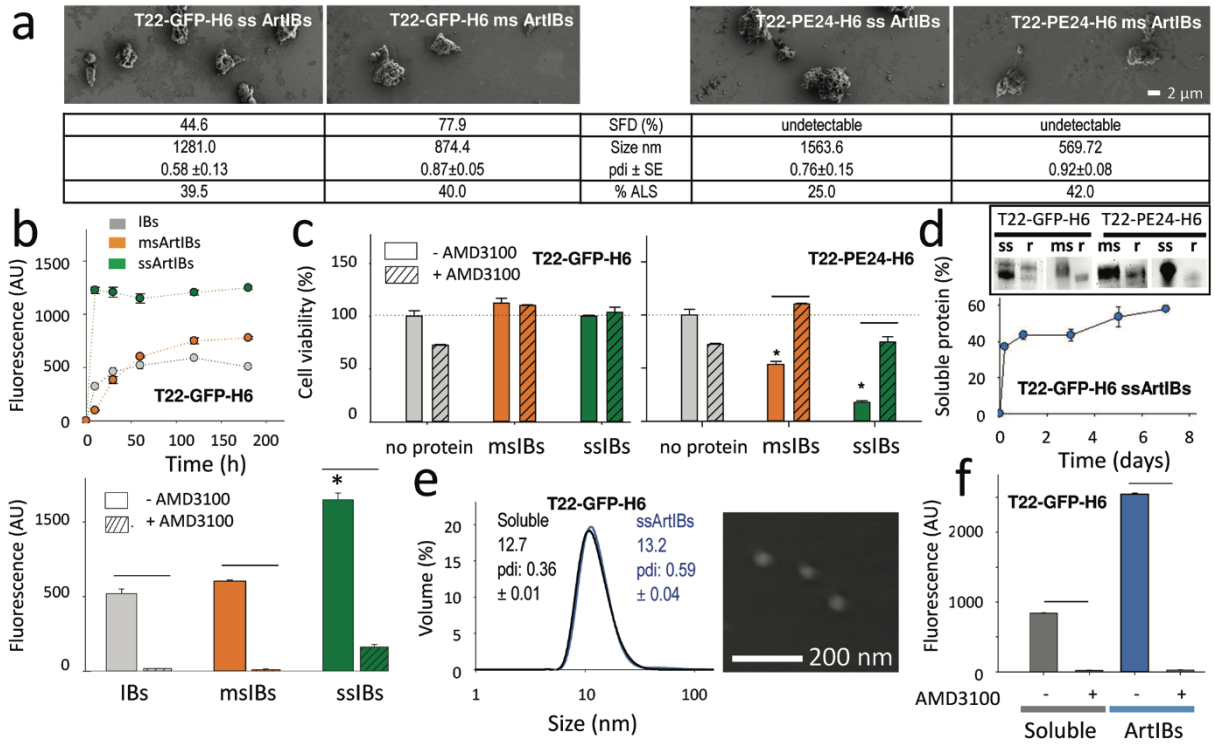

Figure 2. Characterization of ArtIBs formed by modular proteins. a) FESEM images of CXCR4-targeted ArtIBs, all recorded at the same magnification. At the bottom of each image, specific fluorescence decay (SFD), hydrodynamic size peak (pdi ± s.e.m.) and percentage of ALS are shown. b) Internalization of T22-GFP-H6 ArtIBs in cultured HeLa cells, recorded at different times after exposure through intracellular green fluorescent protein (GFP) fluorescence (top). Bottom: AMD3100-mediated inhibition of ArtIB internalization. c) Viability of cultured HeLa cells upon 96 h of T22-GFP-H6 and T22-PE24-H6 ArtIB exposure in presence or absence of AMD3100. d) Stain-free protein detection of released soluble protein (r) from ArtIBs, 7 days after incubation in physiological buffer. In the plot, kinetics of soluble protein release from T22-GFP-H6 ssArtIBs. e) Hydrodynamic mode size peak of T22-GFP-H6 nanoparticles released from ssArtIBs, compared to equivalent soluble nanoparticles after purification from recombinant bacteria (those used for ArtIB fabrication). In the inset, an FESEM image of those nanoparticles released from ArtIBs. f) AMD3100-mediated inhibition of HeLa cell internalization of recombinant soluble and ArtIBs-released nanoparticles. Symbols indicate significant differences to the control (*, $p < 0.05$, Tukey test) and between samples with or without AMD3100 (¯, $p < 0.05$, two tail, t-test).

T22-PE24-H6,[17] that are targeted to the cell-surface cytokine receptor CXCR4[18] through the N-terminal tumor homing peptide T22.[19] The size of these materials was smaller than that of those formed by the previously tested enzymes (Figure 1), a fact that, considering potential medical applications, could generally favor molecular and cell interactivity and protein release, by increasing the surface/volume ratio. When exposed to cultured CXCR4$^+$ Hela cells, T22-GFP-H6 ArtIBs internalized very efficiently as in the case of IB-based nanopills,[10] by a CXCR4-dependent route that is inhibited by the CXCR4 antagonist AMD3100[20] (Figure 2b). Cell viability was not affected by T22-GFP-H6 ArtIBs (Figure 2c), but it was instead dramatically compromised, in a CXCR4-dependent fashion, by the *Pseudomonas aeruginosa* exotoxin (PE24) contained in T22-PE24-H6 ArtIBs. As in the case of IBs, ArtIBs steadily released a fraction of the forming protein in soluble form when incubated in physiological buffer, at least for 7 days (Figure 2d). T22-GFP-H6 solubilized in vitro from ArtIBs was fluorescent (1039.83 AU mg^{-1}), it assembled as 13 nm nanoparticles indistinguishable in size from soluble T22-GFP-H6 (Figure 2e), and this material was equally able to penetrate cultured HeLa cells in a CXCR4-dependent way (Figure 2f). This fact unveiled a potential of ArtIBs as chemically homogenous protein reservoirs for prolonged in vivo delivery of tumor-targeted, nanostructured protein drugs.

In this context, different categories of T22-GFP-H6 ArtIBs were implanted subcutaneously (SC) in a CXCR4$^+$ colorectal cancer mouse model, releasing fluorescent material from the implantation point, followed by selective uptake by a remote CXCR4$^+$ tumor, with specific kinetics for each ArtIB type. A preliminary screening of T22-GFP-H6 msArtIBs and T22-GFP-H6 ssArtIBs (Zn^{2+}, at 100:1 ratio of zinc to protein) showed slow release and negligible or a small amount of material accumulated in the tumor by 21 days (**Figure 3a**). Lowering the proportion of Zn^{2+} (50:1) or using alternative cations to induce ssArtIBs formation, improved protein release and tumor uptake. In particular, ss ArtIBs formed by Ca^{+2} were more efficient than ArtIBs (Zn^{+2} 50:1) in maintaining a faster and progressive protein release from the SC injection site leading to a higher accumulation and longer residence time (starting at day 3 and at least until day 10) in the remote CXCR4$^+$ tumor (Figure 3b). Further, T22-PE24-H6 ArtIBs Ca^{2+}, containing

© 2019 The Authors. Published by WILEY-VCH Verlag GmbH & Co. KGaA, Weinheim

ADVANCED SCIENCE NEWS
www.advancedsciencenews.com

ADVANCED SCIENCE Open Access
www.advancedscience.com

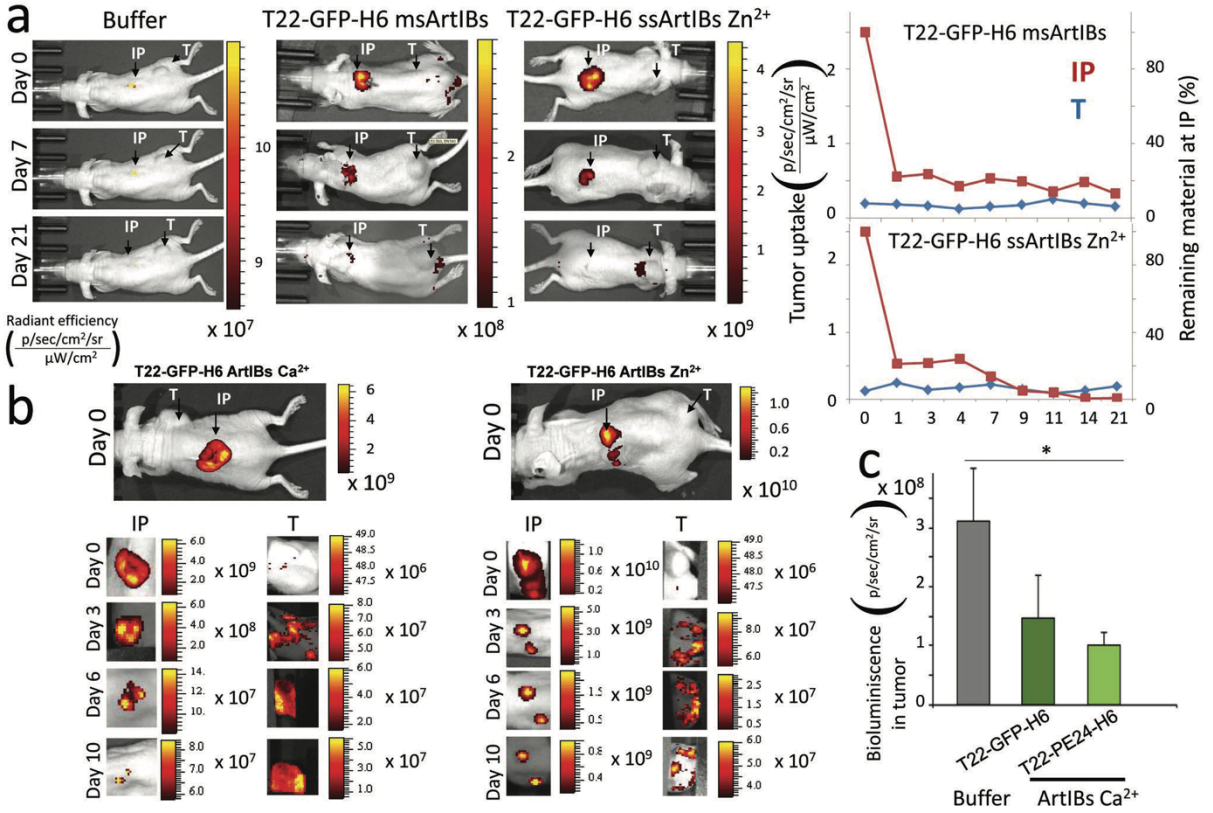

Figure 3. ArtIBs material release, tumor uptake and antitumor activity in a CXCR4$^+$ colorectal cancer model. a) Preliminary screening of released material and tumor uptake after subcutaneous implantation of T22-GFP-H6 msArtIBs, T22-GFP-H6 ssArtIBs (Zn^{2+} 100:1) or PBS. b) Representative FLI images obtained at the injection point (IP) and at the remote tumor (T), along time (day 0, 3, 6, and 10) after T22-GFP-H6 ssArtIBs Ca^{2+}, T22-GFP-H6 ssArtIBs Zn^{2+} (1:50) or buffer SC administration. c) Antitumor effect, measured as bioluminiscence emission by cancer cells along time, in the CXCR4$^+$ SW1417-luci tumor model, after SC injection of 1 mg dose per mouse of T22-GFP-H6 Ca^{2+}ArtIBs, T22-PE24-H6 Ca^{2+} ArtIBs or control PBS (*, $p < 0.05$, Tukey test). Fluorescence in (a) and (b), or bioluminescence in (c) intensity were measured using IVIS Spectrum and expressed as $\bar{x} \pm$ SE of average radiant efficiency.

the CXCR4-targeted cytotoxic polypeptide PE, induced an ($p = 0.083$) inhibition of tumor growth ($n = 3$, $1.0 \pm 0.2 \times 10^8$) stronger than T22-GFP-H6 Ca^{2+} ArtIBs ($n = 3$, $1.5 \pm 0.7 \times 10^8$), as compared to the control buffer-treated group ($n = 2$, $2.6 \pm 1.0 \times 10^8$) (Figure 3c). This fact occurred in absence of systemic toxicity (lack of histopathological alterations in hematoxylin and eosin (H&E)-stained liver and kidney at the end of the experiment, not shown). These observations fully confirmed both the secretion-like prolonged protein release and the precise cell targeting of functional materials through the blood stream, from a remote location.

In summary, ArtIBs can be fabricated in vitro as a new type of biomimetic material, from pure protein and by simple physicochemical methods. These protein particles reproduce IB properties that are relevant to potential uses in biomedicine, especially protein release, but their potential use would fully prevent the immunotoxic reactions potentially associated to the administration of IBs, that contain bacterial debries at variable but significant proportions. On the other hand, since protein drugs used in clinics have a human origin,[21] their administration in an ArtIBs format is not expected to pose significant immune concerns, or to enhance any putative immune reaction over those associated to the repeated, conventional administration regimens of soluble protein drugs (such as insulin, interferons, and many others). In particular, the simpler ss fabrication method allows engineering the strength of protein–protein interactions in the material by means of the stoichiometric control of metal or nonmetal divalent cations. In contrast to other excellent and biocompatible materials developed as micro- or nanoparticles for the slow and sustained drug release,[22] such as those based on PLA or PLGA,[23] ArtIBs are chemically homogeneous and show no chemical distinction between carrier and cargo, thus acting as self-contained, self-released drug materials. Then, the protein drug itself acts, in addition, as a scaffold material, what results in intriguing, totally novel and chemically homogenous drug delivery systems with simpler fabrication processes as opposite to hybrid platforms. ArtIBs might not only replace IBs as functional protein reservoirs and offer homogeneous materials for drug-oriented development, but they will enable, in addition, the packaging of glycosylated proteins of mammalian cell origin as IB-like materials. Since these proteins would be never produced in bacteria

© 2019 The Authors. Published by WILEY-VCH Verlag GmbH & Co. KGaA, Weinheim

ADVANCED SCIENCE NEWS
www.advancedsciencenews.com

ADVANCED SCIENCE Open Access
www.advancedscience.com

in functional forms, ArtIBs will then expand, as a universal platform, the catalogue of enzymes or protein drugs that could be formulated as pure microscale biocatalysts or as secretory protein granules.

Experimental Section

Fabrication of ArtIBs: To produce msArtIBs, 1 mg of pure soluble protein was denatured and concomitantly precipitated by heating at 100 °C in $NaCl_2$ (500×10^{-3} M), $ZnCl_2$ (26.4×10^{-3} M), and $MgCl_2$ (18.4×10^{-3} M) in distilled H_2O. The precipitate was centrifuged at 15 000 × *g* for 15 min at 4 °C, isolated from the soluble fraction and resuspended with 1 mg of phosphatidylcholine with chloroform/methanol 2:1 v/v in a final volume of 300 µL. The excess of organic solvent (OS) was removed by a continuous N_2 flow inducing the formation of a protein–lipid film phase that acted as scaffold. The scaffold was afterwards resuspended in 1 mg mL^{-1} of previous soluble protein diluted in phosphate buffered saline (PBS) at 4 °C overnight. Finally, the sample was centrifuged, and soluble fraction discarded. The manufacturing of ssArtIBs was approached by diluting pure soluble protein in distilled H_2O at a final concentration of 2 mg mL^{-1} and final volume of 200 µL. Protein samples (0.196×10^{-3} M) were subsequently mixed with $ZnCl_2$, at a 100:1 ratio of zinc to protein. After 10 min of incubation at room temperature, samples were centrifuged at 15 000 × *g* for 15 min and soluble fraction discarded to obtain the final product. Alternatively, zinc at a ratio 50:1 and calcium at a ratio 300:1 (in form of $CaCl_2$) were used for the in vivo experimental. β-Gal [EC3.2.1.23] and AP [EC3.1.3.1], both from *Escherichia coli*, were purchased from Sigma-Aldrich. T22-GFP-H6 and T22-PE24-H6 were produced as recombinant proteins and purified by single step chromatography as reported.[17]

Determination of Enzymatic Activity: Between 3.7 and 21.3 ng of pure soluble β-Gal protein or β-Gal ArtIBs were mixed with 5×10^{-3} M of *ortho*-nitrophenylgalactopiranoside in a final volume of 500 µL of PBS. The mixture was incubated for 15 min at 37 °C, the reaction stopped by adding 200 µL of Na_2CO_3 (2.8 M) and the product amount determined by measuring absorbance at 420 nm ($\varepsilon_{420} = 4530\ M^{-1}\ cm^{-1}$) in a UV–vis spectrophotometer (Ultrospec 1000E, Pharmacia Biotech). On the other hand, between 3.9 and 92 ng of pure soluble AP protein or AP ArtIBs were mixed with 20×10^{-3} M of *para*-nitrophenylphosphate (pNPP) in a final volume of 500 µL of PBS. The mixture was incubated for 15 min at 37 °C, the reaction stopped by adding 200 µL of NaOH (1 M) and activity determined by measuring p-nitrophenyl phosphate absorbance at 405 nm ($\varepsilon_{405} = 18\ 000\ M^{-1}\ cm^{-1}$) in a UV–vis spectrophotometer (Ultrospec 1000E, Pharmacia Biotech).

Determination of Specific Fluorescence: Pure soluble T22-GFP-H6 or ArtIB versions were diluted in PBS at concentrations ranging from 0.2 to 1 mg mL^{-1}. The excitation wavelength (λ_{ex}) was set at 488 nm and the emission (λ_{em}) at 510 nm, meanwhile the excitation slit was set at 2.5 nm and the emission slit at 5 nm. Fluorescence was measured in a Cary Eclipse Fluorescence Spectrophotometer (Agilent Technologies) by using a quartz cell with a 10 mm path of light. The intrinsic fluorescence of each sample was then represented referred to protein concentration, defining the SFD mathematically represented as a slope. The % of SFD (%SFD) represents the relationship of the parameter with the SFD of soluble T22-GFP-H6 protein.

Size Distribution Analysis: Volume size distribution of all nanostructures was determined at 633 nm and 25 °C in a Zetasizer Nano ZS (Malvern Instruments Limited) by using ZEN2112 3 mm quartz batch cuvettes. Protein samples dissolved in PBS from 0.2 to 1 mg mL^{-1} were measured in triplicate and mode size peak and polydispersion index (pdi ± s.e.m.) obtained.

Electron Microscopy: Ultrastructural morphometry (size and shape) of ArtIBs was characterized at nearly native state with field emission scanning electron microscopy (FESEM). Drops of 20 µL of each sample diluted at 0.3 mg mL^{-1} in their respective buffers were directly deposited on silicon wafers (Ted Pella Inc.) for 30 s and immediately observed without coating with an FESEM Zeiss Merlin (Zeiss) operating at 1 kV and equipped with a high resolution secondary electron detector. Representative images of a general fields and nanoparticle detail were captured at magnifications ranging between 5500× and 8500× and a working distance of 3.5 mm.

Attenuated Total Reflectance: The most suitable concentration of ArtIBs was placed and dried with a continuous N_2 flow on spectroscopic crystal surfaces. Total reflectance spectroscopy was detected 15 times as spectra by using a scan rate of 50 $cm^{-1}\ min^{-1}$ and a nominal resolution of 2 cm^{-1} in a Tensor 27 Bruker spectrometer coupled to a Specac Golden Gate ATR accessory. All measurements were performed at 25 °C, the absorbance obtained was corrected against the background and the PBS buffer signal was subtracted. Fourier deconvolution of the spectra and the second derivative allow the identification of the different band components. Fitting of the components to the original (not deconvolved) spectrum was essentially performed according to a described procedure.[24] Peak height, band width, and peak position of the components were allowed to vary one at a time in this order. A Gaussian shape was assumed.

Cell Culture: $CXCR4^+$ cervical cancer cell lines (HeLa ATCC-CCL-2) were used to study the performance of ArtIBs in vitro. Cells were routinely cultured in Eagle's minimum essential medium (Gibco), supplemented with 10% fetal bovine serum (FBS, Gibco) and incubated in a humidified atmosphere at 37 °C and 5% of CO_2.

Protein Internalization: HeLa $CXCR4^+$ cells were cultured in 24-well plates in MEM Alpha 1× GlutaMAX medium (Gibco) supplemented with foetal bovine serum (FBS) at 37 °C in a 5% CO_2 humidified atmosphere until 70% of confluence was reached. The medium was then exchanged for serum free OptiPro medium (Gibco) before the addition of the protein. Protein uptake was determined at different times ranging from 10 min to 24 h at a final concentration of 2.5 µg. Cells were detached, and external hooked protein removed by Trypsin-EDTA (Gibco) at 1 mg mL^{-1} exposure for 15 min at 37 °C. Intracellular protein fluorescence was detected by flow cytometry using a FACS-Canto system (Becton Dickinson) with an air-cooled argon ion laser (15 mW) exciting at 488 nm and a D detector (530/30 nm as band pass filter). In addition, the internalization specificity through CXCR4 receptor was tested by exposing cells to the CXCR4 antagonist AMD3100[25] 1 h prior protein incubation at (protein/AMD3100) 1:10 ratio.

Cell Viability: HeLa (ATCC-CCL-2) cell line was cultured in opaque-walled 96-well plates at a final concentration of 6000 cells per well for 24 h. MEM Alpha GlutaMAX medium (Gibco) supplemented with FBS was used at 37 °C in a 5% CO_2 humidified atmosphere, until 70% of confluence was reached. ArtIBs were incubated at 1×10^{-6} M for 96 h using MEM Alpha GlutaMAX medium (Gibco). Cell viability was measured by CellTiter-Glo Luminescent Cell Viability Assay (Promega) in a Multilabel Plater Reader Victor3 (Perkin Elmer).

Soluble Protein Release from Artificial IBs: ArtIBs were resuspended in 1 mL of PBS 1× reaching a final concentration of 1 mg mL^{-1} and incubated at 37 °C without agitation. 100 µL were taken from each sample at different times ranging from 0 to 7 days and centrifuged for 15 min at 15 000 × g at 4 °C to isolate soluble and insoluble fractions. Soluble protein was then stain-free detected by TGX (TGX FastCast Acrylamide Kit) and subsequently quantified by ImageLab software to determine the % of released protein.

In Vivo Release of Fluorescent Material by Subcutaneously Implanted ArtIBs and Their Tumor Uptake: Four-week-old female mice of the Swiss nude strain, in the 18–20 g body weight range (Charles River, L-Abreslle, France), maintained in pathogen-free conditions, were used for the in vivo experiments. All experimental procedures were approved by the Hospital de Sant Pau Animal Ethics Committee and performed according to European Council directives. To generate the $CXCR4^+$ SW1417 CRC cancer model, a 10 mg aliquot of SW1417-luci tumor tissue was obtained from donor animals and deposited in the anterior or posterior flank subcutis of the animals. When tumors reached ≈120–200 mm^3 volume, animals were randomly allocated and implanted in the subcutis of the mouse lumbar region with a pellet of T22-GFP-H6 msArtIBs or T22-GFP-H6 ssArtIBs Zn^{2+} in a preliminary study, at a single dose injection of 1 mg per mouse, suspended in a 150 µL PBS buffer,

© 2019 The Authors. Published by WILEY-VCH Verlag GmbH & Co. KGaA, Weinheim

ADVANCED SCIENCE NEWS
www.advancedsciencenews.com

ADVANCED SCIENCE Open Access
www.advancedscience.com

whereas in a second study, T22-GFP-H6 Zn^{2+} ArtIBs or of T22-GFP-H6 Ca^{2+} ArtIBs were implanted at the same dose. Control buffer injection was used as a negative control. The ArtIBs IP was selected to position it as far away as possible from the tumor in the same mouse, being located either in the anterior or posterior flanks.

After ArtIBs pellet injection, the IVIS Spectrum equipment (PerkinElmer Inc.) was used to monitor the GFP-emitted fluorescence by the SC implants in whole-body mouse by registering immediately (0 h) and at specific time points (3, 6, and 10 days) after the administration to determine the fluorescence remaining in the subcutaneous ArtIBs implants, as well as the fluorescent material that reached the remote tumor along time, in each mouse. Fluorescent signal was digitalized, displayed as pseudocolor overlay, and expressed as radiant efficiency. The fluorescence intensity (FLI) ratio was calculated dividing the signal from the IBs-treated mice by the FLI autofluorescent signal of buffer-administered control mice either in the injection point or in the tumor.

In Vivo Antitumor Activity of SC Implanted ArtIBs: The $CXCR4^+$ SW1417 CRC cancer model used to test antitumor activity was generated as described above. The expression of luciferase by cancer cells in this model allowed for the noninvasive follow-up of tumor growth along time. A week before the deposition of the tumor aliquot in the mouse subcutis, mice were randomly allocated to be SC administered in the mouse lumbar region with 1 mg per mouse dose of T22-GFP-H6 Ca^{2+} ArtIBs or T22-PE24-H6 Ca^{2+} ArtIBs suspended in a 150 µL of PBS buffer or buffer-treated control mice.

After IBs administration, mouse body weight was recorded, and bioluminescent image intensity in the tumor, measured using the IVIS Spectrum equipment (PerkinElmer Inc.), was digitalized and expressed as radiant efficiency. Tumor tissue, liver, and kidney were formalin-fixed and paraffin-embedded for histology. To that aim, four-micrometer-thick sections were stained with H&E, and analyzed for possible histological alterations by two independent observers. Representative images were taken using CellΛB software (Olympus Soft Imaging v. 3.3).

Statistical Analysis: All analyses were performed with SPSS versus version 11.0 (IBM) software. One-way ANOVA and *t*-tests were performed to assess differences in assays with a minimum $n = 3$. The Holme–Sidak test was applied for equal variance and Tukey or Mann Whitney U test for unequal variance (indicated in the figure legend). Two tail *t*-test was also used for individual comparisons. Data were presented as means ± standard error of the mean (s.e.m). Differences between the protein samples were considered significant at $p \leq 0.05$.

Acknowledgements

J.M.S., H.L.L., and P.A. contributed equally to this work. The authors are indebted to Agencia Estatal de Investigación (AEI) and to Fondo Europeo de Desarrollo Regional (FEDER) (Grant No. BIO2016-76063-R, AEI/FEDER, UE) to A.V., AGAUR (2017SGR-229) to A.V., and 2017SGR-865 GRC to R.M. CIBER-BBN (project NANOPROTHER) granted to A.V. and CIBER-BBN project 4NanoMets to R.M. ISCIII (PI15/00272 cofounding FEDER) to E.V. and ISCIII (cofounding FEDER) PIE15//00028 and PI18/00650 to R.M., and to EU COST Action CA 17140. The authors are also indebted to the Networking Research Center on Bioengineering, Biomaterials and Nanomedicine (CIBER-BBN) that is an initiative funded by the VI National R&D&I Plan 2008–2011, Iniciativa Ingenio 2010, Consolider Program, CIBER Actions and financed by the Instituto de Salud Carlos III, with assistance from the European Regional Development Fund. Protein production was performed in part by the ICTS "NANBIOSIS," more specifically by the Protein Production Platform of CIBER in Bioengineering, Biomaterials & Nanomedicine (CIBER-BBN)/IBB, at the UAB sePBioEs scientific-technical service (http://www.nanbiosis.es/portfolio/u1-protein-production-platform-ppp/) and the nanoparticle size analysis by the Biomaterial Processing and Nanostructuring Unit. Biodistribution studies were performed by the ICTS "NANBIOSIS," Nantoxicology Unit (http://www.nanbiosis.es/portfolio/u18-nanotoxicology-unit/). Electron microscopy studies were performed by the Servei de Microscòpia at the UAB. A.V. received an ICREA ACADEMIA award. H.L.L. received a predoctoral fellowship from AGAUR (2019 FI_B 00352) and U.U. was supported by PERIS program from the Health Department of la Generalitat de Catalunya.

Conflict of Interest

E.V., R.M., and A.V. are cofounders of NANOLIGENT, devoted to develop antitumoral drugs based on proteins. J.M.S., H.L-L., P.A., E.V., R.M. and A.V. are co-inventors in a patent covering the use of ArtIBs.

Keywords

biomimetic materials, cancer, drug release, microparticles, recombinant proteins

Received: September 5, 2019
Revised: October 30, 2019
Published online: November 27, 2019

[1] U. Rinas, E. Garcia-Fruitos, J. L. Corchero, E. Vazquez, J. Seras-Franzoso, A. Villaverde, *Trends Biochem. Sci.* **2017**, *42*, 726.
[2] A. de Marco, N. Ferrer-Miralles, E. Garcia-Fruitos, A. Mitraki, S. Peternel, U. Rinas, M. A. Trujillo-Roldan, N. A. Valdez-Cruz, E. Vazquez, A. Villaverde, *FEMS Microbiol. Rev.* **2019**, *43*, 53.
[3] N. S. de Groot, R. Sabate, S. Ventura, *Trends Biochem. Sci.* **2009**, *34*, 408.
[4] N. Gonzalez-Montalban, E. Garcia-Fruitos, A. Villaverde, *Nat. Biotechnol.* **2007**, *25*, 718.
[5] C. Slouka, J. Kopp, O. Spadiut, C. Herwig, *Appl. Microbiol. Biotechnol.* **2019**, *103*, 1143.
[6] C. Slouka, J. Kopp, S. Hutwimmer, M. Strahammer, D. Strohmer, E. Eitenberger, A. Schwaighofer, C. Herwig, *Microb. Cell Fact.* **2018**, *17*, 148.
[7] O. Cano-Garrido, E. Rodriguez-Carmona, C. Diez-Gil, E. Vazquez, E. Elizondo, R. Cubarsi, J. Seras-Franzoso, J. L. Corchero, U. Rinas, I. Ratera, N. Ventosa, J. Veciana, A. Villaverde, E. Garcia-Fruitos, *Acta Biomater.* **2013**, *9*, 6134.
[8] E. Hrabarova, L. Achbergerova, J. Nahalka, *Insoluble Proteins: Methods Protoc.* **2015**, *1258*, 411.
[9] Y. Loo, M. Goktas, A. B. Tekinay, M. O. Guler, C. A. Hauser, A. Mitraki, *Adv. Healthcare Mater.* **2015**, *4*, 2557.
[10] E. Vazquez, J. L. Corchero, J. F. Burgueno, J. Seras-Franzoso, A. Kosoy, R. Bosser, R. Mendoza, J. M. Martinez-Lainez, U. Rinas, E. Fernandez, L. Ruiz-Avila, E. Garcia-Fruitos, A. Villaverde, *Adv. Mater.* **2012**, *24*, 1742.
[11] S. K. Maji, M. H. Perrin, M. R. Sawaya, S. Jessberger, K. Vadodaria, R. A. Rissman, P. S. Singru, K. P. Nilsson, R. Simon, D. Schubert, D. Eisenberg, J. Rivier, P. Sawchenko, W. Vale, R. Riek, *Science* **2009**, *325*, 328.
[12] a) M. V. Cespedes, Y. Fernandez, U. Unzueta, R. Mendoza, J. Seras-Franzoso, A. Sanchez-Chardi, P. Alamo, V. Toledo-Rubio, N. Ferrer-Miralles, E. Vazquez, S. Schwartz, I. Abasolo, J. L. Corchero, R. Mangues, A. Villaverde, *Sci. Rep.* **2016**, *6*, 35765; b) M. Pesarrodona, T. Jauset, Z. V. Díaz-Riascos, A. Sánchez-Chardi, M. E. Beaulieu, J. Seras-Franzoso, L. Sánchez-García, R. Baltà-Foix, S. Mancilla, Y. Fernández, U. Rinas, S. Schwartz, L. Soucek, A. Villaverde, I. Abasolo, E. Vázquez, *Adv. Sci.* **2019**, *6*, 1900849; c) U. Unzueta, M. V. Cespedes, R. Sala, P. Alamo,

© 2019 The Authors. Published by WILEY-VCH Verlag GmbH & Co. KGaA, Weinheim

A. Sanchez-Chardi, M. Pesarrodona, L. Sanchez-Garcia, O. Cano-Garrido, A. Villaverde, E. Vazquez, R. Mangues, J. Seras-Franzoso, *J. Controlled Release* **2018**, *279*, 29.
[13] E. Garcia-Fruitos, N. Gonzalez-Montalban, M. Morell, A. Vera, R. M. Ferraz, A. Aris, S. Ventura, A. Villaverde, *Microb. Cell Fact.* **2005**, *4*, 27.
[14] R. S. Jacob, S. Das, S. Ghosh, A. Anoop, N. N. Jha, T. Khan, P. Singru, A. Kumar, S. K. Maji, *Sci. Rep.* **2016**, *6*, 23370.
[15] Q. Luo, C. Hou, Y. Bai, R. Wang, J. Liu, *Chem. Rev.* **2016**, *116*, 13571.
[16] F. Rueda, M. V. Cespedes, O. Conchillo-Sole, A. Sanchez-Chardi, J. Seras-Franzoso, R. Cubarsi, A. Gallardo, M. Pesarrodona, N. Ferrer-Miralles, X. Daura, E. Vazquez, E. Garcia-Fruitos, R. Mangues, U. Unzueta, A. Villaverde, *Adv. Mater.* **2015**, *27*, 7816.
[17] L. Sanchez-Garcia, N. Serna, P. Alamo, R. Sala, M. V. Cespedes, M. Roldan, A. Sanchez-Chardi, U. Unzueta, I. Casanova, R. Mangues, E. Vazquez, A. Villaverde, *J. Controlled Release* **2018**, *274*, 81.
[18] F. Balkwill, *Semin. Cancer Biol.* **2004**, *14*, 171.
[19] H. Tamamura, M. Imai, T. Ishihara, M. Masuda, H. Funakoshi, H. Oyake, T. Murakami, R. Arakaki, H. Nakashima, A. Otaka, T. Ibuka, M. Waki, A. Matsumoto, N. Yamamoto, N. Fujii, *Bioorg. Med. Chem.* **1998**, *6*, 1033.
[20] J. Kim, K. L. Connelly, E. M. Unterwald, S. M. Rawls, *Brain, Behav., Immun.* **2016**, *62*, 30.
[21] L. Sanchez-Garcia, L. Martin, R. Mangues, N. Ferrer-Miralles, E. Vazquez, A. Villaverde, *Microb. Cell Fact.* **2016**, *15*, 33.
[22] a) P. Davoodi, L. Y. Lee, Q. Xu, V. Sunil, Y. Sun, S. Soh, C. H. Wang, *Adv. Drug Delivery Rev.* **2018**, *132*, 104; b) C. Helary, M. F. Desimone, *Curr. Pharm. Biotechnol.* **2015**, *16*, 635; c) O. S. Fenton, K. N. Olafson, P. S. Pillai, M. J. Mitchell, R. Langer, *Adv. Mater.* **2018**, *30*, 1705328.
[23] a) D. da Silva, M. Kaduri, M. Poley, O. Adir, N. Krinsky, J. Shainsky-Roitman, A. Schroeder, *Chem. Eng. J.* **2018**, *340*, 9; b) D. Ding, Q. Zhu, *Mater. Sci. Eng., C* **2018**, *92*, 1041.
[24] V. Nolan, J. M. Sanchez, M. A. Perillo, *Colloids Surf., B* **2015**, *136*, 1202.
[25] Y. H. Jung, D. Y. Lee, W. Cha, B. H. Kim, M. W. Sung, K. H. Kim, S. H. Ahn, *Head Neck* **2016**, *38*, 1479.

 © 2019 The Authors. Published by WILEY-VCH Verlag GmbH & Co. KGaA, Weinheim

Study 5

In Vitro Fabrication of Microscale Secretory Granules

Hèctor López-Laguna, Eloi Parladé, Patricia Álamo, Julieta M. Sánchez, Eric Voltà-Durán, Naroa Serna, Laura Sánchez-García, Olivia Cano-Garrido, Alejandro Sánchez-Chardi, Antonio Villaverde, Ramón Mangues, Ugutz Unzueta, and Esther Vázquez

Advanced Functional Materials 2021 · Impact factor (19.924) · Quartile (Q1)

Objective 2.a

To develop a new and fully transversal biochemical approach to manufacture **protein-based insoluble microparticles** using multidomain proteins to construct secretory granules.

As well as in study 1, the formulation of versatile insoluble protein-based microparticles has been only supported by a short set of protein candidates. Therefore, in order to test the transversality, scalability and robustness of the platform, a wide range of different and unrelated polypeptides must be tested.

Thus, this work has been focused on using certain concentrations of Zn^{2+} (ranging from 5 to 30 mM) to trigger histidine tagged building blocks (from different natures) crosslinking into secretory granule-like structures able to release nanostructured functional protein. Their physicochemical stability and functional properties were also assessed.

The obtained data resulted in a vast set of microparticulated protein-based structures with different aggregation profiles able to release functional nanoparticles (tested in mouse models). The structures are stable, homogeneous in composition, and made by a simple, easy-to-produce and reproducible procedure. In addition, the microparticles' release profile of nanoparticles can be modified by the stoichiometric manipulation of Zn^{2+}.

RESEARCH ARTICLE

ADVANCED FUNCTIONAL MATERIALS
www.afm-journal.de

In Vitro Fabrication of Microscale Secretory Granules

Hèctor López-Laguna, Eloi Parladé, Patricia Álamo, Julieta M. Sánchez, Eric Voltà-Durán, Naroa Serna, Laura Sánchez-García, Olivia Cano-Garrido, Alejandro Sánchez-Chardi, Antonio Villaverde, Ramón Mangues,* Ugutz Unzueta,* and Esther Vázquez*

Advanced medical treatments involving drug delivery require fully biocompatible materials with the ability to release functional drugs in a time-prolonged way. Ideally, the delivered molecules should be self-contained as chemically homogenous entities to prevent the use of potentially toxic scaffolds or hold matrices. In nature, peptidic hormones are self-stored in protein-only secretory granules formed by the reversible coordination of Zn^{2+} and histidine residues. Inspired by this concept, an in vitro transversal procedure is developed, analyzed, and comparatively applied for the fabrication of protein-only secretory granules at the microscale. These materials can be produced from any polyhistidine-tagged protein using physiological concentrations of Zn^{2+} as a potent and versatile glue-like agent. The screening of granules formed by 12 engineered and nonengineered proteins at different Zn^{2+} concentrations revealed optimal fabrication conditions and the consequent release profiles. Moreover, the functional and structural properties of the delivered protein are fully validated using a drug-targeting protein platform in a mouse model of human colorectal cancer. In summary, short histidine tags allow the packaging of structurally and functionally dissimilar polypeptides, which supports the proposed fabrication method as a powerful protocol extensible to diverse clinical scenarios in which slow protein drug delivery is required.

1. Introduction

The capability of a material to release drugs in a sustained way is appealing in the clinical setting, as its use might provide steady drug concentrations at local or systemic levels without repeated dose administration or under a lower dosing frequency.[1] Because of saved costs and improved patient comfortability, new drug delivery platforms based on this concept are under development. For that, matrices constructed with selected materials are being generated so that when arranged in a sponge-like form, they are ready to entrap different types of drug molecules for their time-prolonged delivery, once implanted in the body.[2] Therefore, the final form of such usable structures is a hybrid composite formed by the scaffold and the drug. As in the case of nanocarriers for intracellular drug delivery,[3] the material used as container might present toxicity issues thus posing severe regulatory concerns[4] and

H. López-Laguna, Dr. E. Parladé, Dr. J. M. Sánchez, E. Voltà-Durán, Dr. N. Serna, Dr. L. Sánchez-García, Prof. A. Villaverde, Dr. E. Vázquez
Institut de Biotecnologia i de Biomedicina
Universitat Autònoma de Barcelona
Bellaterra, Barcelona 08193, Spain
E-mail: antoni.villaverde@uab.cat

H. López-Laguna, Dr. E. Parladé, Dr. P. Álamo, E. Voltà-Durán, Dr. N. Serna, Dr. L. Sánchez-García, Prof. A. Villaverde, Dr. U. Unzueta, Dr. E. Vázquez
Departament de Genètica i de Microbiologia
Universitat Autònoma de Barcelona
Bellaterra, Barcelona 08193, Spain
E-mail: uunzueta@santpau.cat

H. López-Laguna, Dr. E. Parladé, Dr. P. Álamo, E. Voltà-Durán, Dr. N. Serna, Dr. L. Sánchez-García, Prof. A. Villaverde, Prof. R. Mangues, Dr. U. Unzueta, Dr. E. Vázquez
CIBER de Bioingeniería
Biomateriales y Nanomedicina (CIBER-BBN)
C/Monforte de Lemos 3–5, Madrid 28029, Spain
E-mail: rmangues@santpau.cat

Dr. P. Álamo, Prof. R. Mangues, Dr. U. Unzueta
Instituto de Investigación Biomédica Sant Pau (IIB Sant Pau)
Sant Antoni Mª Claret 167, Barcelona 08025, Spain

The ORCID identification number(s) for the author(s) of this article can be found under https://doi.org/10.1002/adfm.202100914.

Dr. P. Álamo, Prof. R. Mangues, Dr. U. Unzueta
Instituto de Investigación contra la Leucemia Josep Carreras
Barcelona 08025, Spain

Dr. J. M. Sánchez
Instituto de Investigaciones Biológicas y Tecnológicas (IIBYT)
(CONICET-Universidad Nacional de Córdoba)
ICTA & Cátedra de Química Biológica
Departamento de Química
FCEFyN, UNC. Av. Velez Sarsfield 1611, Córdoba X 5016GCA, Argentina

Dr. O. Cano-Garrido
Nanoligent SL
Edifici Eureka
Universitat Autònoma de Barcelona
Bellaterra, Barcelona 08193, Spain

Dr. A. Sánchez-Chardi
Servei de Microscòpia
Universitat Autònoma de Barcelona
Bellaterra, Barcelona 08193, Spain

Dr. A. Sánchez-Chardi
Departament de Biologia Evolutiva
Ecologia i Ciències Ambientals
Facultat de Biologia
Universitat de Barcelona
Av. Diagonal 643, Barcelona 08028, Spain

DOI: 10.1002/adfm.202100914

© 2021 Wiley-VCH GmbH

ADVANCED SCIENCE NEWS
www.advancedsciencenews.com

ADVANCED FUNCTIONAL MATERIALS
www.afm-journal.de

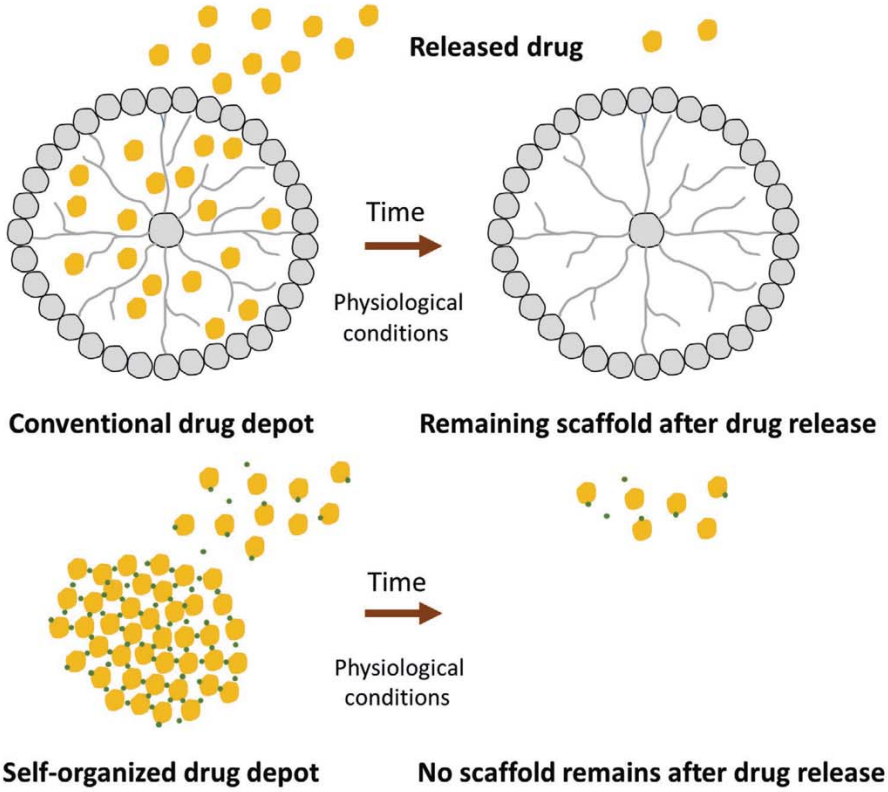

Figure 1. The concept of artificial secretory granules for time-prolonged drug release. Conventional drug depots (top) are based on a scaffold structure (gray material) constructed by polymers, hydrogels, matrices, or in general, porous composites that entrap the drug (yellow balls) in a reversible way. The drugs are then released along time in a passive fashion, while the scaffold itself remains as a stable entity. On the other hand, the scaffold imposes fabrication costs and additional complexity in the fabrication process, apart from biological risks associated with limited biocompatibility and toxicity of the material. On the contrary, the spectrum of payload drugs is potentially broad. In contrast, artificial secretory granules (bottom) are formed in the absence of heterologous scaffolds, and polypeptides of a single species act as both scaffolds and releasable protein drugs. The material, that is mechanically stable, is constructed by the simple coordination of Zn^{2+} cations (small green dots) with histidine-rich stretches of the protein, in absence of additional agents or complex fabrication settings. The protein is slowly released under physiological conditions by still unknown mechanisms, which mimic the secretion of peptide hormones in the mammalian endocrine systems. Therefore, the whole granule disintegrates along with protein release, without leaving any remaining structure. The system is then limited to protein drugs, but it offers high versatility regarding the spectrum of suitable protein species as it is fully regulatable through the addition and engineering of Histidine tags to the desired protein.

then, its use should be desirably avoided. In the case of nanoconjugates, "taking the vehicle out"[3] of the delivery system would involve the design of self-assembled, self-delivered drugs, a goal that has been reached at different extents and by taking different strategies,[5,6] and that is particularly suited for protein-based therapies of cancer.[7] Regarding sustained delivery systems, avoiding a scaffold in the drug reservoir would imply developing platforms in which the drug is self-clustered in absence of any supportive matrix, into mechanically stable but disintegrable materials from which the building blocks should be progressively released (**Figure 1**).

In nature, the appropriate levels of peptide and protein hormones are reached by their delivery into blood from secretory granules,[8] namely, nontoxic amyloidal clusters formed by the hormone itself.[9,10] The Zn ion (Zn^{2+}) is the molecular glue involved in hormone packaging through its divalent coordination with histidine residues from different polypeptides.[11] Being Zn^{2+} a nontoxic metal largely occurring in the human body for multiple functions,[12] its in vitro use as a glue-like agent for the generation of protein-only clusters, mimicking secretory granules, should be perfectly feasible. In fact, the exploration of Zn^{2+} for the generation of artificial protein complexes at both nano- or microscales has already started from different approaches and aimed at different biomedical uses,[13–15] resulting in progressively developed procedures for the fabrication of promising protein materials.[14] Recently, Zn^{2+} and other divalent cations have been adapted to generate protein-only microparticles through the coordination with overhanging histidine rich tails or even with intrinsic histidine-rich regions.[16,17] In vitro, these protein clusters release the forming protein in a time sustained way during a slow disintegration process,[16,17] that is mirrored in vivo upon subcutaneous implantation of the material.[17] The released protein is functional and capable of clinically oriented activities such as precise tumor cell targeting and selective destruction of

© 2021 Wiley-VCH GmbH

ADVANCED SCIENCE NEWS
www.advancedsciencenews.com

ADVANCED FUNCTIONAL MATERIALS
www.afm-journal.de

cancer tissues through highly cytotoxic microbial toxins.[17] In fact, these protein clusters, sizing a few micrometers, have been named artificial inclusion bodies (ArtIBs),[17] as they are structurally and functionally similar to a category of nontoxic functional amyloids (namely, natural IBs) found in recombinant bacterial cells.[18,19] Upon injection in animal models, such natural IBs act as dynamic depots of the forming protein,[20] but their heterogenous composition (that includes undetermined amounts of bacterial macromolecules) prevent their systemic use in humans.

Regarding the ability of artificial protein granules to disintegrate in functional building blocks, it would be interesting to explore to which extent, the capability to release functional protein can be tailored, envisaging particular clinical purposes for which different protein drug releasing rates would be convenient.

2. Results and Discussion

To explore the above possibility, we have constructed Zn^{2+}-induced clusters of T22-GFP-H6 to investigate them as depots of releasable protein and to test the regulatable nature of the disintegration process. T22-GFP-H6 (**Figure 2**A) is a modular protein previously developed as a targeting agent in cancer therapies that contains the green fluorescent protein (GFP).[21,22] Zn^{2+} was mixed with protein solutions at increasing concentrations of the metal by a simple procedure (Figure 2A), rendering the fast formation of increasing amounts of insoluble aggregates (Figure 2B). A complete precipitation of the soluble protein was already achieved at around 10×10^{-3} M of the metal, conforming pellets that were fully fluorescent in all cases (Figure 2B). This fact indicated a proper folding of GFP even in such clustered form. In this regard, it has

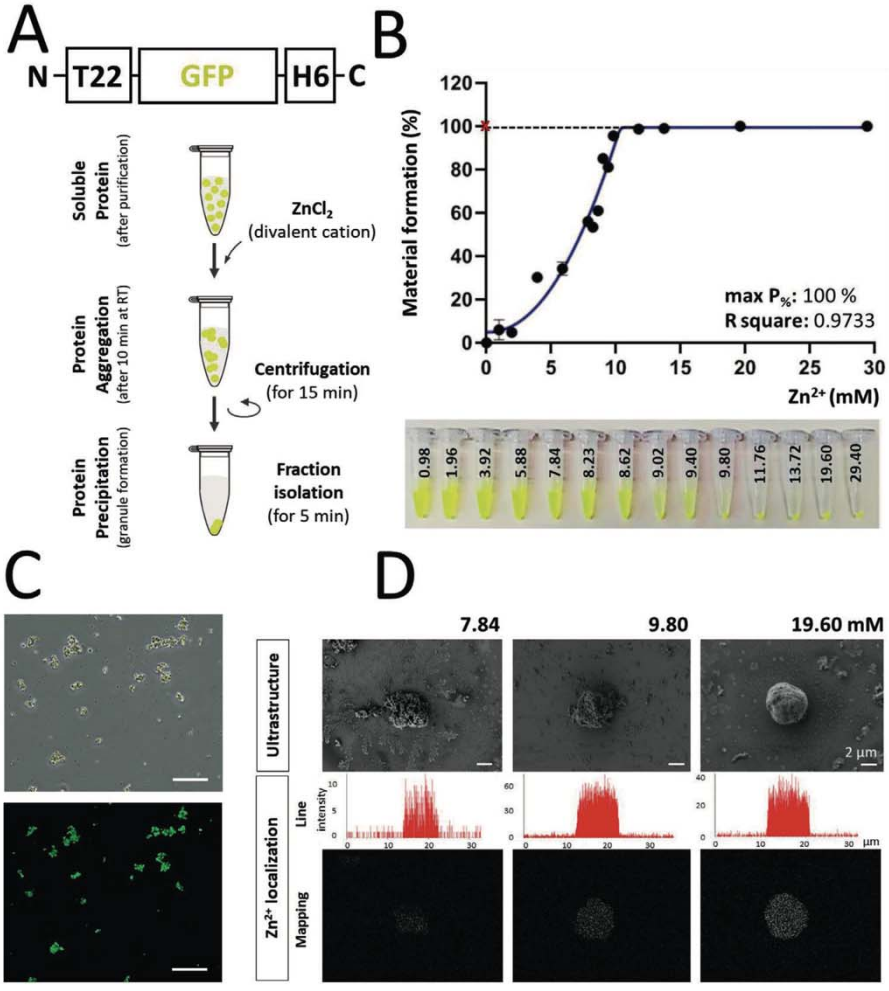

Figure 2. Fabrication of secretory granules using the T22-GFP-H6 modular protein as a model. A) Schematic representation of the modular T22-GFP-H6 protein and the manufacturing process (30 min of duration as standard). B) Protein precipitation curve represented as the % of the formed material relative to Zn^{2+} concentration (in $\times 10^{-3}$ M, black), with the respective *R* square value. The corresponding nonlinear fitting curve (asymmetric sigmoidal 5 parameters logistic; PL) is represented in blue. The maximum % of protein in the aggregate is expressed as (max $P_{\%}$) and indicated in the *y*-axes with a red cross. Additionally, the picture displays the fluorescent pellet that is usually obtained by this process at different concentrations or the ionic Zn ($\times 10^{-3}$ M). C) Optical imaging and fluorescence detection of granules. White bar corresponds to 100 µm. D) Representative high-resolution images linking the granule ultrastructure with 2D (line scan) and 3D (mapping) Zn^{2+} localization at different constructive doses of the metal.

© 2021 Wiley-VCH GmbH

ADVANCED SCIENCE NEWS
www.advancedsciencenews.com

ADVANCED FUNCTIONAL MATERIALS
www.afm-journal.de

been recently shown that the GFP oligomerization does not disturb the emission capacity of the protein, whose stability might be even enhanced.[23] The aggregated material appeared as discrete fluorescent particles with slightly irregular surfaces (Figure 2C), with round or oblong shapes and of around 4–5 µm in diameter (Figure 2D). In these particles, Zn^{2+} was detected homogenously only in the bulk structure and clearly dependent on the Zn^{2+} concentration used for fabrication (Figure 2D). The surface of the microparticles slightly changed from rough to smooth, at increasing concentrations of the crosslinking metal (Figure 2D), indicative of a more compact architecture and protein packaging as the availability of metal increases.

During incubation with conventional physiological phosphate-buffered saline (PBS) and under gentle agitation, microparticles formed by different Zn^{2+} amounts progressively released the forming protein until the loss of 100% of the material and the full disintegration of the cluster (**Figure 3**A). The lowest concentration of Zn^{2+}, however, generates granules with a fast protein leakage, while the highest metal doses result in more stable materials with a smoother protein release profile. This finding indicates how the compactness and stability of the original material can be regulated by adjusting the amount of the linking divalent cation during the fabrication process. Concentrations of Zn^{2+} around 10×10^{-3} M showed an intermediate behavior, resulting in materials with tightly attachment but still highly releasable protein. In all cases, the solubilized T22-GFP-H6 occurs as small oligomers of around 13 nm in size (Figure 3B), similar to the form adopted by the soluble T22-GFP-H6.

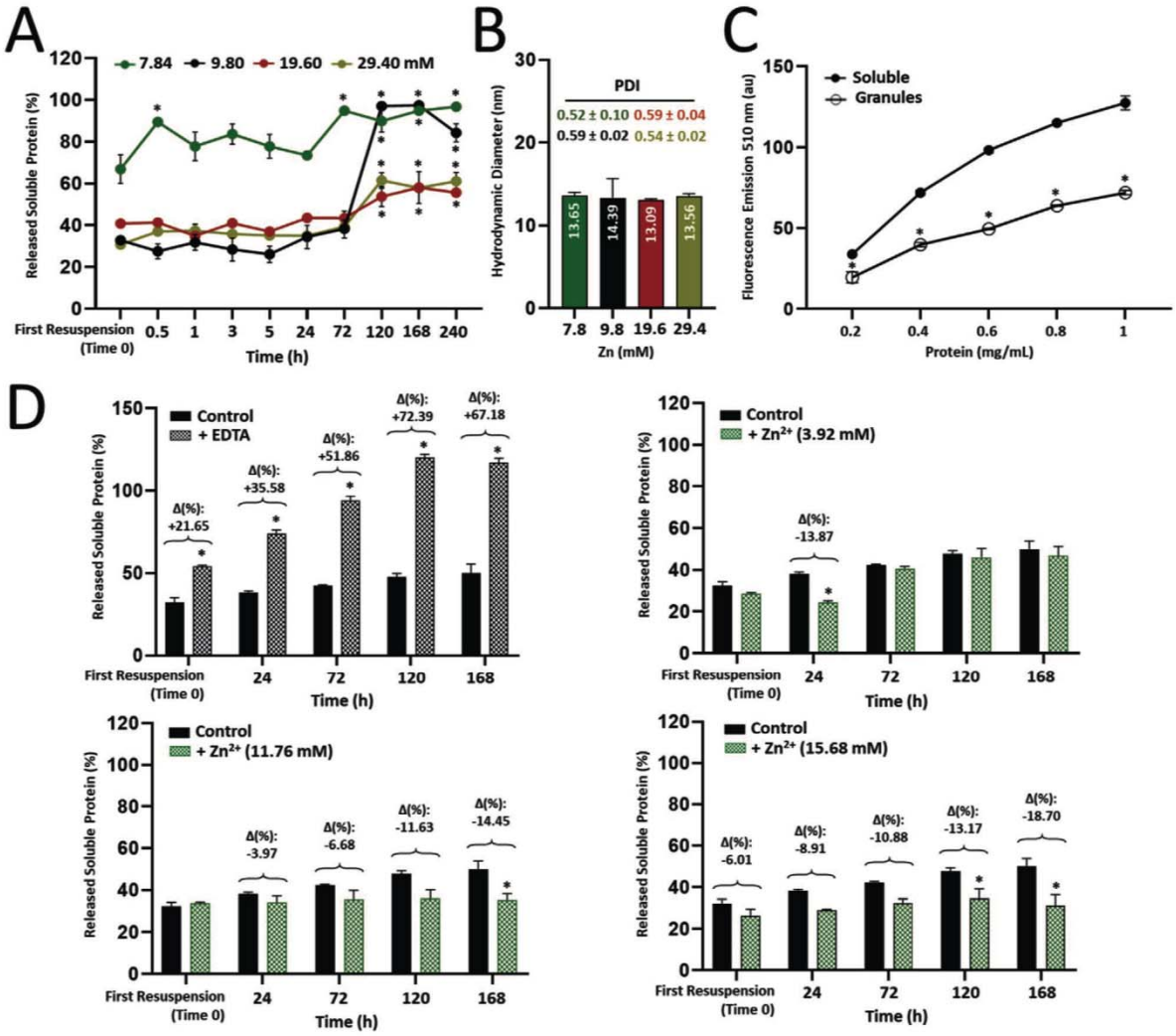

Figure 3. In vitro physicochemical analysis of protein released from T22-GFP-H6 granules. A) Percentage of released protein (in regard to pellet signal after first resuspension) at different times in granules formed at different Zn^{2+} doses (in $\times 10^{-3}$ M, each colored line). B) Hydrodynamic diameter (in nm) of released protein from panel (A). PDI and mean ± SEM are also shown. C) Fluorescence of granules and soluble protein given in arbitrary units (au). D) Percentage of released protein from granules formed by 19.6×10^{-3} M Zn^{2+} after different times of incubation in alternative buffers (+EDTA or $+Zn^{2+}$). The increase or decrease % (Δ%) of soluble protein is also shown. Data are expressed as mean ± SEM, $n = 3$ and statistical comparisons in relation to the control group for panels (A), (C), and (D) ($^*p < 0.05$).

© 2021 Wiley-VCH GmbH

ADVANCED SCIENCE NEWS
www.advancedsciencenews.com

ADVANCED FUNCTIONAL MATERIALS
www.afm-journal.de

This protein, when purified from producing bacterial cells, forms regular toroid nanoparticles of this size.[24] It must be noted that the protein packaged as granules showed slightly lower fluorescent emission than the soluble version (Figure 3C). This fact could be due to a self-quenching event occurring in protein clusters, although minor conformational changes linked to dissociation from the bulk material cannot be discarded, as the protein is structurally flexible.[25] Granule disintegration was, as expected, stimulated by ethylenediaminetetraacetic acid (EDTA) but progressively inhibited by Zn^{2+} (Figure 3D) at increasing concentrations, an observation that fully confirmed the structural role of the metal in the cluster architecture.

All the above data clearly demonstrated the feasibility to control both the architecture at the microscale and the protein release profile of Zn^{2+}-driven microparticles, which behave as depot materials with stable secretion properties. However, to evaluate at which extent the proposed technological platform is extensible to proteins other than the used model, a set of protein species related and unrelated to T22-GFP-H6 was selected for further testing (**Figure 4**). Most of them carry a conventional

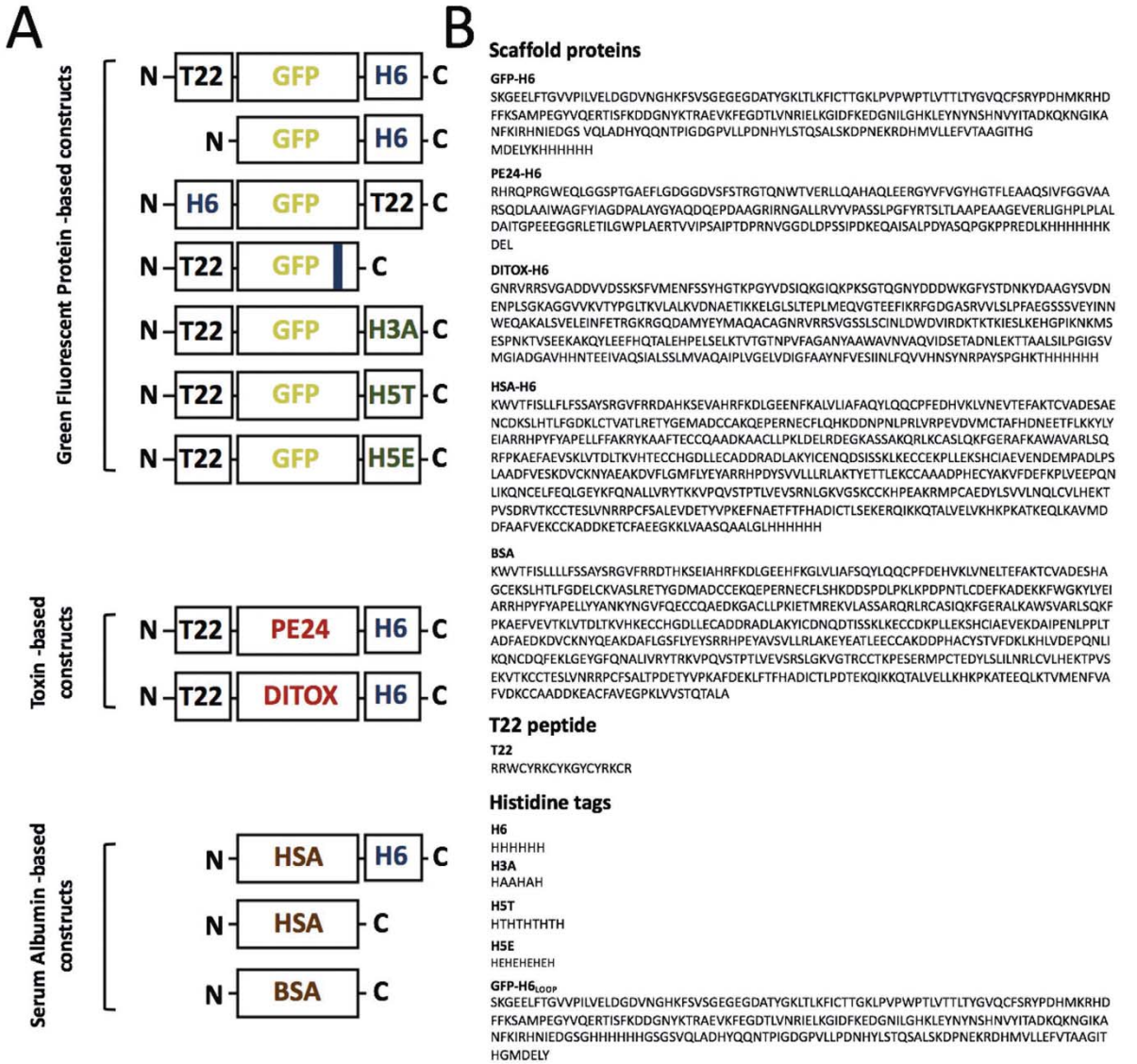

Figure 4. Domain organization of the fusion proteins used in the study and amino acid sequences of relevant modules. A) Modular organization of fusion proteins. The conventional His tag (hexahistidine or H6) is displayed in blue, the modified His tag versions in green and T22 peptide in black. Box sizes are only indicative. PE24 is a fragment of the *Pseudomonas aeruginosa* exotoxin and DITOX a fragment of the diphtheria toxin.[5] HSA is the human serum albumin and BSA is the bovine serum albumin. Additional information about GFP-based constructs can be found elsewhere.[15,24,35] B) Sequences of protein scaffolds and peptidic tags. Note that a spacer sequence (GGSSRSS) was accommodated between T22 and each scaffold protein in all cases (not displayed in the modular scheme). More details about the modified His tags used here can be found elsewhere.[36]

© 2021 Wiley-VCH GmbH

ADVANCED SCIENCE NEWS
www.advancedsciencenews.com

ADVANCED FUNCTIONAL MATERIALS
www.afm-journal.de

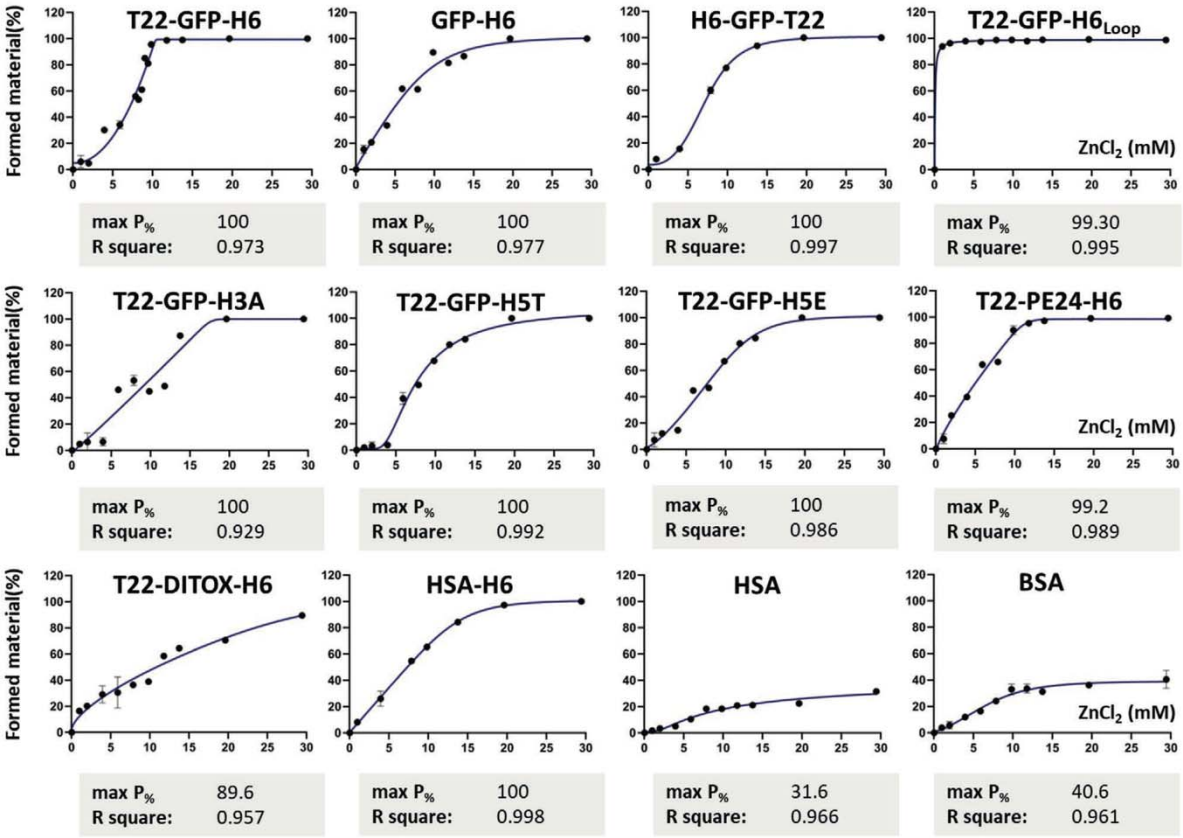

Figure 5. Analytical modeling of granule formation. Protein precipitation curves represented as the % of material formation versus Zn^{2+} concentration in $\times 10^{-3}$ M (black). Respective statistical fittings by nonlinear curve model (asymmetric sigmoidal of 5 parameters logistics; PL) are represented in continuous blue lines. For each plot, the *R* square and the maximum percentage of protein that can precipitate (max $P_{\%}$) are displayed. Data are expressed as mean ± SEM ($n = 3$).

hexahistidine (H6) tag either placed at the N- or C-terminus or accommodated in the protein core, whereas other ones carry the unconventional H3A, H5T, and H5E tags, with a lower number of histidine residues. Moreover, the histidine-containing, tagless human serum albumin (HSA) and bovine serum albumin (BSA) were also included. When tested for their capability to precipitate as Zn^{2+}-driven microparticles, all these proteins responded to the presence of the divalent cation by aggregating in concentration-dependent profiles comparable to that of the control T22-GFP-H6 (**Figure 5**). However, the responsiveness to the crosslinking properties of Zn^{2+} was clearly distinguishable among the protein set, ranging from a very sensitive, aggregation-prone protein (namely, T22-GFP-$H6_{LOOP}$, with a nonterminal solvent-exposed H6 tag) to the hardly clustering tagless HSA and BSA (Figure 5). Proteins carrying the unconventional histidine tags were equally responsive than T22-GFP-H6. Protein sensitivity to Zn^{2+} as a crosslinker was numerically determined by calculating a max $P_{\%}$ (the maximum percentage of protein precipitated by a defined Zn^{2+} concentration), that rendered a scale of tendencies by which proteins could be ordered. A numerical analysis of these data confirmed that the presence of a histidine tag (vs the naturally occurring histidines in the primary protein sequence) dramatically favored aggregation (**Figure 6**A). On the other hand, neither the scaffold (Figure 6B), the presence of a highly cationic peptide (Figure 6C), nor the particular number of histidine residues in the protein sequence (Figure 6D) presented a statistically significant influence on microparticle formation. However, clear tendencies were indeed observed, where the capacity to reach maximum precipitation decreased compared to the model T22-GFP-H6 (Figure 6).

To fully assess the proposed methodology as a feasible fabrication process for usable pharmacological biomaterials, we selected T22-GFP-H6 as a fluorescent model protein for a final analysis. This polypeptide self-assembles as CXCR4-targeted, 12 nm nanoparticles that have been recently used to selectively deliver conventional antitumoral drugs[21] and cytotoxic fusion proteins[26] to $CXCR4^+$ human cancers. A 9.8×10^{-3} M cationic Zn concentration (corresponding to a metal:protein ratio of 50:1) was selected for the fabrication test. This cation dose promotes an efficient aggregation process (Figure 1B) that renders stable, well-formed microparticles (Figure 1D), with a robust, time-prolonged protein release profile (Figure 3A). In vitro, protein liberation initiated at 5 h, and all the forming protein was released within a 6–7 day period. Then, the granules constructed under these conditions appear as an optimal

© 2021 Wiley-VCH GmbH

ADVANCED SCIENCE NEWS
www.advancedsciencenews.com

ADVANCED FUNCTIONAL MATERIALS
www.afm-journal.de

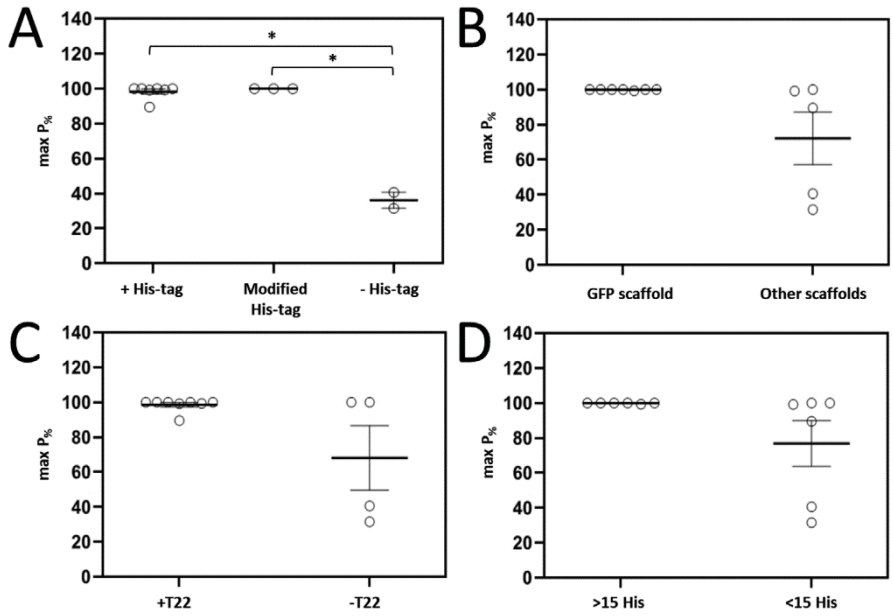

Figure 6. Statistical analysis comparing parameters involved in protein aggregation with intrinsic characteristics of each protein. A) Analysis of max $P_{\%}$ depending on the presence, absence, or modification of histidine tag. B) Analysis of max $P_{\%}$ depending on the type of protein scaffold (GFP-based vs other scaffolds). C) Analysis of max $P_{\%}$ depending on the presence or absence of T22. D) Analysis of max $P_{\%}$ depending on the number of histidine residues in the protein sequence (more or less than 15). Data are expressed as scattered dot plots with mean ± SEM, $n = 3$ and significance ($^*p \leq 0.05$).

intermediate architecture between that promoting an immediate disintegration of the material (<8 × 10^{-3} M) and that showing too tight protein retention (>19 × 10^{-3} M) for a drug depot (Figure 3A).

The fabrication process of T22-GFP-H6 granules rendered a very repetitive efficiency in the packaging of the protein as regular microparticles (**Figure 7**A), with a packaging efficiency higher than 75% and with less than 10% variability between six independent fabrication batches. The granule size was also reproducible comparing those batches (around 1 µm, Figure 7B), with only a moderate reduction upon sonication (Figure 7B). This fact reflects the mechanical stability inherent to the protein material that was confirmed by the stability of its fluorescence emission (Figure 7A, inset). The protein released in vitro by these granules is organized in 11–12 nm oligomers, which resulted also stable in front of the mechanical stress posed by sonication (Figure 7C). The released nanoparticles kept the CXCR4-targeting conferred by the N-terminal peptide T22,[27] as demonstrated by the inhibition of protein internalization into $CXCR4^+$ cells by the CXCR4 antagonist AMD3100[28] (Figure 7D). Then, since the T22 targeting was fully functional in the released material, we decided testing the tumor targeting properties of T22-GFP-H6 administered to animals in form of secretory granules. For that, 1 mg of secretory granules were subcutaneously injected in a mouse model of human $CXCR4^+$ colorectal cancer, in an injection point remote to the tumor. At different times, GFP fluorescence emission from tumor, liver, and kidney was recorded ex vivo. As observed (Figure 7E), the fluorescence levels at the injection point decreased progressively at least during 10 days, while a fluorescent signal concomitantly increased in tumor but not in liver or kidney (Figure 7E). The weight of the administered animals increased normally without differences comparing to a control group injected only with buffer (Figure 7F), indicative of absence of acute toxicity associated with the subcutaneous administration of secretory granules.

Divalent cation coordination mainly based on Zn^{2+} but also on other cations (such as Cu^{2+} and Ca^{2+}) is a natural mechanism to assemble proteins, and in fact, it is the molecular basis of amyloid formation and stable architecture.[29] Among nonfunctional amyloids, whose occurrence and relevance as natural regulators is progressively revealed in a diversity of organisms and systems,[10,30,31] an important fraction of them acts as physiological protein depots, whose components are progressively released to the medium upon appropriate stimuli.[8,11,32] Mainly because of their structural properties, amyloids are explored as components of novel biomaterials with supportive functions,[31,33] but their potential as disintegrable depots has been much more neglected. Here, we demonstrate the feasibility to generate, in a controlled fabrication process, microscale protein-only particles by using physiological concentrations of Zn ion and by means of simple procedures. These particles mimic in morphology and molecular architecture the category of bacterial amyloids named IBs[18] but also the secretory granules of the human endocrine system whose activities are modulated by the Zn^{2+}-histidine coordination. By the appropriate setting of the in vitro fabrication conditions, both the protein clustering (Figure 2) and further release (Figures 3 and 5) kinetics can be easily controlled. In addition, the comparative examination of 12 related and unrelated proteins (Figures 4 and 5) has revealed important key factors in the performance of such artificial secretory granules, mainly related to the presence, nature,

© 2021 Wiley-VCH GmbH

ADVANCED SCIENCE NEWS
www.advancedsciencenews.com

ADVANCED FUNCTIONAL MATERIALS
www.afm-journal.de

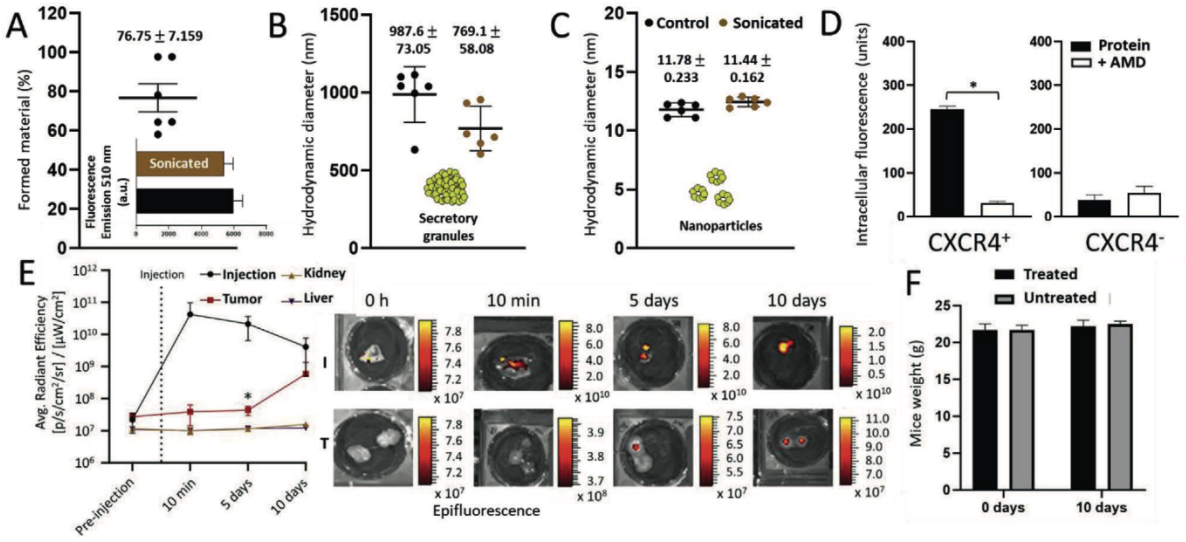

Figure 7. Global validation of the depot/secretion platform, selecting 9.8×10^{-3} M cationic Zn (metal: protein ratio of 50:1) as a convenient model. A) Reproducibility of the fabrication process tested through the percentage of aggregated material. The insert displays the emitted fluorescence from replicates at 510 nm of both control (black) and sonicated (brown) versions of secretory granules. Data derive from fully independent processes in a sixtiplicate experiment. B) Hydrodynamic diameter, expressed in nm, of sonicated and nonsonicated secretory granules. C) Hydrodynamic diameter, expressed in nm, of released protein nanoparticles. D) Protein (released nanoparticles) internalization into cultured SW1417 cells, overexpressing and nonexpressing CXCR4, in the presence and absence of the CXCR4 antagonist AMD3100. Intracellular material was determined by GFP fluorescence. E) Kinetic analysis of GFP fluorescence in the injection point, tumor, and relevant major organs, at different times post-administration. At the right, an example of IVIS images at the injection point and the tumor, in a representative animal. F) Comparative weight of treated and untreated animals before and after injection. Data expressed as mean ± SEM, $n = 6$, and statistical analysis performed in relation to the control group ($^*p \leq 0.05$).

and positioning of a histidine tag (Figure 6). By the appropriate selection of the metal concentration, secretory granules with a release profile convenient for in vivo applications have been constructed, through a simple, robust, and reproducible fabrication process. In this context, the feasibility of the applicability of the proposed platform has been fully validated from the biofabrication side and also regarding the in vivo performance and biosafety of the resulting protein depots (Figure 7).

Of course, the platform proposed here is restricted to protein drugs and it excludes chemicals (Figure 1), but the increasing prevalence of proteins approved by clinical use[34] shows a wide spectrum of potential clinical landscapes and markets. These insights should make possible a semirational design of protein-only artificial secretory granules (formed by the drug as the unique component) for sustained protein drug release, aimed to overcome the obstacles potentially posed by external drug holders such as hydrogels, porous materials, and polymers regarding biodegradability and biosafety issues.

3. Conclusion

The feasibility to produce artificial secretory granules as functional depots for protein drugs has been experimentally supported by the controlled coordination of ionic Zn^{2+} and histidine-rich regions, naturally present or engineered in such proteins. By simple physicochemical procedures combined with plain protein engineering, the aggregation properties of a target protein and its ability to be released from the aggregates can be controlled. The data set presented here totally supports the development of disintegrable microscale protein materials, fully usable in vivo, in which the unique building block is the protein drug itself. The convenience of these secretory granules for clinical application relies in the absence of xenobiotic or potentially toxic holding matrices combined with the enormous versatility of the Zn^{2+}-His platform, which is suited to fine tailoring to specific purposes by simple protein engineering approaches.

4. Experimental Section

Protein Genetic Design, Production, and Purification: Tested proteins were grouped in three different major categories defined as green fluorescent protein, toxin, and serum albumin-based constructs. First, HSA (hemoderivative) and BSA (bovine serum albumin fraction V) proteins without any histidine tag were commercially provided by Grifols and Merck, respectively. The other proteins (except HSA-H6) were designed as *Escherichia coli* codon optimized genes, introduced into a pET22b using NdeI and HindIII restriction enzymes and provided by GeneArt (ThermoFisher). Recombinant plasmids were then transformed in *E. coli* Origami B cells (BL21, OmpT–, Lon–, TrxB, Gor–; Novagen) by thermal shock for 45 s at 42 °C, bacterial cells were grown in lysogenic broth (LB) medium supplemented with 100 μg mL^{-1} ampicillin, 12.5 μg mL^{-1} tetracycline, and 15 μg mL^{-1} kanamycin, and protein was produced at 20 °C overnight (T22-GFP-H6, GFP-H6, T22-GFP-$H6_{LOOP}$, T22-GFP-H3A, T22-GFP-H5T, T22-GFP-H5E, T22-PE24-H6, and T22-DITOX-H6) or 37 °C during 3 h (H6-GFP-T22) upon induction with 0.1×10^{-3} M of isopropyl-β-D-thiogalactopyranoside (IPTG). Cells were then harvested by centrifugation for 15 min at 5000 g, resuspended in Wash buffer (20×10^{-3} M Tris-HCl, 500×10^{-3} M NaCl, 10×10^{-3} M imidazole, pH 8)

© 2021 Wiley-VCH GmbH

ADVANCED SCIENCE NEWS
www.advancedsciencenews.com

ADVANCED FUNCTIONAL MATERIALS
www.afm-journal.de

in the presence of protease inhibitors (Complete EDTA-free, Roche Diagnostics) and disrupted by two rounds of 1200 psi in a French Press (Thermo FA-078A). Soluble fraction from bacterial cell extract was finally collected by centrifugation (45 min at 15 000 *g*) for subsequent protein purification. HSA-H6 protein was also designed as a human codon optimized gene and provided by GeneArt (ThermoFisher) into a pTriex6 plasmid. Transient transfection of human HEK-293F cells was achieved upon addition of PEI:plasmid complexes (3:1 ratio) in Freestyle 293 medium when cell concentration reached 10^6 cells mL^{-1}. Cells were subsequently grown and secretion signal peptide containing protein was produced in the presence of 4×10^{-3} M Valproic acid for 6 days (37 °C, 70% humidity, 8% CO_2 and 120 rpm). Finally, extracellular medium was collected by centrifugation (15 min at 300 *g*) for subsequent purification of the secreted protein.

All proteins were purified by Immobilized Metal Affinity Chromatography (IMAC) using HisTrap HP 1 or 5 mL columns (GE Healthcare) in an Äkta Pure System (GE Healthcare). Protein elution was achieved by a linear gradient of Elution buffer (20×10^{-3} M Tris-HCl, 500×10^{-3} M NaCl, 500×10^{-3} M imidazole, pH 8) and recovered proteins were dialyzed against sodium carbonate (166 mmol L^{-1} $NaHCO_3$, pH 8) with or without salt (333×10^{-3} M NaCl) buffers.

Protein Concentration, Purity, and Integrity: Protein purity was determined after purification by sodium dodecyl sulfate-polyacrylamide gel electrophoresis (SDS-PAGE) using TGX Stain-Free FastCast Acrylamide Kit, 12% (BioRad), followed by a subsequent transference into polyvinylidene fluoride membranes by Trans-Blot Turbo Transfer System (BioRad). Protein bands were finally immunodetected by Western Blot (WB) using the corresponding monoclonal antibodies (1/5000 dilution for both an Anti-GFP Ab for GFP scaffold-based; Clontech, and an anti-His Ab for toxin or serum albumin-based proteins; Santa Cruz Biotechnology). Protein concentration was determined by Bradford assay and integrity assessed by matrix-assisted laser desorption ionization time-of-flight mass spectrometry.

Fabrication of Protein Particles: Pure soluble protein was initially adjusted at 2 mg mL^{-1} and aliquoted in fixed final volumes of 250 µL. Then, a 0.22 µm filtered version of $ZnCl_2$ solution was added in each Eppendorf tube at increasing divalent cation:protein proportions in which 1:1 corresponds to 0.196×10^{-3} M. The overall selected precipitation conditions were (5:1, 20:1, 40:1, 50:1, 70:1, 100:1, 150:1) besides for some constructions was extended to (5:1, 10:1, 20:1, 30:1, 40:1, 50:1, 70:1, 100:1, 150:1) or (5:1, 10:1, 20:1, 30:1, 40:1, 42:1, 44:1, 46:1, 48:1, 50:1, 70:1, 100:1, 150:1) depending on the experimental needs. Mixtures were then gently vortexed for 5 s and centrifuged for 15 min at 15 000 *g* and soluble and insoluble fractions isolated. Remaining protein in the soluble fraction was quantified by Bradford assay and percentage of precipitated protein thus estimated. Pellets were then stored at −80 °C for further use.

Physicochemical Characterization: Fluorescence of different concentrations (from 0.2 to 1 mg mL^{-1}) of T22-GFP-H6 particle samples was determined at 510 nm upon excitation at 488 nm with a 5 nm emission slit in a cary eclipse fluorescence spectrophotometer (Agilent Technologies) in comparison to its respective T22-GFP-H6 soluble protein version by using quartz cells with a 10 mm path of light. The same samples were afterward imaged and the fluorescence was detected at 0.5 mg mL^{-1} final concentration and 10x magnifications in a Nikon-Eclipse Ts2R-FL fluorescence microscope by using the same previous wavelength conditions. For stability experiments, protein particles were resuspended in 250 µL of respective storage buffer and sonicated (0.5 on and 0.5 off) for 40 s at 10% of amplitude in a Bransons Digital Sonifier.

Morphometric and Analytical Imaging: High-resolution imaging of granule morphology (size and shape) and elemental analyses at nearly native state were performed with a rapid method for field emission scanning electron microscopy (FESEM). Pellets of the material were resuspended in deionized water, and 10 µL of each sample was placed in silicon wafers (Ted Pella) for 2 min, air-dried, and observed in an FESEM Merlin (Zeiss). The microscope was equipped with a standard secondary electron (SE) detector operating at 1 kV for morphological assessment and an energy dispersive X-rays (EDX) detector (Oxford Instruments) working at 18 kV for analytical evaluation. For the same particles, images of morphological and both 2D (line scan, 300 s) and 3D (mapping, 500 s) analyses of Zn localization were obtained to link morphology with elemental distribution.

Release of Soluble Protein: Among all manufacturing conditions, 40:1, 50:1, 100:1, and 150:1 ratios were selected to test the capacity of the resulting particles to release soluble protein. Stored pellets were thawed at room temperature for several minutes and softly resuspended in 1 mL of PBS. Samples were placed at 37 °C without agitation (mimicking subdermal conditions in living systems) and aliquots of 75 µL were collected at 0, 0.5, 1, 3, 5, 24, 72, 120, 168, and 240 h. Soluble and insoluble fractions were isolated after centrifugation for 15 min at 15 000 *g* and protein mobility and integrity were assessed by SDS-PAGE using TGX Stain-Free FastCast Acrylamide Kit, 12% (BioRad). Protein bands were immunodetected by WB. Band intensity was then quantified by Image Lab software, what allowed to calculate the percentage of released protein.

Rational Control of Soluble Protein Release: Among all manufacturing conditions, 100:1 was selected to test the capacity to release soluble protein in the presence of different chemical compounds, namely, EDTA and $ZnCl_2$, acting as stimulators or inhibitors of protein delivery, respectively. Stored pellets were thawed at room temperature for several minutes and softly resuspended in 1 mL of PBS in the presence of 19.6×10^{-3} M of EDTA or increasing $ZnCl_2$ concentrations (3.92×10^{-3}, 11.76×10^{-3}, and 15.68×10^{-3} M). Samples were placed at 37 °C without agitation as previously mentioned and aliquots of 75 µL were collected at times 0, 24, 72, 120, and 168 h. Then, soluble and insoluble fractions were isolated thanks to a centrifugation process for 15 min at 15 000 *g* and protein mobility and integrity were equally assessed by SDS-PAGE using TGX Stain-Free FastCast Acrylamide Kit, 12% (BioRad) and by WB. Image Lab software (Bio-Rad) was used to quantify band intensity and the difference (Δ) of released protein (in percentage) between control and treated samples was calculated.

Size Characterization of Microparticles and Released Protein: The hydrodynamic diameter (in nm) of soluble protein released in previous experiments was determined by dynamic light scattering at 25 °C and 633 nm in a Zetasizer NanoZS (Malvern Instruments Limited) using ZEN2112 3 mm quartz batch cuvettes. The run duration value was 10 s for released protein and 4 s for microparticles. Size was determined by volume for released protein nanoparticles and by intensity for microparticles. The polydispersion index (PDI) was also obtained.

Internalization of Released Protein: Protein internalization was monitored in SW1417 colorectal cancer cell lines both patient-derived $CXCR4^+$ and ATCC CCL-238 $CXCR4^-$. Cells were cultured in 24-well plates (120 000 cells per well for $CXCR4^+$ and 180 000 cells per well for $CXCR4^-$) for 24 h in Dulbecco's modified Eagle medium (1X) GlutaMAX (4.5 g L^{-1} D-Glucose and 0.11 g L^{-1} Pyruvate; Gibco) supplemented with fetal bovine serum at 37 °C and 5% CO_2 humidified atmosphere until a confluence of 70% was reached. Protein was incubated at 0.1×10^{-6} M for 1 h in both cell lines. Cells were then detached, and the external attached protein was removed by adding Trypsin-EDTA (Gibco) at 1 mg mL^{-1} for a harsh digestion for 15 min at 37 °C. Such protocol was designed to remove all potential externally attached protein. Protein internalization, detected as intracellular fluorescence, was then determined by flow cytometry using a FACS-Canto system (Becton Dickinson) at 15 mW with an air-cooled argon laser exciting at 488 nm. Receptor mediated internalization was assessed by adding AMD3100 at 10×10^{-6} M that blocked CXCR4 and prevented its interaction with the CXCR4 ligand T22, 1 h prior protein incubation.

Standardization of the Precipitation Curve and Statistical Analyses: A protein precipitation curve was represented for each modular protein type as percentage of material formation in respect of Zn^{2+} concentration (in $\times 10^{-3}$ M), and statistically analyzed by an asymmetric sigmoidal 5 parameter logistic (PL) model. From curve fitting, *R* square (R^2) and maximum percentage of precipitated protein (max $P_{\%}$) were numerically obtained and graphically represented as displayed in Figure 1B. Max $P_{\%}$ protein values were compared with the presence or absence of T22 ligand, histidine tag, protein scaffold, or number of histidines in the primary sequence, respectively. An initial variety of normality and

© 2021 Wiley-VCH GmbH

ADVANCED SCIENCE NEWS
www.advancedsciencenews.com

ADVANCED FUNCTIONAL MATERIALS
www.afm-journal.de

lognormality tests (Anderson–Darling, D'Agostino & Pearson, Shapiro–Wilk, and Kolmogorov–Smirnov) were used to determine the well-modeled normal distribution of all data sets. For parametric data, a *t*-test (single comparisons) or one/two-way analysis of variance (multiple comparisons) tests were used, meanwhile for nonparametric data, a Mann–Whitney test was used. All statistical analyses were performed in comparison with the control or initial specified time = 0, respectively ($^*p \leq 0.05$), expressed as mean ± standard error of the mean (SEM) and at least in triplicate ($n = 3$).

In Vivo Kinetic Biodistribution from Subcutaneously Implanted Protein Particles: In vivo experiments were approved by the Animal Ethics Committee at the Hospital de la Santa Creu i Sant Pau (protocol nº FUE-2020-01732218, granted to Prof. Ramón Mangues by the Generalitat de Catalunya) and performed according to European Council directives. Four weeks old female mice of the Swiss nude strain, in the 18–20 g body weight range (Charles River, L-Abreslle, France), maintained in pathogen-free conditions, were used for the in vivo experiments. To generate the $CXCR4^+$ SW1417 CRC cancer model, 5×10^6 $CXCR4^+$ SW1417 human CRC cells, resuspended in 150 µL of media, were injected in the mouse flank ($n = 12$). When tumors reached approximately a 120–200 mm^3 volume, animals were randomly allocated to the different groups and administered in the subcutis of the mouse lumbar region, at the site contralateral to the tumor site, with a pellet of 1 mg of T22-GFP-H6 Zn^{2+} granules suspended in a 150 µL PBS buffer. Buffer injection was used as a negative control. 10 min, and 5 or 10 days after the administration, ≈1 mL of blood in EDTA anticoagulated collection tubes was drawn. In these samples, the exact volume of obtained plasma and their fluorescent emission at each studied time were measured, and the concentration of nanoparticle as referred to the total fluorescence emitted by the administered dose was calculated. Each mouse was euthanized, the kidney, liver, and tumor and the tissue surrounding the injection point were resected. Following, the intensity of the fluorescence was ex vivo registered emitted by the nanoparticles released by the protein particles and biodistributed to tumor and nontumor organs and also the fluorescence remaining at the IP, using the IVIS 200-Spectrum (PerkinElmer). Fluorescent signal was digitalized, displayed as pseudocolor overlay, and expressed as radiant efficiency. Statistical analysis was performed in GraphPad Prism (v8.0.2). Unpaired *t*-test was used to evaluate differences between means of the average radiant efficiencies extracted from each IVIS images, and at least three replicates were analyzed for each time-point.

Acknowledgements

The authors are indebted to Agencia Estatal de Investigación (AEI) and to Fondo Europeo de Desarrollo Regional (FEDER) (grant BIO2016-76063-R, AEI/FEDER, UE) to A.V., AEI (PID2019-105416RB-I00/AEI/10.13039/501100011033) to E.V., and PI18/00650 AEI/FEDER to R.M., AGAUR (2017SGR-229 to A.V. and 1027SGR-865 to R.M.), and CIBER-BBN (project NANOPROTHER granted to A.V., project 4NanoMets to R.M., and project NANOREMOTE granted to E.V.). The authors are also indebted to the CERCA programme from la Generalitat de Catalunya and to the Networking Research Center on Bioengineering, Biomaterials and Nanomedicine (CIBER-BBN) that is an initiative funded by the VI National R&D&I Plan 2008–2011, Iniciativa Ingenio 2010, Consolider Program, CIBER Actions and financed by the Instituto de Salud Carlos III, with assistance from the European Regional Development Fund. Protein production has been partially performed by the ICTS "NANBIOSIS," more specifically by the Protein Production Platform of CIBER in Bioengineering, Biomaterials & Nanomedicine (CIBER-BBN)/IBB, at the UAB sePBioEs scientific-technical service, the in vivo experimental work by the Nanotoxicology Unit, and the nanoparticle size analysis by the Biomaterial Processing and Nanostructuring Unit. Electron microscopy studies were performed by the Servei de Microscòpia in the UAB. A.V. received an ICREA ACADEMIA award. U.U. was supported by Miguel Servet contract (CP19/00028) from ISCIII cofounded by European Social Fund (ESF investing in your future). L.S.G. and H.L.L. were supported by a predoctoral fellowship from AGAUR (2018FI_B2_00051 and 2019FI_B00352, respectively) and E.V.D. by a predoctoral fellowship from Ministerio de Ciencia, Innovación y Universidades (FPU18/04615).

Conflict of Interest

A. Villaverde, E. Vazquez, H. López-Laguna, J.M. Sanchez and R. Mangues are coauthors of a patent covering the use of artificial secretory granules.

Data Availability Statement

Research data are not shared.

Keywords

divalent cations, drug release, microparticles, protein materials, secretory granules

Received: January 27, 2021
Published online:

[1] a) C. Helary, M. F. Desimone, *Curr. Pharm. Biotechnol.* **2015**, *16*, 635; b) G. Acharya, K. Park, *Adv. Drug Delivery Rev.* **2006**, *58*, 387; c) A. S. Hoffman, *J. Controlled Release* **2008**, *132*, 153.
[2] a) J. Li, D. J. Mooney, *Nat. Rev. Mater.* **2016**, *1*, 16071; b) T. A. Esquivel-Castro, M. C. Ibarra-Alonso, J. Oliva, A. Martinez-Luevanos, *Mater. Sci. Eng., C* **2019**, *96*, 915; c) R. Narayan, U. Y. Nayak, A. M. Raichur, S. Garg, *Pharmaceutics* **2018**, *10*, 118; d) A. Ali, S. Ahmed, *Int. J. Biol. Macromol.* **2018**, *109*, 273; e) N. T. T. Uyen, Z. A. A. Hamid, N. X. T. Tram, N. Ahmad, *Int. J. Biol. Macromol.* **2020**, *153*, 1035.
[3] J. Shen, J. Wolfram, M. Ferrari, H. Shen, *Mater. Today* **2017**, *20*, 95.
[4] a) H. Park, K. Park, *Pharm. Res.* **1996**, *13*, 1770; b) S. Al-Jawadi, P. Capasso, M. Sharma, *Pharm. Dev. Technol.* **2018**, *23*, 953; c) D. da Silva, M. Kaduri, M. Poley, O. Adir, N. Krinsky, J. Shainsky-Roitman, A. Schroeder, *Chem. Eng. J.* **2018**, *340*, 9.
[5] L. Sanchez-Garcia, N. Serna, P. Alamo, R. Sala, M. V. Cespedes, M. Roldan, A. Sanchez-Chardi, U. Unzueta, I. Casanova, R. Mangues, E. Vazquez, A. Villaverde, *J. Controlled Release* **2018**, *274*, 81.
[6] a) P. Huang, D. Wang, Y. Su, W. Huang, Y. Zhou, D. Cui, X. Zhu, D. Yan, *J. Am. Chem. Soc.* **2014**, *136*, 11748; b) Y. Zhao, W. Wang, S. Guo, Y. Wang, L. Miao, Y. Xiong, L. Huang, *Nat. Commun.* **2016**, *7*, 11822; c) J. E. Chung, S. Tan, S. J. Gao, N. Yongvongsoontorn, S. H. Kim, J. H. Lee, H. S. Choi, H. Yano, L. Zhuo, M. Kurisawa, J. Y. Ying, *Nat. Nanotechnol.* **2014**, *9*, 907; d) N. Serna, P. Alamo, P. Ramesh, D. Vinokurova, L. Sanchez-Garcia, U. Unzueta, A. Gallardo, M. V. Cespedes, E. Vazquez, A. Villaverde, R. Mangues, J. P. Mederna, *J. Controlled Release* **2020**, *320*, 96.
[7] N. Serna, L. Sanchez-Garcia, U. Unzueta, R. Diaz, E. Vazquez, R. Mangues, A. Villaverde, *Trends Biotechnol.* **2018**, *36*, 318.
[8] S. K. Maji, M. H. Perrin, M. R. Sawaya, S. Jessberger, K. Vadodaria, R. A. Rissman, P. S. Singru, K. P. Nilsson, R. Simon, D. Schubert, D. Eisenberg, J. Rivier, P. Sawchenko, W. Vale, R. Riek, *Science* **2009**, *325*, 328.
[9] M. P. Badtke, N. D. Hammer, M. R. Chapman, *Sci. Signaling* **2009**, *2*, pe43.
[10] D. Otzen, R. Riek, *Cold Spring Harbor Perspect. Biol.* **2019**, *11*, a033860.
[11] a) R. S. Jacob, S. Das, S. Ghosh, A. Anoop, N. N. Jha, T. Khan, P. Singru, A. Kumar, S. K. Maji, *Sci. Rep.* **2016**, *6*, 23370; b) R. Jacob,

© 2021 Wiley-VCH GmbH

ADVANCED SCIENCE NEWS
www.advancedsciencenews.com

ADVANCED FUNCTIONAL MATERIALS
www.afm-journal.de

A. Anoop, S. Maji, *Protein Nanofibrils as Storage Forms of Peptide Drugs and Hormones*, Vol. *1174*, Springer, Singapore **2019**.

[12] a) G. A. Rutter, P. Chabosseau, E. A. Bellomo, W. Maret, R. K. Mitchell, D. J. Hodson, A. Solomou, M. Hu, *Proc. Nutr. Soc.* **2016**, *75*, 61; b) M. A. Zoroddu, J. Aaseth, G. Crisponi, S. Medici, M. Peana, V. M. Nurchi, *J. Inorg. Biochem.* **2019**, *195*, 120; c) Y. Cherasse, Y. Urade, *Int. J. Mol. Sci.* **2017**, *18*, 2334; d) Y. Ogawa, M. Kinoshita, S. Shimada, T. Kawamura, *Nutrients* **2018**, *10*, 199; e) K. Kerns, M. Zigo, P. Sutovsky, *Int. J. Mol. Sci.* **2018**, *19*, 4097; f) H. Wu, Y. Shen, D. Wang, H. Herrmann, R. D. Goldman, D. A. Weitz, bioRxiv (CSH Laboratory) **2019**, https://doi.org/10.1101/844167.

[13] a) H. K. Munch, J. Nygaard, N. J. Christensen, C. Engelbrekt, M. Ostergaard, T. Porsgaard, T. Hoeg-Jensen, J. Zhang, L. Arleth, P. W. Thulstrup, K. J. Jensen, *Angew. Chem.* **2016**, *55*, 2378; b) I. W. Hamley, *Biomacromolecules* **2019**, *20*, 1829; c) B. Maniaci, C. H. Lipper, D. L. Anipindi, H. Erlandsen, J. L. Cole, B. Stec, T. Huxford, J. J. Love, *Biochemistry* **2019**, *58*, 2199; d) I. Tunn, M. J. Harrington, K. G. Blank, *Biomimetics* **2019**, *4*, 25; e) M. Yang, W. J. Song, *Nat. Commun.* **2019**, *10*, 5545; f) A. S. Knight, J. Larsson, J. M. Ren, R. Bou Zerdan, S. Seguin, R. Vrahas, J. Liu, G. Ren, C. J. Hawker, *J. Am. Chem. Soc.* **2018**, *140*, 1409; g) S. Zechel, M. D. Hager, T. Priemel, M. J. Harrington, *Biomimetics* **2019**, *4*, 20.

[14] H. López-Laguna, J. Sánchez, U. Unzueta, R. Mangues, E. Vázquez, A. Villaverde, *Trends Biochem. Sci.* **2020**, *45*, 992.

[15] H. Lopez-Laguna, U. Unzueta, O. Conchillo-Sole, A. Sanchez-Chardi, M. Pesarrodona, O. Cano-Garrido, E. Volta, L. Sanchez-Garcia, N. Serna, P. Saccardo, R. Mangues, A. Villaverde, E. Vazquez, *Acta Biomater.* **2019**, *83*, 257.

[16] T. Y. Chen, W. J. Cheng, J. C. Horng, H. Y. Hsu, *Colloids Surf., B* **2019**, *187*, 110644.

[17] J. M. Sanchez, H. Lopez-Laguna, P. Alamo, N. Serna, A. Sanchez-Chardi, V. Nolan, O. Cano-Garrido, I. Casanova, U. Unzueta, E. Vazquez, R. Mangues, A. Villaverde, *Adv. Sci.* **2020**, *7*, 1902420.

[18] A. de Marco, N. Ferrer-Miralles, E. Garcia-Fruitos, A. Mitraki, S. Peternel, U. Rinas, M. A. Trujillo-Roldan, N. A. Valdez-Cruz, E. Vazquez, A. Villaverde, *FEMS Microbiol. Rev.* **2019**, *43*, 53.

[19] U. Rinas, E. Garcia-Fruitos, J. L. Corchero, E. Vazquez, J. Seras-Franzoso, A. Villaverde, *Trends Biochem. Sci.* **2017**, *42*, 726.

[20] a) M. V. Cespedes, O. Cano-Garrido, P. Alamo, R. Sala, A. Gallardo, N. Serna, A. Falgas, E. Volta-Duran, I. Casanova, A. Sanchez-Chardi, H. Lopez-Laguna, L. Sanchez-Garcia, J. M. Sanchez, U. Unzueta, E. Vazquez, R. Mangues, A. Villaverde, *Adv. Mater.* **2020**, *32*, 1907348; b) M. Pesarrodona, T. Jauset, Z. V. Díaz-Riascos, A. Sánchez-Chardi, M. E. Beaulieu, J. Seras-Franzoso, L. Sánchez-García, R. Baltà-Foix, S. Mancilla, Y. Fernández, U. Rinas, S. Schwartz, L. Soucek, A. Villaverde, I. Abasolo, E. Vázquez, *Adv. Sci.* **2019**, *6*, 1900849; c) U. Unzueta, M. V. Cespedes, R. Sala, P. Alamo, A. Sanchez-Chardi, M. Pesarrodona, L. Sanchez-Garcia, O. Cano-Garrido, A. Villaverde, E. Vazquez, R. Mangues, J. Seras-Franzoso, *J. Controlled Release* **2018**, *279*, 29; d) M. V. Cespedes, Y. Fernandez, U. Unzueta, R. Mendoza, J. Seras-Franzoso, A. Sanchez-Chardi, P. Alamo, V. Toledo-Rubio, N. Ferrer-Miralles, E. Vazquez, S. Schwartz, I. Abasolo, J. L. Corchero, R. Mangues, A. Villaverde, *Sci. Rep.* **2016**, *6*, 35765.

[21] M. V. Cespedes, U. Unzueta, A. Avino, A. Gallardo, P. Alamo, R. Sala, A. Sanchez-Chardi, I. Casanova, M. A. Mangues, A. Lopez-Pousa, R. Eritja, A. Villaverde, E. Vazquez, R. Mangues, *EMBO Mol. Med.* **2018**, *10*, 8772.

[22] a) A. Falgas, V. Pallares, U. Unzueta, M. V. Cespedes, I. Arroyo-Solera, M. J. Moreno, J. Sierra, A. Gallardo, M. A. Mangues, E. Vazquez, A. Villaverde, R. Mangues, I. Casanova, *Haematologica* **2020**, *105*, 741; b) A. Falgas, V. Pallares, N. Serna, L. Sanchez-Garcia, J. Sierra, A. Gallardo, L. Alba-Castellon, P. Alamo, U. Unzueta, A. Villaverde, E. Vazquez, R. Mangues, I. Casanova, *Theranostics* **2020**, *10*, 5169.

[23] U. Unzueta, M. Roldan, M. Pesarrodona, R. Benitez, A. Sanchez-Chardi, O. Conchillo-Sole, R. Mangues, A. Villaverde, E. Vazquez, *Acta Biomater.* **2020**, *103*, 272.

[24] F. Rueda, M. V. Cespedes, O. Conchillo-Sole, A. Sanchez-Chardi, J. Seras-Franzoso, R. Cubarsi, A. Gallardo, M. Pesarrodona, N. Ferrer-Miralles, X. Daura, E. Vazquez, E. Garcia-Fruitos, R. Mangues, U. Unzueta, A. Villaverde, *Adv. Mater.* **2015**, *27*, 7816.

[25] J. M. Sanchez, L. Sanchez-Garcia, M. Pesarrodona, N. Serna, A. Sanchez-Chardi, U. Unzueta, R. Mangues, E. Vazquez, A. Villaverde, *Biomacromolecules* **2018**, *19*, 3788.

[26] a) N. Serna, M. V. Cespedes, L. Sánchez-García, U. Unzueta, R. Sala, A. Sánchez-Chardi, F. Cortés, N. Ferrer-Miralles, R. Mangues, E. Vázquez, A. Villaverde, *Adv. Funct. Mater.* **2017**, *27*, 1700919; b) N. Serna, O. Cano-Garrido, L. Sánchez-García, M. Pesarrodona, U. Unzueta, A. Sánchez-Chardi, R. Mangues, E. Vázquez, A. Villaverde, *Part. Part. Syst. Charact.* **2020**, *37*, 2000040.

[27] a) H. Tamamura, R. Arakaki, H. Funakoshi, M. Imai, A. Otaka, T. Ibuka, H. Nakashima, T. Murakami, M. Waki, A. Matsumoto, N. Yamamoto, N. Fujii, *Bioorg. Med. Chem.* **1998**, *6*, 231; b) H. Tamamura, M. Imai, T. Ishihara, M. Masuda, H. Funakoshi, H. Oyake, T. Murakami, R. Arakaki, H. Nakashima, A. Otaka, T. Ibuka, M. Waki, A. Matsumoto, N. Yamamoto, N. Fujii, *Bioorg. Med. Chem.* **1998**, *6*, 1033.

[28] a) S. Poty, P. Desogere, C. Goze, F. Boschetti, T. D'Huys, D. Schols, C. Cawthorne, S. J. Archibald, H. R. Maecke, F. Denat, *Dalton Trans.* **2015**, *44*, 5004; b) Y. H. Jung, D. Y. Lee, W. Cha, B. H. Kim, M. W. Sung, K. H. Kim, S. H. Ahn, *Head Neck* **2016**, *38*, 1479.

[29] a) P. Faller, C. Hureau, O. Berthoumieu, *Inorg. Chem.* **2013**, *52*, 12193; b) E. Jozsa, K. Osz, C. Kallay, P. de Bona, C. A. Damante, G. Pappalardo, E. Rizzarelli, I. Sovago, *Dalton Trans.* **2010**, *39*, 7046; c) M. Rana, A. K. Sharma, *Metallomics* **2019**, *11*, 64.

[30] a) L. Molina-Garcia, F. Gasset-Rosa, M. Moreno-Del Alamo, M. E. Fernandez-Tresguerres, S. Moreno-Diaz de la Espina, R. Lurz, R. Giraldo, *Sci. Rep.* **2016**, *6*, 25425; b) S. Shin, S. Cherry, *Immunity* **2017**, *47*, 604; c) M. P. Jackson, E. W. Hewitt, *Biomolecules* **2017**, *7*, 71; d) A. Piscitelli, P. Cicatiello, A. M. Gravagnuolo, I. Sorrentino, C. Pezzella, P. Giardina, *Biomolecules* **2017**, *7*, 45; e) A. Hewetson, H. Q. Do, C. Myers, A. Muthusubramanian, R. B. Sutton, B. J. Wylie, G. A. Cornwall, *Biomolecules* **2017**, *7*, 46; f) N. Van Gerven, S. E. Van der Verren, D. M. Reiter, H. Remaut, *J. Mol. Biol.* **2018**, *430*, 3657; g) K. Schwartz, A. K. Syed, R. E. Stephenson, A. H. Rickard, B. R. Boles, *PLoS Pathog.* **2012**, *8*, e1002744; h) P. Falabella, L. Riviello, M. Pascale, I. D. Lelio, G. Tettamanti, A. Grimaldi, C. Iannone, M. Monti, P. Pucci, A. M. Tamburro, M. Deeguileor, S. Gigliotti, F. Pennacchio, *Insect Biochem. Mol. Biol.* **2012**, *42*, 203; i) M. S. Dueholm, D. Otzen, P. H. Nielsen, *PLoS One* **2013**, *8*, e76630; j) B. Guyonnet, N. Egge, G. A. Cornwall, *Mol. Cell. Biol.* **2014**, *34*, 2624; k) J. D. Taylor, S. J. Matthews, *Front. Cell. Infect. Microbiol.* **2015**, *5*, 33; l) T. Seviour, S. H. Hansen, L. Yang, Y. H. Yau, V. B. Wang, M. R. Stenvang, G. Christiansen, E. Marsili, M. Givskov, Y. Chen, D. E. Otzen, P. H. Nielsen, S. Geifman-Shochat, S. Kjelleberg, M. S. Dueholm, *J. Biol. Chem.* **2015**, *290*, 6457; m) S. M. Lyons, P. Anderson, *Dev. Cell* **2016**, *39*, 131; n) R. D. Rameau, D. N. Jackson, A. Beaussart, Y. F. Dufrene, P. N. Lipke, *mBio* **2016**, *7*, e01815.

[31] M. F. Gebbink, D. Claessen, B. Bouma, L. Dijkhuizen, H. A. Wosten, *Nat. Rev. Microbiol.* **2005**, *3*, 333.

[32] R. A. Akhtar, M. C. Perry, *Bioch. Biophys. Acta* **1979**, *585*, 117.

[33] a) S. Mankar, A. Anoop, S. Sen, S. K. Maji, *Nano Rev.* **2011**, *2*, 6032; b) T. P. J. Knowles, R. Mezzenga, *Adv. Mater.* **2016**, *28*, 6546; c) P. K. R. Tay, P. Q. Nguyen, N. S. Joshi, *ACS Synth. Biol.* **2017**, *6*, 1841; d) G. Wei, Z. Su, N. P. Reynolds, P. Arosio, I. W. Hamley, E. Gazit, R. Mezzenga, *Chem. Soc. Rev.* **2017**, *46*, 4661.

[34] a) L. Sanchez-Garcia, L. Martin, R. Mangues, N. Ferrer-Miralles, E. Vazquez, A. Villaverde, *Microb. Cell Fact.* **2016**, *15*, 33;

© 2021 Wiley-VCH GmbH

b) H. A. Lagasse, A. Alexaki, V. L. Simhadri, N. H. Katagiri, W. Jankowski, Z. E. Sauna, C. Kimchi-Sarfaty, *F1000Research* **2017**, *6*, 113.
[35] E. Voltà-Durán, O. Cano-Garrido, N. Serna, H. López-Laguna, L. Sánchez-García, M. Pesarrodona, A. Sánchez-Chardi, R. Mangues, A. Villaverde, E. Vázquez, U. Unzueta, *Sci. China Mater.* **2020**, *63*, 147.
[36] a) H. López-Laguna, R. Sala, J. M. Sánchez, P. Álamo, U. Unzueta, A. Sánchez-Chardi, N. Serna, L. Sánchez-García, E. Voltà-Durán, R. Mangues, A. Villaverde, E. Vázquez, *Part. Part. Syst. Charact.* **2019**, *36*, 1900304; b) H. López-Laguna, R. Cubarsi, U. Unzueta, R. Mangues, E. Vázquez, A. Villaverde, *Sci. China Mater.* **2020**, *63*, 644.

 © 2021 Wiley-VCH GmbH

Study 6

Ion-dependent slow protein release from in vivo disintegrating micro-granules

Patricia Álamo*, Eloi Parladé*, Hèctor López-Laguna*, Eric Voltà-Durán, Ugutz Unzueta, Esther Vázquez, Ramon Mangues, and Antonio Villaverde

Drug Delivery 2021 · Impact factor (6.819) · Quartile (Q1) · *Equally contributed

Objective 3.b

To test the biomedical applications of **protein-based insoluble microparticles** in mouse models (Biodistribution).

The studies (4 and 5) have revealed our capacity to construct insoluble protein-based microparticles able to liberate nanoparticles in a sustained manner. The system is robust, versatile and easy-to-execute, but its kinetic releasing profiles have been shortly exploited.

Thus, this work has been focused on modulating the fabrication procedure of protein-based microparticles with the idea of changing the material's releasing kinetics and see how it affects the final targeting and specific accumulation tendencies in the desired tissues. In this regard, and aside from testing the gold standard Zn^{2+}, other divalent cations such as Ca^{2+}, Mg^{2+}, and Mn^{2+}, with different chemical reactivities, were tested to induce protein aggregation and subsequent protein release. The obtained data suggested an interesting tendency of Zn^{2+} and Ca^{2+} -based microparticles to liberate in a more sustained way stable protein-based nanoparticles able to target and reach the desired tissue without significant accumulation in off-target tissues. On the other hand, other combinations of divalent cations presented faster kinetics.

DRUG DELIVERY
2021, VOL. 28, NO. 1, 2383–2391
https://doi.org/10.1080/10717544.2021.1998249

Taylor & Francis
Taylor & Francis Group

RESEARCH ARTICLE

OPEN ACCESS Check for updates

Ion-dependent slow protein release from *in vivo* disintegrating micro-granules

Patricia Álamo[a,b,c*], Eloi Parladé[c,d*], Hèctor López-Laguna[c,d,e*], Eric Voltà-Durán[c,d,e], Ugutz Unzueta[a,b,c,e], Esther Vazquez[c,d,e], Ramon Mangues[a,b,c] and Antonio Villaverde[d,e]

[a]Biomedical Research Institute Sant Pau (IIB Sant Pau), Barcelona, Spain; [b]Josep Carreras Leukaemia Research Institute (IJC Campus Sant Pau), Barcelona, Spain; [c]CIBER de Bioingeniería, Biomateriales y Nanomedicina (CIBER-BBN), Madrid, Spain; [d]Institut de Biotecnologia i de Biomedicina, Universitat Autònoma de Barcelona, Bellaterra, Spain; [e]Departament de Genètica i de Microbiologia, Universitat Autònoma de Barcelona, Bellaterra, Spain

ABSTRACT

Through the controlled addition of divalent cations, polyhistidine-tagged proteins can be clustered in form of chemically pure and mechanically stable micron-scale particles. Under physiological conditions, these materials act as self-disintegrating protein depots for the progressive release of the forming polypeptide, with potential applications in protein drug delivery, diagnosis, or theragnosis. Here we have explored the *in vivo* disintegration pattern of a set of such depots, upon subcutaneous administration in mice. These microparticles were fabricated with cationic forms of either Zn, Ca, Mg, or Mn, which abound in the mammalian body. By using a CXCR4-targeted fluorescent protein as a reporter building block we categorized those cations regarding their ability to persist in the administration site and to sustain a slow release of functional protein. Ca^{2+} and specially Zn^{2+} have been observed as particularly good promoters of time-prolonged protein leakage. The released polypeptides result is available for selective molecular interactions, such as specific fluorescent labeling of tumor tissues, in which the protein reaches nearly steady levels.

ARTICLE HISTORY
Received 3 October 2021
Revised 14 October 2021
Accepted 18 October 2021

KEYWORDS
Protein materials; microparticles; protein depots; self-disintegrating materials; tumor targeting

Introduction

Many pharmacological treatments for chronic diseases, such as cancer would benefit from a time-prolonged drug supply aiming at reaching constant or nearly constant levels at the site of action (Natarajan et al., 2014; Koshy et al., 2018; Cross et al., 2019). This is in contrast with the common therapeutic protocols that are based on repetitive drug administrations, frequently given with a few-day time intervals, resulting in oscillating drug concentrations and irregular therapeutic impact (Wen et al., 2015; Zou et al., 2020). Approaching steady drug concentrations in blood is expected to minimize side effects in off-target tissues and to support a potent therapeutic action (Rosen & Abribat, 2005; Wen et al., 2015; Li et al., 2019; Zou et al., 2020), while non-repetitive administrations would reduce the exploitation of sanitary resources (Pareek et al., 2019). Diverse strategies for sustained drug delivery are under exploration, mainly based on porous materials, hydrogels, matrices, or other types of macroscopic, microscale, or nanoscale containers that hold the drug for its progressive leakage (Gilmore et al., 2016; Li & Mooney, 2016; Ali & Ahmed, 2018; Ghalei et al., 2018; Koshy et al., 2018; Wu et al., 2018; Meng et al., 2019). Such methodologies involve a non-drug-containing material that increases the complexity of the system and the fabrication process, often imposing chemical constraints and toxicological concerns (Sharma et al., 2012; Palombo et al., 2014; Aragao-Santiago et al., 2016; Shen et al., 2017). Recently, self-contained, self-disintegrating protein material in form of microparticles have been developed (Chen et al., 2020; Sánchez et al., 2020), suited for a slow protein release *in vivo* (Sánchez et al., 2020; Serna et al., 2020; López-Laguna et al., 2021). These artificial structures mimic the molecular organization and functionality of the secretory granules from the mammalian endocrine system, which contain and release peptidic hormones to the bloodstream (Maji et al., 2009; Mankar et al., 2011; Jacob et al., 2016; Jacob et al., 2019). Such artificial material is based on pure preparations of a single polypeptide species with a fused histidine-rich peptide, and that is clustered as granules around the microscale, by the external addition of Zn^{2+}. The divalent cation generates cross-molecular interactions between histidine-rich domains of adjacent polypeptide chains, which remain attached by such interactions in form of a mechanically stable protein network (López-Laguna et al., 2020). Upon *in vitro* incubation under physiological conditions or by subcutaneous administration *in vivo*, the

CONTACT Ramon Mangues rmangues@santpau.cat Biomedical Research Institute Sant Pau (IIB Sant Pau), Sant Antoni Mª Claret 167, Barcelona, 08025, Spain; Antonio Villaverde antoni.villaverde@uab.cat CIBER de Bioingeniería, Biomateriales y Nanomedicina (CIBER-BBN), C/Monforte de Lemos 3–5, Madrid, 28029, Spain
*These authors contributed equally to this work.

Supplemental data for this article can be accessed here.

© 2021 The Author(s). Published by Informa UK Limited, trading as Taylor & Francis Group.
This is an Open Access article distributed under the terms of the Creative Commons Attribution License (http://creativecommons.org/licenses/by/4.0/), which permits unrestricted use, distribution, and reproduction in any medium, provided the original work is properly cited.

protein granules spontaneously disintegrate, probably by progressive chelation of the clustering ions. This fact allows a slow leakage of the protein building blocks, in a functional form, ready for interactivity or any other biological activity. Divalent non-toxic cations other than Zn^{2+} are, in principle, potentially suited for protein clustering (López-Laguna et al., 2020). By exploring these alternatives, a diversity of related materials could be generated whose properties, regarding the kinetics of protein release, functionality and bioavailability, are presumed to be differential.

Materials and methods

Manufacture of secretory granules and release of soluble protein

Pure soluble T22-GFP-H6 [Figure 1(A), fully described elsewhere (Rueda et al., 2015)], was aliquoted in 250 μL at 2 mg/mL in the storage buffer (166 mM NaCO3H + 333 mM NaCl). Protein precipitation as secretory granules was induced by the direct addition of divalent cations to protein solutions. Different cation: protein molar proportions (and therefore working ion concentrations) were used for the different types of granules, depending on the crosslinking ions. The molar protein amount refers to the molar amount of histidine residues in the overhanging H6 tag (that is, the raw protein molar value x 6). For the construction of Zn-based depots we used a molar ratio 50:1 (at 10 mM Zn^{2+}); for ZnMn-based depots, the ratios were 30:1 (Zn^{2+}) and 70:1 (Mn^{2+}) (at 6 mM Zn^{2+} and 14 mM Mn^{2+}); for ZnMg-based depots, 30:1 Zn^{2+} and 470:1 Mg^{2+} (at 6 mM Zn^{2+} and 94 mM Mg^{2+}); for MnMg depots, 150:1 Mn^{2+} and 350:1 Mg^{2+} (at 30 mM Mn^{2+} and 70 mM Mg^{2+}); for Ca-based depots, the ratio was 350:1 (using 70 mM Ca^{2+}); for CaMn-based depots, ratios were 200:1 Ca^{2+} and 100:1 Mn^{2+} (at 40 mM Ca^{2+} and 20 mM Mn^{2+}); for CaZn-based depots, 270:1 Ca^{2+} and 30:1 Zn^{2+} (at 54 mM Ca^{2+} and 6 mM Zn^{2+}) (see Figure 1(B)). Proportion 1:1 refers to 0.2 mM of both protein and ion. Samples were then incubated at room temperature for 10 min and subsequently centrifuged at 10,000 g and room temperature for 10 min to separate the soluble from the insoluble protein fractions. The insoluble fraction (namely secretory granules) was collected and stored at −80 °C for further use, and the soluble fraction was quantified by Bradford's assay (Maniatis et al., 1989) to determine the amount of precipitated protein in mg. Bacterial inclusion bodies formed by T22-GFP-H6 were prepared by standard bacterial production procedures (Cespedes et al., 2020).

The release of soluble protein from secretory granules was triggered *in vitro* by the direct addition of 250 μL of storage buffer (166 mM $NaCO_3H$ +333 mM NaCl) into the thawed insoluble fraction (namely secretory granules). Samples were properly mixed using a pipette for several minutes and centrifuged at 10,000 g and room temperature for 10 min to collect the soluble fraction (namely released soluble protein).

Size determination of secretory granules and the released soluble protein

The hydrodynamic diameter (in nm) of secretory granules and soluble protein released *in vitro* was determined by dynamic light scattering (DLS) at 25 °C (633 nm), run duration (0.839 s), the number of runs 15, using the forward scatter (for secretory granules) and backscatter (for released soluble protein) detectors, in a Zetasizer NanoZS (Malvern Instruments Limited) using ZEN2112 3 mm quartz batch cuvettes.

In vivo kinetic biodistribution of fluorescent material by subcutaneously implanted granules

In vivo experiments were approved by the Animal Ethics Committee at Hospital de la Santa Creu i Sant Pau (procedure 115_9721) and performed according to European Council directives. To generate the $CXCR4^+$ SW1417 CRC cancer model, four-week-old female mice of the Swiss nude strain, in the 18–20 g body weight range (Charles River, L-Abreslle, France) and maintained in pathogen-free conditions, were used. We injected subcutaneously in the mouse flank (n=) 5×10^6 $CXCR4^+$ SW1417 $CXCR4^+$ human CRC cells, resuspended in 150 μL of media. When tumors reached approximately a 120–200 mm^3 volume, animals were randomly allocated to the different groups and administered in the subcutis of the mouse lumbar region, at the side contralateral to the tumor site, with a pellet of 1 mg of T22-GFP-H6 granules suspended in a 150 μL PBS buffer. Inclusion bodies formed by a recombinant T22-GFP-H6 and purified from bacteria or PBS buffer were injected as controls.

Ten minutes, 5, 10, 24, 48, 120, or 600 h after the administration, mice were registered *in vivo*. The mouse was euthanized, and the kidney, liver, tumor, and tissues surrounding the injection point were resected. Following, we *ex vivo* registered the intensity of the fluorescence emitted by the protein released by the protein depots and biodistributed to the tumor and non-tumor organs and also the fluorescence remaining the injection site, using the IVIS® 200-Spectrum (PerkinElmer, Waltham, MA, USA). The fluorescent signal was digitalized, displayed as pseudocolor overlay, and expressed as radiant efficiency. All experimental data points were corrected by subtracting the mean average radiant efficiency of each respective tissue from mice injected with PBS. Preliminary screening was conducted with one mouse per condition while the final *ex vivo* assay was, at least, performed in duplicate.

Statistical analyses

All statistical analyses and data representation were performed in Graph Pad Prism (v8.0.2).

Results and discussion

To refine the design of such disintegrable protein drug depots with potential for therapeutic applications we have

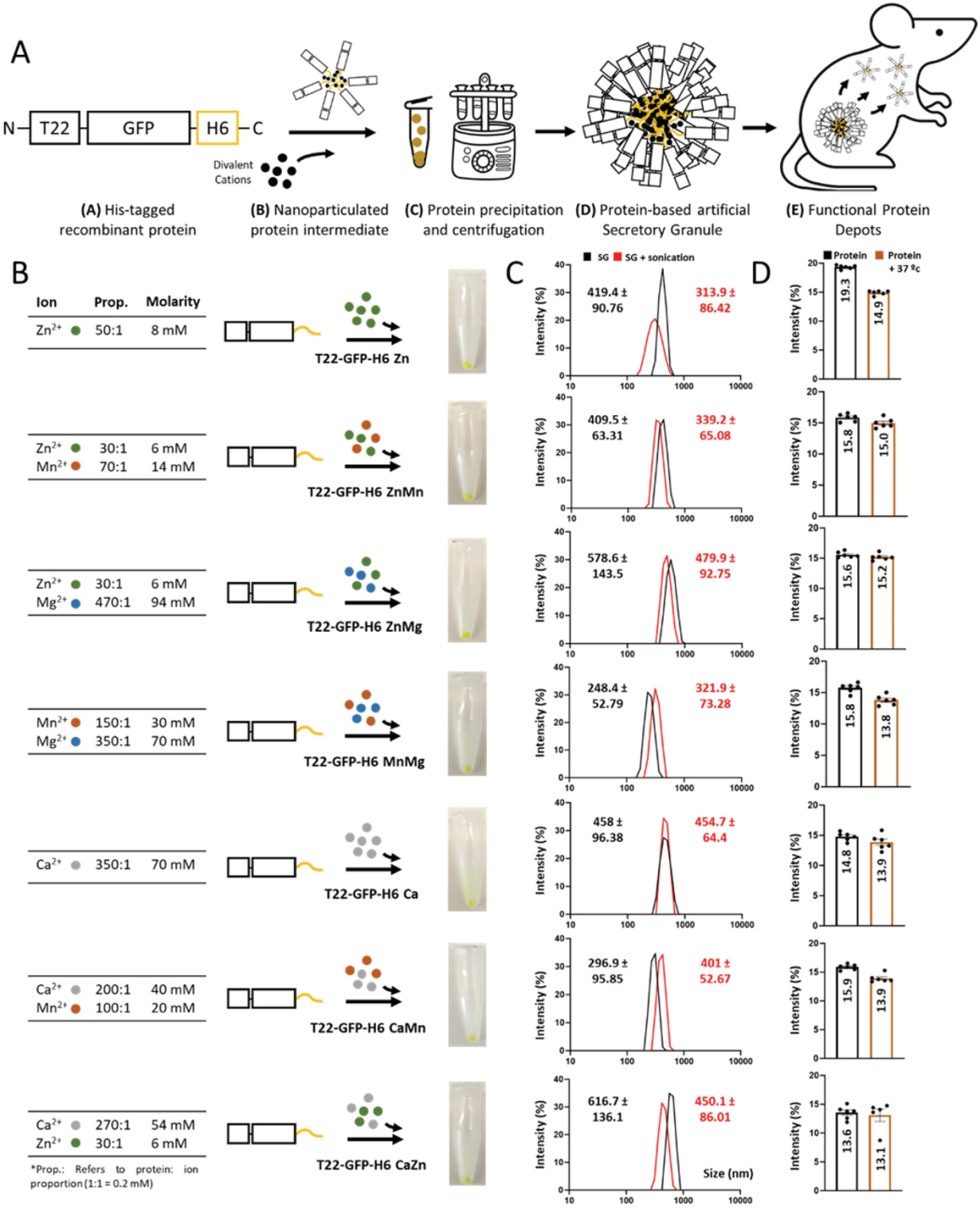

Figure 1. Formulation and physicochemical characterization of secretory granules using different combinations of divalent cations. (A) Schematic representation of the manufacturing process. Architectonically stable protein stages are depicted down below each picture. More details about the organization of final and intermediate materials can be found elsewhere (López-Laguna et al., 2021). (B) Methodological procedure of secretory granules displaying different types of divalent cations and concentrations. Pictures of the resultant pellets are also displayed. (C) Size determination (in nm) by DLS after the preparation of secretory granules (black). Size determination upon sonication (1 min, 10% amplitude, and 0.5 s on/off) to address mechanical stability (red). SG refers to Secretory Granule. Displayed values correspond to peak sizes. (D) Size determination (in nm) by DLS of released soluble protein from secretory granules (black). Size determination upon thermal exposure (37 °C for 24 h) to address thermal stability (brown). All measurements were performed in sextuplicate, and data was represented as mean ± SEM (standard error of the mean).

explored here the use of different divalent cations for the construction of secretory granules of a reporter fluorescent protein (T22-GFP-H6, Figure 1(A)) produced and purified from recombinant bacteria. This has been done to comparatively evaluate how the forming building blocks leak from the depot at the subcutaneous injection site. Several divalent cations, namely those of Zn, Ca, Mn, and Mg, found at relatively high concentrations in living beings, were selected to prevent potential toxicity issues linked to the molecular glue. These physiological linkers were applied to generate, *in vitro*, secretory granules of the modular protein T22-GFP-H6, through a process in which homomeric nanoparticles are intermediates (López-Laguna et al., 2021, Figure 1(A)). This polypeptide contains an enhanced GFP as a core protein for straightforward monitoring of biodistribution, flanked by a C-terminal hexahistidine tail (H6) and an N-terminal cationic peptide, T22. T22 is a ligand of the tumoral marker CXCR4 (Tamamura et al., 1993, 1998a, 1998b), that in form of a recombinant fusion version promotes a highly selective binding and penetration into $CXCR4^+$ cells. Also, it's *in vivo* accumulation in tumoral tissues is detectable through fluorescence (Cespedes et al., 2018; Falgas et al., 2020a, 2020b; Pallares et al., 2020). The combination of T22 and GFP in a single modular polypeptide is then suitable to estimate not only the protein leakage from the injection site but also its final fate when using animal models of $CXCR4^+$ cancers. Also, T22-GFP-H6, in contrast to other previously tested proteins (López-Laguna et al., 2021), is well-aggregated *in vitro* by Zn^{2+} as mechanically stable materials (López-Laguna et al., 2021). In physiological buffer, these clusters release oligomers of the protein (Figure 1(A)) sizing around 13–14 nm (López-Laguna et al., 2021), a size very similar to that reached by the soluble protein version upon a spontaneous self-assembling process (around 12 nm) (Lopez-Laguna et al., 2019).

In this regard, seven versions of T22-GFP-H6 (Figure 1(B)), clustered as mechanically stable micron-scale protein granules (Figure 1(C)) were generated through alternative cations or cation mixtures for subcutaneous administration, a route that allows entry of any leaked protein into the bloodstream but also a local permanence of the remaining material as a depot (Unzueta et al., 2018). The elements selected for clustering were Zn and Ca, alone or as mixtures with Mg and Mn, namely ZnMn, ZnMg, MnMg, CaMn, and CaZn (Figure 1(B)). These cations were selected for their regular presence and relative abundance in living beings (Knape et al., 2017; Pilchova et al., 2017; Al Alawi et al., 2018; Li & Yang, 2018; Pazirandeh et al., 2020; Santos et al., 2020), thus skipping toxicities potentially linked to rarer oligoelements. These ions also cover a wide range in the Irving-Williams (Milicevic et al., 2011) series, which predicts differential stability of the complexes formed by those cations through coordination with histidine residues. In addition, we tested growing cation: protein molar ratios to further expand the range of protein outflow (Figure 1(B)). By using these cations and mixtures we looked for the generation of granules with distinct leakage properties and therefore, different therapeutic potential and applicability in living systems. All the generated granules, with sizes ranging between 300 and 600 nm, resulted mechanically stable as they resisted sonication with only slight size modifications (Figure 1(C)). Also, they exclusively leak, *in vitro*, nanoparticles (but not monomers) of around 13–15 nm that are also structurally stable upon *in vitro* incubation in the physiological buffer for at least 24 h at 37 °C (Figure 1(D)). This observation suggested that the leaked material could be also stable in physiological fluids.

For a fast initial screening, 1 mg of each sample was subcutaneously injected in the CXCR4-expressing SW1417 human colorectal cancer mouse model, as a single dose, in a contralateral remote area regarding the tumor location (Figure 2(A)). The material remaining at the injection point was monitored through fluorescence as an indication of protein loss, during 10 days upon administration. As observed, an inclusion body version of the protein that also releases fluorescent protein material (Unzueta et al., 2018) acting as naturally produced secretory amyloids (Unzueta et al., 2018; Cespedes et al., 2020), was unable to stay at the injection point for long time periods post-administration (Figure 2(B)). In contrast, and in general terms, all the clustered materials were observed as valid depots from which the forming protein was progressively released in comparison to the control, soluble non-clustered protein (Figure 2(B)). However, clear dissimilarities in the protein release rate were also observed. While with some differences, Zn- and Ca-containing materials tended to lose fluorescence more progressively. In contrast, materials in which Mn and Mg participated, including the MnMg combination, showed a tendency to release the protein in a faster way. The MnMg combination resulted in fact in the material disintegrating more rapidly (Figure 2(B)).

Although these data resulted only just from a preliminary screening, the rather consistent negative impact of Mn^{2+} and Mg^{2+} on the permanence of the material at the injection site made us presume that the materials resulting from those ions are more unstable than their counterparts. Then, looking for a time-prolonged release, we took a deeper exploration of the depot potential of Zn- and Ca-based materials. Granules formed with the assistance of either Zn, Ca or a CaZn combination of divalent cations was administered again in the mouse model of human, $CXCR4^+$ SW1417 colorectal cancer, in a larger number of animals. The administration was done in the contralateral area relative to subcutaneous tumors (Figure 2(A)). The loss of fluorescence at the injection point was monitored during relatively long periods of time in whole animals, spanning from the immediate administration to 10 days post-injection (Figure 3). Again, the immediate visualization of fluorescence at the injection point was indicative of an extended permanence of the material in the subcutaneous depot, being Zn^{2+} the clustering ion supporting a slower protein release. However, the whole animal imaging was not precise enough for a fine quantification, and for observing the fate of the released materials. Expectedly, if our starting hypothesis was correct, the protein resulting from the depot disintegration should generate steady fluorescence levels in the $CXCR4^+$ tumor, because of the presence of T22 as a targeting agent (Figure 1(A)).

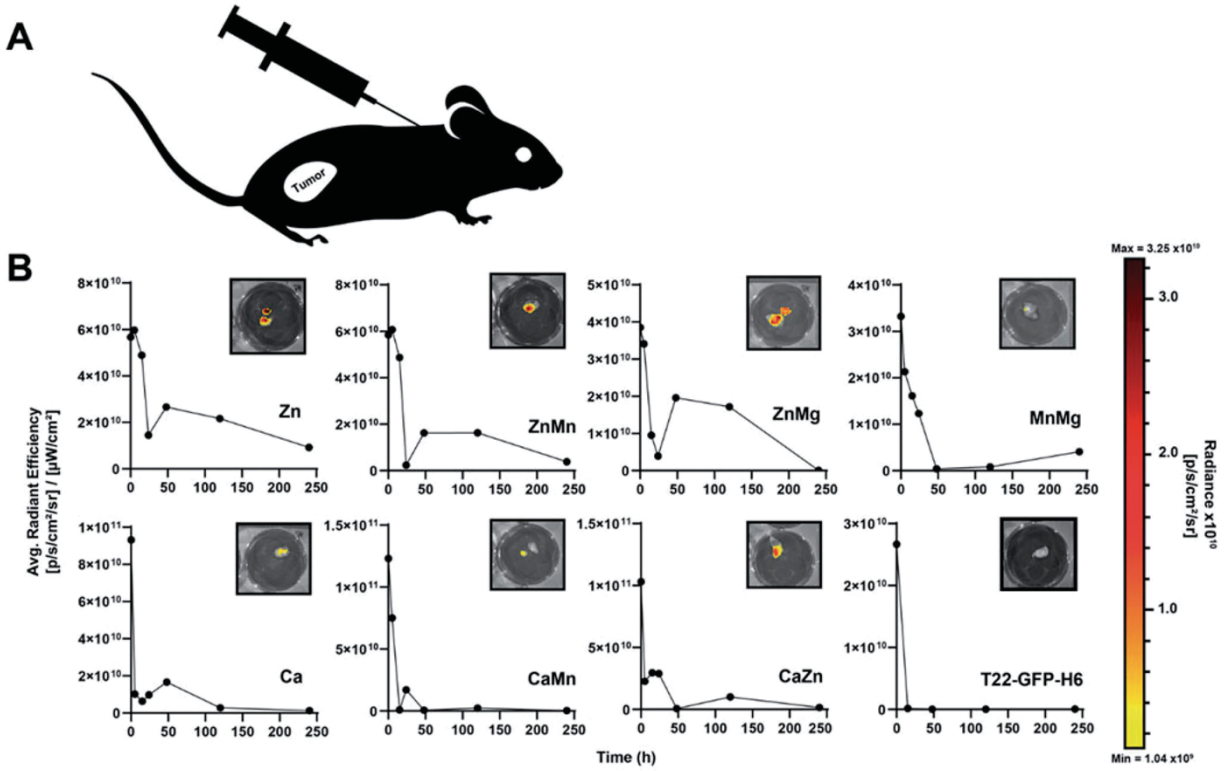

Figure 2. Preliminary screening of protein leakage from the secretory granules. (A) Representation of the injection site, in a contralateral area regarding the tumor in the SW1417 colorectal cancer model. (B) Temporal loss of protein material at the injection point monitored *in vivo* through the emitted fluorescence. In the insets, IVIS images were recorded at 5 days (120 h) post-administration. The scale color bar reflects the radiance expressed as (p/s/cm^2/sr).

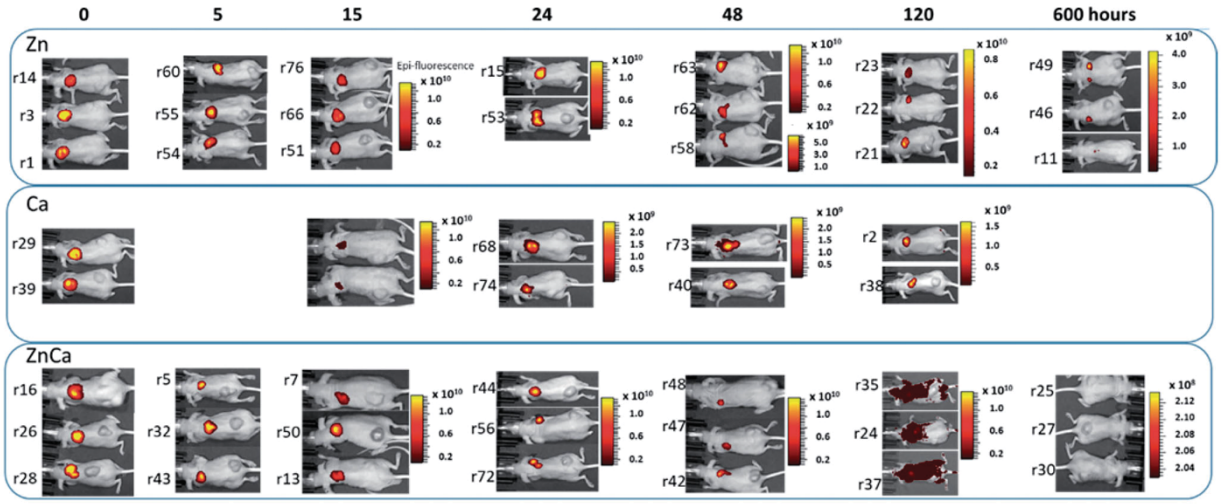

Figure 3. Whole animal IVIS imaging in which the administered material confers fluorescence at the injection point. The administered protein was clustered with divalent cations of either Zn, Ca, or a CaZn mixture as indicated in Figure 1. Numbers at left indicate the particular animal from which the final *ex vivo* reading was recorded (see Supplementary Figure 1). The scale color bar reflects the radiance expressed as (p/s/cm^2/sr).

For that, at the times indicated in Figure 3, animals were euthanized for the *ex vivo* determination of GFP fluorescence in the depots and in the target tumor (Supplementary Figure 1). By the analysis of these *ex vivo* data, the release kinetics of each type of depot was determined. As observed (Figure 4(A,B)), in contrast to inclusion body T22-GFP-H6 that dropped immediately from the injection site, the artificial submicron granules generated with the assistance of ions allowed a sustained protein release, keeping significant amounts of the starting material at the injection point 10 days upon administration (Figure 4, Supplementary Figure 1). Ca-based materials tended to be less supportive of protein permanence than Zn-based counterparts. Then, at a few hours upon administration, an important leakage of the

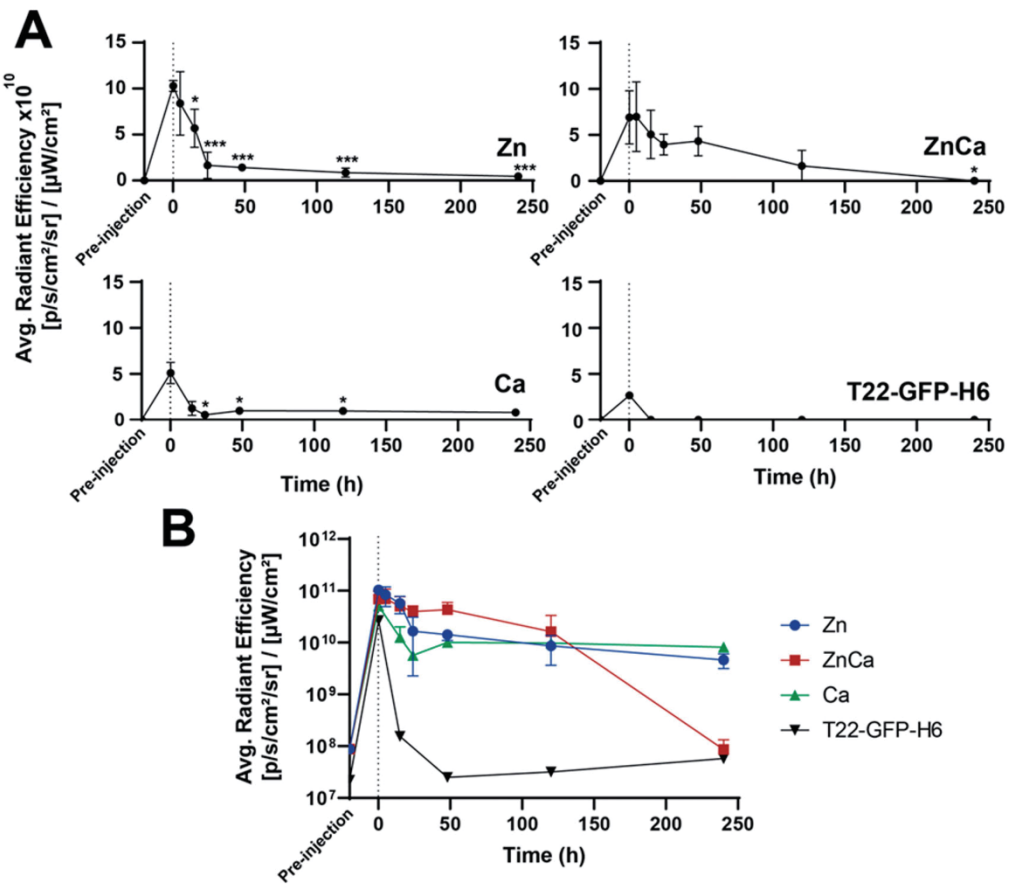

Figure 4. Kinetics of protein depot leakage upon *ex vivo* examination, no background subtraction. (A) Individual kinetics of protein leakage upon subcutaneous administration of either Zn-, Ca-, or CaZn-based granules. Soluble T22-GFP-H6 (in form of nanoparticles) was injected as a control. (B) A comparative plotting of the above data. Differences with data at time 0; $^{*}p \leq .05$, $^{***}p \leq .001$.

protein was observed followed by a smoother release phase (Figure 4(A,B)). In the hybrid CaZn-clustered material, Ca appeared as a negative regulator of protein retention, favoring release. This is an interesting observation as it appears that this cation could be used as a modulator to adjust the leakage rate if designing very precise kinetics is envisaged.

Noting this long permanence of the aggregated protein at the injection site, it would be interesting to know the fate of the released fraction and especially, if the granule-based protein delivery might ensure a steady level of the removed protein at the target site. Such target tissue is, in this system, the $CXCR4^{+}$ tumor toward which the T22 peptide is directed. The *ex vivo* analysis of the fluorescence in the tumor revealed steady levels of fluorescence along the monitored time (Figure 5(A); Supplementary Figure 1). The intensity of the fluorescence in the tumor was between 200 and 300 times lower than those observed at the injection site. An exception was the animals treated with CaZn granules in which the fluorescence at the depot dropped dramatically 10 days upon injection. Interestingly, the observed sets of fluorescence values were rather similar in the three types of tested materials (Figure 5(A)). The protein released from Ca-based granules was particularly steady, as the fluorescence values in the tumor were very constant from a few hours upon injection on, compared to the slightly fluctuating values in the two alternative systems. Because of such stability, we selected the Ca-based model to evaluate, in parallel, the occurrence of GFP fluorescence in two main off-targeted organs, namely the kidney and liver. In this regard, the fluorescence in the tumor was three times higher than that observed in these organs, as evaluated visually by plain kinetic curves (Figure 5(D)), or numerically through the area below the curve (Figure 5(E)). Therefore, T22-GFP-H6 was not only released from the subcutaneous depots during at least 10 days, but the leaked protein also reached steady levels in a target tissue, which are significantly higher than background levels in the kidney and in the liver.

Altogether, these data indicate a promising pattern of the slow disintegration of subcutaneously administered secretory granules, fabricated *in vitro* by the use of divalent cations as protein clustering agents. Importantly, the offered data indicates that the selection of the involved ion determines the strength of the protein-protein contacts and therefore, the rate of protein release during *in vivo* disintegration of the material (Figures 1–3). Importantly, the protein is released from these depots for at least 10 days (Figures 2–4), and it reaches the target organ in a functional form, ensuring steady local levels during the whole experimental time (Figure 5).

We had previously demonstrated that bacterial inclusion bodies, a type of non-toxic amyloids found in recombinant

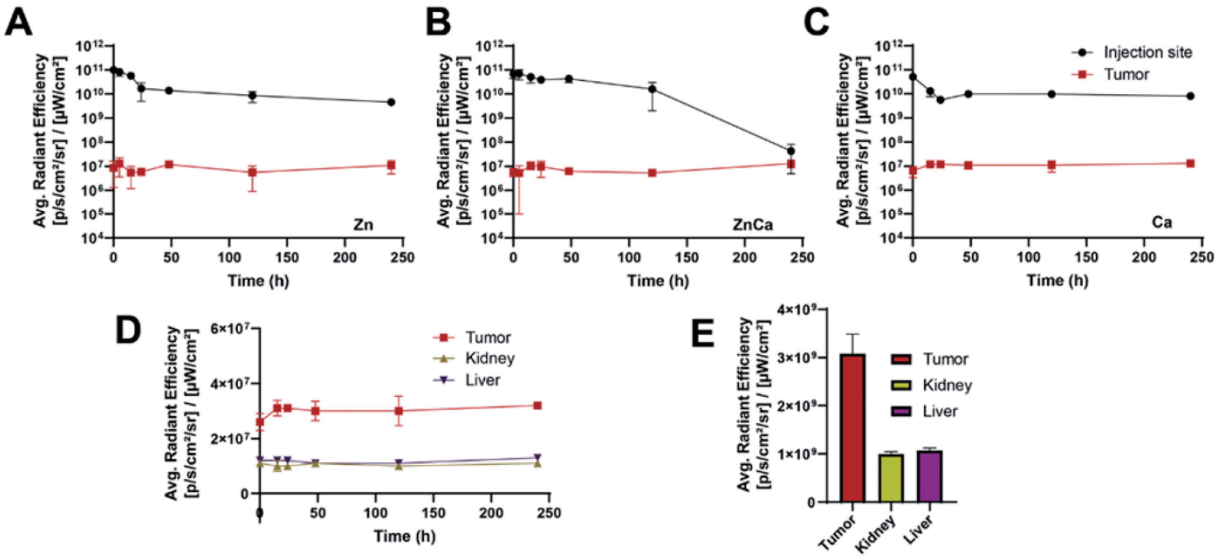

Figure 5. Protein levels at the CXCR4^{+} target tumor. Comparative plotting of fluorescence levels at both the injection site and in tumor upon *ex vivo* analysis, for Zn-based (A), Ca-based (B), or CaZn-based protein depots (C). In Ca-based depots, fluorescence levels in the tumor are plotted together with those in the liver or kidney (D), and the global area under those curves in the monitored time interval is represented for a simple comparison (E).

bacteria (de Marco et al., 2019), can release the forming protein in a functional form, upon local (Cespedes et al., 2016; Pesarrodona et al., 2019) or remote (Unzueta et al., 2018; Cespedes et al., 2020) administration to animals, for a therapeutic effect in breast and colorectal cancer models (Pesarrodona et al., 2019; Cespedes et al., 2020). However, inclusion bodies are highly heterogeneous materials regarding composition, and they trap, during the aggregation of the recombinant protein in the bacterial cytoplasm and the further purification process, numerous bacterial molecules including proteins, nucleic acids, and cell wall components (de Marco et al., 2019). This fact might pose regulatory limitations to the clinical applicability of this material, whose natural formation in the cells cannot be controlled externally and the disintegration process appears to be too fast for a true time-prolonged delivery system (Figure 2). The materials presented here, that are mimetics of those natural inclusion bodies (Sánchez et al., 2020; Sanchez et al., 2021), undergo a chemically controlled fabrication process from a purified protein that is clustered, in a controlled process, by physiological concentrations of divalent cations present in the body. Importantly, the results reported in the present study indicate that the release kinetics from these materials, upon subcutaneous administration, is time-sustained enough to represent a promising candidate for a slow drug delivery system. Importantly, the disintegration process can be regulated in the upstream section of the fabrication by the proper selection of the clustering ion. Among those tested (Figure 1(B)), Zn^{2+} and Ca^{2+} resulted in especially promising as they favor the retention of the polypeptides in the depot and extend their release into the body (Figure 5). The released protein is fluorescent and fully targeted to the tumor in an animal model of human colorectal cancer, accumulating in such a fluorescent form in tumor tissues (Figure 5, Supplementary Figure 1). This fact indicates that apart from mere therapeutic uses, secretory granules might be also used in theragnosis as the time-prolonged release of tumor-targeted protein markers from remote repositories allows a precise visualization of tumor foci. Other strategies have been already developed that use metal coordination to stabilize different categories of nanoparticles for drug delivery (He et al., 2019, 2020), taking advantage of the coordination capacities of Zn and other metals (López-Laguna et al., 2020). On the other hand, metal coordination with polyhistidine stretches has allowed the controlled oligomerization of peptide and protein materials *in vitro*, for the construction of nanostructured immunogens (Manuel-Cabrera et al., 2016), nanotubes (Yewdall et al., 2018), and nanowires (Zhang et al., 2012), among many others (López-Laguna et al., 2020). The exploitation and adaptation of metal and non-metal divalent cations to construct self-disintegrating secretory granules opens a spectrum of possibilities in therapy and diagnosis that could be hardly reached by alternative systems, offering in addition an important extent of versatility regarding the used ion and its capability to retain and leak the protein building blocks.

Altogether, these data and concepts point out synthetic protein granules composed of ion-clustered his-tagged proteins as a regulatable secretory platform for clinical applications that being self-disintegrating, does not need, compared to alternative approaches (Petlin et al., 2017; Ali & Ahmed, 2018; Saghazadeh et al., 2018; Stewart et al., 2018; Safdar et al., 2019), any scaffold material for drug hosting.

Disclosure statement

R.M., E.V., and A.V. are co-founders of NANOLIGENT SL, a company developing tumor-targeted protein-based drugs.

Funding

We are indebted to AGAUR (INVITA, grant 2020PANDE00003), AGAUR (2017SGR-229) and CIBER-BBN (projects NANOPROTHER) granted to A.V. E.V. received support from AEI (PID2019-105416RB-I00/AEI/10.13039/501100011033) and CIBER-BBN (project NANOREMOTE). R.M. received support from ISCIII-AEI (PI18/00650, co-funding FEDER), CIBER-BBN (4NanoMets project), and AGAUR (2017 SGR 865 GRC). U.U. was supported by Miguel Servet contract (CP19/00028) from ISCIII co-funded by European Social Fund (ESF investing in your future) and H.L.L. by a predoctoral fellowship from AGAUR (2019FI_B00352). E.V.D. was supported by a predoctoral fellowship from Ministerio de Ciencia, Innovación y Universidades (FPU18/04615). A.V. received an ICREA ACADEMIA award. U.U received support from ISCIII-AEI (PI20/00400) co-funded by FEDER (a way to make Europe) and Miguel Servet contract (CP19/00028) from ISCIII co-funded by European Social Fund (ESF investing in your future).Protein production was partially performed by the ICTS 'NANBIOSIS,' more specifically by the Protein Production Platform of CIBER in Bioengineering, Biomaterials & Nanomedicine (CIBER-BBN)/IBB, at the UAB (http://www.nanbiosis.es/portfolio/u1-protein-production-platform-ppp/). The *in vivo* work was performed by the ICTS NANBIOSIS of the CIBER-BBN Nanotoxicology Unit (http://www.nanbiosis.es/portfolio/u18-nanotoxicology-unit/).

Data availability statement

The data that support the findings of this study are openly available in DDD (UAB) at https://doi.org/10.5565/ddd.uab.cat/249709 or https://ddd.uab.cat/record/249709.

References

Al Alawi AM, Majoni SW, Falhammar H. (2018). Magnesium and human health: perspectives and research directions. Int J Endocrinol 2018: 9041694.

Ali A, Ahmed S. (2018). A review on chitosan and its nanocomposites in drug delivery. Int J Biol Macromol 109:273–86.

Aragao-Santiago L, Bohr A, Delaval M, et al. (2016). Innovative formulations for controlled drug delivery to the lungs and the technical and toxicological challenges to overcome. Curr Pharm Des 22:1147–60.

Cespedes MV, Cano-Garrido O, Alamo P, et al. (2020). Engineering secretory amyloids for remote and highly selective destruction of metastatic foci. Adv. Mater 32:1907348.

Cespedes MV, Fernandez Y, Unzueta U, et al. (2016). Bacterial mimetics of endocrine secretory granules as immobilized *in vivo* depots for functional protein drugs. Sci Rep 6:35765.

Cespedes MV, Unzueta U, Avino A, et al. (2018). Selective depletion of metastatic stem cells as therapy for human colorectal cancer. EMBO Mol Med 10:e8772.

Chen TY, Cheng WJ, Horng JC, Hsu HY. (2020). Artificial peptide-controlled protein release of Zn(2+)-triggered, self-assembled histidine-tagged protein microparticle. Colloids and Surfaces. B, Biointerfaces 187:110644.

Cross LM, Carrow JK, Ding X, et al. (2019). Sustained and prolonged delivery of protein therapeutics from two-dimensional nanosilicates. ACS Appl Mater Interfaces 11:6741–50.

de Marco A, Ferrer-Miralles N, Garcia-Fruitos E, et al. (2019). Bacterial inclusion bodies are industrially exploitable amyloids. FEMS Microbiol Rev 43:53–72.

Falgas A, Pallares V, Serna N, et al. (2020a). Selective delivery of T22-PE24-H6 to $CXCR^{4+}$ diffuse large B-cell lymphoma cells leads to wide therapeutic index in a disseminated mouse model. Theranostics 10: 5169–80.

Falgas A, Pallares V, Unzueta U, et al. (2020b). A CXCR4-targeted nanocarrier achieves highly selective tumor uptake in diffuse large B-cell lymphoma mouse models. Haematologica 105:741–53.

Ghalei S, Nourmohammadi J, Solouk A, Mirzadeh H. (2018). Enhanced cellular response elicited by addition of amniotic fluid to alginate hydrogel-electrospun silk fibroin fibers for potential wound dressing application. Colloids Surf B Biointerfaces 172:82–9.

Gilmore KA, Lampley MW, Boyer C, Harth E. (2016). Matrices for combined delivery of proteins and synthetic molecules. Adv Drug Deliv Rev 98:77–85.

He Z, Hu Y, Gui Z, et al. (2019). Sustained release of exendin-4 from tannic acid/Fe (III) nanoparticles prolongs blood glycemic control in a mouse model of type II diabetes. J Control Release 301:119–28.

He Z, Nie T, Hu Y, et al. (2020). A polyphenol-metal nanoparticle platform for tunable release of liraglutide to improve blood glycemic control and reduce cardiovascular complications in a mouse model of type II diabetes. J Control Release 318:86–97.

Jacob R, Anoop A, Maji S. (2019). Protein nanofibrils as storage forms of peptide drugs and hormones. Vol. 1174. Singapore: Springer, 265–90.

Jacob RS, Das S, Ghosh S, et al. (2016). Amyloid formation of growth hormone in presence of zinc: relevance to its storage in secretory granules. Sci Rep 6:23370.

Knape MJ, Ballez M, Burghardt NC, et al. (2017). Divalent metal ions control activity and inhibition of protein kinases. Metallomics 9:1576–84.

Koshy ST, Zhang DKY, Grolman JM, et al. (2018). Injectable nanocomposite cryogels for versatile protein drug delivery. Acta Biomater 65: 36–43.

Li C, Wang J, Wang Y, et al. (2019). Recent progress in drug delivery. Acta Pharm Sin B 9:1145–62.

Li J, Mooney D. (2016). Designing hydrogels for controlled drug delivery. Nat Rev Mater 1:16071.

Li L, Yang X. (2018). The essential element manganese, oxidative stress, and metabolic diseases: links and interactions. Oxid Med Cell Longev 2018:7580707.

López-Laguna H, Parladé E, Álamo P, et al. (2021). *In vitro* fabrication of microscale secretory granules. Adv Funct Mater 31:2100914.

López-Laguna H, Sánchez J, Unzueta U, et al. (2020). Divalent cations: a molecular glue for protein materials. Trends Biochem Sci 45: 992–1003.

López-Laguna H, Sánchez JM, Carratalá JV, et al. (2021). Biofabrication of functional protein nanoparticles through simple His-tag engineering. ACS Sustain Chem Eng 9:12341–54.

Lopez-Laguna H, Unzueta U, Conchillo-Sole O, et al. (2019). Assembly of histidine-rich protein materials controlled through divalent cations. Acta Biomater 83:257–64.

Maji SK, Perrin MH, Sawaya MR, et al. (2009). Functional amyloids as natural storage of peptide hormones in pituitary secretory granules. Science 325:328–32.

Maniatis T, Fritsch EF, Sambrook J, Engel J. (1989). Molecular cloning: a laboratory manual. New York, NY: Cold Spring Harbor Laboratory Press.

Mankar S, Anoop A, Sen S, Maji SK. (2011). Nanomaterials: amyloids reflect their brighter side. Nano Rev 2:6032.

Manuel-Cabrera CA, Vallejo-Cardona AA, Padilla-Camberos E, et al. (2016). Self-assembly of hexahistidine-tagged tobacco etch virus capsid protein into microfilaments that induce IgG2-specific response against a soluble porcine reproductive and respiratory syndrome virus chimeric protein. Virol J 13:196.

Meng D, Lei H, Zheng X, et al. (2019). A temperature-sensitive phase-change hydrogel of tamoxifen achieves the long-acting antitumor activation on breast cancer cells. Onco Targets Ther 12:3919–31.

Milicevic A, Branica G, Raos N. (2011). Irving-Williams order in the framework of connectivity index $^{3}\chi v$ enables simultaneous prediction of stability constants of bivalent transition metal complexes. Molecules 16:1103–12.

Natarajan JV, Nugraha C, Ng XW, Venkatraman S. (2014). Sustained-release from nanocarriers: a review. J Control Release 193:122–38.

Pallares V, Unzueta U, Falgas A, et al. (2020). An Auristatin nanoconjugate targeting $CXCR^{4+}$ leukemic cells blocks acute myeloid leukemia dissemination. J Hematol Oncol 13:36.

Palombo M, Deshmukh M, Myers D, et al. (2014). Pharmaceutical and toxicological properties of engineered nanomaterials for drug delivery. Annu Rev Pharmacol Toxicol 54:581–98.

Pareek SP, Kumawat S, Sharma V, et al. (2019). Review on sustained release technology. Int J Pharma Biol Sci Archiv 7:29–38.

Pazirandeh S, Burns D, Griffin U. (2020). Overview of dietary trace elements [last accessed 25 Jul 2020].

Pesarrodona M, Jauset T, Díaz-Riascos ZV, et al. (2019). Targeting antitumoral proteins to breast cancer by local administration of functional inclusion bodies. Adv Sci 6:1900849.

Petlin DG, Tverdokhlebov SI, Anissimov YG. (2017). Plasma treatment as an efficient tool for controlled drug release from polymeric materials: a review. J Control Release 266:57–74.

Pilchova I, Klacanova K, Tatarkova Z, et al. (2017). The involvement of Mg^{2+} in regulation of cellular and mitochondrial functions. Oxid Med Cell Longev 2017:6797460.

Rosen H, Abribat T. (2005). The rise and rise of drug delivery. Nat Rev Drug Discov 4:381–5.

Rueda F, Cespedes MV, Conchillo-Sole O, et al. (2015). Bottom-up instructive quality control in the biofabrication of smart protein materials. Adv Mater 27:7816–22.

Safdar R, Omar AA, Arunagiri A, et al. (2019). Potential of Chitosan and its derivatives for controlled drug release applications – a review. J Drug Delivery Sci Technol 49:642–59.

Saghazadeh S, Rinoldi C, Schot M, et al. (2018). Drug delivery systems and materials for wound healing applications. Adv Drug Deliv Rev 127:138–66.

Sánchez J, López-Laguna H, Álamo P, et al. (2020). Artificial inclusion bodies for clinical development. Adv Sci 7:1902420.

Sanchez JM, López-Laguna H, Serna N, et al. (2021). Engineering the performance of artificial inclusion bodies built of catalytic β-galactosidase. ACS Sustain Chem Eng 9:2552–8.

Santos HO, Teixeira FJ, Schoenfeld BJ. (2020). Dietary vs. pharmacological doses of zinc: a clinical review. Clin Nutr 39:1345–53.

Serna N, Cano-Garrido O, Sanchez JM, et al. (2020). Release of functional fibroblast growth factor-2 from artificial inclusion bodies. J Control Release 327:61–9.

Sharma A, Madhunapantula SV, Robertson GP. (2012). Toxicological considerations when creating nanoparticle-based drugs and drug delivery systems. Expert Opin Drug Metab Toxicol 8:47–69.

Shen J, Wolfram J, Ferrari M, Shen H. (2017). Taking the vehicle out of drug delivery. Mater Today 20:95–7.

Stewart SA, Domínguez-Robles J, Donnelly RF, Larrañeta E. (2018). Implantable polymeric drug delivery devices: classification, manufacture, materials, and clinical applications. Polymers 10:1379.

Tamamura H, Arakaki R, Funakoshi H, et al. (1998a). Effective lowly cytotoxic analogs of an HIV-cell fusion inhibitor, T22 ([Tyr5,12, Lys7]-polyphemusin II). Bioorg Med Chem 6:231–8.

Tamamura H, Imai M, Ishihara T, et al. (1998b). Pharmacophore identification of a chemokine receptor (CXCR4) antagonist, T22 ([Tyr(5,12),Lys7]-polyphemusin II), which specifically blocks T cell-line-tropic HIV-1 infection. Bioorg Med Chem 6:1033–41.

Tamamura H, Kuroda M, Masuda M, et al. (1993). A comparative study of the solution structures of tachyplesin I and a novel anti-HIV synthetic peptide, T22 ([Tyr5,12, Lys7]-polyphemusin II), determined by nuclear magnetic resonance. Biochim Biophys Acta 1163:209–16.

Unzueta U, Cespedes MV, Sala R, et al. (2018). Release of targeted protein nanoparticles from functional bacterial amyloids: a death star-like approach. J Control Release 279:29–39.

Wen H, Jung H, Li X. (2015). Drug delivery approaches in addressing clinical pharmacology-related issues: opportunities and challenges. AAPS J 17:1327–40.

Wu J, Li P, Dong C, et al. (2018). Rationally designed synthetic protein hydrogels with predictable mechanical properties. Nat Commun 9: 620.

Yewdall NA, Allison TM, Pearce FG, et al. (2018). Self-assembly of toroidal proteins explored using native mass spectrometry. Chem Sci 9: 6099–106.

Zhang W, Luo Q, Miao L, et al. (2012). Self-assembly of glutathione S-transferase into nanowires. Nanoscale 4:5847–51.

Zou H, Banerjee P, Leung SSY, Yan X. (2020). Application of pharmacokinetic-pharmacodynamic modeling in drug delivery: development and challenges. Front Pharmacol 11:997.

Study 7

Divalent Cations: A Molecular Glue for Protein Materials

Hèctor López-Laguna, Julieta Sánchez, Ugutz Unzueta, Ramón Mangues, Esther Vázquez, and Antonio Villaverde

Trends in Biochemical Sciences 2020 · Impact factor (13.807) · Quartile (Q1)

Objective 4

To review all the extracted knowledge and condense it as practical guidelines for the scientific community.

After all the extensive studies exposed so far in which the histidine tag-divalent cation principle allows to formulate well-defined, scalable, biocompatible, and efficient protein-based materials in a reproducible manner, we wanted to perform a detailed overview on how divalent cations appear as highly versatile gluing entities to create novel purpose-tailored functional devices. Thus, this work has been focused on describing practical guidelines for the scientific community to address the unmet clinical needs in precision medicine using this simplistic type of biochemical-based technology.

Trends in Biochemical Sciences

CellPress
REVIEWS

Review

Divalent Cations: A Molecular Glue for Protein Materials

Hèctor López-Laguna,[1,2,3] Julieta Sánchez,[1,2,4] Ugutz Unzueta,[2,3,5,6,*] Ramón Mangues,[3,5,6] Esther Vázquez,[1,2,3] and Antonio Villaverde[1,2,3,*]

Among inorganic materials, divalent cations modulate thousands of physiological processes that support life. Their roles in protein assembly and aggregation are less known, although they are progressively being brought to light. We review the structural roles of divalent cations here, as well as the novel protein materials that are under development, in which they are used as glue-like agents. More specifically, we discuss how mechanically stable nanoparticles, fibers, matrices, and hydrogels are generated through their coordination with histidine-rich proteins. We also describe how the rational use of divalent cations combined with simple protein engineering offers unexpected and very simple biochemical approaches to biomaterial design that might address unmet clinical needs in precision medicine.

Highlights

Divalent cations are essential agents in life with myriads of molecular functions and lesser known structural roles, acting as glue-like agents.

By exploiting the architectonic properties of Zn^{2+} and others, novel protein materials are generated, including particles, fibers, matrices, and a diversity of ordered and amorphous clusters.

These materials result from the controlled coordination of divalent cations, at physiological concentrations, with histidine-rich proteins.

Among them, soluble self-assembling oligomers serve as protein-only nanomedicines or nanocarriers for intravenous administration.

Amyloidal protein clusters mimic the function of endocrine secretory granules, releasing protein drugs.

Functional protein materials assembled by divalent cations offer unexpected tools in precision medicines through biocompatible scaffolds, drugs, and drug delivery agents.

Divalent Cations in Living Systems

Apart from oxygen and nitrogen, which delineate 98% of our atmosphere and sustain all living organisms, there is a long list of elements that, in the form of **ions** (see Glossary), exhibit critical roles in biological survival and adaptability and support essential biochemical functions [1–3]. In fact, **inorganic molecules** are deeply interdigitated with **organic molecules** at the cell level (Figure 1) to perform complex biological functions [3–6]. Among all existing ions, **divalent cations** present protruding roles in life because of their versatility and interactivity. Those chemical elements are key players in a plethora of cellular and subcellular processes, including structural coordination, function and metabolism of proteins [7], DNA [8] and RNA [9], and in myriads of molecular, cellular, and organic processes. This makes them essential for the proper functioning of neuromuscular, digestive, hormonal, renal, metabolic, and cardiovascular systems. For this reason, alterations in their physiological concentrations break the organic **homeostasis**. This is associated with several major human illnesses (summarized in Table 1), most derived from dietary deficiencies but some of them being clearly iatrogenic. For instance, the intake of calcium is very common for prevention and treatment of osteoporosis, but uncontrolled supplementation can lead to myocardial infarction, constipation, colorectal neoplasms, and kidney stones [10]. Manganese poisoning is common in at-risk populations such as miners, welders, and steel makers and it is associated, as in deficiency, with metabolic and neuropsychiatric disorders [11]. Cobalt, a constituent of vitamin B12 and various enzymes, can be overloaded in different ways; occupationally, to increase sport performance, as a treatment for anemia, or by medical implants, resulting in nonischemic cardiomyopathies [12]. Cobalt deficiency is very rare since only traces are required for homeostasis [12]. Magnesium, zinc, and copper act as enzyme cofactors (among other functions) and their relatively common dietary deficiencies are associated with metabolic and organic dysfunctions [13–15] (Table 1). Importantly, the link between some elements and neurodegenerative diseases (Table 1) is based on structural roles of these elements, as divalent cations, supporting the architecture of multiprotein complexes. This will be discussed in detail in the next section, focusing on the unexpected possibilities that divalent cations offer for the generation of bio-inspired protein materials.

[1]Institut de Biotecnologia i de Biomedicina, Universitat Autònoma de Barcelona, Bellaterra, 08193, Barcelona, Spain
[2]Departament de Genètica i de Microbiologia, Universitat Autònoma de Barcelona, Bellaterra, 08193, Barcelona, Spain
[3]CIBER de Bioingeniería, Biomateriales y Nanomedicina (CIBER-BBN), Madrid, Spain
[4]Instituto de Investigaciones Biológicas y Tecnológicas (IIBYT) (CONICET-Universidad Nacional de Córdoba), ICTA & Cátedra de Química Biológica, Departamento de Química, FCEFyN, X 5016GCA, Córdoba, Argentina

© 2020 Elsevier Ltd. All rights reserved.

Trends in Biochemical Sciences

CellPress
REVIEWS

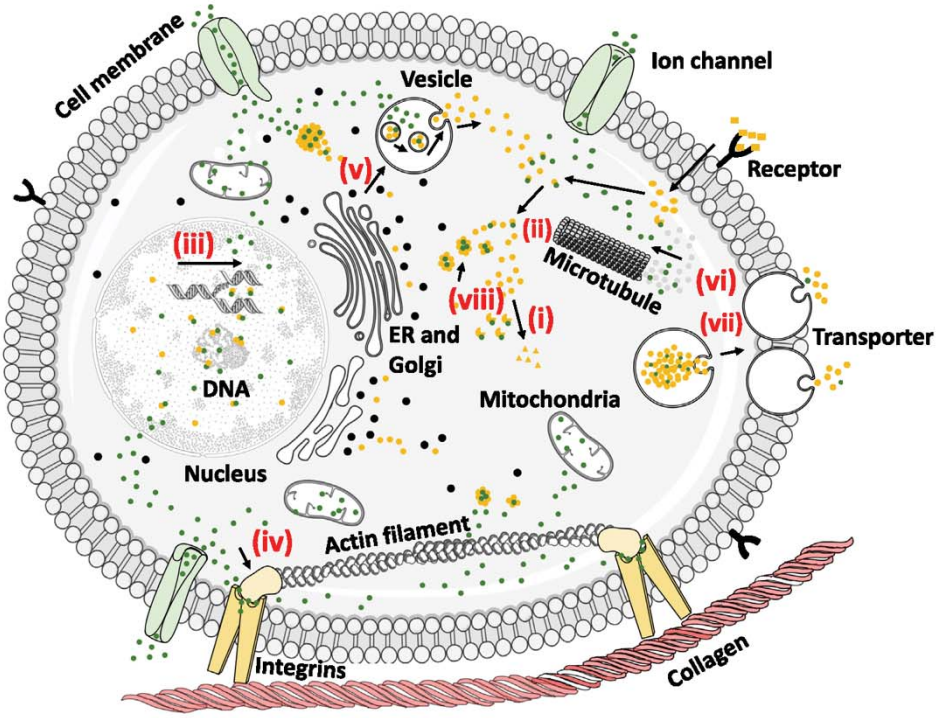

Figure 1. Categories of Physiological Functions of Divalent Cations in Cells. (i) Ions are involved in enzymatic reactions, acting as Lewis acids, accepting electron pairs and constituting the catalytic sites, to promote hydrolysis, hydration, phosphorylation, and carboxylation, among other transformations. (ii) Also, they participate in protein signaling, playing critical roles in kinase and pseudokinase activation. This fact ensures protein phosphorylation, a key event in the regulation of the eukaryotic signal transduction. (iii) DNA synthesis and cell proliferation are modulated by ions, which reduce the energy barrier of the transition state necessary to promote DNA synthesis by DNA polymerases. (iv) Regarding cell adhesion, they play pivotal roles in integrin–ligand affinity, by modulating cell–cell, cell–matrix, and cell–pathogen interactions. (v) In intracellular trafficking, ions regulate the assembling of actin filaments due to a tight interaction with ATP phosphates bound to actin. Acting filaments are the major structures that determine the dynamics of cell cytoskeleton, which is ultimately supported by the structural role of cations. (vi) Another structural role involves the assembling of microtubules by tailoring tubulin conformation. (vii) The hormone aggregation, storage, and secretion by ions is the basis of the artificial secretory granules that are described in the main text. Divalent cations act as an ionic framework in which different types of endocrine hormones, including amylin, glucagon, gastrin, oxytocin, insulin, or growth hormone are stored for further release. (viii) Finally, divalent cations are involved in different modalities of protein oligomerization inside the cell, forming supramolecular complexes that, again, inspire artificial protein constructs aimed at clinical applications. Divalent cations are displayed as green dots, proteins as yellow dots, and ribosomes as black dots. Compartment or organelle names are correspondingly indicated. Abbreviation: ER, Endoplasmic reticulum.

Divalent Cations in Natural and Networking Processes

Amidst all different elements in the periodic table, transition **cations** such as iron, copper, zinc, manganese, cobalt, and nickel, and alkaline-earth cations such as magnesium and calcium, are the major executors of essential cellular roles (Figure 1). Starting from the cell surface, calcium ion (Ca^{2+}) induces bent-like conformational changes into integrins, avoiding their proper anchoring to the cell membrane and preventing proper cell adhesion. Meanwhile, integrin activation and attachment occurs by displacement of Ca^{2+} with magnesium (Mg^{2+}) or manganese (Mn^{2+}) ions [16]. Moving inwards, divalent cations regulate and maintain the cell cytoskeleton through crosslinking and assembling intermediate filaments such as vimentin. Low zinc ion (Zn^{2+}) concentrations leads to a strong bundle network formation, not altered at higher concentrations. In contrast, Ca^{2+} needs a concentration two orders of magnitude higher to achieve the same effect.

[5]Biomedical Research Institute Sant Pau (IIB-Sant Pau), Hospital de la Santa Creu i Sant Pau, 08041 Barcelona, Spain
[6]Josep Carreras Research Institute, 08041 Barcelona, Spain

*Correspondence:
uunzueta@santpau.cat (U. Unzueta) and
Antoni.Villaverde@uab.cat
(A. Villaverde).

Trends in Biochemical Sciences

CellPress REVIEWS

Table 1. Description of the Main Physiological Functions and Plausible Abnormalities Linked to the Divalent Cations That Are Essential in Life

Ion	Group nature	Physiological function	Abnormality	Refs
Fe^{2+}	Transition metal	Part of hemoglobin, myoglobin, cytochrome proteins, myeloperoxidase, NO synthase, coenzyme Q10, respiratory complex, etc.	Deficit: anemia Overload: hemochromatosis, thalassemia, myelodysplastic syndromes, liver and cardiovascular diseases	[84]
Cu^{2+}	Transition metal	Catalytic cofactor in redox chemistry of proteins, important in growth and development	Deficit: multisystem affectation by altered energy production, metabolism, and oxidative damage Overload: Wilson and Menkes disease, Alzheimer's disease	[13]
Zn^{2+}	Transition metal	Required for the function of around 300 enzymes and 1000 transcription factors	Deficit: infections, diarrhea, eye and skin lesions, altered immunity and cognition Overload: neurotoxicity and Ca^{2+} deregulation	[15]
Mn^{2+}	Transition metal	Essential in activation of enzymes and regulator of metabolism and oxidative stress	Related to: neuropsychiatric and metabolic diseases	[11]
Co^{2+}	Transition metal	Key constituent of vitamin B12, methionine aminopeptidase 2, and nitrile hydratase	Overload: cancer and cardiomyopathy	[12]
Ni^{2+}	Transition metal	Cofactor for carbon monoxide dehydrogenase, acetyl-CoA synthase, and nickel superoxide dismutase	Related to: cancer, allergy, cardiovascular and kidney diseases, and in lung fibrosis	[11,85]
Mg^{2+}	Alkaline earth metal	Cofactor of around 300 enzymes, regulates muscle contraction, neuromuscular conduction, glycemia, etc.	Deficit: multisystem disorder Overload: associated to higher mortality	[14]
Ca^{2+}	Alkaline earth metal	Essential in maintenance of skeleton, vascular hormonal secretion, transmission of nerve impulse	Dysregulated in: neurodegenerative, cardiovascular, gastrointestinal, and renal diseases Overload: myocardial infarction, constipation, colorectal neoplasms, and kidney stones	[10]

This finding suggests a competitive binding between the two cations with vimentin, whereas specific cation regulation may control the cell cytoplasmic mechanics [17]. Divalent cations are also involved in the control of signal transduction by protein kinases. As an example, Mg^{2+}, Zn^{2+}, and Mn^{2+} assist in substrate binding and phosphoryl transfer by protein kinase A (PKA). However, while Mg^{2+} stabilizes PKA in an active conformation, accelerating the product release and turnover catalysis, Zn^{2+} and Mn^{2+} induce a catalytically unproductive conformation, crucial to maintain a noncatalytic state [18]; although, Mg^{2+} is a cofactor for ATPases involved in ion transport. It also alters the electrophysiology of Ca^{2+} and potassium ion (K^+) channels and affects the Ca^{2+} capacity to assemble specific Ca^{2+}-binding proteins such as calmodulin, S100, troponin C, and parvalbumin. More importantly, Mg^{2+} plays essential roles inside the mitochondria in conjunction with Ca^{2+}, conforming these organelles as important intracellular stores of Mg^{2+} [19]. Finally, the proper function of DNA polymerases A and B is rooted thanks to the coordination with an octahedral complex formed by Mg^{2+} and Mn^{2+}, as this complex is essential for nucleotidyl transfer reaction, base excision, and proofreading [8]. Notably, ions participate in 70% of binding sites and active sites of intracellular enzymes [20], becoming then main regulators of the whole metabolism (Figure 1).

Glossary

Aβ aggregates: insoluble amyloid aggregates based on a β-sheet secondary structure.
Aβ oligomers: quaternary structure of Aβ peptide and the precursor of Aβ aggregates.
Amyloidosis: group of diseases produced by the abnormal protein aggregation into amyloid fibrils.
Antimetastatic effect: inhibition of migration and/or implantation of tumoral cells to healthy tissues.
β-sheet: common secondary structure motif based of three backbone hydrogen bonds forming a generally twisted, pleated sheet.
Cation: ionic species with a positive charge.
Cross β-sheet: parallel β-strands arranged perpendicularly to the fibril axis.
Divalent cation: ionic species with $^{2+}$ cationic valence.
EDTA: ethylenediaminetetraacetic acid; chelating agent of metal complexes and ions in solution.
Floxuridine: chemotherapeutical antimetabolite drug used to treat cancer.
Fourier-transform infrared spectroscopy (FTIR): infrared spectrum obtained from absorption or emission processes of a solid, liquid, or gas molecule. Particularly, it is applied to detect the secondary structure in proteins.
Functional amyloids: a category of amyloids, not involved in diseases, that shows biological roles in life, such as functional regulation or protein storage.
GFP: a green fluorescent protein from the *Aequorea victoria* jellyfish.
Hexahistidine (H6): amino acid peptide that consists of six sequential histidine residues.
His-rich proteins: proteins with high percentage of histidine residues in its amino acid sequence.
His-tagged proteins: proteins with an added histidine-rich peptide usually fused to either its N or C terminus.
Homeostasis: the dynamic ability or tendency of a living organism or cell to keep internal stable conditions, despite environmental variability.
Inorganic molecules: chemical compounds devoid of carbon–hydrogen bonds.
Ion: an electrically charged atom or groups of atoms formed by the gain or loss of electrons.

Trends in Biochemical Sciences

CellPress
REVIEWS

Divalent Cations in Natural Protein Aggregation Processes

Noting some of the functions previously described (Figure 1), divalent cations show the intrinsic capacity to promote different extents of **protein aggregation** and several categories of supramolecular protein complexes in all biological systems, including viruses [21]. Amongst them, **amyloidosis** (Figure 2) is of special interest because of the stability of the resulting structures (usually inert amyloid fibrils) and because of the toxicity that such aggregates show on cells and tissues, that, triggered by the final aggregated forms or some intermediate oligomers, result in severe degenerative diseases [22]. Amyloid materials are formed *in vitro* and *in vivo* with the participation of divalent cations, through diverse aggregation routes that involve the protein quality control machinery (Figure 2). Protein functionalities are observed in a particular category of amyloid materials, so-called **functional amyloids** [23], that are formed by controlled aggregation processes inside the cell (Figure 2) and that are generally nontoxic. Functional amyloids keep the biological activities of the forming protein or gain novel functionalities conferred by such structured form, acting in several regulatory circuits [23].

Several cations are involved in different amylogenic processes that result in either toxic or functional amyloids. For instance, Ca^{2+} and copper (Cu^{2+}) ions induce structural transition of α-synuclein (α-Syn) monomers that prompt a rapid fibrillation and subsequent interfibrillar aggregation via electrostatic and hydrophobic interactions [24,25]. That is why Cu^{2+} is commonly associated with α-synucleinopathies presenting a high binding affinity to α-Syn (K_d ~10^{-6}–10^{-10} M) in a unique binding site at the N terminus and a histidine residue at position 50. In contrast, Ca^{2+} shows lower binding affinity (K_d ~10^{-3} M) to α-Syn [26]. The difference in the binding affinities

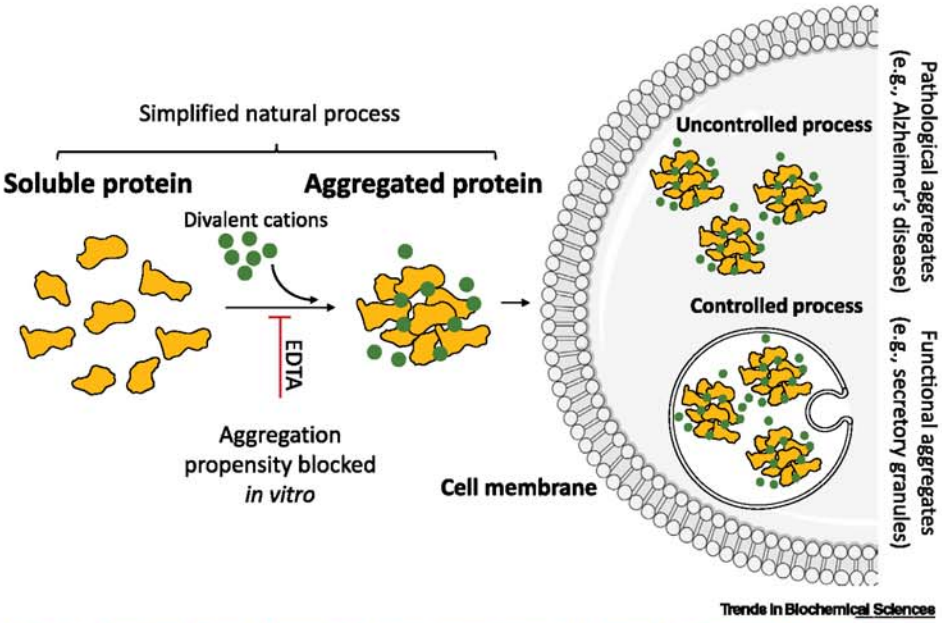

Figure 2. Simplified Natural Process in Which Coordination of Divalent Cations with Proteins Induces Subsequent Aggregation, Which Can Be Avoided by Addition of EDTA into the Solution. In living systems, if protein aggregation results from uncontrolled nonphysiological protein misfolding, it leads to cell death and tissue damage (e.g., neuronal death and tissue damage in Alzheimer's disease). Under cell regulation, protein aggregation is used to store functional proteins in the form of secretory granules through a physiological oligomerization and aggregation that ensures later protein secretion. Both protein oligomerization and aggregation *in vivo* are surveilled by the protein quality control system [93–96], a complex machinery mainly composed of chaperones and proteases that manage protein folding, misfolding, and integrity.

Microparticles: particles with a generic diameter between 100 and 1000 nanometers.
Inclusion bodies (IBs): protein aggregates usually formed in recombinant bacteria.
Nanobiochemistry: scientific field in which biochemistry and nanoscience are combined to produce nanoscale biological compounds with biotechnological and medical applications.
Nanoparticles: particles with a generic diameter between 1 and 100 nanometers.
Organic molecules: chemical compounds based on carbon–hydrogen bonds.
Protein aggregation: phenomenon by which misfolded proteins accumulate and clump together into a rather amorphous larger structure.
Protein assembly: gathering process in which different proteins are added progressively to form a well-defined larger structure.
Recommended dietary allowance (RDA): the recommended average amounts of daily dietary intake believed to meet the nutritional requirements in healthy adults.
Toroidal architecture: structural disposition of a material forming a solid body with a hole in the center, like a doughnut or a circle.

Trends in Biochemical Sciences

CellPress REVIEWS

must be due to the inorganic properties of the cations rather than their nature. Among divalent first row transition metals, Cu^{2+} forms the highest stable complexes (Irving-William series) [27]. However, a similar event is observed in Alzheimer's disease, in which an amyloid β peptide (Aβ) is the precursor of the succeeding plaque-like and tangle structures that cause an obvious toxic effect in the brain [28]. In this case, divalent cations are thought to induce the formation of **Aβ oligomers**, taking advantage of peptide misfolding and inducing aggregation, which yields fibril-like precipitates. Specifically, the stabilization of Aβ oligomers depends on three histidine residues in the amino terminus, which are coordinated with divalent cations [29]. Still, there is no consensus regarding the specific roles of each divalent cation. Some authors propose that Cu^{2+} is the major stabilizer of the smallest soluble oligomers that induce neuron death, whereas Zn^{2+} would induce the formation of larger and less toxic amyloid **Aβ aggregates**. Other researchers propose that both cations are essential throughout all of the aggregation process [30].

Protein Aggregation Offers Live-Supporting Functions

Likewise, divalent cations exhibit crucial roles in nonpathological amylogenesis that results in protein clusters involved in physiological regulation (Figure 2). Among nontoxic functional amyloids, secretory granules in the human endocrine system ensure the storage and slow release of peptide and protein hormones into the bloodstream [31]. In the case of the growth hormone (GH), Zn^{2+}, present at significant amounts in the granules [32], initiates early protein oligomerization into **cross β-sheet** fibrillar aggregates, prompting the subsequent amyloid formation as secretory granules inside the pituitary gland. This gland is sensitive to somatotrophs, so that it releases GH monomers when stimulation occurs. The involvement of Zn^{2+} in GH amyloid formation was confirmed when **EDTA** addition to the media blocked amyloidosis [32]. In a similar way, insulin is stored in pancreatic secretory granules in the form of inactive aggregated-like hexamers, which crystallize at low pH in presence of Zn^{2+} [33]. B10-chain histidine residues of three insulin monomers were established as strong binding sites, allowing Zn^{2+} coordination and subsequent aggregation [34]. Ca^{2+} has also been implicated as a stabilizer of the hexameric form by screening the repulsion between the negatively charged groups of the structure [34].

Cation-Modulated, Amyloid Formation Supported by Histidine Residues

The formation of amyloid fibrils can be divided into nucleation, elongation, and stationary phases [22]. In the nucleation phase, oligomers form a nucleus that can recruit other monomers [35]. A β-strand rotation, which converts antiparallel β-structure in oligomers to parallel **β-sheet** structure in fibril nuclei has been suggested as the mechanism underlying this nucleated conformational conversion [36]. As fibrils grow they can shatter, producing new aggregation-prone species to elongate the fibril [35]. β-Strands of an amyloid fibril are arranged in parallel. Side chains from the same position of each chain align, facilitating metal chelation when the amino acid residues are good metal ligand [35]. The hydrophobic interface is stabilized by polar side chains from adjacent sheets, whereas the hydrated polar interface houses the Zn^{2+}-binding histidine residues with binding geometries unusual in proteins. Each Zn^{2+} has two bis-coordinated histidine ligands, which bridge adjacent strands to form an infinite metal–ligand chain along the fibril axis. However, histidine residues are not the only requirement for Zn^{2+} coordination by proteins since other amino acids can fulfill the coordination sphere of varying metal ions. The hydroxyl of tyrosine and the carbonyl oxygen of the peptide backbone from asparagine or glutamine can also provide stable Zn^{2+} complexes [37].

Divalent Cations in Manufacturing Processes

Understanding the role of divalent cations in natural **protein assembly** and the relevance of histidines in such processes opens a set of possibilities for the rational design of supramolecular

Trends in Biochemical Sciences

CellPress
REVIEWS

protein complexes, within both nano- and microscales, through controlled cation coordination (Table 2). Although other residues are suitable for coordination with divalent cations, polyhistidine peptides are particularly appealing. Firstly, histidine-rich tags are commonly used in the purification of recombinant proteins by Ni^{2+}-based affinity chromatography [38], which offers a solid background about fusion strategies, convenient accommodation sites, and potential functional impact on the target proteins that facilitate protein engineering. Also, metals such as Ni^{2+} interact with the nucleophilic alone-paired electrons from the imidazole ring of histidine residues [39], allowing a particularly stable binding that supports mechanically competent protein oligomers. In such context of methodological simplicity, divalent cations offer potential advantages compared with standard organic linkers, for instance, by achieving a wide range of geometries and coordination numbers [40], accessing different redox states [41], modifying the thermodynamic and kinetics of ligand-based reactions [42], and tuning structures or assembling processes [43]. In the development of biocompatible materials, proteins are considered as especially promising building blocks for medical applications because of their functionality, versatility, and manipulability, apart from their intrinsic lack of toxicity [21,44]. The cation-mediated self-assembling tendency of **His-tagged proteins** has been empirically exploited to construct soluble tumor-targeted protein nanocarriers with **toroidal architecture** [45] (see Figure I in Box 1). They act as stable nanoscale vehicles in precision drug delivery (Table 2), upon chemical conjugation with antitumoral drugs [46,47]. This is exemplified by a potent **antimetastatic effect** achieved in mouse models of human colorectal cancer by the selective delivery of **floxuridine** to metastatic cancer stem cells, driven by an assembled His-tagged **GFP** [46]. Ni^{2+}, Cu^{2+}, Zn^{2+}, and Ca^{2+} were tested as linkers to control the formation of those protein nanocarriers, but the residual Ni^{2+} amounts, released from the chromatographic columns used in protein purification, are sufficient to promote their self-assembling. With such trace amounts, intrinsically therapeutic **nanoparticles** were constructed as formed by tumor-targeted, **hexahistidine (H6)**-tagged microbial toxins: the *Pseudomonas aeruginosa* exotoxin (PE24, [48]), plant toxins (ricin, [49]), scorpion toxins (chlorotoxin, [50]), and venoms [51], resulting in potent self-assembled, self-delivered antitumoral drugs. The H6-mediated self-assembling of these cytotoxic proteins allowed for the first time, an innovative concept in nanomedicine, namely the design of nanoparticulated drugs without heterologous vehicles [52] in which the drug itself self-organizes into nanoscale cell-targeted entities. These nanoparticles, usually ranging between 10 and 30 nm in diameter, disassemble upon EDTA addition and reassemble in the presence of Ni^{2+}, but also other divalent cations such as Ca^{2+}, Zn^{2+}, or Cu^{2+}. Interestingly, the nanoparticle size is sensitive to the concentration of these ions, which confers some potential for structural regulation and manipulability of the material geometry [45]. While Ni^{2+} is toxic for mammals at those experimental doses [53], other divalent metal and non-metal ions such as Zn^{2+}, Ca^{2+}, Mn^{2+}, or Mg^{2+} are present in organisms as oligoelements, at low but significant concentrations, and are therefore suitable for the construction of biomedicine-oriented materials. This issue is discussed later in more detail, paying attention to the **recommended dietary allowance** (RDA) of such elements [54]. Humanized versions of polyhistidine tails also result in proper self-assembling as nanoparticles [55], a promising observation regarding potential regulatory concerns.

By using the same principle applied to soluble protein nanoparticles but based on free H6 peptides (in the absence of linked full proteins) and metal ions such as Zn^{2+}, similar but larger peptidic particles have been recently developed as drug loadable delivery systems [56]. From a more academic view, **His-rich proteins** have been recently dimerized by Zn^{2+} [57,58], His-containing tripeptides aggregated with Cu^{2+} and Ni^{2+} [59], and His-containing coiled coils stabilized with Ni^{2+} [60], which resulted in a wide range of materials (Table 2). Inspired by mussel proteins and other natural products (Table 2), diverse categories of protein or protein-containing hybrid materials have been developed in which Zn^{2+} coordinates with His-rich proteins [61],

Trends in Biochemical Sciences

CellPress REVIEWS

Table 2. Representative Examples of Synthetic Protein Materials Fabricated with the Assistance of Divalent Cations, According to the Final Size and Geometry of the Material

Nano-scale materials						
Material	Size (nm)	Cation	Building block	Coordinating ligand	Applications	Refs
Nanodiscs	~8–20	Zn^{2+} Fe^{2+}	Insulin	His Bipy-Lys	Potential controlled release depots	[86]
Nanocapsules	20	Ni^{2+}	Triblock co-polypeptide of CCMV	His	Potential drug delivery system	[87]
Nanoparticles	60	Zn^{2+}	Hexa-histidine peptide	His	Drug delivery system	[56]
Nanorings	~100–350	Ni^{2+}	GST_{His} homodimer	His	Functional biomaterials	[63]
Nanoparticles	100–200	Mg^{2+}	BCA-P_{11}4	Glu	Functional biomaterials	[88]
Nanoparticles	10–15	Ni^{2+}, Zn^{2+}, Cu^{2+}, Ca^{2+}	T22-GFP-H6	His	Targeted drug delivery	[45]
Micro-scale materials						
Material	Size (μm)	Cation	Building block	Coordinating ligand	Applications	Refs
Auxetic 2D array	~1	Zn^{2+}, Cu^{2+}	$RhuA_{His}$	His	Auxetic biomaterial	[62]
1D Fibrils and 2D planes	~1	Ni^{2+}	Acetyltransferase homohexamer	Bpy-Ala	Functional biomaterials	[89]
Hexagonal prism crystals	0.5–4	Zn^{2+}, Cu^{2+} Co^{2+}	Coiled-coil helical GCN4-p2 trimer	NTA His	Potential drug delivery system	[90]
Hollow nanotubes	~2.5	Mg^{2+}, Ca^{2+}, Co^{2+}, Zn^{2+}, Mn^{2+}	$GroEL_{SP/MC}$ tetradecamer	SP/MC-Cys	Potential biocontainer for drug delivery	[64]
Microparticles	~2	Zn^{2+}	His-GFP	His	Sustained drug release system	[69]
Microparticles	~0.45	Zn^{2+}	Interferon-α-2b	Glu	Sustained drug release system	[67]
Microflorettes	~10	Zn^{2+}	NcoH	NTA His	Sustained drug release system	[65]
Microparticles	~1.5	Zn^{2+}, Ca^{2+}	T22-GFP-H6 T22-PE24-H6	His	Sustained drug release system	[66,74]
Multiple size materials and fibers						
Material	Size	Cation	Building block	Linker	Applications	Refs
1D, 2D, and 3D microarrays	MS	Zn^{2+}	RIDC3	His	Tunable functional biomaterial	[91]
Films	MS	Zn^{2+}, Cu^{2+}	Mussel byssal thread HRD protein	His	Tunable polymeric biomaterial	[71]
Interfacial films	MS	Zn^{2+}	AM1 amphipathic peptide	His	Foam and emulsion based products	[92]
Helical nanotubes	MS	Zn^{2+}	RIDC3-derived Zn_8R_4 tetramer	His	Mechanically tunable biomaterial	[70]
Nanowires	MS	Ni^{2+}	GST_{His} homodimer	His	Functional biomaterials	[68]

Abbreviations: AM1, Amphipathic peptide Lac21 peptide mutant; BCA-P_{11}4, bovine carbonic anhydrase linked with a P_{11}4 peptide; Bipy-Lys, 2,2′-bipyridine functionalized lysine; Bpy-Ala, bipyridyl-alanine; CCMV, cowpea chlorotic mottle virus; Glu, glutamic acid; $GroEL_{SP/MC}$, GroEL mutant bearing conjugated SP/MC photocromic units; GST_{His}, glutathione S-transferase N-term His mutant; His, histidine; HRD, histidine-rich domain; MS, multiple size; NcoH, triple helical collagen-like protein with N-ter NTA and C-ter His-tag; NTA, nitrilotriacetic acid; PE24, *Pseudomonas aeruginosa* exotoxin; $RhuA_{His}$, L-rhamnulose-1-phosphate aldolase H63/H98 mutant; RIDC3, rossetta interface designed cytochrome 3; SP/MC-Cys, photochromic spiropyran (SP)/merocyanine (MC) functionalized cysteine residues; T22-GFP-H6, T22 ligand fused, His-tagged green fluorescent protein; T22-PE24-H6, T22 ligand fused, His-tagged *Pseudomonas aeruginosa* exotoxin PE24; Zn_8R_4, RIDC3-derived H59/C96 mutant that forms tetramers by the coordination of eight Zn^{2+} ions.

including nanoparticles [56,62,63], **microparticles** [64–69], and diverse fibrous structures [68,70] (Table 2). Some of these constructs have also proved to have potential biomedical or biotechnological applications in the form of films [71] and hydrogels [72,73] (Table 2).

Trends in Biochemical Sciences

CellPress
REVIEWS

Box 1. Manufacturing of Supramolecular Protein Materials Assisted by Divalent Cations

The manufacturing process starts from the recombinant production and subsequent purification of soluble protein from the cell factory (Figure I). Thereafter, different concentrations of pure divalent cations, in the form of chloride salt, are added to samples of soluble H6-tagged proteins, depending on the desired architecture of the final material. For protein nanoparticles, divalent cation:protein molar bases proportions range from 1:1 to 4:1, and for microscale protein aggregates from 50:1 to 500:1, depending also on the initial protein concentration (1:1 corresponds to 0.2 mM). After cation addition, samples are mixed and incubated at room temperature for several minutes, allowing the coordination to proceed. Once completed, samples are centrifuged at 15 000 *g* for 20 min. Proteins in the soluble fraction with low cation concentration are organized in form of soluble nanoparticles. Instead, microparticles are collected from the insoluble fraction from the mixture at high cation concentration.

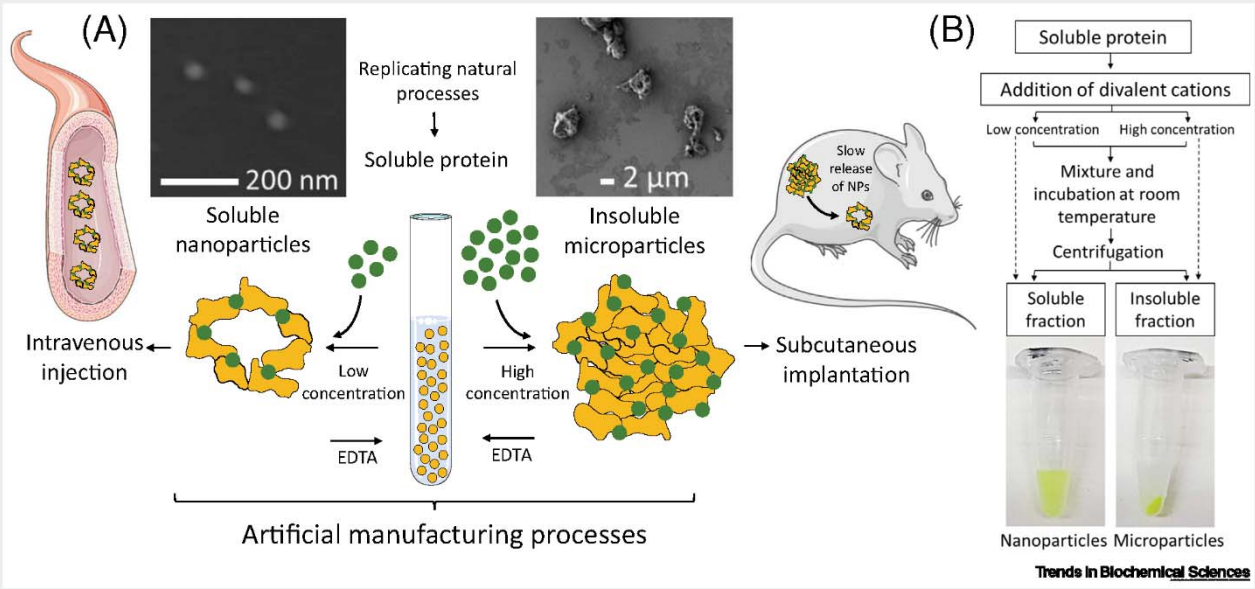

Figure I. Properties and Uses of Synthetic Nano- and Microparticulated Protein Materials Organized with the Assistance of Divalent Cations. (A) A generic procedure for the fabrication of nano- and microparticles using His-tagged proteins as building blocks is depicted, using T22-GFP-H6 [97] as a model. Those agents are intended as soluble nanostructured protein drugs (left, [48,82]) for straight intravenous administration, or as insoluble secretory protein materials for subcutaneous administration as drug reservoirs (right, [74]). Micrographs are modified from [74]. (B) A generic protocol for the fabrication of both type of materials, as illustrated by a fluorescent, His-tagged GFP (T22-GFP-H6). The chemical process that stands in this manufacture takes advantages of the electronic configuration of d orbitals and the octahedral and tetrahedral geometries of divalent cations. Among the different types of plausible interactions between divalent cations and amino acid residues, the histidine-divalent cation coordination is thought to be the major one. This type of interaction is already used to prepare the conventional immobilized metal affinity chromatography (IMAC) purification columns, where Ni^{2+} is stacked inside the column and histidine-tagged proteins are passed through to be attached. This coordination occurs because divalent cations interact with the nucleophilic a lone pair of electrons exposed in the ∂1-nitrogen of the His imidazole ring, producing a coordination type bond [44]. Interestingly, this bond is permanent and sufficiently strong to support the mechanics of an oligomerized structure. Abbreviations: NPs, nanoparticles.

Divalent Cations in Artificial Microparticles or Amyloid-like Secretory Structures

When testing the potential of divalent cations as cross-molecular protein linkers for the design of fine materials, their ability to precipitate, at high molar ratios, H6-tagged proteins in functional forms into large insoluble protein clusters has been noticed (see Figure I in Box 1; Table 2). Enzymes with His-rich stretches, namely alkaline phosphatase and β-galactosidase, were clustered by the controlled addition of Zn^{2+} or Ca^{2+}, as micron-scale protein particles that are mechanically stable and retain enzymatic functionalities of their components [74]. Therefore, these clusters act as self-immobilized enzymatic materials, usable in multicycle reaction processes. Interestingly, those microparticles show a **Fourier-transform infrared spectroscopy (FTIR)** pattern compatible with a partial amyloidal content and their surface roughness and morphology match a type of functional amyloid found in recombinant bacteria, namely **inclusion bodies** (**IBs**) [75]. In such bacterial structures, also within the micron scale,

Trends in Biochemical Sciences

CellPress
REVIEWS

functional and amyloid forms of single forming protein species are combined [76]. Like natural IBs, Zn^{2+}-supported artificial IBs might have a role in industrial biotechnology as particulate catalysts [75] but also as unexpected drug delivery systems, since under physiological conditions they slowly release the forming protein [77]. As a significant example, when Zn^{2+}-supported microparticles formed by precipitation of a CXCR4-targeted version of the potent PE24 toxin from *P. aeruginosa* [78] are implanted subcutaneously in a mouse model of human $CXCR4^{+}$ colorectal cancer, a significant fraction of the protein is released from the injection site and reaches the remote tumoral tissue, via the bloodstream [74]. Because of the H6 tags, these proteins themselves are released in the form of assembled and soluble toroid nanoparticles, as described earlier. The antitumoral effect mediated by the toxin is comparable with that shown by natural IBs in a similar experiment [79], confirming the robustness of the platform as a slow delivery protein depot. However, Zn^{2+}-based artificial material benefits from their pure chemical composition, in contrast to the heterogeneous nature of bacterial IBs. These natural particles, enriched with bacterial cell contaminants, are unsuited for clinical applications. The concept of protein-release from Zn^{2+}-based microparticles fabricated *in vitro* has been independently assessed by using His-tagged GFP [69] that, upon ion-mediated clustering, slowly release their components *in vitro* under physiological conditions. On the basis of such observations, artificial Zn^{2+}-based microparticles are structurally and functionally similar to secretory granules of the human endocrine system [31,80], in which protein hormones are stored in a Zn^{2+}-supported amyloidal architecture [31,32,81] and released from the bulk amyloidal material [32].

Safety Considerations

The possible use, in humans, of protein materials assembled with divalent cations raises safety concerns, regarding the potential induced imbalance of ion levels in the body. As mentioned earlier, the physiological concentrations of divalent cations are within quite defined ranges and their excesses are associated with mild-to-severe pathologies (Table 1). Facing the diverse types of protein material and potential regimens of administration, a generic evaluation of side effects associated with over-administration of cations might be not feasible. However, supported by independent studies, and by our own preclinical experience in cation-assisted protein drugs, it is possible to identify low and high divalent cation content categories of materials and to define threshold doses of those ions. Self-assembling toxins (and also proapoptotic factors) are organized as tumor-targeted nanoparticles [48,82,83], with low ion content that is in the equimolar range with the protein building blocks [45]. These drugs are intravenously administered to model animals, at repeated dose schedules up to 5 mg/kg per dose, in the absence of observable systemic toxicity. Then, once scaled up to adult humans, the protein mass in such drug doses would be around 350 mg and the amount of coordinating cation around 2.8 mg for Ca^{2+}, 3.9 mg for Fe^{2+}, and 1.7 mg for Mg^{2+} [45]. Those materials would be fully safe after intravenous injection since the daily dose would be 80–1000 times lower than the RDA for these elements [54]. Nanoparticles coordinated by Zn^{2+} (carrying around 4.6 mg of the metal) would be still in the safe range, since the recommended daily dose of this metal is 8 mg for adult women and 11 mg for adult men, with the upper tolerable level at 40 mg/day. The equivalent mass of Mn^{2+} in the nanoparticle dose, 3.8 mg, would be still 2.9-fold lower than the upper tolerable level (11 mg/day). In contrast, the administration of 350 mg nanoparticles coordinated by Cu^{2+} (4.4 mg), Ni^{2+} (4.1 mg), or Co^{2+} (4.1 mg) will not be safe since the amount of administered cations for these elements would be 15–5000 times higher than their RDA [54]. The use of such metals as coordinating agents should be then avoided.

At the other end of the cation content range, artificial secretory granules, formulated as sustained-protein release systems for subcutaneous injection, are constructed with a 50-fold molar excess

Trends in Biochemical Sciences

CellPress
REVIEWS

of ions regarding protein building blocks [74]. Therefore, Ca^{2+}, Fe^{2+}, and Mg^{2+} would be clearly usable as inorganic glue-like agents. Precise analyses of the *in vivo* protein and cation release kinetics from administered materials would be necessary to establish the appropriate dosing and to ensure the safety of Zn^{2+}- and Mn^{2+}-based materials.

Concluding Remarks

Divalent cations have been revealed as unexpected agents for the controlled fabrication of nanoscale and microscale protein materials, from pure protein components with histidine-rich domains. Combining serendipitous, rational design and biological inspiration, the fabrication of nano- and microparticles has advanced to generate drug carriers, self-assembled, self-delivered protein drugs, and secretory protein materials. Among those applications and others potentially arising in the future, the fabrication of secretory materials capable of releasing protein drugs upon administration by nonintravenous parenteral routes is of particular interest. Under the unmet needs of fully biocompatible materials for use in the clinical setting and aimed at selective drug targeting, the combination of divalent cations and engineered proteins allows the construction of artificial secretory granules for highly selective and remote delivery of functional proteins. The controlled use of divalent cations, common in living beings and within physiological ranges, offers a convenient and technologically simple approach to mimic the endocrine secretion of protein hormones for therapeutic purposes, posing, at the same time, challenging issues (see Outstanding Questions). In this way, the manipulation of divalent cations in form of emerging **nanobiochemistry** offers a plethora of so far unexplored possibilities in material sciences and in biomedical nanotechnologies.

Outstanding Questions

Are the very simple processes for ion-based fabrication of materials controllable during scale-up production?

Are the crossmolecular bounds provided by divalent cations strong enough to maintain the stability of the protein materials for a prolonged circulation in blood?

Which toxicological issues will challenge the use of soluble oligomeric nanoparticles and artificial secretory granules based on divalent cations?

Could divalent cations play an assisting therapeutic role by themselves as members of an assembled protein complex?

Acknowledgments

The authors appreciate the financial support to their activities devoted to the design of protein materials for medical applications. In particular, they are indebted to Agencia Estatal de Investigación (AEI) and Fondo Europeo de Desarrollo Regional (FEDER) (grant BIO2016-76063-R, AEI/FEDER, UE, to A.V. and PID2019-105416RB-I00 to E.V.), AGAUR (2017SGR-229 to A.V. and 2017SGR-865 GRC to R.M.), ISCIII (co-founding FEDER) PIE15//00028 and PI18/00650 to R.M., and to EU COST Action CA 17140. We are also indebted to the Networking Research Center on Bioengineering, Biomaterials and Nanomedicine (CIBER-BBN) that is an initiative funded by the VI National R&D&I Plan 2008–2011, Iniciativa Ingenio 2010, Consolider Program, CIBER Actions and financed by the Instituto de Salud Carlos III, with assistance from the European Regional Development Fund. A.V. received an ICREA ACADEMIA award. H.L.L. received a predoctoral fellowship from AGAUR (2019 FI_B 00352) and U.U. was supported by the Miguel Servet program (CP19/00028) from ISCIII (cofounded Fondo Social Europeo, FSE). The authors also appreciate the free availability of medical frames and images to construct the figures from Smart Servier Medical Art platform.

References

1. Farrell, N.P. (2020) Medicinal inorganic chemistry: new perspectives and targets for the periodic table. *Adv. Inorg. Chem.* 75, 57–86
2. Fiore, M. (2019) The origin and early evolution of life: prebiotic chemistry. *Life* 9, 73
3. Haraguchi, H. (2017) Metallomics: the history over the last decade and a future outlook. *Metallomics* 9, 1001–1013
4. Lin, J. *et al.* (2019) Regulations of organism by materials: a new understanding of biological inorganic chemistry. *J. Biol. Inorg. Chem.* 24, 467–481
5. Bertini, I. and Rosato, A. (2003) Bioinorganic chemistry in the postgenomic era. *Proc. Natl. Acad. Sci. U. S. A.* 100, 3601–3604
6. Maret, W. (2016) The metals in the biological periodic system of the elements: concepts and conjectures. *Int. J. Mol. Sci.* 17, 66
7. Zhao, H. (2016) Protein stabilization and enzyme activation in ionic liquids: specific ion effects. *J. Chem. Technol. Biotechnol.* 91, 25–50
8. Vashishtha, A.K. *et al.* (2016) Different divalent cations alter the kinetics and fidelity of DNA polymerases. *J. Biol. Chem.* 291, 20869–20875
9. Nguyen, H.T. *et al.* (2019) Theory and simulations for RNA folding in mixtures of monovalent and divalent cations. *Proc. Natl. Acad. Sci. U. S. A.* 116, 21022–21030
10. Li, K. *et al.* (2018) The good, the bad, and the ugly of calcium supplementation: a review of calcium intake on human health. *Clin. Interv. Aging* 13, 2443–2452
11. Li, L. and Yang, X. (2018) The essential element manganese, oxidative stress, and metabolic diseases: links and interactions. *Oxidative Med. Cell. Longev.* 2018, 7580707
12. Packer, M. (2016) Cobalt cardiomyopathy: a critical reappraisal in light of a recent resurgence. *Circ. Heart Fail.* 9, e003604
13. Ackerman, C.M. and Chang, C.J. (2018) Copper signaling in the brain and beyond. *J. Biol. Chem.* 293, 4628–4635
14. Al Alawi, A.M. *et al.* (2018) Magnesium and human health: perspectives and research directions. *Int. J. Endocrinol.* 2018, 9041694
15. Cherasse, Y. and Urade, Y. (2017) Dietary zinc acts as a sleep modulator. *Int. J. Mol. Sci.* 18, E2334
16. Tiwari, S. *et al.* (2011) Divalent cations regulate the folding and activation status of integrins during their intracellular trafficking. *J. Cell Sci.* 124, 1672–1680
17. Wu, H. *et al.* (2019) Effect of the divalent cations zinc and calcium on the structure and mechanics of reconstituted vimentin intermediate filaments. *bioRxiv* Published online November 15, 2019. https://doi.org/10.1101/844167

Trends in Biochemical Sciences

CellPress REVIEWS

18. Knape, M.J. *et al.* (2017) Divalent metal ions control activity and inhibition of protein kinases. *Metallomics* 9, 1576–1584
19. Pilchova, I. *et al.* (2017) The involvement of Mg(2+) in regulation of cellular and mitochondrial functions. *Oxidative Med. Cell. Longev.* 2017, 6797460
20. Petukh, M. and Alexov, E. (2014) Ion binding to biological macromolecules. *Asian J. Phys.* 23, 735–744
21. Korpi, A. *et al.* (2020) Highly ordered protein cage assemblies: a toolkit for new materials. *Wiley Interdiscip. Rev. Nanomed. Nanobiotechnol.* 12, e1578
22. Iadanza, M.G. *et al.* (2018) A new era for understanding amyloid structures and disease. *Nat. Rev. Mol. Cell Biol.* 19, 755–773
23. Otzen, D. and Riek, R. (2019) Functional amyloids. *Cold Spring Harbor Perspect. Biol.* 11 pii: a033860
24. Kaur, A. *et al.* (2020) Characterization of Cu(2+) and Zn(2+) binding sites in SUMO1 and its impact on protein stability. *Int. J. Biol. Macromol.* 151, 204–211
25. Lautenschlager, J. *et al.* (2018) C-terminal calcium binding of alpha-synuclein modulates synaptic vesicle interaction. *Nat. Commun.* 9, 712
26. Han, J.Y. *et al.* (2018) Molecular role of Ca(2+) and hard divalent metal cations on accelerated fibrillation and interfibrillar aggregation of alpha-synuclein. *Sci. Rep.* 8, 1895
27. Irving, H. and Williams, R.J.P. (1953) (1953) The stability of transition-metal complexes. *J. Chem. Soc. (Resumed)* 3192–3210
28. Chen, G.F. *et al.* (2017) Amyloid beta: structure, biology and structure-based therapeutic development. *Acta Pharmacol. Sin.* 38, 1205–1235
29. Rana, M. and Sharma, A.K. (2019) Cu and Zn interactions with abeta peptides: consequence of coordination on aggregation and formation of neurotoxic soluble abeta oligomers. *Metallomics* 11, 64–84
30. Cristovao, J.S. *et al.* (2016) Metals and neuronal metal binding proteins implicated in Alzheimer's disease. *Oxidative Med. Cell. Longev.* 2016, 9812178
31. Maji, S.K. *et al.* (2009) Functional amyloids as natural storage of peptide hormones in pituitary secretory granules. *Science* 325, 328–332
32. Jacob, R.S. *et al.* (2016) Amyloid formation of growth hormone in presence of zinc: relevance to its storage in secretory granules. *Sci. Rep.* 6, 23370
33. Rutter, G.A. *et al.* (2016) Intracellular zinc in insulin secretion and action: a determinant of diabetes risk? *Proc. Nutr. Soc.* 75, 61–72
34. Duboue-Dijon, E. *et al.* (2018) Binding of divalent cations to insulin: capillary electrophoresis and molecular simulations. *J. Phys. Chem. B* 122, 5640–5648
35. Zhang, X. *et al.* (2018) The early events that initiate β-amyloid aggregation in Alzheimer's disease. *Front. Aging Neurosci.* 10, 359
36. Fu, Z. *et al.* (2015) Mechanism of nucleated conformational conversion of abeta42. *Biochemistry* 54, 4197–4207
37. Erthal, L.C. *et al.* (2016) Regulation of the assembly and amyloid aggregation of murine amylin by zinc. *Biophys. Chem.* 218, 58–70
38. Kosobokova, E.N. *et al.* (2016) Overview of fusion tags for recombinant proteins. *Biochem. Mosc.* 81, 187–200
39. Valenti, L.E. *et al.* (2006) The binding of Ni(II) ions to hexahistidine as a model system of the interaction between nickel and His-tagged proteins. *J. Inorg. Biochem.* 100, 192–200
40. Danielsen, E. *et al.* (1997) Coordination geometries for monovalent and divalent metal ions in [His121]azurin–studies using perturbed angular correlations of gamma-rays from 111Ag and 111mCd. *Eur. J. Biochem.* 250, 249–259
41. Wang, C.K. *et al.* (2011) Divalent cations and redox conditions regulate the molecular structure and function of visinin-like protein-1. *PLoS One* 6, e26793
42. Orzel, L. *et al.* (2017) Factors controlling the reactivity of divalent metal ions towards pheophytin a. *J. Biol. Inorg. Chem.* 22, 941–952
43. Rad, B. *et al.* (2015) Ion-specific control of the self-assembly dynamics of a nanostructured protein lattice. *ACS Nano* 9, 180–190
44. Hamley, I.W. (2019) Protein assemblies: nature-inspired and designed nanostructures. *Biomacromolecules* 20, 1829–1848
45. Lopez-Laguna, H. *et al.* (2019) Assembly of histidine-rich protein materials controlled through divalent cations. *Acta Biomater.* 83, 257–264
46. Cespedes, M.V. *et al.* (2018) Selective depletion of metastatic stem cells as therapy for human colorectal cancer. *EMBO Mol. Med.* 10 pii: e8772
47. Pallares, V. *et al.* (2020) An auristatin nanoconjugate targeting CXCR4+ leukemic cells blocks acute myeloid leukemia dissemination. *J. Hematol. Oncol.* 13, 36
48. Serna, N. *et al.* (2020) Nanostructured toxins for the selective destruction of drug-resistant human CXCR4(+) colorectal cancer stem cells. *J. Control. Release* 320, 96–104
49. Diaz, R. *et al.* (2018) Selective CXCR4(+) cancer cell targeting and potent antineoplastic effect by a nanostructured version of recombinant ricin. *Small* 14, e1800665
50. Díaz, R. *et al.* (2019) Engineering a recombinant chlorotoxin as cell-targeted cytotoxic nanoparticles. *Sci. China Mater.* 62, 892–898
51. Serna, N. *et al.* (2020) Engineering protein venoms as self-assembling CXCR4-targeted cytotoxic nanoparticles. *Part. Part. Syst. Charact.* 37, 2000040
52. Shen, J. *et al.* (2017) Taking the vehicle out of drug delivery. *Mater. Today* 20, 95–97
53. Maroney, M.J. and Ciurli, S. (2014) Nonredox nickel enzymes. *Chem. Rev.* 114, 4206–4228
54. Pazirandeh, S. *et al.* (2020) *Overview of Dietary Trace Elements*, Wolters Kluwer
55. López-Laguna, H. *et al.* (2020) Endosomal escape of protein nanoparticles engineered through humanized histidine-rich peptides. *Sci. China Mater.* 63, 644–653
56. Huang, W. *et al.* (2019) Hexahistidine-metal assemblies: a promising drug delivery system. *Acta Biomater.* 90, 441–452
57. Maniaci, B. *et al.* (2019) Design of high-affinity metal-controlled protein dimers. *Biochemistry* 58, 2199–2207
58. Haglin, E.R. *et al.* (2017) His-tag mediated dimerization of chemoreceptors leads to assembly of functional nanoarrays. *Biochemistry* 56, 5874–5885
59. Dunbar, R. *et al.* (2018) Transition metal(II) complexes of histidine-containing tripeptides: structures, and infrared spectroscopy by IRMPD. *Int. J. Mass Spectrom.* 429, 198–205
60. Tunn, I. *et al.* (2018) Tuning coiled coil stability with histidine-metal coordination. *Nanoscale* 10, 22725–22729
61. Zechel, S. *et al.* (2019) Healing through histidine: bioinspired pathways to self-healing polymers via imidazole(-)metal coordination. *Biomimetics* 4, 20
62. Suzuki, Y. *et al.* (2016) Self-assembly of coherently dynamic, auxetic, two-dimensional protein crystals. *Nature* 533, 369–373
63. Bai, Y. *et al.* (2013) Highly ordered protein nanorings designed by accurate control of glutathione S-transferase self-assembly. *J. Am. Chem. Soc.* 135, 10966–10969
64. Biswas, S. *et al.* (2009) A tubular biocontainer: metal ion-induced 1D assembly of a molecularly engineered chaperonin. *J. Am. Chem. Soc.* 131, 7556–7557
65. Pires, M.M. *et al.* (2011) Selective decoration and release of His-tagged proteins from metal-assembled collagen peptide microflorettes. *Biomacromolecules* 12, 2429–2433
66. Serna, N. *et al.* (2020) Release of functional fibroblast growth factor-2 from artificial inclusion bodies. *J. Control. Rel.* 327, 61–69
67. Jiang, Y. *et al.* (2011) Protamine modified metal ion-protein chelate microparticles for sustained release of interferon. *Int. J. Pharm.* 407, 31–37
68. Zhang, W. *et al.* (2012) Self-assembly of glutathione S-transferase into nanowires. *Nanoscale* 4, 5847–5851
69. Chen, T.Y. *et al.* (2019) Artificial peptide-controlled protein release of Zn(2+)-triggered, self-assembled histidine-tagged protein microparticle. *Colloids Surf. B: Biointerfaces* 187, 110644
70. Brodin, J.D. *et al.* (2015) Designed, helical protein nanotubes with variable diameters from a single building block. *J. Am. Chem. Soc.* 137, 10468–10471
71. Jehle, F. *et al.* (2018) Metal-tunable self-assembly of hierarchical structure in mussel-inspired peptide films. *ACS Nano* 12, 2160–2168
72. Trapaidze, A. *et al.* (2018) Exploring mussel byssus fabrication with peptide-polymer hybrids: role of pH and metal coordination in self-assembly and mechanics of histidine-rich domains. *Eur. Polym. J.* 109, 229–236
73. Tunn, I. *et al.* (2019) Bioinspired histidine(-)Zn(2+) coordination for tuning the mechanical properties of self-healing coiled coil cross-linked hydrogels. *Biomimetics* 4, 25

Trends in Biochemical Sciences

CellPress REVIEWS

74. Sánchez, J. *et al.* (2020) Artificial inclusion bodies for clinical development. *Adv. Sci.* 7, 1902420
75. Rinas, U. *et al.* (2017) Bacterial inclusion bodies: discovering their better half. *Trends Biochem. Sci.* 42, 726–737
76. de Marco, A. *et al.* (2019) Bacterial inclusion bodies are industrially exploitable amyloids. *FEMS Microbiol. Rev.* 43, 53–72
77. Unzueta, U. *et al.* (2018) Release of targeted protein nanoparticles from functional bacterial amyloids: a death star-like approach. *J. Control. Release* 279, 29–39
78. Michalska, M. and Wolf, P. (2015) Pseudomonas exotoxin A: optimized by evolution for effective killing. *Front. Microbiol.* 6, 963
79. Cespedes, M.V. *et al.* (2020) Engineering secretory amyloids for remote and highly selective destruction of metastatic foci. *Adv. Mater.* 32, 1907348
80. Dannies, P.S. (2012) Prolactin and growth hormone aggregates in secretory granules: the need to understand the structure of the aggregate. *Endocr. Rev.* 33, 254–270
81. Jacob, R.S. *et al.* (2019) Protein nanofibrils as storage forms of peptide drugs and hormones. *Adv. Exp. Med. Biol.* 1174, 265–290
82. Sanchez-Garcia, L. *et al.* (2018) Self-assembling toxin-based nanoparticles as self-delivered antitumoral drugs. *J. Control. Release* 274, 81–92
83. Sánchez-García, L. *et al.* (2020) A refined cocktailing of pro-apoptotic nanoparticles boosts anti-tumor activity. *Acta Biomaterialia* 113, 584–596
84. Dev, S. and Babitt, J.L. (2017) Overview of iron metabolism in health and disease. *Hemodial. Int.* 21, S6–S20
85. Zamble, D. (2017) Introduction to the biological chemistry of nickel. In *The Biological Chemistry of Nickel* (Zamble, D. *et al.*, eds), pp. 1–11, Royal Society of Chemistry
86. Munch, H.K. *et al.* (2016) Construction of insulin 18-mer nanoassemblies driven by coordination to iron(II) and zinc(II) ions at distinct sites. *Angew. Chem.* 55, 2378–2381
87. van Eldijk, M.B. *et al.* (2016) Metal ion-induced self-assembly of a multi-responsive block copolypeptide into well-defined nanocapsules. *Small* 12, 2476–2483
88. Shanbhag, B.K. *et al.* (2018) Understanding the interplay between self-assembling peptides and solution ions for tunable protein nanoparticle formation. *ACS Nano* 12, 6956–6967
89. Yang, M. and Song, W.J. (2019) Diverse protein assembly driven by metal and chelating amino acids with selectivity and tunability. *Nat. Commun.* 10, 5545
90. Nepal, M. *et al.* (2016) Accessing three-dimensional crystals with incorporated guests through metal-directed coiled-coil peptide assembly. *J. Am. Chem. Soc.* 138, 11051–11057
91. Brodin, J.D. *et al.* (2012) Metal-directed, chemically tunable assembly of one-, two- and three-dimensional crystalline protein arrays. *Nat. Chem.* 4, 375–382
92. Dexter, A.F. *et al.* (2006) Reversible active switching of the mechanical properties of a peptide film at a fluid-fluid interface. *Nat. Mater.* 5, 502–506
93. Sontag, E.M. *et al.* (2017) Mechanisms and functions of spatial protein quality control. *Annu. Rev. Biochem.* 86, 97–122
94. Wentink, A. *et al.* (2019) Modulation of amyloid states by molecular chaperones. *Cold Spring Harb. Perspect. Biol.* 11, a033969
95. Brandman, O. and Hegde, R.S. (2016) Ribosome-associated protein quality control. *Nat. Struct. Mol. Biol.* 23, 7–15
96. Joazeiro, C.A.P. (2019) Mechanisms and functions of ribosome-associated protein quality control. *Nat. Rev. Mol. Cell Biol.* 20, 368–383
97. Rueda, F. *et al.* (2015) Bottom-up instructive quality control in the biofabrication of smart protein materials. *Adv. Mater.* 27, 7816–7822

Additional referenced studies

The following studies have been involved in the thesis storyline, placed in the annex section, and mentioned during the discussion:

Annex 1 (Objective 3.c)

To test the biomedical applications of protein-based insoluble microparticles in tissue engineering (wound healing).

Release of functional fibroblast growth factor-2 from artificial inclusion bodies

Journal of Controlled Release 2020 · Impact factor (9.776) · Quartile (Q1)

Annex 2 (Objective 3.d)

To test the biomedical applications of protein-based insoluble microparticles in tissue engineering (osteogenesis).

BFGF-2-releasing secretory granules as functional topographies in cell growth and osteogenic differentiation

Manuscript in progress

Annex 3 (Objective 3.e)

To test the biomedical applications of protein-based insoluble microparticles in biocatalysis.

Engineering the Performance of Artificial Inclusion Bodies Built of Catalytic β-Galactosidase

ACS Sustainable Chemistry and Engineering (2021) · Impact Factor (9.224) · Quartile (Q1)

Annex 4 (Objective 3.f)

To test the biomedical applications of protein-based insoluble microparticles in the treatment of infectious diseases.

Nanostructured AMPs, released from protein-only microscale depots, confer protection against pathogenic bacteria

Manuscript in progress

Annex 5 (Objective 4)

To review all the extracted knowledge and condense it as practical guidelines for the scientific community.

Insights on the emerging biotechnology of histidine-rich peptides

Biotechnology Advances (2021) · Impact Factor (17.681) · Quartile (Q1)

DISCUSSION

The development of fully tunable and biocompatible drug delivery systems to selectively deliver therapeutic drugs to the desired tissue, without causing major deleterious effects, is highly desirable, even mandatory, for our current needs in precision medicine [122,217,224,226].

Among the different smart material possibilities (e.g., liposomes, polymers, dendrimers, or even magnetic nanoparticles) [163,213,233,238], protein-based assemblies appear as ones with great potential to gather almost all the desirable properties (e.g., biocompatibility, easy to administer, targeting possibilities, proper biodistribution, stability…) [240,249,262] to be used as efficient and safe clinical products.

Particularly, there are two major highly exploited strategies, already explained throughout the introductory section: **strategy 1** (protein-based nanoparticles assembled by a cationic peptide-histidine tag principle) and **strategy 2** (natural occurring protein-based microparticles, so called inclusion bodies), which exhibit formidable properties to be considered as promising drug delivery agents, including (1) efficient delivery of the therapeutic drug (meaning targeting), (2) effective biodistribution (meaning avoidance of renal cut-off), (3) therapeutic versatility (meaning applicability in different biomedical fields), and (4) stability (meaning chemical and thermal stability, especially at 37 °C). But still, they present certain critical concerns which make them unsuitable for clinical purposes such as (1) low reproducibility between batches (meaning size control), (2) low assembling control (meaning procedure control), (3) restricted formulation versatility (meaning applicability to different protein candidates), (4) biocompatibility issues (meaning proper biodegradability and low toxicity), (5) limited formulation in a cost-effective manner (meaning manufacturing simplicity) and (6) product homogeneity issues (meaning level of purity; recall **introduction**, **figures 13 and 14**).

Thus, a novel manufacturing platform based on a simple biochemical principle has been developed to create complex protein-based biomaterials following every architectonic stage (meaning from protein building blocks to protein-based nanoparticles and protein-based microparticles) and tackling every set of mentioned clinical concerns. A schematic illustration is subsequently shown depicting the formulation's workflow of both strategies, in which

different amounts of divalent cations appear as molecular gluing agents of histidine tagged recombinant proteins (**figure 15**).

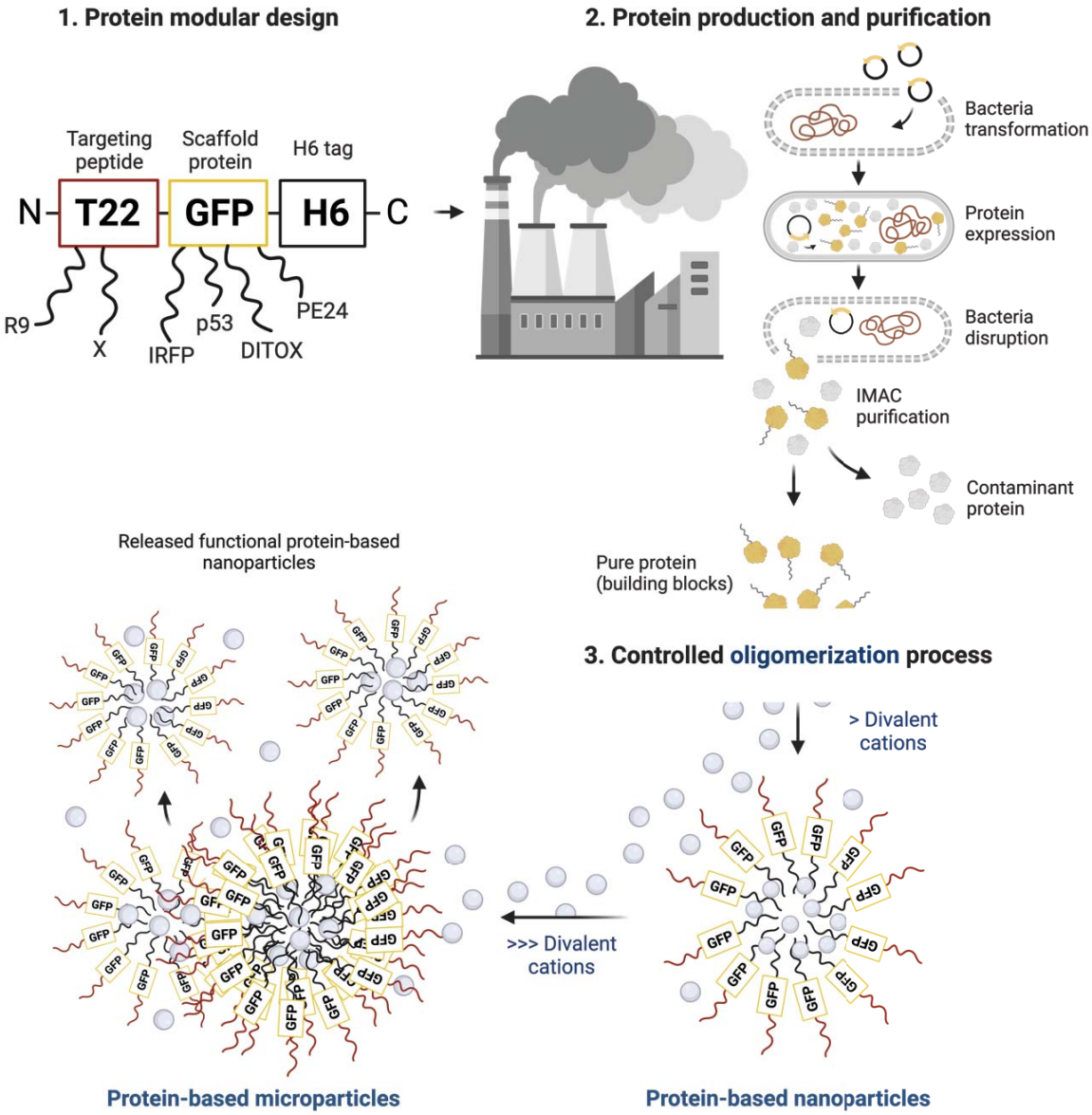

Figure 15. A concise diagram illustrating the novel histidine tag-divalent cation principle. The engineering workflow includes (1) a histidine tagged protein modular design (*a-la-carte* selection of the desired scaffold or targeting peptides), (2) the recombinant protein production and purification (using microbial cell factories and IMAC methodology), and (3) the controlled protein oligomerization process (by increasing concentrations of divalent cations, especially Zn^{2+}). Protein-based nano and micro -particles are formed as a result of this method, no extra steps are required, and a clear gluing of histidine tags by divalent cations is revealed. The example is illustrated with the T22-GFP-H6 protein as a gold standard.

That being said, each presented study already exhibits a detailed discussion highlighting the pros and cons of our technology when compared to the current state of the art. Still, a summarized all-in-one version of the discussion will be subsequently disclosed.

Two main topics will be considered, including (A) the formulation of protein-based nanoparticles, and (B) the formulation of protein-based microparticles. In addition, a still ongoing (C) biomedical assessment of their respective plausible technological applications will be commented in different fields (e.g., tissue engineering, biocatalysis, antimicrobial activity…). Finally, an extended biotechnological review, framed in each basic component (histidine tag and divalent cations), will be also included (D).

(A) The formulation of protein-based nanoparticles (objective 1 – Studies 1, 2 and 3, and objective 3 – Study 2)

The design of a novel self-assembling platform of protein-based nanoparticles which tackles size control, reproducibility between batches, and manufacturing simplicity (Study 1)

The first aim was to look for a transversal and easy way to promote the spontaneous self-assembly of histidine tagged recombinant proteins into toroid-like nanoparticles, using a simple biochemical principle, and ensuring product's controlled size, reproducibility, and low costs. The assembling of protein-derived materials has been largely documented [240], specially for drug delivery [217,226,227] in which virus-inspired complex formats gathered high relevance in the field [275,276].

Study 1 was born from this analysis, in which the histidine's cross-reactivity and the gluing ability of divalent cations [86] was used as an architectonic force to create a bigger-in-size suprastructures, mimicking natural processes [34], and becoming the central foundation of the storyline.

In order to address this unmet engineering need, our gold standard protein-based nanoparticles T22-GFP-H6 [255] (self-assembled following the cationic-histidine tag platform depicted in strategy 1) was studied, and particularly, the interactions supporting its structure. Two new clones were initially designed from N to C -terminus (GFP-H6 and T22-GFP), and size measured (**study 1, figures 1A and B**). The results showed how both T22 and H6 tags were crucial to drive the oligomeric process [255] as oligomers were only observed for T22-GFP-H6 (around 11.7 nm). Protein-based toroidal-like structures were additionally confirmed by SEM and *in-silico* predicted (**study 1, figures 1C and 1D**).

These results were not indicative of any *de novo* assembling biochemical principle, and only reaffirmed the already mentioned cationic peptide-histidine tag strategy. Thus, the next phase was framed on trying to find out the occurring architectonic interactions [17] by testing different disassembling agents. Free -histidine, arginine, tryptophan, and tyrosine amino acids were selected as candidates, each of one related to a specific type of coordinative, electrostatic, and hydrophobic interactions, and set as assembling competitors (**study 1, figure 2A**). The results showed how only free histidine residues were able to trigger

nanostructure disruption [85] at a ratio-concentration dependent manner (from 11.7 to 7.5 and 6.5 nm).

The displayed 1:1 ratio means the equivalent amount (in molarity) of divalent cations to reach the amount of histidines per histidine tag from all recombinant proteins in solution (e.g., for a 30 KDa protein is generally 0.2 mM). In addition, the oligomeric size (expressed as volume size distribution, for nanoparticles, in nm) displayed throughout the project, was determined by dynamic light scattering (DLS) as the gold standard technique. From an experimental point of view, protein sizes of around 4 to 6 nm are indicative of monomeric structures, 6 to 7.5 nm of dimeric/trimeric structures and >8 to 9 nm are indicative of what we call nanoparticles (for a 30 KDa molecular weight protein as well). This is an essential criterion to keep in mind to understand further results (especially discontinuous line thresholds). Adequate resultant sizes ensure, at least, the suitability of the platform to avoid renal cut-off filtration (around <6nm) [170,171,261]. PDI (polydispersion index) was also extracted from these measurements, informing how the protein population distribution size changes upon certain scenarios (meaning 0.9 highly polydisperse and 0.1 slightly polydisperse) [277].

The cross-reactivity role of histidine tag in protein assembling was emerging, but still, the governing biochemical principles triggering the assembling process were unclear. To shed some light on this regard, the overall recombinant protein production and purification process was studied [103,116], looking for crucial chemical elements able to trigger histidine tag attachment, arrangement, or gluing. The traditional IMAC purification methodology was the first candidate, as divalent cations (especially Ni^{2+}) are widely used to entrap histidine tagged proteins using coordinative bonds and being sufficiently strong to support a continuous flow of buffer [86]. Indeed, we wondered if Ni^{2+} metal ions could be dragged out from the column [121] and be used by our T22-GFP-H6 gold standard to self-assemble spontaneously. Firstly, T22-based protein nanoparticles size was assessed in the presence of EDTA (a chelator of divalent cations [278] and used in the purification field to remove the packed divalent cation from the affinity column) and secondly, a semiquantitative nickel measurement was performed directly in the protein solution by ICP-MS methodology [279]. Results clearly showed how EDTA was able to induce a fast nanostructure disruption (approx. at twice of 1:1 ratio concentration, meaning 0.6 to 1 mM) strongly competing with histidine tags for Ni^{2+} coordination (**study 1, figure 2B**), meaning from 11.7 nm to 6.5 nm. EDTA was clearly breaking the major architectonical force sustaining the protein-based structure. In regard to Ni^{2+} measurements, samples presented between 0.8 to 1 μg of metal ion per mg of protein,

being nearly undetectable in the presence of EDTA (**study 1, figure 4C bottom**). The scenario was confirmed by *in situ* visualization of backscattered electron bright signals, coming from heavy atoms (though we can't say they were coming from Ni^{2+} atoms), on assembled T22-based nanoparticles. None of those signals was detected in presence of EDTA (**study 1, figure 4C top**).

In addition, we wondered if divalent cations could directly promote the assembling of EDTA-disrupted T22-based nanoparticles. A wide opened spectrum of ions comprehending different natures (metallic, or non-metallic) and valences (mono or di -valent) was tested, including Ni^{2+}, Cu^{2+}, Zn^{2+}, Ca^{2+}, Cs^{+} (cesium), and K^{+} (potassium). The results clearly showed how only divalent cations were able to induce the reassembling process of T22-GFP-H6 building blocks, irrespective of their natures, with non-significant differences observed for monovalent (**study 1, figure 2B**). A linear correlation between protein size and divalent cation ratio was found as well. Meaning, the more we increase divalent cation concentration, the bigger the resultant structure, until reaching a plateau (**study 1, figure 3A**). This plateau seems to be slightly alike for similar-in-nature divalent cations, and slightly different for Ca^{2+} (increased variability, **studies 1 and 2, figures 2C and 6A**) and different protein candidates (ranging from 0.2 to 0.5 mM, **study 2 figure 4A**).

Finally, we also wanted to assess how and when T22-based nanoparticles were formed during the overall engineering process without the external addition of divalent cations. Studying the size measurements of consecutive collected samples throughout the traditional preparation, elution, and buffer exchange (dialysis) of IMAC processing, we found out that nanoparticles were structured during the exchange buffer step (when certain concentrations of imidazole, 10 mM and NaCl, 500 mM were discarded; **study 1, figure 3B**). Additional studies performed in the lab have shown how moderate to high concentrations of both imidazole and NaCl were able to disrupt the nanoparticle's architecture [280]. Meaning histidine tag-divalent cation coordination acts as a major assembling force (as both EDTA and free -histidines are able to break the architecting forces by themselves), but still other forces could be used to stabilize the final protein architecture, such as electrostatic interaction [281] coming from the cationic peptide T22. This idea could explain why purified GFP-H6 proteins, without divalent cation supplementation, were not able to self-assemble (**study 1, figure 1B**).

Exploring the plausible second source of divalent cations able to trigger protein nanostructuring, microbial factories appear as the only last option [282,283], after IMAC metal leakage. Studying the reassembling capacities of soluble bacteria crude extracts, T22-GFP-

H6 disrupted samples were able to oligomerize up to 9 nm. What is more, non-denaturing gels showed a big-in-size motility pattern, higher in comparison to the building block pattern, of samples coming from inside bacteria. All these results are indicative of a plausible assembling process occurring inside microbial cell factories (**study 1, figures 4A and B**).

Surely, study 1 has allowed us to identify a simple biochemical principle to construct higher-in-complexity T22-GFP-H6 protein-based nanoparticles in a controlled-size manner, being re-confirmed over and over again. Using histidine tags as crosslinking agents with divalent cations seems to be a suitable platform to avoid low sized proteins which anticipate high renal filtration scenarios [284]. A 3D *in-silico* model (**study 1, figure 5A**), of the interaction principle, was predicted in which the δ1-nitrogen of the histidine imidazole ring could share an unpaired group of electrons to nucleophilic divalent cations [86], permanently and strongly held into the structure, and induce histidine tagged protein crosslinking.

Tackling the platform's transversality, and methodological robustness to construct nanoparticles from different origins (Study 2)

Surely, the exhibited findings so far have established the essential pillars of the biochemical assembling principle, but still its capacity to be translated to other protein candidates has been poorly explored, especially outside from our gold standard protein. In order to expand the transversality of the platform, a set of slightly different candidates, meaning different origins, was selected to ensure the solely histidine tag role in the protein re-arranging [85].

Initially, two histidine tagged candidates, HSA (human serum albumin) [285] and GFP [286], were studied in detail. The results showed protein-based oligomeric structures in the presence of 0.4 mM of Zn^{2+} from 9.5 to 15.5 nm, being above renal cut off. Oligomers were also stable upon buffer exchange (dialysis) for several hours (**study 2, figures 1D top and G**) and were disrupted once incubated with 0.8 mM of EDTA (**study 2, figure 1E**). Interestingly, protein candidates without His tag did not respond to Zn^{2+} treatment, reaffirming how both the His tag and divalent cations are the main and essential actors of the assembling scene (see a simplified assembling scheme in **study 2, figure 1B**). This fact was statistically reconfirmed when a variety of dissimilar modular proteins with divergent properties (meaning presence or absence of His tag, ligand, GFP scaffold, or number of total histidines) were plotted against their SIF (size increase factor), being the histidine tag the only peptidic sequence with

statistical significance (**study 2, figure 7**). Resultant polydispersity values were similar as for T22-based gold standard from study 1 ranging from 0.4 to 0.6.

Z-potential was also studied, as an additional stability parameter, measuring the resultant net surface nanoparticle charge (meaning from -20 to -25 in mV), as well as overall protein proclivity to aggregate [287] and define biodistribution tendencies [227]. Indeed, the more negative the surface charge is, and far from 0, the less tendency of our nanoparticles to agglomerate and less plausible non targeted off-targeting effects once administered [288] (as cells generally present negative surface charges; **study 2, figure 1D bottom**). Protein oligomeric stability was also measured at increasing temperatures (from 4 to 50 °C) without major changes, and morphology imaged by TEM and SEM, in presence or absence of Zn^{2+} (**study 2, figures 2A and B**). The structural re-arranging was observed as well when seeing changes in the protein secondary structure [289], being indicative of an architectonical change (**study 2, figure 2C**). All in all, the different methodologies repeatedly confirmed the system's robustness, and so our capacity to consistently obtain stable protein-based nanoparticles.

Long story short, Zn^{2+} was selected as a gold standard gluing agent for the studies to come, as less variability was observed between experiments (already mentioned; **studies 1 and 2, figures 2C and 6A**) and also being biocompatible with the human body at working ratios, meaning 4.6 mg of Zn^{2+} per injected dose of protein-based nanoparticles with a max tolerable level of 40 mg/Kg of Zn^{2+} per day [290] (**study 7**).

Continuing with this common thread, an even wider group of proteins was set to be studied, following the same oligomerization and stability experiments, and with a broader selection of different protein natures, including enzymes (β-galactosidase-H6) [291,292], nanobodies (A1, B4, and F7 -GFP-H6) [293], pro-apoptotic proteins (BAK-GFP-H6) [294], cytokines (TRX-H6-hLIF) [295], tumor-targeted proteins (H6-GFP-T22), and carrier proteins (STM-H6 [296]; **study 2, figures 3A and B**). Zn^{2+} and EDTA were used to promote assembling and disassembling respectively, showing a great tendency, in all cases, to conform protein-based nanoparticles at standard concentrations (**study 2 figure 4A**) and with an oligomeric size increase of at least 34 to 50% (expressed as SIF; **study 2, figure 4B**). A certain variability between final sizes was also detected (being approx. 10.5 nm as average and above renal cut off). This could be explained as a result of different protein molecular weights (from 12 KDa the smallest, to ~41 KDa the biggest), meaning, smaller in molecular weight proteins tend to

construct smaller nanoparticles, and the bigger the protein molecular weights the bigger the nanoparticles, until reaching a size threshold or plateau (as previously mentioned). The SIF, in non-His tagged proteins, was dramatically compromised, but still present, being indicatory of a plausible presence of histidine residue clusters in the protein surfaces which could induce divalent cation gluing. Z-potential was also measured for all candidates and showed negative values while being slightly different from nanoparticle to nanoparticle. Once again, the oligomeric stability at increasing temperatures (4 to 50 °C) was studied, showing overall greater stability in comparison to the control un-assembled sample, and especially at physiological temperatures 37 °C (**study 2, figure 4C and 5**). In addition, protein-based nanoparticle functionality was studied to make sure it was not lost during the assembling process, neither by the presence of Zn^{2+}. Several tests were executed including (1) enzymatic activity (**study 2, inset figure 4C**), (2) fluorescence (**study 2, figure 4D**), and (3) *in vivo* biodistribution in larvae Zebra fish (**study 2, figure 6F**). The obtained data showed no significant functional changes when compared to the control, meaning all resultant protein-based nanoparticles ended up being functional despite the biochemical assembling treatment.

Finally, exploratory experiments were performed to see if even higher concentrations of Zn^{2+} (meaning changing from 0.2-0.5 to 8-10 mM) could induce the architecting of even bigger-in-size structures, already implied in study 1 and presented in **study 2, figures 1B and 6B** illustrations. The particularization into micro-sized structures of histidine tagged recombinant proteins was easily accomplished (**study 2, figure 1F and 6C**), and surprisingly, those new biomaterials were able to release soluble protein-based nanoparticles when resuspended in buffer (**study 2, figure 6D**). The released entities were the same size as previously mentioned in study 2, and equally stable upon increasing temperatures (**study 2, figure 6E**). All these initial insights will be furtherly used in microparticle manufacturing trying to mimic the human secretory granule system [27] (studies 4, 5 and 6).

Definitely, study 2 has shown how histidine tagged recombinant proteins, from completely different origins, can be repetitively oligomerized into stable protein-based nanoparticles, by simply using a robust biochemical principle, and still maintain the functional properties to be used as efficient smart biomaterials.

Considering the platform's ability to formulate highly biocompatible and stable nanoparticles (Study 3)

Having extensively studied how this platform is able to easily manufacture stable protein-based nanoparticles in a simple, cost-effective, and reproducible manner, there were still unsolved issues related to the plausible non-desired interactions [146,183,297], especially in proteins from outsourced origins, with the human body [297]. The idea was to thoroughly assess if this platform was able to oligomerize proteins coming from the human microbiome [298], with low predictable interactivity with human tissues and improved stability.

In this regard, three histidine tagged proteins, namely HCP1 [299], MCP3 [300] and PLD [301] were designed (**study 3, figure 1A**), produced as recombinant versions in microbial cell factories and purified at great levels of purity (**study 3, figure 1B**). Their oligomeric structure was also assessed in presence or absence of Zn^{2+} (**study 3, figure 1C and 2E**), being compatible with their respective resolved 3D structures (**study 3, figure 1E**). The results showed a wide diversity of sizes, especially for MCP3-H6, which displayed an initial size of around 24 nm ± 0.471 at room temperature (meaning 25 °C), maybe due to its intrinsic structural capacity to self-assemble, which slightly increased when increasing concentrations of Zn^{2+} (0.1 and 0.2 mM) were supplied (approx. 49.9 nm). A similar scenario was observed for HCP1-H6, but with higher responsiveness to increasing Zn^{2+} ratios (meaning from initial 8.6 to 34.9 nm). Finally, PLD1-H6 did not effectively respond to Zn^{2+}, at any ratio. Indeed, the only way to induce nanoparticle formation was upon thermal exposure (especially at 45 °C). Those nanostructures remained stable even when cooling down (**study 3, figure 2B**).

What is more, all protein candidates showed great stability in thermal profiles (**study 3, figure 2A**), and even greater when incubated with Zn^{2+}, especially for HCP1-H6 (in which the oligomeric structure was maintained) and MCP3-H6 (in which the thermal stability was increased at physiological temperature, 37 °C; **study 3, figure 2C and D**). Slight changes in Centre of Mass (CSM) suggested an architectonical rearrangement, which could be also translated into a bigger-in-size architecture and the major stability upon thermal exposure (**study 3, figure 2F**). Still, Z-potential measurements remained negative and PDI values were between 0.15 and 0.3, as for all the already studied protein candidates (studies 1 and 2), reaffirming the system's robustness (**study 3, figure 2G**). The oligomeric stability was also addressed in presence of alternative physicochemical conditions, meaning physical (thawing and cooling) and chemical (NaCl, EDTA and Imidazole). Results showed a great structural

stability of all proteins in nearly all chemical conditions (as well as for thawing and cooling) at exception of HCP1 in presence of EDTA; an expected phenomenon as HCP1 was the most sensitive candidate to Zn^{2+}. Moderate changes were also observed for HCP1 and MCP3 upon thermal exposure for 24h and presence of OptiPro medium without substantial structural implications. Oligomers where additionally corroborated by SEM and TEM depicting different types of morphologies (**study 3, figure 3B**).

In short, the histidine tag-divalent cations principle has allowed us to undoubtedly construct smart functional protein-based biomaterials, within the nanoscale, following a reproducible, robust, and simple procedure. The system versatility was confirmed over and over again, biocompatibility issues considered, and the vast majority of critical concerns from the original strategy 1 solved (**figure 16**). But still, this platform is not perfect, and a continuous iterative optimization process needs to be made to keep up with the constant evolving clinical needs [146,302]. That is why a series of concerns will be subsequently discussed.

Ongoing issues

Developing novel drugs for biomedical purposes implies a constant process of finding and minimizing product's weaknesses and optimizing the formulation processes to obtain their best possible version, ensuring safety and efficacy. This is not an exception.

- Even if safety has been a focus all over the experimental design, direct immunogenicity detailed tests must be performed in immunocompetent *in vivo* models, as well as long term protein biodegradability studies. For sure, those will be absolutely mandatory when these protein-based nanoparticles will be moved to the pre-clinical stage.
- Considering protein engineering and assembling as the primordial target of the project, a deeper understanding of biomaterial's functionality underlying pharmaco-kinetic and dynamic properties in *in vivo* systems must be assessed.
- Protein candidates with intrinsic abilities to self-assemble into nanostructures by scaffold cross-reactivity, are not equally sensitive to divalent cations gluing, even when tagged with histidines. This must be considered when rationally designing and planning new projects. Ideally, further assembling studies of a wider spectrum of His tagged proteins (from different natures) should be planned to look for structural patterns or primary sequence peculiarities to shed some light on this issue.
- Zn^{2+} was found as the gold standard cross-linking agent so far, but still there is an additional set of Irving-William series metal ions (Mn^{2+}, Fe^{2+}, Co^{2+}, Ni^{2+} and Cu^{2+}) which were lightly exploited and could give additional intriguing functional and structural properties to our biomaterials.
- Even if the formulation process has been carefully simplified to minimize the overall number of steps, there is not a standardized protocol to automatize all the process (e.g., the external addition of Zn^{2+} to induce assembling). This should be considered for scale up purposes.

Some of these issues have been already tackled and contingency plans launched.

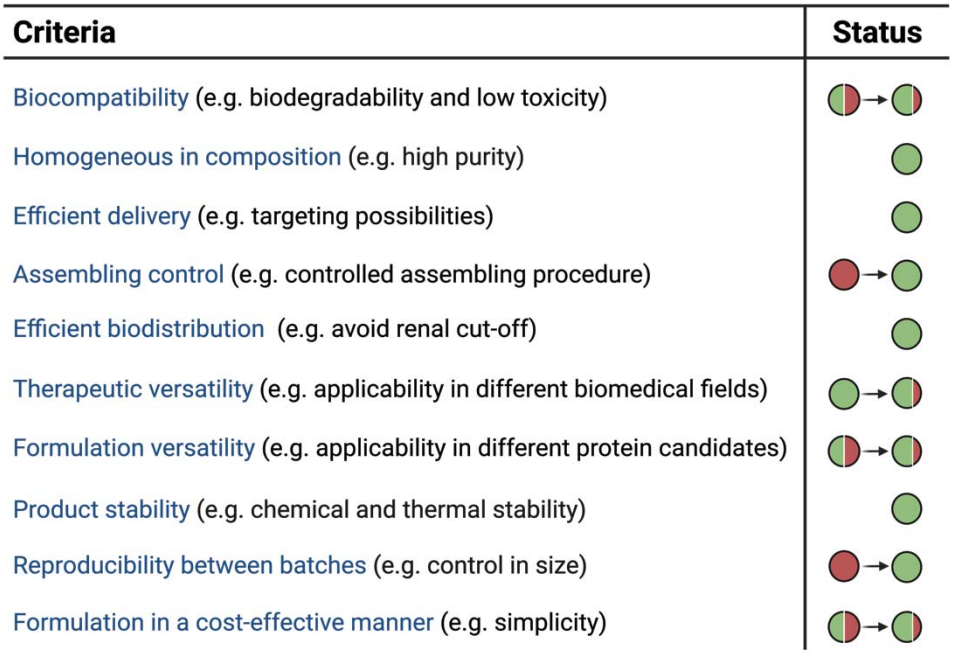

Figure 16. A qualitative evaluation following (Figure 10 list) of strategy 1 (A cationic – histidine tag principle for protein self-assembling), meaning green (accomplished), red (not accomplished), and green-red (further studies needed). The resultant status (right) evaluates the novel protein assembling strategy based on histidine tag-divalent cations gluing. Black arrows refer to the status transition from original strategy 1 to the new one which completely solves (green) or partially solves (major green-minor red) the vast majority of issues.

(B) The formulation of protein-based microparticles (objective 2 – Studies 4, 5 and 6)

The optimization of the novel self-assembling platform to construct particles mimicking the naturally occurring inclusion bodies, while ensuring reproducibility, assembling control, and sample homogeneity (study 4)

The second essential aim was to further expand the biomedical applicability of the so far described biochemical principle (histidine tag-divalent cations) to create even more-in-complexity biomaterials with certain functional peculiarities. The idea was to adapt our simple protein engineering protocol to create submicron/micro-sized materials able to mimic naturally occurring inclusion bodies (IBs; original strategy 2) [28,241,242,268], while keeping functional secretory properties (just like the human secretory granule system), and still solving their major limitations (meaning reproducibility, sample homogeneity, and procedure control).

Study 4 was born to target all these limitations, and surprisingly showed how increased Zn^{2+} concentrations, meaning from 0.2-0.5 mM (for protein-based nanoparticles manufacturing, ratios 1:1 to 2.5:1) to 10-20 mM (for protein-based microparticles manufacturing, ratios 50:1 to 100:1), were able to trigger histidine tagged Alkaline Phosphatase (AP) [303] and β-galactosidase (β-Gal) [291] microparticularization (so called single step protocol in this article, ss). The resultant oligomeric structures (expressed as intensity size distribution; ISD, for all tested microparticles during subsequent studies) sized around 1.72 and 5.56 μm respectively (**study 4, figures 1A; green and C**), which were confirmed by SEM (**study 4, figure 1B**). It is important to highlight that Zn^{2+} was again chosen as the cross-linking gold standard, and insoluble microparticles were obtained right after protein centrifugation and isolation.

What is more, an additional multi step (ms) manufacturing protocol was designed to see if lipid matrices were able to improve even more the resultant microparticle's properties (**study 4, figure 1A**). Slightly smaller microparticle sizes (1.11 to 1.99 μm), in comparison to ss protocol, were observed in both DLS and SEM (**study 4, figures 1A; orange and C**) and no dramatic functional changes were detected when studying their enzymatic activity (**study 4, figure 1D**).

For the next step, T22-GFP-H6 was also used as a gold standard [255] to determine protein structure, release and targeting applicability using both protocols. After the assembling

procedure, resultant sizes were in the same range (meaning 1.28 to 0.88 μm) as for previous candidates (**study 4, figure 2A bottom**) also confirmed by SEM imaging (**study 4, figure 2A top**). The specific fluorescence decay (SFD) was additionally determined to assess structural rearrangement, as well as cross-β-sheet amyloid like motives (ALS) content [26]. Results showed how the single step protocol displayed lesser SFD decay but similar β-amyloid structures (of around 40 %) when compared to ms (**study 4, figure 2A bottom**), meaning a huge secondary and tertiary structural reorganization has taken place. PDI values were higher than the ones for protein-based nanoparticles (0.6 to 0.9), being indicative of an intrinsic tendency of this platform to create simultaneously multiple populations, as expected for insoluble biomaterials. Their functional capabilities were also explored in HeLa cells, starting by specific receptor-based internalization (triggered by T22-CXCR4 receptor interaction). Results showed an increased internalization rate for ss protocol (**study 4, figure 2B top**), in comparison to both ms and natural T22-based IBs (established as control), being receptor-specific as the entrance was blocked in presence of AMD3100 (a molecular inhibitor of CXCR4 receptor) [304] in all cases (**study 4, figure 2B bottom**). Cell viability was additionally assessed to ensure material's safety, without major significant changes when compared to the control (**study 4, figure 2C left**). Surprisingly, soluble protein was released from T22-based microstructures once resuspended in buffer for both ss and ms protocols (**study 4, figure 2D top**), and release was sustained for 7 days at 37 °C until reaching a 60 % of liberated protein for the ss protocol (**study 4, figure 2D bottom**). The oligomeric analysis of released proteins confirmed them to be oligomerized into usual protein-based nanoparticles with equivalent sizes and PDI values (**study 4, figure 2E**), and even greater specific internalization rates, when compared to the control (meaning soluble nanoparticles obtained right after the IMAC purification; **study 4, figure 2F**).

To conclude the *in vitro* analysis, an additional standard protein namely, T22-PE24-H6 [263], with intrinsic cytotoxic activity was used as a functional candidate to assess cell death. The physicochemical studies revealed similar size measurements, PDI values and morphology as for T22-based microparticles, and slightly different ALS content especially for ss methodology (from 40 to 25 %; **study 4, figure 2A right**). HeLa viability assays confirmed clear killing tendencies at 1 μM of PE24-based microparticles up to approx. 50 % of cell viability for ms protocol and approx. 20 % for ss protocol after 96h. The cytotoxic activity was receptor specific as it was reverted in presence of AMD3100 (**study 4, figure 2C right**).

Finally, the microparticle's capacity to release active soluble protein-based nanoparticles was studied in detail in *in vivo* CXCR4+ colorectal cancer mouse models (Swiss nude). A preliminary screening, looking for specific protein accumulation in tumoral cells was assessed, using both ss (at 100:1 ratio) and ms protocols. Results showed an initial fast reduction of protein fluorescence coming from the injection point, followed by a constant and subtle fluorescence increase in the tumoral foci until day 21, especially for ss protocol (**study 4, figure 3A**). It is important to highlight that both tumoral cells and microparticles were subcutaneously implanted in distal regions, far from each other. At that point, we decided to move forward with the ss protocol, due to its simplicity and low-cost, and as no significant improvements were detected for the ms protocol.

Prior the second *in vivo* experiment with the ss protocol, a concentration readjustment was performed as poor accumulation signal was detected from the previous experiment. That is why, we moved from 100:1 (20 mM) to 50:1 ratio (10 mM) of Zn^{2+} to architect the insoluble T22-based microparticles. An additional divalent cation namely Ca^{2+} (at 300:1 ratio; 60 mM) was used to create a second testing group which would present plausible different protein release dynamics. Following the same injecting criteria, results showed greater and clearer accumulation signals in the tumoral foci, as well as proper microparticle disintegration in the injection point up to 10 days (**study 4, figure 3B**). The platform's capacity to have an effect on tumoral tissues was finally corroborated when T22-PE24-H6 [263] microparticles, made of Ca^{2+}, were able to significantly reduce tumoral growth once implanted. Ca^{2+} was selected for this experiment as presented the best releasing and accumulation tendencies. No off-target toxicity was observed so far, at any case or any time point, due to insoluble microparticle's implantation. Whole animal IVIS imaging was the gold standard technique to detect accumulated fluorescence in both injection point or tumoral foci upon time, as well as *ex vivo* fluorescence detection when the experiment was finished, and animals euthanized.

As for protein-based nanoparticles, we have been able to expand the scope of a straightforward assembling biochemical principle (histidine tag-divalent cations) by simply increasing Zn^{2+} concentration, to manufacture higher-in-complexity protein-based microparticles ensuring reproducibility, sample homogeneity, and procedural control. Its functionality has been tested over and over again in both *in vitro* and *in vivo* models showing promising results, and without manifesting any kind of undesired toxicity [181,183]. The Ca^{2+} case will be shortly discussed under ongoing issues.

Tackling the platform's transversality, and methodological robustness to construct sub and micro -scaled particles from different origins (Study 5)

As for protein-based nanoparticles, we wondered if the already displayed histidine tag-divalent cation principle, the so called single step protocol (ss), could transversely induce protein self-assembling into micro-scaled particles when coming from a wide spectrum of different origins, and if the procedure could still maintain its methodological robustness without the need of additional supportive matrices [305] (**study 5, figure 1**).

The microparticularization workflow was optimized, step by step, looking for the best protein release, stability, and precipitation conditions. The gold standard protein T22-GFP-H6 [255] was initially used as proof of concept for the assessment (**study 5, figure 2A**). A detailed study on progressive protein aggregation was performed creating a final precipitation profile (expressed as material formation in percentage; **study 5, figure 2B top**) and exemplifying how this particular protein candidate responded to increasing concentrations of Zn^{2+} (from 0.1 to approx. 30 mM). The results showed a sigmoidal type of behavior, with a clear tendency to induce pellet formation (**study 5, figure 2B bottom**) at medium to high concentrations (meaning from 8 to 20 mM). Two statistical parameters were also extracted from the analysis, namely max $P_{\%}$ (meaning the maximum percentage of aggregated protein) and R square (meaning how close the data fits with the regression line; the higher R square values the better regression fit). In this particular case, T22-based standard protein perfectly responded to increasing Zn^{2+} concentrations up to a 100 % of precipitation with a nearly 1 square values. The resultant product morphology was also determined by both SEM and optical imaging (in which fluorescence signals were additionally obtained). Results clearly suggested equal type of amorphous structures (**study 5, figure 2 C and D top**) as for previously seen analysis (**study 4, figures 1B and 2A top**). The same SEM studies allowed to perform an *in situ* Zn^{2+} localization following 2D (lines) and 3D (mapping) dimensions, displaying an evident colocalization between proteins and Zn^{2+}at increasing doses (**study 5, figure 2D bottom**).

Following up, the releasing tunability and stability of T22-based microparticles was firstly monitored at increasing concentrations of Zn^{2+} (ratios 40:1, 50:1, 100:1 and 150:1) upon 37 °C incubation for several days (from 0.5 to 240h) after granule resuspension. Interestingly, the higher the amount of Zn^{2+} the lesser liberated protein, being 50:1 the most versatile ratio, which fluctuated between both releasing thresholds (too fast or too slow delivery), especially at day 3 (**study 5, figure 3A**). The resuspension buffer's composition was also key to assess

the releasing control. EDTA-based buffers exhibited greater releasing predisposition (acting as stimulators) rather than Zn^{2+} resuspension buffers, which prompted protein withholding (acting as inhibitors; **study 5, figure 3D**). The nano-scaled size of delivered proteins and PDI values were again reconfirmed for all Zn^{2+} concentrations (being around 13.5 to 14.4 nm and 0.52 to 0.59 respectively), and a fluorescence decrease noted for micro-sized particles (**study 5, figures 3B and C**). The mechanical stability (particularly for Zn^{2+} 50:1 ratio) was studied upon sonication for both micro and released nano -particles, showing no significant differences (**study 5, figures 7A and B**). Internalization experiments of liberated protein nanoparticles also showed receptor specific internalization in CXCR4+ SW1417 cells (reverted in presence of AMD3100) and no entrance in CXCR4- SW1417 cells (**study 5, figure 7D**). *In vivo* studies, performed following the same implantation and detection procedures as for (**study 4, figure 3A**), displayed a significant and specific protein accumulation, from T22-bases microparticles (50:1 ratio), in tumoral tissues up to 10 days (**study 5, figure 7E**) without causing any major changes in mice weight (**study 5, figure 7F**).

A transversality assessment of microparticle formation was performed for dissimilar fusion proteins with or without both targeting ligands or histidine tag, and with alternate GFP [286], PE24 [262] and DITOX [263], HSA and BSA [296,306] scaffolds (**study 5, figure 4**). Precipitation profiles were obtained for all candidates at increasing Zn^{2+} concentrations and max $P_{\%}$ and R values extracted (**study 5, figure 5**). Results clearly showed how histidine tags strongly stimulated protein cross-linking and subsequent precipitation into granulated structures (meaning max $P_{\%}$ values between 90 to 100 % for all His tagged proteins) in comparison to non-histidine tagged proteins (meaning max $P_{\%}$ values between 30 to 40 %). Interestingly, the aggregation kinetics moderately changed in each particular case, but without any further implications. The only statistically significant parameter involved in protein aggregation was the presence or absence of the histidine tag (**study 5, figure 6**).

Beyond any doubt, the simple histidine tag-divalent cation principle has allowed us to repetitively formulate a wide set of different-in-origin protein-based microparticles mimicking the human secretory granule system which could be easily constructed by recombinant candidates approved for clinical use [307]. The platform's robustness has been confirmed over and over again, and the functional capacities and stability of released entities fully demonstrated.

Considering the platform's ability to change the delivery kinetics of stable functional nanoparticles from sub and micro -scaled particles (Study 6)

Going a step further, study 6 was built up as the basic pillar for a thorough assessment of modified delivery kinetics of protein-based microparticles without the need of any external hosting structures as well [308–310]: a platform which has exhibited great versatile, easy-to-execute, transversal, and reproducible results.

The idea was to modify the usual single step fabrication procedure (**study 6, figure 1A**), by the rational combination of alternative divalent cations, and monitor changes in material's releasing kinetics, final targeting, and accumulation tendencies. Aside from the usual gold standard Zn^{2+}, other divalent cations like Ca^{2+}, Mg^{2+}, Mn^{2+} and combinations (ZnMn, ZnMg, MnMg, CaMn, CaZn) were tested at different ratios (**study 6, figure 1B**) to architect T22-GFP-H6 microgranules. Those ratios were obtained from qualitative assays, and detailed precipitation studies are currently ongoing. Protein aggregation, and so microparticle formation (imaged as a pellet) was obtained for all conditions (**study 6, figure 1B right**), with sizes ranging from 0.250 to 0.620 μm. Interestingly, Zn^{2+}-based microparticles, even in combination with other divalent cations, tended to present bigger structures than Ca^{2+} or Mn^{2+} -based mixtures. Microparticles remained mechanically stable, with no significant changes once sonicated (**study 6, figure 1C**) and released entities structured at the nanoscale (meaning from 13 to 20 nm), even after 37 °C incubation (**study 6, figure 1D**).

An initial *in vivo* screening was performed with all different mixtures in CXCR4+ colorectal cancer mouse models (Swiss nude) using, again, the same implantation and injection conditions as in studies 4 and 5 (**study 6, figure 2A**). The temporal loss of the injected material, meaning microparticle disintegration was monitored up to 10 days (240h) and the *ex vivo* fluorescence was measured for each injection point at day 5 (120h). Results showed how Zn^{2+}, Ca^{2+} and CaZn T22-based microparticles displayed slower releasing tendencies. That is why, a second and more detailed *in vivo* experiment was designed monitoring time-based injection point protein signals (**study 6, figure 3**) and an extensive *ex vivo* examination was performed. Results showed a clear initial peak signal phase for all conditions, followed by a subsequent progressive fluorescence decrease (meaning protein nanoparticle release) up to day 10, especially and significantly sustained by Zn^{2+} and Ca^{2+} -based particles (**study 5, figure 4A**). The remaining signal at the injection point was 100 times greater for all T22-based microparticles, compared to its soluble T22-based counterpart, which exhibited a fast clearance at day 5 (**study 5, figure 4B**). These results were indicative of a clear direct

correlation between material format (meaning soluble protein-based nanoparticles or insoluble protein-based microparticles) and sustained delivery. Finally, averaged fluorescence signals comparing both injection point and tumor, revealed a continued accumulation of protein in tumoral foci, and a progressive reduction of fluorescence at the injection point, accentuated for the CaZn condition (**study 6, figures 5A, B and C**). No cumulative fluorescence signals were observed in tumors so far, as could be expected. This phenomenon might be explained by the existence of an equilibrium between the amount of protein reaching the tumor, and the speed of protein degradation inside the targeted cell which creates a linear correlation (meaning the degradation speed plausibly equals the homing and internalization speed). Finally, the protein signal in tumor from Ca^{2+}-based depots, was three times greater than protein signals coming from non-targeted tissues (kidney and liver), being indicative of a clear effective targeting and sustained delivery of the therapeutic drug (**study 6, figures 5D and E**).

In short, not only the histidine tag-divalent cations principle has allowed us to construct smart protein-based nanoparticles, but also fully functional insoluble protein-based microparticles able to mimic naturally occurring secretory granules [28,241,268]. The system is reproducible, robust, transversal and creates a sustained releasing scenario of therapeutical entities able to reach the targeted tissues without the need of external matrices. All in all, product's composition remained homogeneous, no undesirable *in vivo* issues have been detected so far, and the manufacturing simplicity was maintained. In addition, the vast majority of the critical concerns from the original strategy 2 have been solved (**figure 17**). But still, and as for protein-based nanoparticles, the system requires a continuous iterative process of optimization to keep up with the constant evolving clinical needs [146,302]. That is why a full section of concerns will be subsequently listed.

Ongoing issues

Protein-based microparticles are no exception either. Among the overall advantages described so far, there is still a set of remaining weaknesses to be tackled to achieve the best possible product version, ensuring above all, safety, and efficacy.

- Though material's safety was persistently considered, direct immunogenicity experiments must be planned in immunocompetent *in vivo* models (not Swiss nude). This is absolutely mandatory if protein-based microparticles should be translated towards clinics.
- A large group of different-in-nature histidine tagged proteins has been assembled into micro-sized depots, and there have been size and precipitation discrepancies in response to divalent cations (especially for Ca^{2+}, for which final precipitated protein yields are quite variable). That is why, the ideal divalent cation formula (meaning ion type and concentration) must be optimized for each particular case to ensure maximum agglomeration outputs, and subsequent efficacy when functionally tested.
- The formulation process has been carefully simplified and improved, but still, there is not a final protocol to automatize the aggregation process upon divalent cation addition. This should be considered for scale up purposes.
- Micro-scaled particles' size and physical traits are not properly measured by DLS, as they tend to precipitate when the measurement is taking place. For that reason, additional techniques (meaning TEM, SEM or Flow Cytometry) should be explored to minimize the final size measurement variability.

Some of these issues have been already tackled and contingency plans launched.

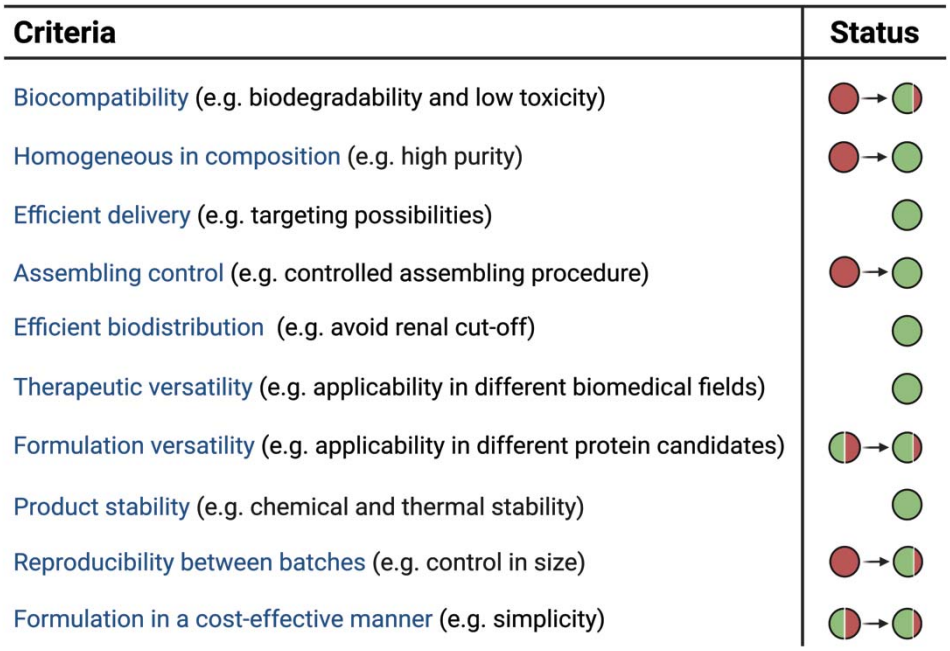

Figure 17. A qualitative evaluation following (Figure 10 list) of strategy 2 (A physicochemical self-assembling principle of protein-based insoluble microparticles, meaning naturally occurring inclusion bodies), meaning green (accomplished), red (not accomplished), and green-red (further studies needed). The resultant status (right) evaluates the novel protein assembling strategy based on histidine tag-divalent cations gluing. Black arrows refer to the status transition from original strategy 2 to the new one which completely solves (green) or partially solves (major green-minor red) the vast majority of issues.

(C) Protein-based nano and micro -particles biomedical assessment (objective 3 – Annex 1, 2, 3 and 4)

The biomedical assessment of the developed platform was essential, as the platform's biochemical simplicity and versatility pushed us to look for different biotechnological models (e.g., wound healing, osteogenesis, biocatalysis and antimicrobial activity) and see how the system responds upon different stimuli. The goal is to develop robust and reproducible technologies that could be translated into the clinics. Only the most remarkable results will be discussed here.

Biomedical applicabilities of sub and micro -scaled protein-based particles as secretory entities in wound healing (Annex 1)

The study focused on producing and purifying [103] a well-studied growth factor, namely the human fibroblast growth factor [311] (hFGF2-H6; **figure 1**) and compared its proliferative and wound healing abilities when assembled into natural bacteria inclusion bodies [242] (original strategy 1) or divalent cation-based (Zn^{2+}, Ca^{2+}, and Mn^{2+}) microparticles (novel histidine tag-divalent cation principle). Physicochemical experiments revealed common size measurements, as previously observed in discussion's section B (**figure 2A**), usual morphologies (**figure 2B**), and high purity levels (particularly for formulated microparticles; **figure 2C**). *In vitro* experiments disclosed both increased proliferation (for 48h, especially for Zn^{2+} and Ca^{2+} microparticles in comparison to both soluble or natural IBs FGF2-H6 formats), and survival (upon starvation medium for 2 to 6 days) of NIH3T3 fibroblast cells (**figures 3A and B**). Released protein from microparticles was additionally monitored at 37 °C for 7 days, proliferation capacity was confirmed (for 48h), comparable to the endocrine system [26,77], and structural stability assessed (at increasing temperatures, from 25 to 80 °C). Results showed how Zn^{2+}-based microparticles were the most efficient biomaterials for those purposes (**figure 4**). In addition, wound healing studies (**figure 5**), measured as the percentage of healed wound area, revealed how hFGF2-H6 Zn^{2+} microparticles also displayed the greatest healing capacity (up to 55 %), in comparison to the soluble (22 %) and GFP Zn^{2+} microparticles control (38 %) after 2 and 4 days. In short, zinc-based FGF2-H6 microparticles appeared as the best disintegrating materials to induce fibroblast-based wound healing, and still, maintaining adequate physicochemical properties.

Biomedical applicabilities of sub and micro -scaled protein-based particles as secretory entities in osteogenesis (Annex 2)

A similar study was unfolded for Annex 2, in which the same human FGF2-H6 recombinant protein was formulated as disintegrating microparticles in presence of Zn^{2+} but with the idea to be used as a functional topography [312] for mesenchymal stem cells (MSCs) growth and differentiation [13,313]. FGF2-H6 recombinant protein was produced in microbial cell factories [116,314], re-purified by IMAC chromatography [86], and several oligomeric and physicochemical parameters determined (such as Z-potential, size, purity, integrity, thermal stability, etc.; **figure 1**). Results showed how both protein-based nano and micro -particles adequately responded to Zn^{2+} as expected, and stability and protein release experiments also displayed suitable results (**figure 2**). All this data reinforced again the robustness and reproducibility of the overall biochemical platform. What is more, the designed topographies were set up on glass coverslips which were initially functionalized with a PEA-fibronectin (FN) layers [315]. Insoluble microparticles were subsequently adsorbed on top (with greater adsorption values than its soluble counterparts, with a 20 % increase) and MSCs seeded (**figure 2F**). *In vitro* results undoubtably showed improved MSCs proliferative tendencies for FGF2-H6 microparticles (after 7 to 14 days and 50 ng/mL) up to 40 % compared to the controls (**figures 3 B and D, and 4E**). Imaged MSCs additionally exhibited exceptional internalization tendencies of disintegrating microparticles (**figure 3A**). Finally, the MSCs differentiation capacity was also confirmed, showing how osteogenic markers such as Runx2, osteonectin (OSN) or Osteopontin (OSP) were expressed without major issues [316] (**figure 4**). Again, zinc-based FGF2-H6 microparticles clearly appear as suitable disintegration biomaterials to promote, in this case, osteogenesis.

Biomedical applicabilities of sub and micro -scaled protein-based particles as secretory entities in biocatalysis (Annex 3)

Changing the field of study, we wondered if micro-scale particles constructed by divalent cation crosslinking were able to improve enzymatic stability, reusability, and catalytic properties. β-galactosidase was chosen as the gold standard enzyme [291], from which the catalytic activity, measured as ONPg (o-nitrophenyl- β-D-galactopyranoside) hydrolysis [292] (**figure 1A**), was assessed for micrometric particles (**figure 1C**). As for other applications, several divalent cations (namely Zn^{2+}, Ca^{2+}, Mg^{2+} and Mn^{2+}) were chosen to construct those

disintegrating entities displaying both precipitating and functional discrepancies (**figures 1D and E**). Meanwhile Zn^{2+} appeared as one of the best precipitators, it also dramatically compromised the enzymatic performance. A similar scenario was observed for Mn^{2+} and Ca^{2+} but with less activity reduction. Mg^{2+} solely appeared as an optimal functional activator with low precipitating tendencies. All in all, the enzymatic activity of two different sets of microparticles (Mn^{2+}-based or a combination of Ca^{2+}:Mg^{2+}-based) was assessed in reusability conditions; meaning a reusable enzymatic cartridge was manufactured (**figure 2B**) avoiding protein loss (translated as activity decrease) during each reaction cycle (**figure 2A**). In all cases, a greater hydrolysis rate was observed cycle by cycle for the micro-scaled entities, in comparison to the control soluble protein (**figures 2C and D**). In addition, when the optimal Ca^{2+}:Mg^{2+} combination was found (meaning ratio 2:1, **figure 3A**), the fastest and most efficient kinetic properties were exhibited (**figures 3C and D**) translated as K_M (from control 0.14 to 0.21 mM CaMg microstructures) and Vmax (from control 2.44 to 4.03 nmol/min CaMg microstructures) [317]. Finally, structural studies revealed more active moieties (protein more hydrated) in micro-scale particles, and greater thermal stability [318] translated as melting temperature, Tm (from control 55.5 to 63.1 °C CaMg Art IBs; **figures 4A and B**). Long story short, the obtained data suggested how reusable β-Gal microparticles increased in thermal stability and performance compared to its soluble counterpart when the adequate divalent cation mixture was found.

Biomedical applicabilities of sub and micro -scaled protein-based particles as antimicrobial secretory entities (Annex 4)

The bactericide capacity of antimicrobial peptide (AMPs) [319,320] -based microparticles was also tested in the infectious field. Indeed, four different histidine tagged recombinant proteins, based on a fluorescent GFP scaffold, were designed with different positively charged AMPs (namely T22 [321], Pt5 [322], PaD [323] and GWH1 [324], **figures 1A and B**). Proteins were produced [314], purified and 3D structures predicted, especially for the AMPs. They all exhibited quiet standard physicochemical properties, meaning common amino acidic length (between 18 to 55 Aa residues) and number of positive charges (between 4 and 9). In addition, α-helix structures were predicted in all cases excepting T22, which a β-strand was observed (**figure 1B**). Size measurements displayed structural discrepancies between protein candidates; nanoparticles ranging from 12 to 54 nm were observed for T22, GWH1 and PaD, and smaller structures (from 5 to 7 nm) were detected for Pt5 (**figure 1C**) with usual

Pdi values (from 0.14 to 0.5). Zn^{2+}-based microparticles were manufactured following the standard protocol (**figure 2A**) for all protein candidates as Zn^{2+}-based exhibited the highest antimicrobial activity (against *S. aureus*) compared to Mn^{2+} and Fe^{2+} -based formulations (**figure 2B**). Particle size remained stable between 150 and 570 nm as expected, and the release of protein-based nanoparticles of 12 to 21 nm (**figure 2F**) was sustained for 168h, being Pt5 and GWH1 the most progressive ones (**figure 2D**). Additional *in vitro* studies revealed GWH1 and T22 Zn^{2+}-based secretory granules as the most effective ones against *S. aureus* at 10 μM (**figure 2H**) and *in vivo* biodistribution assays of all constructs displayed gastrointestinal, pancreas and intestinal accumulation in Zebrafish larvae at 50 μg/mL for 48h (**figure 2I**). No fluorescence signals were observed for the control so far. Finally, a humanized version [296] of the GWH1-GFP-H6 construction, meaning GWH1-NIDO-H6, was designed (as the one with the most promising results), produced and purified without major issues (**figure 3A**). No significant changes were observed when analyzing the physicochemical properties of the resultant protein-based nanoparticles (of around 35 nm), although smaller submicrometric Zn^{2+}-based particles were detected (of around 80 nm, **figure 3B**). *In vivo* survival studies performed in *S. maltophilia* (K279) adult Zebrafish infection models revealed how Zn^{2+}-based GWH1-NIDO-H6 secretory granules were able to both significantly kill and protect Zebrafish from the infection. The optimal dose was set at 50 μg and survival rate (in percentage) determined 6 days post-infection. No off-targeting deleterious effects [169,181] were spotted so far (**figures 3C, D E and F**).

(D) The extracted knowledge (objective 4 – Study 7 and Annex 5)

The narrative comes to an end, and last but not least, our final contribution to the scientific community. Two main actors have showed up on the scene, namely histidine tag and divalent cations. Each of those with chemical peculiarities that surprisingly cooperate to assemble higher-in-complexity protein-based nano and micro -structures. But there is more than we think when all the puzzle tiles are pulled together. That is why, a personalized review has been performed for each component to discover their overall biomedical applicabilities.

Each technical discussion has been displayed in each review (**study 7 and annex 5**).

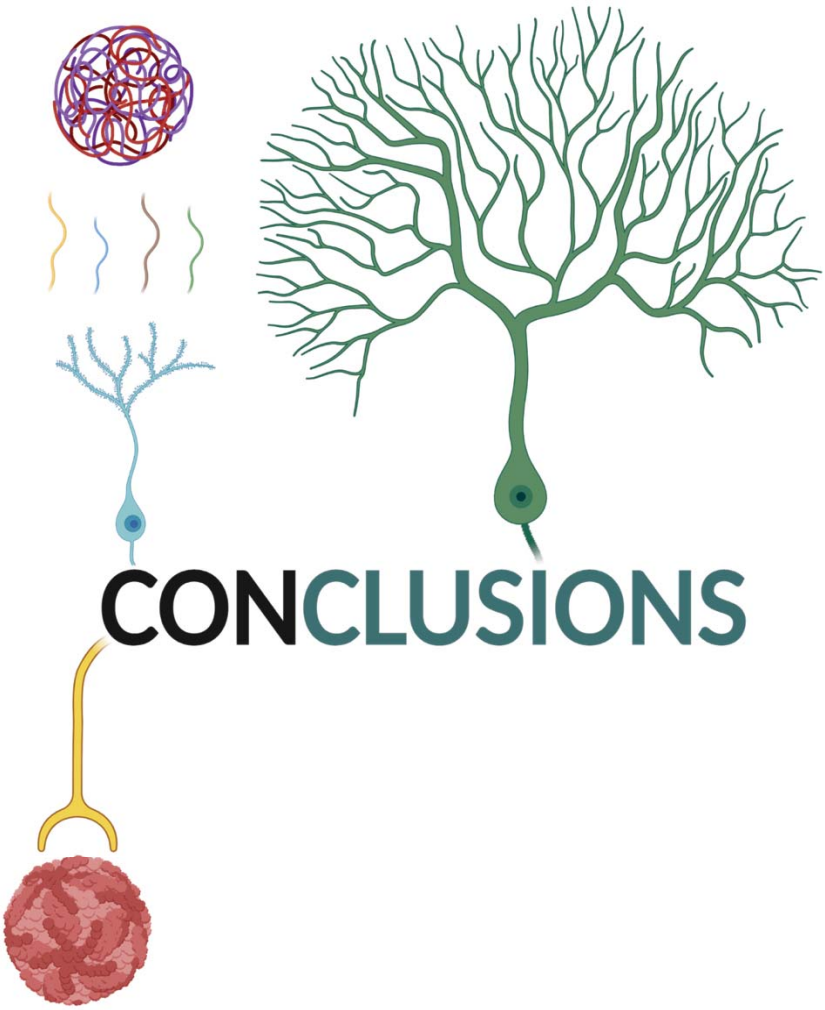

CONCLUSIONS

All in all, there is a short set of take home messages that summarize the whole story's vision. Simple ideas that would, maybe, stick in the readers' mind after having surfed on this tide of data:

1. A novel and simple biochemical principle, meaning the interaction between the histidine tag and divalent cations, has been rationally designed to spontaneously self-assemble higher-in-complexity protein-based nano and micro -sized materials.

2. The resultant nano and micro -sized materials have remained:
    a. Homogeneous in composition (high purity).
    b. Stable upon thermal and chemical treatment.
    c. Reproducible between batches.

3. The implemented platform beholds:
    a. High therapeutic versatility (applicability in different biomedical fields).
    b. High formulation versatility (applicability in different protein candidates).
    c. A great improvement in regard to previous outdated assembling strategies.

4. The design and manufacturing processes fall upon:
    a. Controllable assembly.
    b. Efficient delivery (targeting possibilities).
    c. Efficient biodistribution (avoidance of renal filtration).
    d. Cost-effective formulation (simplicity).
    e. Biocompatible formulation.

5. The platform matures in a continuous optimization and improvement process, in which material's issues are continuously solved and products updated.

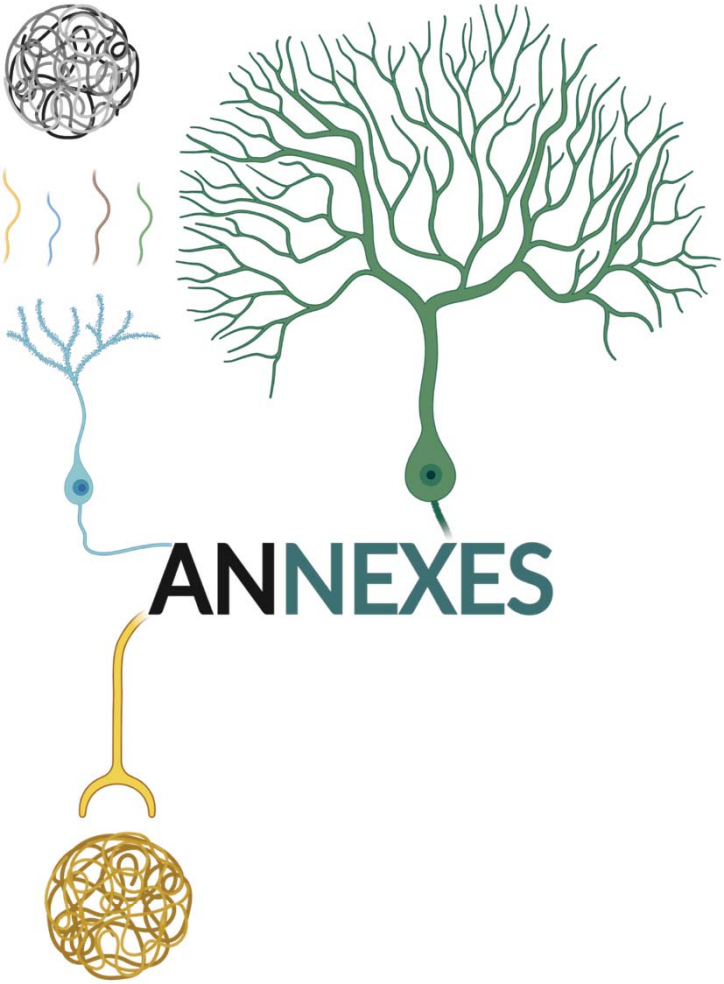

ANNEXES

Referenced studies

Annex 1

Release of functional fibroblast growth factor-2 from artificial inclusion bodies

Naroa Serna, Olivia Cano-Garrido, Julieta M. Sánchez, Alejandro Sánchez-Chardi, Laura Sánchez-García, Hèctor López-Laguna, Ester Fernández, Esther Vázquez, and Antonio Villaverde

Journal of Controlled Release 2020 · Impact factor (9.776) · Quartile (Q1)

Objective 3.c

To test the biomedical applications of **protein-based insoluble microparticles** in tissue engineering (wound healing).

Having extensively studied the manufacturing mechanisms of insoluble protein-based microparticles able to deliver, in a sustained manner, functional protein-based nanoparticles, we wondered how this platform could be used in tissue engineering, particularly in wound healing.

Thus, this work has been focused on testing microparticle's capacity to stimulate fibroblast growth and subsequent wound healing in an *in vitro* model, based on growth factors release. The obtained data suggests how artificial microparticles behave as disintegrating secretory granules for the prolonged administration of growth factors. Being chemically homogeneous, compliant with regulatory restrictions, and more efficient restoring the damaged tissue than its soluble counterparts.

Journal of Controlled Release 327 (2020) 61–69

Contents lists available at ScienceDirect

Journal of Controlled Release

journal homepage: www.elsevier.com/locate/jconrel

Release of functional fibroblast growth factor-2 from artificial inclusion bodies

Naroa Serna[a,b,c], Olivia Cano-Garrido[a,b,c,1], Julieta M. Sánchez[a,b,c,d], Alejandro Sánchez-Chardi[e,f], Laura Sánchez-García[a,b,c], Hèctor López-Laguna[a,b,c], Ester Fernández[g], Esther Vázquez[a,b,c,*], Antonio Villaverde[a,b,c,*]

[a] Institut de Biotecnologia i de Biomedicina, Universitat Autònoma de Barcelona, Bellaterra, 08193 Barcelona, Spain
[b] Departament de Genètica i de Microbiologia, Universitat Autònoma de Barcelona, Bellaterra, 08193 Barcelona, Spain
[c] CIBER de Bioingeniería, Biomateriales y Nanomedicina (CIBER-BBN), Spain
[d] Instituto de Investigaciones Biológicas y Tecnológicas (IIBYT) (CONICET-Universidad Nacional de Córdoba) ICTA & Cátedra de Química Biológica Departamento de Química FCEFyN, UNC. Av. Velez Sarsfield 1611, X 5016GCA Córdoba, Argentina
[e] Servei de Microscòpia, Universitat Autònoma de Barcelona, Bellaterra, 08193 Barcelona, Spain
[f] Departament de Biologia Evolutiva, Ecologia i Ciències Ambientals, Facultat de Biologia, Universitat de Barcelona, Av. Diagonal 643, 08028 Barcelona, Spain
[g] Departament de Biologia Cel·lular, Fisiologia i Immunologia, Universitat Autònoma de Barcelona, Bellaterra, 08193 Barcelona, Spain

ARTICLE INFO

Keywords:
Secretory granules
Protein materials
Extended drug release
Wound healing
hFGF-2

ABSTRACT

Growth factors are required for cell proliferation and differentiation under physiological conditions but especially in the context of regenerative medicine. The time-prolonged administration of those factors has been explored using different sustained drug delivery systems. These platforms include natural materials such as bacterial inclusion bodies (IBs) that contain chaperones and other bacterial components that might favour protein release. Being successful from a functional point of view, IBs pose regulatory concerns to clinical applications because of the mentioned presence of bacterial cell components, including endotoxins. We have here explored the release and activity of the human fibroblast growth factor-2 (hFGF-2) from a novel synthetic material, namely artificial IBs. Being chemically homogenous and compliant with regulatory restrictions, we wondered if these materials would effectively release functional proteins in absence of accompanying bacterial agents. The data provided here fully supports that artificial hFGF-2 IBs act as true and efficient secretory granules and they slowly disintegrate in cell culture to promote wound healing in an in vitro wound healing model. Free from undesired bacterial components, artificial inclusion bodies show promises as delivery agents in regenerative medicine.

1. Introduction

Delivery systems for therapeutic proteins are required in different clinical fields, to avoid or delay repeated protein dosing that might become inconvenient or unreachable. Protein replacement therapies and especially regenerative medicine are among the main clinical targets for protein delivery systems. Many strategies are based on the design of biocompatible matrices or networks to be used as protein holders. Built with organic or inorganic composites, these structures pursue a regulatable and time-sustained release of the embedded protein in absence of toxicities linked to the material forming the matrix [1–6].

In this context, the secretory granules of the human endocrine system, that release peptidic hormones, are of particular interest. These structures are proteinaceous materials in which the protein components themselves are physiologically released by a slow disintegration process [7]. This is based on a particular architecture of such secretory agents, which are in fact functional amyloids [8,9]. From them, the building block itself, that is, the protein hormone, is slowly released by a process that involves molecular chaperones [7]. Mimetics of those secretory materials would be then very useful in biomedicine, as their use would not require any heterologous matrix or supporting scaffold to release the functional protein. In this regard, bacterial inclusion bodies (IBs), that are micro-scale protein aggregates formed in recombinant bacteria by the product of the cloned gene, behave, in many aspects, like those secretory granules [10]. Being intriguing protein depots [11], IBs have

* Corresponding authors at: Institut de Biotecnologia i de Biomedicina, Universitat Autònoma de Barcelona, Bellaterra, 08193 Barcelona, Spain.
E-mail addresses: esther.vazquez@uab.cat (E. Vázquez), Antoni.Villaverde@uab.cat (A. Villaverde).
[1] Nanoligent SL. Edifici Eureka, Universitat Autònoma de Barcelona, Bellaterra, 08193 Barcelona, Spain.

https://doi.org/10.1016/j.jconrel.2020.08.007
Received 14 February 2020; Received in revised form 21 June 2020; Accepted 4 August 2020
Available online 05 August 2020
0168-3659/ © 2020 Elsevier B.V. All rights reserved.

been tailored as a source of functional proteins in cell culture, to release growth factors [12,13], chaperones [13], cytoskeleton components [14] and anti-oxidant proteins [13]. In two different mouse models of human cancers, the local or remote administration of IBs formed by anti-tumoral proteins show potent antitumoral [15] and antimetastatic effects [16] respectively. Being structural and functional mimetics of secretory granules, IBs show promise as protein delivery systems [17], but their bacterial origin imposes the presence of molecular contaminants and endotoxins whose full elimination is unapproachable by industrially compliant methods. Therefore, the use of IBs results non-appropriate for most of clinical applications. Very recently [18], micron sized artificial IBs (ArtIBs) have been generated by very simple in vitro fabrication approaches, using divalent ions as molecular cross-linkers and a functional protein as a unique building block. If efficiently releasing the forming protein, such ArtIBs might represent better mimetics of secretory granules than IBs. Being fabricated out of pure protein, they are chemically homogeneous and with a defined composition, what is highly appealing in clinics. However, since they are generated in vitro by the controlled assembly of one single protein species and free from any bacterial component, they are also devoid of chaperones from the bacterial quality system that are associated to natural IBs [19]. Whether IB-associated bacterial chaperones are necessary for the release of functional protein from these functional amyloids has been not yet determined. Therefore, the ability of ArtIBs to deliver functional growth factors (and other clinically relevant proteins) should be assessed before further development and even before any detailed in vivo analyses of functionality. In this context, we have designed, fabricated and fully characterized ArtIBs formed by the hFGF-2 in an in vitro wound healing model, and evaluated the potential of these materials as functional protein depots for a time-prolonged healing effect.

2. Materials and methods

2.1. Plasmid, culture & protein production

The synthetic hFGF-2-H6 gene (Low Molecular Weight isoform; 18 KDa) and the control GFP-H6 gene were designed in house to be inserted into the prokaryotic expression vector pET22b and obtained from GeneArt (Thermo Fisher Scientific). The amino acid sequences of the encoded proteins hFGF-2-H6 and GFP-H6 are MAAGSITTLPALPEDGGSGAFPPGHFKDPKRLYCKNGGFFLRIHPDGRVDGVREKSDPHIKLQLQAEERGVVSIKGVCANRYLAMKEDGRLLASKCVTDECFFFERLESNNYNTYRSRKYTSWYVALKRTGQYKLGSKTGPGQKAILFLPMSAKSHHHHHH and MSKGEELFTGVVPILVELDGDVNGHKFSVSGEGEGDATYGKLTLKFICTTGKLPVPWPTLVTTLTYGVQCFSRYPDHMKRHDFFKSAMPEGYVQERTISFKDDGNYKTRAEVKFGDTLVNRIELKGIDFKEDGNILGHKLEYNYNSHNVYITADKQKNGIKANFKIRHNIEDGSVQLADHYQQNTPIGDGPVLLPDNHYLSTQSALSKDPNEKRDHMVLLEFVTAAGITHGMDELYKHHHHHH), respectively. H6 stands for the carboxy-hexahistidine tail, which simultaneously serves for protein purification, for divalent cation coordination and for ArtIB fabrication.

The *Escherichia coli (E. coli)* strain BL21 (DE3) was used for the production of bacterial IBs and soluble protein, once transformed by heat shock with the recombinant pET22b vectors. The *E. coli* cultures were kept at 37 °C and 250 rpm up to 0.5 OD units. In order to promote the protein deposition as bacterial IBs, gene expression was induced for 3 h at 37 °C upon isopropyl-D-thiogalactoside (IPTG) at 1 mM. For soluble protein production, cells were cultured overnight at 20 °C and the gene expression was induced with IPTG at 0.1 mM. Then, bacterial cells were harvested by centrifugation (5000 *g* at 4 °C, 15 min) and freezed at −80 °C.

2.2. Bacterial IBs and ArtIBs fabrication

Bacterial hFGF-2-H6 IBs were isolated by a combination of enzymatic and soft mechanical cell lysis by a protocol described elsewhere [20]. IB proteins were quantified by Western Blot using an anti-His antibody (1:5000 Anti-His Santa Cruz Biotechnology, ref.: sc-57,598). Sample protein amounts were inferred from standard curves with known amounts of hFGF-2-H6 protein using the Quantity One software.

hFGF-2-H6 and non-functional GFP-H6 ArtIBs were fabricated from pure soluble proteins. For purification of these soluble recombinant proteins, bacterial cells were resuspended in wash buffer (20 mM Tris-HCl, 500 mM NaCl and 10 mM imidazole pH 8), containing an EDTA-free protease inhibitor cocktail (Roche). Afterwards, *E. coli* cells were disrupted by three rounds at 1200 psi in a French press (Thermo FA-078A). Both proteins hFGF-2-H6 and GFP-H6 were purified by His-tag affinity chromatography using 1 mL HiTrap Chelating HP columns (GE Healthcare) through an ÄKTA pure FPLC (GE Healthcare). Fractionation was made by a linear gradient of elution buffer (20 mM Tris-HCl, 500 mM NaCl and 500 mM imidazole pH 8). Purified protein fractions were dialyzed against carbonate buffer (166 mM $NaCO_3H$, pH 8). Soluble protein was then stain-free detected by TGX (TGX FastCast Acrylamide Kit) technology and protein amounts were determined by Bradford's assay. Finally, formation of ArtIBs was approached by diluting pure soluble proteins in distilled H_2O at a final concentration of 2 mg mL^{-1} and a final volume of 200 μL. Afterwards, protein samples were mixed by default with $ZnCl_2$, at a zinc:protein molar ratio of 50:1 for hFGF-2 ArtIBs and at 100:1 for GFP ArtIBs (1:1 ratio stands for 0.196 mM). Then, samples were incubated 10 min at room temperature and centrifuged at 15.000 *g* for 15 min. Finally, the soluble fraction was discarded to obtain the final product. The discarded soluble protein was quantified by Bradford assay to determine the exact concentration of artificial inclusion bodies that correspond to the remaining protein. Alternatively, other divalent cations namely $CaCl_2$ and $MnCl_2$ were used at cation:protein molar ratio of 200:1 and 400:1 for hFGF-2 ArtIB, and at 300:1 and 500:1for the control GFP ArtIBs formation.

2.3. Ultrastructural characterization

Volume size distribution of bacterial IBs and ArtIBs was determined by dynamic light scattering (DLS) at 633 nm in a Zetasizer Nano ZS (Malvern Instruments Limited) using ZEN2112 3 mm quartz batch cuvettes. Protein samples dissolved in deionized water at 1 mg mL^{-1} were measured in triplicate and mode size peak and polydispersion index (PDI; expressed as mean ± standard error of the mean) were obtained.

Ultrastructural morphometry (size and shape) of bacterial IBs and ArtIBs was visualized at nearly native state with electron microscopy. Drops of 20 μL of IBs resuspended in deionized water were directly deposited on silicon wafers (Ted Pella Inc.) for 2 min, excess of liquid blotted, air dried, and immediately observed without coating in a field emission scanning electron microscope (FESEM) Merlin (Zeiss) operating at 1 kV and equipped with a standard secondary electron detector. Representative images of general fields and nanostructure details were captured at three high magnifications (10,000×, 40,000× and 80,000×).

2.4. Thioflavin T fluorescence in ArtIBs

The interaction of Thioflavin T with ArtIBs was explored to evaluate the amyloidal nature of the protein material. Protein aliquots (30 μL) were added to 25 μM Thioflavin T (Sigma Aldrich) (Thio T) (30 μL) in carbonate buffer (166 mM $NaCO_3H$, pH 8). The final protein concentration was 0.1 mg/mL. ThioT fluorescence was excited at 450 nm and the fluorescence emission spectra were recorded with a Varian Cary Eclipse spectrofluorimeter. The cross-beta sheet structure of the hFGF-2 within ArtIBs was monitored by the enhancement of the free dye fluorescence emission caused by the interaction with amyloidogenic

proteins.

2.5. Soluble protein release

Bacterial IBs and ArtIBs were resuspended in 1 mL of PBS reaching a final concentration of 2 mg mL^{-1} and incubated at 37 °C without agitation. Then, 100 μL were taken from each sample at 24, 72, 120 and 168 h time points and centrifuged for 10 min at 15,000 g to separate soluble and insoluble fractions. Then, soluble protein was detected by stain-free TGX (TGX FastCast Acrylamide Kit) and by Western Blot using an anti-His monoclonal antibody (1:5000 Anti-His Santa Cruz Biotechnology, ref.: sc-57,598). The percentage of released protein was quantified by Image Lab software.

2.6. Thermal stability of the released proteins

Fluorescence spectra were recorded in a Cary Eclipse spectrofluorimeter (Agilent Technologies), using a quartz cell with 2 mm path length and a thermostated holder. The excitation and emission slits were set at 5 nm. Excitation wavelength (λ_{ex}) was set at 295 nm. Emission spectra were acquired between 310 and 450 nm in hFGF-2 samples at 0.1 mg mL^{-1}, dissolved in carbonate buffer (166 mM $NaCO_3H$, pH 8) upon release from ArtIBs. The temperature-dependent behavior of proteins was determined between 25 and 80 °C. The Centre of Spectral Mass (CSM), a weighted average of the fluorescence spectrum peaks [21] was calculated for comparison. The CSM is also related with the relative exposure of the tryptophan (Trp) to the protein environment. The maximum red-shift in the CSM of Trp is compatible with large solvent accessibility and unfolding [22]. The protein thermal stability was analyzed by the onset temperature (T_{onset}). This parameter indicate the temperature where the CSM start to increase.

2.7. Cell proliferation and survival assay

Biological activity of bacterial IBs, ArtIBs, soluble protein and cations ($ZnCl_2$, $CaCl_2$ and $MnCl_2$) was analyzed by measuring cell proliferation and survival of the murine cell line NIH3T3. NIH3T3 cells were routinely maintained in D-Minimum Essential Medium Eagle (D-MEM) supplemented with 10% Fetal Bovine Serum (FBS) and 2 mM L-glutamine at 37 °C and 10% CO_2 in a humidified incubator.

For proliferation studies, bacterial IBs and ArtIBs were resuspended in cell culture medium with 1% FBS at different concentrations. ArtIBs formed by the fluorescent protein GFP-H6 were included as negative control and recombinant soluble hFGF-2 was used as a positive control. 96-well plates were decorated with IBs and ArtIBs, adding 50 μL of IB suspension per well at final concentration of 0.1, 1, 100 and 1000 μg mL^{-1}. These plates were incubated at 4 °C overnight in order to allow IBs and ArtIBs sedimentation. 4×10^3 NIH3T3 cells were seeded per well and cultured for 48 h at 37 °C and 10% CO_2 in a humidified incubator. Cell proliferation was determined by CellTiter-Glo Luminescent Cell Viability Assay (Promega) in a Multilabel Plater Reader Victor3 (Perkin Elmer). All experiments were done with three replicates.

For cell survival assay, 96-well plates were decorated with bacterial IBs and ArtIBs at a final concentration of 1 μg mL^{-1}. Then, NIH3T3 cells were seeded at 4×10^3 cells per well and cell survival was measured at different days (0, 1, 2, 3, 4, and 6) by adding 100 μL of the CellTiter-Glo® Reagent (Promega).

The positive control soluble hFGF-2 was added together with NIH3T3 cells. It was incubated for 48 h at final concentration of 0.1 and 1 μg mL − 1 for proliferation studies and at 1 μg mL^{-1} for cell survival assay. All experimental data were measured in triplicate.

2.8. Wound healing assay

Wound healing assays were performed by decorating the cell culture surface with GFP and hFGF-2 ArtIBs Zn^{+2} and soluble hFGF-2 protein. Briefly, ArtIBs and soluble protein aliquots were defrosted and resuspended in culture medium. 70 μL of this solution was added to each of the two compartments of a silicone insert (culture-insert, 2-wells 24-well plate, ibiTreat; Ibidi), resulting in a final concentration of 1 μg mL^{-1}. The coating was incubated for 4 h at 4 °C. Then cells were seeded with a cell density of 4×10^4 cells mL^{-1} and after 24 h the medium was changed to starvation medium containing only 1% FBS. Cells were grown further and after 24 h the culture-inserts were removed using sterile tweezers resulting in a 500 μm-wide gap. More starvation medium was added to cover the whole well of the 24-well plate. The subsequent healing process was recorded using an optical microscope (Leica). Images of the starting conditions (~ 500 μm gaps) and at different time points for at least two wells were taken and all wells of the 24-well plate were checked visually for any irregularities. Wound sizes were determined from four independent wells from two plates, using Image J software with the MRI wound healing tool macAhro.

2.9. Statistical analyses

Pairwise comparisons of protein cell viability effect were analyzed by Student's *t*-test and multiple comparisons to detect differences between control and experimental groups of proliferation and wound healing by Tukey's method. All statistical tests were performed using GraphPad Prism version 8.0. All quantitative values were expressed as mean ± standard error of the mean ($\bar{x} \pm$ SEM). Differences among groups were considered significant at $p < 0.05$ and relevant divergences were marked as * ($p < 0.01$) or # ($p < 0.05$).

3. Results and discussion

A H6-tagged hFGF-2 (Fig. 1A, top) was produced in recombinant bacteria under conventional (mild) production conditions or under conditions promoting conformational stress (Fig. 1A). Mild conditions favoured the production of soluble protein versions, that upon purification, were further used for ArtIB fabrication (Fig. 1A). The purified soluble hFGF-2 was proteolytically stable (Fig. 1B,C), and it showed a tendency to oligomerization (Fig. 1C). For protein precipitation as ArtIBs, we used three different divalent cations at the respective molar proportions that lead to full protein precipitation, meaning that remaining soluble protein was undetectable (Fig. 1D). On the other hand, the stress-prone culture conditions (Fig. 1A) favoured the formation of bacterial IBs that were isolated and straightforward used in the experimental. Such bacterial IBs exhibited around 600 nm (Fig. 2A), while ArtIBs (those generated with Zn^{2+} cation and named ArtIBs Zn) doubled this size, indicative of a successful His- and Zn-mediated assembly of the His-tagged hFGF-2. GFP-H6 ArtIBs were also fabricated as experimental controls, sizing around 1.8 μm (Fig. 2A). Morphologically, hFGF-2 IBs and ArtIBs Zn were very similar, showing the typical rough surface of conventional IBs [23]. The purity of ArtIBs, formed by a single immunoreactive protein species, contrasted with the extreme heterogeneity in the protein composition of IBs, as revealed by the broad brand spectrum of these materials (Fig. 2C). Such heterogeneity had been previously reported in IBs during early proteomic studies of such materials [19,24], and the presence of different types of bacterial chaperones (holding, folding and disaggregating) also repeatedly confirmed as a part of the IB proteome [19,24–29]. In addition to the morphological similarity with conventional IBs, the amyloid nature of ArtIBs was evaluated by the interaction of Thioflavin T, showing a significant extent of cross beta secondary structure (Fig. 2D) that was in agreement with previous data obtained with different ArtIB species [30].

To start the hFGF-2 ArtIB characterization, we decorated with different types of protein clusters cell culture plates where NIH3T3 were further seeded. Control GFP ArtIBs formed with the assistance of

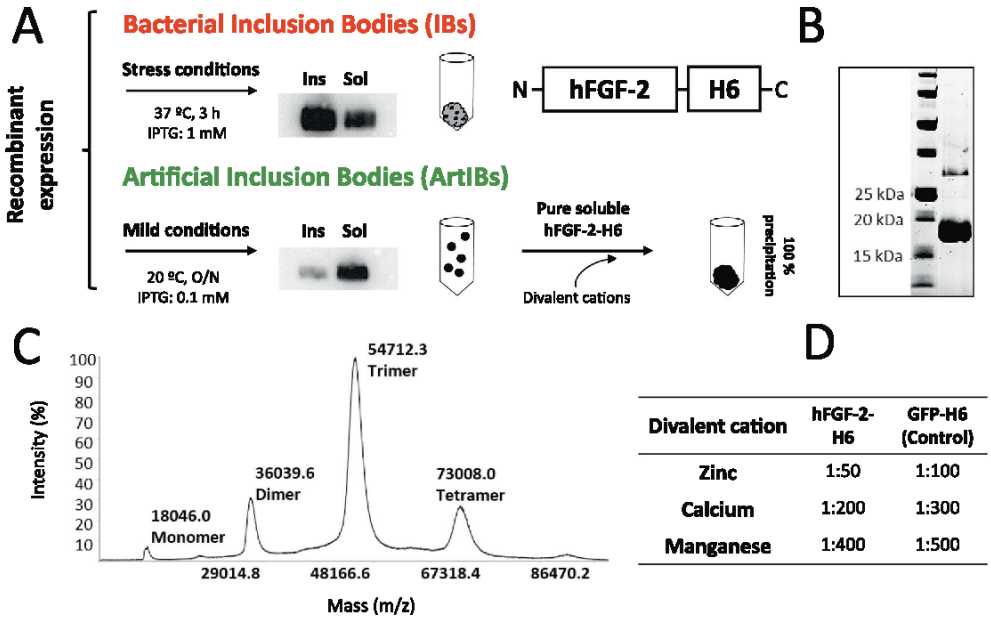

Divalent cation	hFGF-2-H6	GFP-H6 (Control)
Zinc	1:50	1:100
Calcium	1:200	1:300
Manganese	1:400	1:500

Fig. 1. Production of bacterial IBs and ArtIBs based on hFGF-2. A. The modular scheme of hFGF-2-H6 is shown, indicating the amino (N) and carboxy (C) terminal ends. Note that sizes of the boxes are only approximate. GFP-H6 has the same modular scheme in which hFGF-2 is replaced by GFP [59]. The recombinant protein was produced in *E. coli* under a set of mild or stressful conditions (indicated), that resulted in a different fractioning between soluble (Sol) and insoluble (Ins) protein fractions (shown here by anti-H6 Western blots). Natural IBs were straightforward recovered from the insoluble protein fraction produced under stress conditions. Purified soluble protein obtained under mild production conditions was used to fabricate ArtIBs as described [18]. B. The hFGF-2 soluble protein sample submitted to denaturing SDS-PAGE and further TGX protein staining, revealing the integrity of the protein (18 kDa) and the absence of degradation bands. The molecular weight of markers (left line) is indicated. C. MALDI-TOF analysis of the same hFGF-2 sample, indicating different oligomeric states of the protein in its native state. D. Molar ratio (protein:cation) of the tested divalent cations that resulted in 100% of ArtIB formation in hFGF-2-H6 and the control protein GFP-H6.

different ions did not show any proliferative effect, and cell growth over them was fully comparable to control cell cultures in absence of additional materials (Fig. 3A). However, hFGF-2 ArtIBs clearly stimulated cell proliferation at levels similar to those promoted by the soluble hFGF-2 and slightly higher than those promoted by hFGF-2 bacterial IBs (Fig. 3A). Such effect was observed at two different concentrations of the protein material, and the nature of the ion used as cross-linker did not show clear influences on the biological impact of the material (Fig. 3A). Then Zn cation was at this point selected as a default ion for fabrication of the protein granules. The fact that ArtIBs tended to stimulate cell growth with more intensity than IBs, was indicative of a higher bioavailability of hFGF-2 in the artificial materials compared to natural versions, at a similar extent than that offered by the plain soluble protein version. At this stage, we wondered how hFGF-2 ArtIBs would behave in a cell survival assay, in which cells were cultured in a starving medium. Again, the biological impact of ArtIBs was fully comparable to that of the soluble protein, since both agents rescued with matching profiles starving cells, which died in a few days in the presence of GFP materials or without any additive (Fig. 3B). The rescuing ability of both forms of hFGF-2 was confirmed by microscopy of cultured cells 4 days upon the starting of the starving period (Fig. 3C).

hFGF-2 can execute its biological activities from outside the target cell by canonical receptor-based tyrosine kinase signalling or upon internalization and nuclear uptake [20], as this factor combines paracrine and nuclear activities in its biological function [31]. ArtIBs, as their natural counterparts, can penetrate mammalian cells upon exposure in absence of any intrinsic cytotoxicity [13,18]. In an attempt to evaluate the potential delivery of hFGF-2 from chemically pure ArtIBs, we determined the amount of protein released to the media upon incubation of the protein granules under physiological conditions. As observed, a significant portion of the growth factor was released from the insoluble hFGF-2 artificial material and detectable in the soluble fraction of the ArtIBs suspension, at 24 h of incubation (Fig. 4A). Protein release was specifically notable in ArtIBs Zn^{+2} and ArtIBs Ca^{+2}, while it was hardly detectable in the case of ArtIBs Mn^{+2}. These release kinetics would be especially helpful in assisting the design of specific applications for those materials when intended for protein depots with time-prolonged supply of the contained growth factors. When cultured cells were exposed to such soluble fraction containing ArtIBs-released protein, stimulation of cell proliferation over the control, non-treated cells (100%) was specially apparent when using ArtIBs Zn-solubilized protein, and at decreasing extents with ArtIBs formed with the assistance of Ca^{2+} and Mn^{2+} (Fig. 4B). This is in agreement with the release kinetics shown in Fig. 4A in which Mn-based materials were less able to deliver the growth factor than the other ArtIB variants, indicative of a tighter clustering induced by this particular cation. At that point, we also investigated the conformational quality of the growth factor once removed from the particles. Importantly, the intrinsic fluorescence caused by exciting the protein with 295 nm ultraviolet light revealed no changes in the thermal profile of hFGF-2 released from ArtIBs. However, the CSM values at 25 °C indicated a subtle change, suggesting conformational differences between the released proteins in comparison to the soluble version. Those results demonstrated a stability similar, if not higher, of the released protein compared to the original soluble hFGF-2 ($T_{onset,\ release\ hFGF\text{-}2} > T_{onset,\ soluble\ hFGF\text{-}2}$) (Fig. 4C).

This set of results confirmed the correct selection of Zn^{2+} as default building ion, but also revealed that ArtIBs are good secretion materials, since the forming protein is progressively released without an immediate or a fast disintegration of the whole bulk material. These data also confirm the biological (and therefore structural) stability of hFGF-2 when submitted to packaging as ArtIBs and upon the subsequent release from them. Why some cations seem to favour better than others protein release, is an issue that remains to be solved. In this regard, protein release is inversely related to the binding strength between each cation-protein interaction. Distinct binding constants (Kb) have been demonstrated for Cu^{2+} and Ca^{2+} towards α-synuclein [32]. Also, the

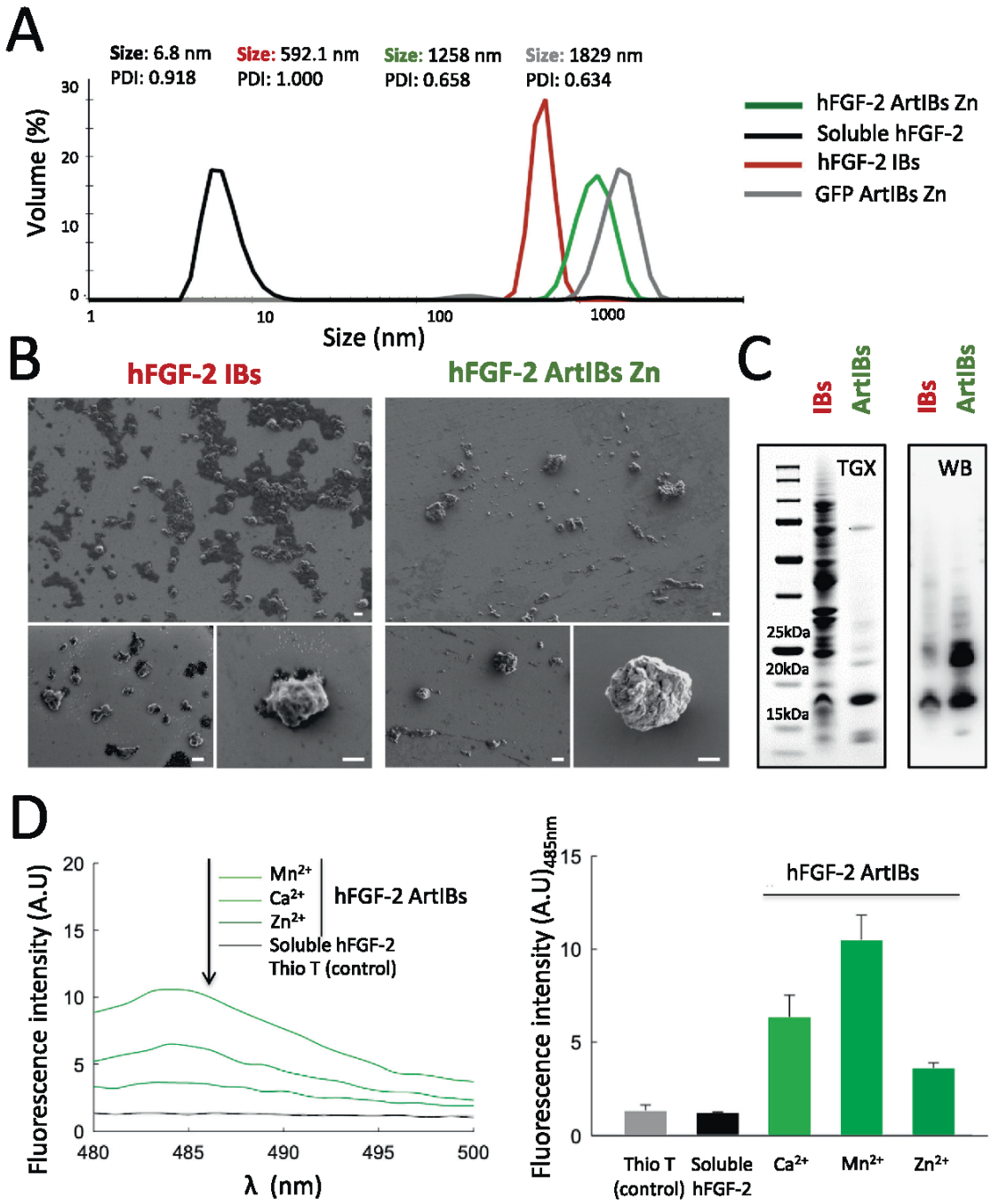

Fig. 2. Characterization of hFGF-2 IBs and hFGF-2 ArtIBs. A. Hydrodynamic size of hFGF-2 IBs and hFGF-2 ArtIBs based on Zn^{2+}. Numbers indicate the peak of the DLS plot (size) and the polydispersion index (PDI). GFP-H6 ArtIBs Zn and soluble hFGF-2 were used as control. B. Representative FESEM images at three magnifications showing from broad fields to IBs detail of isolated hFGF-2 IBs and hFGF-2 ArtIBs Zn. Bars indicate 500 nm. C. SDS-PAGE and further TGX protein staining or Western blot immunodetection of both hFGF-2 bacterial IBs and hFGF-2 ArtIBs based on Zn^{2+}. The molecular weight of markers is also indicated. The migration of the soluble protein is shown in Fig. 1 B. D. Thio T fluorescence emission spectra recorded at λ_{ex} = 450 nm. Left: Thio T spectra of hFGF-2 ArtIBs indicated by its cationic composition. The control represents the fluorescence of Thioflavin T in carbonate buffer. Thio T interacting with soluble hFGF-2 was also included. Right: Thio T fluorescence emission intensity at 485 nm.

structure-function effect of a particular cation on a given protein might be also and unique, as demonstrated by Cu^{2+} that activate pro-angiogenic growth factors such fibroblast growth factor 2 [33]. Irrespective of that the precise mechanics of the observed differences, Zn^{2+}, Ca^{2+} and Mn^{2+} (and other divalent cations) are all present at important amounts in the human body [34–37] and the clinical use of materials containing any of them would be completely plausible.

In vitro wound healing models are convenient tools to quickly evaluate the therapeutic potential of growth factors [38], and they have been specifically applied to examine the regenerative potential of the

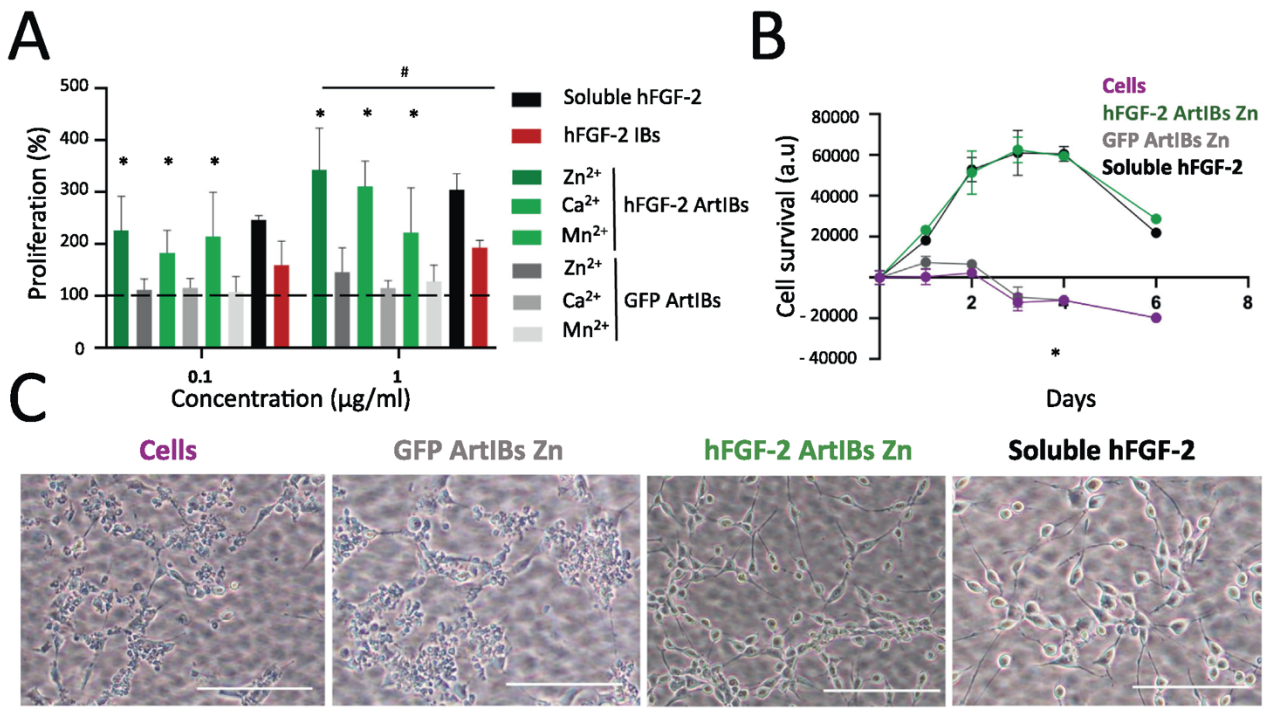

Fig. 3. Biological effects of hFGF-2 ArtIBs. A. Proliferation of NIH3T3 cells cultured on hFGF-2 IBs and hFGF-2 ArtIBs during 48 h, at final concentrations of 0.1 and 1 µg mL^{-1}. GFP-H6 ArtIBs were used as negative control and soluble hFGF-2 as positive control. Significant differences with the respective GFP ArtIB controls are indicated (* $p < 0.01$). Differences between hFGF-2 ArtIBs and hFGF-2 bacterial IBs are also indicated (# $p < 0.05$). B. Survival of NIH3T3 cells cultured on starvation medium containing 1% FBS in the presence of 1 µg mL^{-1} of hFGF-2 ArtIBs Zn, GFP-H6 ArtIBs Zn and soluble hFGF-2. Data within upper and lower curves are significantly different to each other in the interval from day 2 to day 6 ($p < 0.01$).C. Representative light microscopy images of cells at day 4 of the cell survival assay showing the morphological changes induced by hFGF-2 ArtIBs Zn and soluble hFGF-2. Bars indicate 50 µm.

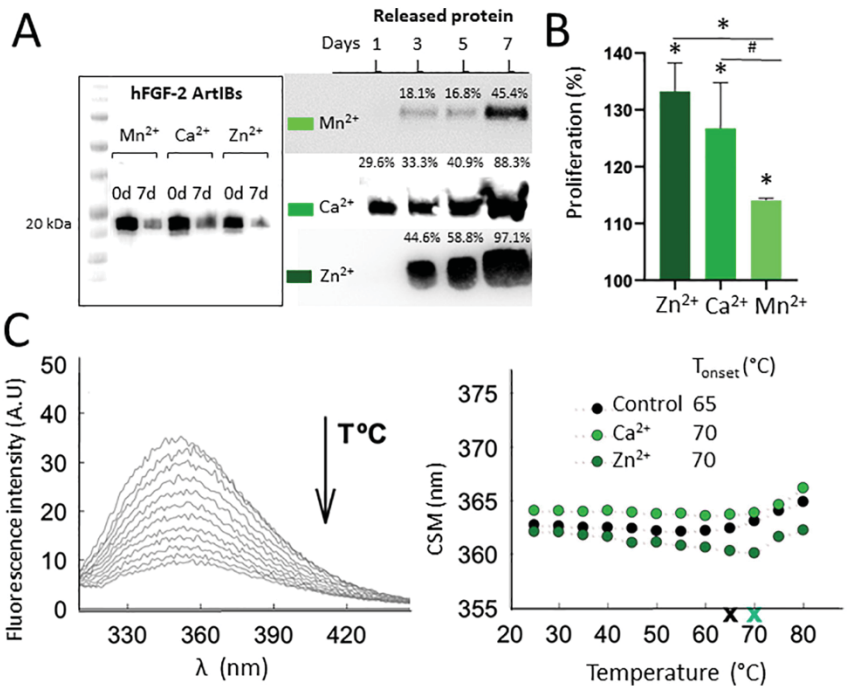

Fig. 4. Release of soluble protein from hFGF-2 ArtIBs. A. Western blot detection of hFGF-2 ArtIBs (formed by alternative cations) before and after incubation at 37 °C for 7 days. Western blot detection and the percentage of the released soluble protein after incubation of those ArtIBs at 37 °C for 1, 3, 5 and 7 days is also shown. B. Proliferation of NIH3T3 cells treated with the soluble hFGF-2 released from hFGF-2 ArtIBs during 48 h. The cross-linking cations are indicated in each case. The symbols indicate significant differences (* $p < 0.01$, # $p < 0.05$) with untreated cells or between cells treated with released protein from diverse materials. C. Thermal stability of released soluble hFGF-2 from ArtIBs. Left: Typical intrinsic fluorescence spectra of soluble hFGF-2 recorded at different temperatures. The arrow indicates the heating direction. Right: CSM vs temperature. The black cross indicates the onset temperature (T_{onset}) of the soluble protein and the green cross indicates the T_{onset} of the protein released from ArtIBs. (For interpretation of the references to colour in this figure legend, the reader is referred to the web version of this article.)

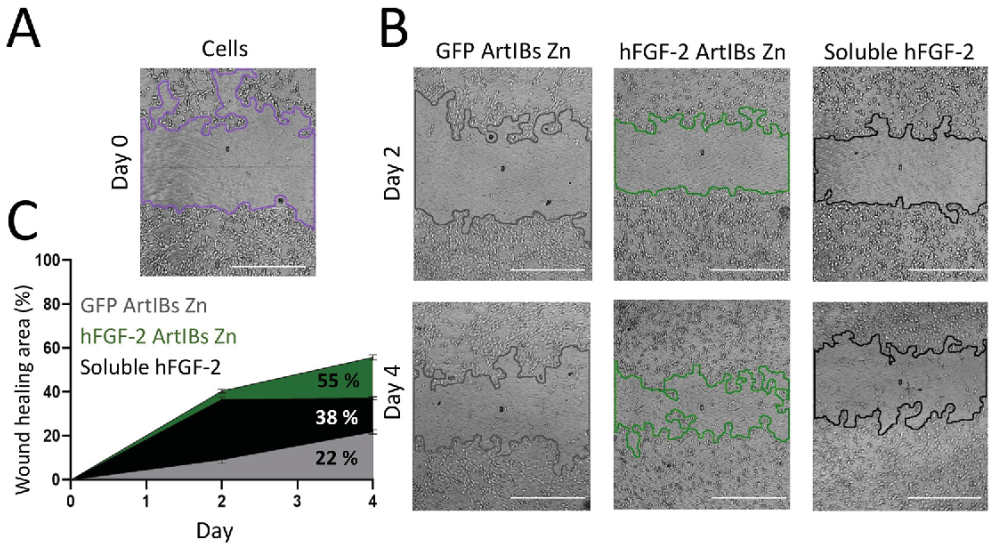

Fig. 5. Wound healing activity. A. Measurement of wound area after culture-insert removal. B. Measurement of wound areas coating with 1 μg mL ^{1} of hFGF-2 ArtIBs Zn, negative control GFP-H6 ArtIBs Zn and treatment with positive control, soluble hFGF-2. Bars indicate 50 μm. All measurements were done using the MRI wound healing tool macro for ImageJ. C. Wound closure area % determined in the wound healing assay after 2 and 4 days. On the last day of the experiment, the differences in these areas are significantly different between soluble hFGF-2 and GFP ArtIB ($p < 0.01$), and between hFGF-2 ArtIB and GFP ArtIB ($p < 0.01$). Wound closure area is also significantly different between soluble hFGF-2 and hFGF-2 ArtIB ($p < 0.05$).

axolotl lipoxygenase administered as bacterial IBs [12]. A similar wound model (Fig. 5A) was applied to scrutinize the activity of hFGF-2 ArtIBs Zn, compared to the soluble version of the growth factor. As observed (Fig. 5B,C), hFGF-2 ArtIBs Zn were more efficient than the soluble protein version in expanding the wound closure area, while the non-functional GFP ArtIBs Zn had only mild positive effects. These data, apart from being promising regarding the potential use of ArtIBs as carriers of growth factors, strongly suggest that the administration of hFGF-2 from ArtIBs could be more efficient than that of the soluble protein version (see also the supporting data in Fig. 3A). This is probably associated to the depot effect of the protein granules, which extend the bioavailability of the growth factor for a longer time than when the protein is supplied in the soluble conventional form. The slow protein release from the material (Fig. 4), that appears to be very stable, can of course account for this effect.

ArtIBs, as fully proved here, can release plain soluble and functional protein for a biological role, in absence of bacterial contaminants that like chaperones, are expected to contribute to protein release from natural IBs because of their disaggregating activities [39,40]. The amount of released protein is enough for enhanced cell proliferation (Fig. 3A) and prolonged cell survival under starving conditions (Fig. 3 B,C), and this material favoured wound healing in an in vitro wound healing model (Fig. 5). Such biological effects are superior than those obtained when exposing cells to either conventional IBs or soluble growth factor, supporting the further development of ArtIBs as a tremendously interesting biomaterial. The main relevance of ArtIBs is based on their pure composition. In contrast with the extremely heterogeneous nature of natural IBs, that contain cell wall components, nucleic acids, lipids and proteins as impurities from the producing cells [19,24,41,42], these analogous artificial versions are uniquely formed by a single protein species assembled under defined physicochemical conditions. Being then chemically pure, synthetic protein depots are much less controversial regarding the potential toxicity of associated contaminants. The purification of soluble protein species (the building blocks for ArtIBs) is an scalable procedure at industrial level that has not posed any obstacle to the approval and generic clinical of recombinant proteins as drugs [43–45]. Therefore, the ArtIB packaging of recombinant protein drugs of human origin, namely enzymes, hormones, growth factors and others, irrespective of the cell factory used for the production of the soluble building blocks, should not envisage any problem related with immunotoxicity or poor biocompatibility. Therefore, ArtIBs would be functionally equivalent to functional secretory granules and applied in clinics in this context.

In addition, the properties of natural IBs are strongly dependent on the physiological conditions, nature and genetic background of the bacterial cell factory where they have been produced [46]. Among other observed influences, the culture conditions strongly affect the protein release capability [47], while the genetic background is a potent influencer of size, geometry, wettability, stiffness and other physicochemical parameters affecting IB performance [48,49]. In this context, ArtIBs benefit from the controlled fabrication process from purified protein, but also from the possibility to expand the source of the pure recombinant protein used for the generation of the materials. With a few exceptions, IBs are essentially produced in gram-negative bacteria, and therefore, restricted to non-glycosylated proteins [17], the polypeptides used for ArtIB fabrication can be obtained from bioproduction in any suitable cell factory, including yeast [50], plant [51] and mammalian cells [52], apart from any less-conventional microorganism or eukaryotic cells [50,53–56]. This fact largely expands the categories of proteins that can be packaged in form of secretory materials, including a large fraction of human proteins that are non-active or poorly active when produced in *Escherichia coli* [53].

As materials, ArtIBs are generated by a very easy fabrication process involving the protein itself and the linking ion, in mild environment-friendly conditions, that results in peculiar protein microparticles in which the unique forming protein shows a dual role as a scaffold and functional agent. The non-toxic amyloid composition of ArtIBs [18], that appears to be similar to that of natural IBs [57] and comparable to that of endocrine secretory granules [7,9], confers mechanical stability and a protein network that engulfs or traps functional versions of the same protein. Protein release from ArtIBs can be then observed as a slow disintegration process during which building blocks of the material are progressively released from it, in a rate potentially regulatable by the divalent cation used in the fabrication. A similar protein release process supported by Zn^{2+} has been recently described for the natural secretion of the human growth hormone [58]. Being chemically pure,

the further development of ArtIBs as storage/delivery micron sized granules for growth factors and other functional proteins should not face the constricting regulatory issues imposed to the chemically heterogeneous bacterial IBs and it opens a wide spectrum of possibilities for the controlled delivery of therapeutic proteins in many in vivo clinical contexts.

Declaration of Competing Interest

None.

Acknowledgements

We are indebted to Agencia Estatal de Investigación (AEI) and to Fondo Europeo de Desarrollo Regional (FEDER) (grant PID2019-105416RB-I00 to EV and grant BIO2016-76063-R to AV, AEI/FEDER, UE) and AGAUR (2017SGR-229, to AV). We are also indebted to the Networking Research Center on Bioengineering, Biomaterials and Nanomedicine (CIBER-BBN) that is an initiative funded by the VI National R&D&I Plan 2008–2011, Iniciativa Ingenio 2010, Consolider Program, CIBER Actions and financed by the Instituto de Salud Carlos III, with assistance from the European Regional Development Fund. Protein production has been partially performed by the ICTS "NANBIOSIS", more specifically by the Protein Production Platform of CIBER in Bioengineering, Biomaterials & Nanomedicine (CIBER-BBN)/IBB, at the UAB sePBioEs scientific-technical service (http://www.nanbiosis.es/portfolio/u1-protein-production-platform-ppp/) and the particle size analysis by the Biomaterial Processing and Nanostructuring Unit. Electron microscopy studies were performed by the Servei de Microscòpia at the UAB. Cell culture experiments were performed at the Cell Culture Service at the UAB (SCAC). AV received an ICREA ACADEMIA award. HLL and LSG supported by predoctoral fellowships from AGAUR (2019 FI_B_00352) and (2018FI_B2_00051), respectively.

References

[1] K.A. Gilmore, M.W. Lampley, C. Boyer, E. Harth, Matrices for combined delivery of proteins and synthetic molecules, Adv. Drug Deliv. Rev. 98 (2016) 77–85.
[2] J. Li, D.J. Mooney, Designing hydrogels for controlled drug delivery, Nat. Rev. Mater. 1 (2016).
[3] M.S. Hasnain, A.K. Nayak, M. Singh, M. Tabish, M.T. Ansari, T.J. Ara, Alginate-based bipolymeric-nanobioceramic composite matrices for sustained drug release, Int. J. Biol. Macromol. 83 (2016) 71–77.
[4] A. Bolhassani, Improvements in chemical carriers of proteins and peptides, Cell Biol. Int. 43 (2019) 437–452.
[5] L.M. Cross, J.K. Carrow, X. Ding, K.A. Singh, A.K. Gaharwar, Sustained and prolonged delivery of protein therapeutics from two-dimensional nanosilicates, ACS Appl. Mater. Interfaces 11 (2019) 6741–6750.
[6] S. Kapoor, S.C. Kundu, Silk protein-based hydrogels: promising advanced materials for biomedical applications, Acta Biomater. 31 (2016) 17–32.
[7] S.K. Maji, M.H. Perrin, M.R. Sawaya, S. Jessberger, K. Vadodaria, R.A. Rissman, et al., Functional amyloids as natural storage of peptide hormones in pituitary secretory granules, Science 325 (2009) 328–332.
[8] M.P. Badtke, N.D. Hammer, M.R. Chapman, Functional amyloids signal their arrival, Sci. Signal. 2 (2009) (pe43).
[9] S. Mankar, A. Anoop, S. Sen, S.K. Maji, Nanomaterials: amyloids reflect their brighter side, Nano Rev. 2 (2011).
[10] A. de Marco, N. Ferrer-Miralles, E. Garcia-Fruitos, A. Mitraki, S. Peternel, U. Rinas, et al., Bacterial inclusion bodies are industrially exploitable amyloids, FEMS Microbiol. Rev. 43 (2019) 53–72.
[11] P. Singhvi, A. Saneja, S. Srichandan, A.K. Panda, Bacterial Inclusion Bodies: A Treasure Trove of Bioactive Proteins. Trends in biotechnology, (2020).
[12] A. Stamm, S. Strauss, P. Vogt, T. Scheper, I. Pepelanova, Positive in vitro wound healing effects of functional inclusion bodies of a lipoxygenase from the Mexican axoloti, Microb. Cell Factories 17 (2018) 57.
[13] E. Vazquez, J.L. Corchero, J.F. Burgueno, J. Seras-Franzoso, A. Kosoy, R. Bosser, et al., Functional inclusion bodies produced in bacteria as naturally occurring nanopills for advanced cell therapies, Adv. Mater. 24 (2012) 1742–1747.
[14] M. Liovic, M. Ozir, A.B. Zavec, S. Peternel, R. Komel, T. Zupancic, Inclusion bodies as potential vehicles for recombinant protein delivery into epithelial cells, Microb. Cell Factories 11 (2012) 67.
[15] M. Pesarrodona, T. Jauset, Z.V. Díaz-Riascos, A. Sánchez-Chardi, M.E. Beaulieu, J. Seras-Franzoso, et al., Targeting antitumoral proteins to breast cancer by local administration of functional inclusion bodies, Adv. Sci. (2019), https://doi.org/10.1002/advs.201900849.
[16] M.V. Cespedes, O. Cano-Garrido, P. Alamo, R. Sala, A. Gallardo, N. Serna, et al., Engineering secretory amyloids for remote and highly selective destruction of metastatic foci, Adv. Mater. 32 (2020) 1907348.
[17] A. Villaverde, E. Garcia-Fruitos, U. Rinas, J. Seras-Franzoso, A. Kosoy, J.L. Corchero, et al., Packaging protein drugs as bacterial inclusion bodies for therapeutic applications, Microb. Cell Factories 11 (2012) 76.
[18] J. Sánchez, H. López-Laguna, P. Álamo, N. Serna, A. Sánchez-Chardi, V. Nolan, et al., Artificial inclusion bodies for clinical development, Adv. Sci. 7 (2020) 1902420.
[19] U. Rinas, F. Hoffmann, E. Betiku, D. Estape, S. Marten, Inclusion body anatomy and functioning of chaperone-mediated in vivo inclusion body disassembly during high-level recombinant protein production in Escherichia coli, J. Biotechnol. 127 (2007) 244–257.
[20] J. Seras-Franzoso, K. Peebo, E. Garcia-Fruitos, E. Vazquez, U. Rinas, A. Villaverde, Improving protein delivery of fibroblast growth factor-2 from bacterial inclusion bodies used as cell culture substrates, Acta Biomater. 10 (2014) 1354–1359.
[21] J.M. Sanchez, L. Sanchez-Garcia, M. Pesarrodona, N. Serna, A. Sanchez-Chardi, U. Unzueta, et al., Conformational conversion during controlled oligomerization into nonamylogenic protein nanoparticles, Biomacromolecules 19 (2018) 3788–3797.
[22] A.D. Ferrao-Gonzales, S.O. Souto, J.L. Silva, D. Foguel, The preaggregated state of an amyloidogenic protein: hydrostatic pressure converts native transthyretin into the amyloidogenic state, Proc. Natl. Acad. Sci. U. S. A. 97 (2000) 6445–6450.
[23] M.V. Cespedes, Y. Fernandez, U. Unzueta, R. Mendoza, J. Seras-Franzoso, A. Sanchez-Chardi, et al., Bacterial mimetics of endocrine secretory granules as immobilized in vivo depots for functional protein drugs, Sci. Rep. 6 (2016) 35765.
[24] U. Rinas, J.E. Bailey, Protein compositional analysis of inclusion bodies produced in recombinant Escherichia coli, Appl. Microbiol. Biotechnol. 37 (1992) 609–614.
[25] M.M. Carrio, A. Villaverde, Localization of chaperones DnaK and GroEL in bacterial inclusion bodies, J. Bacteriol. 187 (2005) 3599–3601.
[26] S.P. Allen, J.O. Polazzi, J.K. Gierse, A.M. Easton, Two novel heat shock genes encoding proteins produced in response to heterologous protein expression in Escherichia coli, J. Bacteriol. 174 (1992) 6938–6947.
[27] J.G. Thomas, F. Baneyx, Roles of the Escherichia coli small heat shock proteins IbpA and IbpB in thermal stress management: comparison with ClpA, ClpB, and HtpG in vivo, J. Bacteriol. 180 (1998) 5165–5172.
[28] A. Mogk, E. Deuerling, S. Vorderwulbecke, E. Vierling, B. Bukau, Small heat shock proteins, ClpB and the DnaK system form a functional triade in reversing protein aggregation, Mol. Microbiol. 50 (2003) 585–595.
[29] M. Matuszewska, D. Kuczynska-Wisnik, E. Laskowska, K. Liberek, The small heat shock protein IbpA of Escherichia coli cooperates with IbpB in stabilization of thermally aggregated proteins in a disaggregation competent state, J. Biol. Chem. 280 (2005) 12292–12298.
[30] J.M. Sanchez, H. Lopez-Laguna, P. Alamo, N. Serna, A. Sanchez-Chardi, V. Nolan, et al., Artificial inclusion bodies for clinical development, Adv. Sci. 7 (2020) 1902420.
[31] B. Forthmann, C. Grothe, P. Claus, A nuclear odyssey: fibroblast growth factor-2 (FGF-2) as a regulator of nuclear homeostasis in the nervous system, Cell. Mol. Life Sci. 72 (2015) 1651–1662.
[32] J.Y. Han, T.S. Choi, H.I. Kim, Molecular role of Ca(2+) and hard divalent metal cations on accelerated fibrillation and interfibrillar aggregation of alpha-synuclein, Sci. Rep. 8 (2018) 1895.
[33] M.P. Stelling, J.M. Motta, M. Mashid, W.E. Johnson, M.S. Pavao, N.P. Farrell, Metal ions and the extracellular matrix in tumor migration, FEBS J. 286 (2019) 2950–2964.
[34] W. Maret, Zinc biochemistry: from a single zinc enzyme to a key element of life, Adv. Nutr. 4 (2013) 82–91.
[35] M.J. Leonhard, E.T. Chang, A.E. Loccisano, M.R. Garry, A systematic literature review of epidemiologic studies of developmental manganese exposure and neurodevelopmental outcomes, Toxicology 420 (2019) 46–65.
[36] K. Fijorek, M. Puskulluoglu, D. Tomaszewska, R. Tomaszewski, A. Glinka, S. Polak, Serum potassium, sodium and calcium levels in healthy individuals - literature review and data analysis, Folia Med. Cracov. 54 (2014) 53–70.
[37] S.M. Glasdam, S. Glasdam, G.H. Peters, The importance of magnesium in the human body: a systematic literature review, Adv. Clin. Chem. 73 (2016) 169–193.
[38] A. Guerra, J. Belinha, R.N. Jorge, Modelling skin wound healing angiogenesis: a review, J. Theor. Biol. 459 (2018) 1–17.
[39] J. Weibezahn, B. Bukau, A. Mogk, Unscrambling an egg: protein disaggregation by AAA+ proteins, Microb. Cell Factories 3 (2004) 1.
[40] J. Weibezahn, C. Schlieker, P. Tessarz, A. Mogk, B. Bukau, Novel insights into the mechanism of chaperone-assisted protein disaggregation, Biol. Chem. 386 (2005) 739–744.
[41] P.F. Neubauer, H. Lilie, A. Villaverde, Protein Inclusion Bodies in Recombinant Bacteria, Springer, 2006.
[42] B. Jurgen, A. Breitenstein, V. Urlacher, K. Buttner, H. Lin, M. Hecker, et al., Quality control of inclusion bodies in Escherichia coli, Microb. Cell Factories 9 (2010) 41.
[43] L. Sanchez-Garcia, L. Martin, R. Mangues, N. Ferrer-Miralles, E. Vazquez, A. Villaverde, Recombinant pharmaceuticals from microbial cells: a 2015 update, Microb. Cell Factories 15 (2016) 33.
[44] H.A. Lagasse, A. Alexaki, V.L. Simhadri, N.H. Katagiri, W. Jankowski, Z.E. Sauna, et al., Recent advances in (therapeutic protein) drug development, F1000Research 6 (2017) 113.
[45] G. Walsh, Pharmaceutical biotechnology products approved within the European Union, Eur. J. Pharm. Biopharm. 55 (2003) 3–10.

[46] E. Garcia-Fruitos, E. Vazquez, C. Diez-Gil, J.L. Corchero, J. Seras-Franzoso, I. Ratera, et al., Bacterial inclusion bodies: making gold from waste, Trends Biotechnol. 30 (2012) 65–70.
[47] S. Peternel, J. Grdadolnik, V. Gaberc-Porekar, R. Komel, Engineering inclusion bodies for non denaturing extraction of functional proteins, Microb. Cell Factories 7 (2008) 34.
[48] C. Diez-Gil, S. Krabbenborg, E. Garcia-Fruitos, E. Vazquez, E. Rodriguez-Carmona, I. Ratera, et al., The nanoscale properties of bacterial inclusion bodies and their effect on mammalian cell proliferation, Biomaterials 31 (2010) 5805–5812.
[49] E. Garcia-Fruitos, J. Seras-Franzoso, E. Vazquez, A. Villaverde, Tunable geometry of bacterial inclusion bodies as substrate materials for tissue engineering, Nanotechnology 21 (2010) 205101.
[50] D. Mattanovich, P. Branduardi, L. Dato, B. Gasser, M. Sauer, D. Porro, Recombinant protein production in yeasts, Methods Mol. Biol. 824 (2012) 329–358.
[51] S.M. Rozov, E.V. Deineko, Strategies for optimizing recombinant protein synthesis in plant cells: classical approaches and new directions, Mol. Biol. 53 (2019) 179–199.
[52] L.M. Barnes, A.J. Dickson, Mammalian cell factories for efficient and stable protein expression, Curr. Opin. Biotechnol. 17 (2006) 381–386.
[53] J.L. Corchero, B. Gasser, D. Resina, W. Smith, E. Parrilli, F. Vazquez, et al., Unconventional microbial systems for the cost-efficient production of high-quality protein therapeutics, Biotechnol. Adv. 31 (2013) 140–153.
[54] S. Rebello, A. Abraham, A. Madhavan, R. Sindhu, P. Binod, A. Karthika Bahuleyan, et al., Non-conventional yeast cell factories for sustainable bioprocesses, FEMS Microbiol. Lett. 365 (2018).
[55] A.A. Song, L.L.A. In, S.H.E. Lim, R.A. Rahim, A review on Lactococcus lactis: from food to factory, Microb. Cell Factories 16 (2017) 55.
[56] A.M. Vieira Gomes, T. Souza Carmo, L. Silva Carvalho, F. Mendonca Bahia, N.S. Parachin, Comparison of yeasts as hosts for recombinant protein production, Microorganisms 6 (2018).
[57] O. Cano-Garrido, E. Rodriguez-Carmona, C. Diez-Gil, E. Vazquez, E. Elizondo, R. Cubarsi, et al., Supramolecular organization of protein-releasing functional amyloids solved in bacterial inclusion bodies, Acta Biomater. 9 (2013) 6134–6142.
[58] R.S. Jacob, S. Das, S. Ghosh, A. Anoop, N.N. Jha, T. Khan, et al., Amyloid formation of growth hormone in presence of zinc: relevance to its storage in secretory granules, Sci. Rep. 6 (2016) 23370.
[59] E. Vazquez, M. Roldan, C. Diez-Gil, U. Unzueta, J. Domingo-Espin, J. Cedano, et al., Protein nanodisk assembling and intracellular trafficking powered by an arginine-rich (R9) peptide, Nanomedicine 5 (2010) 259–268.

Annex 2

BFGF-2-releasing secretory granules as functional topographies in cell growth and osteogenic differentiation

Manuscript in progress

Objective 3.d

To test the biomedical applications of **protein-based insoluble microparticles** in tissue engineering (osteogenesis).

Keeping on track with the previous study (Annex 1), we wondered how SG-mimicking microparticles could be used to, not only promote fibroblast proliferation, but also osteogenic differentiation.

Thus, this work has been focused on developing zinc-based microparticles to stimulate osteogenesis from mesenchymal stem cells (MSCs) using fibronectin-PEA$_{\text{(Polyethylene adipate)}}$ functionalized surfaces. The obtained data suggests how protein-based microparticles, added on top of fibronectin-PEA surfaces, are able to simultaneously increase MSCs proliferation (greater than its soluble counterpart) while maintaining its capacity to differentiate into osteogenic cells, and still conserve the rest of their properties.

This work has been executed in collaboration with the University of Glasgow under the supervision of Professor Matthew Dalby.

BFGF-2-releasing secretory granules as functional topographies in cell growth and osteogenic differentiation

Hèctor López-Laguna[¥], Monica P Tsimbouri[¥], Vineetha Jayawarna, Ioanna Rigou, Naroa Serna, Eric Voltà-Durán, Ugutz Unzueta, Esther Vázquez, Antonio Villaverde* and Matthew J Dalby*

[¥] Equally contributed

Introduction

Because of their mechanical stability, proteins take, among many other roles, scaffolding functions that support the structure and assist the positioning of cells, tissues and whole organisms [1]. An important category of artificial protein materials, including particles, layers, fibers and complex matrices seek to mimic the complex functionality of the natural extracellular matrix (ECM) and other natural settings [2-8]. Therefore, such materials offer enormous potential for functional and structural versatility linked to protein engineering, that allow the incorporation of novel activities of interest (for instance, catalysis or precise cross-molecular binding) based upon precise design approaches [9,10]. The ability to tune and adapt these properties through protein engineering allow us to envisage clinical applications if the fabrication process can be made regulatory compliant.

Among the spectrum of clinically appealing protein materials found in nature the secretory granules from the endocrine system release peptide hormones offering control of the cellular milieu [11]. As with many other agents in the body, they are functional amyloids [12-15] that act as both protein reservoirs and protein-releasing structures. In these depots, peptide chains cluster together through the coordination of cationic Zn and solvent-exposed histidine residues or histidine-rich segments [16,17]. Taking the inspiration from the protein-clustering properties of divalent cations [18] and the versatility in the engineering of histidine-rich segments in recombinant proteins [19] we have developed an approach to fabricate, in vitro, from pure protein and by using a simple coordination protocol, micro-scale protein depots with time sustained, protein-releasing properties [20,21]. These materials are similar in micro-scale size and structural composition to bacterial inclusion bodies [22,23], protein aggregates naturally occurring in recombinant bacteria when actively producing foreign polypeptides. Although the protein-releasing activities of inclusion bodies make them appealing as time-sustained drug-delivery systems [24], their heterogeneous composition and recalcitrant contamination with bacterial cell components prevent them from entering clinical studies.

The protein secretion properties of artificial secretory granules have been already validated in oncology, through the subcutaneous administration of materials releasing cancer cell-targeted cytotoxic nanoparticles and the resulting selective destruction of tumor tissues [22]. However, apart from secretion, the amyloid content of these granules and the consequently conferred mechanical stability should also provide scaffolding properties. Then, we have explored here the performance of secretory granules releasing BFGF-2 as functional topographies and how they could be properly displayed for the growth and differentiation of human mesenchymal stem cells. In this context, we further draw on the natural design of

the ECM, where structural proteins, such as fibronectin (FN) have cryptic binding sites that open when the protein is under tension in fibrillar conformation (Klotzsch et al. 2009). For that, we have developed a simple polymer coating, poly(ethyl acrylate) (PEA) where, upon absorption, FN molecules elongate and form nanonetworks, revealing $FNIII_{12-14}$ that is known to bind growth factors including BFGF-2 and $FNIII_{9-10}$ that contains the RGD cell adhesion sequence (Martino et al. 2010, 2011, Llopis-Hernández et al. 2016, Cheng et al. 2019). The growth factor binding to open FN and solid phase presentation in synergy to integrin binding sites is considered to potentiate the growth factor potency (Llopis-Hernández et al. 2016, Cheng et al. 2019). Thus, aiming at expanding the functionalities and clinical potential of secretory granules as an emerging category of protein materials, we have utilized a cell microenvironment comprising PEA organized FN with synthetic BFGF-2 releasing granules to further enhance cell response to the growth factor release.

Results

The hexahistidine H6 was added to the C-terminus of BFGF-2 to confer cation-mediated clustering properties to the protein with a minimal impact on the BFGF-2 structure and function. This was done to allow the in vitro fabrication, based on purified protein, of self-disintegrating pure protein granules. The resulting fusion was modeled as a regularly folded polypeptide with molecular dimensions predicted around up to 7 nm (Figure 1A). The fusion protein was well produced in *E. coli* and purified through IMAC, resulting in proteins fractions in which a monomeric form was especially abundant (Figure 2B). The molecular mass of the protein was as theoretically predicted (18 kDa), its purity reached 99.3 %, and the protein preparations were stable and free from contaminating DNA (Figure 2C). The MALDI-TOF analysis revealed the minor occurrence of a trimeric form (Figure 2D), not observed by Western Blot upon denaturing SDS-PAGE (Figure 2B). Such tendency to oligomerization might be favored by the polar distribution of electrostatic charges on the protein surface (Figure 2E) and it was seen as positive regarding controlled protein clustering using cation-histidine coordination. In this regard, cationic Zn added to the protein solution (peaking at the monomer size of 7 nm) at equimolar amounts with histidine residues from H6, generated nanoparticles with a hydrodynamic size of 13.5 nm (Figure 1F), similar in range to other oligomeric constructs obtained by the same procedure (BOTTOM-up instructive). Nanoparticles are considered to be intermediates in the cation-mediated clustering process of His-tagged proteins that ends up in the formation of secretory granules (Biofabrication of functional protein nanoparticles through simple His-tag engineering). These nanoscale materials were further disassembled by EDTA to the original size (Figure 1F), proving the reversibility of the assembly process and the critical intervention of Zn in it. Nanoparticles showed a more negative Z potential than plain soluble protein (Figure 1G), when indicates enhanced solubility in contrast to the more aggregation-prone plain polypeptides. The nanoparticles were also more thermally resistant than the unassembled version, which aggregated between 40 and 50 ºC (Figure 1H). All these data confirmed that in global, the oligomers were structurally more stable than their uncoordinated building blocks.

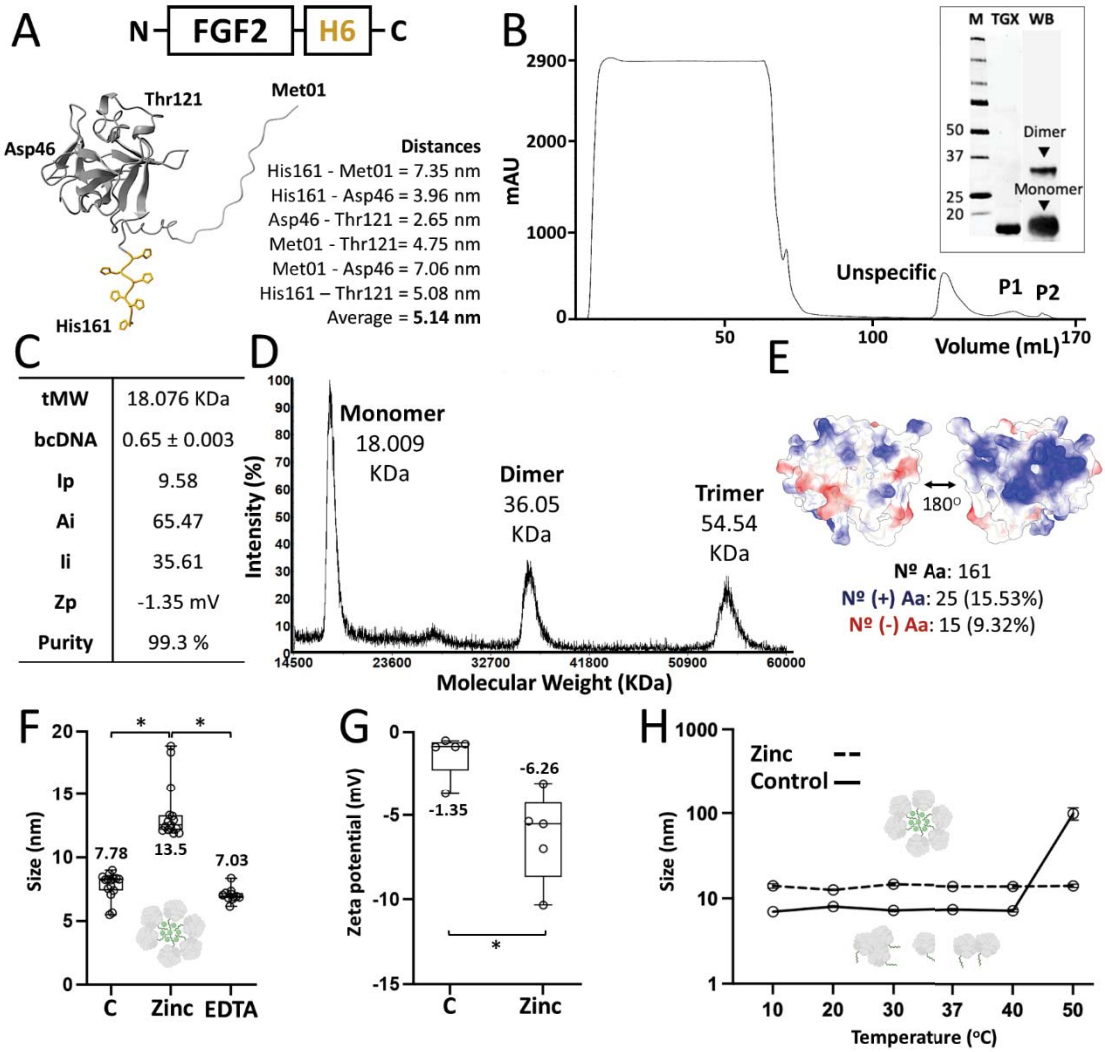

Figure 1. Physicochemical characterization of purified FGF2-H6. **A**. Modular representation of recombinant FGF2-H6 protein from N- to C-terminus. Bottom. 3D structure prediction by Alpha fold. The hexahistidine tag H6 is displayed in yellow. Distances in nm between edging amino acid residues are also displayed (namely histidine 161, threonine 121, methionine 1 and aspartic acid 46). An average monomeric size was afterwards calculated. **B**. Protein purification chromatogram expressed as mAU (milli absorbance units) vs volume in mL. The protein was eluted in two (P1 and P2) populations. Protein integrity and purity levels displayed in the inset by SDS-PAGE (TGX) and western blot (WB). **C.** Protein physicochemical properties showing theoretical molecular weight (tMW), measured bicatenary DNA content (bcDNA), isoelectric point (Ip), aliphatic index (Ai), instability index (Ii), measured zeta potential (Zp) and calculated purity levels. **D**. MALDI-TOF spectra represented by the intensity (in %) vs the molecular weight (in KDa). Monomeric, dimeric and trimeric structures were detected. Numbers on top of peaks refer to respective molecular weights. **E**. Surface charge distribution was predicted using the 3D structure from panel A displaying both protein sides. Positive amino acid residues are displayed in blue, negatively charged in red. The corresponding percentages are also displayed. **F**. Volume size distribution in nm of soluble FGF2-H6 in presence of 0.4 mM zinc II (Zn^{2+}) and after the subsequent addition of 1 mM of EDTA. **G**. Zeta potential in mV of soluble FGF2-H6 in presence or absence of 0.4 mM Zn^{2+}. **H**. Volume size distribution in nm of soluble FGF2-H6 upon increasing temperature (from 10 to 50 ºC) in presence or absence of 0.4 mM of Zn^{2+}. C refers to the control protein free of additives for panels F, G and H. Data expressed as mean ± standard error of the mean (SEM). Statistical significance ($p < 0.05$) is represented as (*).

As stated above, nanoparticles assembled through Zn-His coordination are expected to be intermediates in a clustering process that conduces to higher order micrometric particles (Figure 2A). The ability of these materials to release the intermediate nanoparticles is what make them appealing as secretory protein depots, and these concepts were to be tested here for the H6-tagged FGF2 version. At molar excess amounts of ionic Zn, FGF2-H6 clustered as discrete materials around 1 μm, that pelleted as insoluble material at low speed centrifugation (Figure 2B). Resuspended in physiological buffer, a progressive leakage of full-length protein to the soluble fraction was determined from the microparticles during at least 7 days (Figure 2C), these granules being indeed observed as disintegrating structures (Figure 2D). An accurate TEM analysis of the soluble fraction confirmed the occurrence of nanoparticles (Figure 2E), with sizes (between 11 and 20 nm) in range of but slightly higher than those found in the oligomeric material intermediate in the construction of granules (Figure 1F). These FGF2-based secretory granules were then moved a step forward for the functionalization of PEA-fibronectin surfaces (Figure 2F), to be further tested as a novel category of functional, FGF2-releasing topographies.

Human mesenchymal stem cells (MSCs), when cultured over such functional surfaces, showed an excellent adhesion and a deep interaction with the attached microparticles (Figure 3A). In this hybrid platform, cell proliferation was faster (determined at 7 days) when the growth factor was used in the particulate format than in a plain soluble format (Figure 3B). This difference was observed within a wide range of tested protein concentrations, among which the values between 20 and 50 ng/ml comprised the highest cell density values and a higher biological effect of FGF2 SGs (Figure 3C). The stimulation of cell proliferation was evidenced at least up to 14 days, while at 21 days the culture started to decline (Figure 3 D). GFP-based materials represented, as expected for soft micro-scale topographies with adhesion properties (Surface cell growth engineering assisted by a novel bacterial nanomaterial), a slighter cell growth support that is apparently complemented through the function of FGF2, that renders higher cell densities (Figure 3D).

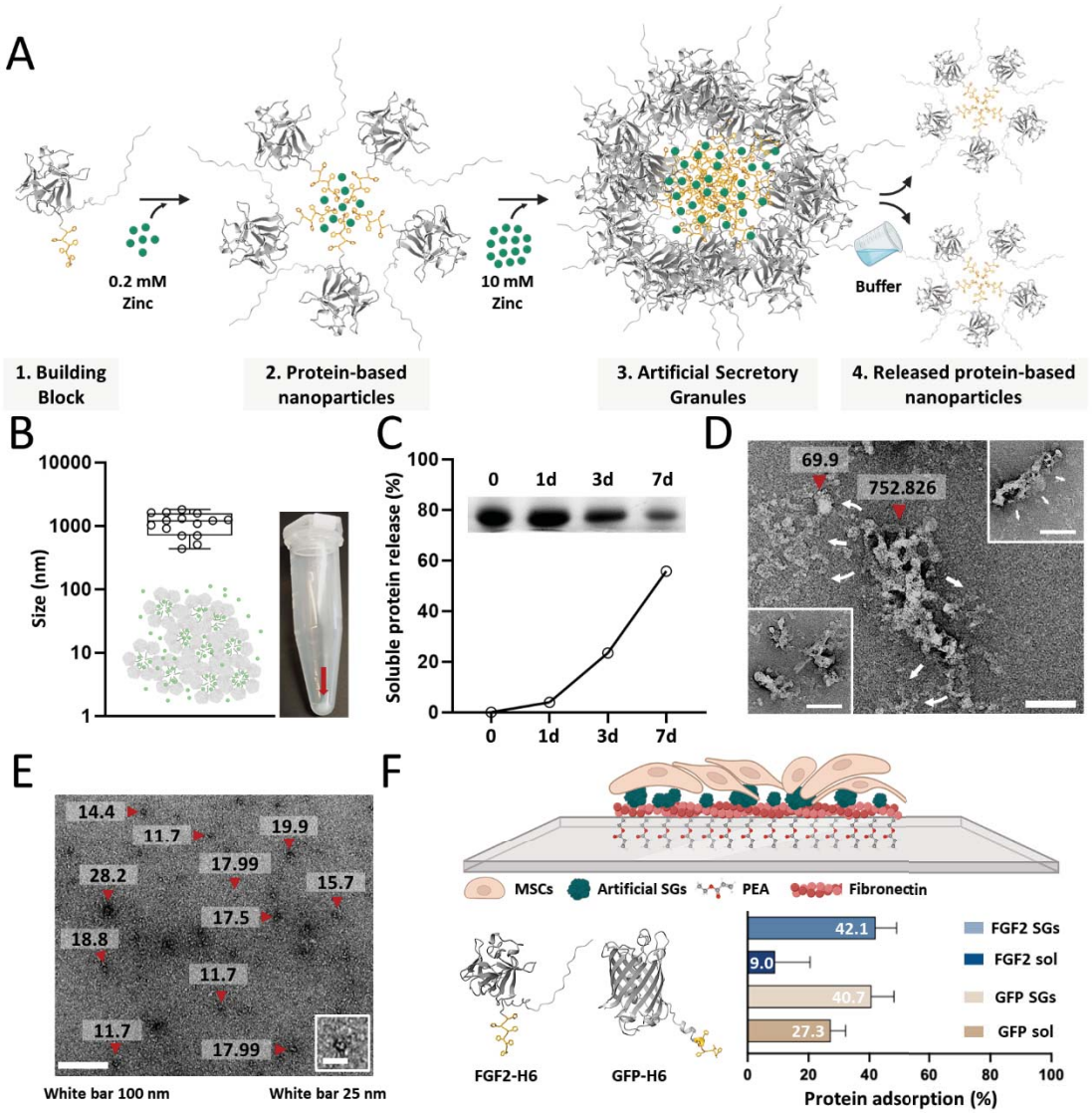

Figure 2. Formulation and physicochemical characterization of FGF2-H6 secretory granules (SGs). **A**. Schematic representation of the SGs manufacturing process from building blocks (step 1) to SGs (step 3). This is done for the further release of soluble nanoparticles (step 4). The histidine tag is displayed in yellow and zinc in green. **B**. Volume size distribution of FGF2-H6 SGs as determined in different DLS lectures. Right. Picture displaying the resultant SGs pellet. **C**. Soluble protein release in percentage from FGF2-H6 SGs upon 37ºC incubation for several days (from 1 to 7 days). Inset. SDS-PAGE showing the disintegration of SGs during this process. **D**. Imaging of FGF2-H6 SGs in buffer by transmission electron microscopy (TEM). White bar refers to 100 nm. Representative sizes in nm displayed on top of each structure. Insets. Additional pictures of the same sample of artificial FGF2-H6 SGs. White bars in the insets refer to 200 nm. White arrows refer to the suspected disintegrating direction of the material. **E**. Imaging of released FGF2-H6 nanoparticles from SGs by transmission electron microscopy (TEM). White bar refers to 100 nm. Nanoparticle size in nm is displayed on top. Inset. A closer view of the nanoparticle architecture. White bar in the inset refers to 25 nm. **F**. Schematic representation of the functionalization of PEA-fibronectin surfaces with artificial SGs. Mesenchymal stem cells (MSCs) are to be added on top. Down left. 3D structure prediction by Alpha fold of FGF2-H6 and GFP-H6 proteins. GFP-H6 was used as control protein. Histidine tag is displayed in yellow. Down right. Protein adsorption in percentage of both H6-taggd FGF2 (blue) and GFP (brown) SGs (pale colors) and soluble protein (sol; dark colors) on top of PEA-fibronectin surfaces. White numbers represent the protein adsorption in percentage for each condition. Data are expressed as mean ± standard error of the mean (SEM).

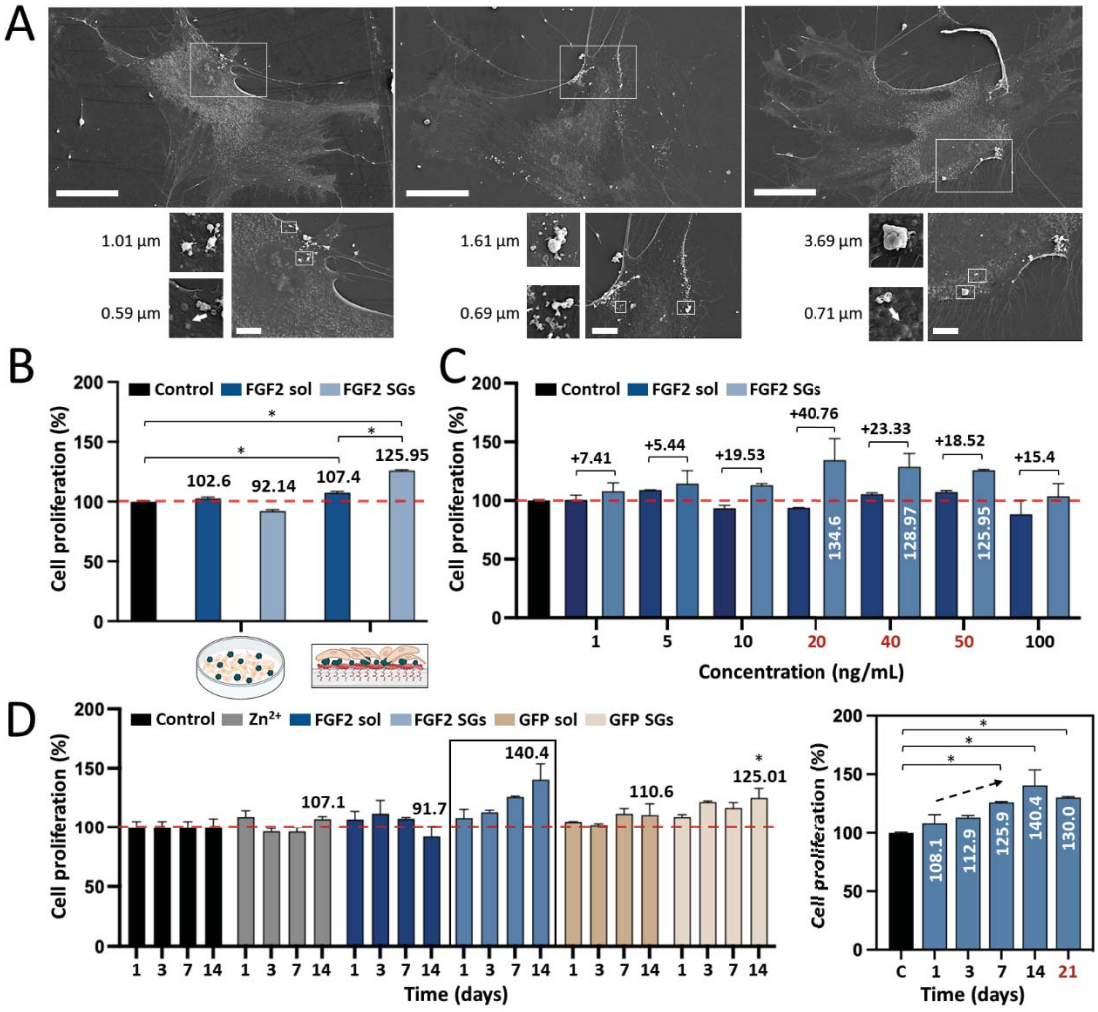

Figure 3. Mesenchymal stem cell (MSC) proliferation and interaction with FGF2-H6 SGs PEA-fibronectin surfaces. **A**. Imaging of MSCs by scanning electron microscopy (SEM) in presence of FGF2-H6 SGs (white dots). White bars refer to 50 µm. White squares display observed regions in the insets (down). White bars in the insets refer to 10 µm. Down left. Closer pictures of FGF2-H6 SGs with size numbers. White arrows indicate the measured SGs. **B**. MSCs proliferation analysis (in percentage) upon exposure to FGF2-H6 soluble (dark blue) and artificial SGs (pale blue) samples at 50 ng/mL for 7 days. Left legend corresponds to the seeding gold standard technique, and the right legend to the PEA-fibronectin surfaces. Pointed red line displays the 100 % proliferation threshold. Peak numbers correspond to each cell proliferation percentage. **C**. MSCs proliferation analysis (in percentage) upon exposure to FGF2-H6 soluble (dark blue) and artificial SGs (pale blue) samples at increasing concentrations (from 1 to 100 ng/mL) for 7 days. Pointed red line displays the 100% proliferation threshold. Peak numbers correspond to the increased percentage of cell growth comparing artificial FGF2-H6 SGs with soluble FGF2-H6. The highest cell growth concentrations for artificial FGF2-H6 SGs (namely 20, 40 and 50 ng/mL) are displayed in red and specific growth percentages indicated as white numbers. **D**. MSCs proliferation analysis (in percentage) upon exposure to FGF2-H6 soluble (dark blue), artificial FGF2-H6 SGs (pale blue), free Zn^{2+} (grey), GFP-H6 soluble (dark brown) and artificial GFP-H6 SGs (pale brown) samples at 50 ng/mL for 1, 3, 7 and 14 days. Pointed red line displays the 100% proliferation threshold. Peak numbers correspond to the cell proliferation percentage at day 14. Right. The same squared cell proliferation graph with an additional time point (day 21) highlighted in red. Control of MSCs is displayed in black in all cases. Data expressed as mean ± standard error of the mean (SEM), and statistical significance achieved when $p < 0.05$ represented as (*) in respect to the control.

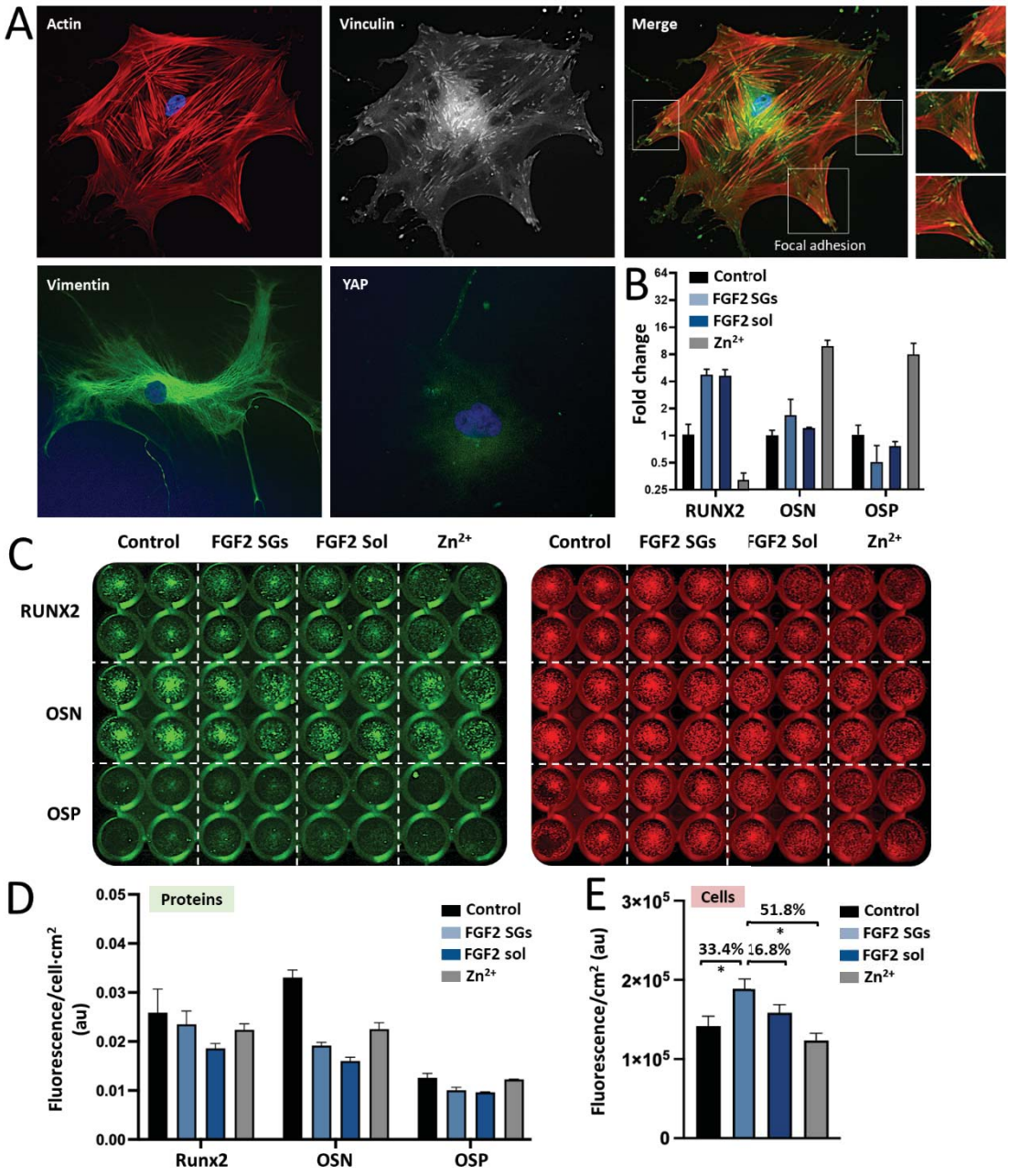

Figure 4. Mesenchymal stem cell (MSCs) differentiation in cultures over artificial FGF2-H6 SGs PEA-fibronectin surfaces. **A**. Imaging of MSCs by fluorescence microscopy (FLM) in presence of artificial FGF2-H6 SGs at 50 ng/mL, for 14 days. Actin, vinculin, vimentin and YAP were selected as cell markers. Merge refers to actin and vinculin combined fluorescence signals. White squares highlight cell focal adhesions. Closer pictures of focal adhesions are displayed on the right panels. **B**. Fold change on mRNA content (meaning RUNX2, OSN; osteonectin, and OSP; osteopontin gene expression) in MSCs upon incubation with soluble FGF2-H6 (dark blue), artificial FGF2-H6 SGs (pale blue) and free Zn^{2+} (grey) at 50 ng/mL and 14 days. **C**. Western blot immunodetection of RUNX2, OSN and OSP proteins in MSCs extracts upon incubation over soluble FGF2-H6, artificial FGF2-H6 SGs and free Zn^{2+} (grey) at 50 ng/mL and 14 days. Protein signal is displayed in green and

cell signal in red. **D**. Statistical analysis of protein signal (green from panel C) expressed as fluorescence per cell and cm^2 in absorbance units (au). **E**. Statistical analysis of protein signal (red from panel C) expressed as fluorescence per cm^2 in absorbance units (au). Peak numbers correspond to the increased percentage of cell growth comparing artificial FGF2-H6 SGs (pale blue) with soluble FGF2-H6 (dark blue), free Zn^{2+} (grey) and MSCs control (black). Data expressed as mean ± standard error of the mean (SEM), and statistical significance achieved when $p < 0.05$ represented as (*).

References

1. Cano-Garrido, O.; Serna, N.; Unzueta, U.; Parlade, E.; Mangues, R.; Villaverde, A.; Vazquez, E. Protein scaffolds in human clinics. *Biotechnology advances* **2022**, *61*, 108032, doi:10.1016/j.biotechadv.2022.108032.
2. Delfi, M.; Sartorius, R.; Ashrafizadeh, M.; Sharifi, E.; Zhang, Y.; De Berardinis, P.; Zarrabi, A.; Varma, R.S.; Tay, F.R.; Smith, B.R.; et al. Self-assembled peptide and protein nanostructures for anti-cancer therapy: Targeted delivery, stimuli-responsive devices and immunotherapy. *Nano today* **2021**, *38*, 101119, doi:https://doi.org/10.1016/j.nantod.2021.101119.
3. Gopalakrishnan, S.; Xu, J.; Zhong, F.; Rotello, V.M. Strategies for Fabricating Protein Films for Biomaterial Applications. *Advanced Sustainable Systems* **2021**, *5*, 2000167, doi:https://doi.org/10.1002/adsu.202000167.
4. Shim, J.; Zhou, C.; Gong, T.; Iserlis, D.A.; Linjawi, H.A.; Wong, M.; Pan, T.; Tan, C. Building protein networks in synthetic systems from the bottom-up. *Biotechnology advances* **2021**, *49*, 107753, doi:https://doi.org/10.1016/j.biotechadv.2021.107753.
5. Li, J.; Li, S.; Huang, J.; Khan, A.Q.; An, B.; Zhou, X.; Liu, Z.; Zhu, M. Spider Silk-Inspired Artificial Fibers. *Advanced science* **2021**, e2103965, doi:10.1002/advs.202103965.
6. Korpi, A.; Anaya-Plaza, E.; Valimaki, S.; Kostiainen, M. Highly ordered protein cage assemblies: A toolkit for new materials. *Wiley interdisciplinary reviews. Nanomedicine and nanobiotechnology* **2020**, *12*, e1578, doi:10.1002/wnan.1578.
7. Ulijn, R.V.; Lampel, A. Order/Disorder in Protein and Peptide-Based Biomaterials. *Israel Journal of Chemistry* **2020**, *n/a*, doi:10.1002/ijch.201900051.
8. Xu, X.; Chen, X.; Li, J. Natural protein bioinspired materials for regeneration of hard tissues. *Journal of materials chemistry. B* **2020**, *8*, 2199-2215, doi:10.1039/d0tb00139b.
9. DiMarco, R.L.; Heilshorn, S.C. Multifunctional materials through modular protein engineering. *Advanced materials* **2012**, *24*, 3923-3940.
10. Wang, Y.; Katyal, P.; Montclare, J.K. Protein-Engineered Functional Materials. *Advanced healthcare materials* **2019**, *8*, e1801374, doi:10.1002/adhm.201801374.
11. Maji, S.K.; Perrin, M.H.; Sawaya, M.R.; Jessberger, S.; Vadodaria, K.; Rissman, R.A.; Singru, P.S.; Nilsson, K.P.; Simon, R.; Schubert, D.; et al. Functional amyloids as natural storage of peptide hormones in pituitary secretory granules. *Science* **2009**, *325*, 328-332, doi:10.1126/science.1173155.
12. Mankar, S.; Anoop, A.; Sen, S.; Maji, S.K. Nanomaterials: amyloids reflect their brighter side. *Nano reviews* **2011**, *2*, 6032, doi:10.3402/nano.v2i0.6032.

13. Otzen, D.; Riek, R. Functional Amyloids. *Cold Spring Harbor perspectives in biology* **2019**, *11*, pii: a033860, doi:10.1101/cshperspect.a033860.

14. Jackson, M.P.; Hewitt, E.W. Why are Functional Amyloids Non-Toxic in Humans? *Biomolecules* **2017**, *7*, doi:10.3390/biom7040071.

15. Badtke, M.P.; Hammer, N.D.; Chapman, M.R. Functional amyloids signal their arrival. *Science signaling* **2009**, *2*, pe43, doi:10.1126/scisignal.280pe43.

16. Jacob, R.; Anoop, A.; Maji, S. *Protein Nanofibrils as Storage Forms of Peptide Drugs and Hormones*; Springer, Singapore: Singapore, 2019; Volume 1174: 265-290

17. Jacob, R.S.; Das, S.; Ghosh, S.; Anoop, A.; Jha, N.N.; Khan, T.; Singru, P.; Kumar, A.; Maji, S.K. Amyloid formation of growth hormone in presence of zinc: Relevance to its storage in secretory granules. *Scientific reports* **2016**, *6*, 23370, doi:10.1038/srep23370.

18. López-Laguna, H.; Sánchez, J.; Unzueta, U.; Mangues, R.; Vázquez, E.; Villaverde, A. Divalent Cations: A Molecular Glue for Protein Materials. *Trends in biochemical sciences* **2020**, *45*, 992-1003, doi:https://doi.org/10.1016/j.tibs.2020.08.003.

19. Lopez-Laguna, H.; Volta-Duran, E.; Parlade, E.; Villaverde, A.; Vazquez, E.; Unzueta, U. Insights on the emerging biotechnology of histidine-rich peptides. *Biotechnology advances* **2022**, *54*, 107817, doi:10.1016/j.biotechadv.2021.107817.

20. Alamo, P.; Parlade, E.; Lopez-Laguna, H.; Volta-Duran, E.; Unzueta, U.; Vazquez, E.; Mangues, R.; Villaverde, A. Ion-dependent slow protein release from in vivo disintegrating micro-granules. *Drug delivery* **2021**, *28*, 2383-2391, doi:10.1080/10717544.2021.1998249.

21. López-Laguna, H.; Parladé, E.; Álamo, P.; Sánchez, J.M.; Voltà-Durán, E.; Serna, N.; Sánchez-García, L.; Cano-Garrido, O.; Sánchez-Chardi, A.; Villaverde, A.; et al. In Vitro Fabrication of Microscale Secretory Granules. *Advanced Functional Materials* **2021**, *31*, 2100914, doi:https://doi.org/10.1002/adfm.202100914.

22. Sánchez, J.; López-Laguna, H.; Álamo, P.; Serna, N.; Sánchez-Chardi, A.; Nolan, V.; Cano-Garrido, O.; Casanova, I.; Unzueta, U.; Vazquez, E.; et al. Artificial inclusion bodies for clinical development *Advanced science* **2020**, *7*, 1902420, doi:DOI: 10.1002/advs.201902420.

23. Sánchez, J.M.; Carratalá, J.V.; Serna, N.; Unzueta, U.; Nolan, V.; Sánchez-Chardi, A.; Voltà-Durán, E.; López-Laguna, H.; Ferrer-Miralles, N.; Villaverde, A.; et al. The Poly-Histidine Tag H6 Mediates Structural and Functional Properties of Disintegrating, Protein-Releasing Inclusion Bodies. *Pharmaceutics* **2022**, *14*, 602.

24. Cespedes, M.V.; Cano-Garrido, O.; Alamo, P.; Sala, R.; Gallardo, A.; Serna, N.; Falgas, A.; Volta-Duran, E.; Casanova, I.; Sanchez-Chardi, A.; et al. Engineering Secretory Amyloids for Remote and Highly Selective Destruction of Metastatic Foci. *Advanced materials* **2020**, *32*, e1907348, doi:10.1002/adma.201907348.

Annex 3

Engineering the Performance of Artificial Inclusion Bodies Built of Catalytic β-Galactosidase

Julieta M. Sánchez, Hèctor López-Laguna, Naroa Serna, Ugutz Unzueta, Pedro D. Clop, Antonio Villaverde, and Esther Vázquez

ACS Sustainable Chemistry and Engineering (2021) · Impact Factor (9.224) · Quartile (Q1)

Objective 3.e

To test the biomedical applications of **protein-based insoluble microparticles** in biocatalysis.

Changing the scope of action, we wondered how artificial protein-based microparticles will behave as biocatalytic entities, ensuring enzyme stability and reusability in industrial processes.

Thus, this work has been focused on developing an immobilized enzymatic platform, using different combinations of crosslinking divalent cations, to enhance protein stability, reusability, and catalytic capacity. The obtained data suggested how reusable β-galactosidase-base microparticles increased in performance and thermal stability compared to its soluble counterpart, and when the adequate divalent cation mixture was found.

ACS Sustainable Chemistry & Engineering

pubs.acs.org/journal/ascecg

Research Article

Engineering the Performance of Artificial Inclusion Bodies Built of Catalytic β-Galactosidase

Julieta M. Sanchez,* Hèctor López-Laguna, Naroa Serna, Ugutz Unzueta, Pedro D. Clop, Antonio Villaverde,* and Esther Vazquez*

Cite This: ACS Sustainable Chem. Eng. 2021, 9, 2552−2558

Read Online

ACCESS | Metrics & More | Article Recommendations

ABSTRACT: One of the most critical bottlenecks in the application of industrial enzymes is the preservation of protein stability throughout the catalytic reaction, which often requires protein engineering and/or process optimization. In this context, we have designed and deeply characterized an efficient, stable, and reusable enzymatic platform based on the *Escherichia coli* β-galactosidase. The enzyme was assembled *in vitro*, by using divalent cations as molecular linkers, as stable protein microparticles showing catalytic activity. In this assembled microstructure, β-galactosidase exhibits a particular conformation within the microparticles, sharing structural traits (a high cross-parallel beta-sheet content) with the bacterial inclusion bodies and secretory amyloids from the mammalian endocrine system. This fact confers enhanced thermal stability compared to the soluble protein version and ensures high reusability in industry-oriented processes. On the other hand, among the catalog of cations tested as molecular linkers, a mixture of Ca^{2+} and Mg^{2+} offers the best performance to the catalytic particle. Altogether, these data offer clues for the application of a self-immobilized enzymatic platform with transversal applicability and enormous potential in biotechnology and biomedicine.

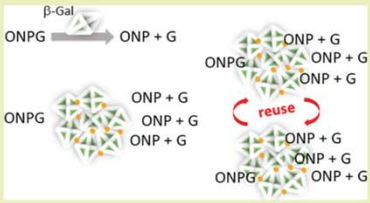

KEYWORDS: *artificial inclusion bodies, catalytic microparticles, reusability, thermostability*

INTRODUCTION

In order to exploit the full potential of industrial enzymes, either protein re-engineering or process optimization is needed to ensure a high enzymatic performance for given applications.[1] One of the most critical tasks for the use of enzymes in industry is the preservation of the protein stability while submitted to catalytic processes. Fortunately, enzyme features can be redesigned by computing approaches and the modified versions produced by recombinant technologies at the laboratory scale or at large scale.[2−4] On the other hand, a powerful strategy to enhance stability is enzyme immobilization. The attachment of a biocatalyst to a material with desired physical, chemical, electrical, or mechanical properties usually improves its activity and stability under different operating conditions.[5−7] Also, the immobilization of enzymes facilitates their separation from the reaction mixture, thus allowing the enzymatic device to be reused in additional reaction cycles. This fact largely minimizes the cost associated with production and purification.[8]

Since the discovery of the biological activity associated to bacterial inclusion bodies (IBs),[9,10] these protein particles have been exploited as self-immobilized catalysts for chemical and biotechnology industries.[11−13] IBs are protein aggregates naturally occurring under recombinant gene expression, as a consequence of the conformational stress posed to the protein quality control machinery.[14−17] The transgene protein product being their main component, they are mechanically stable soft proteinaceous materials,[15] with dimensions in between nano- and microscales (usually ranging from 50 to 1500 nm in size). A fraction of the recombinant IB protein is organized as nontoxic amyloid fibers, whereas the remaining protein component is found as a proteinase-K-sensitive, functional, or quasi-functional form.[18] The functionalities of IBs result then from the co-aggregation of functional (conformationally competent) and nonfunctional polypeptides (mechanically rigid amyloidal fibrils) under defined culture and gene expression conditions inside the bacterial cell.[19] Because of such unusual combination of mechanical stability and functionality, IBs have also been applied as protein carriers for intracellular delivery of functional proteins, in the form of nanopills.[20,21] As an issue of concern, IBs are not chemically homogeneous as they do contain significant amounts of nonprotein macromolecules and proteins derived from the bacterial cell, entrapped in the cluster of recombinant proteins.[22,23]

Recently, an alternative IB-mimetic material has been developed, namely artificial inclusion bodies (ArtIBs), sized,

Received: November 15, 2020
Revised: January 14, 2021
Published: February 1, 2021

ACS Publications © 2021 American Chemical Society

https://dx.doi.org/10.1021/acssuschemeng.0c08345
ACS Sustainable Chem. Eng. 2021, 9, 2552−2558

ACS Sustainable Chemistry & Engineering pubs.acs.org/journal/ascecg Research Article

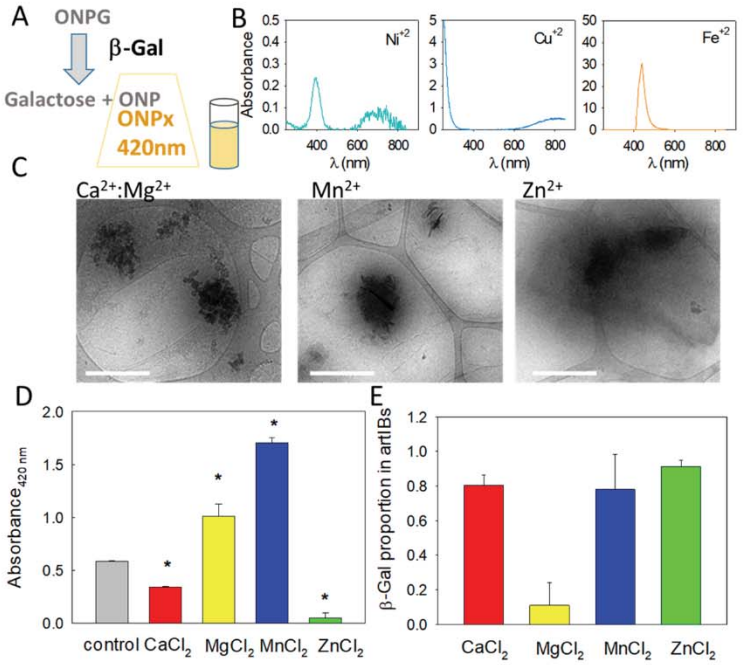

Figure 1. (A) ONPG hydrolysis catalyzed by β-Gal. ONPx is the reaction product measured by UV−vis spectrophotometry at 420 nm. (B) Absorbance spectrum of divalent cation salts (400 mM). (C) Representative cryo-TEM images of β-Gal ArtIBs. White bars correspond to 1 μm. (D) Divalent cation salt effect on β-Gal activity measured as the absorbance of ONPx at 420 nm. (*) Statistically significant ($p \leq 0.02$). (E) β-Gal proportion within ArtIBs with respect to the initial amount of protein at the beginning of the ArtIB preparation process.

as their natural counterparts, a few microns in diameter. The advantage of these particles lies in the fact that they are built up of pure proteins from any type of cell factory, bacterial or not. The methodology to fabricate ArtIBs has been described in detail elsewhere,[24,25] and it is based on the coordination of divalent cations to proteins containing histidine tags. In the preliminary development of ArtIBs, zinc ion (Zn^{2+}) was used as a choice of molecular glue-like agent because of its high efficiency to promote the supramolecular arrangement of proteins.[25] However, it is known that the nature of the divalent cation might modulate, in different manners, protein functionality.[26] As an example, the use of Zn^{2+} to produce alkaline phosphatase microparticles was more profitable for the enzyme activity, while being detrimental for the activity of β-galactosidase in the form of such microparticles.[24]

In this work, we tested the ability of divalent cations to improve the functionality and stability of catalytic β-galactosidase (β-Gal) ArtIBs, to set transversal clues in this novel approach to produce functional protein materials for catalytic applications.

MATERIALS AND METHODS

Spectroscopic Analysis of Divalent Cation Salts. Each divalent chloride-based cation salt resuspended in ultrapure water (400 mM) was placed in a quartz cuvette to measure the UV−visible-spectra recorded with a NanoDrop spectrophotometer (Thermo Fisher Scientific).

Divalent Cation Effect on the Enzymatic Activity. A 10 μL of soluble β-Gal (20 ng) was mixed with 30 μL of divalent cation salt solution (400 mM) for 10 min at 4 °C. Then, *ortho*-nitrophenyl-galactopyranoside (ONPG) of 5 mM was added, and the incubation volume of 550 μL was buffered during 15 min with phosphate-buffered saline (PBS) 1× pH 7.4 at 37 °C. These pH and temperature values are the optimal conditions of Mg-*Escherichia coli* β-Gal activity.[27,28] The enzymatic reaction was stopped by adding 200 μL of Na_2CO_3 (2.8 M). In this condition, *ortho*-nitrophenol (ONP), one of the reaction products (Figure 1A), predominates, in the *ortho*-nitrophenoxide (ONPx) form. The enzyme activity was determined, measuring the ONPx absorbance at 420 nm in a UV−visible spectrophotometer (Ultrospec 1000E, Pharmacia Biotech), as illustrated in Figure 1A. Before reading the absorbance, the sample was centrifuged for 15 min at 10,000*g* to avoid light scattering induced by the precipitates.

Manufacturing of Artificial Inclusion Bodies. Once the cationic effect was analyzed on β-Gal activity, 60 μL of soluble β-Gal (0.2 g/L or less in PBS) was mixed with 60 μL of pure or a mixture of divalent cations salts (400 mM). After 10 min of incubation at 4 °C, the sample was centrifuged at 10,000*g* for 15 min, and the protein in the soluble fraction, if present, was discarded to obtain the pellet containing ArtIBs.

Linker Ability of Divalent Cations. The total amount of protein within ArtIBs was calculated from the difference between the initial quantity of soluble β-Gal and the protein that remains in the soluble fraction after ArtIB formation. Both, the initial and final proteins in the soluble fraction were quantified by UV−vis spectrophotometry at 280 nm.

Morphometry of ArtIBs. For cryoTEM experiments, a perforated holey carbon film on a 400 mesh copper grid was applied. After glow discharge to make the holey film hydrophilic, a 4 μL (micro) drop of the ArtIB sample was deposited onto the film. The grid was mounted on a plunger (Leica EM GP) and blotted with Whatman no. 4 filter paper for 0.6 s. The aqueous suspension of lipoplex within the holes was immediately vitrified by rapid immersion in liquid ethane at −175 °C. The specimen grid under liquid nitrogen was mounted on a Gatan 626 cryotransfer system. Images were obtained with a JEOL JEM 2011 cryoelectron microscope operated at 200 kV under low-dose conditions and using different degrees of defocus (500−700 nm) to obtain an adequate phase contrast. Images were recorded on a Gatan 794 ultrascan digital camera, and files were saved in .dm3 format. The CCD images were processed and analyzed with Digital Micrograph version 1.8.0.

https://dx.doi.org/10.1021/acssuschemeng.0c08345
ACS Sustainable Chem. Eng. 2021, 9, 2552−2558

Enzymatic Activity of Reusable ArtIBs. The enzymatic activity was measured as previously described, and the catalytic reaction stopped by decreasing the temperature to 4 °C, followed by centrifugation at 10,000*g* during 15 min. The supernatant was removed, and the pellet was washed with PBS buffer and maintained at 4 °C until the next enzymatic determination. ONP present in the supernatant was mixed with 200 μL of Na_2CO_3 (2.8 M) and quantified at 420 nm.

The next round of enzymatic determination started when the pellet was hydrated with an ONPG solution at 5 mM. After 15 min, at 37 °C, the enzymatic reaction was stopped, as previously described. We repeat the process several times within 2 days, in order to evaluate the enzymatic activity of the pellet.

Reusable Enzymatic Cartridge. An enzymatic cartridge was constructed to avoid the protein loss from the ArtIBs sample. The cartridge was built from an Eppendorf tube with a hole in the lid; meanwhile, ArtIBs were previously prepared. A measure of 490 ng of β-Gal and 0.04 mmol of divalent cation salts were diluted in 1 mL and kept for 10 min at 4 °C. After this, the cartridge tubes were filled with 300 μL of soluble β-Gal or the ArtIBs sample up to the top, and a dialysis membrane was used to cover the tube and was firmly locked with the lid. To evaluate the activity of ArtIBs, we incorporated the cartridge to the reaction system containing 500 μL of 5 mM ONPG. The cartridge was placed in an inverted way to favor the interchange of ONPG and ONP through the dialysis membrane. Because of the diffusional restriction, the reaction was maintained for 2 h at 37 °C. After this, the cartridge was removed, and 200 μL of Na_2CO_3 (2.8 M) was added to the reaction volume. Before reading the absorbance of ONPx at 420 nm, the sample was centrifuged for 15 min at 10,000*g* to avoid light scattering induced by the precipitation of divalent cations.

The cartridge containing the ArtIBs was washed two times in PBS buffer containing 40 mM of divalent cation salts (the same divalent cation concentration within the cartridge). Finally, the catalytic cartridge was kept in the wash solution overnight (ON) until it was used. A cartridge containing the protein without salts was applied as the control.

Calibration Curve of ONPx in the Presence of Divalent Cations. Aliquots of ONPx in the range of 0−0.07 mM were incubated with water or solutions of divalent cation salts of 30 μL (400 mM). Then, 200 μL of Na_2CO_3 (2.8 M) was added, resulting in a final volume of 0.75 mL, in which the absorbance at 420 nm was recorded. The ONPx extinction coefficient (ε) was determined with a linear regression analysis. Before reading the absorbance of ONPx at 420 nm, the sample was centrifuged for 15 min at 10,000*g* to avoid light scattering induced by the precipitation of divalent cations.

Effect of Divalent Cations on the Kinetic Parameters of β-Gal. β-Gal in soluble or ArtIBs forms (20 ng) was mixed with ONPG in a range of concentrations from 0 to 4.5 mM. The incubation volume of 550 μL was buffered with PBS pH 7.4. The reaction was incubated for 15 min at 37 °C and stopped by adding 200 μL of Na_2CO_3 (2.8 M). The enzyme activity was determined by measuring the ONPx absorbance at 420 nm with a UV−visible spectrophotometer (Ultrospec 1000E, Pharmacia Biotech). Before reading the absorbance, the sample was centrifuged for 15 min at 10,000*g* to avoid light scattering induced by ArtIBs.

Determination of Kinetic Parameters of β-Galactosidase. The values of Michaelis constant (K_M) and the maximal velocity (V_{max}) were determined by fitting the experimental data from the initial velocity (V_0) versus substrate concentration plot to the equation of Michaelis−Menten by a computer-aided nonlinear regression analysis by the least-squares method.

Volume Size Distribution of ArtIBs. Volume size distribution of ArtIBs was determined at 633 nm and 25 °C in a Zetasizer Nano ZS system (Malvern Instruments Ltd.) by using 3 mm ZEN2112 quartz batch cuvettes. Measurements were performed in triplicate, and the sample concentration was 0.2 mg/mL.

Conformation Studies of β-Gal ArtIBs in Relation to Soluble Enzyme. Fluorescence spectra were recorded in a Cary Eclipse spectrofluorometer (Agilent Technologies), using a quartz cell with a 3 mm path length and a thermostatic holder. The excitation and emission slits were set at 5 nm; the excitation wavelength (λ_{ex}) was set at 295 nm; and the emission spectra were acquired between 310 and 450 nm in soluble β-Gal samples or in the form of ArtIBs at 0.1 mg/mL. The center of spectral mass (CSM), a weighted average of the fluorescence spectrum peaks, was calculated for comparison. The CSM is also related with the relative exposure of tryptophan (Trp) to the protein environment. The maximum red shift in the CSM of Trp is compatible with the large solvent accessibility or hydration and unfolding.[29]

The thermal stability profile was analyzed from 25 to 80 °C. The CSM of soluble β-Gal or in the form of ArtIBs (0.1 mg/mL) was determined in a spectral range of 318−450 nm. The fluorescence intensity values between 310 and 317 were underestimated because of the dispersion exerted by the divalent cations. A nonlinear regression was applied to the experimental point of CSM versus temperature spectrum, and the melting temperature (T_m) was estimated. With a nonlinear regression analysis, applying a sigmoidal model of four parameters, we determined the T_m value for the soluble and ArtIB β-Gal.

Thioflavin T Fluorescence in ArtIBs. The interaction of Thioflavin T (Thio T) with ArtIBs was explored to evaluate the amyloidal nature of the protein material. A 0.1 mg/mL of the protein sample was added to 25 μM of Thio T (Sigma-Aldrich) in PBS. ThioT fluorescence was excited at 450 nm, and the fluorescence emission spectra were recorded with a Varian Cary Eclipse spectrofluorometer in the 470−500 nm range. The cross-beta-sheet structure of β-Gal within ArtIBs was monitored by the enhancement of the free dye fluorescence emission caused by the interaction with amyloidogenic proteins.

Statistical Analysis. T tests assuming unequal variances were performed to assess the differences in assays with a minimum $n = 3$. The Shapiro−Wilk test was used to compare the enzymatic specific activity using Sigma Plot software. All quantitative values were expressed as mean ± standard error of the mean. The significance of the statistical difference was included in each experiment.

Nonlinear regression analysis was developed to determine not only the kinetic parameters (K_M and V_{max}) but also the melting temperature (T_m) of β-Gal in both formats, applying a hyperbolic or a sigmoidal model, respectively.

RESULTS AND DISCUSSION

Before starting the fabrication and characterization of β-Gal ArtIBs, several technical issues were considered. The functional analysis of β-Gal activity is based on the hydrolysis of ONPG and the spectrophotometric quantification of the reaction product ONP (Figure 1A). Then, any optical interference by experimental reagents could offer wrong interpretations. In this context, we first explored the optical behavior of several types of divalent cation salts intended for ArtIB fabrication, namely $CaCl_2$, $CuCl_2$, $MgCl_2$, $FeCl_2$, $MnCl_2$, $NiCl_2$, and $ZnCl_2$. Among this set of salts, $CuCl_2$, $FeCl_2$, and $NiCl_2$ absorbed light in the UV−vis range (Figure 1B) and were consequently discarded for further experiments. On the other hand, the microscale size and shape of ArtIBs (Figure 1C) might scatter light and hinder the correct ONP determination in the reaction mixtures. To solve this problem, the quantification of ONP was set to be done over samples centrifuged at 10,000*g* for 15 min.

Our interest was to select the best salt composition that allows ArtIB formation and that favors enzyme functionality. The inactivation of β-Gal activity by calcium ions (Ca^{2+}) and Zn^{2+} and the activation induced by manganese ions (Mn^{2+}) and magnesium ions (Mg^{2+}) (Figure 1D) agrees with other studies.[30,31] On the other hand, the precipitation of the enzyme as an insoluble material was demonstrated for all the tested cations, with the exception of Mg^{2+} that instead appeared as an enzyme activator (Figure 1D,E). These results encouraged us to first explore Mn^{2+} as a linker to form β-Gal

https://dx.doi.org/10.1021/acssuschemeng.0c08345
ACS Sustainable Chem. Eng. 2021, 9, 2552−2558

ACS Sustainable Chemistry & Engineering pubs.acs.org/journal/ascecg Research Article

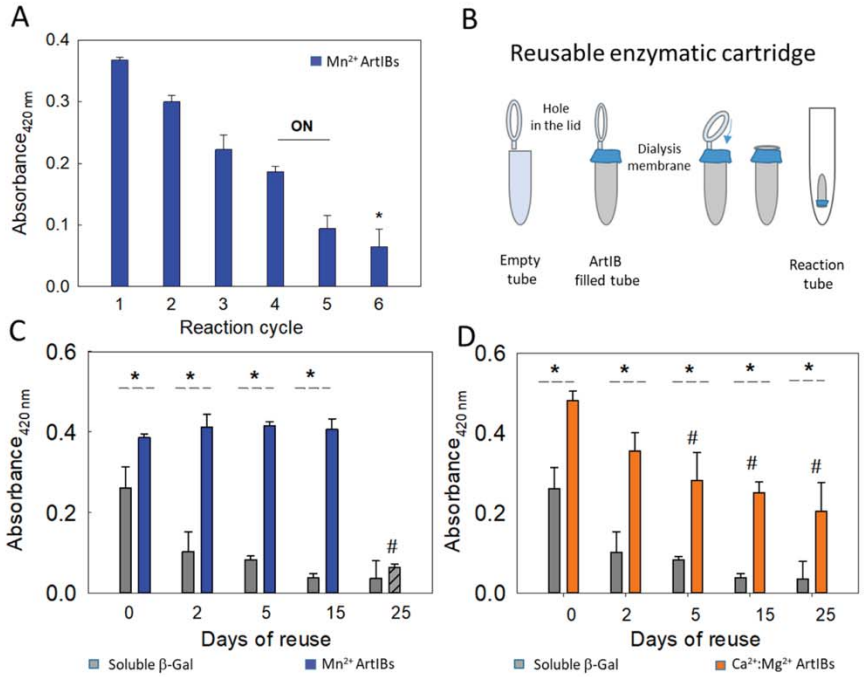

Figure 2. (A) ONPx absorbance at 420 nm at the successive reaction cycles of ArtIBs. ON: overnight, (*) statistically different from the initial measurement ($p \leq 0.006$). (B) Construction scheme of the reusable cartridge. (C) ONPx absorbance at 420 nm measured repeated times to evaluate the reusable properties of ArtIBs made with Mn^{2+}. (*) Statistically different from the control without Mn^{2+} ($p \leq 0.015$). The last reuse cartridge (25 days) was washed three times with water, and it was statistically different from the rest of ArtIB treatment (#, $p \leq 0.001$). (D) ONPx absorbance at 420 nm measured repeated times to evaluate the reusable properties of ArtIBs made with Ca^{2+} and Mg^{2+} (2:1 molar rates). (*) Statistically different from the control without salt ($p \leq 0.025$). (#) Statistically different from the initial treatment with salt ($p \leq 0.001$).

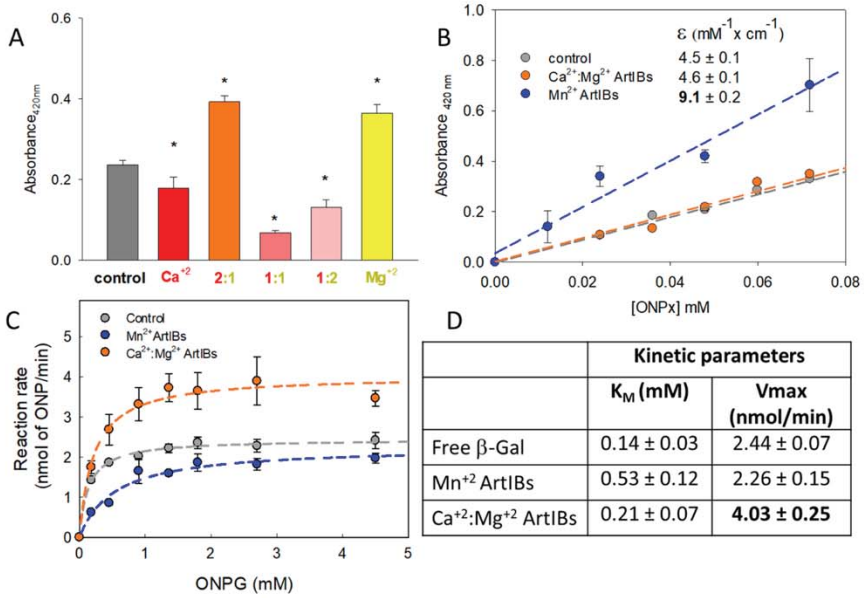

	Kinetic parameters	
	K_M (mM)	Vmax (nmol/min)
Free β-Gal	0.14 ± 0.03	2.44 ± 0.07
Mn^{+2} ArtIBs	0.53 ± 0.12	2.26 ± 0.15
Ca^{+2}:Mg^{+2} ArtIBs	0.21 ± 0.07	**4.03 ± 0.25**

Figure 3. (A) Combination effect of different molar rates of the Ca^{2+}/Mg^{2+} mixture on the β-Gal activity determined as ONPx absorbance at 420 nm. (*) Statistically different from the control without salt ($p \leq 0.028$) (in yellow: number of moles of Mg^{2+}; in red: number of moles of Ca^{2+}). (B) Calibration curves of ONPx in the presence of divalent cation salts. The extinction coefficient (ε) was determined with the slope of the curve, and the value for each condition is incorporated in the plot. The ε value under Mn^{2+} treatment is highlighted. (C) Substrate curve of soluble (gray line) and ArtIBs (colored lines). In all cases, the Michaelian behavior was observed. (D) Kinetic parameters determined by a nonlinear regression from each hyperbolic curve. The highest V_{max} from Ca^{2+}/Mg^{2+} ArtIBs was highlighted.

https://dx.doi.org/10.1021/acssuschemeng.0c08345
ACS Sustainable Chem. Eng. 2021, 9, 2552−2558

ACS Sustainable Chemistry & Engineering pubs.acs.org/journal/ascecg Research Article

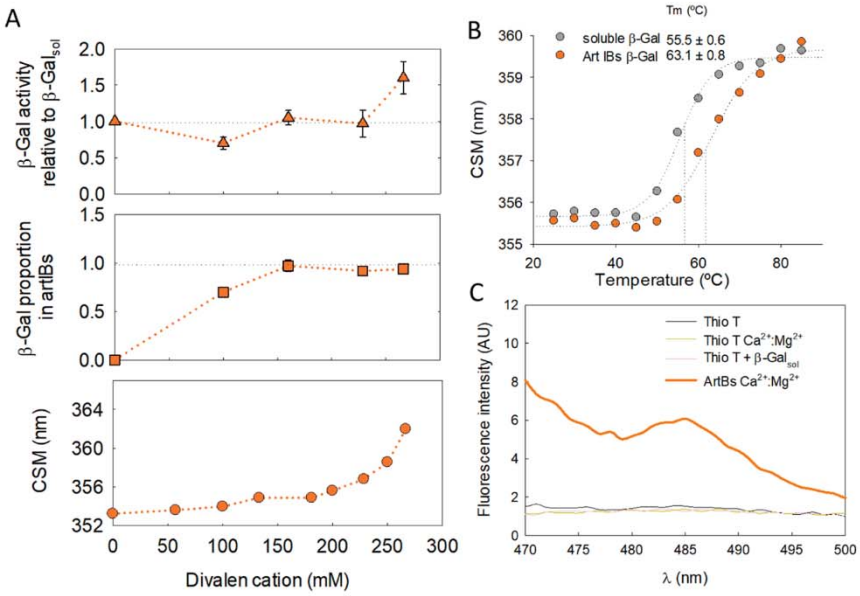

Figure 4. (A) Effect of the 2:1 Ca^{2+}/Mg^{2+} divalent cation salt concentration on the ArtIB enzymatic activity (triangle symbols) relative to the soluble β-Gal (β-Gal$_{sol}$), enzyme proportion within ArtIBs (square symbols), and CSM (circle symbols). (B) Thermal profile of ArtIBs and soluble β-Gal. The T_m value of each protein was indicated in the plot. (C) ThioT spectrum in the presence of different β-Gal samples. λ_{ex} was 450 nm, and the emission spectra ranged from 470 to 500 nm (β-Gal$_{sol}$: soluble β-Gal).

ArtIBs. In this context, when the ArtIB pellets were washed by successive centrifugations (at 10,000g for 15 min) and resuspended in buffer, a progressive decay in the β-Gal activity (Figure 2A) was observed, which might be due to the release and loss of soluble protein from ArtIBs in each reaction cycle, as described elsewhere.[24−26] From these results, we designed a reusable cartridge to prevent protein losses (Figure 2B), in which the functionality of the enzyme would remain unchanged (Figure 2C). It must be noted that each wash step was done in the buffer containing the same concentration of $MnCl_2$ that was initially present in the cartridge to restore the salt concentration and ensure the integrity of β-Gal ArtIBs, as the protein functionality dropped abruptly when washed with low-salt buffers (see dashed bar in Figure 2C). On the other hand, the no-salted cartridge, only filled with the soluble protein, exhibited a decrease in the catalytic activity, reinforcing the stable condition exerted by the ArtIBs (gray bars in Figure 2C).

The stability of ArtIBs was also explored when fabricated with a mixture of $MgCl_2$ (an enzyme activator) (as shown in Figure 1D) and $CaCl_2$ (an aggregator). Ca^{2+} is an excellent protein linker (Figure 1E), and its inactivating effect on β-Gal was only modest compared to $ZnCl_2$ (see Figure 1D). In these new ArtIBs, a discreet inactivation during reusing was observed, but the recorded activity was always higher in comparison to the soluble protein version (Figure 2D). The optimal molar $CaCl_2$:$MgCl_2$ ratio was 2:1 (Figure 3A) because this proportion offered an activation comparable only with $MgCl_2$ but in a microstructured β-Gal induced by $CaCl_2$. It seems that the inactivating/aggregating dual role of Ca^{2+} could be modulated by the cation proportion in the $CaCl_2/MgCl_2$ mixture. At low amounts, Ca^{2+} prevails as an inactivating agent in the reaction mechanism, but as the proportion of this cation increases, the linker (but not inactivating) activity also takes place. Hence, we applied a 2:1 cation molar ratio to the next experiments. The use of Ca^{2+} and Mg^{2+} in ArtIBs is very convenient because of the abundance in which both cations are found in our body, which improves the biocompatibility and lack of toxicity of the proteins presented in this new format.[25]

With the aim to establish the kinetic parameters of ArtIBs, we construct the ONPx calibration curve under the used salt formulations. The curve was developed in alkaline conditions (pH = 12, achieved with Na_2CO_3) to ensure that all ONP in the sample exists in the ONPx form. Taking into account the possible light scattering effect of salts, we centrifuged each sample before reading the ONPx absorbance at 420 nm. We demonstrated that Mn^{2+} but not Ca^{2+}/Mg^{2+} had an impact on the extinction coefficient of ONPx, with a great increase in its value (Figure 3B). These results could explain the high values of absorbance at 420 nm in the samples containing Mn^{2+} observed in previous experiments (Figures 1D and 2A,C). With the real amount of ONPx in the reaction system, we could construct the initial reaction rate (V_0) versus ONPG concentration plot to further determine the kinetic parameters, namely the Michaelis constant (K_M) and the maximal velocity (V_{max}) of β-Gal. In all the supramolecular formats, the enzyme exhibited a Michaelian behavior that was adjusted to a hyperbolic curve by a nonlinear regression. Mn^{2+} ArtIBs presented a lower V_{max} than the soluble β-Gal, but Ca^{2+}/Mg^{2+} ArtIBs were more active ($V_{max,CaMgArtIBs} > V_{max,soluble\ \beta\text{-Gal}}$) compared to the soluble protein (Figure 3C,D). Besides, although Mn^{2+} ArtIBs exhibited a lower affinity than the soluble enzyme toward the substrate ($K_{M,MnArtIBs} > K_{M,soluble\ \beta\text{-Gal}}$), Ca^{2+}/Mg^{2+} ArtIBs showed the same affinity with respect to the soluble β-Gal toward ONPG (Figure 3D). Once the desired ArtIB composition was reached, we wondered if the protein underwent any conformational change and/or if these ArtIBs would present the same properties that have been described for other ArtIBs.[24,26] We observed that as the Ca^{2+}/Mg^{2+} concentration increased over 150 mM, the

https://dx.doi.org/10.1021/acssuschemeng.0c08345
ACS Sustainable Chem. Eng. 2021, 9, 2552−2558

CSM values remarkably grew up too, indicating that the protein tended to be more hydrated (circle symbols, Figure 4A), especially when all the protein in the sample is in the aggregated form (revealed by the unity value in the *y*-axis; square symbols, Figure 4A). At this stage, a supramolecular arrange with a mean size of 1138 ± 364 nm and a polydispersion index of 0.23. Concomitantly, as the cation concentration increased, the protein acquired a more active moiety (triangle symbols, Figure 4A).

The new conformation of the protein within ArtIBs could alter its stability. Then, we explored the thermal profile of the soluble and the ArtIBs protein (Figure 4B) and proved that beyond the highly expanded structure of β-Gal in ArtIBs, the T_m value was higher than the one obtained from the soluble protein. Our results suggest that the protein was greatly resistant to thermal unfolding within ArtIBs. The cross-parallel β structure described for other ArtIBs[24,26] was also proved here (Figure 4C) by the increase in the Thio T fluorescence, confirming the presence of such secondary structure patterns in ArtIBs.

CONCLUSIONS

In this study, we have designed an efficient, stable, and reusable enzymatic device. Based on the divalent cations as architectonic elements to form functional β-Gal microparticles, we offer a highly simple methodology to produce catalytic devices with increased efficiency, robust reusability, and high thermal stability acquired by the enzyme during the formation of the microscale particulate version.

AUTHOR INFORMATION

Corresponding Authors

Julieta M. Sanchez − *Institut de Biotecnologia i de Biomedicina, Universitat Autònoma de Barcelona, 08193 Barcelona, Spain; Departament de Genètica i de Microbiologia, Universitat Autònoma de Barcelona, 08193 Barcelona, Spain; Instituto de Investigaciones Biológicas y Tecnológicas (IIBYT) (CONICET-Universidad Nacional de Córdoba), Departamento de Química, FCEFyN, ICTA & Cátedra de Química Biológica, X 5016GCA Córdoba, Argentina;* orcid.org/0000-0001-6676-5776; Email: julieta.sanchez@unc.edu.ar

Antonio Villaverde − *Institut de Biotecnologia i de Biomedicina, Universitat Autònoma de Barcelona, 08193 Barcelona, Spain; Departament de Genètica i de Microbiologia, Universitat Autònoma de Barcelona, 08193 Barcelona, Spain; CIBER de Bioingeniería, Biomateriales y Nanomedicina (CIBER-BBN), 28029 Madrid, Spain;* orcid.org/0000-0002-2615-4521; Email: antoni.villaverde@uab.cat

Esther Vazquez − *Institut de Biotecnologia i de Biomedicina, Universitat Autònoma de Barcelona, 08193 Barcelona, Spain; Departament de Genètica i de Microbiologia, Universitat Autònoma de Barcelona, 08193 Barcelona, Spain; CIBER de Bioingeniería, Biomateriales y Nanomedicina (CIBER-BBN), 28029 Madrid, Spain;* Email: esther.vazquez@uab.cat

Authors

Hèctor López-Laguna − *Institut de Biotecnologia i de Biomedicina, Universitat Autònoma de Barcelona, 08193 Barcelona, Spain; Departament de Genètica i de Microbiologia, Universitat Autònoma de Barcelona, 08193 Barcelona, Spain; CIBER de Bioingeniería, Biomateriales y Nanomedicina (CIBER-BBN), 28029 Madrid, Spain*

Naroa Serna − *Institut de Biotecnologia i de Biomedicina, Universitat Autònoma de Barcelona, 08193 Barcelona, Spain; Departament de Genètica i de Microbiologia, Universitat Autònoma de Barcelona, 08193 Barcelona, Spain; CIBER de Bioingeniería, Biomateriales y Nanomedicina (CIBER-BBN), 28029 Madrid, Spain*

Ugutz Unzueta − *Departament de Genètica i de Microbiologia, Universitat Autònoma de Barcelona, 08193 Barcelona, Spain; CIBER de Bioingeniería, Biomateriales y Nanomedicina (CIBER-BBN), 28029 Madrid, Spain; Biomedical Research Institute Sant Pau (IIB Sant Pau), 08025 Barcelona, Spain*

Pedro D. Clop − *Instituto de Investigaciones Biológicas y Tecnológicas (IIBYT) (CONICET-Universidad Nacional de Córdoba), Departamento de Química, FCEFyN, ICTA & Cátedra de Química Biológica, X 5016GCA Córdoba, Argentina*

Complete contact information is available at: https://pubs.acs.org/10.1021/acssuschemeng.0c08345

Notes

The authors declare no competing financial interest.

ACKNOWLEDGMENTS

The authors are indebted to Agencia Estatal de Investigación (AEI) and to Fondo Europeo de Desarrollo Regional (FEDER) (PID2019 105416RB-I00/AEI/10.13039/501100011033 to E.V.) and AGAUR (2017SGR-229, to A.V.). The authors are also indebted to the Networking Research Center on Bioengineering, Biomaterials and Nanomedicine (CIBER-BBN) through the NANOREMOTE intramural project that is an initiative funded by the VI National R&D&I Plan 2008−2011, Iniciativa Ingenio 2010, Consolider Program, CIBER Actions, and financed by the Instituto de Salud Carlos III, with assistance from the European Regional Development Fund. The authors appreciate the assistance of the Protein Production Platform of CIBER in Bioengineering, Biomaterials & Nanomedicine (CIBER-BBN)/IBB, at the UAB sePBioEs scientific-technical service (http://www.nanbiosis.es/portfolio/u1-protein-production-platform-ppp/) and particle size analysis by the Biomaterial Processing and Nanostructuring Unit. Electron microscopy studies were performed by Servei de Microscòpia at the UAB. A.V. received an ICREA ACADEMIA award. HLL is supported by a predoctoral fellowship from AGAUR (2019FI_B00352). U.U. is supported by Miguel Servet contract (CP19/00028) from ISCIII co-funded by European Social Fund (ESF investing in your future).

REFERENCES

(1) Markel, U.; Essani, K. D.; Besirlioglu, V.; Schiffels, J.; Streit, W. R.; Schwaneberg, U. Advances in Ultrahigh-Throug Put Screening for Directed Enzyme Evolution. *Chem. Soc. Rev.* **2020**, *49*, 233−262.

(2) Copley, S. D. An Evolutionary Biochemist's Perspective on Promiscuity. *Trends Biochem. Sci.* **2015**, *40*, 72−78.

(3) Wu, Z.; Jennifer Kan, S. B.; Lewis, R. D.; Wittmann, B. J.; Arnold, F. H. Machine Learning-Assisted Directed Protein Evolution with Combinatorial Libraries. *Proc. Natl. Acad. Sci. U.S.A.* **2019**, *116*, 8852.

(4) Ribeiro, A. J. M.; Tyzack, J. D.; Borkakoti, N.; Holliday, G. L.; Thornton, J. M. A Global Analysis of Function and Conservation of Catalytic Residues in Enzymes. *J. Biol. Chem.* **2020**, *295*, 314−324.
(5) Zhang, B.; Weng, Y.; Xu, H.; Mao, Z. Enzyme Immobilization for Biodiesel Production. *Appl. Microbiol. Biotechnol.* **2012**, *93*, 61−70.
(6) Jesionowski, T.; Zdarta, J.; Krajewska, B. Enzyme Immobilization by Adsorption: A Review. *Adsorption* **2014**, *20*, 801−821.
(7) Weltz, J. S.; Kienle, D. F.; Schwartz, D. K.; Kaar, J. L. Dramatic Increase in Catalytic Performance of Immobilized Lipases by Their Stabilization on Polymer Brush Supports. *ACS Catal.* **2019**, *9*, 4992−5001.
(8) Gennari, A.; Mobayed, F. H.; da Silva Rafael, R.; Rodrigues, R. C.; Sperotto, R. A.; Volpato, G.; Volken de Souza, C. F. Modification of Immobead 150 Support for Protein Immobilization: Effects on the Properties of Immobilized Aspergillus Oryzae β-Galactosidase. *Biotechnol. Prog.* **2018**, *34*, 934−943.
(9) González-Montalbán, N.; García-Fruitós, E.; Villaverde, A. Recombinant Protein Solubility - Does More Mean Better? [4]. *Nat. Biotechnol.* **2007**, *25*, 718−720.
(10) Flores, S. S.; Nolan, V.; Perillo, M. A.; Sánchez, J. M. Superactive Beta-Galactosidase Inclusion Bodies. *Colloids Surf., B* **2019**, *173*, 769−775.
(11) Hrabárová, E.; Achbergerová, L.; Nahálka, J. *Insoluble Protein Applications: The Use of Bacterial Inclusion Bodies as Biocatalysts*; Springer: New York, 2015.
(12) Krauss, U.; Jäger, V. D.; Diener, M.; Pohl, M.; Jaeger, K. E. Catalytically-Active Inclusion Bodies—Carrier-Free Protein Immobilizates for Application in Biotechnology and Biomedicine. *J. Biotechnol.* **2017**, *258*, 136.
(13) Jäger, V. D.; Kloss, R.; Grünberger, A.; Seide, S.; Hahn, D.; Karmainski, T.; Piqueray, M.; Embruch, J.; Longerich, S.; Mackfeld, U.; Jaeger, K. E.; Wiechert, W.; Pohl, M.; Krauss, U. Tailoring the Properties of (Catalytically)-Active Inclusion Bodies. *Microb. Cell Factories* **2019**, *18*, 33−53.
(14) Kopito, R. R. Aggresomes, Inclusion Bodies and Protein Aggregation. *Trends Cell Biol.* **2000**, *10*, 524−530.
(15) Rinas, U.; Garcia-Fruitós, E.; Corchero, J. L.; Vázquez, E.; Seras-Franzoso, J.; Villaverde, A. Bacterial Inclusion Bodies: Discovering Their Better Half. *Trends Biochem. Sci.* **2017**, *42*, 726−737.
(16) Rodríguez-Carmona, E.; Mendoza, R.; Ruiz-Cánovas, E.; Ferrer-Miralles, N.; Abasolo, I.; Schwartz, S.; Villaverde, A.; Corchero, J. L. A Novel Bio-Functional Material Based on Mammalian Cell Aggresomes. *Appl. Microbiol. Biotechnol.* **2015**, *99*, 7079−7088.
(17) Carratalá, J. V.; Cano-Garrido, O.; Sánchez, J.; Membrado, C.; Pérez, E.; Conchillo-Solé, O.; Daura, X.; Sánchez-Chardi, A.; Villaverde, A.; Arís, A.; Garcia-Fruitós, E.; Ferrer-Miralles, N. Aggregation-Prone Peptides Modulate Activity of Bovine Interferon Gamma Released from Naturally Occurring Protein Nanoparticles. *New Biotechnol.* **2020**, *57*, 11−19.
(18) Cano-Garrido, O.; Rodríguez-Carmona, E.; Díez-Gil, C.; Vázquez, E.; Elizondo, E.; Cubarsi, R.; Seras-Franzoso, J.; Corchero, J. L.; Rinas, U.; Ratera, I.; Ventosa, N.; Veciana, J.; Villaverde, A.; García-Fruitós, E. Supramolecular Organization of Protein-Releasing Functional Amyloids Solved in Bacterial Inclusion Bodies. *Acta Biomater.* **2013**, *9*, 6134−6142.
(19) Lamm, R.; Jäger, V. D.; Heyman, B.; Berg, C.; Cürten, C.; Krauss, U.; Jaeger, K.-E.; Büchs, J. Detailed Small-Scale Characterization and Scale-up of Active YFP Inclusion Body Production with Escherichia Coli Induced by a Tetrameric Coiled Coil Domain. *J. Biosci. Bioeng.* **2020**, *129*, 730−740.
(20) Vázquez, E.; Corchero, J. L.; Burgueño, J. F.; Seras-Franzoso, J.; Kosoy, A.; Bosser, R.; Mendoza, R.; Martínez-Láinez, J. M.; Rinas, U.; Fernández, E.; Ruiz-Avila, L.; García-Fruitós, E.; Villaverde, A. Functional Inclusion Bodies Produced in Bacteria as Naturally Occurring Nanopills for Advanced Cell Therapies. *Adv. Mater.* **2012**, *24*, 1742−1747.
(21) Céspedes, M. V.; Cano-Garrido, O.; Álamo, P.; Sala, R.; Gallardo, A.; Serna, N.; Falgàs, A.; Voltà-Durán, E.; Casanova, I.; Sánchez-Chardi, A.; López-Laguna, H.; Sánchez-García, L.; Sánchez, J. M.; Unzueta, U.; Vázquez, E.; Mangues, R.; Villaverde, A. Engineering Secretory Amyloids for Remote and Highly Selective Destruction of Metastatic Foci. *Adv. Mater.* **2020**, *32*, 1907348.
(22) De Marco, A.; Ferrer-Miralles, N.; Garcia-Fruitós, E.; Mitraki, A.; Peternel, S.; Rinas, U.; Trujillo-Roldán, M. A.; Valdez-Cruz, N. A.; Vázquez, E.; Villaverde, A. Bacterial Inclusion Bodies Are Industrially Exploitable Amyloids. *FEMS Microbiol. Rev.* **2019**, *43*, 53−72.
(23) Wasmer, C.; Benkemoun, L.; Sabaté, R.; Steinmetz, M. O.; Coulary-Salin, B.; Wang, L.; Riek, R.; Saupe, S. J.; Meier, B. H. Solid-State NMR Spectroscopy Reveals That E. Coli Inclusion Bodies of HET-s(218-289) Are Amyloids. *Angew. Chem. Int. Ed.* **2009**, *48*, 4858−4860.
(24) Sánchez, J. M.; López-Laguna, H.; Álamo, P.; Serna, N.; Sánchez-Chardi, A.; Nolan, V.; Cano-Garrido, O.; Casanova, I.; Unzueta, U.; Vazquez, E.; Mangues, R.; Villaverde, A. Artificial Inclusion Bodies for Clinical Development. *Adv. Sci.* **2020**, *7*, 1902420.
(25) López-Laguna, H.; Sánchez, J.; Unzueta, U.; Mangues, R.; Vázquez, E.; Villaverde, A. Divalent Cations: A Molecular Glue for Protein Materials. *Trends Biochem. Sci.* **2020**, *45*, 992−1003.
(26) Serna, N.; Cano-Garrido, O.; Sánchez, J. M.; Sánchez-Chardi, A.; Sánchez-García, L.; López-Laguna, H.; Fernández, E.; Vázquez, E.; Villaverde, A. Release of Functional Fibroblast Growth Factor-2 from Artificial Inclusion Bodies. *J. Control. Release* **2020**, *327*, 61−69.
(27) Tomizawa, M.; Tsumaki, K.; Sone, M. Characterization of the Activity of β-Galactosidase from Escherichia Coli and Drosophila Melanogaster in Fixed and Non-Fixed Drosophila Tissues. *Biochim. Open* **2016**, *3*, 1−7.
(28) Tenu, J.-P.; Viratelle, O. M.; Yon, J. Kinetic Study of the Activation Process of B-Galactosidase from Escherichia Coli by Mg2+. *Eur. J. Biochem.* **1972**, *26*, 112−118.
(29) Sánchez, J. M.; Sánchez-García, L.; Pesarrodona, M.; Serna, N.; Sánchez-Chardi, A.; Unzueta, U.; Mangues, R.; Vázquez, E.; Villaverde, A. Conformational Conversion during Controlled Oligomerization into Nonamylogenic Protein Nanoparticles. *Biomacromolecules* **2018**, *19*, 3788−3797.
(30) Ustok, F. I.; Tari, C.; Harsa, S. Biochemical and Thermal Properties of β-Galactosidase Enzymes Produced by Artisanal Yoghurt Cultures. *Food Chem.* **2010**, *119*, 1114−1120.
(31) Banerjee, G.; Ray, A.; Hasan, K. N. Is Divalent Magnesium Cation the Best Cofactor for Bacterial β-Galactosidase? *J. Biosci.* **2018**, *43*, 941−945.

https://dx.doi.org/10.1021/acssuschemeng.0c08345
ACS Sustainable Chem. Eng. 2021, 9, 2552−2558

Annex 4

Nanostructured AMPs, released from protein-only microscale depots, confer protection against pathogenic bacteria

Manuscript in progress

Objective 3.f

To test the biomedical applications of **protein-based insoluble microparticles** in the treatment of infectious diseases.

Following the idea of testing the microparticle-based platform transversality in biomedicine, we wondered how SG-like microparticles could be used to fight infectious disease, taking advantage of the slow and sustained release of antimicrobial peptides (AMP).

Thus, this work has been focused on developing disintegrating AMP-based microparticles able to release efficient protein-based nanoparticles to kill bacteria. The obtained data suggested how AMP-based microscale depots are able to release stable nanoparticles in a sustained manner and promote a better survival rate in an infectious *in vivo* zebrafish model.

Nanostructured AMPs, released from protein-only microscale depots, confer protection against pathogenic bacteria

Naroa Serna [1,2,3*±¥], Hèctor López-Laguna [1,2,3±], Patricia Aceituno [1,4±], Eloi Parladé [1,2,3], Eric Voltà-Durán [1,2], Carlos Martínez-Torró [1], Julieta M. Sánchez [1,2], Angela di Somma [1], José Vicente Carratalá [1,2,3], Neus Ferrer-Miralles [1,2,3], Esther Vázquez [1,2,3], Ugutz Unzueta [1,2,3,5], Nerea Roher [1,3,4*], Antonio Villaverde [1,2,3*]

[1] Institut de Biotecnologia i de Biomedicina (IBB), Universitat Autònoma de Barcelona, Barcelona, Spain.

[2] Departament de Genètica i de Microbiologia, Universitat Autònoma de Barcelona, Barcelona, Spain.

[3] Centro de Investigación Biomédica en Red de Bioingeniería, Biomateriales y Nanomedicina, Instituto de Salud Carlos III, Barcelona, Spain.

[4] Departament de Biologia Cel·lular, Fisiologia Animal i Immunologia, Universitat Autònoma de Barcelona, Barcelona 08193, Spain

± Equally contributed

¥ Present address: NS, Nanoligent SL, Edifici Eureka, Universitat Autònoma de Barcelona, Barcelona, Spain.

* Corresponding authors: NR, nerea.roher@uab.cat; AV, antonio.villaverde@uab.cat

Abstract

Both nanostructure and multivalency enhance the biological activities of antimicrobial peptides (AMPs), whose mechanism of action is cooperative. In addition, the efficacy of a particular AMP should benefit from a steady concentration at the local place of action, and therefore, from a slow release after a dynamic repository. In the context of emerging multi-resistant bacterial infections and the urgent need for novel and effective (AM) drugs, we have tested these concepts through the engineering of four AMPs into supramolecular complexes. For that, GWH1, T22, Pt5 and PaD, produced as GFP- or nidogen-based His-tagged fusion proteins, have been engineered as self-assembling oligomeric nanoparticles ranging from 10 to 70 nm and further packaged into nanoparticle-leaking sub-micron granules. Since these materials slowly release functional nanoparticles during their time-sustained unpackaging they are suited as drug depots *in vivo*. In this context, a particular AMP version (GWH1-NIDO-H6) was selected for *in vivo* validation in a zebra-fish model of a complex bacterial infection. The GWH1-NIDO-H6-secreting protein granules are protective in zebra fish in front of infection by the multiresistant bacteria *Stenotrophomonas maltophilia*, proving the potential of innovative formulations based on nanostructured and slowly released recombinant AMPs in the fight against bacterial infections.

Introduction

Infectious diseases represent an increasing health treat, expected to acquire immense proportions in the next decades. The abuse and misuse of antibiotics has pushed towards the accumulation of drug-resistance genes in single bacterial strains that allow them to escape the activity of diverse sets of antibiotics (Ventola, 2015). These multi-drug resistant pathogens are responsible for high impact, live-threating infections whose incidence is expected to gear up in forthcoming decades (Klemm et al., 2018; Martens & Demain, 2017; Medina & Pieper, 2016; Roca et al., 2015). Beyond conventional antibiotics, unconventional AM agents are either being identified from nature (Laport et al., 2009; Rafal et al., 2018; Wu et al., 2018) and/or further developed in the lab, through diverse engineering approaches (Bhattacharjya & Straus, 2020; Tacconelli et al., 2018; Torres et al., 2018). This is aiming at enhancing their effectiveness and to offer a new spectrum of clinically realistic alternatives and formulations usable as operative AM drugs [1,2]. AMPs are among such new likely agents [3-5], usually produced by chemical synthesis but also suited for recombinant production in microbial cells via fusion to carrier proteins [6,7] or through tandem arrangements [8-10]. Of course, the recombinant biofabrication of AMPs in prokaryotic cell factories offers, as in the case of any other protein drug [11], fully scalable, eco-friendly and cost-effective methodologies [12-14] compatible with a sustainable circular economy [15]. Also, recombinant AMPs benefit from the generic properties of protein drugs, namely excellent biocompatibility and biodegradability and the possibility of functional and structural adjustment through conventional genetic engineering [16-19]. Since protein drugs are broadly used in human clinics [11,20], the possibility to develop recombinant AM pharmaceuticals is highly promising as a main strategic route.

In the global route to improve the effectiveness of AMPs, two main conclusions have been drawn. Frist, AMP presentation as nanoscale versions ensures particularly good tissue penetrability, stability and retention in contrast to monomeric soluble versions, being multivalence and local cooperativity (in homomeric AMP oligomers) a highly desirable parameter [21-24]. Furthermore, as in the case of many other drugs, a time-sustained AMP release might enhance effectiveness, prompting the development of suited materials, devices and holding matrices accordingly [25-27]. In this context, we have previously generated recombinant versions of distinct AMPs, that in form of self-assembling fusion proteins can be easily produced in *Escherichia coli* as multivalent nanoscale oligomers [22,28,29] on which the displayed AMP is fully functional. On the other hand, we have recently developed a protein-only type of submicron/micron material [30] in which monomeric or oligomeric

protein versions are clustered by the coordination between histidine residues of hexahistidine tags (H6) and divalent cations (such as Zn^{2+} or Ca^{2+}) (Álamo et al., 2021; López-Laguna et al., 2021; Sánchez et al., 2020, 2022). Those ions act as a molecular glue between overhanging histidine residues from different polypeptides (López-Laguna et al., 2020, 2022). Then, the AMPs are self-contained in microparticles that in absence of any holding matrices, slowly disintegrate under physiological conditions by the spontaneous chelation of the cations. This fact, that mimics the release of peptidic hormones from the human endocrine system (Jacob et al., 2016, 2019; Maji et al., 2009; Seuring et al., n.d.), results in a steady leakage of the building block protein, in cell culture (Serna et al., 2020) or in vivo (Álamo et al., 2021). The present study was designed to evaluate the AMP performance, in vitro and in vivo, as a formulation that combine these concepts, namely recombinant AMPs versions organized as multimeric nanoparticles, slowly delivered from protein-only dynamic depots. The presented data fully support the usability and clinical potential of recombinant AMPs administered in such a novel protein-only depot formulation based on a very simple fabrication process.

Results and discussion

Four AMPs, namely T22 [28], GWH1 [31], PaD [32] and Pt5 [33], were selected to be displayed on nanoscale oligomers, through N-terminal fusions to a H6-tagged GFP (Figure 1A, B). The cationic character of these peptides favours cation-assisted oligomerization, through cross-molecular contacts that involve histidine residues from the H6 tails [34]. All proteins were produced in good yields in *Escherichia coli*, in form of full-length fusions of expected molecular mass (Figure 1B), and they spontaneously assembled, upon purification from bacterial cell extracts, as nanoparticles of different sizes (Figure 1C). The molecular basis for the oligomerization is the combination of an N-terminal cationic peptide and a C-terminal histidine-rich peptide, with the intervention of divalent cations. Under the tested conditions, the parental construct GFP-H6, used here as a negative control, did not assemble (Figure 1C).

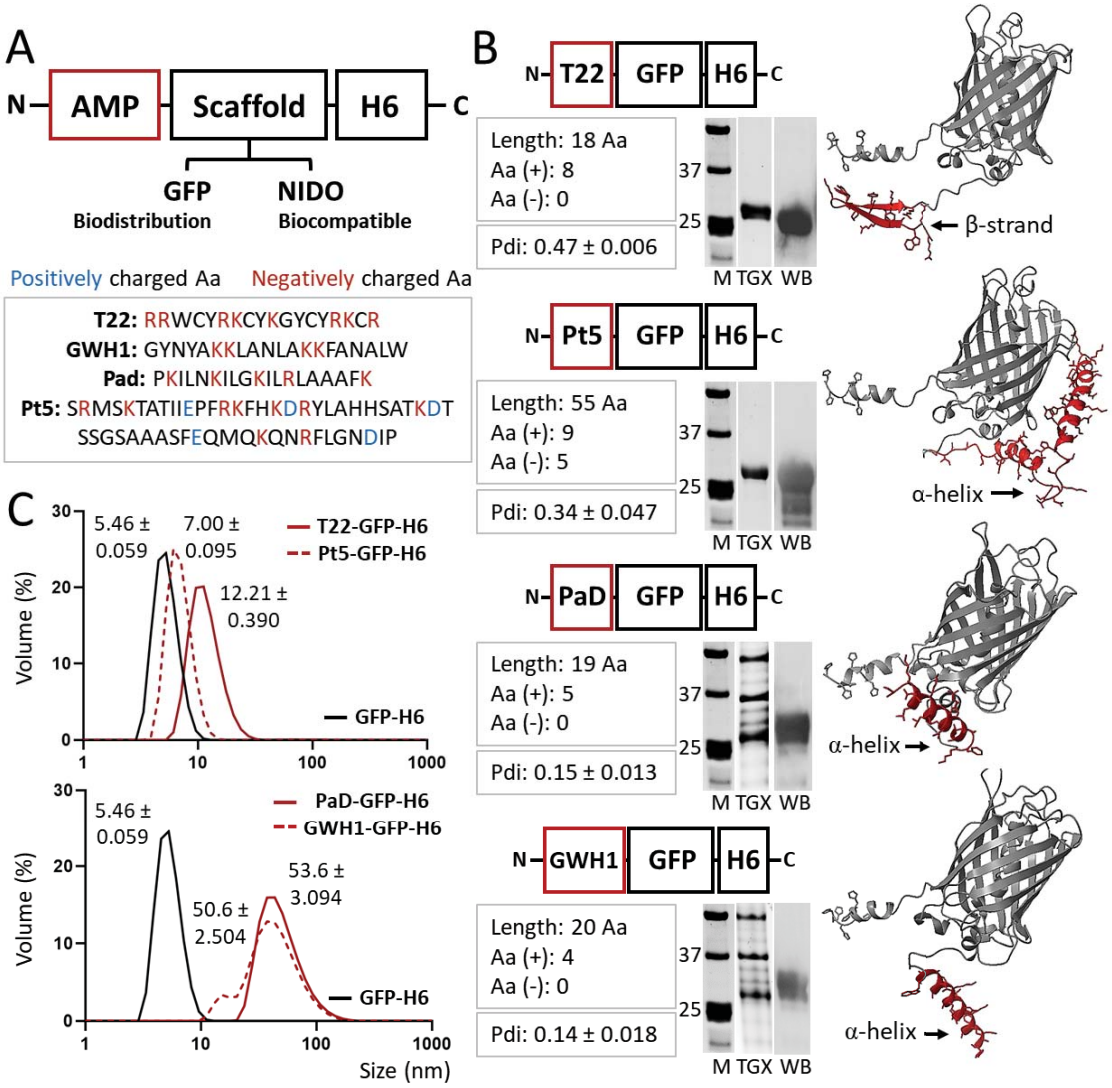

Figure 1. Physicochemical characterization of AMP-based recombinant proteins. **A**. Schematic representation of the modular design of the protein-based platform. The GFP scaffold is intended to be used as reporter in biodistribution. NIDO, being a human protein segment, is a promising scaffold envisaging clinical uses. **B**. Schematic modular representation of each protein construction based on an N -terminal AMP (namely T22, Pt5, PaD and GWH1). Right. 3D structure prediction of each protein (AMP sequence displayed in red). Center. Protein integrity and purity analyzed by SDS-PAGE electrophoresis (TGX) and Western Blot (WB) respectively. Marker sizes are displayed in between 37 and 25 KDa. Left. A short primary sequence description of each AMP, indicating peptide length and the charge of charged amino acids. **C**. Volume size distribution (in nm) of the resulting nanoparticles. Peak values are displayed ± standard error of the mean. The parental construct GFP-H6, which under the used conditions does not assemble into nanoparticles, is also displayed in black as a reference. The polydispersity index (Pdi) for each material is also displayed underneath the description box, in the panel B.

Using these nanoparticles as starting components, the fabrication of larger-order microscale particles was approached by testing alternative divalent cations as cross-molecular linkers (Figure 2A). In this regard, chloride salt versions of Zn, Fe and Mn were tested as a supply of molar excess divalent cations for protein clustering, using T22-GFP-H6 as an indicator of AM activity (Figure 1B). All these cations were able, with variable efficacies, to promote protein precipitation because of the overhanging H6 tags in them [35]. Because of the robustness of Zn^{2+} as a crosslinking agent and since the materials formed with Zn show a clearer AM activity (Figure 2B), this cation was selected for further fabrication of protein granules out of soluble nanoparticles. As observed (Figure 2C), at the tested conditions, the newly formed supramolecular complexes of all the constructs occurred at the submicron scale, between 150 and 600 nm. At that point, protein release was monitored from these materials along time, and in physiological buffer, revealing protein-dependent variability in this process (Figure 2D). This was indicative of different compactness and leakage availability of AMPs from them, which might of course influence the final clinical applicability. While T22-based material was released very rapidly, PaD and specially GWH1 rendered more progressive release patterns. The different amounts of Zn retained by the particles during formation (Figure 2E) did not offered clues for the differential release kinetics observed in Figure 2D.

To determine potential toxicities of these materials and to evaluate their distribution *in vivo*, we employed a zebrafish larvae model that being simple, is fully validated for toxicology. In this context, the exposure of zebrafish larvae to 50 μg/ml of all versions of AMP-based granules for 48 h did not resulted in any sign of toxicity. Also, after 48 h of immersion, the materials derived from T22, PaD, and Pt5 were found in the gastrointestinal tract and pancreas of zebrafish larvae, whereas the fluorescence of GWH1-based granules was only observed in the intestine. Interestingly, in larvae treated with soluble GFP-H6, no fluorescent

signal was observed (Figure 2I). To further move towards a functional analysis, the same in vivo model was used to determine the AM properties of these materials. In particular, granules formed by GWH1 were the ones that rendered a more constant and steady protein release (namely, Figure 2D) and also, they showed a more localized biodistribution. Therefore, they were observed as interesting for further analyses.

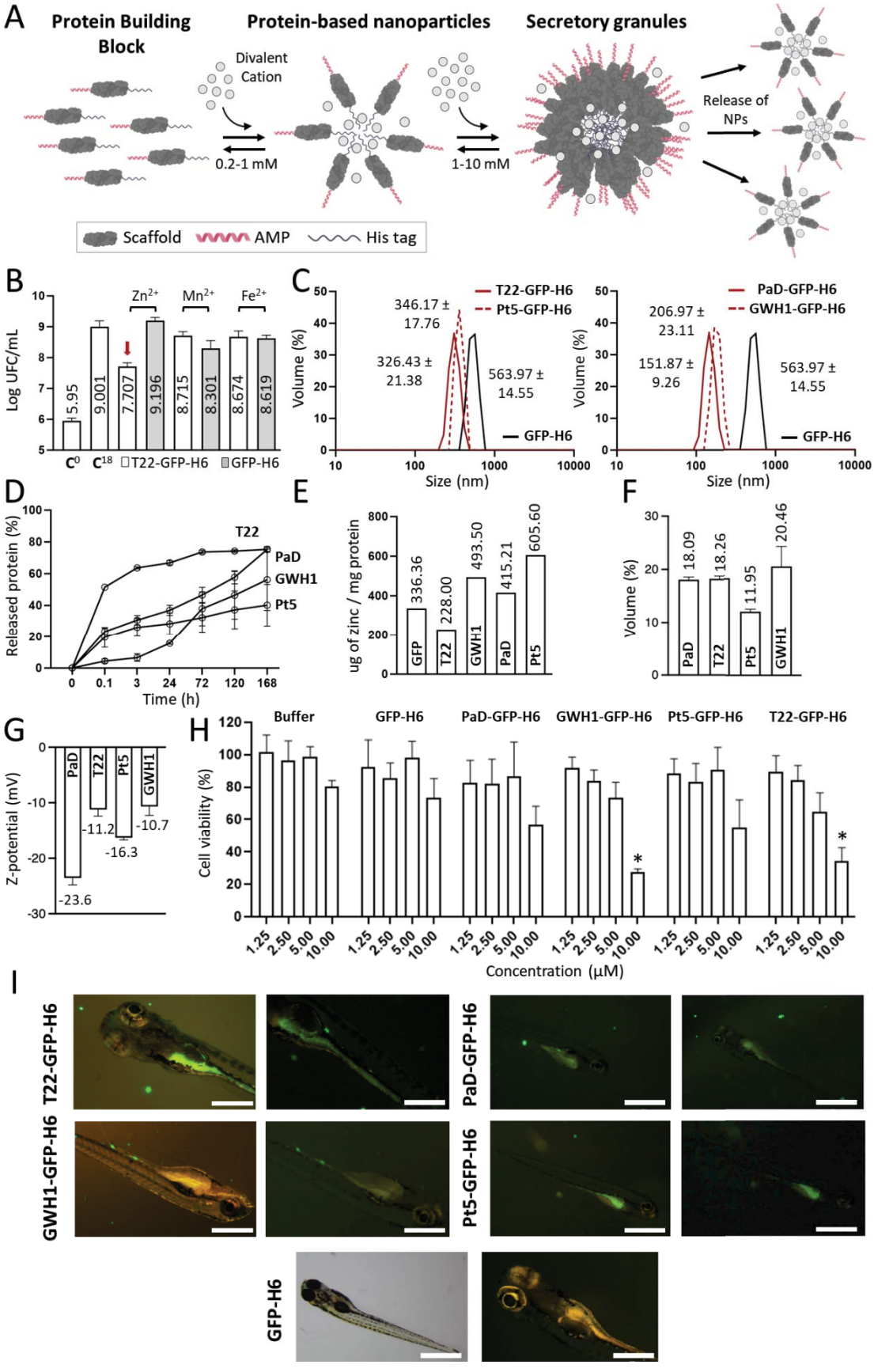
A
Protein Building Block
Protein-based nanoparticles
Secretory granules
Divalent Cation
0.2-1 mM
1-10 mM
Release of NPs
Scaffold
AMP
His tag
B
Log UFC/mL
Zn2+
Mn2+
Fe2+
5.95
9.001
7.707
9.196
8.715
8.301
8.674
8.619
C0
C18
T22-GFP-H6
GFP-H6
C
Volume (%)
T22-GFP-H6
Pt5-GFP-H6
346.17 ± 17.76
326.43 ± 21.38
563.97 ± 14.55
GFP-H6
Size (nm)
PaD-GFP-H6
GWH1-GFP-H6
206.97 ± 23.11
151.87 ± 9.26
563.97 ± 14.55
GFP-H6
Size (nm)
D
Released protein (%)
T22
PaD
GWH1
Pt5
Time (h)
E
ug of zinc / mg protein
336.36
228.00
493.50
415.21
605.60
GFP
T22
GWH1
PaD
Pt5
F
Volume (%)
18.09
18.26
11.95
20.46
PaD
T22
Pt5
GWH1
G
Z-potential (mV)
PaD
T22
Pt5
GWH1
-23.6
-11.2
-16.3
-10.7
H
Buffer
GFP-H6
PaD-GFP-H6
GWH1-GFP-H6
Pt5-GFP-H6
T22-GFP-H6
Cell viability (%)
Concentration (µM)
I
T22-GFP-H6
PaD-GFP-H6
GWH1-GFP-H6
Pt5-GFP-H6
GFP-H6

Figure 2. Manufacturing of AMP-based secretory granules (SGs) and in vivo biodistribution. **A**. Schematic representation of the formulation process upon divalent cations addition (from recombinant proteins acting as building blocks to artificially created SGs which release functional protein). Ranges of divalent cations are displayed underneath the left pointing arrows. Scaffold is displayed in dark grey, AMP structure in red and histidine tag in pale grey. **B.** *S. aureus* bacterial growth (log UFC/mL) after 18h in presence of T22-GFP-H6 (white bars) or GFP-H6 (grey bars) artificial SGs constructed by different divalent cations (namely zinc II, manganese II and Iron II). C^0 refers to the amount of bacterial initial colonies, and C^{18} after 18h of incubation. Numbers inside bars refer to log UFC/mL for each material. Red arrow displays the most effective condition. **C**. Volume size distribution analysis (nm) by DLS of each zinc-based artificial SG. Peak values are displayed ± standard error of the mean. A positive control of protein microparticularization, namely GFP-H6, is also displayed in black. **D**. Protein release (in percentage) at 37 ºC from each zinc-based artificial SG upon time (from 0 to 168h). **E**. Chemical detection of zinc II (in μg) for each artificial SG. Peak values refer to the number of ug per mg of protein for each condition. **F**. Volume size distribution analysis (in nm; peak values displayed on top) by DLS of released soluble protein from each zinc-based artificial SG upon 24h and 37 ^{0}C incubation. **G**. Z-potential analysis (in mV; peak values displayed on top) of released soluble protein from panel F. **H**. *S. aureus* viability (in percentage) after 24h and 37 ^{0}C in presence of increasing concentrations (from 1.25 to 10 μM) of PaD, Pt5, T22 and GWH1 -GFP-H6 soluble proteins. Statistical significance achieved when $p < 0.05$ and expressed as * in respect to the control (0 concentration of soluble protein). **I**. *In vivo* biodistribution of zinc-based artificial SGs in Zebrafish larvae at 50 μg /mL for 48h. White bar refers to 600 μm.

For that, a humanized version of the GWH1 fusion protein was generated in which GFP was replaced by an human structural analogue (Figure 1A, 3A), namely the beta barrel domain of the human nidogen [36]. This protein segment had been successfully used by us as an structural replacement of GFP as scaffold for nanoparticle formation out of multidomain proteins acting as drug carries in cancer and it seemed adequate as scaffold for peptide display in nanoscale oligomers [37]. The resulting GWH1-NIDO-H6 nanoparticles of around 34 nm formed, upon addition of cationic Zn, higher order materials with final sizes comparable to those based on GFP (Figure 3B).

In non-infected larvae, neither the resulting granules nor soluble Zn, at molar amounts equivalent to those present in the granules, showed any sign toxicity (Figure 3C). When exposing the soluble protein nanoparticles to larvae infected with *S. maltophilia* the AM of the construct was confirmed as it reduced the rate of death promoted by the bacterial infection in a dose-dependent fashion (Figure 3D). When using 50 μg of GWH1-NIDO-H6 in form of secretory granules, the survival of the larvae was slightly higher (but not statistically significant) than when exposing the larvae to the plain soluble format of the construct (Figure 3E). Interestingly, the AM activity of the GWH1-NIDO-H6 granules was still detectable upon their addition to the media 24 h before infection, also rendering an important reduction in the mortality of infected larvae (Figure 3 F).

The results presented here demonstrate that the oligomeric assembly of AMP-containing, modular, H6-tagged proteins (Figure 1) does not prevent their biological activity (Figure 2, 3), that is retained even when these proteins form complex supramolecular materials at the submicron/micron scales and under complex media (Figure 3). In vitro, such materials allow the steady release of the forming protein in a oligomeric form (Figure 2 A, D), through kinetic patterns that are distinguishable depending on the cation used for assembly as clusters. Ionic Zn, as clustering agent, promotes a regular released in vitro during the testing period (almost three days; Figure 2D), and it is the agent, among those tested (also cationic Fe and Mg), for which the generated granules appear as more functional (Figure 2B). The slow release of drugs or antigens is an emerging strategy in innovative medicines especially appealing for the immune stimulation (Time is of the essence for vaccine success) of for the treatment of chronic or prolonged conditions (https://doi.org/10.1016/j.addr.2021.113957; https://doi.org/10.1007/s10544-019-0389-6). In this regard, developing biocompatible holding matrices is a main bottleneck (https://doi.org/10.1016/j.bioactmat.2021.09.033; https://doi.org/10.1155/2021/9011226, 10.30476/TIPS.2019.81604.1002). The use of Zn or related divalent cations as protein clustering agents allows the construction of micro-scale materials, which through their slow physiological disintegration release the forming building block protein, that is, the drug itself. Such a mechanism is found in nature as used by peptidic hormones in their body storage through secretory granules, mostly based on Zn. The absence of chemically heterogeneous holding materials represents an advantage over analogous systems. We have previously tested this principle in oncology, always under physiological conditions, namely subcutaneous injection. The secretion granules, ten, had been never tested out of the body (or cell culture). The plain nanoparticle version and the granular secretory versions, in the aquatic media inherent to the in vivo model tested here are similar in their capacity to protect zebrafish larvae from infection (Figure 3E). However, the tendency towards a stronger effect in the granular version (Figure 3E) combined with the stability of the granules in complex media (Figure 3F) allow envisaging AMPs, in such clustered formulation, as valuable therapeutic agents. This concept should not only apply in aquaculture but also in other clinical settings in which a slow protein drug release and multivalence might be required, especially in complex media.

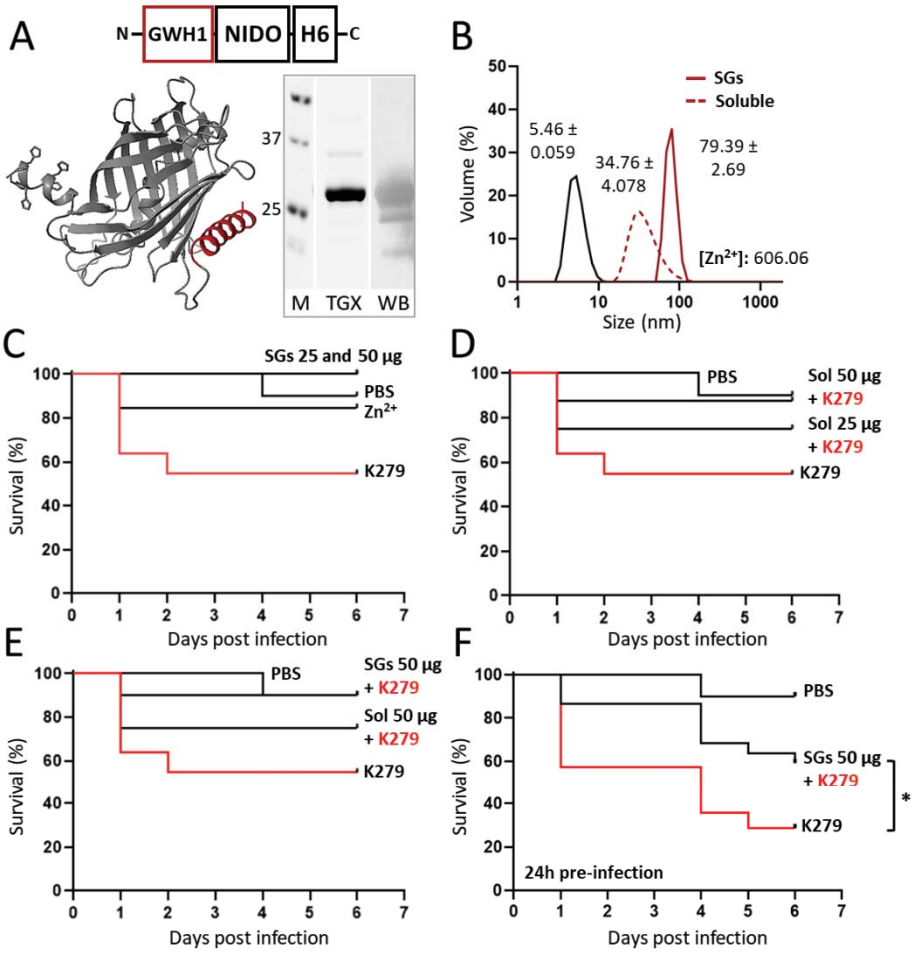

Figure 3. Humanizing AMP-based SGs, physicochemical characterization and in vivo AM effects. A. Schematic modular representation of the protein-based construction. Right. Integrity and purity analyzed by SDS-PAGE electrophoresis (TGX) and Western Blot (WB) respectively. Marker sizes are displayed in between 37 and 25 KDa. Left. 3D structure prediction. AMP sequence displayed in red. B. Volume size distribution analysis (nm) by DLS of both AMP-based nanoparticles and artificial SGs. Peak values are displayed ± standard error of the mean. A negative control of protein assembling, namely GFP-H6, is also displayed in black. The amount of zinc II chemically detected, [Zn^{2+}], is also displayed in (µg/mg of protein). C. Toxicity assay expressed as organism survival (in percentage) in adult Zebrafish upon 25-50 µg of artificial GWH1-NIDO-H6 SGs and free zinc until day 6 without infection. PBS is displayed as positive survival control and K279 (infective bacteria) as negative control. D. Effective dose screening expressed as organism survival (in percentage) in adult Zebrafish upon 25 and 50 µg of soluble GWH1-NIDO-H6 nanoparticles until day 6 post-infection with K279. PBS is displayed as positive survival control and K279 as negative control. E. Antibiotic effect expressed as organism survival (in percentage) in adult Zebrafish upon 50 µg of both soluble nanoparticles and artificial SG of GWH1-NIDO-H6 until day 6 post-infection with K279. PBS is displayed as positive survival control and K279 as negative control. F. Antibiotic effect expressed as organism survival (in percentage) in adult Zebrafish upon 50 µg of artificial SG of GWH1-NIDO-H6 (administered 24h pre-infection) until day 6 post-infection with K279. PBS is displayed as positive survival control and K279 as negative control. Statistical significance achieved when $p<0.05$ (*).

Acknowledgments

We are indebted to Agencia Estatal de Investigación (AEI) and to Fondo Europeo de Desarrollo Regional (FEDER) (grant PID2019-105416RB-I00/AEI/10.13039/501100011033 to EV and grant PID2020-116174RB-I00 to AV). This research was also supported by CIBER -Consorcio Centro de Investigación Biomédica en Red- (CB06/01/0014), Instituto de Salud Carlos III, Ministerio de Ciencia e Innovación. Protein production and nanoparticle characterization have been partially performed by the ICTS "NANBIOSIS", more specifically by the Protein Production Platform and by the Biomaterial Processing and Biostructuring Unit of CIBER in Bioengineering, Biomaterials & Nanomedicine (CIBER-BBN)/ IBB, at the UAB sePBioEs scientific-technical service (http://www.nanbiosis.es/portfolio/u1-protein-production-platform-ppp/). Molecular graphics and analyses were performed with UCSF Chimera, developed by the Resource for Biocomputing, Visualization, and Informatics at the University of California, San Francisco, with support from NIH P41- GM103311. AV received an ICREA ACADEMIA award.

References

1. Smerkova, K.; Dolezelikova, K.; Bozdechova, L.; Heger, Z.; Zurek, L.; Adam, V. Nanomaterials with active targeting as advanced antimicrobials. *WIREs Nanomedicine and Nanobiotechnology* **2020**, *12*, e1636, doi:https://doi.org/10.1002/wnan.1636.
2. Coates, A.; Hu, Y.; Bax, R.; Page, C. The future challenges facing the development of new antimicrobial drugs. *Nature Reviews Drug Discovery* **2002**, *1*, 895-910, doi:10.1038/nrd940.
3. Casciaro, B.; Cappiello, F.; Verrusio, W.; Cacciafesta, M.; Mangoni, M.L. Antimicrobial Peptides and Their Multiple Effects at Sub-Inhibitory Concentrations. *Current topics in medicinal chemistry* **2020**, doi:10.2174/1568026620666200427090912.
4. Chen, C.H.; Lu, T.K. Development and Challenges of Antimicrobial Peptides for Therapeutic Applications. *Antibiotics (Basel, Switzerland)* **2020**, *9*, doi:10.3390/antibiotics9010024.
5. Bhopale, G.M. Antimicrobial Peptides: A Promising Avenue for Human Healthcare. *Current pharmaceutical biotechnology* **2020**, *21*, 90-96, doi:10.2174/1389201020666191011121722.
6. Cao, J.; de la Fuente-Nunez, C.; Ou, R.W.; Torres, M.D.T.; Pande, S.G.; Sinskey, A.J.; Lu, T.K. Yeast-Based Synthetic Biology Platform for Antimicrobial Peptide Production. *ACS synthetic biology* **2018**, *7*, 896-902, doi:10.1021/acssynbio.7b00396.
7. Ashcheulova, D.O.; Efimova, L.V.; Lushchyk, A.Y.; Yantsevich, A.V.; Baikov, A.N.; Pershina, A.G. Production of the recombinant antimicrobial peptide UBI18-35 in Escherichia coli. *Protein Expres Purif* **2018**, *143*, 38-44, doi:https://doi.org/10.1016/j.pep.2017.10.011.

8. Liu, Y.; Zhan, Z.; Zhu, B.; Zheng, R.; Cheng, H.; Nie, Z. [Tandem expression and activity determination of antibacterial peptide Spinosan-C from Paa spinosa]. *Sheng wu gong cheng xue bao = Chinese journal of biotechnology* **2018**, *34*, 132-139, doi:10.13345/j.cjb.170153.

9. Dong, B.; Cheng, R.-Q.; Liu, Q.-Y.; Wang, J.; Fan, Z.-C. Multimer of the antimicrobial peptide Mytichitin-A expressed in Chlamydomonas reinhardtii exerts a broader antibacterial spectrum and increased potency. *J Biosci Bioeng* **2018**, *125*, 175-179, doi:https://doi.org/10.1016/j.jbiosc.2017.08.021.

10. Rezaei, S.; Hadadian, S.; Khavari-Nejad, R.A.; Norouzian, D. Recombinant Tandem Repeated Expression of S3 and SΔ3 Antimicrobial Peptides. *Reports of biochemistry & molecular biology* **2020**, *9*, 348-356, doi:10.29252/rbmb.9.3.348.

11. Sanchez-Garcia, L.; Martin, L.; Mangues, R.; Ferrer-Miralles, N.; Vazquez, E.; Villaverde, A. Recombinant pharmaceuticals from microbial cells: a 2015 update. *Microbial cell factories* **2016**, *15*, 33, doi:10.1186/s12934-016-0437-3.

12. Yatmaz, E.; Turhan, I. Carob as a carbon source for fermentation technology. *Biocatalysis and Agricultural Biotechnology* **2018**, *16*, 200-208, doi:https://doi.org/10.1016/j.bcab.2018.08.006.

13. Said, S.D.; Zaki, M.; Asnawi, T.M.; Novita, E. Single cell protein production by a local Aspergillus niger in solid state fermentation using rice straw pulp as carbon source: effects of fermentation variables. *IOP Conference Series: Materials Science and Engineering* **2019**, *543*, 012002, doi:10.1088/1757-899x/543/1/012002.

14. Amorim, C.C.; Farinas, C.S.; Miranda, E.A. Liquefied wheat bran as carbon source and inducer in high-solids submerged cultivation of Aspergillus niger for xylanase production. *Biocatalysis and Agricultural Biotechnology* **2019**, *21*, 101346, doi:https://doi.org/10.1016/j.bcab.2019.101346.

15. Wollensack, L.; Budzinski, K.; Backmann, J. Defossilization of pharmaceutical manufacturing. *Current Opinion in Green and Sustainable Chemistry* **2022**, *33*, 100586, doi:https://doi.org/10.1016/j.cogsc.2021.100586.

16. Agyei, D.; Ahmed, I.; Akram, Z.; Iqbal, H.M.; Danquah, M.K. Protein and Peptide Biopharmaceuticals: An Overview. *Protein and peptide letters* **2017**, *24*, 94-101, doi:10.2174/0929866523666161222150444.

17. Doll, T.A.P.F.; Dey, R.; Burkhard, P. Design and optimization of peptide nanoparticles. *J Nanobiotechnol* **2015**, *13*, doi:ARTN 73 10.1186/s12951-015-0119-z.

18. Overton, T.W. Recombinant protein production in bacterial hosts. *Drug discovery today* **2014**, *19*, 590-601, doi:10.1016/j.drudis.2013.11.008.

19. Lagasse, H.A.; Alexaki, A.; Simhadri, V.L.; Katagiri, N.H.; Jankowski, W.; Sauna, Z.E.; Kimchi-Sarfaty, C. Recent advances in (therapeutic protein) drug development. *F1000Research* **2017**, *6*, 113, doi:10.12688/f1000research.9970.1.

20. Ferrer-Miralles, N.; Domingo-Espin, J.; Corchero, J.L.; Vazquez, E.; Villaverde, A. Microbial factories for recombinant pharmaceuticals. *Microbial cell factories* **2009**, *8*, 17, doi:10.1186/1475-2859-8-17.

21. Thapa, R.K.; Diep, D.B.; Tønnesen, H.H. Nanomedicine-based antimicrobial peptide delivery for bacterial infections: recent advances and future prospects. *Journal of Pharmaceutical Investigation* **2021**, *51*, 377-398, doi:10.1007/s40005-021-00525-z.

22. Serna, N.; Carratalá, J.V.; Parladé, E.; Sánchez-Chardi, A.; Aviñó, A.; Unzueta, U.; Mangues, R.; Eritja, R.; Ferrer-Miralles, N.; Vazquez, E.; et al. Developing Protein–Antitumoral Drug Nanoconjugates as Bifunctional Antimicrobial Agents. *ACS applied materials & interfaces* **2020**, *12*, 57746-57756, doi:10.1021/acsami.0c18317.

23. Teixeira, M.C.; Carbone, C.; Sousa, M.C.; Espina, M.; Garcia, M.L.; Sanchez-Lopez, E.; Souto, E.B. Nanomedicines for the Delivery of Antimicrobial Peptides (AMPs). *Nanomaterials* **2020**, *10*, doi:10.3390/nano10030560.

24. Li, Y.; Wang, Y.; Huang, G.; Gao, J. Cooperativity Principles in Self-Assembled Nanomedicine. *Chemical reviews* **2018**, *118*, 5359-5391, doi:10.1021/acs.chemrev.8b00195.

25. Ghaeini-Hesaroeiye, S.; Boddohi, S.; Vasheghani-Farahani, E. Dual responsive chondroitin sulfate based nanogel for antimicrobial peptide delivery. *International journal of biological macromolecules* **2020**, *143*, 297-304, doi:https://doi.org/10.1016/j.ijbiomac.2019.12.026.

26. Parilti, R.; Caprasse, J.; Riva, R.; Alexandre, M.; Vandegaart, H.; Bebrone, C.; Dupont-Gillain, C.; Howdle, S.M.; Jérôme, C. Antimicrobial peptide encapsulation and sustained release from polymer network particles prepared in supercritical carbon dioxide. *Journal of colloid and interface science* **2018**, *532*, 112-117, doi:https://doi.org/10.1016/j.jcis.2018.07.125.

27. Yang, G.; Huang, T.; Wang, Y.; Wang, H.; Li, Y.; Yu, K.; Dong, L. Sustained Release of Antimicrobial Peptide from Self-Assembling Hydrogel Enhanced Osteogenesis. *Journal of biomaterials science. Polymer edition* **2018**, *29*, 1812-1824, doi:10.1080/09205063.2018.1504191.

28. Serna, N.; Carratalá, J.V.; Conchillo-Solé, O.; Martínez-Torró, C.; Unzueta, U.; Mangues, R.; Ferrer-Miralles, N.; Daura, X.; Vázquez, E.; Villaverde, A. Antibacterial Activity of T22, a Specific Peptidic Ligand of the Tumoral Marker CXCR4. *Pharmaceutics* **2021**, *13*, doi:10.3390/pharmaceutics13111922.

29. Carratala, J.V.; Brouillette, E.; Serna, N.; Sanchez-Chardi, A.; Sanchez, J.M.; Villaverde, A.; Aris, A.; Garcia-Fruitos, E.; Ferrer-Miralles, N.; Malouin, F. In Vivo Bactericidal Efficacy of GWH1 Antimicrobial Peptide Displayed on Protein Nanoparticles, a Potential Alternative to Antibiotics. *Pharmaceutics* **2020**, *12*, doi:10.3390/pharmaceutics12121217.

30. Sánchez, J.; López-Laguna, H.; Álamo, P.; Serna, N.; Sánchez-Chardi, A.; Nolan, V.; Cano-Garrido, O.; Casanova, I.; Unzueta, U.; Vazquez, E.; et al. Artificial inclusion bodies for clinical development *Advanced science* **2020**, *7*, 1902420, doi:DOI: 10.1002/advs.201902420.

31. Chen, Y.L.; Li, J.H.; Yu, C.Y.; Lin, C.J.; Chiu, P.H.; Chen, P.W.; Lin, C.C.; Chen, W.J. Novel cationic antimicrobial peptide GW-H1 induced caspase-dependent apoptosis of hepatocellular carcinoma cell lines. *Peptides* **2012**, *36*, 257-265, doi:10.1016/j.peptides.2012.05.011.

32. Irazazabal, L.N.; Porto, W.F.; Fensterseifer, I.C.M.; Alves, E.S.F.; Matos, C.O.; Menezes, A.C.S.; Felicio, M.R.; Goncalves, S.; Santos, N.C.; Ribeiro, S.M.; et al. Fast and potent bactericidal membrane lytic activity of PaDBS1R1, a novel cationic antimicrobial peptide. *Biochimica et biophysica acta. Biomembranes* **2019**, *1861*, 178-190, doi:10.1016/j.bbamem.2018.08.001.

33. Ding, Y.; Liu, X.; Bu, L.; Li, H.; Zhang, S. Antimicrobial–immunomodulatory activities of zebrafish phosvitin-derived peptide Pt5. *Peptides* **2012**, *37*, 309-313, doi:https://doi.org/10.1016/j.peptides.2012.07.014.

34. Lopez-Laguna, H.; Unzueta, U.; Conchillo-Sole, O.; Sanchez-Chardi, A.; Pesarrodona, M.; Cano-Garrido, O.; Volta, E.; Sanchez-Garcia, L.; Serna, N.; Saccardo, P.; et al. Assembly of histidine-rich protein materials controlled through divalent cations. *Acta biomaterialia* **2019**, *83*, 257-264, doi:10.1016/j.actbio.2018.10.030.

35. López-Laguna, H.; Sánchez, J.M.; Carratalá, J.V.; Rojas-Peña, M.; Sánchez-García, L.; Parladé, E.; Sánchez-Chardi, A.; Voltà-Durán, E.; Serna, N.; Cano-Garrido, O.; et al. Biofabrication of functional protein nanoparticles through simple His-tag engineering. *ACS Sustainable Chemistry & Engineering* **2021**, *9*, 12341-12354, doi:10.1021/acssuschemeng.1c04256.

36. Human Nidogen: Complete Amino Acid Sequence and Structural Domains Deduced from cDNAs, and Evidence for Polymorphism of the Gene. *DNA* **1989**, *8*, 581-594, doi:10.1089/dna.1989.8.581.

37. Alamo, P.; Cedano, J.; Conchillo-Sole, O.; Cano-Garrido, O.; Alba-Castellon, L.; Serna, N.; Avino, A.; Carrasco-Diaz, L.M.; Sanchez-Chardi, A.; Martinez-Torro, C.; et al. Rational engineering of a human GFP-like protein scaffold for humanized targeted nanomedicines. *Acta biomaterialia* **2021**, doi:10.1016/j.actbio.2021.06.001.

Annex 5

Insights on the emerging biotechnology of histidine-rich peptides

Hèctor López-Laguna, Eric Voltà-Durán, Eloi Parladé, Antonio Villaverde, Esther Vázquez, and Ugutz Unzueta

Biotechnology Advances (2021) · Impact Factor (17.681) · Quartile (Q1)

Objective 4

To review all the extracted knowledge and condense it as practical guidelines for the scientific community.

As for the already presented study 7, the histidine tag-divalent cation principle allows to formulate scalable, biocompatible, well-defined, and efficient protein-based materials in a reproducible manner. An extensive study of divalent cation's versatility as gluing entities for biomedical purpose has been presented, but not for the histidine tag.

Thus, and with the aim to expose the two sides of the same coin, this work has been focused on describing practical guidelines for the scientific community to address the use of histidine tag, as gold standard, to manufacture efficient biomaterials for precision medicine, exposing all its biochemical potential.

Biotechnology Advances 54 (2022) 107817

Contents lists available at ScienceDirect

Biotechnology Advances

journal homepage: www.elsevier.com/locate/biotechadv

Research review paper

Insights on the emerging biotechnology of histidine-rich peptides

Hèctor López-Laguna [a,b,c,1], Eric Voltà-Durán [a,b,c,1], Eloi Parladé [a,b,c,1], Antonio Villaverde [a,b,c,*], Esther Vázquez [a,b,c,*], Ugutz Unzueta [b,c,d,*]

[a] Institut de Biotecnologia i de Biomedicina, Universitat Autònoma de Barcelona, Bellaterra, 08193 Barcelona, Spain
[b] Departament de Genètica i de Microbiologia, Universitat Autònoma de Barcelona, Bellaterra, 08193 Barcelona, Spain
[c] CIBER de Bioingeniería, Biomateriales y Nanomedicina (CIBER-BBN), Spain
[d] Biomedical Research Institute Sant Pau (IIB Sant Pau), Sant Antoni Mª Claret 167, 08025 Barcelona, Spain

ARTICLE INFO

Keywords:
Recombinant protein
Modular protein
Biomaterials
Biosensing
Nanobiotechnology

ABSTRACT

In the late 70's, the discovery of the restriction enzymes made possible the biological production of functional proteins by recombinant DNA technologies, a fact that largely empowered both biotechnological and pharmaceutical industries. Short peptides or small protein domains, with specific molecular affinities, were developed as purification tags in downstream processes to separate the target protein from the culture media or cell debris, upon breaking the producing cells. Among these tags, and by exploiting the interactivity of the imidazole ring of histidine residues, the hexahistidine peptide (H6) became a gold standard. Although initially used almost exclusively in protein production, H6 and related His-rich peptides are progressively proving a broad applicability in novel utilities including enzymatic processes, advanced drug delivery systems and diagnosis, through a so far unsuspected adaptation of their binding capabilities. In this context, the coordination of histidine residues and metals confers intriguing functionalities to His-rich sequences useable in the forward-thinking design of protein-based nano- and micro-materials and devices, through strategies that are comprehensively presented here.

1. Introduction

Protein purification is an essential practice in biotechnology, drug development and proteomics, and a late downstream step in the recombinant protein production task flow (Garg et al., 1991; Gräslund et al., 2008). Considering the diversity of cell factories and target proteins in the protein production scenario, simple, one-step separation protocols are ideally required to fulfill the demands for generality, scalability, and high throughput (Fig. 1A). In this context, affinity tags, namely peptides or proteins with selectivity for specific binders have been incorporated to recombinant proteins by genetic fusion, usually at either the amino or carboxy termini, to selectively retain the whole fusion in affinity chromatography systems based on immobilized ligands (Amarasinghe and Jin, 2015; Kimple and Sondek, 2004; Mishra, 2020). Essentially, any pair of interactors involving at least a peptidic partner should be suitable for the design of entrapment protocols to retain a specific protein among complex molecular mixtures such as cell lysates or culture media.

Since the 70's (Porath et al., 1975) and along decades (Gaberc-Porekar and Menart, 2001; Porath, 1992; Riguero et al., 2020; Spriestersbach et al., 2015; Sulkowski, 1985), immobilized metal affinity chromatography (IMAC) has proved to be a robust choice method for preparative protein purification because of its versatility, cost effectiveness, scalability and simplicity, compliant with high-throughput requirements. The IMAC concept is supported by the relatively strong interactions between transition metal ions (namely Ni^{2+}, Cu^{2+}, Zn^{2+} and Co^{2+}) and the side chains of some particular amino acids. Among them, the amino acid histidine is the tightest binder through the electron donor group on its imidazole ring, that forms coordination bonds with the metal (Watly et al., 2014). If immobilized in a matrix, the metal acts as a molecular hook for histidine-rich protein segments, that can be further eluted from the matrix by adjusting the buffer pH or by adding excess imidazole. Since series of consecutive histidine residues confer a much tighter binding than isolate amino acids (Bornhorst and Falke, 2000; Gaberc-Porekar and Menart, 2005), polyhistidine stretches and specially H6, have become gold standard affinity tags for protein purification

* Corresponding authors.
E-mail addresses: antoni.villaverde@uab.cat (A. Villaverde), esther.vazquez@uab.cat (E. Vázquez), uunzueta@santpau.cat (U. Unzueta).
[1] Equally contributed.

https://doi.org/10.1016/j.biotechadv.2021.107817
Received 10 April 2021; Received in revised form 16 July 2021; Accepted 16 August 2021
Available online 19 August 2021
0734-9750/© 2021 The Author(s). Published by Elsevier Inc. This is an open access article under the CC BY-NC-ND license (http://creativecommons.org/licenses/by-nc-nd/4.0/).

(Table 1). In this sense, smaller tags with three to five histidine residues can also serve for this purpose (López-Laguna et al., 2019) at the expense of a weaker binding. On the other hand, longer histidine tags (e.g. H8 or H10) are also an alternative when high purity is needed and optimization of H6-tags is not sufficient (Grisshammer and Tucker, 1997). Several downsides, however, include the possibility of inhibiting protein functions, inducing conformational changes, decreasing the protein expression, or requiring higher imidazole concentrations to elute, which ultimately lead to unstable proteins in the solution (Mohanty and Wiener, 2004). Nevertheless, it is historically assumed that H6 is an appropriate choice when designing recombinant proteins unless previous concerns regarding the desired number of histidine residues exist. The binding mediated by histidine residues occurs since at physiological pH, the molecular coordinative foci of imidazole rings are found in the δ1-Nitrogen atom, which is capable to act as a nucleophilic center and share two unpaired electrons with the desired targeting molecule, which will act as an electrophilic Lewis acid. In particular, the d-orbitals of these electrophiles allow the formation of coordinative bonds whose geometrical structures promote the simultaneous gluing of several imidazole rings from adjacent His residues (Valenti et al., 2006). This type of interaction is strongly held into the structure formed by the molecular partners in the complex, supporting mechanical forces that sustain the applicability of polyhistidine tails as molecular ligands (Lopez-Laguna et al., 2019).

2. Advanced systems for protein purification

The traditional IMAC, with divalent cations immobilized on agarose resin beads, basically Sepharose, remains as a conventional protocol (Loughran et al., 2017). Here, several divalent cations (Co^{2+}, Cu^{2+}, Zn^{2+}, Ni^{2+}) are useful for purification purposes and each of them shows different binding affinity towards histidine. Its choice therefore, depends on the final application. Co^{2+} for example, forms less stable coordination bonds with histidine residues and is especially suitable when high protein purity is required. On the other hand, Cu^{2+} has the greatest affinity and is useful for enriching low abundant proteins from crude lysates, prior to other purification steps. Ni^{2+} and Zn^{2+} have an intermediate affinity, being nickel the most extended choice (Riguero et al., 2020). In all these cases, divalent cations might suffer from leakage from IMAC columns and elute with the protein of interest. For some particular applications, the presence of metal ions may affect protein activity or promote undesired reactions. Therefore, in these cases, we must ensure that the final product is free of divalent cations. In this sense, some commercial protein purification companies have already developed resins that show tighter bonds with the divalent cation and propose strategies to diminish its presence in the eluted fractions (e.g. using prepacked columns, pre-washing the column with elution buffer prior to protein purification or connecting an uncharged column just after the purification column,in series, to catch leaked ions). An alternative solution is to eliminate eluted ions during the protein dialysis step using a chelator such as EDTA, although this chemical compound can also be a contaminant for the protein of interest and it must be subsequently removed (Mónico et al., 2017).

Advanced strategies based on this principle have been developed to purify His-tagged proteins in a more efficient, sustainable, easier or cheaper manner. In this regard, magnetic nanoparticles have emerged as a simple, fast, and high-throughput system to purify proteins from complex bacterial or animal cell lysates by magnetic separation when functionalized with linker-chelating metal ions (Xu et al., 2004), nickel silicate (Wang et al., 2014a) or simply a nickel coating (Minkner et al., 2020). In 2019, Schwaminger and collaborators went a step further with a proof of principle of a magnetic one-step purification system, using non-functionalized bare iron oxide nanoparticles (BIONs) (Schwaminger et al., 2019). Besides IMAC, liquid-liquid extraction with affinity ionic liquids has been also used for the same purpose, resulting in a suitable method for large-scale purification (Ren et al., 2015). His-tagging has served for the purification of structures more complex than single polypeptides, such as bacterial outer membrane vesicles (OMVs) (Alves et al., 2017), virus-like particles (Gupta et al., 2020) or bacteriophages (Ceglarek et al., 2013).

An additional step in the enhancement of IMAC purification exploits nitrilotriacetic (NTA)-Ni^{2+}-His tag coordination complexes (Fig. 1B). NTA is an aminopolycarboxylic acid with a tripodal tetradentate nature, able to form coordinative interactions with divalent metal ions in a bonding type called chelation. The NTA-metal ion complexes can specifically interact with certain chemically compatible amino acid residues. Among all different options, imidazole rings from histidine residues are extremely good targets, as they offer two non-bonded valences on their surface that are available for further metal ion coordination. In a general manner, more-than-two NTA (bis or tris) structures are needed to ensure a sufficient strong binding between ion and histidine (Fig. 1B). As a result, ternary bis or tris NTA-metal ion-histidine stable complexes are formed. From here, the chemical versatility of NTA allows this technology to be used in a plethora of different protein engineering fields (Wijeratne et al., 2016).

Although poorly studied in general terms, His-rich tags are suspected to have potential undesired impacts on the structure, function and immunogenicity of some of the target proteins (Khan et al., 2012; Singh et al., 2020). Such side-effects of His-tagging, mild and case-dependent, can be solved by the proteolytic removal of the peptide upon purification, driven by a protease target site introduced during the genetic fusion (Goh et al., 2017) or by regulatable, Ni^{2+}-mediated hydrolysis (Abd Elhameed et al., 2019). More details about the potential bottlenecks generated by His-tagging are discussed below. Because of these issues, alternative affinity tags have been extensively used, such as small peptides (FLAG, c-Myc, Strep-Tag) or longer polypeptidic ligands such

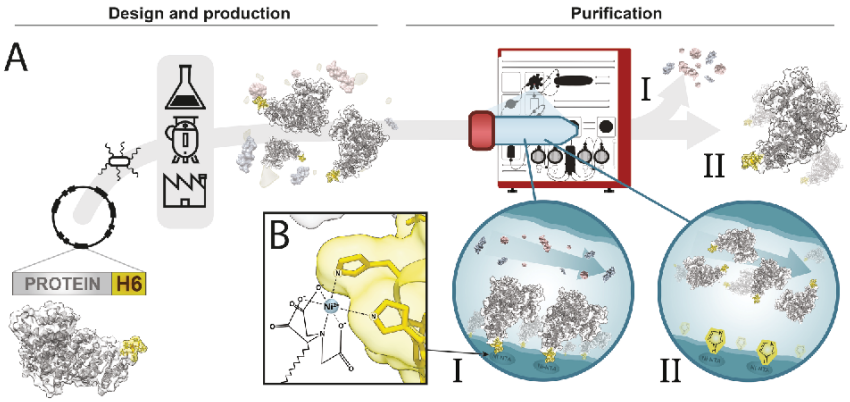

Fig. 1. A. Schematic process to obtain a pure recombinant polypeptide (e.g. His-tagged Human Serum Albumin, PDB: 1AO6) by means of a His-tag genetically fused to the target protein. The sequence of activities involves gene design (in which the desired protein-encoding gene is fused to the selected tag), cloning, transformation in a capable cell factory, production in an adequate scale (lab, pilot or industrial), His-tag based immobilization in an IMAC column (I) and subsequent displacement using imidazole (II). B. Zoomed representation of the coordination bonding between Ni-NTA and the histidine imidazole ring.

Table 1
A summary of applications of His-rich tags in protein sciences.

Application category	Strategy	Used material or technical basis	Approaches	Representative references
Protein purification	Traditional Chromatography	Immobilized Metal Ion Affinity Chromatography (IMAC)	Sepharose beads with immobilized divalent metal ions	Loughran et al. (2017)
	Alternative Material-based strategies	Magnetic NPs	- Linker chelated metal ion NPs. - Nickel (II) Silicate NPs. - Nickel (II) Coated NPs. - Iron oxide NPs (BIONs).	Minkner et al. (2020); Schwaminger et al. (2019); Wang et al. (2014a); Xu et al. (2004)
	Alternative Liquid-based strategies	Affinity ionic liquid (AIL)	Liquid-liquid extraction with affinity ionic liquids	Ren et al. (2015)
Protein labelling and detection	Traditional Ab-protein recognition	Western Blot	Anti His-tag Abs emitting detectable signals	Hirano (2012); Kreisig et al. (2014)
	His-tag radiolabeling	$^{99m}Tc(CO)_3$-His-tag	Technetium-99 attached to His-tags, emitting radioactive signals	Garousi et al. (2020)
	scFv-Bioimaging	Histidine tagged monoclonal scFv	scFv Abs recognizing biological compounds and His-rich tags allowing cell or tissue imaging (e.g. by immunofluorescence, immunoelectron microscopy, ELISA or Western Blot)	Min and Yamabhai (2020)
	Mono or Tris NTA-based complexes	Signaling compound-NTA-Ni^{2+}-His-tag	NTA- Ni^{2+} complexes label His-tagged proteins and conjugated compounds (e.g. $ATTO_X$, $ALEXA_X$, OG488, FEW_{646}, BODIPY, arylazide, QD and gold nanoparticles) emit detectable signals	Banerjee et al. (2016); Chao et al. (2017); Kitai et al. (2011); Kollmannsperger et al. (2016); Soh (2008); Wang et al. (2014b); Zheng et al. (2016)
Protein immobilization	Basic Immobilization strategies for biosensing	Surface-NTA-Ni^{2+}-His tagged proteins	NTA-Ni^{2+} complexes conjugated to chemically adequate surfaces allowing the detection of His-tagged proteins, nucleic acids, biomarkers, toxins, immunoglobulins or pesticides	Dai et al. (2018); Kang et al. (2017); Liu et al. (2010); Mikula et al. (2018); Povedano et al. (2020); Ravikumar et al. (2018); Vallina-Garcia et al. (2007); Zhang et al. (2014)
	Alternative Immobilization strategies for biosensing	Au-coated probes-NTA-Co^{3+}-His-tagged proteins	Au-coated probes conjugated with NTA-Co^{3+} complexes used to create SPR Optic biosensors immobilizing His-tagged antigens	Horta et al. (2020)
		Chitosan-Zn^{2+}-His-tagged proteins in a quartz crystal microbalance (QCM)	Chitosan-Zn^{2+} complex immobilize and allow the detection of His tagged mycotoxin in hapten biosensors using the QCM technology	Soleri et al. (2015)
	Biocatalysis in glass surfaces	Fe^{3+} porosity glass carriers with immobilized His-tagged enzymes	Controlled porosity Fe^{3+} glass carriers used to immobilize His-tagged enzymes to catalyze reactions	Pellis et al. (2017)
	Biocatalysis in self-immobilized insoluble enzymes	Zn^{2+} assisted generation of reusable insoluble protein microgranules	Generation of H6-tagged β-galactosidase microscale granules with enhanced stability	Sanchez et al. (2021)
	Biocatalysis in bioreactors	Semicontinuous or continuous -flow bioreactors with His-tag immobilized enzymes	His-tagged enzymes immobilized in different functioning bioreactors promoting successive and multi-step product transformations	Britton et al. (2017); Plz et al. (2020)
		Microfluidic bioreactors with magnetic beads attaching His-tagged enzymes	Microfluidic packed-bed bioreactors using magnetic beads to attach His-tagged enzymes to perform desired enzymatic reactions	Peschke et al. (2019)
	Bioengineering	Glass-plate Ni^{2+} chelated surface with immobilized His-tagged growth factor	Glass-plate Ni^{2+} surfaces used to enhance *in vitro* proliferation of human mesenchymal cells by immobilizing FGF	Shakya et al. (2020)
Protein site-specific conjugation	Site specific conjugation by metal cation-coordination.	Desired compound-NTA-Ni^{2+}-His-tagged proteins	Biological compounds or materials such as DNA, nanolipoproteins (MPLA-NiNLP), Au-polymer NPs or QD can be chemically attached to NTA-Ni^{2+} complexes and be specifically coordinated to His-rich tags from proteins	Goodman et al. (2009); Rai et al. (2016); Shimada et al. (2008); Wilkins et al. (2019); Zheng et al. (2016)
	Site specific conjugation by alkynyl group addition	Baylis-Hillman ester - ternary NTA-Ni^{2+}	Ternary NTA-Ni^{2+} complexes can be used to bring an alkynyl group-carrying ester moiety near the imidazole ring of a desired histidines for its two stage derivatization with molecules.	Liu and Melman, 2013)
	Site specific conjugation by histidines *bis*-alkylation	Cation free Sulfone – His *bis*-alkylation.	Sulfone-mediated bis-alkylation of PEG-*bis*-sulfone or PEG_{10}-mono-sulfone molecules to His-tag in desired proteins (e.g. interferon α-2a or anti-TNFα domain Ab)	Cong et al. (2012); Peciak et al. (2019)
	Site specific conjugation by cyclic ketone generation	Michael addition of 2-cyclohexanone in His residue.	Orthogonal late-stage installation of aminooxy functionalized NMR tags or dyes in exposed His residues on protein surface (e.g. lysozyme C)	Joshi and Rai (2019)
	Site specific conjugation by histidine acylation.	D-gluconic acid δ-lactone (GDL) and 4-methoxyphenil esters for specific acylation of amino-terminal His-tags ($GHHH_n$).	Site specific acylation allows the direct addition of a biotin or an azide functional group for its subsequent reaction with DBCO-functionalized molecules into His-rich tags of different proteins (e.g. GFP, MBP or SUMO).	Martos-Maldonado et al. (2018)
Protein assembling	Ion-based protein gluing to manufacture soluble nanostructures	His-tag/divalent cation/His-tag	Divalent cations used as coordinative agents of His-tags (interacting with the δ1 nitrogen of the histidine imidazole ring) and promoting	Bai et al. (2013); Brodin et al. (2015); Cespedes et al. (2018); Dexter et al. (2006); Diaz et al. (2018); Haglin et al. (2017);

(*continued on next page*)

Table 1 (*continued*)

Application category	Strategy	Used material or technical basis	Approaches	Representative references
			adequate nanostructuring (10-350 nm, e.g. dimers, coiled coils, nanodiscs, nanocapsules, nanorings, helical nanotubes, nanowires, interfacial films or tumor targeted NPs) in a reversible way (upon addition of EDTA)	Maniaci et al. (2019); Serna et al. (2020a); Serna et al. (2020c); Tunn et al. (2018); Unzueta et al. (2020); van Eldijk et al. (2016); Zhang et al. (2012)
	Ion-based protein gluing to manufacture insoluble functional depots	His-tag/divalent cation/His-tag	Divalent cations used as precipitator agents to create functional secretory-like granules at the microscale in a reversible way (upon addition of EDTA)	Chen et al. (2019); Jiang et al. (2011); Sanchez et al. (2020); Serna et al. (2020b)

Ab: Antibody; scFv: Single-chain variable fragments; Ni^{2+}: Nickel (II); NTA: Nitrilotriacetic acid; $ATTO_X$ & $ALEXA_X$: $ATTO_{565}$ or $ATTO_{655}$ and $ALEXA_{647}$ or $ALEXA_{488}$; QD: Quantum Dots; SPR: Surface plasmon resonance; Au: Gold; Co^{3+}: Cobalt (III); FGF: Fibroblast growth factor; DTPC: DNA-template protein conjugation strategy; PEG: Polyethylene Glycol; NMR: Nuclear magnetic resonance; GFP: Green fluorescent protein; MBP: Maltose-binding protein; SUMO: Small ubiquitin-like modifier protein; EDTA: Ethylenediaminetetraacetic acid; DBCO: Dibenzocyclooctyne.

as Maltose Binding Protein (MBP) or Glutathione S-Transferase (GST) (Pina et al., 2014). Also, several novel tags are already under development (Spy Tag, Strach Binding Protein, Fluropatite, Diatomite, Beta-GRP) trying to reduce protein contaminants and/or production costs (Khairil Anuar et al., 2019; Wood, 2014). Related to that, a specific solution to increase His-tagged protein purity is the use of low background cell factory strains, such as *Escherichia coli* LOBSTR, which is engineered to eliminate major His-rich contaminants (Andersen et al., 2013).

3. Protein labelling and detection

3.1. Protein immunodetection

Specific protein recognition appears as a prior method in proteomic profiling, and monoclonal or polyclonal antibody (Ab)-protein immunodetection has raised as one of the most popular methodologies for protein identification (Signore et al., 2017). Upon Western Blot, protein detection ensures adequate polypeptide identification and quantification even in complex samples (Obermaier et al., 2015). Considering the large number of H6-tagged recombinant proteins (Loughran et al., 2017), the importance of using anti-polyhistidine tag antibodies has emerged in parallel (Kreisig et al., 2014). In anti-H6-based detection techniques (Table 1), a primary monoclonal Ab recognizes the H6 tail, followed by a secondary Ab that recognizes the first attached Ab (Fig. 2A). Primary (or secondary, binding to primary) Abs are typically labelled with organic fluorophores (e.g. Alexa Fluor) or enzymes (e.g. alkaline phosphatase and peroxidase) that emit a measurable signal (Hirano, 2012) allowing its quantitative detection.

3.2. Tracking oriented protein labelling

Interestingly, the popularity of using NTA-Ni^{2+}-His tag coordination complexes in protein purification has uplifted in novel protein engineering fields (Johnson and Martin, 2005) and single molecule imaging, along with recent H6 radiolabeling (e.g. $^{99m}Tc(CO)_3$) (Garousi et al., 2020) and single-chain variable fragments (scFv) of monoclonal Abs bioimaging (Min and Yamabhai, 2020). Novel formulations of NTA-based complexes are being designed to ensure precise protein detection at sub-nanomolar concentrations and to create clear pictures of protein spatiotemporal behavior under physiological conditions (Kollmannsperger et al., 2016). The specific conjugation of chromophores (e.g. $ATTO_{565}$, $ATTO_{655}$, $ALEXA_{647}$, $ALEXA_{488}$, OG_{488}, and FEW_{646} (Kollmannsperger et al., 2016; Soh, 2008)), small molecules (e.g. distylryl BODIPY or arylazide crosslinkers (Chao et al., 2017)) and other nanoscale materials (e.g. quantum dots, QD (Banerjee et al., 2016) or gold nanoparticles (Kitai et al., 2011)) to these complexes allows exploring biological fundamental processes such as viral infections, protein dynamics and mobility (e.g. QD-NTA-Ni^{2+} labelling respiratory syncytial virus (Zheng et al., 2016), or Au NPs NTA-Ni^{2+} labelling dynactin subunit p62 (Kitai et al., 2011)), protein function (e.g. labelling the DNA repair protein XPA122 (Chao et al., 2017)), subcellular location (e.g. tracing extracellular and intracellular histidine-tagged proteins (Wang et al., 2014b), protein targeting, biodistribution and general protein pharmacokinetics (Garousi et al., 2020). The tripodal tetradentate nature of NTA allows the eventual interaction with exposed H6 tails (Raghunath and Dyer, 2019). Besides the binding affinity of mono-NTA is sufficient for IMAC needs (K_D: 10×10^{-6} M), the molecular labelling of polyhistidine-tagged proteins requires tighter associations to form stable complexes useful in biological conditions. Because of that, three NTAs are usually associated, named Tris-NTA, to provide sufficient binding affinity (K_D: 20×10^{-9} M (Huang et al., 2006)) and to increase the complex stability up to 4 orders of magnitude, thanks to the multivalency of the system. Tris-NTA-Ni^{2+} coordinated complexes are being used by the scientific community to interact with inner-cell histidine tagged proteins without affecting endogenous processes, presenting high specificity and low cell toxicity (Kollmannsperger et al., 2016). These complexes can be bound to H6-tagged cell penetrating peptides (CPPs) to promote cell entrance, and afterwards, spontaneously change its preference to bind H10-tagged proteins of interest inside the cell, due to the 10-fold higher binding affinity of the longer tag (Schneider and Hackenberger, 2017). Also, NTA-Ni^{2+}-red fluorescent probes or similar (e.g. AB or BODIPY) complexes can enter into bacteria cells to selectively label histidine-tagged proteins by using appropriate amounts of detergents (e.g. Tween 80 (Chao et al., 2017)). The traditional proteomic profiling techniques, together with protein radio-labelling methods and NTA-Ni^{2+}-based complexes (Fig. 2B), outpoint the huge versatility and applicability of using H6 (or related tags) as labelling target for protein characterization and *in situ* functional imaging.

4. Protein immobilization in biosensing, biocatalysis and bioengineering

Protein immobilization onto solid surfaces has several applications in protein-based biocatalysis, biosensing and bioengineering (Table 1). In this sense, among the growing variety of developed protein immobilization methods, including entrapment, adsorption, cross-linking or covalent binding, affinity techniques provide a highly specific, controllable, and reversible way to anchor proteins to surfaces without losing their functional structure (Ley et al., 2011; Zhang et al., 2014). Additional benefits of this approach are protein stabilization, protection against environmental stresses and reusability in successive processes (Rodrigues et al., 2013). Taking advantage of their affinity towards divalent metal cations, surfaces or nanomaterials can be decorated with His-tagged proteins, rendering uniformly oriented protein layers with controlled spatial distribution and without multipoint attachments that could impair their functionality (Ley et al., 2011). This chemistry works well under mild conditions, at physiological pH and in presence of salts,

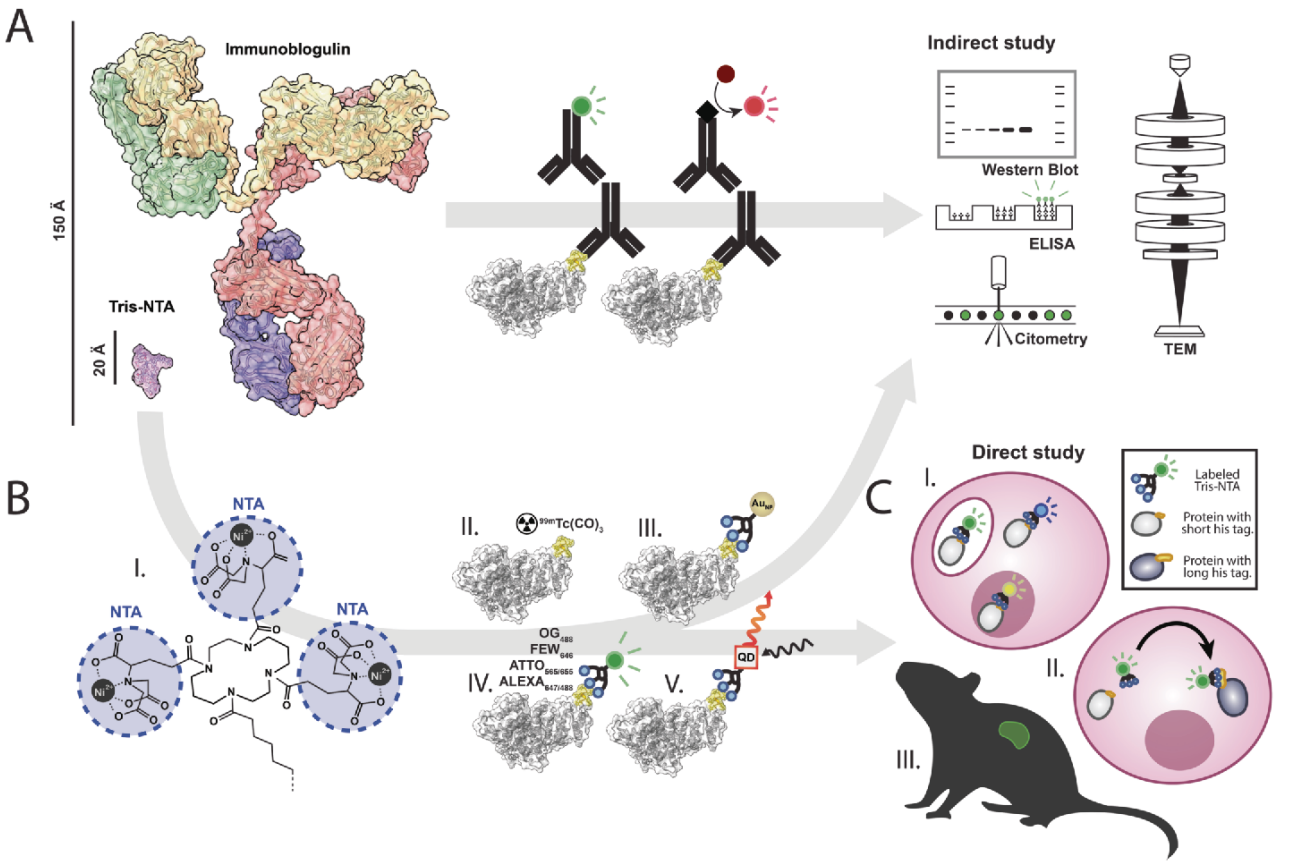

Fig. 2. A. Overview of size, common labeling strategies, and popular detection techniques available for the study of His-tagged proteins using antibodies. B. Size comparison and structure of the Tris-NTA ligand (I), along with common labeling approaches (radiolabeling with Technetium 99m (II) or Tris-NTA-based labeling with gold nanoparticles (III), fluorescent dyes (IV) and quantum dots (V)). C. Schematic representation of direct techniques to study subcellular localization of his-tagged proteins *in vitro* (I), co-localization of different his-tagged proteins *in vitro* (II), or protein bioaccumulation in *in vivo* models (III).

making it appropriate for applications in biological interfaces (Wegner et al., 2016). The conventional procedure to immobilize His-tagged proteins involves an earlier step of surface functionalization with NTA, followed by the incorporation of the divalent cation, typically Ni^{2+} (Liu et al., 2010). In such process, a deep consideration of surface pretreatment, metal leaching and unwanted dissociation of the His-rich tag from the divalent cation-NTA pair is suited (Ravikumar et al., 2018). In this regard, a plethora of procedures are emerging to solve these issues whilst maintaining the benefits of His-tagged immobilization. For instance, alternative strategies involve the use of multiple NTA groups (Lata et al., 2005), longer His-rich tags (Lata et al., 2005), different chelators (e.g. chitosan (Ravikumar et al., 2018)), acbztacn (Johnson and Martin, 2005), 1-acetato-4-benzyl-triazacyclononane (Wollenberg et al., 2014), iminodiacetatic acid (Zhao et al., 2017), NiO (Jia et al., 2016) and polydopamine (Yang et al., 2015)) or the conversion to different metal oxidation states (namely Fe^{3+} (Pellis et al., 2017) and Co^{3+} (Wegner et al., 2016)). In this last case, the process requires a first-step of complexation between histidines and a Co^{2+} ion, followed by a subsequent Co^{2+} ion oxidation into Co^{3+}, resulting in a tight immobilized complex.

4.1. Biosensing

In biosensors, His-tagged proteins have been broadly used in optical (Auer et al., 2017; Avsar et al., 2020; Faccio et al., 2016; Horta et al., 2020; Lata et al., 2005; Ravikumar et al., 2018) and electrochemical (Dai et al., 2018; Povedano et al., 2020; Vallina-Garcia et al., 2007; Zhang et al., 2014) devices and also in piezoelectric transducers (Baltus et al., 2007; Li et al., 2016; Nam et al., 2013; Wegner et al., 2016). Optical biosensors, mainly based on Surface Plasmon Resonance (SPR) or Biolayer Interferometry (BLI), are extensively employed to detect the interaction of an immobilized His-tagged protein with its ligand, due to a change in the light properties (Fig. 3A). For example, Horta and co-workers have recently developed an optical-fiber-based SPR biosensor to detect autoantibodies in autoimmune diseases, by immobilizing His-tagged antigens on Co^{3+}-NTA Au-coated probes (Horta et al., 2020). A similar approach, involving Co^{3+}-His complexes, has been used for immobilizing virus-like particles in a BLI biosensor that detects norovirus antibodies from human serum samples (Auer et al., 2017). Moreover, the chemokine receptor CXCR4 has been successfully immobilized for studying its interaction with nanobody-Fc ligands, which represents an important progress in the study of G protein-coupled receptors involved in a broad range of diseases (Boonen et al., 2020). Electrochemical biosensors tend to be sensitive, fast, simple, cheap, and easy-to-miniaturize devices that detect a change in electrical properties in the media (Dai et al., 2018; Ley et al., 2011). Their use is specially promising in point-of-care facilities, but their susceptibility to electrochemical interferences such as pH or ionic strength changes must be faced. His-tagged proteins in electrochemical biosensors have been used for the detection of nucleic acids (Dai et al., 2018; Povedano et al., 2020), biomarkers (Ta et al., 2016), toxins (Vallina-Garcia et al., 2007), immunoglobulins (Kang et al., 2017; Mikula et al., 2018) or pesticides (Zhang et al., 2014). The quartz crystal microbalance (QCM) is a simple, label-free, real-time, and efficient tool for the detection of biomolecular

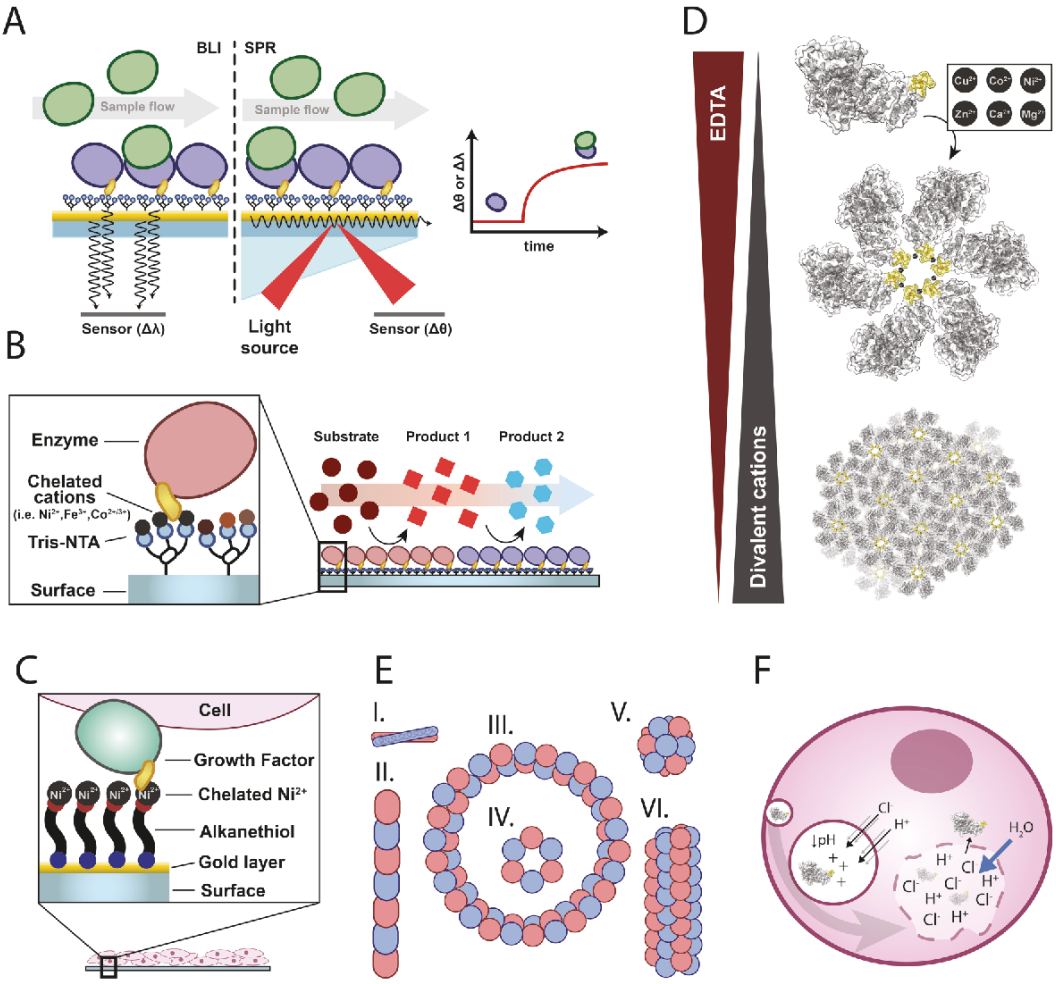

Fig. 3. A. Schematic representation of biolayer interferometry (left) and surface plasmon resonance (right) in his-tag based biosensing. B. Schematic disposition of immobilized enzymes for a sequential biocatalysis in which the product of the first reaction acts as substrate for the second reaction. Common cations used in immobilization are Ni^{2+}, Fe^{3+}, Co^{2+} or Co^{3+}. C. His-tagged protein coating as a bioengineering strategy to enhance cell growth. D. Schematic representation of how histidine residues promote protein assembly and secretory granule-like structures with the addition of divalent cations. E. Representation of the wide range of nanoscale protein materials that can be assembled by histidine coordination with metal cations such as coiled coils (I), nanowires (II), nanorings (III), toroids (IV), nanocapsules (V) and nanotubes (VI). F. Proton sponge effect; illustration of how the decrease in pH in endosomes in presence of his-tagged proteins results in the endosomal disruption and subsequent protein liberation.

interactions that is based in the measurement of the frequency decrease caused by a mass increase (upon interaction) in the functionalized surface (Nam et al., 2013). Its major drawback is the lack of sensitivity for small molecules. In a recent report it has been demonstrated the feasibility of QCM to explore the binding properties of a GPCR to its immobilized partner, which provides the basis for studying other similar interactions through this technique (Avsar et al., 2020). Finally, mycotoxin recognition peptides have been also immobilized over Zn^{2+} adsorbed chitosan foam via His-rich tag for the development of hapten biosensors (Soleri et al., 2015).

4.2. Biocatalysis

In biocatalysis, immobilization enhances enzymatic stability and facilitates product recovery and enzyme reusability. His-rich tag-based immobilization has been used for many different reactions in different supports. For example, EnginZyme® has developed Fe^{3+}-chelated glass carriers with controlled porosity in which His-tagged enzymes can be successfully immobilized and perform their activities (Pellis et al., 2017). Also, H6-tagged β-galactosidase has been self-immobilized using a molar excess of Zn^{2+} as mechanically stable microscale granules, a format that allows reusability and that enhances the operational stability of the enzyme (Sanchez et al., 2021). On the other hand, there is a growing tendency to synchronize purification and immobilization of His-tagged enzymes in one-step procedures, avoiding the initial on-column step and directly working with complex protein mixtures derived from cell lysates (Wang et al., 2017). Britton and collaborators developed a continuous-flow bioreactor with a 10-min synchronized purification and immobilization strategy (Britton et al., 2017). Moreover, they were able to produce a multi-step bioreactor that allows successive transformations by controlling spatial distribution of each enzyme throughout the bioreactor surface (Fig. 3B). The same principle has been applied in semi-continuous bioreactors (Plz et al., 2020). Magnetic nanoparticles have been widely used for such dual purpose for both intracellular and extracellular proteins obtaining great enzyme reusability indexes after several batches (Yang et al., 2015; Zhao et al., 2017; Zhou et al., 2017). Peschke and co-workers have exploited the use of magnetic beads in a microfluidic packed-bed bioreactor with His-tagged loaded ketoreductase (Peschke et al., 2019). The use of miniaturized reactors may be notably important in the future development of

sustainable production processes.

4.3. Bioengineering

His-tagged protein immobilization is also useful for bioengineering (Fig. 3C). For example, the Fibroblast Growth Factor (FGF) was immobilized onto the surface of a Ni^{2+} chelated glass-plate to enhance *in vitro* proliferation of human mesenchymal stem cells (Shakya et al., 2020). The successful outcome can be directly attributed to the structural integrity of the FGF domain in the fusion protein. As it has been done for biosensors, Ni^{2+} has been replaced by Co^{3+} to stabilize the bond between His-rich tag and NTA. Di Russo and co-workers proved that such replacement results in the development of a higher and broader range of E-cadherin adhesion forces, leading to extended cell spreading and colony organization (Di Russo et al., 2019). This principle is highly relevant for further development of functionalized surfaces for cell culture.

5. Site-specific conjugation

The functionalities of proteins or protein nanomaterials can be tuned by the conjugation of drugs or different organic molecules. As a representative example, in the Antibody Drug Conjugates (ADCs) the therapeutic molecule is covalently attached to a protein nanocarrier for its targeted delivery. Usually, protein nanomaterials are also linked to different organic molecules such as Polyethylene Glycol (PEG) to improve their pharmacokinetic properties, stability or immunogenicity. In all cases, site-directed conjugation is very convenient, not only because it would allow molecular binding in a desired and controlled position of the protein, but also since such strategies generate more homogeneous products with low batch-to-batch variability and with higher stoichiometric control. In this sense, engineering of histidine-rich motifs within the protein also plays an important role as site-specific conjugation targets.

5.1. Divalent transition metal ion coordination

As the most explored approach, many molecules chelated to divalent transition metal ions such as Ni^{2+} or Zn^{2+} have been attached to different nanomaterials (Table 1). This is done by the generation of ternary complexes with the unpaired electrons in imidazole rings of specific histidine residues as previously described. In this sense, NTA-modified DNA molecules have been conjugated to proteins such as Green Fluorescent Protein (GFP) (Goodman et al., 2009) or alkaline phosphatase (Shimada et al., 2008) using Ni^{2+} ion coordination as a molecular glue. This strategy has been also used to attach different types of molecules such as monophospharyl lipid A adjuvants containing nanolipoprotein particles (MPLA:NiNLP) to His-tagged foot-and-mouth disease virus capsids (Rai et al., 2016), or NTA-modified quantum dots to progeny virus capsids (Zheng et al., 2016). Further, NTA-modified gold-polymer nanoparticles have been also conjugated to His-tagged antifreeze peptides to generate new active nanomaterials (Wilkins et al., 2019).

5.2. Templated addition of alkynyl group or lysine conjugation

Hexahistidine tags can be also used as templates for a first-step temporal cation-coordinated molecular binding and subsequent covalent bonding with a neighboring histidine residue within the protein. In this sense, templated alkylation of an imidazole residue in a H6 tag can be achieved using Baylis-Hillman esters tethered to NTA in presence of divalent cations. Here, Ni^{2+}-coordinated ternary complex is generated between NTA and two adjacent histidine residues. This event brings the reactive double bond of the Baylis-Hillman ester into the vicinity of another free imidazole ring for its covalent binding and subsequent breaking of the previous NTA bond. This methodology allows the successful derivatization of recombinant proteins with a reactive alkynyl group that undergo subsequent cycloaddition of molecules (Liu and Melman, 2013).

As a similar approach, the DNA-template protein conjugation strategy (DTPC) allows the initial direction of an NTA-modified oligonucleotide to a His-tagged protein. This serves then as a template for complementary N-hydroxysuccinimide (NHS)-bearing molecule conjugation to a lysine residue, in the close proximity of the histidine-rich tag (Rosen et al., 2014).

5.3. Bis-alkylation of histidine residues

A more sophisticated His-rich tag specific conjugation methodology relies on the *bis*-alkylation of two histidine residues located close together in the target protein by sulfone-containing molecules, without the need of any metal chelator. Following this strategy, molecules such as PEG have been successfully attached to different His-tagged proteins using PEG-*bis*-sulfone or PEG_{10}-mono-sulfone molecules. Moreover, this type of conjugation was successfully achieved using different types of polyhistidine tags containing both continuous (H2, H6, H8) or discontinuous (-HGH or -HGHGHG) histidine residues (Cong et al., 2012; Peciak et al., 2019).

5.4. Generation of cyclic ketone

The use of an electrophile molecule such as 2-cyclohexanone has also allowed cation-free site-selective modification of surface-accessible histidine residues on a protein. This Michael addition generates a cyclic ketone able to form an oxime by the addition of aminooxy-derivative probes. Using this methodology, different types of molecules including nuclear magnetic resonance (NMR) tags, fluorescent dyes or biotin have been successfully attached to a His-tagged protein (Joshi and Rai, 2019).

5.5. Histidine acylation

Finally, in a similar approach, specific acylation of an optimized amino-terminal histidine tag ($GHHH_n$) has been also reported using D-gluconic acid δ-lactone (GDL) and 4-methoxyphenil esters. This His-rich tag specific acylation methodology has allowed the introduction of small reactive groups such as azides in different proteins including GFP, maltose-binding protein (MBP) or the small ubiquitin-like modifier protein (SUMO) for further reaction with DBCO-functionalized molecules or direct conjugation of biotin (Martos-Maldonado et al., 2018).

6. Refined protein assembling and functional protein aggregation

Artificial but largely bioinspired nanostructured materials have been developed based on protein building blocks, with high precision and structural complexity, integrating order and dynamics into the system (Hamley, 2019; Korpi et al., 2020). Among the different protein-based assembling approaches, simple fusion protein engineering permits the incorporation of peptidic cross-interactors and the facile synthesis of *de novo* multimeric nanomaterials. This is done by bottom-up fabrication approaches that ensure a control over the range of biochemical (e.g. specificity, bioactivity or biodegradability) and physical (e.g. small size, conformation or multivalency) properties (Mendes et al., 2013). His-rich tags in recombinant fusion proteins have been empirically tested to construct regular, stable and highly versatile nanocarriers with pseudospherical architectures (Lopez-Laguna et al., 2019), highly suited for precision intracellular drug delivery (Falgas et al., 2020; Pallares et al., 2020). One of the most exploited chemical mechanisms that drives the assembling process based on H6 tags is the ion-based gluing (Lopez-Laguna et al., 2020). In this regard, divalent cations (e.g. Ni^{2+}, Mg^{2+}, Cu^{2+}, Co^{2+}, Zn^{2+}, and Ca^{2+}) are able to simultaneously coordinate more-than-one histidine residues from overhanging histidine tails,

promoting building block recruitment and adequate protein organization at the nanoscale (Fig. 3D). This process, usually renders materials ranging between 10 and 350 nm, which are efficiently disassembled by EDTA (Lopez-Laguna et al., 2020). The gluing process takes place when the respective ion interacts with the nucleophilic electron pair from δ1 nitrogen of the histidine imidazole ring and accommodates at least 2 near-in-space building blocks into the final oligomeric structure. These interactions could also take place when carboxyl groups from asparagine and glutamine amino acid residues are close by (Erthal et al., 2016; Lopez-Laguna et al., 2019). When envisaged for biomedical applications, engineering ionic doses should be appropriately adjusted to avoid possible systemic toxicity as stated in the recommended dietary allowance (RDA) (Lopez-Laguna et al., 2020). A huge variety of different H6-tagged materials have been lately constructed (Table 1) with different morphologies and pointing to different applications (Fig. 3E).

In this sense metal-controlled protein dimers have been generated upon zinc binding to designed histidine residues (Maniaci et al., 2019), which in some particular cases such as CheA/W chemoreceptors can further assemble into ternary complexes to generate functional arrays (Haglin et al., 2017). The bioengineering of strategically placed metal-coordinating histidine residues has also allowed the generation of synthetic coiled coil structures (Tunn et al., 2018). Going still further, the combination of specifically oriented metal coordinating histidines with additional intrinsic non-covalent interactions has allowed the generation of more sophisticated nanostructures. These include linear nanowires of different lengths (Zhang et al., 2012), circular nanorings whose diameters can be regulated by tuning the strength of the non-covalent interactions (Bai et al., 2013), or even multi-responsive triblock copolypeptides that self-assemble as 20 nm diameter nanocapsules (van Eldijk et al., 2016). Other sophisticated structures, generated through metal-histidine interaction, also include helical nanotubes, whose widths can be controlled by solution conditions (Brodin et al., 2015), stimuli-responsive interfacial films (Dexter et al., 2006) or toroid nanoparticles (e.g. toxin-based (Diaz et al., 2018; Serna et al., 2020a), venom-based (Serna et al., 2020c) GFP-based (Cespedes et al., 2018; Pallares et al., 2020; Unzueta et al., 2020) or human nidogen-based (Alamo et al., 2021), either being intrinsically toxic or delivering coupled antitumoral drugs (e.g. floxuridine or monomethyl auristatin E). Finally, in a step further regarding structural complexity, functional secretory-like granules at the micro scale have been generated also through controlled protein aggregation via H6 tag–divalent cation coordination. These artificial aggregates permit the slow release of a protein drug in a prolonged manner, then acting as a sustained drug release systems aimed at reducing the need of repeated doses (Chen et al., 2019; Jiang et al., 2011; López-Laguna et al., 2021; Sanchez et al., 2020; Serna et al., 2020b).

7. Systemic administration for therapeutic applications

When proteins with histidine tails are meant to be used for biomedical purposes, it is essential to know whether histidine tails could change the behavior of therapeutic proteins when they are applied *in vivo*. It is especially critical to study whether histidines play a role in protein biodistribution as well as subcellular localization. To this purpose, different clarifying studies have been carried out, the results of which are described below.

7.1. Biodistribution

Because of their universal use as purification tags, the potential impact of His-rich tails in the biodistribution of systemically administered proteins and their implication in drug delivery have been carefully explored in different experimental settings. In these studies, the role of the amino acid composition of the histidine-rich tail has been evaluated, using intercalated hydrophobic or hydrophilic amino acids with different charges and upon an H-X-H-X-H-X arrangement (Hofstrom et al., 2013), which still allows an efficient purification through immobilized metal affinity chromatography (Knecht et al., 2009). Besides this, the influence of the position of the tag at the carboxy or amino terminal end of the protein has been studied (Hofstrom et al., 2013; Hofstrom et al., 2011; Tolmachev et al., 2010; Vorobyeva et al., 2019) by using radioactive labeling, to determine their organ biodistribution in mouse models. The resulting data indicated that variations in the body localization of the materials do not rely exclusively on the histidine tail, but also on the presence of charges and hydrophobic patches on the scaffold protein and the way they are distributed (local vs. overall) on the protein surface (Hofstrom et al., 2011; Lindbo et al., 2016; Tolmachev et al., 2010). Even though the different studies are not comparable due to the use of different chimeric scaffold proteins such as affibodies (Altai et al., 2016; Hofstrom et al., 2011; Mitran et al., 2015; Tolmachev et al., 2010), nanobodies (Singh et al., 2014), scFvs (Casey et al., 1995), toxins (Altai et al., 2016), uniCAR target modules (Jureczek et al., 2019), ADAPT scaffolds (Lindbo et al., 2016), DARPIN scaffold (Vorobyeva et al., 2019) and also due to different linker chemistry for radioactive tagging (Lindbo et al., 2016), it can be globally inferred that hydrophobic domains and positively charged areas favors liver uptake (Altai et al., 2016; Hofstrom et al., 2013; Mitran et al., 2015; Singh et al., 2014; Tolmachev et al., 2010). In this sense, His-based tails like (HE)3, hydrophilic and negatively charged, could help to counterbalance the hydrophobicity and positive charges of the area (Hofstrom et al., 2013; Hofstrom et al., 2011; Mitran et al., 2015; Tolmachev et al., 2010), while (HT)5, uncharged, gets mostly cleared by kidneys (López-Laguna et al., 2019). Also, poly-histidine tails at the amino terminal end show, in general, a low level of nonspecific organ uptake, especially in kidney (Hofstrom et al., 2013; Hofstrom et al., 2011; Vorobyeva et al., 2019). In contrast, other studies show that the histidine tail does not affect significantly the biodistribution of the protein (Casey et al., 1995; Jureczek et al., 2019; Lindbo et al., 2016), indicating again that changes of the protein fate in the body depend more on the overall distribution of charged and hydrophobic amino acids of the His-tagged protein than on the mere presence and nature of the His-rich tag (López-Laguna et al., 2020). Of course, all these concepts and considerations have important implications in the therapeutic applications of His-tagged proteins.

7.2. Intracellular trafficking

His-rich tags have been exploited as endosomal escape enhancers to deliver proteins or nucleic acids to the cytosol due to their ability to trigger osmotic swelling and endosomal disruption (Ferrer-Miralles et al., 2011). Since the pKa of their lateral chain imidazole group is around 6.0, histidine residues undergo protonation state change from neutral to positive when endosomal lumen becomes acidic. In consequence, not only H^+ protons enter the lysosomes, but Cl anions also do it likewise in order to equilibrate charges, which generates an osmotic pressure that ends up with membrane disruption, namely the proton sponge effect (Fig. 3F). Following this mechanism, His-tagged proteins can promote higher cytosolic delivery of their cargo molecule (e.g. nucleic acids and other drugs (Ferrer-Miralles et al., 2011)) into the cytosol. Also, based on their selective protonation at acidic pH, histidines has resulted attractive in the design of novel endosomolytic peptides (Boeckle et al., 2006; Paray et al., 2021). In this regard, the number of histidine residues, their distribution in the primary sequence and the endosomal vesicle size and membrane leakiness, has been described to affect this process (Ahmad et al., 2019; Kichler et al., 2007; Lo and Wang, 2008; López-Laguna et al., 2020; Vermeulen et al., 2018). (Munsell et al., 2016; Smith et al., 2019). Therefore, His-rich tag-dependent proton sponge effect can be considered a lysosome-specific membrane disruption system, although its real impact in promoting endosomal burst remains still controversial

8. Bottlenecks associated to polyhistidine tags

Because of the chemical versatility of His-rich tags, a plethora of different functional materials and surfaces have been constructed following bottom-up rational approaches. In this sense, although no intrinsic signs of cytotoxicity has been reported in the literature for polyhistidine tags, its potential influence over the protein structure, stability or function should be precisely considered when designing devices for biotechnological or biomedical applications (Zhao and Huang, 2016). Interestingly, while B-factor values (reflecting thermal motion) were usually slightly higher in His-tagged proteins, no significant structural effects have been generically observed neither in both resolution or R-factor (reliability factor) when considering a broad spectrum of crystallographic 3D protein structures with or without fused His tags (Carson et al., 2007). Similar results were obtained in recombinant GFP-based fusion proteins, in which H6 was placed in either the amino or carboxy termini or in a permissive solvent-exposed loop of the GFP barrel. In all cases, protein fluorescence remained intact and purification took place without any technical issues (Voltà-Durán et al., 2019).

8.1. Conformational impact

However, the influence of H6 tags on structural propensities and internal dynamics of small peptides might be more noticeable. While small peptides are highly mobile with no unique preferred spatial conformation, the addition of certain peptides such as His-based tags, triggers small chemical shifts and changes relaxation properties, being translated into long-range effect on overall structural propensities (Bräuer et al., 2019). This possibility was demonstrated when studying the His-rich tag effects on zinc finger proteins, in which the addition of those peptides either at their amino or carboxy-terminal positions promoted changes in their native or complexed-with-zinc CD spectra, unfolding profiles under urea degeneration tests, and protein functionality (Zhao and Huang, 2016). Alike influences were observed in disulfide bond structures but not in the binding behavior of the rat corticotropin-releasing factor receptor 2a in a His-rich tag carrying version (Klose et al., 2004). In this regard, while a huge catalogue of proteins should not be nearly affected by His-rich tag fusion, enzymes appear as a special and particular group sensitive to small structural changes by either creating or depleting functional scenarios. In this context, the carboxy-terminal tagging of tropinone reductase enzyme impaired its enzymatic activity while the amino-terminal tagged version remained fully active (Freydank et al., 2008). In agreement with that, *in silico* modelling of the protein structure showed an interference of the H6-tag with the enzyme active site by steric and electrostatic interactions only when placed at the carboxy terminal (Freydank et al., 2008). Similar scenarios were also described in L-lactate dehydrogenase, in the molybdoenzyme YedY, in secretory leukocyte protease inhibitors (SLPIs) and in hormone-sensitive lipases (HSL), in which the carboxy-terminal (Halliwell et al., 2001; Munadziroh et al., 2020; Sabaty et al., 2013) or the amino terminal (Wang et al., 2019) tagging resulted in reduced activities. The H6 tag fusion can also elicit a modulatory influence on the enzymatic activity of certain proteins and be used therefore as an advantage, as observed in the catalytic capacity of the nuclease domain of the Colicin E7 metallonuclease (NColE7) from E. coli, an enzyme used by *E. coli* to kill competing bacteria under stress conditions (Abd Elhameed et al., 2020). In this regard, the interference of the oligohistidine peptide tag with the Zn^{2+} containing active center was used for the regulation and fine tuning of the enzymatic activity. From another point of view, scanning fluorimetry profiles displayed both beneficial and deleterious effects on the thermal stability of the protein, depending on the presence or absence of a H6 in the amino-terminus (Booth et al., 2018) possibly due to an occasional architectonic rearrangement of the final protein structure. Mild and case-associated modulation of protein solubility have been also occasionally observed upon His-rich tag fusion (Woestenenk et al., 2004).

The variability of the already presented conformational scenario opens up to the idea of using small peptide linkers to reduce the conformational impact of fusion his-rich tags and to ensure an adequate conformational structure thus refining the design of bioactive fusion proteins. In this sense, three major categories of linkers can be found according to their physicochemical or functional properties (flexible, rigid or in vivo cleavable), which can be selected depending on the particular scientific needs. In fact, these linkers could not only contribute to minimize the conformational impact of introduced tags over the protein but also improve the biological properties of the tagged protein by increasing their production yields, by achieving desirable pharmacokinetic profiles or by improving their biological activity. In this regard, flexible linkers appear as the most appropriate ones to reduce the conformational impact of the histidine tag, as they confer sufficient mobility and flexibility to such tag. Flexible linkers are generally composed by small and either polar (e.g. Serine; Ser or Threonine; Thr) or non-polar (Glycine; Gly) amino acid residues. Their small size allows the protein sequence being sufficiently mobile, and their polarity contribute to protein stability in aqueous solution not only by forming hydrogen bonds with water molecules, but reducing the unfavored interactions between other protein regions. The most commonly used flexible linkers include (Gly-Gly-Gly-Gly-Ser)n or (Gly-Ser)n sequences. In this sense, the n value could be adjusted for an optimized separation between functional domains, or to maintain necessary inter-domain interactions. Although Gly and Ser are the most used amino acids, Thr and Alanine (Ala) could be also introduced to maintain sufficient structural flexibility and Lysine (Lys) and Glutamine (Glu) to improve sequence solubility. In all cases, the rational design should be supported by experimental data, ensuring the optimization of the linker sequence, in order to fit with the particular needs linked to the recombinant protein (Argos, 1990; Chen et al., 2013).

8.2. Immunogenicity

On the other hand, immunogenicity assessment is paramount to ensure the safe and effective development of therapeutic proteins (Ishii-Watabe et al., 2018), since mitigation or full ablation of immunological-based adverse events such as anaphylaxis, cytokine release syndrome, and cross-reactive neutralization of endogenous proteins is mandatory (Lau and Dunn, 2018; Tourdot and Hickling, 2019). Indeed, immunogenic responses correspond to the most common non-desired side effects of proteins in clinics. In this scenario, protein-based drugs are currently transforming the pharmaceutical industry, displaying an unpreceded potential specially in precision medicines (Sanchez-Garcia et al., 2016; Serna et al., 2018) and promoting the development of highly effective treatments (Lagasse et al., 2017). Then, immunogenicity of potential tags used in production might be a critical issue (Tourdot and Hickling, 2019). From here, a dichotomy appears; while a large catalogue of manufactured proteins with clinical potential are His-tagged, a public concern shows up in which the use of H6 tag is discouraged by the Food and Drug Administration (FDA) and the European Medicines Agency (EMA) due to its potential non-desired immune response, although no official specifications are publicly indicated. In this context, alternative histidine-rich tags have been designed and tested with the aim of solving these regulatory concerns. For that, humanized versions, alternative to the traditional H6, were constructed derived from BLAST-ed human proteins namely H3A (HAAHAH), H5T (HTHTHTHTH) and H5E (HEHEHEHEH). Interestingly, all humanized His-tag versions maintained their protein production, purification and functional properties, displaying a huge potential to be used in humanized biomedicines (López-Laguna et al., 2020).

From a technical point of view, part of the scientific community considers H6 sequences as safe tags, due to its small size (0.84 kDa), absence of electric charge (non-interactive material), and low cell

toxicity and immunogenicity (Loughran et al., 2017). This is of course in addition to the very convenient potential of His-rich segments as purification tags, at low costs and under mild imidazole-promoted elution and native or denaturing conditions (Lau and Dunn, 2018; Loughran et al., 2017), making feasible the industrial production of protein drugs. Notably, protein BLASTs also shows coincidences in more-than-six consecutive histidine segments found in human proteins, hinting that human immune system is not expected to react when administering H6-tagged formulations (López-Laguna et al., 2020). Besides this conceptual consideration, there is no huge quantity and detailed experimental facts describing H6 immunogenicity, neither *in vivo* nor *in vitro*. In addition, His-rich tags have been included in multiple vaccine candidates against malaria (Angov et al., 2003; Dutta et al., 2002; Otsyula et al., 2013), proceeding as far as phase IIb in clinical trials without apparent safety concerns in vaccinated children (Jin et al., 2017). A similar scenario was observed in tandem phase I studies evaluating reactogenicity, safety and immunogenicity of His-tagged antigens (*Plasmodium falciparum* surface protein; $MSP1_{42}$) administered intramuscularly with AS01 as adjuvant (Otsyula et al., 2013). On the other way around, the amino-terminal His-tagged *Streptococcus pneumoniae* surface protein SP08456 promoted undesired immunogenic responses when administered intramuscularly, in comparison to its non-tagged version for bacteria immunization in Balb/c mice (Singh et al., 2020). In short, there are not experimental concluding remarks that support or preclude the use of His-tagged drugs into clinics.

8.3. Catalytic activity of imidazole rings

The addition of His-tags in recombinant proteins for purification or other purposes may not be as innocuous as previously thought. Imidazole rings appear to be reactive species able to catalyze specific enzymatic reactions, and so changing the resulting properties of the His-tagged protein material.

In this sense, the catalytic function of the imidazole ring has been reported since 1956 in several scenarios, in which different types of polymers, nanoparticles, peptide bundles and nanofibers have been involved (Bai et al., 2011; Chadha and Zhao, 2013; Giusti et al., 2014; Guler and Stupp, 2007). Indeed, this chemical group has been described as able to catalyze the transformation of p-nitrophenyl acetate hydrolysis (p-NPA) (Denmark et al., 1990), as well as, having a capital role in aldol-based and RNA cleavage reactions (Anslyn and Breslow, 1989; Breslow, 1994; Kirby and Marriott, 1995; Markert et al., 2009; Scheffler and Mahrwald, 2012). Its chemical versatility (especially when conforming the side chain of the histidine amino acid) lies in its amphoteric nature. Thus, the imidazole ring is able to lose a proton via its pros nitrogen atom or to accept a proton via its tele nitrogen atom at pHs close to 7 (Schneider, 1978). Because of that, histidine residues are suitable for both nucleophilic and base catalysis reactions, in addition to the traditional metal coordination functions.

Therefore, due to this intrinsic chemical reactivity of the imidazole ring, His-tags might be not biologically inert when fused to a protein. Among the different experimentally described scenarios, the His-tag can present esterase activity as reported in a GFP-H6 protein model, being able to convert p-NPA to p-nitrophenol and acetic acid in a linear concentration dependent way, and in an aqueous PBS-based solution (Schoonen et al., 2017). This esterase catalytic activity was also observed with other esterase substrates such as p-nitrophenyl butyrate (p-NPB), polyethylene glycol MW 800-modifed p-NPA (p-NPA-PEG) and carboxyfuorescein diacetate (CFDA). In addition, an increase in His-tag-mediated esterase activity was observed upon assembling of an His-tagged cowpea chlorotic mottle virus (CCMV), showing that the bigger the protein-based structure, the higher the activity. The activity increase upon protein assembling could be associated with a cooperative effect between close-in-space imidazole rings of the His-tag from each protein building block. Besides, this plausible cooperative effect between adjacent imidazole rings was discarded, as very small activity changes were observed at alternative increasing number-of-histidines His-tags, namely H-His-NH_2, H-His6-NH_2 and H-His12-NH_2. This was indicative of the irrespective influence of the number of close histidines into the final catalytic capacity of the tag. Finally, in a further step, the addition of a His-tag into an enzyme structure can generate additional functions (dual-active enzymes) as reported in a His-tagged phenylacetone monooxygenase (His6-PAMO) able to hydrolyze p-nitroacetophenone to p-NP (via p-NPA), apart from its intrinsic natural oxidoreductase activity (from phenylacetone to benzyl acetate). Interestingly, this gain of function was inhibited in presence of a molar excess of $NiCl_2$, which was able to specifically bind to the imidazole ring and block its catalytic reactivity (Schoonen et al., 2017).

Because of that, the catalytic propensity of his-tags must also be considered when designing novel protein-based materials, to address undesired scenarios of gain of function.

9. Concluding remarks

Although short histidine-rich peptides were initially developed as tags for recombinant protein purification, their pleiotropic nature has facilitated their progressive and expansive adaptation as functional and structural agents in multiple biotechnological and biomedical fields that are sustained by protein-based materials. They range from catalysis to drug development, but include dozens of different refined uses such as designing advanced smart micro- and nano-scale materials, tools for precision medicines or for fine diagnosis approaches. Such innovative applications open exciting possibilities to tailor proteins as powerful devices with unexpected regulatable properties, as purpose-tailored functional devices.

Declaration of competing interest

The authors declare that there is no conflict of interest.

Acknowledgments

The authors are indebted to Agencia Estatal de Investigación (AEI) and to Fondo Europeo de Desarrollo Regional (FEDER) BIO2016-76063-R, AEI/FEDER, UE to A.V. and PID2019-105416RB-I00/AEI/10.13039/501100011033 to E.V., AGAUR 2017SGR-229 GRC to A.V., CIBER-BBN (projects NANOPROTHER and VENOM4CANCER to A.V., NANO-REMOTE to E.V. and NANOSCAPE and NANOLINK to U.U.), and to Instituto de Salud Carlos III (ISCIII) PI20/00400 co-funded by European Regional Development Fund (A way to make Europe) to U.U., for their research in protein production and in functional protein materials. The authors are also indebted to CERCA programme from la generalitat de Catalunya, Spain and to the Networking Research Center on Bioengineering, Biomaterials and Nanomedicine (CIBER-BBN), Spain that is an initiative funded by the VI National R&D&I Plan 2008–2011, Iniciativa Ingenio 2010, Consolider Program, CIBER Actions and financed by the Instituto de Salud Carlos III, with assistance from the European Regional Development Fund. Molecular graphics and analyses were performed with UCSF ChimeraX, developed by the Resource for Biocomputing, Visualization, and Informatics at the University of California, San Francisco, with support from National Institutes of Health R01-GM129325 and the Office of Cyber Infrastructure and Computational Biology, National Institute of Allergy and Infectious Diseases. H.L.L. was supported by a predoctoral fellowship from AGAUR (2019FI_B00352), and E.V.D. was supported by a predoctoral fellowship from Ministerio de Ciencia e Innovación, Spain (FPU18/04615). U.U. was supported by a Miguel Servet contract (CP19/00028) from ISCIII co-funded by European Social Fund (ESF investing in your future). A.V. received an ICREA ACADEMIA award.

References

Abd Elhameed, H.A.H., Hajdu, B., Balogh, R.K., Hermann, E., Hunyadi-Gulyás, É., Gyurcsik, B., 2019. Purification of proteins with native terminal sequences using a Ni (II)-cleavable C-terminal hexahistidine affinity tag. Protein Expr. Purif. 159, 53–59. https://doi.org/10.1016/j.pep.2019.03.009.

Abd Elhameed, H.A.H., Hajdu, B., Jancso, A., Keri, A., Galbacs, G., Hunyadi-Gulyas, E., Gyurcsik, B., 2020. Modulation of the catalytic activity of a metallonuclease by tagging with oligohistidine. J. Inorg. Biochem. 206, 111013. https://doi.org/10.1016/j.jinorgbio.2020.111013.

Ahmad, A., Khan, J.M., Haque, S., 2019. Strategies in the design of endosomolytic agents for facilitating endosomal escape in nanoparticles. Biochimie 160, 61–75. https://doi.org/10.1016/j.biochi.2019.02.012.

Alamo, P., Cedano, J., Conchillo-Sole, O., Cano-Garrido, O., Alba-Castellon, L., Serna, N., Avino, A., Carrasco-Diaz, L.M., Sanchez-Chardi, A., Martinez-Torro, C., Gallardo, A., Cano, M., Eritja, R., Villaverde, A., Mangues, R., Vazquez, E., Unzueta, U., 2021. Rational engineering of a human GFP-like protein scaffold for humanized targeted nanomedicines. Acta Biomater. https://doi.org/10.1016/j.actbio.2021.06.001.

Altai, M., Liu, H., Orlova, A., Tolmachev, V., Graslund, T., 2016. Influence of molecular design on biodistribution and targeting properties of an Affibody-fused HER2-recognising anticancer toxin. Int. J. Oncol. 49 (3), 1185–1194. https://doi.org/10.3892/ijo.2016.3614.

Alves, N.J., Turner, K.B., DiVito, K.A., Daniele, M.A., Walper, S.A., 2017. Affinity purification of bacterial outer membrane vesicles (OMVs) utilizing a His-tag mutant. Res. Microbiol. 168 (2), 139–146. https://doi.org/10.1016/j.resmic.2016.10.001.

Amarasinghe, C., Jin, J.P., 2015. The use of affinity tags to overcome obstacles in recombinant protein expression and purification. Protein Pept. Lett. 22 (10), 885–892. https://doi.org/10.2174/0929866522666150728115307.

Andersen, K.R., Leksa, N.C., Schwartz, T.U., 2013. Optimized *E. coli* expression strain LOBSTR eliminates common contaminants from His-tag purification. Proteins 81 (11), 1857–1861. https://doi.org/10.1002/prot.24364.

Angov, E., Aufiero, B.M., Turgeon, A.M., Van Handenhove, M., Ockenhouse, C.F., Kester, K.E., Walsh, D.S., McBride, J.S., Dubois, M.C., Cohen, J., Haynes, J.D., Eckels, K.H., Heppner, D.G., Ballou, W.R., Diggs, C.L., Lyon, J.A., 2003. Development and pre-clinical analysis of a *Plasmodium falciparum* Merozoite Surface Protein-1(42) malaria vaccine. Mol. Biochem. Parasitol. 128 (2), 195–204. https://doi.org/10.1016/s0166-6851(03)00077-x.

Anslyn, E., Breslow, R., 1989. Geometric evidence on the ribonuclease model mechanism. J. Am. Chem. Soc. 111 (15), 5972–5973. https://doi.org/10.1021/ja00197a085.

Argos, P., 1990. An investigation of oligopeptides linking domains in protein tertiary structures and possible candidates for general gene fusion. J. Mol. Biol. 211 (4), 943–958. https://doi.org/10.1016/0022-2836(90)90085-z.

Auer, S., Azizi, L., Faschinger, F., Blazevic, V., Vesikari, T., Gruber, H.J., Hytönen, V.P., 2017. Stable immobilisation of His-tagged proteins on BLI biosensor surface using cobalt. Sensors Actuators B Chem. 243, 104–113. https://doi.org/10.1016/j.snb.2016.11.090.

Avsar, S.Y., Kapinos, L.E., Schoenenberger, C.A., Schertler, G.F.X., Muhle, J., Meger, B., Lim, R.Y.H., Ostermaier, M.K., Lesca, E., Palivan, C.G., 2020. Immobilization of arrestin-3 on different biosensor platforms for evaluating GPCR binding. Phys. Chem. Chem. Phys. 22 (41), 24086–24096. https://doi.org/10.1039/d0cp01464h.

Bai, Y., Ling, Y., Shi, W., Cai, L., Jia, Q., Jiang, S., Liu, K., 2011. Heteromeric assembled polypeptidic artificial hydrolases with a six-helical bundle scaffold. ChemBioChem 12 (17), 2647–2658. https://doi.org/10.1002/cbic.201100311.

Bai, Y., Luo, Q., Zhang, W., Miao, L., Xu, J., Li, H., Liu, J., 2013. Highly ordered protein nanorings designed by accurate control of glutathione S-transferase self-assembly. J. Am. Chem. Soc. 135 (30), 10966–10969. https://doi.org/10.1021/ja405519s.

Baltus, R.E., Carmon, K.S., Luck, L.A., 2007. Quartz crystal microbalance (QCM) with immobilized protein receptors: comparison of response to ligand binding for direct protein immobilization and protein attachment via disulfide linker. Langmuir 23 (7), 3880–3885. https://doi.org/10.1021/la0628468.

Banerjee, A., Pons, T., Lequeux, N., Dubertret, B., 2016. Quantum dots-DNA bioconjugates: synthesis to applications. Interface Focus 6 (6), 20160064. https://doi.org/10.1098/rsfs.2016.0064.

Boeckle, S., Fahrmeir, J., Roedl, W., Ogris, M., Wagner, E., 2006. Melittin analogs with high lytic activity at endosomal pH enhance transfection with purified targeted PEI polyplexes. J. Control. Release 112 (2), 240–248. https://doi.org/10.1016/j.jconrel.2006.02.002.

Boonen, A., Singh, A.K., Hout, A.V., Das, K., Loy, T.V., Noppen, S., Schols, D., 2020. Development of a novel SPR assay to study CXCR4-ligand interactions. Biosensors 10 (10). https://doi.org/10.3390/bios10100150.

Booth, W.T., Schlachter, C.R., Pote, S., Ussin, N., Mank, N.J., Klapper, V., Offermann, L. R., Tang, C., Hurlburt, B.K., Chruszcz, M., 2018. Impact of an N-terminal polyhistidine tag on protein thermal stability. ACS Omega 3 (1), 760–768. https://doi.org/10.1021/acsomega.7b01598.

Bornhorst, J.A., Falke, J.J., 2000. [16] Purification of proteins using polyhistidine affinity tags. In: Methods in Enzymology. Academic Press, pp. 245–254.

Bräuer, M., Zich, M.T., Önder, K., Müller, N., 2019. The influence of commonly used tags on structural propensities and internal dynamics of peptides. Monatsh. Chem. Chem. Mon. 150 (5), 913–925. https://doi.org/10.1007/s00706-019-02401-x.

Breslow, R., 1994. Bifunctional acid—base catalysis by imidazole groups in enzyme mimics. J. Mol. Catal. 91 (2), 161–174. https://doi.org/10.1016/0304-5102(94)00046-8.

Britton, J., Dyer, R.P., Majumdar, S., Raston, C.L., Weiss, G.A., 2017. Ten-minute protein purification and surface tethering for continuous-flow biocatalysis. Angew. Chem. 56 (9), 2296–2301. https://doi.org/10.1002/anie.201610821.

Brodin, J.D., Smith, S.J., Carr, J.R., Tezcan, F.A., 2015. Designed, helical protein nanotubes with variable diameters from a single building block. J. Am. Chem. Soc. 137 (33), 10468–10471. https://doi.org/10.1021/jacs.5b05755.

Carson, M., Johnson, D.H., McDonald, H., Brouillette, C., Delucas, L.J., 2007. His-tag impact on structure. Acta Crystallogr. D Biol. Crystallogr. 63 (Pt 3), 295–301. https://doi.org/10.1107/S0907444906052024.

Casey, J.L., Keep, P.A., Chester, K.A., Robson, L., Hawkins, R.E., Begent, R.H., 1995. Purification of bacterially expressed single chain Fv antibodies for clinical applications using metal chelate chromatography. J. Immunol. Methods 179 (1), 105–116. https://doi.org/10.1016/0022-1759(94)00278-5.

Ceglarek, I., Piotrowicz, A., Lecion, D., Miernikiewicz, P., Owczarek, B., Hodyra, K., Harhala, M., Gorski, A., Dabrowska, K., 2013. A novel approach for separating bacteriophages from other bacteriophages using affinity chromatography and phage display. Sci. Rep. 3, 3220. https://doi.org/10.1038/srep03220.

Cespedes, M.V., Unzueta, U., Avino, A., Gallardo, A., Alamo, P., Sala, R., Sanchez-Chardi, A., Casanova, I., Mangues, M.A., Lopez-Pousa, A., Eritja, R., Villaverde, A., Vazquez, E., Mangues, R., 2018. Selective depletion of metastatic stem cells as therapy for human colorectal cancer. EMBO Mol. Med. 10 (10) https://doi.org/10.15252/emmm.201708772 pii: e8772.

Chadha, G., Zhao, Y., 2013. Histidine-functionalized water-soluble nanoparticles for biomimetic nucleophilic/general-base catalysis under acidic conditions. Org. Biomol. Chem. 11 (39), 6849–6855. https://doi.org/10.1039/c3ob41485j.

Chao, A., Jiang, N., Yang, Y., Li, H., Sun, H., 2017. A Ni-NTA-based red fluorescence probe for protein labelling in live cells. J. Mater. Chem. B 5 (6), 1166–1173. https://doi.org/10.1039/c6tb02848a.

Chen, X., Zaro, J.L., Shen, W.C., 2013. Fusion protein linkers: property, design and functionality. Adv. Drug Deliv. Rev. 65 (10), 1357–1369. https://doi.org/10.1016/j.addr.2012.09.039.

Chen, T.Y., Cheng, W.J., Horng, J.C., Hsu, H.Y., 2019. Artificial peptide-controlled protein release of Zn(2+)-triggered, self-assembled histidine-tagged protein microparticle. Colloids Surf. B: Biointerfaces 110644. https://doi.org/10.1016/j.colsurfb.2019.110644.

Cong, Y., Pawlisz, E., Bryant, P., Balan, S., Laurine, E., Tommasi, R., Singh, R., Dubey, S., Peciak, K., Bird, M., Sivasankar, A., Swierkosz, J., Muroni, M., Heidelberger, S., Farys, M., Khayrzad, F., Edwards, J., Badescu, G., Hodgson, I., Heise, C., Somavarapu, S., Liddell, J., Powell, K., Zloh, M., Choi, J.W., Godwin, A., Brocchini, S., 2012. Site-specific PEGylation at histidine tags. Bioconjug. Chem. 23 (2), 248–263. https://doi.org/10.1021/bc200530x.

Dai, T., Pu, Q., Guo, Y., Zuo, C., Bai, S., Yang, Y., Yin, D., Li, Y., Sheng, S., Tao, Y., Fang, J., Yu, W., Xie, G., 2018. Analogous modified DNA probe and immune competition method-based electrochemical biosensor for RNA modification. Biosens. Bioelectron. 114, 72–77. https://doi.org/10.1016/j.bios.2018.05.018.

Denmark, S.E., Dappen, M.S., Sear, N.L., Jacobs, R.T., 1990. The vinylogous anomeric effect in 3-alkyl-2-chlorocyclohexanone oximes and oxime ethers. J. Am. Chem. Soc. 112 (9), 3466–3474. https://doi.org/10.1021/ja00165a034.

Dexter, A.F., Malcolm, A.S., Middelberg, A.P., 2006. Reversible active switching of the mechanical properties of a peptide film at a fluid-fluid interface. Nat. Mater. 5 (6), 502–506. https://doi.org/10.1038/nmat1653.

Di Russo, J., Young, J.L., Balakrishnan, A., Benk, A.S., Spatz, J.P., 2019. NTA-Co(3+)-His6 versus NTA-Ni(2+)-His6 mediated E-Cadherin surface immobilization enhances cellular traction. Biomaterials 192, 171–178. https://doi.org/10.1016/j.biomaterials.2018.10.042.

Diaz, R., Pallares, V., Cano-Garrido, O., Serna, N., Sanchez-Garcia, L., Falgas, A., Pesarrodona, M., Unzueta, U., Sanchez-Chardi, A., Sanchez, J.M., Casanova, I., Vazquez, E., Mangues, R., Villaverde, A., 2018. Selective CXCR4(+) cancer cell targeting and potent antineoplastic effect by a nanostructured version of recombinant ricin. Small 14 (26), e1800665. https://doi.org/10.1002/smll.201800665.

Dutta, S., Lalitha, P.V., Ware, L.A., Barbosa, A., Moch, J.K., Vassell, M.A., Fileta, B.B., Kitov, S., Kolodny, N., Heppner, D.G., Haynes, J.D., Lanar, D.E., 2002. Purification, characterization, and immunogenicity of the refolded ectodomain of the *Plasmodium falciparum* apical membrane antigen 1 expressed in *Escherichia coli*. Infect. Immun. 70 (6), 3101–3110. https://doi.org/10.1128/iai.70.6.3101-3110.2002.

Erthal, L.C., Marques, A.F., Almeida, F.C., Melo, G.L., Carvalho, C.M., Palmieri, L.C., Cabral, K.M., Fontes, G.N., Lima, L.M., 2016. Regulation of the assembly and amyloid aggregation of murine amylin by zinc. Biophys. Chem. 218, 58–70. https://doi.org/10.1016/j.bpc.2016.09.008.

Faccio, G., Bannwarth, M.B., Schulenburg, C., Steffen, V., Jankowska, D., Pohl, M., Rossi, R.M., Maniura-Weber, K., Boesel, L.F., Richter, M., 2016. Encapsulation of FRET-based glucose and maltose biosensors to develop functionalized silica nanoparticles. Analyst 141 (13), 3982–3984. https://doi.org/10.1039/c5an02573g.

Falgas, A., Pallares, V., Serna, N., Sanchez-Garcia, L., Sierra, J., Gallardo, A., Alba-Castellon, L., Alamo, P., Unzueta, U., Villaverde, A., Vazquez, E., Mangues, R., Casanova, I., 2020. Selective delivery of T22-PE24-H6 to CXCR4(+) diffuse large B-cell lymphoma cells leads to wide therapeutic index in a disseminated mouse model. Theranostics 10 (12), 5169–5180. https://doi.org/10.7150/thno.43231.

Ferrer-Miralles, N., Corchero, J.L., Kumar, P., Cedano, J.A., Gupta, K.C., Villaverde, A., Vazquez, E., 2011. Biological activities of histidine-rich peptides; merging biotechnology and nanomedicine. Microb. Cell Factories 10, 101. https://doi.org/10.1186/1475-2859-10-101.

Freydank, A.C., Brandt, W., Drager, B., 2008. Protein structure modeling indicates hexahistidine-tag interference with enzyme activity. Proteins 72 (1), 173–183. https://doi.org/10.1002/prot.21905.

Gaberc-Porekar, V., Menart, V., 2001. Perspectives of immobilized-metal affinity chromatography. J. Biochem. Biophys. Methods 49 (1-3), 335–360.

Gaberc-Porekar, V., Menart, V., 2005. Potential for using histidine tags in purification of proteins at large scale. Chem. Eng. Technol. 28 (11), 1306–1314. https://doi.org/10.1002/ceat.200500167.

Garg, V.K., Costello, M.A., Czuba, B.A., 1991. Purification and production of therapeutic grade proteins. Bio/Technology 12, 29–54.

Garousi, J., Orlova, A., Frejd, F.Y., Tolmachev, V., 2020. Imaging using radiolabelled targeted proteins: radioimmunodetection and beyond. EJNMMI Radiopharm. Chem. 5 (1), 16. https://doi.org/10.1186/s41181-020-00094-w.

Giusti, L.A., Medeiros, M., Ferreira, N.L., Mora, J.R., Fiedler, H.D., 2014. Polymers containing imidazole groups as nanoreactors for hydrolysis of esters. J. Phys. Org. Chem. 27 (4), 297–302. https://doi.org/10.1002/poc.3263.

Goh, H.C., Sobota, R.M., Ghadessy, F.J., Nirantar, S., 2017. Going native: complete removal of protein purification affinity tags by simple modification of existing tags and proteases. Protein Expr. Purif. 129, 18–24. https://doi.org/10.1016/j.pep.2016.09.001.

Goodman, R.P., Erben, C.M., Malo, J., Ho, W.M., McKee, M.L., Kapanidis, A.N., Turberfield, A.J., 2009. A facile method for reversibly linking a recombinant protein to DNA. ChemBioChem 10 (9), 1551–1557. https://doi.org/10.1002/cbic.200900165.

Gräslund, S., Nordlund, P., Weigelt, J., Hallberg, B.M., Bray, J., Gileadi, O., Knapp, S., Oppermann, U., Arrowsmith, C., Hui, R., Ming, J., dhe-Paganon, S., Park, H.-w., Savchenko, A., Yee, A., Edwards, A., Vincentelli, R., Cambillau, C., Kim, R., Kim, S.-H., Rao, Z., Shi, Y., Terwilliger, T.C., Kim, C.-Y., Hung, L.-W., Waldo, G.S., Peleg, Y., Albeck, S., Unger, T., Dym, O., Prilusky, J., Sussman, J.L., Stevens, R.C., Lesley, S.A., Wilson, I.A., Joachimiak, A., Collart, F., Dementieva, I., Donnelly, M.I., Eschenfeldt, W.H., Kim, Y., Stols, L., Wu, R., Zhou, M., Burley, S.K., Emtage, J.S., Sauder, J.M., Thompson, D., Bain, K., Luz, J., Gheyi, T., Zhang, F., Atwell, S., Almo, S.C., Bonanno, J.B., Fiser, A., Swaminathan, S., Studier, F.W., Chance, M.R., Sali, A., Acton, T.B., Xiao, R., Zhao, L., Ma, L.C., Hunt, J.F., Tong, L., Cunningham, K., Inouye, M., Anderson, S., Janjua, H., Shastry, R., Ho, C.K., Wang, D., Wang, H., Jiang, M., Montelione, G.T., Stuart, D.I., Owens, R.J., Daenke, S., Schütz, A., Heinemann, U., Yokoyama, S., Büssow, K., Gunsalus, K.C., Structural Genomics, C., Architecture et Fonction des Macromolécules, B, Berkeley Structural Genomics, C, China Structural Genomics, C, Integrated Center for, S, Function, I, Israel Structural Proteomics, C, Joint Center for Structural, G, Midwest Center for Structural, G, New York Structural Genomi, X.R.C.f.S.G, Northeast Structural Genomics, C, Oxford Protein Production, F, Protein Sample Production Facility, M.D.C.f.M.M, Initiative, R.S.G.P, Complexes, S, 2008. Protein production and purification. Nat. Methods 5 (2), 135–146. https://doi.org/10.1038/nmeth.f.202.

Grisshammer, R., Tucker, J., 1997. Quantitative evaluation of neurotensin receptor purification by immobilized metal affinity chromatography. Protein Expr. Purif. 11 (1), 53–60. https://doi.org/10.1006/prep.1997.0766.

Guler, M.O., Stupp, S.I., 2007. A self-assembled nanofiber catalyst for ester hydrolysis. J. Am. Chem. Soc. 129 (40), 12082–12083. https://doi.org/10.1021/ja075044n.

Gupta, J., Kaul, S., Srivastava, A., Kaushik, N., Ghosh, S., Sharma, C., Batra, G., Banerjee, M., Shalimar, Nayak, B., Ranjith-Kumar, C.T., Surjit, M., 2020. Expression, purification and characterization of the hepatitis E virus like-particles in the *Pichia pastoris*. Front. Microbiol. 11, 141. https://doi.org/10.3389/fmicb.2020.00141.

Haglin, E.R., Yang, W., Briegel, A., Thompson, L.K., 2017. His-Tag-mediated dimerization of chemoreceptors leads to assembly of functional nanoarrays. Biochemistry 56 (44), 5874–5885. https://doi.org/10.1021/acs.biochem.7b00698.

Halliwell, C.M., Morgan, G., Ou, C.P., Cass, A.E., 2001. Introduction of a (poly)histidine tag in L-lactate dehydrogenase produces a mixture of active and inactive molecules. Anal. Biochem. 295 (2), 257–261. https://doi.org/10.1006/abio.2001.5182.

Hamley, I.W., 2019. Protein assemblies: nature-inspired and designed nanostructures. Biomacromolecules 20 (5), 1829–1848. https://doi.org/10.1021/acs.biomac.9b00228.

Hirano, S., 2012. Western blot analysis. Methods Mol. Biol. 926, 87–97. https://doi.org/10.1007/978-1-62703-002-1_6.

Hofström, C., Orlova, A., Altai, M., Wangsell, F., Graslund, T., Tolmachev, V., 2011. Use of a HEHEHE purification tag instead of a hexahistidine tag improves biodistribution of affibody molecules site-specifically labeled with (99m)Tc, (111)In, and (125)I. J. Med. Chem. 54 (11), 3817–3826. https://doi.org/10.1021/jm200065e.

Hofstrom, C., Altai, M., Honarvar, H., Strand, J., Malmberg, J., Hosseinimehr, S.J., Orlova, A., Graslund, T., Tolmachev, V., 2013. HAHAHA, HEHEHE, HIHIHI, or HKHKHK: influence of position and composition of histidine containing tags on biodistribution of [(99m)Tc(CO)3](+)-labeled affibody molecules. J. Med. Chem. 56 (12), 4966–4974. https://doi.org/10.1021/jm400218y.

Horta, S., Qu, J.H., Dekimpe, C., Bonnez, Q., Vandenbulcke, A., Tellier, E., Kaplanski, G., Delport, F., Geukens, N., Lammertyn, J., Vanhoorelbeke, K., 2020. Co(III)-NTA mediated antigen immobilization on a fiber optic-SPR biosensor for detection of autoantibodies in autoimmune diseases: application in immune-mediated thrombotic *Thrombocytopenic purpura*. Anal. Chem. 92 (20), 13880–13887. https://doi.org/10.1021/acs.analchem.0c02586.

Huang, Z., Park, J.I., Watson, D.S., Hwang, P., Szoka Jr., F.C., 2006. Facile synthesis of multivalent nitrilotriacetic acid (NTA) and NTA conjugates for analytical and drug delivery applications. Bioconjug. Chem. 17 (6), 1592–1600. https://doi.org/10.1021/bc0602228.

Ishii-Watabe, A., Shibata, H., Nishimura, K., Hosogi, J., Aoyama, M., Nishimiya, K., Saito, Y., 2018. Immunogenicity of therapeutic protein products: current considerations for anti-drug antibody assay in Japan. Bioanalysis 10 (2), 95–105. https://doi.org/10.4155/bio-2017-0186.

Jia, S., Li, P., Koh, K., Chen, H., 2016. A cytosensor based on NiO nanoparticle-enhanced surface plasmon resonance for detection of the breast cancer cell line MCF-7. Microchim. Acta 183 (2), 683–688. https://doi.org/10.1007/s00604-015-1700-8.

Jiang, Y., Shi, K., Xia, D., Piao, H., Quan, P., Song, T., Cui, F., 2011. Protamine modified metal ion-protein chelate microparticles for sustained release of interferon. Int. J. Pharm. 407 (1-2), 31–37. https://doi.org/10.1016/j.ijpharm.2011.01.003.

Jin, J., Hjerrild, K.A., Silk, S.E., Brown, R.E., Labbe, G.M., Marshall, J.M., Wright, K.E., Bezemer, S., Clemmensen, S.B., Biswas, S., Li, Y., El-Turabi, A., Douglas, A.D., Hermans, P., Detmers, F.J., de Jongh, W.A., Higgins, M.K., Ashfield, R., Draper, S.J., 2017. Accelerating the clinical development of protein-based vaccines for malaria by efficient purification using a four amino acid C-terminal 'C-tag'. Int. J. Parasitol. 47 (7), 435–446. https://doi.org/10.1016/j.ijpara.2016.12.001.

Johnson, D.L., Martin, L.L., 2005. Controlling protein orientation at interfaces using histidine tags: an alternative to Ni/NTA. J. Am. Chem. Soc. 127 (7), 2018–2019. https://doi.org/10.1021/ja045084g.

Joshi, P.N., Rai, V., 2019. Single-site labeling of histidine in proteins, on-demand reversibility, and traceless metal-free protein purification. Chem. Commun. 55 (8), 1100–1103. https://doi.org/10.1039/c8cc08733d.

Jureczek, J., Bergmann, R., Berndt, N., Koristka, S., Kegler, A., Puentes-Cala, E., Soto, J. A., Arndt, C., Bachmann, M., Feldmann, A., 2019. An oligo-His-tag of a targeting module does not influence its biodistribution and the retargeting capabilities of UniCAR T cells. Sci. Rep. 9 (1), 10547. https://doi.org/10.1038/s41598-019-47044-4.

Kang, D., Sun, S., Kurnik, M., Morales, D., Dahlquist, F.W., Plaxco, K.W., 2017. New architecture for reagentless, protein-based electrochemical biosensors. J. Am. Chem. Soc. 139 (35), 12113–12116. https://doi.org/10.1021/jacs.7b05953.

Khairil Anuar, I.N.A., Banerjee, A., Keeble, A.H., Carella, A., Nikov, G.I., Howarth, M., 2019. Spy&Go purification of SpyTag-proteins using pseudo-SpyCatcher to access an oligomerization toolbox. Nat. Commun. 10 (1), 1734. https://doi.org/10.1038/s41467-019-09678-w.

Khan, F., Legler, P.M., Mease, R.M., Duncan, E.H., Bergmann-Leitner, E.S., Angov, E., 2012. Histidine affinity tags affect MSP142 structural stability and immunodominance in mice. Biotechnol. J. 7 (1), 133–147. https://doi.org/10.1002/biot.201100331.

Kichler, A., Leborgne, C., Danos, O., Bechinger, B., 2007. Characterization of the gene transfer process mediated by histidine-rich peptides. J. Mol. Med. 85 (2), 191–201. https://doi.org/10.1007/s00109-006-0119-4.

Kimple, M.E., Sondek, J., 2004. Overview of affinity tags for protein purification. In: Current Protocols in Protein Science. https://doi.org/10.1002/0471140864.ps0909s36. Chapter 9, Unit 9 9.

Kirby, A.J., Marriott, R.E., 1995. Mechanism of RNA cleavage by imidazole. Catalysis vs medium effects. J. Am. Chem. Soc. 117 (2), 833–834. https://doi.org/10.1021/ja00107a034.

Kitai, T., Watanabe, Y., Toyoshima, Y.Y., Kobayashi, T., Murayama, T., Sakaue, H., Suzuki, H., Takahagi, T., 2011. Simple method of synthesizing Nickel–nitrilotriacetic acid gold nanoparticles with a narrow size distribution for protein labeling. Jpn. J. Appl. Phys. 50 (9), 095002 https://doi.org/10.1143/jjap.50.095002.

Klose, J., Wendt, N., Kubald, S., Krause, E., Fechner, K., Beyermann, M., Bienert, M., Rudolph, R., Rothemund, S., 2004. Hexa-histidin tag position influences disulfide structure but not binding behavior of in vitro folded N-terminal domain of rat corticotropin-releasing factor receptor type 2a. Protein Sci. 13 (9), 2470–2475. https://doi.org/10.1110/ps.04835904.

Knecht, S., Ricklin, D., Eberle, A.N., Ernst, B., 2009. Oligohis-tags: mechanisms of binding to Ni2+-NTA surfaces. J. Mol. Recog. 22 (4), 270–279. https://doi.org/10.1002/jmr.941.

Kollmannsperger, A., Sharei, A., Raulf, A., Heilemann, M., Langer, R., Jensen, K.F., Wieneke, R., Tampe, R., 2016. Live-cell protein labelling with nanometre precision by cell squeezing. Nat. Commun. 7, 10372. https://doi.org/10.1038/ncomms10372.

Korpi, A., Anaya-Plaza, E., Valimaki, S., Kostiainen, M., 2020. Highly ordered protein cage assemblies: a toolkit for new materials. Wiley interdisciplinary reviews. Nanomed, Nanobiotechnol. 12 (1), e1578 https://doi.org/10.1002/wnan.1578.

Kreisig, T., Prasse, A.A., Zscharnack, K., Volke, D., Zuchner, T., 2014. His-tag protein monitoring by a fast mix-and-measure immunoassay. Sci. Rep. 4, 5613. https://doi.org/10.1038/srep05613.

Lagasse, H.A., Alexaki, A., Simhadri, V.L., Katagiri, N.H., Jankowski, W., Sauna, Z.E., Kimchi-Sarfaty, C., 2017. Recent advances in (therapeutic protein) drug development. F1000Research 6, 113. https://doi.org/10.12688/f1000research.9970.1.

Lata, S., Reichel, A., Brock, R., Tampe, R., Piehler, J., 2005. High-affinity adaptors for switchable recognition of histidine-tagged proteins. J. Am. Chem. Soc. 127 (29), 10205–10215. https://doi.org/10.1021/ja050690c.

Lau, J.L., Dunn, M.K., 2018. Therapeutic peptides: Historical perspectives, current development trends, and future directions. Bioorg. Med. Chem. 26 (10), 2700–2707. https://doi.org/10.1016/j.bmc.2017.06.052.

Ley, C., Holtmann, D., Mangold, K.M., Schrader, J., 2011. Immobilization of histidine-tagged proteins on electrodes. Colloids Surf. B: Biointerfaces 88 (2), 539–551. https://doi.org/10.1016/j.colsurfb.2011.07.044.

Li, X., Song, S., Pei, Y., Dong, H., Aastrup, T., Pei, Z., 2016. Oriented and reversible immobilization of His-tagged proteins on two- and three-dimensional surfaces for study of protein–protein interactions by a QCM biosensor. Sensors Actuators B Chem. 224, 814–822. https://doi.org/10.1016/j.snb.2015.10.096.

Lindbo, S., Garousi, J., Astrand, M., Honarvar, H., Orlova, A., Hober, S., Tolmachev, V., 2016. Influence of Histidine-containing Tags on the biodistribution of ADAPT scaffold proteins. Bioconjug. Chem. 27 (3), 716–726. https://doi.org/10.1021/acs.bioconjchem.5b00677.

Liu, X.X., Melman, A., 2013. Templated alkylation of hexahistidine with Baylis-Hillman esters. Chem. Commun. 49 (79), 9042–9044. https://doi.org/10.1039/c3cc43271h.

Liu, Y.C., Rieben, N., Iversen, L., Sorensen, B.S., Park, J., Nygard, J., Martinez, K.L., 2010. Specific and reversible immobilization of histidine-tagged proteins on

functionalized silicon nanowires. Nanotechnology 21 (24), 245105. https://doi.org/10.1088/0957-4484/21/24/245105.
Lo, S.L., Wang, S., 2008. An endosomolytic Tat peptide produced by incorporation of histidine and cysteine residues as a nonviral vector for DNA transfection. Biomaterials 29 (15), 2408–2414. https://doi.org/10.1016/j.biomaterials.2008.01.031.
López-Laguna, H., Sala, R., Sánchez, J.M., Álamo, P., Unzueta, U., Sánchez-Chardi, A., Serna, N., Sánchez-García, L., Voltà-Durán, E., Mangues, R., Villaverde, A., Vázquez, E., 2019. Nanostructure empowers active tumor targeting in ligand-based molecular delivery. In: Particle and Particle Characterization System.
Lopez-Laguna, H., Unzueta, U., Conchillo-Sole, O., Sanchez-Chardi, A., Pesarrodona, M., Cano-Garrido, O., Volta, E., Sanchez-Garcia, L., Serna, N., Saccardo, P., Mangues, R., Villaverde, A., Vazquez, E., 2019. Assembly of histidine-rich protein materials controlled through divalent cations. Acta Biomater. 83, 257–264. https://doi.org/10.1016/j.actbio.2018.10.030.
López-Laguna, H., Cubarsi, R., Unzueta, U., Mangues, R., Vázquez, E., Villaverde, A., 2020. Endosomal escape of protein nanoparticles engineered through humanized histidine-rich peptides. Sci. China Mater. 63 (4), 644–653. https://doi.org/10.1007/s40843-019-1231-y.
Lopez-Laguna, H., Sanchez, J., Unzueta, U., Mangues, R., Vazquez, E., Villaverde, A., 2020. Divalent cations: a molecular glue for protein materials. Trends Biochem. Sci. 45 (11), 992–1003. https://doi.org/10.1016/j.tibs.2020.08.003.
López-Laguna, H., Parladé, E., Álamo, P., Sánchez, J.M., Voltà-Durán, E., Serna, N., Sánchez-García, L., Cano-Garrido, O., Sánchez-Chardi, A., Villaverde, A., Mangues, R., Unzueta, U., Vázquez, E., 2021. In vitro fabrication of microscale secretory granules. Adv. Funct. Mater. 2100914. https://doi.org/10.1002/adfm.202100914.
Loughran, S.T., Bree, R.T., Walls, D., 2017. Purification of polyhistidine-tagged proteins. Methods Mol. Biol. 1485, 275–303. https://doi.org/10.1007/978-1-4939-6412-3_14.
Maniaci, B., Lipper, C.H., Anipindi, D.L., Erlandsen, H., Cole, J.L., Stec, B., Huxford, T., Love, J.J., 2019. Design of high-affinity metal-controlled protein dimers. Biochemistry 58 (17), 2199–2207. https://doi.org/10.1021/acs.biochem.9b00055.
Markert, M., Scheffler, U., Mahrwald, R., 2009. Asymmetric histidine-catalyzed cross-aldol reactions of enolizable aldehydes: access to defined configured quaternary stereogenic centers. J. Am. Chem. Soc. 131 (46), 16642–16643. https://doi.org/10.1021/ja907054y.
Martos-Maldonado, M.C., Hjuler, C.T., Sorensen, K.K., Thygesen, M.B., Rasmussen, J.E., Villadsen, K., Midtgaard, S.R., Kol, S., Schoffelen, S., Jensen, K.J., 2018. Selective N-terminal acylation of peptides and proteins with a Gly-His tag sequence. Nat. Commun. 9 (1), 3307. https://doi.org/10.1038/s41467-018-05695-3.
Mendes, A.C., Baran, E.T., Reis, R.L., Azevedo, H.S., 2013. Self-assembly in nature: using the principles of nature to create complex nanobiomaterials. Wiley Interdiscip. Rev. Nanomed. Nanobiotechnol. 5 (6), 582–612. https://doi.org/10.1002/wnan.1238.
Mikula, E., Silva, C.E., Kopera, E., Zdanowski, K., Radecki, J., Radecka, H., 2018. Highly sensitive electrochemical biosensor based on redox – active monolayer for detection of anti-hemagglutinin antibodies against swine-origin influenza virus H1N1 in sera of vaccinated mice. BMC Vet. Res. 14 (1), 328. https://doi.org/10.1186/s12917-018-1668-9.
Min, T.T., Yamabhai, M., 2020. Human hexa-Histidine-tagged single-chain variable fragments for bioimaging of bacterial infections. ACS Omega 6 (1), 762–774. https://doi.org/10.1021/acsomega.0c05340.
Minkner, R., Xu, J., Takemura, K., Boonyakida, J., Watzig, H., Park, E.Y., 2020. Ni-modified magnetic nanoparticles for affinity purification of His-tagged proteins from the complex matrix of the silkworm fat body. J Nanobiotechnol. 18 (1), 159. https://doi.org/10.1186/s12951-020-00715-1.
Mishra, V., 2020. Affinity tags for protein purification. Curr. Protein Pept. Sci. 21 (8), 821–830. https://doi.org/10.2174/1389203721666200606220109.
Mitran, B., Altai, M., Hofström, C., Honarvar, H., Sandström, M., Orlova, A., Tolmachev, V., Graslund, T., 2015. Evaluation of 99mTc-Z IGF1R:4551-GGGC affibody molecule, a new probe for imaging of insulin-like growth factor type 1 receptor expression. Amino Acids 47 (2), 303–315. https://doi.org/10.1007/s00726-014-1859-z.
Mohanty, A.K., Wiener, M.C., 2004. Membrane protein expression and production: effects of polyhistidine tag length and position. Protein Expr. Purif. 33 (2), 311–325. https://doi.org/10.1016/j.pep.2003.10.010.
Mónico, A., Martínez-Senra, E., Cañada, F.J., Zorrilla, S., Pérez-Sala, D., 2017. Drawbacks of dialysis procedures for removal of EDTA. PLoS One 12 (1), e0169843. https://doi.org/10.1371/journal.pone.0169843.
Munadziroh, E., Ulfa, E.U., Labiqah, A., Asmarani, O., Puspaningsih, N.N.T., 2020. Effect of poly-Histidine Tag position toward inhibition activity of secretory leukocyte protease inhibitor as candidate for material wound healing. Avicenna J. Med. Biotechnol. 12 (1), 32–36.
Munsell, E.V., Ross, N.L., Sullivan, M.O., 2016. Journey to the center of the cell: current nanocarrier design strategies targeting biopharmaceuticals to the cytoplasm and nucleus. Curr. Pharm. Des. 22 (9), 1227–1244. https://doi.org/10.2174/1381612822666151216151420.
Nam, D.H., Lee, J.O., Sang, B.I., Won, K., Kim, Y.H., 2013. Silaffin peptides as a novel signal enhancer for gravimetric biosensors. Appl. Biochem. Biotechnol. 170 (1), 25–31. https://doi.org/10.1007/s12010-013-0161-y.
Obermaier, C., Griebel, A., Westermeier, R., 2015. Principles of protein labeling techniques. Methods Mol. Biol. 1295, 153–165. https://doi.org/10.1007/978-1-4939-2550-6_13.
Otsyula, N., Angov, E., Bergmann-Leitner, E., Koech, M., Khan, F., Bennett, J., Otieno, L., Cummings, J., Andagalu, B., Tosh, D., Waiturmbi, J., Richie, N., Shi, M., Miller, L., Otieno, W., Otieno, G.A., Ware, L., House, B., Godeaux, O., Dubois, M.C., Ogutu, B., Ballou, W.R., Soisson, L., Diggs, C., Cohen, J., Polhemus, M., Heppner Jr., D.G., Ockenhouse, C.F., Spring, M.D., 2013. Results from tandem Phase 1 studies evaluating the safety, reactogenicity and immunogenicity of the vaccine candidate antigen *Plasmodium falciparum* FVO merozoite surface protein-1 (MSP1(42)) administered intramuscularly with adjuvant system AS01. Malar. J. 12, 29. https://doi.org/10.1186/1475-2875-12-29.
Pallares, V., Unzueta, U., Falgas, A., Sanchez-Garcia, L., Serna, N., Gallardo, A., Morris, G.A., Alba-Castellon, L., Alamo, P., Sierra, J., Villaverde, A., Vazquez, E., Casanova, I., Mangues, R., 2020. An Auristatin nanoconjugate targeting CXCR4+ leukemic cells blocks acute myeloid leukemia dissemination. J. Hematol. Oncol. 13 (1), 36. https://doi.org/10.1186/s13045-020-00863-9.
Paray, B.A., Ahmad, A., Khan, J.M., Taufiq, F., Pathan, A., Malik, A., Ahmed, M.Z., 2021. The role of the multifunctional antimicrobial peptide melittin in gene delivery. Drug Discov. Today 26 (4), 1053–1059. https://doi.org/10.1016/j.drudis.2021.01.004.
Peciak, K., Laurine, E., Tommasi, R., Choi, J.W., Brocchini, S., 2019. Site-selective protein conjugation at histidine. Chem. Sci. 10 (2), 427–439. https://doi.org/10.1039/c8sc03355b.
Pellis, A., Vastano, M., Quartinello, F., Herrero Acero, E., Guebitz, G.M., 2017. His-Tag immobilization of cutinase 1 from *Thermobifida cellulosilytica* for solvent-free synthesis of polyesters. Biotechnol. J. 12 (10) https://doi.org/10.1002/biot.201700322.
Peschke, T., Bitterwolf, P., Rabe, K.S., Niemeyer, C.M., 2019. Self-immobilizing oxidoreductases for flow biocatalysis in miniaturized packed-bed reactors. Chem. Eng. Technol. 42 (10), 2009–2017. https://doi.org/10.1002/ceat.201900073.
Pina, A.S., Lowe, C.R., Roque, A.C., 2014. Challenges and opportunities in the purification of recombinant tagged proteins. Biotechnol. Adv. 32 (2), 366–381. https://doi.org/10.1016/j.biotechadv.2013.12.001.
Plz, M., Petrovicova, T., Rebros, M., 2020. Semi-continuous flow biocatalysis with affinity co-immobilized ketoreductase and glucose dehydrogenase. Molecules 25 (18). https://doi.org/10.3390/molecules25184278.
Porath, J., 1992. Immobilized metal ion affinity chromatography. Protein Expr. Purif. 3 (4), 263–281. https://doi.org/10.1016/1046-5928(92)90001-D.
Porath, J., Carlsson, J.A.N., Olsson, I., Belfrage, G., 1975. Metal chelate affinity chromatography, a new approach to protein fractionation. Nature 258 (5536), 598–599. https://doi.org/10.1038/258598a0.
Povedano, E., Ruiz-Valdepenas Montiel, V., Gamella, M., Serafín, V., Pedrero, M., Moranova, L., Bartosik, M., Montoya, J.J., Yanez-Sedeno, P., Campuzano, S., Pingarron, J.M., 2020. A novel zinc finger protein-based amperometric biosensor for miRNA determination. Anal. Bioanal. Chem. 412 (21), 5031–5041. https://doi.org/10.1007/s00216-019-02219-w.
Raghunath, G., Dyer, R.B., 2019. Kinetics of histidine-tagged protein association to nickel-decorated liposome surfaces. Langmuir 35 (38), 12550–12561. https://doi.org/10.1021/acs.langmuir.9b01700.
Rai, D.K., Segundo, F.D., Schafer, E., Burrage, T.G., Rodriguez, L.L., de Los Santos, T., Hoeprich, P.D., Rieder, E., 2016. Novel 6xHis tagged foot-and-mouth disease virus vaccine bound to nanolipoprotein adjuvant via metal ions provides antigenic distinction and effective protective immunity. Virology 495, 136–147. https://doi.org/10.1016/j.virol.2016.04.027.
Ravikumar, R., Chen, L.H., Jayaraman, P., Poh, C.L., Chan, C.C., 2018. Chitosan-nickel film based interferometric optical fiber sensor for label-free detection of histidine tagged proteins. Biosens. Bioelectron. 99, 578–585. https://doi.org/10.1016/j.bios.2017.08.012.
Ren, G., Gong, X., Wang, B., Chen, Y., Huang, J., 2015. Affinity ionic liquids for the rapid liquid–liquid extraction purification of hexahistidine tagged proteins. Sep. Purif. Technol. 146, 114–120. https://doi.org/10.1016/j.seppur.2015.03.025.
Riguero, V., Clifford, R., Dawley, M., Dickson, M., Gastfriend, B., Thompson, C., Wang, S.-C., O'Connor, E., 2020. Immobilized metal affinity chromatography optimization for poly-histidine tagged proteins. J. Chromatogr. A 1629, 461505. https://doi.org/10.1016/j.chroma.2020.461505.
Rodrigues, R.C., Ortiz, C., Berenguer-Murcia, A., Torres, R., Fernandez-Lafuente, R., 2013. Modifying enzyme activity and selectivity by immobilization. Chem. Soc. Rev. 42 (15), 6290–6307. https://doi.org/10.1039/c2cs35231a.
Rosen, C.B., Kodal, A.L., Nielsen, J.S., Schaffert, D.H., Scavenius, C., Okholm, A.H., Voigt, N.V., Enghild, J.J., Kjems, J., Torring, T., Gothelf, K.V., 2014. Template-directed covalent conjugation of DNA to native antibodies, transferrin and other metal-binding proteins. Nat. Chem. 6 (9), 804–809. https://doi.org/10.1038/nchem.2003.
Sabaty, M., Grosse, S., Adryanczyk, G., Boiry, S., Biaso, F., Arnoux, P., Pignol, D., 2013. Detrimental effect of the 6 His C-terminal tag on YedY enzymatic activity and influence of the TAT signal sequence on YedY synthesis. BMC Biochem. 14, 28. https://doi.org/10.1186/1471-2091-14-28.
Sanchez, J.M., Lopez-Laguna, H., Alamo, P., Serna, N., Sanchez-Chardi, A., Nolan, V., Cano-Garrido, O., Casanova, I., Unzueta, U., Vazquez, E., Mangues, R., Villaverde, A., 2020. Artificial inclusion bodies for clinical development. Adv. Sci. 7 (3), 1902420. https://doi.org/10.1002/advs.201902420.
Sanchez, J.M., López-Laguna, H., Serna, N., Unzueta, U., Clop, P.D., Villaverde, A., Vazquez, E., 2021. Engineering the performance of artificial inclusion bodies built of catalytic β-galactosidase. ACS Sustain. Chem. Eng. 9 (6), 2552–2558. https://doi.org/10.1021/acssuschemeng.0c08345.
Sanchez-Garcia, L., Martin, L., Mangues, R., Ferrer-Miralles, N., Vazquez, E., Villaverde, A., 2016. Recombinant pharmaceuticals from microbial cells: a 2015 update. Microb. Cell Factories 15, 33. https://doi.org/10.1186/s12934-016-0437-3.
Scheffler, U., Mahrwald, R., 2012. Histidine-catalyzed asymmetric aldol addition of enolizable aldehydes: insights into its mechanism. J. Organ. Chem. 77 (5), 2310–2330. https://doi.org/10.1021/jo202558f.

Schneider, F., 1978. Histidine in enzyme active centers. Angew. Chem. Int. Ed. Engl. 17 (8), 583–592. https://doi.org/10.1002/anie.197805831.
Schneider, A.F.L., Hackenberger, C.P.R., 2017. Fluorescent labelling in living cells. Curr. Opin. Biotechnol. 48, 61–68. https://doi.org/10.1016/j.copbio.2017.03.012.
Schoonen, L., van Esterik, K.S., Zhang, C., Ulijn, R.V., Nolte, R.J.M., Hest, J., 2017. Alternative application of an affinity purification tag: hexahistidines in ester hydrolysis. Sci. Rep. 7 (1), 14772. https://doi.org/10.1038/s41598-017-15310-y.
Schwaminger, S.P., Fraga-Garcia, P., Blank-Shim, S.A., Straub, T., Hasibeck, M., Muraca, F., Dawson, K.A., Berensmeier, S., 2019. Magnetic one-step purification of His-tagged protein by bare iron oxide nanoparticles. ACS Omega 4 (2), 3790–3799. https://doi.org/10.1021/acsomega.8b03348.
Serna, N., Sanchez-Garcia, L., Unzueta, U., Diaz, R., Vazquez, E., Mangues, R., Villaverde, A., 2018. Protein-based therapeutic killing for cancer therapies. Trends Biotechnol. 36 (3), 318–335. https://doi.org/10.1016/j.tibtech.2017.11.007.
Serna, N., Alamo, P., Ramesh, P., Vinokurova, D., Sanchez-Garcia, L., Unzueta, U., Gallardo, A., Cespedes, M.V., Vazquez, E., Villaverde, A., Mangues, R., Medema, J.P., 2020a. Nanostructured toxins for the selective destruction of drug-resistant human CXCR4(+) colorectal cancer stem cells. J. Control. Release 320, 96–104. https://doi.org/10.1016/j.jconrel.2020.01.019.
Serna, N., Cano-Garrido, O., Sanchez, J.M., Sanchez-Chardi, A., Sanchez-Garcia, L., Lopez-Laguna, H., Fernandez, E., Vazquez, E., Villaverde, A., 2020b. Release of functional fibroblast growth factor-2 from artificial inclusion bodies. J. Control. Release. https://doi.org/10.1016/j.jconrel.2020.08.007.
Serna, N., Cano-Garrido, O., Sánchez-García, L., Pesarrodona, M., Unzueta, U., Sánchez-Chardi, A., Mangues, R., Vázquez, E., Villaverde, A., 2020c. Engineering protein venoms as self-assembling CXCR4-targeted cytotoxic nanoparticles. Part. Part. Syst. Charact. 37 (6), 2000040. https://doi.org/10.1002/ppsc.202000040.
Shakya, A., Imado, E., Nguyen, P.K., Matsuyama, T., Horimoto, K., Hirata, I., Kato, K., 2020. Oriented immobilization of basic fibroblast growth factor: bioengineered surface design for the expansion of human mesenchymal stromal cells. Sci. Rep. 10 (1), 8762. https://doi.org/10.1038/s41598-020-65572-2.
Shimada, J., Maruyama, T., Hosogi, T., Tominaga, J., Kamiya, N., Goto, M., 2008. Conjugation of DNA with protein using His-tag chemistry and its application to the aptamer-based detection system. Biotechnol. Lett. 30 (11), 2001–2006. https://doi.org/10.1007/s10529-008-9784-4.
Signore, M., Manganelli, V., Hodge, A., 2017. Antibody Validation by Western Blotting. Methods Mol. Biol. 1606, 51–70. https://doi.org/10.1007/978-1-4939-6990-6_4.
Singh, A.N., McGuire, M.J., Li, S., Hao, G., Kumar, A., Sun, X., Brown, K.C., 2014. Dimerization of a phage-display selected peptide for imaging of alphavbeta6-integrin: two approaches to the multivalent effect. Theranostics 4 (7), 745–760. https://doi.org/10.7150/thno.7811.
Singh, M., Sori, H., Ahuja, R., Meena, J., Sehgal, D., Panda, A.K., 2020. Effect of N-terminal poly histidine-tag on immunogenicity of *Streptococcus pneumoniae* surface protein SP0845. Int. J. Biol. Macromol. 163, 1240–1248. https://doi.org/10.1016/j.ijbiomac.2020.07.056.
Smith, S.A., Selby, L.I., Johnston, A.P.R., Such, G.K., 2019. The endosomal escape of nanoparticles: toward more efficient cellular delivery. Bioconjug. Chem. 30 (2), 263–272. https://doi.org/10.1021/acs.bioconjchem.8b00732.
Soh, N., 2008. Selective chemical labeling of proteins with small fluorescent molecules based on metal-chelation methodology. Sensors 8 (2), 1004–1024. https://doi.org/10.3390/s8021004.
Soleri, R., Demey, H., Tria, S.A., Guiseppi-Elie, A., Hassine, A.I., Gonzalez, C., Bazin, I., 2015. Peptide conjugated chitosan foam as a novel approach for capture-purification and rapid detection of hapten – example of ochratoxin A. Biosens. Bioelectron. 67, 634–641. https://doi.org/10.1016/j.bios.2014.09.084.
Spriestersbach, A., Kubicek, J., Schafer, F., Block, H., Maertens, B., 2015. Purification of His-tagged proteins. Methods Enzymol. 559, 1–15. https://doi.org/10.1016/bs.mie.2014.11.003.
Sulkowski, E., 1985. Purification of proteins by IMAC. Trends Biotechnol. 3 (1), 1–7. https://doi.org/10.1016/0167-7799(85)90068-X.
Ta, D.T., Guedens, W., Vranken, T., Vanschoenbeek, K., Steen Redeker, E., Michiels, L., Adriaensens, P., 2016. Enhanced biosensor platforms for detecting the atherosclerotic biomarker VCAM1 based on bioconjugation with uniformly oriented VCAM1-targeting nanobodies. Biosensors 6 (3). https://doi.org/10.3390/bios6030034.
Tolmachev, V., Hofstrom, C., Malmberg, J., Ahlgren, S., Hosseinimehr, S.J., Sandstrom, M., Abrahmsen, L., Orlova, A., Graslund, T., 2010. HEHEHE-tagged affibody molecule may be purified by IMAC, is conveniently labeled with [(9)(9)(m)Tc(CO)(3)](+), and shows improved biodistribution with reduced hepatic radioactivity accumulation. Bioconjug. Chem. 21 (11), 2013–2022. https://doi.org/10.1021/bc1002357.
Tourdot, S., Hickling, T.P., 2019. Nonclinical immunogenicity risk assessment of therapeutic proteins. Bioanalysis 11 (17), 1631–1643. https://doi.org/10.4155/bio-2018-0246.
Tunn, I., de Leon, A.S., Blank, K.G., Harrington, M.J., 2018. Tuning coiled coil stability with histidine-metal coordination. Nanoscale 10 (48), 22725–22729. https://doi.org/10.1039/c8nr07259k.
Unzueta, U., Roldan, M., Pesarrodona, M., Benitez, R., Sanchez-Chardi, A., Conchillo-Sole, O., Mangues, R., Villaverde, A., Vazquez, E., 2020. Self-assembling as regular nanoparticles dramatically minimizes photobleaching of tumour-targeted GFP. Acta Biomater. 103, 272–280. https://doi.org/10.1016/j.actbio.2019.12.003.
Valenti, L.E., De Pauli, C.P., Giacomelli, C.E., 2006. The binding of Ni(II) ions to hexahistidine as a model system of the interaction between nickel and His-tagged proteins. J. Inorg. Biochem. 100 (2), 192–200. https://doi.org/10.1016/j.jinorgbio.2005.11.003.
Vallina-Garcia, R., del Mar Garcia-Suarez, M., Fernandez-Abedul, M.T., Mendez, F.J., Costa-Garcia, A., 2007. Oriented immobilisation of anti-pneumolysin Fab through a histidine tag for electrochemical immunosensors. Biosens. Bioelectron. 23 (2), 210–217. https://doi.org/10.1016/j.bios.2007.04.001.
van Eldijk, M.B., Schoonen, L., Cornelissen, J.J., Nolte, R.J., van Hest, J.C., 2016. Metal ion-induced self-assembly of a multi-responsive block copolypeptide into well-defined nanocapsules. Small 12 (18), 2476–2483. https://doi.org/10.1002/smll.201503889.
Vermeulen, L.M.P., Brans, T., Samal, S.K., Dubruel, P., Demeester, J., De Smedt, S.C., Remaut, K., Braeckmans, K., 2018. Endosomal size and membrane leakiness influence proton sponge-based rupture of endosomal vesicles. ACS Nano 12 (3), 2332–2345. https://doi.org/10.1021/acsnano.7b07583.
Voltà-Durán, E., Cano-Garrido, O., Serna, N., López-Laguna, H., Sánchez-García, L., Pesarrodona, M., Sánchez-Chardi, A., Mangues, R., Villaverde, A., Vázquez, E., Unzueta, U., 2019. Controlling self-assembling and tumor cell-targeting of protein-only nanoparticles through modular protein engineering. Sic. China Mater. 63 (1), 147–156. https://doi.org/10.1007/s40843-019-9582-9.
Vorobyeva, A., Schulga, A., Konovalova, E., Guler, R., Lofblom, J., Sandstrom, M., Garousi, J., Chernov, V., Bragina, O., Orlova, A., Tolmachev, V., Deyev, S.M., 2019. Optimal composition and position of histidine-containing tags improves biodistribution of (99m)Tc-labeled DARPin G3. Sci. Rep. 9 (1), 9405. https://doi.org/10.1038/s41598-019-45795-8.
Wang, Y., Wang, G., Xiao, Y., Yang, Y., Tang, R., 2014a. Yolk-shell nanostructured Fe3O4@NiSiO3 for selective affinity and magnetic separation of His-tagged proteins. ACS Appl. Mater. Interfaces 6 (21), 19092–19099. https://doi.org/10.1021/am505041a.
Wang, Z., Ding, X., Li, S., Shi, J., Li, Y., 2014b. Engineered fluorescence tags for in vivo protein labelling. RSC Adv. 4 (14), 7235–7245. https://doi.org/10.1039/C3RA46991C.
Wang, Z., Su, M., Li, Y., Wang, Y., Su, Z., 2017. Production of tartaric acid using immobilized recominant cis-epoxysuccinate hydrolase. Biotechnol. Lett. 39 (12), 1859–1863. https://doi.org/10.1007/s10529-017-2419-x.
Wang, F., Ren, X.F., Chen, Z., Li, X.L., Zhu, H.J., Li, S., Ou, X.H., Zhang, C., Zhang, F.X., Zhu, B.C., 2019. The N-terminal His-tag affects the triglyceride lipase activity of hormone-sensitive lipase in testis. J. Cell. Biochem. 120 (8), 13706–13716. https://doi.org/10.1002/jcb.28643.
Watly, J., Simonovsky, E., Wieczorek, R., Barbosa, N., Miller, Y., Kozlowski, H., 2014. Insight into the coordination and the binding sites of Cu2+ by the Histidyl-6-Tag USING experimental and computational tools. Inorg. Chem. 53 (13), 6675–6683. https://doi.org/10.1021/ic500387u.
Wegner, S.V., Schenk, F.C., Spatz, J.P., 2016. Cobalt(III)-mediated permanent and stable immobilization of histidine-tagged proteins on NTA-functionalized surfaces. Chemistry 22 (9), 3156–3162. https://doi.org/10.1002/chem.201504465.
Wijeratne, S., Liu, W., Dong, J., Ning, W., Ratnayake, N.D., Walker, K.D., Bruening, M.L., 2016. Layer-by-Layer deposition with polymers containing nitrilotriacetate, a convenient route to fabricate metal- and protein-binding films. ACS Appl. Mater. Interfaces 8 (16), 10164–10173. https://doi.org/10.1021/acsami.6b00896.
Wilkins, L.E., Hasan, M., Fayter, A.E.R., Biggs, C., Walker, M., Gibson, M.I., 2019. Site-specific conjugation of antifreeze proteins onto polymer-stabilized nanoparticles. Polym. Chem. 10 (23), 2986–2990. https://doi.org/10.1039/c8py01719k.
Woestenenk, E.A., Hammarstrom, M., van den Berg, S., Hard, T., Berglund, H., 2004. His tag effect on solubility of human proteins produced in *Escherichia coli*: a comparison between four expression vectors. J. Struct. Funct. Genom. 5 (3), 217–229. https://doi.org/10.1023/b:jsfg.0000031965.37625.0e.
Wollenberg, L.A., Kabulski, J.L., Powell, M.J., Chen, J., Flora, D.R., Tracy, T.S., Gannett, P.M., 2014. The use of immobilized cytochrome P4502C9 in PMMA-based plug flow bioreactors for the production of drug metabolites. Appl. Biochem. Biotechnol. 172 (3), 1293–1306. https://doi.org/10.1007/s12010-013-0537-z.
Wood, D.W., 2014. New trends and affinity tag designs for recombinant protein purification. Curr. Opin. Struct. Biol. 26, 54–61. https://doi.org/10.1016/j.sbi.2014.04.006.
Xu, C., Xu, K., Gu, H., Zhong, X., Guo, Z., Zheng, R., Zhang, X., Xu, B., 2004. Nitrilotriacetic acid-modified magnetic nanoparticles as a general agent to bind histidine-tagged proteins. J. Am. Chem. Soc. 126 (11), 3392–3393. https://doi.org/10.1021/ja031776d.
Yang, J., Ni, K., Wei, D., Ren, Y., 2015. One-step purification and immobilization of his-tagged protein via Ni2+-functionalized Fe3O4@polydopamine magnetic nanoparticles. Biotechnol. Bioproc. Eng. 20 (5), 901–907. https://doi.org/10.1007/s12257-015-0136-7.
Zhang, W., Luo, Q., Miao, L., Hou, C., Bai, Y., Dong, Z., Xu, J., Liu, J., 2012. Self-assembly of glutathione S-transferase into nanowires. Nanoscale 4 (19), 5847–5851. https://doi.org/10.1039/c2nr31244a.
Zhang, H., Li, Z.F., Snyder, A., Xie, J., Stanciu, L.A., 2014. Functionalized graphene oxide for the fabrication of paraoxon biosensors. Anal. Chim. Acta 827, 86–94. https://doi.org/10.1016/j.aca.2014.04.014.
Zhao, D., Huang, Z., 2016. Effect of His-Tag on Expression, Purification, and Structure of Zinc Finger Protein, ZNF191(243-368). Bioinorg. Chem. Appl. 2016, 8206854. https://doi.org/10.1155/2016/8206854.
Zhao, X., Hong, H., Cheng, X., Liu, S., Deng, T., Guo, Z., Wu, Z., 2017. One-step purification and immobilization of extracellularly expressed sortase A by magnetic

particles to develop a robust and recyclable biocatalyst. Sci. Rep. 7 (1), 6561. https://doi.org/10.1038/s41598-017-06856-y.

Zheng, L.L., Li, C.M., Zhen, S.J., Li, Y.F., Huang, C.Z., 2016. His-tag based in situ labelling of progeny viruses for real-time single virus tracking in living cells. Nanoscale 8 (44), 18635–18639. https://doi.org/10.1039/c6nr05806j.

Zhou, Y., Yuan, S., Liu, Q., Yan, D., Wang, Y., Gao, L., Han, J., Shi, H., 2017. Synchronized purification and immobilization of his-tagged beta-glucosidase via Fe3O4/PMG core/shell magnetic nanoparticles. Sci. Rep. 7, 41741. https://doi.org/10.1038/srep41741.

Annex 6 (Tables)

Table 1. A taste of protein structural and functional heterogeneity. Several protein-based assemblies and their respective physiological relevance are displayed.

Type of assembly	Physiological relevance
Linear protein assemblies	Give tremendous structural stability, motility and sustenance to cells and tissues (e.g., collagen and actin) [325,326]
Ring protein assemblies	Involved in fundamental biochemical processes related to DNA processivity and structural dynamics (e.g., DNA clamps, helicases, and nucleases) [327–329]
Tubular protein assemblies	Used to create cellular pores or viral tubular structures for host infection and genetic material storage (e.g., tobacco mosaic virus capsid protein and aquaporins) [330,331]
Catenane protein assemblies	Exhibit structural, mechanical, and interactive properties (e.g., peroxiredoxin III and HK79 Bacteriophage Capsid) [332,333]
Knot protein assemblies	Allow the assembly not to be disentangled when pulled from the N and C -termini simultaneously. Although the functional implications are not fully understood (e.g., 3_1 knots) [334]
Protein cage assemblies	Endeavor compartmentalization of organic molecules providing spatial control over certain biological processes (e.g., ferritins, chaperonins and clathrin cages) [335–337]
Bacterial compartments	Allow bacteria to create reaction chambers that enclose enzymes or other proteins (e.g., encapsulins) [338]

Table 2. Classification of chemical elements under the essentiality criteria (abundances, toxicity and pharmacological relevance are also displayed).

<table>
<tr><th>Essentiality criteria</th><th colspan="3">Chemical elements</th></tr>
<tr><td rowspan="3">Essential elements [49]</td><td>Abundant
(99.9% mass)</td><td colspan="2">Oxygen (O); 65 % mass
Carbon (C); 18.5 % mass
Hydrogen (H); 10 % mass
Nitrogen (N); 3.2 % mass
Calcium (Ca); 1.5 % mass
Phosphor (P); 1 % mass
Sulfur (S); 0.3 % mass
Potassium (K); 0.4 % mass
Sodium (Na); 0.2 % mass
Chlorine (Cl); 0.2 % mass
Magnesium (Mg); 0.1 % mass</td></tr>
<tr><td rowspan="2">Less abundant
(<0.1 % mass)</td><td>Traces
(mg)</td><td>Copper (Cu)
Iron (Fe)
Zinc (Zn)</td></tr>
<tr><td>Ultratraces
(<mg)</td><td>Vanadium (V)
Nickel (Ni)
Cobalt (Co)
Molybdenum (Mo)
Manganesium (Mn)
Chromium (Cr)</td></tr>
<tr><td>Toxic elements [70,72]</td><td colspan="3">Cadmium (Cd)
Mercury (Hg)
Lead (Pb)
Uranium (U)
Aluminum (Al)</td></tr>
<tr><td>Non-essential elements [339–344]
(Pharmacological interests) *</td><td colspan="3">Technetium (Tc)
Silver (Ag)
Gold (Au)
Platinum (Pt)
Ruthenium (Ru)
Barium (Ba)
Titanium (Ti)</td></tr>
</table>

*Although these elements are not essential, could be used in quiet safe ranges for pharmacological purposes.

Table 3. Abnormalities linked to metal ion deficiencies or overloads, adapted from [345].

Metal ion	Group nature	Abnormalities
Calcium	Alkaline earth metal	Related to: cardiovascular, gastrointestinal, and neurodegenerative diseases when dysregulated. Kidney stones, myocardial infarction and constipation when overloaded [346]
Magnesium	Alkaline earth metal	Deficiency: Produces a multisystemic disorder [347]
Copper	Transition metal	Deficiency: Altered energy production (metabolism), and oxidative damage Excess: Alzheimer's and Wilson and Menkes diseases [348]
Iron	Transition metal	Deficiency: Anemia disease Excess: Myelodysplastic syndromes, hemochromatosis, thalassemia, and liver and cardiovascular diseases [349]
Zinc	Transition metal	Deficiency: Eye and skin lesions, diarrhea, infections and altered immunity Excess: Calcium deregulation and neurotoxicity [350]
Vanadium	Transition metal	Related to: Glucose metabolism (diabetes) and parasitosis [351]
Nickel	Transition metal	Related to: Lung fibrosis, allergy, and cardiovascular and kidney diseases [352]
Cobalt	Transition metal	Related to: Cardiomyopathy and cancer (especially when overloaded) [353]
Molybdenum	Transition metal	Deficiency: Seizures, lens dislocation and intellectual disability Excess: Brain damage [354]
Manganese	Transition metal	Related to: Metabolic and neurological disorders [355]
Chromium	Transition metal	Deficiency: Peripheral neuropathies, and reduced glucose sensibility (risk of diabetes) [356]

Table 4. Main physiological functions of divalent (2+) metal ions in the human body, adapted from [345].

Metal ion	Physiological function
Calcium	Essential for vascular hormonal secretion, blood clotting, muscle contraction, transmission of nerve impulse and maintenance of the skeleton [346,357]
Magnesium	Essential for neuromuscular conduction, glycemia and blood pressure regulation, and acting as a cofactor of more than 300 enzymes [347]
Copper	Essential in overall body growth and development, red blood cells formation, and acting as a catalytic cofactor in proteins redox chemistry [348]
Iron	Essential to carry oxygen from the lungs throughout the human body (conforming hemoglobin). Iron also acts as a crucial cofactor for several other proteins and enzymes such as myoglobin, cytochrome, myeloperoxidase, NO synthase, and coenzyme Q10, as examples [349,358]
Zinc	Essential for the adequate functioning of the immune system. Zinc also plays crucial roles in cell growth, division, and tissue healing. It is required by 300 enzymes and 1000 transcription factors [290,350]
Vanadium	It is related to blood sugar regulation, heart functioning, and immune stimulation against bacteria and parasites [351]
Nickel	It is directly involved in lipid metabolism and increases hormonal activity [352,359]
Cobalt	Essential for adequate cell functioning as conforms vitamin B12. Cobalt is also involved in the production of anti- bacterial and viral compounds and red blood vessels [360]
Molybdenum	It is involved in the breaking down process of toxins and waste products. Molybdenum also acts as a cofactor for several enzymes being necessary for the adequate processing of proteins and DNA [354]
Manganese	It is related to normal brain and nerve functioning, blood clotting and sex hormones. Manganese also helps to conform connective and bone tissues, and plays a role in fat and carbohydrate metabolism, and calcium and glycemia regulation [355,361]
Chromium	Essential for fat and cholesterol synthesis. Chromium is also important for glucose breakdown, insulin action, and brain function [356,362]

Table 5. A short description on what to consider when injecting nanomaterial-based prototypes into in vivo models.

Physicochemical property	Toxic effect
Aggregation state	Toxic effects observed by sample sedimentation and accumulation. Related to lack of material's stability and frustrated phagocytosis in tissues, provoking chronic inflammation [175,176]
Cationic surface charge	Toxic effects observed by non-specific interaction with negatively charged cell membranes [177,178]
Release of toxic ions	Toxic effects observed when inorganic metal ions with oxidative, allergenic, and carcinogenic capacities are release from the nanomaterial by corrosion [179,180]
Powdered samples	Toxic effects observed when polydisperse in size and shape grans of powder aggregate after resuspension, changing final drug's therapeutical properties [166,182]
Presence of antigens, allergens, or pollutants	Toxic effects observed when nanoparticles unexpectedly present antigenic moieties to the immune system, cause allergenic reactions by the coadministration with stabilization molecules, or contain non-purified pollutants from the manufacturing process [183,184]
Presence of toxic moieties or pollutants	Toxic effects observed when nanomaterials are formulated using stabilizer cationic PEI molecules, or non-removed detergents, affecting final sample structure and functionality [183,184]
Hydrophobicity and clogging	Toxic effects observed when amphiphilic and detergent-like molecules create a vesicle-like coating on top of material's surface or promoting the exposure of its hydrophobic core that triggers unspecific interactions [187,188]
Non desired catalytic reactions	Toxic effects observed when unexpected photocatalysis phenomena occurs inside the organism after light exposure [189]
Lack of targeting	Toxic effects observed when injected nanomaterials lack of directing molecules and end up accumulating in non-desired tissues [190]

Table 6. A short description of the biodistribution limitations of free drugs.

Limitations	Description
Limited circulation time	1 minute as average lifetime in the bloodstream until tissue absorption, renal clearance, or molecule degradation [218]
Undesired accumulation tendencies	Fat-soluble drugs tend to accumulate in fatty tissues e.g., clorazepate, and water-soluble drugs in interstitial or liquid-based regions, e.g., atenolol [219,363]
Undesired penetration tendencies	Fat-soluble drugs tend to rapidly penetrate cell membranes e.g., rifampin which penetrates the brain, meanwhile, water-soluble drugs not e.g., penicillin [364,365]
Undesired interaction with proteins	Drugs with particular tendencies to interact with bloodstream proteins, creating a protein-drug reservoir that remains in the long term [220]
Lack of targeting	Drugs tend to accumulate in non-desired tissues causing off-target effects and due to its intrinsic physicochemical properties, e.g., chemotherapeutic molecules in cancer treatment, in which less than 1% of the administered dose reaches the tumor [221]

Annex 7 (Declared patents)

Patent 1

Therapeutic nanoconjugates and uses thereof

Antonio Villaverde Corrales, Esther Vázquez Gómez, Ugutz Unzueta Elorza, Ramón Mangues Bafalluy, María Virtudes Céspedes Navarro, Isolda Casanova Rigat, and Héctor López Laguna

International patent · Publication number (WO 2020/148398 A8)

From the invention document…

"The present invention relates to nanostructured conjugates, more specifically to nanostructured fusion proteins suitable for the selective delivery of their conjugated therapeutic agents to specific cell and tissue types. It also relates to nanoparticles comprising such nanostructured proteins and the therapeutic uses thereof".

(12) INTERNATIONAL APPLICATION PUBLISHED UNDER THE PATENT COOPERATION TREATY (PCT)

CORRECTED VERSION

(19) World Intellectual Property Organization
International Bureau

(43) International Publication Date
23 July 2020 (23.07.2020)

WIPO | PCT

(10) International Publication Number
WO 2020/148398 A8

(51) International Patent Classification:
A61K 47/64 (2017.01) *A61K 47/69* (2017.01)

(21) International Application Number:
PCT/EP2020/051048

(22) International Filing Date:
16 January 2020 (16.01.2020)

(25) Filing Language: English

(26) Publication Language: English

(30) Priority Data:
19382031.3 17 January 2019 (17.01.2019) EP

(71) Applicants: **UNIVERSITAT AUTONOMA DE BARCELONA (UAB)** [ES/ES]; Oficina de Valorització i Patents (OVP), Edifici A- Rectorat, Campus universitari s/n, 08193 Bellaterra (Cerdanyola del Valles) (ES). **FUNDACIÓ INSTITUT DE RECERCA DE L'HOSPITAL DE LA SANTA CREU I SANT PAU** [ES/ES]; Sant Antoni Mª Claret, 167, 08025 Barcelona (ES). **CONSORCIO CENTRO DE INVESTIGACIÓN BIOMÉDICA EN RED, M.P.** [ES/ES]; Instituto de Salud Carlos III, Monforte de Lemos, 3-5, Pabellón 11, 28029 Madrid (ES).

(72) Inventors: **VILLAVERDE CORRALES, Antonio**; UNIVERSITAT AUTONOMA DE BARCELONA (UAB), IBB, Campus de la UAB, s/n, 08193 Bellaterra (Cerdanyola del Vallès) (ES). **VÁZQUEZ GÓMEZ, Esther**; UNIVERSITAT AUTONOMA DE BARCELONA (UAB), IBB, Campus de la UAB, s/n, 08193 Bellaterra (Cerdanyola del Vallès) (ES). **UNZUETA ELORZA, Ugutz**; HOSPITAL DE LA SANTA CREU I SANT PAU, Antoni Mª Claret, 167, 08025 Barcelona (ES). **MANGUES BAFALLUY, Ramón**; HOSPITAL DE LA SANTA CREU I SANT PAU, Antoni Mª Claret, 167, 08025 Barcelona (ES). **CÉSPEDES NAVARRO, María Virtudes**; HOSPITAL DE LA SANTA CREU I SANT PAU, Antoni Mª Claret, 167, 08025 Barcelona (ES). **CASANOVA RIGAT, Isolda**; CENTRO DE INVESTIGACIÓN BIOMÉDICA EN, RED, Monforte de Lemos, 5, 28029 Madrid (ES). **LÓPEZ LAGUNA, Hector**; UNIVERSITAT AUTONOMA DE BARCELONA (UAB), IBB, Campus de la UAB, s/n, 08193 Bellaterra (Cerdanyola del Vallès) (ES).

(81) Designated States *(unless otherwise indicated, for every kind of national protection available)*: AE, AG, AL, AM, AO, AT, AU, AZ, BA, BB, BG, BH, BN, BR, BW, BY, BZ, CA, CH, CL, CN, CO, CR, CU, CZ, DE, DJ, DK, DM, DO, DZ, EC, EE, EG, ES, FI, GB, GD, GE, GH, GM, GT, HN, HR, HU, ID, IL, IN, IR, IS, JO, JP, KE, KG, KH, KN, KP, KR, KW, KZ, LA, LC, LK, LR, LS, LU, LY, MA, MD, ME, MG, MK, MN, MW, MX, MY, MZ, NA, NG, NI, NO, NZ, OM, PA, PE, PG, PH, PL, PT, QA, RO, RS, RU, RW, SA, SC, SD, SE, SG, SK, SL, ST, SV, SY, TH, TJ, TM, TN, TR, TT, TZ, UA, UG, US, UZ, VC, VN, WS, ZA, ZM, ZW.

(84) Designated States *(unless otherwise indicated, for every kind of regional protection available)*: ARIPO (BW, GH, GM, KE, LR, LS, MW, MZ, NA, RW, SD, SL, ST, SZ, TZ, UG, ZM, ZW), Eurasian (AM, AZ, BY, KG, KZ, RU, TJ, TM), European (AL, AT, BE, BG, CH, CY, CZ, DE, DK, EE, ES, FI, FR, GB, GR, HR, HU, IE, IS, IT, LT, LU, LV, MC, MK, MT, NL, NO, PL, PT, RO, RS, SE, SI, SK, SM, TR), OAPI (BF, BJ, CF, CG, CI, CM, GA, GN, GQ, GW, KM, ML, MR, NE, SN, TD, TG).

Published:
— *with international search report (Art. 21(3))*
— *with sequence listing part of description (Rule 5.2(a))*
— *with information concerning incorporation by reference of missing element or part (Rule 20.6)*

(48) Date of publication of this corrected version:
07 October 2021 (07.10.2021)

(15) Information about Correction:
see Notice of 07 October 2021 (07.10.2021)

(54) Title: THERAPEUTIC NANOCONJUGATES AND USES THEREOF

(57) Abstract: The present invention relates to nanostructured conjugates, more specifically to nanostructured fusion proteins suitable for the selective delivery of their conjugated therapeutic agents to specific cell and tissue types. It also relates to nanoparticles comprising such nanostructured proteins and the therapeutic uses thereof.

WO 2020/148398 A8

Patent 2

Protein nano- or microparticles as artificial inclusion bodies

Antonio Villaverde Corrales, Esther Vázquez Gómez, Héctor López Laguna, Julieta María Sánchez, and Ramón Mangues Bafalluy

International patent · Publication number (WO 2020/208065A1)

From the invention document…

"The present invention relates to protein particles comprising a cluster of one or more types of assembled self-contained protein, wherein the particle has a size from 50 nm to 50 micrometers; is in form of a pellet in aqueous media; is mechanically stable; and it release a particular percentage by weight of the self-contained protein within a predetermined period of time, and any other compound contained in the particle. Particular methods for obtaining the particles are also disclosed, said methods comprising the addition of salts to allow precipitation of proteins. Particular protein particles comprising lipids associated with the assembly of self-contained proteins are also disclosed. The invention also relates to several uses of the particle, in particular medical uses and to pharmaceutical and cosmetic compositions comprising the particles".

(12) INTERNATIONAL APPLICATION PUBLISHED UNDER THE PATENT COOPERATION TREATY (PCT)

(19) World Intellectual Property Organization
International Bureau

(43) International Publication Date
15 October 2020 (15.10.2020)

WIPO | PCT

(10) International Publication Number
WO 2020/208065 A1

(51) International Patent Classification:
C07K 14/00 (2006.01) *A61K 38/00* (2006.01)
B82Y 5/00 (2011.01) *A61K 47/00* (2006.01)

(21) International Application Number:
PCT/EP2020/059994

(22) International Filing Date:
08 April 2020 (08.04.2020)

(25) Filing Language: English

(26) Publication Language: English

(30) Priority Data:
19382271.5 11 April 2019 (11.04.2019) EP
19382909.0 17 October 2019 (17.10.2019) EP

(71) Applicants: **UNIVERSITAT AUTONOMA DE BARCELONA** [ES/ES]; Oficina de Valorització i Patents, Edifici A- Rectorat, Campus universitari s/n, 08193 Bellaterra (Cerdanyola del Valles) (ES). **INSTITUT RECERCA HOSPITAL DE LA SANTA CREU I SANT PAU** [ES/ES]; C/Sant Antoni Maria Claret 167, 08025 BARCELONA (ES). **CONSORCIO CENTRO DE INVESTIGACIÓN BIOMÉDICA EN RED, M.P. (CIBER)** [ES/ES]; Instituto de Salud Carlos III, Monforme de Lemos, 3-5, Pabellón 11, 28029 MADRID (ES).

(72) Inventors: **VILLAVERDE CORRALES, Antonio**; C/ Lluís Millet, 94, El Masnou, 08320 El Masnou (Barcelona) (ES). **VÁZQUEZ GÓMEZ, Esther**; C/ Lluís Millet, 94, El Masnou, 08320 El Masnou (Barcelona) (ES). **LÓPEZ LAGUNA, Héctor**; Guerau de Liost, 1-5, 4º4ª, Badalona, 08915 Badalona (Barcelona) (ES). **SÁNCHEZ, Julieta María**; Carrer de Napols 51-53. Edificio B. 3º1, Barberà del Vallés, 08210 Barberà del Vallès (Barcelona) (ES). **MANGUES BAFALLUY, Ramón**; c/ Marina, 29, 3e, 1a, Barcelona, 08005 Barcelona (ES). **ALAMO, Patricia**; c/ Consell de Cent, 575, 2-3, Barcelona, 08013 Barcelona (ES).

(81) Designated States *(unless otherwise indicated, for every kind of national protection available)*: AE, AG, AL, AM, AO, AT, AU, AZ, BA, BB, BG, BH, BN, BR, BW, BY, BZ, CA, CH, CL, CN, CO, CR, CU, CZ, DE, DJ, DK, DM, DO, DZ, EC, EE, EG, ES, FI, GB, GD, GE, GH, GM, GT, HN, HR, HU, ID, IL, IN, IR, IS, JO, JP, KE, KG, KH, KN, KP, KR, KW, KZ, LA, LC, LK, LR, LS, LU, LY, MA, MD, ME, MG, MK, MN, MW, MX, MY, MZ, NA, NG, NI, NO, NZ, OM, PA, PE, PG, PH, PL, PT, QA, RO, RS, RU, RW, SA, SC, SD, SE, SG, SK, SL, ST, SV, SY, TH, TJ, TM, TN, TR, TT, TZ, UA, UG, US, UZ, VC, VN, WS, ZA, ZM, ZW.

(84) Designated States *(unless otherwise indicated, for every kind of regional protection available)*: ARIPO (BW, GH, GM, KE, LR, LS, MW, MZ, NA, RW, SD, SL, ST, SZ, TZ, UG, ZM, ZW), Eurasian (AM, AZ, BY, KG, KZ, RU, TJ, TM), European (AL, AT, BE, BG, CH, CY, CZ, DE, DK, EE, ES, FI, FR, GB, GR, HR, HU, IE, IS, IT, LT, LU, LV, MC, MK, MT, NL, NO, PL, PT, RO, RS, SE, SI, SK, SM, TR), OAPI (BF, BJ, CF, CG, CI, CM, GA, GN, GQ, GW, KM, ML, MR, NE, SN, TD, TG).

Published:
— *with international search report (Art. 21(3))*
— *before the expiration of the time limit for amending the claims and to be republished in the event of receipt of amendments (Rule 48.2(h))*
— *with sequence listing part of description (Rule 5.2(a))*

WO 2020/208065 A1

(54) **Title:** PROTEIN NANO- OR MICROPARTICLES AS ARTIFICIAL INCLUSION BODIES

(57) **Abstract:** The invention relates to protein particles comprising a cluster of one or more types of assembled self-contained protein, wherein the particle has a size from 50 nm to 50 micrometers; is in form of a pellet in aqueous media; is mechanically stable; and it release a particular percentage by weight of the self-contained protein within a predetermined period of time, and any other compound contained in the particle. Particular methods for obtaining the particles are also disclosed, said methods comprising the addition of salts to allow precipitation of proteins. Particular protein particles comprising lipids associated with the assembly of self-contained proteins are also disclosed. The invention also relates to several uses of the particle, in particular medical uses and to pharmaceutical and cosmetic compositions comprising the particles.

Annex 8 (Studies in collaboration)

The following studies have not been directly discussed throughout the thesis storyline but have taken part in my overall scientific contribution (as co-author) during these years of PhD.

Study 1

López-Laguna H, Sala R, Sánchez JM, Álamo P, Unzueta U, Sánchez-Chardi A, Serna N, Sánchez-García L, Voltà-Durán E, Mangues R, Villaverde A, and Vázquez E. **Nanostructure Empowers Active Tumor Targeting in Ligand-Based Molecular Delivery**. Particle and Particle Systems Characterization. 2019 Nov 1;36(11).

Study 2

Voltà-Durán E, Cano-Garrido O, Serna N, López-Laguna H, Sánchez-García L, Pesarrodona M, Sánchez-Chardi A, Mangues R, Villaverde A, Vázquez E, and Unzueta U. **Controlling self-assembling and tumor cell-targeting of protein-only nanoparticles through modular protein engineering**. Sci China Mater. 2020 Jan 1;63(1):147–56.

Study 3

Céspedes MV, Cano-Garrido O, Álamo P, Sala R, Gallardo A, Serna N, Falgàs A, Voltà-Durán E, Casanova I, Sánchez-Chardi A, López-Laguna H, Sánchez-García L, Sánchez JM, Unzueta U, Vázquez E, Mangues R, and Villaverde A. **Engineering Secretory Amyloids for Remote and Highly Selective Destruction of Metastatic Foci**. Advanced Materials. 2020 Feb 1;32(7).

Study 4

López-Laguna H, Cubarsi R, Unzueta U, Mangues R, Vázquez E, and Villaverde A. **Endosomal escape of protein nanoparticles engineered through humanized histidine-rich peptides**. Sci China Mater. 2020 Apr 1;63(4):644–53.

Study 5

Voltà-Durán E, Serna N, Sánchez-García L, Aviñó A, Sánchez JM, López-Laguna H, Cano-Garrido O, Casanova I, Mangues R, Eritja R, Vázquez E, Villaverde A, and Unzueta U. **Design and engineering of tumor-targeted, dual-acting cytotoxic nanoparticles**. Acta Biomater. 2021 Jan 1;119:312–22.

Study 6

Sánchez-García L, Voltà-Durán E, Parladé E, Mazzega E, Sánchez-Chardi A, Serna N, López-Laguna H, Mitstorfer M, Unzueta U, Vázquez E, Villaverde A, and de Marco A. **Self-Assembled Nanobodies as Selectively Targeted, Nanostructured, and Multivalent Materials**. ACS Appl Mater Interfaces. 2021 Jun 30;13(25):29406–15.

Study 7

Sánchez JM, Carratalá JV, Serna N, Unzueta U, Nolan V, Sánchez-Chardi A, Voltá-Durán E, López-Laguna H, Ferrer-Miralles N, Villaverde A, and Vázquez E. **The Poly-Histidine Tag H6 Mediates Structural and Functional Properties of Disintegrating, Protein-Releasing Inclusion Bodies**. Pharmaceutics. 2022 Mar 1;14(3).

Study 8

Parladé E, Voltà-Durán E, Cano-Garrido O, Sánchez JM, Unzueta U, López-Laguna H, Serna N, Cano M, Rodríguez-Mariscal M, Vázquez E, and Villaverde A. **An In Silico Methodology That Facilitates Decision Making in the Engineering of Nanoscale Protein Materials**. Int J Mol Sci. 2022 May 1;23(9).

Study 9

Voltà-Durán E, Sánchez JM, López-Laguna H, Parladé E, Sánchez-García L, Sánchez-Chardi A, de Marco A, Unzueta U, Vázquez E, and Villaverde A. **The spectrum of building block conformers sustains the biophysical properties of clinically-oriented self-assembling protein nanoparticles**. Sci China Mater. 2022 Jun 1;65(6):1662–70.

Annex 9 (International internship)

University of Glasgow (Scotland, UK)

Advanced Research Centre (ARC)

Centre for the Cellular Microenvironment (CeMi)

3 months internship (meaning 90 days) under the supervision of Professor Matthew Dalby, and scientific manager Monica Tsimbouri; experts in cell and biomedical engineering science and its translation to the clinics.

The project was set up in the frame of osteogenesis and focused on developing disintegrating zinc-based microparticles to stimulate MSCs proliferation and differentiation into osteogenic cells using fibronectin-PEA surfaces.

This collaboration has ended up with a manuscript exposed in Annex 2, and further interlaboratory cooperation.

From: Prof. Matthew Dalby
Centre for the Cellular Microenvironment
Institute of Molecular, Cells and Systems Biology
Advanced Research Centre (ARC),
University of Glasgow, 11 Chapel Lane, Glasgow, UK

30th of June 2022

To whom it may concerns,

I would like to certify that Hèctor López Laguna (DNI: 47442763L), a pre-doctoral researcher attached to the nanobiotechnology group led by Prof. Antonio Villaverde Corrales at the Institute of Biotechnology and Biomedicine (IBB-UAB, Barcelona, Spain), spent a training placement of **3 months** (from April 1st 2022 to June 30th 2022) as a visiting researcher at our laboratory in the University of Glasgow.

Sincerely,

Matthew Dalby

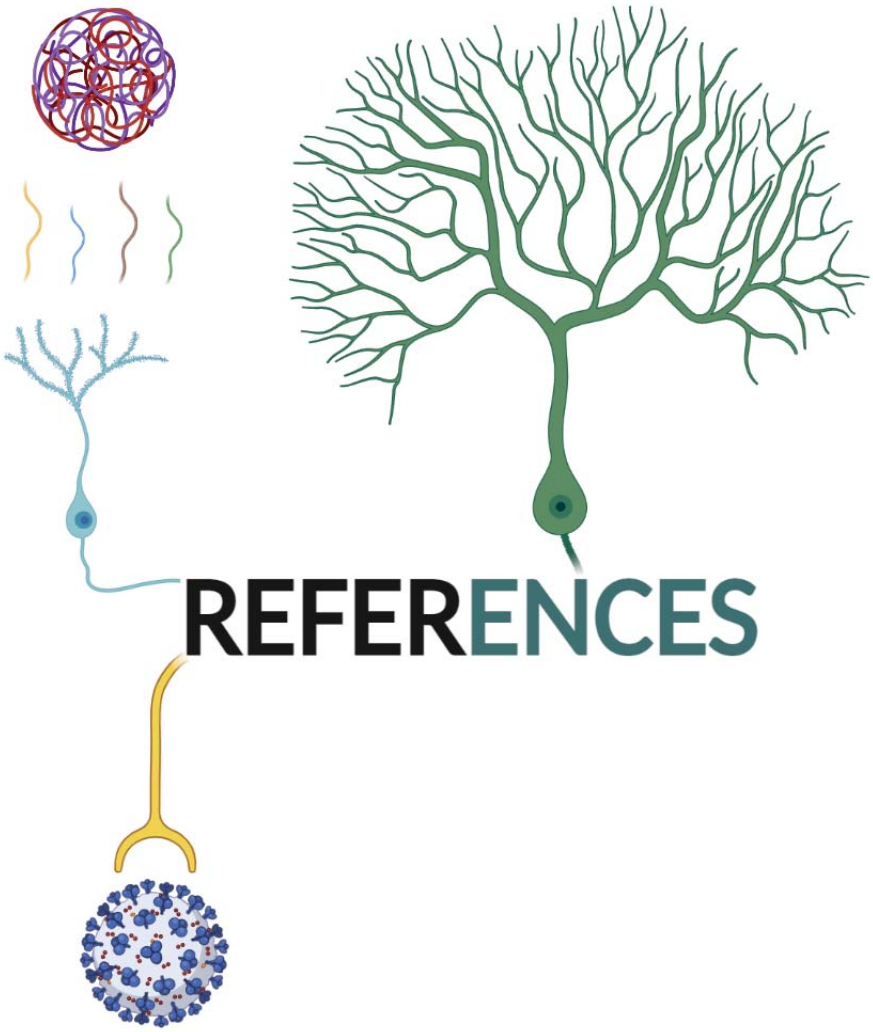

REFERENCES

1. Clery D. Webb reveals early universe's galactic bounty. Science (1979). 2022 Aug 12;377(6607):700–1.

2. Bundell S. The history of the Universe in the blink of an eye. Nature. 2019 Aug 14.

3. Pfalzner S, Bannister MT. A Hypothesis for the Rapid Formation of Planets. Astrophys J. 2019 Apr 8;874(2):L34.

4. Knoll AH, Bergmann KD, Strauss J v. Life: the first two billion years. Philos Trans R Soc Lond B Biol Sci. 2016;371(1707).

5. Kitadai N, Maruyama S. Origins of building blocks of life: A review. Geoscience Frontiers. 2018 Jul;9(4):1117–53.

6. Cowan JJ. A sprinkling of stardust. Nature. 2004 Mar 25;428(6981):369–70.

7. David L. Nelson, Michael M. Cox. Lehninger principles of biochemistry (7th ed.). New York: W. H. Freeman. 2017.

8. Brooks AN, Turkarslan S, Beer KD, Yin Lo F, Baliga NS. Adaptation of cells to new environments. WIREs Systems Biology and Medicine. 2011 Sep 31;3(5):544–61.

9. Fernandez-de-Cossio-Diaz J, Vazquez A. A physical model of cell metabolism. Sci Rep. 2018 Dec 29;8(1):8349.

10. Derényi I, Szöllősi GJ. Hierarchical tissue organization as a general mechanism to limit the accumulation of somatic mutations. Nat Commun. 2017 Apr 23;8(1):14545.

11. Bryant DM, Mostov KE. From cells to organs: building polarized tissue. Nat Rev Mol Cell Biol. 2008 Nov;9(11):887–901.

12. McKee TJ, Perlman G, Morris M, Komarova S v. Extracellular matrix composition of connective tissues: a systematic review and meta-analysis. Sci Rep. 2019 Dec 22;9(1):10542.

13. Murphy MB, Moncivais K, Caplan AI. Mesenchymal stem cells: environmentally responsive therapeutics for regenerative medicine. Exp Mol Med. 2013 Nov 15;45(11):e54–e54.

14. Dergham M, Lin S, Geng J. Supramolecular Self-Assembly in Living Cells. Angewandte Chemie International Edition. 2022 Apr 25;61(18).

15. Harkness V RW, Avakyan N, Sleiman HF, Mittermaier AK. Mapping the energy landscapes of supramolecular assembly by thermal hysteresis. Nat Commun. 2018 Dec 8;9(1):3152.

16. Hobza P, Řezáč J. Introduction: Noncovalent Interactions. Chem Rev. 2016 May 11;116(9):4911–2.

17. Johnson ER, Keinan S, Mori-Sánchez P, Contreras-García J, Cohen AJ, Yang W. Revealing Noncovalent Interactions. J Am Chem Soc. 2010 May 12;132(18):6498–506.

18. Rafelski SM, Marshall WF. Building the cell: design principles of cellular architecture. Nat Rev Mol Cell Biol. 2008 Aug;9(8):593–602.

19. Porras P, Barrera E, Bridge A, del-Toro N, Cesareni G, Duesbury M, et al. Towards a unified open access dataset of molecular interactions. Nat Commun. 2020 Dec 1;11(1):6144.

20. Barbieri L, Luchinat E, Banci L. Protein interaction patterns in different cellular environments are revealed by in-cell NMR. Sci Rep. 2015 Nov 26;5(1):14456.

21. Demarco IA, Periasamy A, Booker CF, Day RN. Monitoring dynamic protein interactions with photoquenching FRET. Nat Methods. 2006 Jul 21;3(7):519–24.

22. WATSON JD, CRICK FHC. Molecular Structure of Nucleic Acids: A Structure for Deoxyribose Nucleic Acid. Nature. 1953 Apr 25;171(4356):737–8.

23. Watson H. Biological membranes. Essays Biochem. 2015 Nov 15;59:43–69.

24. Germanos M, Gao A, Taper M, Yau B, Kebede MA. Inside the Insulin Secretory Granule. Metabolites. 2021 Aug 5;11(8):515.

25. Greenwald J, Riek R. Biology of Amyloid: Structure, Function, and Regulation. Structure. 2010 Oct;18(10):1244–60.

26. Maji SK, Perrin MH, Sawaya MR, Jessberger S, Vadodaria K, Rissman RA, et al. Functional Amyloids As Natural Storage of Peptide Hormones in Pituitary Secretory Granules. Science (1979). 2009 Jul 17;325(5938):328–32.

27. Céspedes MV, Fernández Y, Unzueta U, Mendoza R, Seras-Franzoso J, Sánchez-Chardi A, et al. Bacterial mimetics of endocrine secretory granules as immobilized in vivo depots for functional protein drugs. Sci Rep. 2016 Dec 24;6(1):35765.

28. Rinas U, Garcia-Fruitós E, Corchero JL, Vázquez E, Seras-Franzoso J, Villaverde A. Bacterial Inclusion Bodies: Discovering Their Better Half. Trends Biochem Sci. 2017 Sep;42(9):726–37.

29. Rincheval V, Lelek M, Gault E, Bouillier C, Sitterlin D, Blouquit-Laye S, et al. Functional organization of cytoplasmic inclusion bodies in cells infected by respiratory syncytial virus. Nat Commun. 2017 Dec 15;8(1):563.

30. Chiesa G, Kiriakov S, Khalil AS. Protein assembly systems in natural and synthetic biology. BMC Biol. 2020 Dec 26;18(1):35.

31. Wear MA, Schafer DA, Cooper JA. Actin dynamics: Assembly and disassembly of actin networks. Current Biology. 2000 Dec;10(24):R891–5.

32. Revell CK, Jensen OE, Shearer T, Lu Y, Holmes DF, Kadler KE. Collagen fibril assembly: New approaches to unanswered questions. Matrix Biol Plus. 2021 Dec;12:100079.

33. Kholodenko BN. Cell-signalling dynamics in time and space. Nat Rev Mol Cell Biol. 2006 Mar 15;7(3):165–76.

34. Pieters BJGE, van Eldijk MB, Nolte RJM, Mecinović J. Natural supramolecular protein assemblies. Chem Soc Rev. 2016;45(1):24–39.

35. Huberts DHEW, van der Klei IJ. Moonlighting proteins: An intriguing mode of multitasking. Biochimica et Biophysica Acta (BBA) - Molecular Cell Research. 2010 Apr;1803(4):520–5.

36. Zaretsky JZ, Wreschner DH. Protein multifunctionality: principles and mechanisms. Transl Oncogenomics. 2008 May 15;3:99–136.

37. Horio T, Murata T. The role of dynamic instability in microtubule organization. Front Plant Sci. 2014 Oct 7;5.

38. Dhillon AS, Hagan S, Rath O, Kolch W. MAP kinase signalling pathways in cancer. Oncogene. 2007 May 14;26(22):3279–90.

39. Ciechanover A. Intracellular protein degradation: from a vague idea thru the lysosome and the ubiquitin–proteasome system and onto human diseases and drug targeting. Cell Death Differ. 2005 Sep 11;12(9):1178–90.

40. Yoshida M, Muneyuki E, Hisabori T. ATP synthase — a marvellous rotary engine of the cell. Nat Rev Mol Cell Biol. 2001 Sep;2(9):669–77.

41. Venkatakrishnan AJ, Deupi X, Lebon G, Tate CG, Schertler GF, Babu MM. Molecular signatures of G-protein-coupled receptors. Nature. 2013 Feb 13;494(7436):185–94.

42. Sigal A, Milo R, Cohen A, Geva-Zatorsky N, Klein Y, Liron Y, et al. Variability and memory of protein levels in human cells. Nature. 2006 Nov 1;444(7119):643–6.

43. Lee D, Redfern O, Orengo C. Predicting protein function from sequence and structure. Nat Rev Mol Cell Biol. 2007 Dec;8(12):995–1005.

44. Henzler-Wildman K, Kern D. Dynamic personalities of proteins. Nature. 2007 Dec 13;450(7172):964–72.

45. Williams RJP. The fundamental nature of life as a chemical system: the part played by inorganic elements. J Inorg Biochem. 2002 Feb;88(3–4):241–50.

46. Tampa M, Sarbu I, Matei C, Benea V, Georgescu SR. Brief history of syphilis. J Med Life. 2014 Mar 15;7(1):4–10.

47. Dixon NE, Gazzola C, Blakeley RL, Zerner B. Jack bean urease (EC 3.5.1.5). Metalloenzyme. Simple biological role for nickel. J Am Chem Soc. 1975 Jul 1;97(14):4131–3.

48. Bertini I, Rosato A. Bioinorganic chemistry in the postgenomic era. Proceedings of the National Academy of Sciences. 2003 Apr 24;100(7):3601–4.

49. Zoroddu MA, Aaseth J, Crisponi G, Medici S, Peana M, Nurchi VM. The essential metals for humans: a brief overview. J Inorg Biochem. 2019 Jun;195:120–9.

50. Pace NR. The universal nature of biochemistry. Proceedings of the National Academy of Sciences. 2001 Jan 30;98(3):805–8.

51. Moustakas M. The Role of Metal Ions in Biology, Biochemistry and Medicine. Materials. 2021 Jan 24;14(3):549.

52. Nature Publishing Group (npg). Metals in chemical biology. Nat Chem Biol. 2008 Mar;4(3):143–143.

53. Macedo LJA, Hassan A, Sedenho GC, Crespilho FN. Assessing electron transfer reactions and catalysis in multicopper oxidases with operando X-ray absorption spectroscopy. Nat Commun. 2020 Dec 16;11(1):316.

54. Czyrko J, Sliwiak J, Imiolczyk B, Gdaniec Z, Jaskolski M, Brzezinski K. Metal-cation regulation of enzyme dynamics is a key factor influencing the activity of S-adenosyl-l-homocysteine hydrolase from Pseudomonas aeruginosa. Sci Rep. 2018 Dec 27;8(1):11334.

55. Steffens JJ, Siewers IJ, Benkovic SJ. Catalysis of phosphoryl group transfer. Role of divalent metal ions in the hydrolysis of lactic acid O-phenyl phosphate and salicylic acid O-aryl phosphates. Biochemistry. 1975 Jun;14(11):2431–40.

56. Jeremy N. Harvey, Kevin M. Smith, Rinaldo Poli. Understanding the reactivity of transition metal complexes involving multiple spin states. Coord Chem Rev. 2003;238–239:347–61.

57. Philip P. Power. Main-group elements as transition metals. Nature. 2010;463:171–7.

58. Robert R. Crichton, Roberta J. Ward, Robert C. Hider. Metal Chelation in Medicine. RSC Publishing. 2016 Oct(8).

59. Frenking G, Fröhlich N. The Nature of the Bonding in Transition-Metal Compounds. Chem Rev. 2000 Feb 1;100(2):717–74.

60. MELLOR D, MALEY L. Order of Stability of Metal Complexes. Nature. 1948 March(161):436–7.

61. Wolczanski PT. Structure and reactivity studies of transition metals ligated by tBuSi3X (X = O, NH, N, S, and CC). Chem Commun (Camb). 2009 Feb (7):740–57.

62. Wu X, Zhao L, Jin J, Pan S, Li W, Jin X, et al. Observation of alkaline earth complexes M(CO)8 (M = Ca, Sr, or Ba) that mimic transition metals. Science. 2018;361(6405):912–6.

63. Crans DC, Kostenkova K. Open questions on the biological roles of first-row transition metals. Commun Chem. 2020 Dec 7;3(1):104.

64. Banci L, Bertini I. Metallomics and the Cell: Some Definitions and General Comments. Met Ions Life Sci. 2013(12);1-13.

65. Haraguchi H. Metallomics as integrated biometal science. J Anal At Spectrom. 2004;19(1):5.

66. Chandrangsu P, Rensing C, Helmann JD. Metal homeostasis and resistance in bacteria. Nat Rev Microbiol. 2017 Jun 27;15(6):338–50.

67. Borzelleca JF. Paracelsus: Herald of Modern Toxicology. Toxicological Sciences. 2000 Jan 1;53(1):2–4.

68. Thompson KH. Medicinal Inorganic Chemistry: Continuum of Dose versus Response-From Deficiency through Optimal Intake to Toxicity. Encyclopedia of Inorganic and Bioinorganic Chemistry. Chichester, UK: John Wiley & Sons, Ltd. 2011 Dec.

69. SIMS LS. Uses of the Recommended Dietary Allowances. J Am Diet Assoc. 1996 Jul;96(7):659–62.

70. Jaishankar M, Tseten T, Anbalagan N, Mathew BB, Beeregowda KN. Toxicity, mechanism and health effects of some heavy metals. Interdiscip Toxicol. 2014 Jun 1;7(2):60–72.

71. Mitra S, Chakraborty AJ, Tareq AM, Emran T bin, Nainu F, Khusro A, et al. Impact of heavy metals on the environment and human health: Novel therapeutic insights to counter the toxicity. J King Saud Univ Sci. 2022 Apr;34(3):101865.

72. Crichton RR. Chapter 1 - Metal Toxicity: An Introduction. RSC Publishing. 2016 Oct;1–23. Edited by Crichton RR, Ward RJ, Hider RC.

73. Smethurst DGJ, Shcherbik N. Interchangeable utilization of metals: New perspectives on the impacts of metal ions employed in ancient and extant biomolecules. Journal of Biological Chemistry. 2021 Dec;297(6):101374.

74. Huayin Wu, Yinan Shen, Dianzhuo Wang, Harald Herrmann, Robert D. Goldman, David A. Weitz. Effect of the divalent cations zinc and calcium on the structure and mechanics of reconstituted vimentin intermediate filaments. BioRxiv. 2019.

75. Tiwari S, Askari JA, Humphries MJ, Bulleid NJ. Divalent cations regulate the folding and activation status of integrins during their intracellular trafficking. J Cell Sci. 2011 May 15;124(10):1672–80.

76. Knape MJ, Ballez M, Burghardt NC, Zimmermann B, Bertinetti D, Kornev AP, et al. Divalent metal ions control activity and inhibition of protein kinases. Metallomics. 2017;9(11):1576–84.

77. Otzen D, Riek R. Functional Amyloids. Cold Spring Harb Perspect Biol. 2019 Dec;11(12):a033860.

78. Lautenschläger J, Stephens AD, Fusco G, Ströhl F, Curry N, Zacharopoulou M, et al. C-terminal calcium binding of α-synuclein modulates synaptic vesicle interaction. Nat Commun. 2018 Dec 19;9(1):712.

79. Han JY, Choi TS, Kim HI. Molecular Role of Ca2+ and Hard Divalent Metal Cations on Accelerated Fibrillation and Interfibrillar Aggregation of α-Synuclein. Sci Rep. 2018 Dec 30;8(1):1895.

80. Chen G fang, Xu T hai, Yan Y, Zhou Y ren, Jiang Y, Melcher K, et al. Amyloid beta: structure, biology and structure-based therapeutic development. Acta Pharmacol Sin. 2017 Sep 17;38(9):1205–35.

81. Rana M, Sharma AK. Cu and Zn interactions with Aβ peptides: consequence of coordination on aggregation and formation of neurotoxic soluble Aβ oligomers. Metallomics. 2019;11(1):64–84.

82. Jacob RS, Das S, Ghosh S, Anoop A, Jha NN, Khan T, et al. Amyloid formation of growth hormone in presence of zinc: Relevance to its storage in secretory granules. Sci Rep. 2016 Mar 23;6(1):23370.

83. Rutter GA, Chabosseau P, Bellomo EA, Maret W, Mitchell RK, Hodson DJ, et al. Intracellular zinc in insulin secretion and action: a determinant of diabetes risk? Proceedings of the Nutrition Society. 2016 Feb 14;75(1):61–72.

84. Duboué-Dijon E, Delcroix P, Martinez-Seara H, Hladílková J, Coufal P, Křížek T, et al. Binding of Divalent Cations to Insulin: Capillary Electrophoresis and Molecular Simulations. J Phys Chem B. 2018 May 31;122(21):5640–8.

85. Liao SM, Du QS, Meng JZ, Pang ZW, Huang RB. The multiple roles of histidine in protein interactions. Chem Cent J. 2013 Dec 1;7(1):44.

86. Valenti LE, de Pauli CP, Giacomelli CE. The binding of Ni(II) ions to hexahistidine as a model system of the interaction between nickel and His-tagged proteins. J Inorg Biochem. 2006 Feb;100(2):192–200.

87. WILLIAMS RJP. The symbiosis of metal and protein functions. Eur J Biochem. 1985 Jul;150(2):231–48.

88. Chakrabarti P. Geometry of interaction of metal ions with histidine residues in protein structures. Protein Engineering, Design and Selection. 1990;4(1):57–63.

89. Barh D, Azevedo Vasco. Towards Improving Quality of Life. Omics Technologies and Bio-Engineering (1st edition). Elsevier. 2018 Feb;(2):449–69.

90. Li C, Zhang R, Wang J, Wilson LM, Yan Y. Protein Engineering for Improving and Diversifying Natural Product Biosynthesis. Trends Biotechnol. 2020 Jul;38(7):729–44.

91. Lutz S, Iamurri SM. Protein Engineering: Past, Present, and Future. Methods Mol Biol. 2018;1685:1-12.

92. Dobson CM. Protein folding and misfolding. Nature. 2003 Dec;426(6968):884–90.

93. Koga N, Tatsumi-Koga R, Liu G, Xiao R, Acton TB, Montelione GT, et al. Principles for designing ideal protein structures. Nature. 2012 Nov 7;491(7423):222–7.

94. Caradonna TM, Schmidt AG. Protein engineering strategies for rational immunogen design. NPJ Vaccines. 2021 Dec 17;6(1):154.

95. Pongsupasa V, Anuwan P, Maenpuen S, Wongnate T. Rational-Design Engineering to Improve Enzyme Thermostability. Methods Mol Biol. 2022;2397:159-178.

96. Strack R. Directing evolution in cells. Nat Methods. 2020 May 5;17(5):457–457.

97. Qiu Y, Hu J, Wei GW. Cluster learning-assisted directed evolution. Nat Comput Sci. 2021 Dec 9;1(12):809–18.

98. Renata H, Wang ZJ, Arnold FH. Expanding the Enzyme Universe: Accessing Non-Natural Reactions by Mechanism-Guided Directed Evolution. Angewandte Chemie International Edition. 2015 Mar 9;54(11):3351–67.

99. Wittwer M, Markel U, Schiffels J, Okuda J, Sauer DF, Schwaneberg U. Engineering and emerging applications of artificial metalloenzymes with whole cells. Nat Catal. 2021 Oct 20;4(10):814–27.

100. Liu R, Liang L, Lacerda MP, Freed EF, Eckert CA. Chapter 10 - Advances in protein engineering and its application in synthetic biology. New Frontiers and Applications of Synthetic Biology. Elsevier. 2022:147–58. Edited by Singh V.

101. de la Concepcion JC, Franceschetti M, MacLean D, Terauchi R, Kamoun S, Banfield MJ. Protein engineering expands the effector recognition profile of a rice NLR immune receptor. Elife. 2019 Sep 19;8.

102. Roberts RJ. How restriction enzymes became the workhorses of molecular biology. Proceedings of the National Academy of Sciences. 2005 Apr 26;102(17):5905–8.

103. Gupta V, Sengupta M, Prakash J, Tripathy BC. Production of Recombinant Pharmaceutical Proteins. Basic and Applied Aspects of Biotechnology. Singapore: Springer Singapore. 2017:77–101.

104. Hunt I. From gene to protein: a review of new and enabling technologies for multi-parallel protein expression. Protein Expr Purif. 2005 Mar;40(1):1–22.

105. Malla A, Rosales-Mendoza S, Phoolcharoen W, Vimolmangkang S. Efficient Transient Expression of Recombinant Proteins Using DNA Viral Vectors in Freshwater Microalgal Species. Front Plant Sci. 2021 Apr 7;12.

106. Wurm FM. Production of recombinant protein therapeutics in cultivated mammalian cells. Nat Biotechnol. 2004 Nov 4;22(11):1393–8.

107. Kimple ME, Brill AL, Pasker RL. Overview of Affinity Tags for Protein Purification. Curr Protoc Protein Sci. 2013 Aug 16;73(1).

108. Loughran ST, Bree RT, Walls D. Purification of Polyhistidine-Tagged Proteins. Methods Mol Biol. 2017;1485:275-303.

109. Chadha G, Zhao Y. Histidine-functionalized water-soluble nanoparticles for biomimetic nucleophilic/general-base catalysis under acidic conditions. Org Biomol Chem. 2013;11(39):6849.

110. Meng L, Liu Y, Yin X, Zhou H, Wu J, Wu M, et al. Effects of His-tag on Catalytic Activity and Enantioselectivity of Recombinant Transaminases. Appl Biochem Biotechnol. 2020 Mar 13;190(3):880–95.

111. Signore M, Manganelli V, Hodge A. Antibody Validation by Western Blotting. Methods Mol Biol. 2017;1606:51-70.

112. Ley C, Holtmann D, Mangold KM, Schrader J. Immobilization of histidine-tagged proteins on electrodes. Colloids Surf B Biointerfaces. 2011 Dec;88(2):539–51.

113. Rai DK, Segundo FDS, Schafer E, Burrage TG, Rodriguez LL, de los Santos T, et al. Novel 6xHis tagged foot-and-mouth disease virus vaccine bound to nanolipoprotein adjuvant via metal ions provides antigenic distinction and effective protective immunity. Virology. 2016 Aug;495:136–47.

114. Kollmannsperger A, Sharei A, Raulf A, Heilemann M, Langer R, Jensen KF, et al. Live-cell protein labelling with nanometre precision by cell squeezing. Nat Commun. 2016 Apr 29;7(1):10372.

115. Kimple ME, Brill AL, Pasker RL. Overview of Affinity Tags for Protein Purification. Curr Protoc Protein Sci. 2013;73:Unit-9.9.

116. Structural Genomics Consortium, China Structural Genomics Consortium, Northeast Structural Genomics Consortium, Gräslund S, Nordlund P, Weigelt J, et al. Protein production and purification. Nat Methods. 2008 Feb;5(2):135–46.

117. Mishra V. Affinity Tags for Protein Purification. Curr Protein Pept Sci. 2020 Nov 9;21(8):821–30.

118. Crowe J, Döbeli H, Gentz R, Hochuli E, Stüber D, Henco K. 6xHis-Ni-NTA Chromatography as a Superior Technique in Recombinant Protein Expression/Purification. Methods Mol Biol. 1994;31:371-87.

119. Porath J. Immobilized metal ion affinity chromatography. Protein Expr Purif. 1992 Aug;3(4):263–81.

120. Magnusdottir A, Johansson I, Dahlgren LG, Nordlund P, Berglund H. Enabling IMAC purification of low abundance recombinant proteins from E. coli lysates. Nat Methods. 2009 Jul;6(7):477–8.

121. Glover SD, Tommos C. A Quick and Colorful Method to Measure Low-Level Contaminations of Paramagnetic Ni2+ in Protein Samples Purified by Immobilized Metal Ion Affinity Chromatography. Methods Enzymol. 2019;614:87-106.

122. Yoo JW, Irvine DJ, Discher DE, Mitragotri S. Bio-inspired, bioengineered and biomimetic drug delivery carriers. Nat Rev Drug Discov. 2011 Jul 1;10(7):521–35.

123. Tobin P, Richards D, Callender R, Wilson C. Protein Engineering: A New Frontier for Biological Therapeutics. Curr Drug Metab. 2015 Jan 26;15(7):743–56.

124. Lin CY, Liu JC. Modular protein domains: an engineering approach toward functional biomaterials. Curr Opin Biotechnol. 2016 Aug;40:56–63.

125. Quijano-Rubio A, Yeh HW, Park J, Lee H, Langan RA, Boyken SE, et al. De novo design of modular and tunable protein biosensors. Nature. 2021 Mar 18;591(7850):482–7.

126. Turanli-Yildiz B, Alkim C, Petek Z. Protein Engineering Methods and Applications. Protein Engineering. InTech. 2012 Feb.

127. Mishra S, Kumar Mani A, Singh RB, Ali Mahdi A. A Review on Conventional and Modern Techniques of Protein Engineering and their Applications. Am J Biochem Mol Biol. 2018 Dec 15;9(1):17–28.

128. Brannigan JA, Wilkinson AJ. Protein engineering 20 years on. Nat Rev Mol Cell Biol. 2002 Dec;3(12):964–70.

129. Kazlauskas RJ, Bornscheuer UT. Finding better protein engineering strategies. Nat Chem Biol. 2009 Aug;5(8):526–9.

130. Balaratnasingam C, Dhrami-Gavazi E, McCann JT, Ghadiali Q, Freund KB. Aflibercept: a review of its use in the treatment of choroidal neovascularization due to age-related macular degeneration. Clin Ophthalmol. 2015;9:2355–71.

131. Eklund JW, Kuzel TM. Denileukin diftitox: a concise clinical review. Expert Rev Anticancer Ther. 2005 Jan 10;5(1):33–8.

132. Goffe B, Cather JC. Etanercept: An overview. J Am Acad Dermatol. 2003 Aug;49(2):105–11.

133. Sancho J. Protein Engineering: The Present and the Future. Biophysica. 2022 Apr 29;2(2):111–2.

134. Dobrzański LA. Significance of materials science for the future development of societies. J Mater Process Technol. 2006 Jun;175(1–3):133–48.

135. William D. Callister Jr, David G. Rethwisch. Materials Science and Engineering: An Introduction (10th ed). Wiley. 2018 Jan.

136. Dai Z, Yang X, Wu F, Wang L, Xiang K, Li P, et al. Living fabrication of functional semi-interpenetrating polymeric materials. Nat Commun. 2021 Dec 8;12(1):3422.

137. Gibson UJ, Wei L, Ballato J. Semiconductor core fibres: materials science in a bottle. Nat Commun. 2021 Dec 28;12(1):3990.

138. Gowri S, Narayanasamy K, Krishnamurthy R. Recent developments in ceramic-materials processing and applications. J Mater Process Technol. 1993 Feb;37(1–4):571–82.

139. Axinte E. Glasses as engineering materials: A review. Mater Des. 2011 Apr;32(4):1717–32.

140. Lu K. The Future of Metals. Science (1979). 2010 Apr 16;328(5976):319–20.

141. Othman Z, Cillero Pastor B, van Rijt S, Habibovic P. Understanding interactions between biomaterials and biological systems using proteomics. Biomaterials. 2018 Jun;167:191–204.

142. Du J, Katti D, Thomas V. Interactions between Biomaterials and Biological Tissues and Cells, Part I. JOM. 2022 Sep 28;74(9):3334–5.

143. Morais JM, Papadimitrakopoulos F, Burgess DJ. Biomaterials/Tissue Interactions: Possible Solutions to Overcome Foreign Body Response. AAPS J. 2010 Jun 9;12(2):188–96.

144. Bayda S, Adeel M, Tuccinardi T, Cordani M, Rizzolio F. The History of Nanoscience and Nanotechnology: From Chemical–Physical Applications to Nanomedicine. Molecules. 2019 Dec 27;25(1):112.

145. Sim S, Wong N. Nanotechnology and its use in imaging and drug delivery (Review). Biomed Rep. 2021 Mar 5;14(5):42.

146. Soares S, Sousa J, Pais A, Vitorino C. Nanomedicine: Principles, Properties, and Regulatory Issues. Front Chem. 2018 Aug 20;6.

147. Sanders WC. Basic Principles of Nanotechnology. CRC Press. 2018 Jul.

148. Sharma PK, Dorlikar S, Rawat P, Malik V, Vats N, Sharma M, et al. Chapter 1 - Nanotechnology and its application: a review. Nanotechnology in Cancer Management. Elsevier. 2021:1–33.

149. Rodgers P. Top down, bottom up. Nat Nanotechnol. 2006 Sep 29.

150. Dhiraj Sud, Anil Kumar Singla, Munish Kumar Gupta. Nanomaterials in Manufacturing Processes (1st Edition). CRC Press. 2022 Aug.

151. Saha S, Bansal S, Khanuja M. Classification of nanomaterials and their physical and chemical nature (1st Edition). Nano-enabled Agrochemicals in Agriculture. Elsevier. 2022 Mar:7–34.

152. Avouris P, Chen Z, Perebeinos V. Carbon-based electronics. Nat Nanotechnol. 2007 Oct 30;2(10):605–15.

153. Maeyoshi Y, Saeki A, Suwa S, Omichi M, Marui H, Asano A, et al. Fullerene nanowires as a versatile platform for organic electronics. Sci Rep. 2012 Dec 24;2(1):600.

154. Xiao J, Cheng K, Xie X, Wang M, Xing S, Liu Y, et al. Tandem catalysis with double-shelled hollow spheres. Nat Mater. 2022 May 27;21(5):572–9.

155. Gangatharan PM, Maubane-Nkadimeng MS, Coville NJ. Building carbon structures inside hollow carbon spheres. Sci Rep. 2019 Dec 23;9(1):10642.

156. He X, Htoon H, Doorn SK, Pernice WHP, Pyatkov F, Krupke R, et al. Carbon nanotubes as emerging quantum-light sources. Nat Mater. 2018 Aug 18;17(8):663–70.

157. Efros AL. Quantum dots realize their potential. Nature. 2019 Nov 28;575(7784):604–5.

158. Desireddy A, Conn BE, Guo J, Yoon B, Barnett RN, Monahan BM, et al. Ultrastable silver nanoparticles. Nature. 2013 Sep 19;501(7467):399–402.

159. Lim ZZJ, Li JEJ, Ng CT, Yung LYL, Bay BH. Gold nanoparticles in cancer therapy. Acta Pharmacol Sin. 2011 Aug 11;32(8):983–90.

160. Tsuzuki T. Mechanochemical synthesis of metal oxide nanoparticles. Commun Chem. 2021 Dec 12;4(1):143.

161. Virlan MJR, Miricescu D, Radulescu R, Sabliov CM, Totan A, Calenic B, et al. Organic Nanomaterials and Their Applications in the Treatment of Oral Diseases. Molecules. 2016 Feb 9;21(2).

162. Romero G, Moya SE. Chapter 4 - Synthesis of Organic Nanoparticles. Frontiers of Nanoscience. 2012(4):115–41.

163. Lee CC, MacKay JA, Fréchet JMJ, Szoka FC. Designing dendrimers for biological applications. Nat Biotechnol. 2005 Dec 6;23(12):1517–26.

164. Peng J, Cheng Q. High-Performance Nanocomposites Inspired by Nature. Advanced Materials. 2017 Dec;29(45):1702959.

165. Wennersten R, Fidler J, Spitsyna A. Nanotechnology: A New Technological Revolution in the 21st Century. Handbook of Performability Engineering. London: Springer London. 2088:943–52.

166. Louro H, Silva MJ, editors. Nanotoxicology in Safety Assessment of Nanomaterials. Cham: Springer International Publishing. 2022(1357).

167. Lead JR, Doak SH, Clift MJD, editors. Nanotoxicology in Humans and the Environment. Cham: Springer International Publishing. 2021.

168. Zielińska A, Costa B, Ferreira M v., Miguéis D, Louros JMS, Durazzo A, et al. Nanotoxicology and Nanosafety: Safety-by-Design and Testing at a Glance. Int J Environ Res Public Health. 2020 Jun 28;17(13):4657.

169. Yildirimer L, Thanh NTK, Loizidou M, Seifalian AM. Toxicology and clinical potential of nanoparticles. Nano Today. 2011 Dec;6(6):585–607.

170. Soo Choi H, Liu W, Misra P, Tanaka E, Zimmer JP, Itty Ipe B, et al. Renal clearance of quantum dots. Nat Biotechnol. 2007 Oct 23;25(10):1165–70.

171. Longmire M, Choyke PL, Kobayashi H. Clearance properties of nano-sized particles and molecules as imaging agents: considerations and caveats. Nanomedicine. 2008 Oct;3(5):703–17.

172. Du B, Yu M, Zheng J. Transport and interactions of nanoparticles in the kidneys. Nat Rev Mater. 2018 Oct 3;3(10):358–74.

173. Bastús NG, Puntes V. Nanosafety: Towards Safer Nanoparticles by Design. Curr Med Chem. 2018 Dec 3;25(35):4587–601.

174. Fadeel B, Farcal L, Hardy B, Vázquez-Campos S, Hristozov D, Marcomini A, et al. Advanced tools for the safety assessment of nanomaterials. Nat Nanotechnol. 2018 Jul 6;13(7):537–43.

175. Hotze EM, Phenrat T, Lowry G v. Nanoparticle Aggregation: Challenges to Understanding Transport and Reactivity in the Environment. J Environ Qual. 2010 Nov;39(6):1909–24.

176. Shrestha S, Wang B, Dutta P. Nanoparticle processing: Understanding and controlling aggregation. Adv Colloid Interface Sci. 2020 May;279:102162.

177. Goodman CM, McCusker CD, Yilmaz T, Rotello VM. Toxicity of Gold Nanoparticles Functionalized with Cationic and Anionic Side Chains. Bioconjug Chem. 2004 Jul 1;15(4):897–900.

178. Wei X, Shao B, He Z, Ye T, Luo M, Sang Y, et al. Cationic nanocarriers induce cell necrosis through impairment of Na+/K+-ATPase and cause subsequent inflammatory response. Cell Res. 2015 Feb 23;25(2):237–53.

179. Kirchner C, Liedl T, Kudera S, Pellegrino T, Muñoz Javier A, Gaub HE, et al. Cytotoxicity of Colloidal CdSe and CdSe/ZnS Nanoparticles. Nano Lett. 2005 Feb 1;5(2):331–8.

180. Hahn A, Fuhlrott J, Loos A, Barcikowski S. Cytotoxicity and ion release of alloy nanoparticles. Journal of Nanoparticle Research. 2012 Jan 12;14(1):686.

181. Sharifi S, Behzadi S, Laurent S, Forrest ML, Stroeve P, Mahmoudi M. Toxicity of nanomaterials. Chem Soc Rev. 2012 Mar 21;41(6):2323–43.

182. Oberdörster G, Oberdörster E, Oberdörster J. Nanotoxicology: An Emerging Discipline Evolving from Studies of Ultrafine Particles. Environ Health Perspect. 2005 Jul;113(7):823–39.

183. Yoshioka Y, Hirai T, Tsutsumi Y. Immune Toxicity of and Allergic Responses to Nanomaterials. Allergy and Immunotoxicology in Occupational Health – The Next Step. Current Topics in Environmental Health and Preventive Medicine. 2020:37–46. Edited by Otsuki T, di Gioacchino M, Petrarca C.

184. di Gioacchino M, di Giampaolo L, Mangifesta R, Gangemi S, Petrarca C. Exposure to nanoparticles and occupational allergy. Curr Opin Allergy Clin Immunol. 2022 Apr;22(2):55–63.

185. Calarco A, Bosetti M, Margarucci S, Fusaro L, Nicolì E, Petillo O, et al. The genotoxicity of PEI-based nanoparticles is reduced by acetylation of polyethylenimine amines in human primary cells. Toxicol Lett. 2013 Mar;218(1):10–7.

186. Murugadoss S, Lison D, Godderis L, van den Brule S, Mast J, Brassinne F, et al. Toxicology of silica nanoparticles: an update. Arch Toxicol. 2017 Sep 1;91(9):2967–3010.

187. Soares EV, Soares HMVM. Harmful effects of metal(loid) oxide nanoparticles. Appl Microbiol Biotechnol. 2021 Feb 1;105(4):1379–94.

188. Liu S, Cui M, Li X, Thuyet DQ, Fan W. Effects of hydrophobicity of titanium dioxide nanoparticles and exposure scenarios on copper uptake and toxicity in Daphnia magna. Water Res. 2019 May;154:162–70.

189. Friehs E, AlSalka Y, Jonczyk R, Lavrentieva A, Jochums A, Walter JG, et al. Toxicity, phototoxicity and biocidal activity of nanoparticles employed in photocatalysis. Journal of Photochemistry and Photobiology C: Photochemistry Reviews. 2016 Dec;29:1–28.

190. Rosenblum D, Joshi N, Tao W, Karp JM, Peer D. Progress and challenges towards targeted delivery of cancer therapeutics. Nat Commun. 2018 Dec 12;9(1):1410.

191. Mohammad-Beigi H, Hayashi Y, Zeuthen CM, Eskandari H, Scavenius C, Juul-Madsen K, et al. Mapping and identification of soft corona proteins at nanoparticles and their impact on cellular association. Nat Commun. 2020 Dec 10;11(1):4535.

192. Rampado R, Crotti S, Caliceti P, Pucciarelli S, Agostini M. Recent Advances in Understanding the Protein Corona of Nanoparticles and in the Formulation of “Stealthy” Nanomaterials. Front Bioeng Biotechnol. 2020 Apr 3;8.

193. Kopac T. Protein corona, understanding the nanoparticle–protein interactions and future perspectives: A critical review. Int J Biol Macromol. 2021 Feb;169:290–301.

194. Stepien G, Moros M, Pérez-Hernández M, Monge M, Gutiérrez L, Fratila RM, et al. Effect of Surface Chemistry and Associated Protein Corona on the Long-Term Biodegradation of Iron Oxide Nanoparticles In Vivo. ACS Appl Mater Interfaces. 2018 Feb 7;10(5):4548–60.

195. García-Álvarez R, Hadjidemetriou M, Sánchez-Iglesias A, Liz-Marzán LM, Kostarelos K. In vivo formation of protein corona on gold nanoparticles. The effect of their size and shape. Nanoscale. 2018;10(3):1256–64.

196. Charbgoo F, Nejabat M, Abnous K, Soltani F, Taghdisi SM, Alibolandi M, et al. Gold nanoparticle should understand protein corona for being a clinical nanomaterial. Journal of Controlled Release. 2018 Feb;272:39–53.

197. Lesniak A, Fenaroli F, Monopoli MP, Åberg C, Dawson KA, Salvati A. Effects of the Presence or Absence of a Protein Corona on Silica Nanoparticle Uptake and Impact on Cells. ACS Nano. 2012 Jul 24;6(7):5845–57.

198. Caracciolo G. Liposome–protein corona in a physiological environment: Challenges and opportunities for targeted delivery of nanomedicines. Nanomedicine. 2015 Apr;11(3):543–57.

199. Bertrand N, Grenier P, Mahmoudi M, Lima EM, Appel EA, Dormont F, et al. Mechanistic understanding of in vivo protein corona formation on polymeric nanoparticles and impact on pharmacokinetics. Nat Commun. 2017 Dec 3;8(1):777.

200. Ratner BD. Biomaterials: Been There, Done That, and Evolving into the Future. Annu Rev Biomed Eng. 2019 Jun 4;21(1):171–91.

201. Peppas NA, Khademhosseini A. Make better, safer biomaterials. Nature. 2016 Dec 15;540(7633):335–7.

202. Huebsch N, Mooney DJ. Inspiration and application in the evolution of biomaterials. Nature. 2009 Nov 25;462(7272):426–32.

203. Troy E, Tilbury MA, Power AM, Wall JG. Nature-Based Biomaterials and Their Application in Biomedicine. Polymers (Basel). 2021 Sep 28;13(19):3321.

204. Chun HJ, Park K, Kim CH, Khang G, editors. Novel Biomaterials for Regenerative Medicine. Singapore: Springer Singapore. 2018(1077).

205. Mendes AC, Baran ET, Reis RL, Azevedo HS. Self-assembly in nature: using the principles of nature to create complex nanobiomaterials. Wiley Interdiscip Rev Nanomed Nanobiotechnol. 2013 Nov;5(6):582–612.

206. Yadav S, Sharma AK, Kumar P. Nanoscale Self-Assembly for Therapeutic Delivery. Front Bioeng Biotechnol. 2020 Feb 25;8.

207. Whitesides GM, Mathias JP, Seto CT. Molecular Self-Assembly and Nanochemistry: a Chemical Strategy for the Synthesis of Nanostructures. Science (1979). 1991 Nov 29;254(5036):1312–9.

208. Levin A, Hakala TA, Schnaider L, Bernardes GJL, Gazit E, Knowles TPJ. Biomimetic peptide self-assembly for functional materials. Nat Rev Chem. 2020 Nov 15;4(11):615–34.

209. Wang Y, Yokota T, Someya T. Electrospun nanofiber-based soft electronics. NPG Asia Mater. 2021 Dec 8;13(1):22.

210. Li J, Mooney DJ. Designing hydrogels for controlled drug delivery. Nat Rev Mater. 2016 Dec 18;1(12):16071.

211. Daly AC, Riley L, Segura T, Burdick JA. Hydrogel microparticles for biomedical applications. Nat Rev Mater. 2020 Jan 7;5(1):20–43.

212. Cheng L, Hill AF. Therapeutically harnessing extracellular vesicles. Nat Rev Drug Discov. 2022 May 2;21(5):379–99.

213. Torchilin VP. Recent advances with liposomes as pharmaceutical carriers. Nat Rev Drug Discov. 2005 Feb;4(2):145–60.

214. Han X, Lu Y, Xie J, Zhang E, Zhu H, Du H, et al. Zwitterionic micelles efficiently deliver oral insulin without opening tight junctions. Nat Nanotechnol. 2020 Jul 1;15(7):605–14.

215. Discher DE, Kamien RD. Towards precision micelles. Nature. 2004 Jul 28;430(6999):519–20.

216. Agarwal S, Klocke MA, Pungchai PE, Franco E. Dynamic self-assembly of compartmentalized DNA nanotubes. Nat Commun. 2021 Dec 11;12(1):3557.

217. Fenton OS, Olafson KN, Pillai PS, Mitchell MJ, Langer R. Advances in Biomaterials for Drug Delivery. Advanced Materials. 2018 Jul;30(29):1705328.

218. Hoelder S, Clarke PA, Workman P. Discovery of small molecule cancer drugs: Successes, challenges and opportunities. Mol Oncol. 2012 Apr;6(2):155–76.

219. Bruno CD, Harmatz JS, Duan SX, Zhang Q, Chow CR, Greenblatt DJ. Effect of lipophilicity on drug distribution and elimination: Influence of obesity. Br J Clin Pharmacol. 2021 Aug 16;87(8):3197–205.

220. Wanat K. Biological barriers, and the influence of protein binding on the passage of drugs across them. Mol Biol Rep. 2020 Apr 5;47(4):3221–31.

221. Wilhelm S, Tavares AJ, Dai Q, Ohta S, Audet J, Dvorak HF, et al. Analysis of nanoparticle delivery to tumours. Nat Rev Mater. 2016 May 26;1(5):16014.

222. Han X, Alu A, Liu H, Shi Y, Wei X, Cai L, et al. Biomaterial-assisted biotherapy: A brief review of biomaterials used in drug delivery, vaccine development, gene therapy, and stem cell therapy. Bioact Mater. 2022 Nov;17:29–48.

223. Joyce K, Fabra GT, Bozkurt Y, Pandit A. Bioactive potential of natural biomaterials: identification, retention and assessment of biological properties. Signal Transduct Target Ther. 2021 Dec 19;6(1):122.

224. May M. Why drug delivery is the key to new medicines. Nat Med. 2022 Jun 6;28(6):1100–2.

225. Poon W, Kingston BR, Ouyang B, Ngo W, Chan WCW. A framework for designing delivery systems. Nat Nanotechnol. 2020 Oct 7;15(10):819–29.

226. Mitchell MJ, Billingsley MM, Haley RM, Wechsler ME, Peppas NA, Langer R. Engineering precision nanoparticles for drug delivery. Nat Rev Drug Discov. 2021 Feb 4;20(2):101–24.

227. Blanco E, Shen H, Ferrari M. Principles of nanoparticle design for overcoming biological barriers to drug delivery. Nat Biotechnol. 2015 Sep 1;33(9):941–51.

228. Khanna C, Rosenberg M, Vail DM. A Review of Paclitaxel and Novel Formulations Including Those Suitable for Use in Dogs. J Vet Intern Med. 2015 Jul;29(4):1006–12.

229. Gradishar WJ. Albumin-bound paclitaxel: a next-generation taxane. Expert Opin Pharmacother. 2006 Jun 24;7(8):1041–53.

230. Figueiredo P, Santos HA. Chapter 6 - Requirements and properties of biomaterials for biomedical applications. Lignin-Based Materials for Biomedical Applications. Elsevier. 2021:195–226.

231. Carugo D, Bottaro E, Owen J, Stride E, Nastruzzi C. Liposome production by microfluidics: potential and limiting factors. Sci Rep. 2016 May 19;6(1):25876.

232. Federman N, Denny CT. Targeting Liposomes Toward Novel Pediatric Anticancer Therapeutics. Pediatr Res. 2010 May;67(5):514–9.

233. Jeong B, Gutowska A. Lessons from nature: stimuli-responsive polymers and their biomedical applications. Trends Biotechnol. 2002 Jul;20(7):305–11.

234. Duncan R. The dawning era of polymer therapeutics. Nat Rev Drug Discov. 2003 May;2(5):347–60.

235. Kono K. Dendrimer-based bionanomaterials produced by surface modification, assembly and hybrid formation. Polym J. 2012 Jun 18;44(6):531–40.

236. Zhang H, Ma Y, Xie Y, An Y, Huang Y, Zhu Z, et al. A Controllable Aptamer-Based Self-Assembled DNA Dendrimer for High Affinity Targeting, Bioimaging and Drug Delivery. Sci Rep. 2015 Sep 11;5(1):10099.

237. Lee JH, Jang J tak, Choi J sil, Moon SH, Noh S hyun, Kim J wook, et al. Exchange-coupled magnetic nanoparticles for efficient heat induction. Nat Nanotechnol. 2011 Jul 26;6(7):418–22.

238. Vaughan O. Magnetic nanoparticles: Self-assembly at the limit. Nat Nanotechnol. 2015 Dec.

239. Ye L, Pearson T, Cordeau Y, Mefford OT, Crawford TM. Triggered self-assembly of magnetic nanoparticles. Sci Rep. 2016 Mar 15;6(1):23145.

240. Ferrer-Miralles N, Rodríguez-Carmona E, Corchero JL, García-Fruitós E, Vázquez E, Villaverde A. Engineering protein self-assembling in protein-based nanomedicines for drug delivery and gene therapy. Crit Rev Biotechnol. 2015 Apr 3;35(2):209–21.

241. García-Fruitós E, Vázquez E, Díez-Gil C, Corchero JL, Seras-Franzoso J, Ratera I, et al. Bacterial inclusion bodies: making gold from waste. Trends Biotechnol. 2012 Feb;30(2):65–70.

242. Vázquez E, Corchero JL, Burgueño JF, Seras-Franzoso J, Kosoy A, Bosser R, et al. Functional Inclusion Bodies Produced in Bacteria as Naturally Occurring Nanopills for Advanced Cell Therapies. Advanced Materials. 2012 Apr 3;24(13):1742–7.

243. Thakur G. Designing Protein Self-Assembly for Smart Materials. J Nanomed Res. 2017 Oct 2;6(2).

244. Shen Y, Levin A, Kamada A, Toprakcioglu Z, Rodriguez-Garcia M, Xu Y, et al. From Protein Building Blocks to Functional Materials. ACS Nano. 2021 Apr 27;15(4):5819–37.

245. Ma W, Saccardo A, Roccatano D, Aboagye-Mensah D, Alkaseem M, Jewkes M, et al. Modular assembly of proteins on nanoparticles. Nat Commun. 2018 Dec 16;9(1):1489.

246. Bhattacharya T, Maishu SP, Akter R, Rahman MdH, Akhtar MF, Saleem A, et al. A Review on Natural Sources Derived Protein Nanoparticles as Anticancer Agents. Curr Top Med Chem. 2021 Sep 20;21(12):1014–26.

247. Liu M, Fang X, Yang Y, Wang C. Peptide-Enabled Targeted Delivery Systems for Therapeutic Applications. Front Bioeng Biotechnol. 2021 Jul 1;9.

248. Sadeghi S, Lee WK, Kong SN, Shetty A, Drum CL. Oral administration of protein nanoparticles: An emerging route to disease treatment. Pharmacol Res. 2020 Aug;158:104685.

249. Gagner JE, Kim W, Chaikof EL. Designing protein-based biomaterials for medical applications. Acta Biomater. 2014 Apr;10(4):1542–57.

250. Unzueta U, Ferrer-Miralles N, Cedano J, Zikung X, Pesarrodona M, Saccardo P, et al. Non-amyloidogenic peptide tags for the regulatable self-assembling of protein-only nanoparticles. Biomaterials. 2012 Nov;33(33):8714–22.

251. Serna N, Céspedes MV, Saccardo P, Xu Z, Unzueta U, Álamo P, et al. Rational engineering of single-chain polypeptides into protein-only, BBB-targeted nanoparticles. Nanomedicine. 2016 Jul;12(5):1241–51.

252. Vazquez E, Roldán M, Diez-Gil C, Unzueta U, Domingo-Espín J, Cedano J, et al. Protein nanodisk assembling and intracellular trafficking powered by an arginine-rich (R9) peptide. Nanomedicine. 2010 Feb;5(2):259–68.

253. Céspedes MV, Unzueta U, Tatkiewicz W, Sánchez-Chardi A, Conchillo-Solé O, Álamo P, et al. In Vivo Architectonic Stability of Fully de Novo Designed Protein-Only Nanoparticles. ACS Nano. 2014 May 27;8(5):4166–76.

254. Cano-Garrido O, Álamo P, Sánchez-García L, Falgàs A, Sánchez-Chardi A, Serna N, et al. Biparatopic Protein Nanoparticles for the Precision Therapy of CXCR4+ Cancers. Cancers (Basel). 2021 Jun 11;13(12):2929.

255. Villaverde A, Unzueta, Céspedes, Ferrer-Miralles, Casanova, Cedano, et al. Intracellular CXCR4+ cell targeting with T22-empowered protein-only nanoparticles. Int J Nanomedicine. 2012 Aug;4533.

256. Murakami T, Zhang TY, Koyanagi Y, Tanaka Y, Kim J, Suzuki Y, et al. Inhibitory Mechanism of the CXCR4 Antagonist T22 against Human Immunodeficiency Virus Type 1 Infection. J Virol. 1999 Sep;73(9):7489–96.

257. Habibi N, Mauser A, Ko Y, Lahann J. Protein Nanoparticles: Uniting the Power of Proteins with Engineering Design Approaches. Advanced Science. 2022 Mar 25;9(8):2104012.

258. Martinez-Veracoechea FJ, Frenkel D. Designing super selectivity in multivalent nano-particle binding. Proceedings of the National Academy of Sciences. 2011 Jul 5;108(27):10963–8.

259. Woythe L, Tito NB, Albertazzi L. A quantitative view on multivalent nanomedicine targeting. Adv Drug Deliv Rev. 2021 Feb;169:1–21.

260. Ueda G, Antanasijevic A, Fallas JA, Sheffler W, Copps J, Ellis D, et al. Tailored design of protein nanoparticle scaffolds for multivalent presentation of viral glycoprotein antigens. Elife. 2020 Aug 4;9.

261. Zelepukin I v., Yaremenko A v., Yuryev M v., Mirkasymov AB, Sokolov IL, Deyev SM, et al. Fast processes of nanoparticle blood clearance: Comprehensive study. Journal of Controlled Release. 2020 Oct;326:181–91.

262. Serna N, Sánchez-García L, Unzueta U, Díaz R, Vázquez E, Mangues R, et al. Protein-Based Therapeutic Killing for Cancer Therapies. Trends Biotechnol. 2018 Mar;36(3):318–35.

263. Sánchez-García L, Serna N, Álamo P, Sala R, Céspedes MV, Roldan M, et al. Self-assembling toxin-based nanoparticles as self-delivered antitumoral drugs. Journal of Controlled Release. 2018 Mar;274:81–92.

264. Céspedes MV, Unzueta U, Aviñó A, Gallardo A, Álamo P, Sala R, et al. Selective depletion of metastatic stem cells as therapy for human colorectal cancer. EMBO Mol Med. 2018 Oct 6;10(10).

265. Serna N, Falgàs A, García-León A, Unzueta U, Núñez Y, Sánchez-Chardi A, et al. Time-Prolonged Release of Tumor-Targeted Protein–MMAE Nanoconjugates from Implantable Hybrid Materials. Pharmaceutics. 2022 Jan 14;14(1):192.

266. Pallarès V, Unzueta U, Falgàs A, Sánchez-García L, Serna N, Gallardo A, et al. An Auristatin nanoconjugate targeting CXCR4+ leukemic cells blocks acute myeloid leukemia dissemination. J Hematol Oncol. 2020 Dec 15;13(1):36.

267. Pallarès V, Unzueta U, Falgàs A, Aviñó A, Núñez Y, García-León A, et al. A multivalent Ara-C-prodrug nanoconjugate achieves selective ablation of leukemic cells in an acute myeloid leukemia mouse model. Biomaterials. 2022 Jan;280:121258.

268. de Marco A, Ferrer-Miralles N, Garcia-Fruitós E, Mitraki A, Peternel S, Rinas U, et al. Bacterial inclusion bodies are industrially exploitable amyloids. FEMS Microbiol Rev. 2019 Jan 1;43(1):53–72.

269. García-Fruitós E, González-Montalbán N, Morell M, Vera A, Ferraz RM, Arís A, et al. Aggregation as bacterial inclusion bodies does not imply inactivation of enzymes and fluorescent proteins. Microb Cell Fact. 2005 Dec 12;4(1):27.

270. Arié JP, Miot M, Sassoon N, Betton JM. Formation of active inclusion bodies in the periplasm of Escherichia coli. Mol Microbiol. 2006 Oct;62(2):427–37.

271. Nahalka J, Nidetzky B. Fusion to a pull-down domain: a novel approach of producingTrigonopsis variabilisD-amino acid oxidase as insoluble enzyme aggregates. Biotechnol Bioeng. 2007 Jun 15;97(3):454–61.

272. Rinas U, Hoffmann F, Betiku E, Estapé D, Marten S. Inclusion body anatomy and functioning of chaperone-mediated in vivo inclusion body disassembly during high-level recombinant protein production in Escherichia coli. J Biotechnol. 2007 Jan;127(2):244–57.

273. Villaverde A, Corchero JL, Seras-Franzoso J, Garcia-Fruitós E. Functional protein aggregates: just the tip of the iceberg. Nanomedicine. 2015 Sep;10(18):2881–91.

274. Jürgen B, Breitenstein A, Urlacher V, Büttner K, Lin H, Hecker M, et al. Quality control of inclusion bodies in Escherichia coli. Microb Cell Fact. 2010 Dec 28;9(1):41.

275. Matsuura K. Construction of spherical virus-inspired peptide nanoassemblies. Polym J. 2012 Jun 14;44(6):469–74.

276. Lamarre B, Ryadnov MG. Self-Assembling Viral Mimetics: One Long Journey with Short Steps. Macromol Biosci. 2011 Apr 8;11(4):503–13.

277. Danaei M, Dehghankhold M, Ataei S, Hasanzadeh Davarani F, Javanmard R, Dokhani A, et al. Impact of Particle Size and Polydispersity Index on the Clinical Applications of Lipidic Nanocarrier Systems. Pharmaceutics. 2018 May 18;10(2).

278. SUNDBERG MW, MEARES CF, GOODWIN DA, DIAMANTI CI. Chelating agents for the binding of metal ions to macromolecules. Nature. 1974 Aug 1;250(5467):587–8.

279. Ammann AA. Inductively coupled plasma mass spectrometry (ICP MS): a versatile tool. Journal of Mass Spectrometry. 2007 Apr;42(4):419–27.

280. Unzueta U, Serna N, Sánchez-García L, Roldán M, Sánchez-Chardi A, Mangues R, et al. Engineering multifunctional protein nanoparticles by *in vitro* disassembling and reassembling of heterologous building blocks. Nanotechnology. 2017 Dec 15;28(50):505102.

281. Zhou HX, Pang X. Electrostatic Interactions in Protein Structure, Folding, Binding, and Condensation. Chem Rev. 2018 Feb 28;118(4):1691–741.

282. Outten CE, O'Halloran and T v. Femtomolar Sensitivity of Metalloregulatory Proteins Controlling Zinc Homeostasis. Science (1979). 2001 Jun 29;292(5526):2488–92.

283. Kung FC, Raymond J, Glaser DA. Metal ion content of Escherichia coli versus cell age. J Bacteriol. 1976 Jun;126(3):1089–95.

284. Zhao Z, Ukidve A, Kim J, Mitragotri S. Targeting Strategies for Tissue-Specific Drug Delivery. Cell. 2020 Apr;181(1):151–67.

285. Lomis N, Westfall S, Farahdel L, Malhotra M, Shum-Tim D, Prakash S. Human Serum Albumin Nanoparticles for Use in Cancer Drug Delivery: Process Optimization and In Vitro Characterization. Nanomaterials. 2016 Jun 15;6(6):116.

286. Álamo P, Cedano J, Conchillo-Sole O, Cano-Garrido O, Alba-Castellon L, Serna N, et al. Rational engineering of a human GFP-like protein scaffold for humanized targeted nanomedicines. Acta Biomater. 2021 Aug;130:211–22.

287. Liu L. Aggregation of silica nanoparticles in an aqueous suspension. AIChE Journal. 2015 Jul;61(7):2136–46.

288. Nangia S, Sureshkumar R. Effects of Nanoparticle Charge and Shape Anisotropy on Translocation through Cell Membranes. Langmuir. 2012 Dec 21;28(51):17666–71.

289. Ji YY, Li YQ. The role of secondary structure in protein structure selection. The European Physical Journal E. 2010 May 25;32(1):103–7.

290. Roohani N, Hurrell R, Kelishadi R, Schulin R. Zinc and its importance for human health: An integrative review. J Res Med Sci. 2013 Feb;18(2):144–57.

291. Damin BIS, Kovalski FC, Fischer J, Piccin JS, Dettmer A. Challenges and perspectives of the β-galactosidase enzyme. Appl Microbiol Biotechnol. 2021 Jul 5;105(13):5281–98.

292. Richmond ML, Gray JI, Stine CM. Beta-Galactosidase: Review of Recent Research Related to Technological Application, Nutritional Concerns, and Immobilization. J Dairy Sci. 1981 Sep;64(9):1759–71.

293. Yang EY, Shah K. Nanobodies: Next Generation of Cancer Diagnostics and Therapeutics. Front Oncol. 2020 Jul 23;10.

294. Sánchez-García L, Sala R, Serna N, Álamo P, Parladé E, Alba-Castellón L, et al. A refined cocktailing of pro-apoptotic nanoparticles boosts anti-tumor activity. Acta Biomater. 2020 Sep;113:584–96.

295. Tian H, Matsuo Y, Fukunaga A, Ono R, Nishigori C, Yodoi J. Thioredoxin Ameliorates Cutaneous Inflammation by Regulating the Epithelial Production and Release of Pro-Inflammatory Cytokines. Front Immunol. 2013;4.

296. Cano-Garrido O, Serna N, Unzueta U, Parladé E, Mangues R, Villaverde A, et al. Protein scaffolds in human clinics. Biotechnol Adv. 2022 Dec;61:108032.

297. Dingman R, Balu-Iyer S v. Immunogenicity of Protein Pharmaceuticals. J Pharm Sci. 2019 May;108(5):1637–54.

298. Gilbert JA, Blaser MJ, Caporaso JG, Jansson JK, Lynch S v, Knight R. Current understanding of the human microbiome. Nat Med. 2018 Apr 1;24(4):392–400.

299. Mougous JD, Cuff ME, Raunser S, Shen A, Zhou M, Gifford CA, et al. A Virulence Locus of *Pseudomonas aeruginosa* Encodes a Protein Secretion Apparatus. Science (1979). 2006 Jun 9;312(5779):1526–30.

300. Bamford JKH, Luo C, Juuti JT, Olkkonen VM, Bamford DH. Topology of the Major Capsid Protein P3 of Bacteriophage PRD1: Analysis Using Monoclonal Antibodies and C-Terminally Truncated Proteins. Virology. 1993 Dec;197(2):652–8.

301. Rajagopala S v, Casjens S, Uetz P. The protein interaction map of bacteriophage lambda. BMC Microbiol. 2011;11(1):213.

302. Riehemann K, Schneider SW, Luger TA, Godin B, Ferrari M, Fuchs H. Nanomedicine-Challenge and Perspectives. Angewandte Chemie International Edition. 2009 Jan 19;48(5):872–97.

303. Le-Vinh B, Akkuş-Dağdeviren ZB, Le NN, Nazir I, Bernkop-Schnürch A. Alkaline Phosphatase: A Reliable Endogenous Partner for Drug Delivery and Diagnostics. Adv Ther (Weinh). 2022 Feb 10;5(2):2100219.

304. de Clercq E. AMD3100/CXCR4 Inhibitor. Front Immunol. 2015 Jun 8;6.

305. Kang M, Tuteja M, Centrone A, Topgaard D, Leal C. Nanostructured Lipid-Based Films for Substrate-Mediated Applications in Biotechnology. Adv Funct Mater. 2018 Feb 10;28(9):1704356.

306. Kuten Pella O, Hornyák I, Horváthy D, Fodor E, Nehrer S, Lacza Z. Albumin as a Biomaterial and Therapeutic Agent in Regenerative Medicine. Int J Mol Sci. 2022 Sep 12;23(18):10557.

307. Sanchez-Garcia L, Martín L, Mangues R, Ferrer-Miralles N, Vázquez E, Villaverde A. Recombinant pharmaceuticals from microbial cells: a 2015 update. Microb Cell Fact. 2016 Dec 9;15(1):33.

308. Bai X, Smith Z, Wang Y, Butterworth S, Tirella A. Sustained Drug Release from Smart Nanoparticles in Cancer Therapy: A Comprehensive Review. Micromachines (Basel). 2022 Sep 28;13(10):1623.

309. Petlin DG, Tverdokhlebov SI, Anissimov YG. Plasma treatment as an efficient tool for controlled drug release from polymeric materials: A review. Journal of Controlled Release. 2017 Nov;266:57–74.

310. Saghazadeh S, Rinoldi C, Schot M, Kashaf SS, Sharifi F, Jalilian E, et al. Drug delivery systems and materials for wound healing applications. Adv Drug Deliv Rev. 2018 Mar;127:138–66.

311. Koike Y, Yozaki M, Utani A, Murota H. Fibroblast growth factor 2 accelerates the epithelial–mesenchymal transition in keratinocytes during wound healing process. Sci Rep. 2020 Oct 29;10(1):18545.

312. Mansouri N, SamiraBagheri. The influence of topography on tissue engineering perspective. Mater Sci Eng C Mater Biol Appl. 2016 Apr;61:906–21.

313. Rosenbaum AJ, Grande DA, Dines JS. The use of mesenchymal stem cells in tissue engineering. Organogenesis. 2008 Jan 27;4(1):23–7.

314. Ferrer-Miralles N, Villaverde A. Bacterial cell factories for recombinant protein production; expanding the catalogue. Microb Cell Fact. 2013;12(1):113.

315. Llopis-Hernández V, Cantini M, González-García C, Cheng ZA, Yang J, Tsimbouri PM, et al. Material-driven fibronectin assembly for high-efficiency presentation of growth factors. Sci Adv. 2016 Aug 5;2(8).

316. Shen C, Yang C, Xu S, Zhao H. Comparison of osteogenic differentiation capacity in mesenchymal stem cells derived from human amniotic membrane (AM), umbilical cord (UC), chorionic membrane (CM), and decidua (DC). Cell Biosci. 2019 Dec 11;9(1):17.

317. Choi B, Rempala GA, Kim JK. Beyond the Michaelis-Menten equation: Accurate and efficient estimation of enzyme kinetic parameters. Sci Rep. 2017 Dec 5;7(1):17018.

318. Miotto M, Olimpieri PP, di Rienzo L, Ambrosetti F, Corsi P, Lepore R, et al. Insights on protein thermal stability: a graph representation of molecular interactions. Bioinformatics. 2019 Aug 1;35(15):2569–77.

319. Fjell CD, Hiss JA, Hancock REW, Schneider G. Designing antimicrobial peptides: form follows function. Nat Rev Drug Discov. 2012 Jan 16;11(1):37–51.

320. Mookherjee N, Anderson MA, Haagsman HP, Davidson DJ. Antimicrobial host defence peptides: functions and clinical potential. Nat Rev Drug Discov. 2020 May 27;19(5):311–32.

321. Serna N, Carratalá JV, Conchillo-Solé O, Martínez-Torró C, Unzueta U, Mangues R, et al. Antibacterial Activity of T22, a Specific Peptidic Ligand of the Tumoral Marker CXCR4. Pharmaceutics. 2021 Nov 13;13(11):1922.

322. Wang Y, Cui P, Zhang Y, Yang Q, Zhang S. Augmentation of the antibacterial activities of Pt5-derived antimicrobial peptides (AMPs) by amino acid substitutions: Design of novel AMPs against MDR bacteria. Fish Shellfish Immunol. 2018 Jun;77:100–11.

323. Irazazabal LN, Porto WF, Fensterseifer ICM, Alves ESF, Matos CO, Menezes ACS, et al. Fast and potent bactericidal membrane lytic activity of PaDBS1R1, a novel cationic antimicrobial peptide. Biochimica et Biophysica Acta (BBA) - Biomembranes. 2019 Jan;1861(1):178–90.

324. Carratalá J v., Brouillette E, Serna N, Sánchez-Chardi A, Sánchez JM, Villaverde A, et al. In Vivo Bactericidal Efficacy of GWH1 Antimicrobial Peptide Displayed on Protein Nanoparticles, a Potential Alternative to Antibiotics. Pharmaceutics. 2020 Dec 17;12(12):1217.

325. Bielajew BJ, Hu JC, Athanasiou KA. Collagen: quantification, biomechanics and role of minor subtypes in cartilage. Nat Rev Mater. 2020 Oct 20;5(10):730–47.

326. Dominguez R, Holmes KC. Actin Structure and Function. Annu Rev Biophys. 2011 Jun 9;40(1):169–86.

327. de March M, Merino N, Barrera-Vilarmau S, Crehuet R, Onesti S, Blanco FJ, et al. Structural basis of human PCNA sliding on DNA. Nat Commun. 2017 Apr 28;8(1):13935.

328. Burnham DR, Kose HB, Hoyle RB, Yardimci H. The mechanism of DNA unwinding by the eukaryotic replicative helicase. Nat Commun. 2019 Dec 14;10(1):2159.

329. Nishino T, Morikawa K. Structure and function of nucleases in DNA repair: shape, grip and blade of the DNA scissors. Oncogene. 2002 Dec 16;21(58):9022–32.

330. FRANKLIN RE. Structure of Tobacco Mosaic Virus. Nature. 1955 Feb;175(4452):379–81.

331. Walz T, Hirai T, Murata K, Heymann JB, Mitsuoka K, Fujiyoshi Y, et al. The three-dimensional structure of aquaporin-1. Nature. 1997 Jun 5;387(6633):624–7.

332. Cao Z, Roszak AW, Gourlay LJ, Lindsay JG, Isaacs NW. Bovine Mitochondrial Peroxiredoxin III Forms a Two-Ring Catenane. Structure. 2005 Nov;13(11):1661–4.

333. Helgstrand C, Wikoff WR, Duda RL, Hendrix RW, Johnson JE, Liljas L. The Refined Structure of a Protein Catenane: The HK97 Bacteriophage Capsid at 3.44 Å Resolution. J Mol Biol. 2003 Dec;334(5):885–99.

334. Virnau P, Mallam A, Jackson S. Structures and folding pathways of topologically knotted proteins. Journal of Physics: Condensed Matter. 2011 Jan 26;23(3):033101.

335. Montemiglio LC, Testi C, Ceci P, Falvo E, Pitea M, Savino C, et al. Cryo-EM structure of the human ferritin–transferrin receptor 1 complex. Nat Commun. 2019 Dec 8;10(1):1121.

336. Wang JCY, Chen L. Publisher Correction: Structural basis for the structural dynamics of human mitochondrial chaperonin mHsp60. Sci Rep. 2021 Dec 24;11(1):17372.

337. Halebian M, Morris K, Smith C. Structure and Assembly of Clathrin Cages. Subcell Biochem. 2017;83:551-567.

338. Gabashvili AN, Chmelyuk NS, Efremova M v., Malinovskaya JA, Semkina AS, Abakumov MA. Encapsulins—Bacterial Protein Nanocompartments: Structure, Properties, and Application. Biomolecules. 2020 Jun 26;10(6):966.

339. Kovrlija I, Locs J, Loca D. Incorporation of Barium Ions into Biomaterials: Dangerous Liaison or Potential Revolution? Materials. 2021 Oct 2;14(19):5772.

340. Chen Q, He L, Li X, Xu L, Chen T. Ruthenium complexes boost NK cell immunotherapy via sensitizing triple-negative breast cancer and shaping immuno-microenvironment. Biomaterials. 2022 Feb;281:121371.

341. Lambert JM. The nature of platinum in silicones for biomedical and healthcare use. J Biomed Mater Res B Appl Biomater. 2006 Jul;78B(1):167–80.

342. Bapat RA, Chaubal T v., Dharmadhikari S, Abdulla AM, Bapat P, Alexander A, et al. Recent advances of gold nanoparticles as biomaterial in dentistry. Int J Pharm. 2020 Aug;586:119596.

343. Burdușel AC, Gherasim O, Grumezescu AM, Mogoantă L, Ficai A, Andronescu E. Biomedical Applications of Silver Nanoparticles: An Up-to-Date Overview. Nanomaterials. 2018 Aug 31;8(9):681.

344. Clunie GPR, Bomanji J, Renton P, Edwards JCW, Ell PJ. Technetium-99m human immunoglobulin imaging in patients with subacromial impingement or adhesive capsulitis. Clin Rheumatol. 1998 Sep;17(5):419–21.

345. López-Laguna H, Sánchez J, Unzueta U, Mangues R, Vázquez E, Villaverde A. Divalent Cations: A Molecular Glue for Protein Materials. Trends Biochem Sci. 2020 Nov;45(11):992–1003.

346. Li K, Wang XF, Li DY, Chen YC, Zhao LJ, Liu XG, et al. The good, the bad, and the ugly of calcium supplementation: a review of calcium intake on human health. Clin Interv Aging. 2018 Nov;Volume 13:2443–52.

347. al Alawi AM, Majoni SW, Falhammar H. Magnesium and Human Health: Perspectives and Research Directions. Int J Endocrinol. 2018;2018:1–17.

348. Ackerman CM, Chang CJ. Copper signaling in the brain and beyond. Journal of Biological Chemistry. 2018 Mar;293(13):4628–35.

349. Dev S, Babitt JL. Overview of iron metabolism in health and disease. Hemodialysis International. 2017 Apr;21:S6–20.

350. Cherasse Y, Urade Y. Dietary Zinc Acts as a Sleep Modulator. Int J Mol Sci. 2017 Nov 5;18(11):2334.

351. Rehder D. Vanadium. Its Role for Humans. Met Ions Life Sci. 2013;13:139-69.

352. Zamble D, Rowinska-Zyrek M, Kozlowski H, editors. The Biological Chemistry of Nickel. Royal Society of Chemistry. 2017 Mar.

353. Packer M. Cobalt Cardiomyopathy: A Critical Reappraisal in Light of a Recent Resurgence. Circ Heart Fail. 2016;9(12).

354. Sardesai VM. Molybdenum: An Essential Trace Element. Nutrition in Clinical Practice. 1993 Dec;8(6):277–81.

355. Li L, Yang X. The Essential Element Manganese, Oxidative Stress, and Metabolic Diseases: Links and Interactions. Oxid Med Cell Longev. 2018;2018:1–11.

356. Wallach S. Clinical and biochemical aspects of chromium deficiency. J Am Coll Nutr. 1985 Jan;4(1):107–20.

357. Beto JA. The Role of Calcium in Human Aging. Clin Nutr Res. 2015;4(1):1.

358. Briguglio M, Hrelia S, Malaguti M, Lombardi G, Riso P, Porrini M, et al. The Central Role of Iron in Human Nutrition: From Folk to Contemporary Medicine. Nutrients. 2020 Jun 12;12(6):1761.

359. Genchi G, Carocci A, Lauria G, Sinicropi MS, Catalano A. Nickel: Human Health and Environmental Toxicology. Int J Environ Res Public Health. 2020 Jan 21;17(3):679.

360. Yamada K. Cobalt: Its Role in Health and Disease. Met Ions Life Sci . 2013;13:295-320.

361. Avila DS, Puntel RL, Aschner M. Manganese in Health and Disease. Met Ions Life Sci. 2013;13:1997-227.

362. Cefalu WT, Hu FB. Role of Chromium in Human Health and in Diabetes. Diabetes Care. 2004 Nov 1;27(11):2741–51.

363. Wadworth AN, Murdoch D, Brogden RN. Atenolol. Drugs. 1991 Sep;42(3):468–510.

364. Mindermann T, Zimmerli W, Gratzl O. Rifampin Concentrations in Various Compartments of the Human Brain: A Novel Method for Determining Drug Levels in the Cerebral Extracellular Space. Antimicrob Agents Chemother. 1998 Oct;42(10):2626–9.

365. Levison ME, Levison JH. Pharmacokinetics and Pharmacodynamics of Antibacterial Agents. Infect Dis Clin North Am. 2009 Dec;23(4):791–815.

AKNOWLEDGEMENTS

The author of the thesis is indebted to a predoctoral fellowship from AGAUR (2019FI_B00352) under the supervision of Prof. Antonio Villaverde Corrales and Drs. Esther Váquez Gómez and Ugutz Unzueta Elorza. The experimental work was performed at the Nanobiotechnology Group (Institute of Biotechnology and Biomedicine) from the Autonomous University of Barcelona (UAB). The author is also indebted to the PhD Biotechnology programme supervised by Prof. Francesc Godia Casablancas (Department of Chemical Engineering – UAB) and the Department of Genetics and Microbiology (UAB) supervised by Maria Josep Mas Fages. The Protein Production Platform (PPP – ICS NanBiosis) linked to the Networking Research Center on Bioengineering, Biomaterials and Nanomedicine (CIBER – BBN; in which the nanobiotechnology group is also affiliated) was involved in the protein purification at the UAB sePBioES scientific-technical service. The *in vivo* studies were performed in collaboration with the "Hospital de la Santa Creu i Sant Pau" under the supervision of Prof. Ramon Mangues Bafalluy (Biomedical Research Institute – IIB Sant Pau), and the Evolutive Immunology group (IBB – UAB) under the supervision of Dr. Nerea Armentia Roher. Electron microscopy studies were performed at the "Servei de Microscopia" (UAB) and the *in vitro* experiments at the "Servei de Cultius Celulars, Producció d'Anticossos i Citometria" (SCAC – UAB). Finally, the 3 months internship (meaning 90 days) was performed at the University of Glasgow (Advanced Research Centre, ARC – Centre for the Cellular Microenvironment, CeMi) under the supervision of Prof. Matthew Dalby and scientific manager Monica Tsimbouri.

Article rights and permissions

The rights and permissions of the articles included in the results section and annexes are subsequently disclosed:

- Permissions for **articles 1 and 7, and annexes 1 and 5** are not required. Stated by the publishing journal: "As the author of this Elsevier article, you retain the right to include it in a thesis or dissertation, provided it is not published commercially. Permission is not required, but please ensure that you reference the journal as the original source".
- Permissions for **articles 2, 4, and 6** are not required as well. Stated by the publishing journal: "This is an open access article distributed under the terms of the Creative Commons CC BY license, which permits unrestricted use, distribution, reproduction in any medium, provided the original work is properly cited".

- Permissions for **annex 3** are not required but appropriate credit for the requested material needs to be given. Stated by the publishing journal: "Permission is granted for your request in both print and electronic formats, and translations. If figures and/or tables were requested, they may be adapted or used in part. Please print this page for your records and send a copy of it to your publisher/graduate school. Appropriate credit for the requested material should be given as follows: Reprinted with permission from Julieta M. Sanchez, Hèctor López-Laguna, Naroa Serna, et al. Engineering the Performance of Artificial Inclusion Bodies Built of Catalytic β-Galactosidase. ACS Sustainable Chem. Eng. 2021, 9, 6, 2552–2558. Copyright 2021 American Chemical Society".
- Permissions for **articles 3 and 5** are required. An agreement between Hèctor López-Laguna from the Institute of Biotechnology and Biomedicine (IBB-UAB) and "John Wiley and Sons" has been disclosed and licenses provided by the Copyright Clearance Center. License number 5460140443754 is provided for article 3 and license number 5460140712888 is provided for article 5.

Figure rights and permissions

All presented figures were created with BioRender.com (including front, back and chapter covers), and confirmation documents of Publication and Licensing Rights obtained. Respective agreement numbers are displayed: front cover (SN24VP5T5B), figure 1 (UD24VFYIOB), figure 2 (KZ24VKOJIO), figure 3 (SJ24VKOW7Z), figure 4 (CP24VKP9FA), figure 5 (GN24VKPM8R), figure 6 (YF24VKPX1Q), figure 7 (NF24VKQMUS), figure 8 (PO24VKQUZR), figure 9 (UR24VKR473), figure 10 (VP24VKRCU1), figure 11 (UX24VKRLBJ), figure 12 (MF24VKSJCF), figure 13 (TQ24VKSRTV), figure 14 (FS24VKT111), figure 15 (RB24VKTGJX), figure 16 (CR24VKTS8L), figure 17 (ZN24VKU7CH), chapter cover (BA24VOWI6P) and back cover (ZN24VP18QW).

The team

There is no thesis without a team, no science without a team, no substantial progress without a team, and for sure no home without a team.

There is no other way to end up a journey rather than being grateful for all the experiences lived, all the ups and downs felt, all the strength pulled from failure, and all brightness earned from discussion. There is no other way to say goodbye than remembering all the names and faces along the way. A team that pushes but also lets, that teaches but also listens. People who have put sweat and tears into this journey.

I will use the words that allow me express the best what needs to be expressed.

El que ha sigut: una aventura

"Començaré pels ciments. De la mateixa manera que es comença a construir una casa. Potser, els ciments determinen la fortalesa final, sobretot en temps de tempesta. En el meu cas, els ciments són aquella infraestructura humana que ha permès tirar endavant aquest projecte.

Podria dir que la Rosa ha sigut aquell formigó que ha ajudat a que tota la resta es conformi. Semblant als braços d'un pop. Allà on la Rosa posa energia la cosa funciona. Ben senzill com això. De la mateixa manera que també ho ha fet tot el personal tècnic i administratiu de l'Institut (Francesca, Àngels, Laura...), on he viscut pràcticament més que a casa. M'agradaria oferir un especial agraïment al Miguel; doncs la seva energia a principi i a final del dia t'ajuden a entrar i sortir amb un somriure, sobretot en aquells dies on la ciència va cap a un lloc i tu cap a un altre. També m'agradaria donar les gràcies al Fran, l'Olga, l'Àlex S., i a l'Amable per assessorar-me quan feia falta, especialment en els dies en què feia més hores que un rellotge.

A més, i per increïble que sembli, la Rosa també s'involucra experimentalment en projectes com ho és la Plataforma de Producció de Proteïnes (PPP), on conjuntament amb la Mercè i la Neus, ens ajuden a solucionar els problemes que tenim habitualment amb proteïnes entremaliades. Gràcies per fer-nos la vida purificadora més senzilla.

D'aquests mateixos tentacles energètics neixen tota la resta de criatures científiques. Tant les més novelles com les que no ho són tant. Persones com jo, les quals comencen a entendre què és l'entorn científic. Un entorn que a vegades pot semblar frustrant i incert, però que, un cop et poses les ulleres adequades comences a veure llum rere la foscor. Suposo que és qüestió de pràctica. És interessant pensar que allò que inicialment t'espanta (em refereixo a la pressió selectiva dels primers anys), t'impulsa al mateix temps a cohesionar i fer equip amb

persones de les quals no en saps massa. Com dues coses oposades però que, al mateix temps, sents amb la mateixa intensitat. Em refereixo a una llista de noms. Persones amb les quals a poc a poc comences a crear vincles i viure experiències. Ara recordo els meus inicis amb la Núria i la Laura; podríem dir que va ser aleshores quan es va sembrar la primera llavor d'on passats uns mesos, i amb l'aparició de l'Eric, l'Amanda, l'Andrés i l'Aida, naixeria el conegut popularment com a: *Despachito*. Un ecosistema on el riure i el bon rotllo no faltaven. Potser, aquest indret va ser inconscientment construït per assegurar la nostra pròpia supervivència a la vista dels futurs anys boirosos que ens esperaven. Una ànima de cooperació, ajut i alegria. No puc recordar aquells temps d'una altra manera, i encara que cadascú estigui seguint els seus passos, aquells que el destí o el mateix cos van marcant, l'essència es manté. De fet, encara tenim alguna foto per allà dels nostres inicis.

D'aquí podríem anar tirant del fil, i començar a explicar totes les històries i persones que hi han passat amb personalitats, llenguatges i idees diferents (Elijah, Alejandro, Estera, Mara, Marila, Agus, Andreu, Sara, Marianna, Rubén, Raquel, Diana...) amb les que he compartit anècdotes, hores de debat i fins i tot viatges. No m'endinsaré en relatar-ho tot al peu de la lletra, no vull que aquestes paraules es converteixin en una autobiografia, sinó en una carta d'agraïment al viscut i caminat. Curiosament, aquesta pressió selectiva de la qual abans parlava ens va impulsar a donar la mà quan algú ho necessitava o demanar ajuda quan un se sentia atrapat. A vegades amb una simple conversa o somriure era suficient. Crec que per això es van crear vincles. Vincles en espais i temps determinats que recordes amb alegria i tendresa. Em sembla curiós com a mínim. Potser, representa una mica la naturalesa humana.

Aquesta energia, però, també habitava fora d'aquestes 4 parets (folrades amb imatges eclèctiques representant una mica el caos creatiu de les nostres ments); especialment allà on es feia ciència i on jo em vaig formar com a investigador. De fet, i en el meu cas, un nou espai implica una nova llista de noms. Persones amb experiències passades molts semblants a les que nosaltres, com a joves cadells, estàvem caminant en aquell moment. Em refereixo a l'Olivia, la Naroa, la Laura S., el José Vicente, l'Eloi, la Julieta, el Paolo... Aquesta llista de noms és veritablement especial per mi. L'altre dia parlava amb la Isabel, en una d'aquestes converses on el temps sembla que se t'escapi de les mans. Li expressava la sensació que havia tingut després d'haver caminat aquests últims cinc anys. La sensació que m'havia transformat en una persona que veritablement no sabia que existia. Pot ser, referint-me a trobar allò que ja hi era, però que s'havia perdut per falta d'atenció. Una de les revelacions va ser la gratitud que el meu cos sentia en pensar en totes aquelles persones que m'havien ajudat a fer camí, i que, al cap i a la fi, hi havien i han contribuït al fet que jo fos i sigui capaç de ser i estar on

soc ara. Des de converses profundes, experiències lliures, riures sincers, abraçades intenses, saviesa compartida... Potser, era allò que necessitàvem en cada moment, fent el millor que podíem amb el que teníem. Gràcies i més gràcies. A més, d'aquesta llista de vincles que un va creant a mesura que va fent passes, i hi han alguns que s'intensifiquen, pot ser per energies inexplicables. Qui sap. Teniu una ànima brillant. I no diré més. Potser, cadascú ja sap el que ha de saber.

També m'agradaria donar les gràcies a persones com l'Àlex M., el Pablo, Christos, i en Jezer, que fora de l'ambient universitari ens hem mantingut connectats. Sempre preparats pel que faci falta.

I de la mateixa manera que el vell existeix, també ho fa el nou. M'agradaria aleshores donar les gràcies a tots aquells nous vincles que s'estan creant. Em refereixo a Roger, Tuty, Jara, Carlos, Jan, Ariana, Angela, Chari, Lucía S., Helena, Eddie, Lucía A., Gala, Jaime, Ioanna, Monica, Matt, Seb, Juan, Margaret, Ana Maria, Udesh... Persones que apareixen i comparteixen part del que són; que sumen i no resten. Sou molt macos. De fet, ja començo a compartir moments i vivències amb alguns, similars però diferents de les ja viscudes. Tot sembla una aventura de la qual mai saps on acabaràs. Un cicle que es repeteix. Gràcies per ser-hi.

Si abans parlava del formigó, ara m'agradaria parlar de les estructures que sustenten la casa, que protegeixen i donen aixopluc als éssers que busquen refugi en elles. Em refereixo a aquelles persones que ofereixen un camí als nous deixebles que entren (Pepe, Neus, Ramon, Esther, Toni, Ugutz...). Així, les parets són tan necessàries com el ciment, i viceversa. Gràcies aleshores per oferir-nos a tots l'oportunitat de viure aquest viatge anomenat tesis. En especial m'agradaria parlar de tres d'ells. No acabo de trobar ben bé una paraula que mostri el que el meu cos vol expressar. Podrien ser mentors, o pares/mares científics, però crec que va una mica més enllà, ja que sento que un vincle fort s'ha forjat. Han sigut les tres persones que m'han guiat i acompanyat en una aventura desconeguda per a mi. Un camí replet de llums i foscors, però que al final ha valgut la pena. El meu agraïment seria aleshores tan gran com les experiències viscudes, ja que sense aquesta oportunitat qui sap on jo hagués acabat. Gràcies amb la mà al cor als tres, perquè heu fet que l'Hèctor hagi pogut viure el que ha viscut; i això no té preu. Sempre atents i disposats, escoltant i ensenyant, ajudant i oferint.

Ciments i parets, sembla que estem construint una llar. Però per poder fer-ho, encara falta alguna cosa més, quelcom que doni escalfor i energia. Aquella cosa que fa sentir-te a casa.

Miren, has sigut l'espurna que ha encès la flama. I tot i que ara els nostres camins se separin, el record del viscut i sentit romandrà en el meu cos, allà on hagi de ser. Pot ser, som en part aquelles persones amb què hem fet camí. Només et puc desitjar el millor, més que el millor; que volis ben amunt, allà on neixen les estrelles, i que et deixis emportat per una brisa suau fins a arribar a bon port. Arreveure. Potser, ens tornem a trobar, qui sap.

Papa i mama, les persones que em van portar al món. Aquelles que generen gran part de l'escalfor de la qual parlava. Tinc la sensació que hi ha certes coses que un no pot decidir. A vegades passa el que ha de passar i prou. Aquesta és una d'elles. Gràcies per haver-m'ho donat tot i més, i per haver tingut el valor de dedicar part de la vostra vida (dia i nit) a criar i ensenyar a una criatura, indefensa per si mateixa, a viure una vida. Res no seria si no fos per vosaltres. Amb això tinc suficient potser, una vida.

D'aquí aleshores surt el bitxo. Aix Marina. Saps que t'estimo molt no? La Marina és l'ésser amb qui porto compartint vint-i-dos anys de la meva vida, hem crescut i après junts sota la mateixa ala. Estiguem lluny o a prop, ens tenim, dins nostre. A poc a poc. I ens ho fem saber de la forma en què ens ho fem saber. Un petó gegant. Aquí em tens.

La veritat és que no vull enrotllar-me més, pot ser l'energia que fa sortir aquestes paraules s'està acabant. Suficient és suficient. Agrair, finalment, a la família i a totes aquelles persones que m'han donat suport i ajudat a navegar durant aquests anys. Sense una tripulació crec que és molt difícil trobar la llum del far quant la boira cega. Com més o penso, menys crec que es tracti de jo, i més penso que es tracti de tots; encara que jo una mica més (com diu el Toni). Potser, estem més connectats del que creiem. Qui sap. I així m'acomiado. Fins aviat".

FINAL WORDS

A gift made of words, that strengths my mind and softens my body. I wish you like it.

Alone I set out on the road;
The flinty path is sparkling in the mist;
The night is still. The desert harks to God,
and star with star converses.

The vault is overwhelmed with solemn wonder.
The earth in cobalt aura sleeps. . .
Why do I feel so pained and troubled?
What do I harbor: hope, regrets?

I see no hope in years to come,
have no regrets for things gone by.
All that I seek is peace and freedom!
To lose myself and sleep!

But not the frozen slumber of the grave…
I'd like eternal sleep to leave
my life force dozing in my breast,
gently with my breath to rise and fall;
By night and day, my hearing would be soothed,
by voices sweet, singing to me of love.
And over me, forever green,
a dark oak tree would bend and rustle…

Salgo solo al camino;
En la bruma brilla el sendero pedregoso;
La noche es silenciosa. El desierto escucha a Dios,
y las estrellas hablan entre ellas.

Todo es solemne y misterioso en los cielos.
La tierra duerme en un resplandor azul…
¿Qué es lo que me resulta tan doloroso y difícil?
¿Quizás espero algo? ¿Lamento quizás?

Yo ya de la vida nada espero,
y nada lamento del pasado en absoluto;
¡Busco libertad y tranquilidad!
¡Quisiera olvidar y dormir!

Pero no con ese frío sueño sepulcral…
Quisiera dormir eternamente, de tal forma
que mi pecho guarde el poder de la vida,
y se alce tranquilo al respirar…
Que una dulce voz acaricie mi oído
cantando noche y día sobre el amor; y
que sobre mí reverdezca el roble oscuro
eternamente, y se incline, y susurre…

Mikhail Lermontov

"I Go Out on the Road Alone…"

PHD THESIS 2023

Institute of Biotechnology and Biomedicine
Department of Genetics and Microbiology
Autonomous University of Barcelona

A simple biochemical approach to easily manufacture complex protein-based materials has been rationally designed.

Divalent cations and the histidine tag appear as the main inductors of the recombinant protein gluing and subsequent self-structuring into nano and micro -scaled entities.

The platform's versatility, robustness and transversality has been repetitively confirmed, and product's biocompatibility considered.

Hèctor López Laguna